NATIONAL TECHNICAL UNIVERSITY OF ATHENS

School of Mechanical Engineering

Laboratory of Heterogeneous Mixtures & Combustion Systems

Doctoral Thesis

Investigation of novel emission reduction technologies and use of liquid or gaseous fuels for curbing marine engines environmental impact

Theofanis Chountalas

National Technical University of Athens

Supervisor: Prof. Maria Founti

Athens, July 2023

Abstract

The control of air pollution in all primary industries is the major technological challenge currently and for the upcoming decades. The effect of industrial carbon emissions on global temperature rise is now an undisputed fact, with all major institutions and governmental bodies examining pathways to reduce the amount of CO_2 emitted in the atmosphere. Unless strict measures are implemented, the global average temperature increase is projected to reach levels that will have severe effects on population welfare and the environment. Beyond CO_2, other emissions from fossil fuel powered infrastructure have been found to adversely affect human health and the environment. Some of the most harmful species emitted are NO_x, a product of high temperature combustion and a hurdle of diesel engine design regardless of application.

The marine sector accounts for roughly 3.3% of total anthropogenic CO_2 emissions and is also one of the major sources of NO_x emitted in the atmosphere, both on a global scale and near centres of high human population density. In this thesis solutions to limit the contribution of the marine sector on global emissions are investigated focusing on pollutants from marine internal combustion engines.

Modern emission reduction technologies for the marine industry are examined and evaluated using measurement data collected from marine engines on-site, either on-board vessels or during factory acceptance tests of the engines. The direct measurements were complemented by data acquired using telemetry solutions, if required. The technologies investigated, aim to reduce CO_2 and NO_x emissions by direct or indirect methods. Both emissions are controlled by the International Maritime Organization (IMO) with limits that target total ship carbon and NO_x emissions. The control of carbon emissions is enforceable since the start of 2023 via indexes that penalize high fuel consumption, hence CO_2 emissions. In the case of NO_x, limits have become considerably stricter in specific sailing areas since 2016. The CO_2 reduction technologies examined are the use of natural gas in dual-fuel marine 2-stroke propulsion engines and the use of marine type biofuels. Dual-fuel engines operating on liquified natural gas (LNG) are, in their current form, a relatively new development and the total number of such engines in the field is still limited compared to diesel only designs. High interest for marine grade biofuels started roughly in 2018, with considerable number of tests conducted between 2020 and 2022 to verify compatibility with various types of marine engines and evaluate for potential effect on NO_x emissions. The biofuel used for most of these tests and in the measurements conducted for this thesis contained 30% biodiesel sourced from waste oil feedstock. The NO_x abatement solutions examined are exhaust gas recirculation (EGR) and selective catalytic reduction (SCR). Both technologies started their commercial use in maritime within 2016, with SCR being the solution mostly selected until recently.

The thesis mainly concentrates on the 2-stroke engine which is the primary power source of commercial vessels and has the highest contribution to both CO_2 and NO_x emissions. The 2-stroke engine investigation involved two engines with the same characteristics but with different designs and settings regarding gas injection for the dual-fuel LNG high-pressure gas injection tests. For the biofuel trials five diesel engines of various types were tested. A diesel only engine and a one of the dual-fuel engines were considered for the

EGR tests and four engines were tested using SCR. In addition, seven 4-stroke engines were measured during the biofuel tests. All 2-stroke engines tested were state-of-the-art including automatic control systems. For the above subjects limited information is available in existing literature, especially regarding data from full-scale applications and analysis of potential performance impact of the technologies based on experimental procedures and not mainly simulation results.

The tests conducted included measurement of all major operational data from engines, with priority given in acquiring cylinder pressure traces and data from the engines' control systems. Exhaust gas composition measurements were conducted for all engines to estimate their specific NO_x emissions and acquire CO_2 emission data via a streamlined procedure devised for fast and accurate on-board and on-site tests. The CO_2 emissions were also calculated using fuel carbon content and fuel consumption. The cylinder pressure data were used to conduct heat release rate analysis and estimate the fuel combustion progress. A heat loss model was used to estimate gross heat release and allow calculation of fuel consumption where accurate measurement was not possible. The pressure traces were analysed to derive engine settings, specifically the timing of the exhaust valve opening and closing angle and the fuel injection angle. For the biofuels and EGR analysis, a multizone engine model was utilized to simulate engine performance and emissions. The model was based on pre-existing code that was modified accordingly. The validation of the model was performed using the data from factory acceptance tests (FAT), that are of high quality for engine operation at "conventional" conditions, with standard fuel and with/without EGR.

The technologies found to have the highest impact on engine performance compared to a modern but conventional design were dual-fuel high-pressure LNG and EGR. Dual-fuel operation tests showed both similar and quite different performance compared to diesel only operation, depending on the engine version. For both LNG engines, high combustion "speed" and fuel energy content resulted in increased peak combustion rate and decreased total combustion duration, excluding some cases of high delay between the diesel pilot and main gas injection. Overall, the effect of the pilot injection strategy was found to considerably alter the combustion mechanism. For the EGR equipped engines the presence of recirculated gases resulted to slower combustion and peak combustion rate values were decreased. The combustion duration was increased. For the other two technologies tested, biofuels and SCR, effects on engine performance were rather limited. The use of biofuel did affect combustion to a degree but was in most cases not immediately discernible. The SCR system had minimal impact on engine performance and no effect on the combustion process as it is an exhaust gas aftertreatment device not imposing excessive backpressure.

Analysis of engine tuning showed considerable differences in some approaches, with the highest degree of settings variation found for the EGR equipped engines and the updated version dual-fuel engine. For the dual-fuel engines, the previous generation engine showed a conservative approach regarding pilot fuel injection to limit peak combustion rate, pressure rise and maximum pressure values. The overall tuning resulted to nearly identical performance to diesel only operation. Different tuning approach was found for the newer engine that featured altered EVC timings, considerable pilot injection timing advance and use of a different injection profile for the diesel pilot. During EGR use both EVC and injection timing were considerably altered, as was

the total mass flow in the engines. Other notable differences in engine settings were found for the low-pressure SCR system examined, in contrast with the high-pressure one, that barely affected engine operation. These measures were employed to increase exhaust gas temperature at the catalyst inlet to allow safer operation and improve NO_x conversion efficiency especially at reduced load. The use of biofuels could have presented differences for fuel injection timing due to physical property differences, but only minimal effect was found. The only confirmed difference was earlier ignition due to elevated cetane number.

The variations in tuning and the combustion process affected main operational parameters, specifically compression and peak pressure, pressure increase after fuel ignition and exhaust gas temperature. The total efficiency of the engines was impacted in most cases with increased fuel consumption compared to typical operation. The notable exceptions were both dual-fuel engines. The total fuel mass consumed, and total energy content supplied to the engine were either similar to or considerably lower than diesel-only operation. In the case of the updated version engine considerable improvement of efficiency was found due to advances in injector design and a different tuning approach. The highest fuel consumption penalty was measured during EGR use in the diesel and dual-fuel engines. The main reasons were the reduced rate of the combustion process, prolonged duration and the lower peak pressures achieved. SCR operation caused minimal fuel penalty due to the added backpressure either on the engine of after the turbine and some tuning requirements to increase exhaust gas temperature. The urea consumption, however, was substantial, and its cost may, depending on pricing trends, approach or surpass that of crude oil. This resulted to the SCR being the least desirable NO_x reduction solution in terms of operating expenses, but also featuring the least number of considerations for potential issues on engine operation due to its relative simplicity and minimal effect on performance. The B30 biofuel did affect fuel consumption due to its lower calorific content and a slight combustion efficiency decrease compared to conventional fuels. The level of difference was evaluated as not concerning in terms of operating costs, but the issue of its higher price will remain until production capabilities increase.

The CO_2 emissions were affected by all the tested technological solutions due to the change in fuel consumption and/or the different carbon content of each fuel used. Biofuels showed only a small decrease of carbon tailpipe emissions compared to crude oil, while the lowest tailpipe CO_2 emissions were found for MGO operation. Their benefit towards carbon emission reduction will only result in a well-to-wake basis. On the other hand, their application is simple and requires no engine modifications. LNG use in high-pressure injection dual-fuel engines confirmed its high potential for carbon reduction with both good fuel consumption values and low fuel carbon content. The other two studied technologies resulted in fuel consumption increase that raises CO_2 emissions; despite the low consumption penalty for the SCR its impact was rated as considerable due to the urea production high energy requirements.

The NO_x emissions were not affected for the tested dual-fuel engines and were close to or below diesel-only operation. This is expected due to similar overall in-cylinder conditions and the use of the Diesel cycle principles. The increase in peak combustion rate, most prevalent in the updated dual-fuel engine, did not result in high change of NO_x emissions or exhaust gas temperature. In the case of biofuels, NO_x emissions were

above conventional fuel operation in most cases. This was found for both the 2-stroke and 4-stroke engines tested. The level of increase was moderate, allowing for the NO_x emissions standards of the tested engines to be retained. Due to almost identical engine performance compared to a conventional fuel, the NO_x emission increase was attributed to the oxygen content of the biodiesel, increasing air-fuel ratio in the flame and reaction speed. The use of the multizone engine model confirmed the previous with good predictions of NO_x emissions for biofuel and conventional fuels. Both the SCR and EGR systems were proven capable of substantial NO_x reduction, with the maximum efficiency of the former being slightly higher. It is noted, however, that the SCR catalyst efficiency will decrease with use, and three-to-five-year interval renewals are required. For the SCR system the efficiency of catalysts operating on HFO was also confirmed, with some reservations regarding the system's longevity. The EGR effect on NO_x emissions was investigated in detail using the multizone engine model, with good results in replicating its effect on their formation. The required EGR percentage was also estimated and found on the high side for all loads. The use of the model allowed to determine the actual mechanism for NO_x reduction and to examine of a solution for minimizing the fuel consumption penalty at all engine loads.

Overall, the viability of all technical approaches tested was confirmed, most notably for the case of biofuels that were up to now unproven in the marine field. Tests with the dual-fuel LNG engines demonstrated high versatility on operation capabilities via engine tuning and it was established that high level of advances can be achieved between sequential engine generations. This is strong indication that, as both a short- and mid-term solution, LNG powered vessels will become the go-to approach for low-carbon fuel use. Between the two NO_x abatement measures available and tested for large marine engines, both were found within expectations in real-world applications. Their comparison showed advantages and disadvantages for each system. The main concerns for the EGR system are high complexity, low number of operating hours in the field and high impact on engine operation. The SCR solution was superior in all of the previous terms, but its considerably higher operating costs are unfavourable in return of investment terms.

Acknowledgments

First of all, I would like to thank the supervisor of my thesis Prof. Maria Founti for her immense support in this undertaking. Her deep knowledge provided valuable insight, her support, direction and positive attitude were pivotal to the research involved and its completion. I would also like to extend my gratitude to the other members of my PhD committee Prof. Evangelos Giakoumis and Prof. Lambros Kaiktsis for their thoughtful input and remarks. I greatly appreciate their comments and have made an effort to consider them carefully in the analysis conducted.

Second, I would like to express my outmost gratitude to my family and most of all to my father. His deep knowledge, ever-present support and standing in the Greek marine field were a most substantial contribution to the work involved that would not have been possible at least in this form otherwise. My special thanks goes to my friends and partner for supporting me and enduring along the difficulties encountered in the years of conducting this research.

Last but not least, I would like to express my gratitude to the Technical Departments of the shipping companies that provided this invaluable opportunity in conducting experiments aboard their vessels. I would like to thank especially the vessels' crews and superintendent engineers attending the various trials for welcoming me onboard and being ever available for assistance even long after their official shift end. Their aid in the measurement procedures was crucial to the completion of the numerous tests that culminated to the present thesis.

Contents

Table of Figures

Nomenclature

Abbreviations

AFR	Air Fuel Ratio
aTDC	after Top Dead Centre
AUS40	40% Aqueous Urea Solution
BSFC	Brake Specific Fuel Consumption
bTDC	before Top Dead Centre
CA	Crank Angle
CAPEX	Capital Expenditure
CBV	Cylinder Bypass Valve
CFD	Computational Fluid Dynamics
CI	Compression Ignition
CII	Carbon Intensity Index
DF	Dual Fuel
DI	Direct Injection
ECA	Emission Control Areas
ECS	Engine Control System
EEDI	Energy Efficiency Design Index
EEXI	Energy Efficiency eXisting ship Index
EGB	Exhaust Gas Bypass
EGR	Exhaust Gas Recirculation
ERCS	Emission Reduction Control System
EVC	Exhaust Valve Closing
EVO	Exhaust Valve Opening
FAME	Fatty Acid Methyl Ester
FAT	Factory Acceptance Test
GHG	Green House Gas
HFO	Heavy Fuel Oil
HP	High Pressure
HRR	Heat Release Rate
ICCT	International Council on Clean Transport
IEA	International Energy Agency
IMO	International Maritime Organization
ISO	International Organization for Standardization
LP	Low Pressure
MARPOL	Marine Pollution
MCR	Maximum Continuous Rating
MEPC	Marine Environment Protection Committee
MGO	Marine Gas Oil
NG	Natural Gas
NTC	NOx Technical Code
OPEX	Operating Expense

Pcomp	Compression Pressure
Pign	Pressure at Ignition
Pmax	Maximum Combustion Pressure
SCR	Selective Catalytic Reduction
SGC	Specific Gas Consumption
SOC	Start of Combustion
SOI	Start of Injection
SPC	Specific Pilot fuel Consumption
TDC	Top Dead Centre
THR	Total Heat Rate
VLSFO	Very Low Sulphur Fuel Oil
WTS	Water Treatment System

Latin Symbols

A	effective area, m^2
a	initial spray angle, rad
C_d	discharge coefficient
c_p	specific heat capacity at constant pressure, J/kgK
c_v	specific heat capacity at constant volume, J/kgK
D	cylinder bore, m
d	diameter, m
D_d	droplet diameter, m
DSM	Sauter mean diameter, m
D_t	turbulent diffusivity, s^{-1}
D_v	mass diffusivity, m^2/s
E_c	reduced activation energy, J/kmol
E_m	mean kinetic energy, J
H_a	absolute humidity, g/m^3
h_c	heat transfer coefficient, W/m^2K
I	moment of inertia, kgm^2
k	turbulent kinetic energy, J
k_{hd}	NOx humidity correction factor
L	breakup length of fuel spray, m
l_{car}	characteristic length, m
L_f	fuel latent heat of vaporization, J/kg
m	mass, kg
n	fuel jet axial penetration exponent
P	pressure, pa/Bar
P_{O2}	partial oxygen pressure, bar
P_{tk}	turbulent kinetic energy production rate, W
P_v	vapor partial pressure, bar
Q	heat exchange rate, W
q	flow rate, kg/s
R	gas constant, J/kmolK

r_i	position relative to axis, m
R_i	one way reaction rate for reaction i
r_o	jet cross section radius, m
R_{pos}	radius of position, m
T	temperature, K
t_{break}	time for fuel jet breakup, s
Tr	torque force, N
u	velocity, m/s
u’	turbulent velocity, m/s
U_a	swirl velocity, m/s
u_i	density ratio of species i and total exhaust gas
V	volume, m^3
W	angular velocity, rad/s
w_{ALF}	mass percentage of H in fuel
w_{BET}	mass percentage of C in fuel
w_{EPS}	mass percentage of O in fuel
x	distance, m
X_i	percentage of species i
z	heat transfer correction factor
ε_t	viscus dissipation rate, W

Various Constants & Coefficients

a_c	heat transfer constant
a_{del}	ignition delay constant
A_{eq}	equivalent blowby area, m^2
A_{max}	CBV orifice area
b	heat transfer constant
c	heat transfer coefficient constant
C_{iscav}	scavenging model constant
c_l	fuel jet breakup length constant
c_r	heat transfer constant, W/m^2K^4
fc	fuel carbon factor
f_{fd}	fuel specific constant
K_b	fuel combustion rate constant
k_{if}	forward reaction rate constant
n_{cbv}	CBV valve area coefficient
σ_r	heat transfer constant

Greek Characters

δ	wall jet thickness, m
δ_i	zone i distance from the wall, m
δ_{rc}	equivalent cylinder piston clearance, m
ε_t	viscus dissipation rate per unit mass, W/kg
κ	thermal conductivity, W/mK

λ	air-fuel equivalence ratio
μ	dynamic viscosity, kg/ms
μ_t	turbulent viscosity, kg/ms
ν	kinematic viscosity, m^2/s
Π	pressure ratio
ρ	density, kg/m^3
σ	surface tension, N/m
φ	deg, rad
Φ_{eq}	local equivalence ratio (fuel to air)

Dimensionless Groups

Nu	Nusselt number
Pr	Prandlt number
Re	Reynolds Number
Sc	Schmidt number
Sh	Sherwood number
We	Weber number

Subscripts

a	ambient
car	characteristic
d	dry
e	equilibrium, exhaust
exh	exhaust
f,l	fuel, liquid
g	gas
gross	
inj	injector/injection
inl	unlet
m	mass/mean
net	
o	initial/open
p	cylinder
sc/scav	scavenging
st	stoichiometric
TC	turbocharger
w	wall/wet

Chapter 1 Introduction

1.1 Background & Motivation

Environmental protection and air quality improvement is one of the most important technological challenges of the immediate future and is expected to result in major shifts in all sectors relying on the use of fossil fuels and internal combustion engines. The maritime industry is estimated to account for 15% of NO_x emissions globally and for 16.5% of population exposure in the EU (1,2). In addition, while emissions from vehicles are on the decline, ship emissions show a steadily increasing trend (2). NO_x emissions control is important due to its harmful effect on human health and the environment (3). The CO_2 emissions of marine vessels account for 3.3% of global values and projections point to considerable increase in the immediate future, unless mitigative measures are implemented (4,5). While the percentage compared to total emissions is low, the total green-house-gases (GHGs) emitted by the industry are high, over 1000 million tons annually. Despite the energy crisis during the coronavirus pandemic CO_2 emissions have risen globally and reached a new high in 2022, (6). The International Council on Clean Transportation (ICCT) has declared the immediacy for action to curb carbon emissions in the next 15 years for any chance to limit global warming to 1.5^{o}C above pre-industrial levels to be retained, (7). A scenario of exceeding this limit could result in catastrophic consequences for natural and human systems, (8,9) as has been known since the late 1970s. In Figure 1-1 global temperature anomalies, as recorded by NASA are visualized for the period of 2018 – 2022, with 2016 the warmest and 2019 the second warmest year in the 140 years of global historical records (10,11). Just recently the hottest recorded day record was broken consequently between 5 - 8 July 2023 (12). In Figure 1-2 the CO_2 emissions in the general Europe and African area are visualized by the organization (13) showing the increase of CO_2 concentration in the atmosphere and in Figure 1-3 the global NO_x distribution is given for 1960 and 2021.

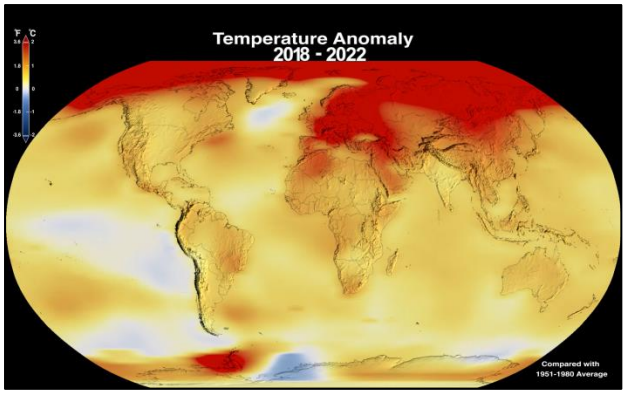

Figure 1-1 Global temperature anomaly events and distribution 2018 - 2022, (11)

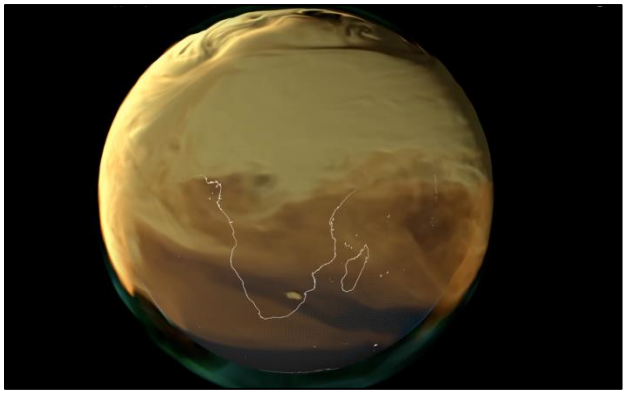

Figure 1-2 CO_2 emissions visualization, Europe and Africa 2022, (13)

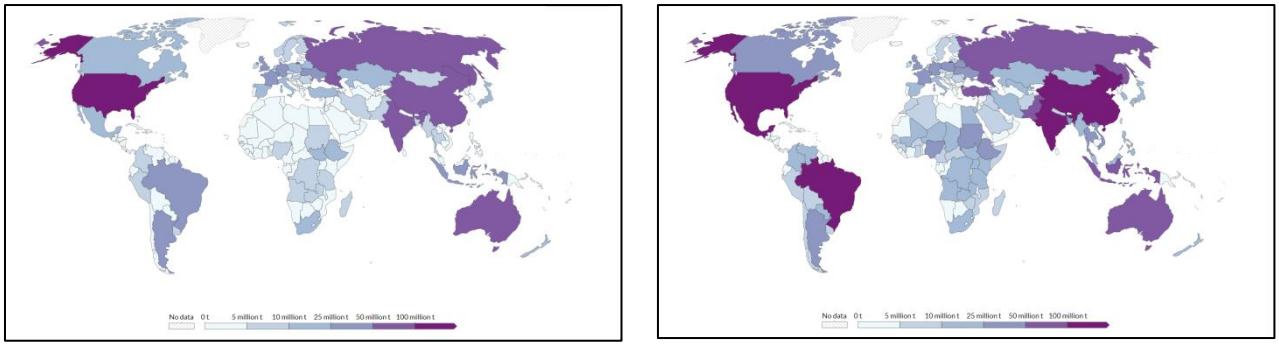

Figure 1-3 Global NOx emissions distribution, 1960 vs 2021, (14)

Further to the previous, marine engines have a very high contribution to SO_2 emissions due to the use of low distillation fuels, that account to 15% of total emissions and at the same time to 11.6% of EU population exposure to the pollutant due to sailing near coastal areas (15,16). As established for decades, the SO_2 emitted by the combustion of high sulfur content fuels can have serious effects on human health and above a certain concentration to the environment (17,18).

The internal combustion engine is the main powertrain solution of the maritime industry and will remain the main technical solution for the next decades as no promising alternatives are immediately available (19). The reasons for this dependence of the industry are the requirements of very high power output and for operation at prolonged periods without stops for refuelling. At the same time, the powertrain selected should not have considerable impact on the cargo capacity of the vessel. The previous makes solutions such as electrification or utilization of renewables very difficult (20,21) with the exception of niche applications that mostly utilize small vessels of low power requirements (22). The variant with the most widespread adoption for the propulsion of seagoing commercial cargo vessels are compression ignition (CI) engines, most commonly large 2-stroke low-speed types. For auxiliary power requirements 4-stroke medium-speed diesel generators are used. The almost universal use of CI engines in these applications is the result of superior thermodynamic efficiency and the ability to run these engines on crude oil variants such as Heavy Fuel Oil (HFO). The sheer power output of propulsion marine engines and consequently their energy requirements, coupled with high runtimes, make fuel costs of outmost importance for vessel operators.

As with all industries relying on fossil fuel combustion, maritime is faced with scrutiny, and changes are demanded by institutional bodies aiming to achieve significant emissions reduction. The International Maritime Organization's (IMO) first efforts regarding pollution control in the industry date back to the MEPC MARPOL 1973 convention (23). Air pollution measures were set in the MARPOL ANNEX VI, initially discussed in 1997, and have been revised multiple times with the 2008 NO_x Technical Code introduction being a major milestone setting the first hard limits for NO_x emissions of marine vessels now designated as Tier-I (23). The latest revision of marine air pollution legislation entered into force in November 2022 including, for the first time, measures aimed at GHG emission control (24). Currently the officially regulated exhaust emissions are NO_x and SO_x, with carbon emissions being indirectly restricted in the form of environmental performance indexes to be achieved by vessels (4). The first measures for emission control of

vessels were imposed in January 2000 by the IMO with the Tier-I standard which set limits for NO_x emissions of marine diesel engines of over 130kW output power, (23). Stricter limits were imposed in January 2011 with the introduction of the Tier-II emission standard. Since January 2016, the Tier-III limitations have been in effect, enforceable in select Emission Control Areas (ECA) zones, while globally the Tier-II limit applies, (25). The emissions limits for large 2-stroke marine engines for each NO_x emissions tier are provided in Figure 1-4. The transition from Tier-II to Tier-III introduced significant challenges demanding NO_x emissions reduction of 77% for low-speed engines compared to the 15% reduction from Tier-I to Tier-II limit, (26,27). Considerable statutory restrictions on SO_x emissions came into effect in 2005 following their 1997 introduction in the MARPOL ANNEX VI. The initial global limit was 4.5 wt. % and since 2020 has been reduced to 0.5 wt.%, while for ECA zones a 0.1 wt.% limit has been in effect since 2015, (28). The SO_x emissions limits through time are given in Figure 1-5 with the depiction of current and possible future ECA zones illustrated in Figure 1-6. Carbon emission restrictions started in January 2023 towards the goal of reducing GHG emissions from vessels by 40% compared to 2008 values until 2030, (4). While no specific limits have been set for CO_2 and other GHGs two indexes were introduced, Energy Efficiency existing ship Index (EEXI) and the Carbon Intensity Index (CII), related to vessel fuel efficiency and carbon output, (29). Depending on the score of the two indexes vessel operators may be forced to limit maximum engine power and sailing speed inhibiting vessels' operational capabilities, (30,31).

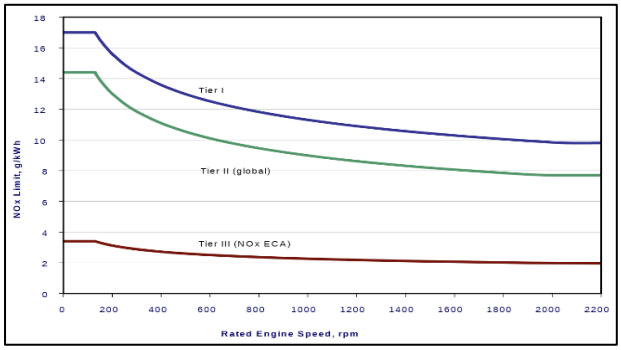

Figure 1-4 Marine NOx emissions limits, (32)

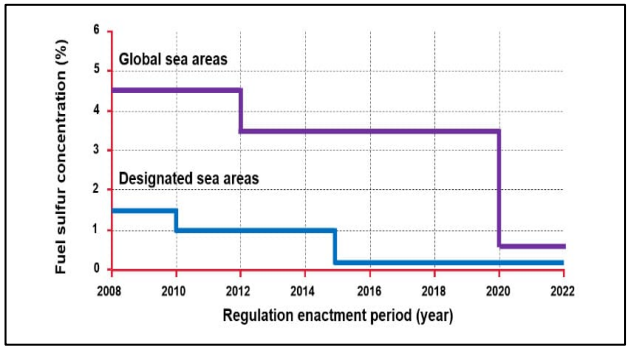

Figure 1-5 Marine SOx emission limits, (33)

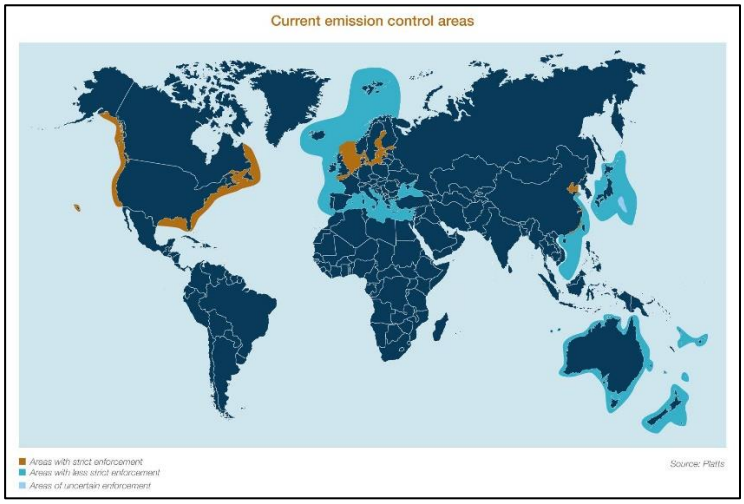

Figure 1-6 Marine Emission Control Areas Map, (34)

Following the drastic changes in environmental policy, major shifts are underway in the maritime industry. The technical solutions to overcome the new restrictions without significantly impacting operational capabilities, fuel economy or availability and vessel acquisition cost are still not fully defined by the regulating bodies (35,36). Vessel operators are concerned for the best strategy for a future fleet composition, evaluating mainly cost, ease of operation, versatility and future proofness of newly acquired vessels should further restrictions be imposed.

1.2 Thesis Objectives & New Contribution to the Field

The regulated exhaust emissions of marine engines are, as mentioned, CO_2, NO_x and SO_2. In this thesis various technical solutions for reduction of the CO_2 and NO_x emissions are investigated, based on applications in the field, in its two main chapters. Regarding SO_2 emissions, the industry has already settled on the use of low sulfur content fuels or the installation of SO_x scrubbers to achieve the required emissions limits. It is noted, however, that the use of certain scrubber systems (open loop) is being banned in various areas (37), and depending on the approach shipowners follow, further traction for research may appear on the subject. This will mostly depend on price and availability of low and very low sulfur content crude oil blends. Regarding CO_2 emissions a clear pathway has not yet been decided by regulators or shipowners (24). For NO_x emissions two main reduction methods are currently in use, each with their individual advantages and disadvantages.

1.2.1 Thesis Main Objective

The main objective of the thesis is to analyse the use of technical solutions for O_2 and NO_x emissions reduction technologies in the marine field focusing on novel solutions. The major requirement for the technologies investigated was to be currently usable in actual commercial operation and to be considered as potent short- and mid-term solutions for marine engines emissions control, while keeping operating expenses within normal limits. The analysis contained in this thesis is focused on measurements to evaluate data from actual operation and utilizes software tools for in-depth analysis, where viable. The aim is to provide a comprehensive evaluation on major, newly introduced, pollution reduction technologies in the marine industry, focusing on their effect on engine operation and performance and primarily relying on data from measurements conducted on the field.

The technologies investigated in the thesis are newly introduced in the marine sector and include in-cylinder measures (internal), exhaust after-treatment devices (external measure) and alternative low carbon content fuels. Specifically for CO_2 emissions reduction liquified natural gas (LNG) use in dual-fuels engines and liquid biofuels were investigated. The NO_x emissions abatement solutions examined were selective catalytic reduction (SCR) and exhaust gas recirculation (EGR). These solutions are either newly applied in the field, or under evaluation by regulators and shipowners. The analysis is based on extensive collection of experimental data acquired from full-scale testing, either on-board vessels or in engine manufacturer facilities.

Experimental results are also used to verify simulation tools that are utilized for further analysis and mainly for the better understanding of the mechanisms that affect pollutant formation.

For the requirements of this thesis experimental data were acquired during full-scale tests with attendance on-board marine vessels. The tests were conducted both on-board vessels during normal operation and official sea trials processes. In addition, attendance and data collection was possible for engine FATs, commonly referred to as Shop Tests in the industry, at the manufacturer facilities. This was achieved in cooperation with engine makers and allowed to have high quality data. The on-site measurement data are complemented by data acquired via telemetry via a specialized methodology in collaboration with shipowners.

1.2.2 Thesis Main Contributions

1.2.2.1 Methodology

Due to the sheer size of most of the engines tested and the low, or relatively low, number of units currently utilizing the examined technologies, data from tests conducted at full-scale are very limited in the literature. The logistics of conducting tests on-board vessels or participating in factory acceptance test (FAT) procedures are challenging. In addition, use of equipment and measurement methods that do not intervene with commercial operation, or other tests conducted in parallel, further complicates the testing of new technologies on marine engines. For this reason, a streamlined procedure for acquisition of performance and emissions data was devised with the aim of fast, efficient, and most importantly accurate measurements that allows for fast verification of acquired data quality. This allowed for the analysis in this thesis to accommodate a high number of engines, 19 in total. Multiple engine types were tested utilizing state-of-the-art technologies in the marine field.

The conduct of these measurements allowed to carry out a subsequent analysis on a basis of hard data and not estimations by simulators as commonly performed. The measurement procedure was performed on modern engine types utilizing the emissions reduction solutions and provided insight on the various tuning changes and compromises required to a degree that is possible by a hypothetical simulation. It also allowed to account for the previous in the theoretical analysis included and provide further insight to the mechanisms involved and influencing engine manufacturer choices. In addition, a combined analysis of the effect on both engine performance and emissions was provided that is rarely contained in previous works on these subjects.

1.2.2.2 Technologies & Fuels Tested

LNG Dual-Fuel Engines

The measurement campaign conducted allowed for this thesis to include direct analysis and comparison of dual-fuel high-pressure gas injection engines of the latest technology. The use of actual data for operation at single (diesel) and dual-fuel (diesel and LNG) and direct comparison allowed to provide concrete estimates regarding emissions and expected benefits. In addition, insight on the combustion mechanism and particular tuning requirements was provided. The use of two sequential generation engines also provided information on

improvements and major changes that can be expected for this technology. Information for dual fuel 2-stroke marine engines is scarce in the available literature, especially for the high-pressure gas injection variant and analyses based on actual measurements.

Marine Biofuels

The investigation conducted for biofuels covers a significant lack of technical and theoretical knowledge regarding use of this fuel type in marine engines. At the time of writing this work (and related published content in scientific journals) provide the first analysis regarding biofuel use in marine engines, especially 2-stroke ones that contain information on performance, combustion and NO_x formation process combining measurement data and computational results.

EGR

The use of EGR is yet relatively uncommon in the marine industry. The measurement data acquired allowed to assess its impact on engine performance, combustion and NO_x formation under actual conditions. The requirements for engine tuning were reviewed to a degree not possible by engine simulators. In addition, the simulation tools utilized were prepared accordingly using the measurement data to allow parametric investigations that are closer to actual conditions. Investigations that use actual measurement data and provide detailed analysis on both engine performance and emissions of large 2-stroke marine engines are scarce in the available literature.

SCR

The extensive investigation of SCR use in multiple engines provided insight on the specific of engine operation and tuning limitations by the catalytic reactor minimum temperature threshold requirements. Data from various cases was collected for specific urea consumption that changes considerably with engine load. This is a value of major interest that is rarely used in detail in most investigations as they rely on flat assumptions for the total engine load range. Last, the trials and subsequent analysis include one of the first tests conducted with HFO in SCR systems, that is a new and quite limited approach.

Overall, a substantial contribution to the subject was provided, including both qualitative and quantitative findings that can also be utilized as a basis or guideline for future applications and analyses.

1.3 Thesis Outline

The introductory part of the thesis continues with two additional chapters, 2 and 3. In chapter 2 a detailed background on CO_2 and NO_x emissions is provided, focusing on the marine industry's approach to their control with the relevant legislation and reduction technologies currently employed and under consideration.
Chapter 3 includes the principles and main formulation of the multizone combustion model used for detailed analysis of the biofuels and EGR effect on performance and in-cylinder combustion and emission formation mechanisms.

Next the two main sections follow that contain the investigated emission control technologies. The sections are divided on a pollutant basis for CO_2 and NO_x. In the case of biofuels, the effect studied applies to both the CO_2 and NO_x emissions. Their categorization is based on the primary emission target that is CO_2.
The main sections are:

Section 2: CO_2 emissions reduction.

- Chapter 4: Dual-fuel high-pressure natural gas engines, a direct approach to carbon emissions reduction.
- Chapter 5: Biodiesel addition in crude oil blends, an indirect approach to carbon emissions reduction.

For both chapters engine performance and tuning are determined and evaluated and the impact of the two fuels, biodiesel and LNG, on the combustion process compared to conventional ones is estimated. For the dual-fuel section two engines of the same type and consecutive generations, with the later generation only recently installed in delivered vessels, are examined and compared. The data presented are exclusively from high-pressure gas injection engines. In the case of the biofuel study, data from both 2-stroke main engines and 4-stroke auxiliary generators are presented. In total five 2-stroke main propulsion engines and seven 4-stroke auxiliary generators using different variants of B30 biofuel were tested. The combustion process analysis is based on measured data, specifically the pressure traces from the cylinders were employed. The combustion analysis is also used to estimate fuel consumption with the required accuracy, which was important in cases where measuring instruments were not installed or measurements proved to lack sufficient accuracy. Emission measurement data are used to assess impact on emissions and verify compliance to regulations and the level of benefits expected regarding carbon output potential. Performance and emissions are compared to findings of other published studies and to data published by engine manufacturers, vessel operators, classification societies, and marine fuel providers. The biofuels study includes a computational investigation using a multi-zone simulation model that was utilized to simulate the effect of an oxygen enriched fuel on the performance and NO_x emissions of a large 2-stroke engine. Direct comparison between the two CO_2 reduction methods is not performed, as biofuels and LNG are aimed at different market segments. Biofuels are considered as a ready to use (drop in) fuel that requires no modification to the engines, fuel storage and handling installations of existing vessels, while LNG use is mainly considered for newly ordered vessels even though also available for retrofit solutions. The ability to conduct a retrofit to enable dual fuel operation is provided by engine manufacturers (38), however, the overall cost and the requirement to also install a separate fuel gas supply system and bunker tank will most probably dissuade ship owners from proceeding to alteration of this scale if other options are available.

Section 3: NO_x emissions reduction to achieve Tier-III standards.

- Chapter 6: Exhaust gas recirculation; an in-engine solution.
- Chapter 7: Selective catalytic reduction devices; an exhaust gas after-treatment solution.

For the two chapters the effect of the methods used to reduce emissions is evaluated regarding NO_x reduction potential and effect on engine performance and fuel efficiency. For the analysis, all data used were also acquired from measurements conducted on full scale applications. All results in this case refer to 2-stroke large engines since these are the main emission contributors. The EGR equipped engines tested were one diesel engine and one of the dual-fuel engines of the CO_2 emissions chapter (the previous generation, as the newer one was equipped with an SCR system for NO_x reduction). In the case of the dual-fuel engine, the effect of EGR was tested both at diesel only mode and during dual-fuel operation but emphasis was made on the dual-fuel mode results. Measurements on SCR equipped engines were conducted on-board multiple vessels and during FATs, with the results from four characteristic cases included. The data from low-pressure (LP) and high-pressure (HP) catalyst installations are reviewed and provided separately. For both the EGR and SCR systems the analysis is aimed at engine tuning changes when the systems are active and their effect on performance and emissions. Performance and combustion analysis is extensively analysed in the EGR part and only an overview is given in the SCR part for reference, due to its minimal effect on performance and no effect on the combustion process. The multizone engine model used above is utilized for analysis of the EGR engine. Its use allowed the estimation of certain implementation specific parameters detailed in Chapter 6, and to provide further insight to its effect on the combustion and NO_x formation mechanisms. Furthermore, it was used to investigate the possibility for fuel consumption penalty reduction via engine tuning.

Extensive modifications were performed to simulate the EGR system during open cycle simulation. This included modifications to account for some changes of engine design and tuning during EGR use. In addition, modifications were applied in the fuel air-mixing mechanism along with the introduction of variable engine settings for the case of electronically controlled 2-stroke engines These modifications are provided in a short subsection of Chapter 6, EGR, following a detailed description of the EGR system and the engine modifications conducted for its incorporation.

In the SCR section the methods used by the system designers to increase exhaust gas temperature at catalyst inlet are analysed. The last part of the chapter includes a direct comparison between the two NO_x abatement solutions where overall complexity, engine operation impact and operating costs of each system are compared. The final chapter contains a combined summary for all four technologies tested, along with the conclusions derived from the analysis.

1.4 Publications & conference presentations

The following publications in peer-reviewed international journals and conferences resulted from the work performed as part of the Thesis:

Journal Publications:

- Provataris S. A., Savva N. S., Chountalas T. D., Hountalas D. T. “Prediction of NOx emissions for high speed DI Diesel engines using a semi-empirical, two-zone model”, Energy Conversion and Management, 153, 2017, p. 659-670, https://doi.org/10.1016/j.enconman.2017.10.007.
- Chountalas T. D., Founti M., Zannis T. “Experimental Investigation to Assess the Performance Characteristics of a Marine Two-Stroke Dual Fuel Engine under Diesel and Natural Gas Mode” *Energies* **2023**, *16*, 3551. https://doi.org/10.3390/en16083551.
- Chountalas T. D., Founti M., Tsalavoutas I. “Evaluation of biofuel effect on performance & emissions of a 2-stroke marine diesel engine using on-board measurements”, Energy, 278, 2023, 127845, https://doi.org/10.1016/j.energy.2023.127845.
- Chountalas T. D., Founti M., Hountalas D. T. "Review of Biofuel Effect on Emissions of Various Types of Marine Propulsion and Auxiliary Engines", *Energies*, 16, 2023, 12: 4647, https://doi.org/10.3390/en16124647.

Conference Proceedings:

- Chountalas T. D., Founti M., “Effect of Low-Sulfur Fuel on Auxiliary Engine Combustion and Performance”, SNAME 7th International Symposium on Ship Operations, Management and Economics, SOME 2021, https://doi.org/10.5957/SOME-2021-010

Chapter 2 Carbon & NO_x Emissions in the Marine Industry

2.1 Pathway to Lower Carbon Emissions in Maritime

Carbon oxide emissions are a natural product of combustion using fossil fuels as they contain significant amount of carbon in their molecular structure. CO_2 in the atmosphere traps part of the long-wave radiation emitted by the earth's surface trapping heat and thereby increasing temperature. The reduction of carbon emissions is of the outmost importance to retain average earth temperature within 2^oC above the pre-industrial levels, as further increase could have catastrophic impact to the current state of earth's biosphere. Currently almost all industries with significant anthropogenic CO_2 emissions are in the process of investigating solutions to their decarbonisation. Efforts have increased since the alarming all-time high for carbon emissions in 2016 that motivated industrial and governmental bodies to adopt a resolute stance regarding decarbonization of human activity, (39). The marine industry is almost entirely dependent on the combustion of fossil fuels for energy production. Over 85% of all merchandise is transported by marine vessels making the industry the backbone of the commercial and transport sector worldwide, (40). Its carbon emissions account to 3.3% of total anthropogenic emissions according to the latest estimates and are set to further increase in the future, (6,41). Due to the size of the industry and the complexity of large vessels' high power requirements, a defined pathway to emissions decrease has yet to be set. For large marine vessels, such as cargo and container ships, bulk carriers and tankers, electrification solutions are not currently feasible and will not become a viable option for the foreseeable future due to the high power concentration and capacity required, (20). This makes a solution utilizing fuel combustion in IC engines the expected approach for the next decades, (42). Thus, the remaining pathways for decarbonization of the industry's powertrains is increasing operational efficiency of vessels and relying on low or zero carbon content fuels. Operational efficiency improvement of vessels is possible, however, the remaining degree for improvement is low, as expected in a well-established industry, (35). In addition, the high cost of fuel in the last two decades has long steered the industry towards optimization to maximize profit margins. The latest development regarding efficiency advances is vessel routing optimization using advanced algorithms such as deep learning and artificial neural networks, but the level of expected improvement is in the single digit region, (43,44). The emission reduction target set by the industry is 40% compared to 2008 by 2030 and by 50% - 70% up to 2050 and these quotas cannot be met through optimization alone. Currently the industry's attention is set on alternative fuels, liquid and mostly gaseous, that can allow achieving low or even zero net carbon emissions (4,45–47). The main fuel to be used is, according to current market position and projections by industry bodies, natural gas, (20,36,48). Other fuels examined are biofuels, ammonia, methanol and e-methane. At this point, apart from LNG, none of the low-carbon fuels have reached a meaningful penetration in the market, (20). For reference, according to estimates, the use of biofuels accounts for roughly 0.1% of the total energy consumption of marine vessels, (49). The adoption of vessels equipped with engines capable of operating on LNG is growing and has reached considerable levels, with an annual growth between 20% - 40% since 2010, (50). Despite the high rate of

adoption as an absolute number the LNG powered fleet remains limited in size when excluding LNG carriers with a total of 173 vessels in operation by 2022, (42). The number of active LNG carriers is roughly 600 vessels and most of them use LNG as primary fuel, (51). With a high number of active orders for both LNG carriers and vessels equipped with LNG-ready engines, industry bodies expect LNG use to lead to midterm efforts of the industry for decarbonization.

Starting roughly around 2018 the marine industry began trials of using biodiesel as a drop in fuel. Biodiesel was tested in blends with very low sulfur fuel oil (VLSFO), for ratios of 20%, 30%, 50% and 100%. The testing was conducted by engine manufacturers and vessel operators in collaboration with classification societies of the industry, focusing mainly on emissions, (52,53). Following initial testing results, international maritime regulations for pollution were updated in mid-2022 to allow operation with fuel blends containing up to 30% biodiesel that was officially classified in the same category as normal HFO/VLSFO. However, ship operators still have concerns regarding the possible effect of biofuel on performance and the present thesis offers a positive contribution in this field.

2.1.1 Legislation for CO_2 Emissions

Official legislation for limiting carbon emissions of commercial vessels came into effect in January 2023, (4). The first two measures implemented refer to the design and operational aspects of vessels with the EEXI and CII indexes respectively. The EEXI calculation is required to be submitted to regulating parties as a once in a lifetime process, unless substantial changes are performed on the vessel. The first periodical survey will be completed in 2023 at the latest for all vessels that are of 400 GT and above with the requirements for EEXI certification having started since November 2022, (29). For each vessel type and particulars, a certain efficiency value has to be achieved. A number of options is provided for cases where improvements are required. The most common is engine power limitation (EPL), which restricts the maximum available engine power. Other popular methods are devises to improve vessel propulsion efficiency, such as ducts, propeller boss cap fins, but the effectiveness of said devices has to be verified by model tests. Additional options can be re-tuning of the engine, which in turn requires revision of its NO_x file to verify that emission standards are attained, and retrofits allowing the use of alternative fuels for example LNG. Last, state of the art efficiency devices that may be used are wind assisting propulsion systems or hull air lubrication systems, (4,24,30,45,54).

The Carbon Intensity Indicator (CII) came into effect in January 2023 to be used as (31,55,56) an indicator of operational efficiency at an annual basis. The CII rating applies to commercial vessels of 5000 GT and above regardless of propulsion type. The rating has five categories from A to E with the threshold of each stage revised and becoming increasingly stringent towards 2030. For vessels that achieve a D rating for three consecutive years or an E in a single year their operators will have to proceed to a corrective action plan. The basis of CII calculation is emitted CO_2 per cargo carrying capacity and nautical mile. The achieved CII rating is primarily the result of fuel consumption and how efficiently the ship is operated. The final rating is affected by vessel speed, engine and hull condition and how effectively the ship is routed based on voyages and

weather conditions. Studies by independent organizations have verified that the impact of speed limitations on vessels can substantially decrease emissions, (57). Considering the CII rating the use of biofuels or other carbon neutral fuels can provide significant improvement of the final evaluation, allowing greater flexibility especially concerning the vessel speed set by charterers. The same applies to vessels operating on natural gas (NG) that has low carbon content and can easily achieve good CII rating, at least until methane emissions monitoring commences.

2.1.2 Carbon Emission Reduction Technologies under Consideration

The pathway to low carbon emissions within 2050, set by the IMO, has led to consideration of multiple technical approaches. These mainly include alternative marine fuels of low-carbon content and the use of advanced technologies, not yet applied in the maritime sector, (35). The short-term ones are technical and operational measures that have taken the form of the CII and EEDI/EEXI indexes to regulate carbon output of existing marine vessels. The mid-term solutions that will be jointly utilized with the aforementioned indexes will be market based measures and the introduction or further adoption of low-carbon fuels. On the long-term, from 2050 and beyond, technologies that are still in the R&D or pilot project stage are expected to make their market entry or to have achieved a meaningful market penetration. Currently industry bodies expect that solutions with most likely market uptake will be LNG and LPG, (42), with currently the highest percentage of both active and on-order (newbuildings) vessels utilizing a low/lower carbon solution, being LNG powered, (36). Biofuel of Fatty Acid Methyl Ester (FAME) content is also projected as able to make a market entry, as recent trials and improvement in its production capacity for marine use have shown potential, (58,59) and marine biofuels are becoming commercially available. Interestingly studies have shown that the conventionally used fuel with the greatest benefit regarding carbon emissions is HFO with the use of a scrubber unit, (42), however the use of scrubbers is progressively being banned in ports worldwide currently, (37).

Beyond solutions existing in the market the alternative fuels that may be adopted by the industry in the future are methanol, biogas, hydrogen (from water or methane) as a fuel or in fuel cells and ammonia, (20,35,47,60). As stated in chapter 1, battery powered propulsion has been mostly excluded as a consideration for large marine vessels due to the very high power density required. Electrification may prove to be a good solution for smaller vessels sailing short routes near coastal areas, (35,61,62). Ammonia is another fuel into consideration that can be used in marine engines as a H_2 carrier, with the first large 2-stroke marine engine expected by 2024, (63), while an extensive proof of concept project has been underway from various industry bodies since 2020, (64). Its use within fuel cells is currently at a premature stage and direct combustion will be the first version of the technology, (35,65,66). Apart from a considerable number of technical challenges, mainly due to the ammonia being toxic and having a lower combustion speed (63), the major problems for its adoption are very limited supply and practically non-existent bunkering infrastructure, (67). No availability exists for ammonia, as the yearly global production is currently consumed by other sectors, mainly agriculture, almost in its entirety, (68). Increase of its production by significant percentage, especially using

renewable sources to achieve a net carbon emission reduction would require profound changes in the worldwide economy. The previous is partly due to the very low efficiency of using electricity to produce ammonia for vessel propulsion; the total cycle efficiency is estimated at around 17%, (65). The next stage would be use of hydrogen, possibly within fuel cells. There is currently no application for such engines in the marine industry, (20). The use of hydrogen is considered as one of the last technologies to reach maturity and to be late-term option possibly beyond 2050 for zero-carbon shipping, (35). The main reasons for this reservation regarding the required time for full scale use of this fuel is the land-based applications that have been met with some accidents, and the challenges of transitioning this technology and its peculiarities to the challenging marine environment, and the engine operation due to the combustion speed of hydrogen, (69) thus the most common way to use the fuel is through either addition to conventional fuels or via its use in fuel cells. However, multiple concerns still exist for fuel cells in marine vessel use ranging through safety to their capability as a main powertrain solution for large vessels due to issues when both high energy density and low energy input are required, (70). In addition, one of the main challenges, hydrogen storage on-board is not solved, (71). The final major hurdle regarding this technology is cost that using current production capabilities and methods will be considerably higher than all other fuels examined for potential use, regardless of the hydrogen production approach, (72,73). Despite the ever-mounting concerns for environmental protection and curbing global temperature rise a non-viable economic solution will not be adopted at a meaningful degree and other options will be examined. The same currently applies to fuel cell use in general, regardless of their technology, (20). The last two fuels under serious consideration are liquefied petroleum gas (LPG) and methanol. The use of LPG is viewed in tandem with LNG as they both require the use of dual fuel engines and actual commercial solutions already available in operating vessels are in the field, (36,42,74) with more than 100 LPG operation capable main propulsion engines sold since 2018 by one of the major two marine engine manufacturers. The CO_2 reduction potential of LPG ranges between 13% - 18% based on estimates from various sources, (20,35,74,75). Its combustion characteristics show stable combustion, low flame temperature and the fuel has a high octane number (75,76), all of which are desirable qualities in a dual fuel engine for the main fuel used (roughly the opposite are required for the fuel triggering the main combustion event). Actual data from researchers that studied existing LPG powered vessels confirm that fuel efficiency was good for these engines and that LPG prices were competitive to conventional fuels, (75,76) (for substantial time periods propane price was comparable to that of Brent oil, (20)). However, as with the use of LNG, concerns exist regarding propane slip to the environment that can negate all CO_2 reduction benefit or even have higher final environmental impact and further evaluation using empirical tests is recommended, (75). In this thesis the use of LNG is examined due to its much faster adoption and most studies considering it as the most viable mid-term fuel use in the future, (20,21,35).

The last alternative fuel considered is methanol that features the lowest carbon content and can be almost completely carbon neutral when produced from electricity via renewable sources or biomass (e-methanol), (77). However, for methanol not produced by renewable sources the carbon emission benefits decrease considerably due to its higher brake specific fuel consumption (BSFC) compared to conventional fuels,

mostly because of a low lower calorific value (LCV), (78). Some studies conducting lifecycle analysis of the fuel have concluded that when methanol is produced from fossil feedstock such as coal and natural gas the life cycle GHG emissions might be above those of typical HFO, (79). Further to the carbon emission benefits the combustion of methanol produces lower NO_x than marine gas oil (MGO) or HFO, (80–82). This is due to the lower combustion temperature of methanol, (83–85). However, the level of emissions is still below the Tier-III standards, (20,86–88). The combustion characteristics of methanol also resulted in very low particulate matter emissions, confirmed by measurements from real world testing in marine methanol engines, (79,82). Currently only one type of methanol capable two-stroke diesel engine for ship propulsion is commercially available and used in marine tankers, (20). According to the manufacturer's data the number of installed engines is 26 in total and exclusively used in methanol carriers, (86). Compared to the other fuels considered for use in dual fuel engines, methanol has multiple benefits regarding handling and storage (87), which place it close to qualifying as a drop in fuel. The main challenge for its use is that for substantial benefits synthetic/green production is required which has currently very low production capabilities unless it has to compete with other sectors for use of renewable feedstock, (35,87). Another substantial technical aspect that needs to be considered is that the low energy content of this fuel, 40% of HFO, that requires high storage capacity, (20,87).

Beyond the use of low carbon fuels, other solutions are examined to improve sailing efficiency of vessels and consequently reduce energy requirements and fuel consumption. A number of those solutions examined by the industry is summarized for the sake of completeness. These solutions include hull efficiency increase measures, such as redesign of hull shape, use of low friction paints and air lubrication, (35,49,89,90). The use of renewable energy is also under consideration with solar panel installation on the vessel board and the utilization of wind assisting devices for propulsion, (20,35,91), but the benefit and use feasibility of employing these solutions on-deck is unknown. Another future technology gaining traction among studies is carbon capture devices (92–95), with researchers examining the potential of CO_2 absorption rate and regulating bodies considering their future application, (35). Currently, pilot projects have shown very poor return of investment due to very high capital expenditure (CAPEX) and operating expenses (OPEX) of the technology, (96). Other major challenges are the very low technical experience of the technology in the marine environment and space constraints requiring liquefication or solidification of the captured CO_2, which requires high energy use, (96,97). If this technology reaches maturity and installation on vessels proves possible without operation issues, it will feature one of the most carbon reducing potentials close to 85%, (93,97), but the overall technology is yet unproven, (35).

2.2 NO_x Emissions Control in the Marine Industry

2.2.1 NO_x Emissions Formation

NO_x formation in CI engines is classified in three categories, thermal NO as the main source, fuel NO_x and prompt NO_x. Fuel and prompt NO_x contribution to total emissions is rather limited, as the former results from the nitrogen content of the fuel and the latter is caused by attack on air content nitrogen from hydrocarbon radicals. The most significant formation mechanism is thermal NO_x, driven by the breakdown of atmospheric nitrogen due to high temperatures, (98). As the name implies, thermal NO_x formation is highly dependent on temperature rising exponentially above 1100ºC. NO_x formation is kinetically controlled and driven mainly by O_2 availability and temperature level. The formation of thermal NO_x is described by the Zeldovich mechanism that proposes two main reaction paths for their formation:

$$O + N_2 \leftrightarrow NO + N \quad (2.1)$$

$$N + O_2 \leftrightarrow NO + O \quad (2.2)$$

The first reaction takes place when O_2 molecules are dissociated to atoms under very high temperatures. The O atoms react with N_2 molecules forming NO and N. The resulting N reacts with nearby O_2, and NO and O are formed. The overall process is mainly controlled by the first reaction's rate, as the second reaction is much faster and occurs immediately after the first reaction. In cases of low oxygen availability and fuel rich conditions the second reaction weakens, and a third reaction is included in the mechanism.

$$N + OH \leftrightarrow NO + H \quad (2.3)$$

The three reactions are known as the extended Zeldovich mechanism, (99). As mentioned, this process initiates at around 1100ºC and is commonly maximised in the region of 1900 – 2000ºC. Since this is the common temperature range for combustion processes thermal NO_x are the main source and most measures employed by manufacturers to limit emissions are focused in reducing the above reaction rates either by lowering the mean combustion chamber temperature or significantly lowering oxygen availability to control the first reaction's rate.

Fuel NO_x are formed by the oxidation of fuel nitric contents. As such the fuel's N content is rather proportional to the amount of NO_x formed. The general reaction for their formation is:

$$R_xN + O_2 \leftrightarrow NO, NO_2, CO_2, H_2O \quad (2.4)$$

The complete mechanism has not been defined, but it is based on two primary formation pathways. In the first during the initial stage of combustion, volatile nitrogen species are oxidized. The second pathway is the result of nitrogen combustion from the char portion produced, however it is a considerably slower reaction than the former pathway. Due to the reduction of most NO_x formed via the second pathway to N by the formed char, the fuel NO_x finally emitted are mostly attributed to the first pathway i.e., the oxidation of volatiles.

2.2.2 Maritime NO_x Emissions Legislation

NO_x emissions of marine engines are currently controlled by the MARPOL ANNEX VI, NO_x Technical Code of 2008. The code has been revised or amended to incorporate even stricter limits and account for newer technologies introduced in the maritime industry. In 2023 three categories of NO_x emission limits are in effect that depend on vessel age, ranging from Tier-I to Tier-III. The Tier-III category applies only in certain areas commonly referred to as Emission Control Areas, which are continuously expanded. Further to the various categories the limits depend on the engine type and size. A breakdown of all applicable NO_x emissions values was presented in Chapter 1 for 2-stroke engines. Before an engine is installed on the vessel a NO_x file has to be registered during a trial run that covers 25%, 50%, 75% and 100% load for large 2-stroke engines and additionally 10% load for 4-stroke auxiliary generators. During this procedure the main operating parameters are registered such as in-cylinder peak pressure, inlet air and exhaust gas temperature along with the flue gas composition. The process is not conducted for all engines manufactured but at least for one of each line of series-produced. The engine series is commonly referred to as family, with the engine selected for testing being the one incorporating the features that will result in the highest emissions designated as the parent engine. Following engine installation on the vessel, the NO_x Technical Code (NTC) includes various methods for future testing the NO_x emissions.

The emissions verification methods to be conducted on-board are the engine parameter check method, the simplified measurement method and the direct measurement and monitoring method, (26,27). The simpler procedure is the parameter check method that is based on the verification that certain engine components, settings and operating values that can affect NO_x emissions are according to the specifications of the engine NO_x file. For engines that are not equipped with NO_x reducing devices i.e., all Tier-I and Tier-II engines no emissions measurements are required in this verification procedure. The simplified measurement method can be conducted during surveys, confirmation tests and renewal procedures. As a minimum, the CO_2 and NO_x concentration in the exhaust gas must be measured along with engine speed, torque and fuel consumption. Additional parameters required are ambient conditions, inlet air and exhaust gas pressure and temperature. The measurement procedure should be conducted at a number of different load points with the approval of the regulators. The direct measurement and monitoring method has similar requirements to the simplified measurement method with stricter requirements regarding the load points of the conducted tests and the measurement time of flue gas composition. The tests should be conducted according to the E2, E3 or D2 cycles depending on the type and use of the engine tested. The E3 and D2 cycles are provided in Table 2-1 and Table 2-2. Both simplified measurement and direct and monitoring methods provide the option for allowance of higher emissions than the limit applicable to the tested engine. Due to the difficulties of the overall procedure an increase of up to 10% over the emission limit may be accepted as detailed but the IMO in the NO_x Technical Code of 2008 (26,27). The same applies when tests are conducted using RM-grade fuel, such as HFO, VLSFO or any other such fuel type. In no case, however, the total added emissions allowance cannot exceed 15%.

Table 2-1 Test Cycle E3 for 2-stroke main engines

Test Cycle Type E3	Speed	100%	91%	80%	63%
	Power	100%	75%	50%	25%
	Weighting Factor	0.2	0.5	0.15	0.15

Table 2-2 Test Cycle D2 for 4-stroke generators

Test Cycle Type D2	Speed	100%	100%	100%	100%	100%
	Power	100%	75%	50%	25%	10%
	Weighting Factor	0.05	0.25	0.3	0.3	0.1

2.2.3 Effect of engine tuning on NO_x Emissions

NO_x emission reduction using engine tuning is a process of compromise between fuel efficiency and regulation limits. The common methods are retarded fuel injection timing and lowering the effective compression ratio via alternating valve timing which have been commonly used by manufacturers to achieve the Tier-I and mostly Tier-II emission standards enforceable since 2011. While the aforementioned techniques have a positive effect regarding NO_x emissions, they can negatively affect other emissions and in most cases decrease fuel efficiency, thus resulting to added CO_2 emissions. In Table 2-3 a summary of the measures used in diesel engines to control most common pollutant emissions is provided along with the methods' advantages and disadvantages.

Table 2-3 Measures for Optimising Diesel Engine Combustion & their Effects on emissions and cnsumption, (100)

Measure	NOx	HC/CO	Soot	bsfc	Noise
Retarded start of injection	+	−	−	−	+
Exhaust gas recirculation	+	−	−	−	+
Cooled EGR	+	−	+	+	0
Supercharging	−	+	+	+	0
Intercooling	+	−	+	+	0
Pilot injection	0	+	−	0	+
Added post-injection	+	0	+	−	0
Injection pressure increase	0	+	+	+	0
Lower compression ratio	+	−	+	0	−

Symbols: +: reduction; −: increase; 0: no change

One of the main measures applied is the adjustment of injection timing. Retarded start of injection will lead to lower NO_x emissions, but also possibly increase soot formation, (100) and BSFC. The goal of retarded injection is to limit the peak pressure and mainly in-cylinder temperature. This occurs because fuel injection takes place closer to expansion, which lowers the pressure. Injection retard reduces peak temperature, however the fuel and air mixing is negatively affected which leads to greater soot formation, (100). The decreased oxidation of soot due to the lower temperatures further increases the soot emissions. For advanced injection timing, combustion initiates the pressure rise when the piston is still moving upwards, thus pressure

also increases due to compression. The higher pressure results to higher peak temperature values, that drive NO_x formation.

The adverse effects of retarded injection timing can be partially alleviated by reducing injection duration. Increasing injection pressure enhances fuel mass flow rate, shortening injection duration. This allows for better mixing of fuel and air so the number and range of fuel rich mixture regions is decreased, leading to lower soot formation. However, the shorter injection duration leads to faster combustion, placing the combustion around Top Dead Centre (TDC), increasing thus peak temperature. The effect of injection timing is presented in Figure 2-1 while the effect of injection pressure is presented in Figure 2-2 received from (100) for a heavy duty diesel engine, as part of the above description.

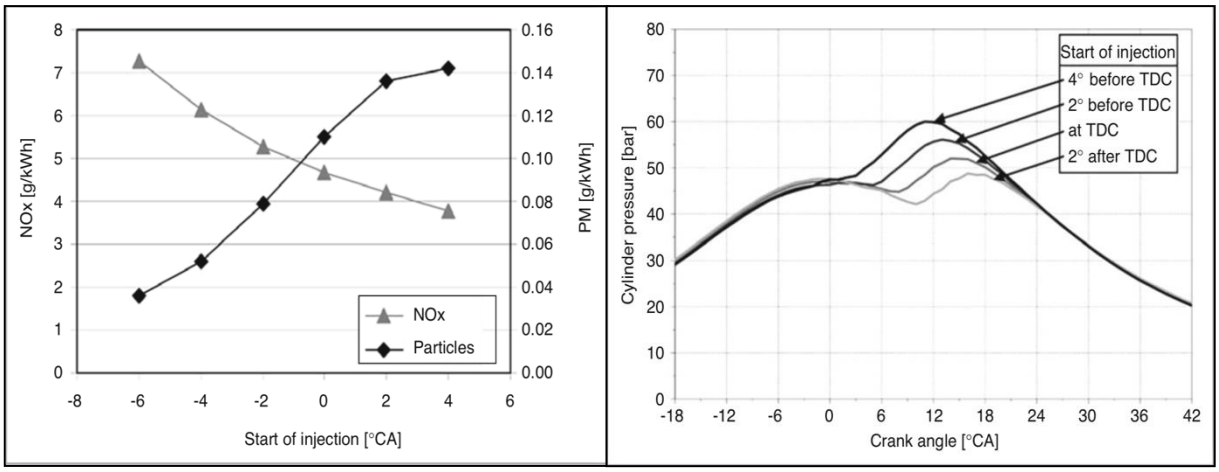

Figure 2-1 Effect of Injection Timing in NOx, Soot and Peak Pressure, (100)

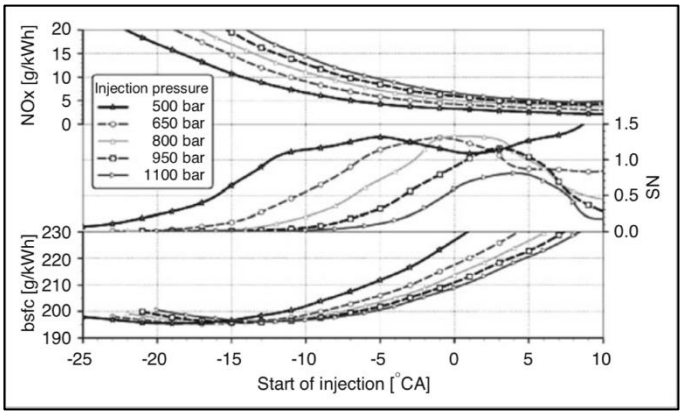

Figure 2-2 Effect of Injection Pressure Relative to Injection Timing on Soot and NOx Formation, (100)

2.2.4 NO_x Emission Reduction Systems in the Marine Industry for the Tier-III Emissions Standard

As established, the main contributor driving NO_x formation is high temperature during combustion. In addition, their formation can also be enhanced by increased oxygen presence at the most intense thermal spots of the combustion chamber. The main methodologies applied by engine manufacturers to limit NO_x emissions are divided into two categories, the in-cylinder measures (internal) and after-treatment devices (external). The in-cylinder measures employed target temperature and oxygen availability. As stated above, to achieve Tier-II

emissions certification the methods applied are exclusively in-cylinder, specifically engine tuning and injection rate/profile. To further reduce NO_x emissions to the newer Tier-III standard new technical solutions, proven in other fields, such as the automotive and energy generation industries, have been introduced in maritime. These involve selective catalytic reduction (SCR), exhaust gas recirculation (EGR) and Otto cycle based duel-fuel engines operating on gaseous fuel with the low-pressure gas admission approach. The first two solutions are studied extensively in this thesis. These solutions are most often employed in tandem with older approaches regarding engine tuning, thus, for Tier-III operational mode usually differs than the one for standard operation. The tuning switch is performed via the engines' electronic control system. The different tuning for Tier-III operation is investigated in depth in each relevant chapter, along with the NO_x abatement systems' effect on engine performance and emissions.

Chapter 3 Multizone Model Description

3.1 General-Model Modifications

Before proceeding to the main section of the thesis, a description of the multizone engine model that was employed to assist in data processing and the overall investigation is provided. The model was mostly used to analyse in detail the effect of the technologies examined on engine performance and emissions.

Various simulation models exist in the literature ranging deform simple zero dimensional, to phenomenological multizone and finally to detailed computational fluid dynamic (CFD) models. For the present work a multizone model emulating both the closed and open part of the engine cycle was used. The model is based on pre-existing code which was focused on the description of 4-stroke engines used for automotive and truck applications. The model was modified for the needs of the thesis to incorporate the novelties of the engines studied and mainly to properly describe 2-stroke marine engine operation. Furthermore, modifications were conducted to improve the air-fuel mixing mechanism and to minimize the necessity of combustion model tuning with engine operating conditions. The modifications conducted to the older multizone model code are provided below:

- Variable injection and exhaust valve timing to account for the electronic control system of modern engines .
- Consideration for fuel composition which allows to examine oxygen enriched fuels.
- Modification of the air entrainment mechanism to use volume based air entrainment instead of momentum which overcomes the necessity of constant tuning with engine load.
- Introduction of EGR for the open cycle simulation, which includes modifications to inlet and outlet system modelling.
- EGR cooler.
- Incorporation of cylinder bypass valve (CBV) in the engine.
- Incorporation of exhaust gas bypass (EGB) valve at the turbine.
- Development of computation procedure to estimate EGR and CBV valve mass flow rates.

As mentioned in chapter 1, the specific the modifications required for emulation of EGR operation are provided in a separate subsection in the relevant chapter as description of the engine and system layout is first required.

3.2 Zone Formation

In the model, the fuel jet is divided in individual volumes or zones with different properties. The cylinder volume is treated separately and is attributed a uniform pressure value in each time step of the simulation, (215). The main approach of the model is the calculation of the conditions in each zone, by applying mass and momentum conservation equations and use of the first thermodynamic law to form a differential equation

which provides the uniform in-cylinder pressure. Following the estimation of the mean cylinder pressure, the first thermodynamic law is employed for each zone to calculate the local temperature. The principle detailed below has been found to perform well in other studies using engine modelling, such as (102).

The consideration of zones is done to acquire a more realistic representation of the actual air-fuel mixing mechanism and the distribution of the investigated parameters inside the fuel jet. This is especially important for the prediction of NO_x which depend on temperature and species, mainly O_2, distribution. A single zone model cannot predict NO_x, while a two zone model can offer NO_x prediction but is limited regarding capability to predict the effect of load, speed and other parameters. The multizone approach offers enhanced prediction capability, important for practical applications.

It is common practice in phenomenological modelling to consider only one fuel jet and assume all others to be the same. The total number of fuel jets is thus equal to: N_{holes} x $N_{injectors}$. The number of zones in the circumferential direction was selected after a sensitivity analysis from the point where NO and performance predictions were stabilized. No zone mixing or jet interaction is considered. This is common practise in phenomenological modelling, and other more resource intensive modelling applications, and is accounted for by the use of correction factors that are determined during the initial calibration procedure using shop test data.

3.2.1 Heat Transfer Model

For the heat transfer mechanism, a turbulent kinetic energy viscous dissipation rate k~ε_t model is used to determine the characteristic velocity of heat transfer calculations (103). The mean flow kinetic energy E_m is supplied to the cylinder chamber during the gas exchange process. The kinetic energy is partially converted to turbulent kinetic energy k through a dissipation process at the rate of P_{tk} and finally to heat through viscous dissipation at a rate of mε_t. The system of two differential equations for E_m and k can be written as:

$$\frac{dE_m}{dt} = \frac{1}{2}\frac{dm}{dt}u_{inl}^2 - P_{tk} - \frac{E_m}{m}\frac{dm}{dt} \quad (3.1)$$

$$\frac{dk}{dt} = P_{tk} - m\varepsilon_t - \frac{k}{m}\frac{dm}{dt} \quad (3.2)$$

with $E_m = \frac{1}{2}m\bar{u}^2$ and $k = \frac{3}{2}m\acute{u}^2$ for isotropic turbulence, and dm/dt the net mass flow rate into the combustion/cylinder chamber.

The turbulent kinetic energy production rate and the viscous dissipation rate ε_t are calculated from the known relations:

$$\varepsilon_t = \left(\frac{k}{1.5m}\right)^{1.5}\frac{1}{l_{car}},\ P_{tk} = 0.09\mu_t\frac{\bar{u}^2}{l_{car}^2} \quad (3.3)$$

with l_{car} being the characteristic length equal to the combustion chamber height at each time step, or the cylinder radius depending on the piston position and μ_t the gas turbulent viscosity that is calculated using:

$$\mu_t = \rho l_{car} \left(\frac{k}{m}\right)^{0.5} \tag{3.4}$$

The heat transfer calculations additionally require the characteristic velocity calculated by:

$$u_{car} = (\bar{u}^2 + \acute{u}^2)^{0.5} \tag{3.5}$$

The Nusselt number is calculated to be used for estimating the heat transfer coefficient:

$$Nu = cRe^{0.8}Pr^{0.33} \tag{3.6}$$

The heat transfer coefficient is calculated by eq. (3.7) and the instantaneous heat rate by eq. (3.8).

$$h_c = cRe^{0.8}Pr^{0.33}\frac{\lambda}{l_{car}} \tag{3.7}$$

$$\dot{Q} = A\left[h_c(T_g - T_w) + \sigma_r c_r\left(T_g^4 - T_w^4\right)\right] \tag{3.8}$$

As also verified in the biofuel results, Chapter 5, the above relation for heat transfer has been tested with very good results for this type of engine. Equation 3.8 contains two unknown parameters, the mean wall temperature T_w and the c constant of the previous eq. 3.7. During its application in the multi-zone model the T_w cannot be used for zones not in contact with the cylinder walls surface. To circumvent this difficulty the first part of eq. 3.8, referring to convective transfer phenomena, is calculated using the bulk average temperature of the jet, provided by:

$$T_g = \frac{\sum_{i=1}^{n_z} m_i c_{vi} T_i}{\sum_{i=1}^{n_z} m_i c_{vi}} \tag{3.9}$$

Then the heat exchange rate calculated in eq. 3.8 is distributed among the jet zones on using the individual zone mass, temperature and heat capacity as distribution basis:

$$d\dot{Q}_{i,d} = \frac{\dot{Q}(m_i c_{vi} T_i)}{\sum_{i=1}^{n_z} m_i c_{vi} T_i} \tag{3.10}$$

Regarding the radiative component of eq. 3.8, zone surface area is used so no further calculations are required and is used as described above.

3.2.2 Cylinder Blowby

Blow-by rate affects the compression pressure diagram. A detailed blowby model is embedded in the present simulation considering for the rings motion in their grooves. However, for the present investigation, the blow-by rate is modelled using a simplified approach assuming an equivalent blow-by area between the cylinder rings and the cylinder liner. The blow-by mass flow rate is calculated using the isentropic compressible flow assumption as follows.

$$\frac{dm}{dt} = C_d A \frac{P_u}{R_u T_u} \sqrt{\frac{2\gamma R_u T_u}{\gamma - 1}\left[\left(\frac{P_d}{P_u}\right)^{\frac{2}{\gamma}} - \left(\frac{P_d}{P_u}\right)^{\frac{\gamma+1}{\gamma}}\right]} \qquad \text{for } \frac{P_d}{P_u} \geq \left(\frac{2}{\gamma+1}\right)^{\frac{\gamma}{\gamma-1}} \tag{3.11a}$$

$$\frac{dm}{dt} = C_d A \frac{P_u}{R_u T_u} \sqrt{\frac{2\gamma R_u T_u}{\gamma - 1}\left[\left(\frac{P_d}{P_u}\right)^{\frac{2}{\gamma}} - \left(\frac{P_d}{P_u}\right)^{\frac{\gamma+1}{\gamma}}\right]} \qquad \text{for } \frac{P_d}{P_u} \leq \left(\frac{2}{\gamma+1}\right)^{\frac{\gamma}{\gamma-1}} \tag{3.11b}$$

where d*m*/d*t* is the blow-by mass flow rate, *P* is the pressure, *T* the temperature, γ is the ratio of the specific heat capacities under constant pressure and volume and C_d the discharge coefficient (index "u" denotes upstream of the flow and index "d" downstream).

The equivalent blow-by area A_{eq} is equal to:

$$A_{eq} = \pi D \delta r \tag{3.12}$$

where δr is referred to as the "equivalent" cylinder-ring clearance. This is considered as one of the model constants and its value should remain fairly the same with operating conditions. The equivalent blow-by area accounts also for the mass loss rate through the engine valves because no distinction is made, in the present analysis, between this mechanism and blow-by.

3.2.3 Air Swirl

Air swirl is required to achieve a high rate of air and injected fuel mixing in the cylinder. In the case of 2-stroke large scale marine engines the swirl motion of the cylinder charge is produced during the scavenging stroke as a result of the inlet port geometry. The effect of swirl on fuel mixing is lower for newer engines due to the advanced injection strategies used. Further to the promotion of fuel and air mixing the swirling motion of entry air assists the scavenging process and gas exchange improving efficiency of this stage of the engine cycles. The previous effect was researched and described in detail in (104,105). The swirling motion of the air is modelled by assuming a hybrid scheme consisting of a solid body core surrounded by a potential flow region, (106,107). In this approach the air viscosity is taken into account, as it creates a boundary layer near the cylinder walls. This requires the use of tangential velocity profile for calculations, such as the one proposed by (107):

$$\begin{aligned} u &= W_p R && \text{for } 0 \leq R \leq R_c \\ u &= W_p R_c (R_c/R)^{0.05} && \text{for } R_c \leq R \leq R_p \end{aligned} \tag{3.13}$$

where R_c is the point to which the solid body rotation ends, given be the following empirical expression:

$$R_c = R_{in}\left(D_b / 2R_p\right) \tag{3.14}$$

with R_p the cylinder radius, D_b the piston bowl diameter (for 2-stroke engine designs with no bowl D_b=D) and R_{in} the cylinder-valve axis distance. For the 2-stroke engine since air flows through the inlet ports Rin is equal to the cylinder radius, Rin=D/2.

The swirl ratio in the present case is considered to be an input and from the aforementioned modeling its variation during the engine cycle is determined. The calculation of swirl is based on the conservation of the flows angular momentum applied to the cylinder during the intake stroke. During the induction stroke angular momentum is continuously added to the cylinder, with a part of it lost due to friction and the remaining forming the flow field. The equation for angular momentum conservation is:

$$\frac{d(IW)}{dt} = I\frac{dW}{dt} + W\frac{dI}{dt} = -T_r \tag{3.15}$$

In eq. 3.15 W is the angular air velocity, I is the moment of inertia of the mass trapped in the cylinder and T_r is the torque force acting on the flow field. T_r is equal to the force due to friction on the cylinder walls, piston crown and cylinder head. By integration of eq. 3.15 the instantaneous angular velocity of the cylinder charge is calculated.

3.2.4 Spray Model

The spray model used has been previously utilized in (108), (109). The main assumptions of this model are detailed presently. Empirical correlations are used to estimate the fuel jet angle and zone penetration in the cylinder. These correlations provide the velocity along the spray axis and its radial component (105), (108). The air swirl effect is also considered by applying the approach of (108). Using the previous and the equations for mass and momentum conservation the position of each zone in the cylinder is estimated for each time step. The analytical model description is presented below.

Following injection, the fuel starts to penetrate into the combustion chamber and the individual zones of the model start to form. The initial conditions at injector nozzle exit are derived from the injection rate which can either be derived from a fuel injection system simulation model or can be predefined as input to the simulation. There are multiple approaches to model the initial behavior of the fuel spray before substantial breakup into droplets, (110) with a relatively simple but efficient approach used in the present thesis. The breakup length is calculated using the well tested test approach of (105,107):

$$L = u_{inj}t_{break} \cong c_l\left(\frac{\rho_l}{\rho_a}\right)^{0.5} d_{inj} \tag{3.16}$$

with c_l a constant and ρ_a and ρ_l the density of air and fuel respectively.

The distribution of spray velocity along its axis is calculated using correlations for spray penetration (106,111) with the following equations used in reference to time of penetration.

$$\begin{aligned} u = u_{inj} &= c_d\left(\frac{2\Delta P}{\rho_l}\right)^{0.5} && \text{for } x < L \\ u &= u_{inj}\left(\frac{L}{x}\right)^{n} && \text{for } x \geq L \end{aligned} \tag{3.17}$$

with c_d above a constant. According to theoretical and experimental data the spray zones located at the fuel jet periphery will have lower axial penetration. To simulate this the following radial distribution of exponent n of eq. 3.16 is assumed:

$$n_i = n_{min} \exp\left[\log^{-1}\left(\frac{n_{max}}{n_{min}}\right)\left(\frac{r_i}{r_o}\right)^2\right] \tag{3.18}$$

where n_i is the local zone exponent, r_i is its position relative to the axis and n_{min}, n_{max} are the minimum and maximum values for the exponent distribution. From a sensitivity analysis and considering the result from application of various engine designs the values are used are 0.7 and 1.0 respectively. For each time step the initial value of the radial velocity for all zones formed is given by:

$$u_{ri} = u_{inj} \tan\left(\frac{a}{r_o} r_i\right) \tag{3.19}$$

with r_o the nozzle hole radius and r_i the radial distance of each zone from the centerline. The angle "a" of the jet is estimated using the widely tested relation:

$$a = 0.05\left(\frac{d_{inj}^2 \rho_a \Delta P}{\mu_a^2}\right)^{0.25} \tag{3.20}$$

To estimate the effect of the cylinder charge swirl on the fuel jet the local components of air velocity in the radial and axial directions are calculated using the conservation of momentum equations in both axes. The air swirl results to deflection of the zones from their original direction, which promotes air entrainment in the zones. Application of the momentum conservation equations shows that axial penetration of the jet decreases and this leads to increased air entrainment rate in the jet zone. The deflection of each zone is calculated using the local air velocity:

$$\begin{aligned} u_{ixt} &= u_{ix} + u_a \sin(\varphi_i) \\ u_{irt} &= u_{ir} - u_a \cos(\varphi_i) \end{aligned} \tag{3.21}$$

In the above equation, u_a is the local swirl velocity and φ_i the angular position of the zone inside the cylinder.

3.2.5 Wall Impingement of Spray Model

An effort was made to calculate the effect of wall impingement on the fuel spray, which is a challenging task for multi-zone models and is better suited to other approaches such as CFD modelling for accurate predictions at the cost of heavily increased computational power and time requirements. The simpler approach is to assume that following wall impingement the zones follow a path parallel to the cylinder walls, even though such an approach would be non-realistic and is unlikely to provide a proper representation of the jet geometry. The wall jet theory of (112) is used to estimate a zone's velocity after it reaches the combustion chamber walls.

$$w_i = w_{oi}\left(\frac{r_{oi}}{r_i}\right) \tag{3.22}$$

In the above eq. 3.22, r_{oi} is the initial radial position of the zone relative to the jet axis after impingement and w_{oi} its initial velocity. The zone is assumed to follow a path adjacent to the wall and its radial distance δ is used to define the thickness of the wall jet, (102,112).

$$\delta_i = \delta_{oi}\left(\frac{r_i}{r_{oi}}\right) \tag{3.23}$$

where δ_{oi} is the initial distance of the zone from the wall following deflection. Before the zones collide with the combustion chamber walls, their velocity is divided into the normal one and one parallel to the cylinder walls. At impingement the parallel velocity component is deflected in total, while the normal component is assumed to be divided in two segments, left and right, (102). The portion of the zone with a velocity vector opposite to the parallel component will now be treated as a new zone created by the impingement. Its initial values for velocity and thickness are determined by applying conservation equations for mass and energy and accounting for the local jet geometry, (102).

3.2.6 Zone Air Entrainment

The air entering the zones is estimated by considering the volume change of each zone through time and momentum conservation. A typical approach for phenomenological multi-zone modeling is to use the momentum approach. But the volume change approach allows to circumvent the issues in accuracy that can be caused by the initial momentum loses due to friction that cannot be easily replicated directly in a model of this type. Furthermore, after a detailed analysis conducted, comparison of simulation results has revealed that with the volume approach no tuning of constant c_a which affects the peak combustion pressure is required with variation of engine operating conditions and load. The air entrainment rate for each zone is calculated by, (102):

$$\frac{dm_{ia}}{dt} = c_a \rho \frac{dV_i}{dt} \tag{3.24}$$

with c_a above a constant specific to the model.

3.2.7 Droplet Breakup and Evaporation

There are multiple models and sub-variations for the modelling of droplet breakup utilizing relations within the multi-zone approach (110,113–115), CFD direct numerical approach (116) and also approaches utilizing stochastic mathematic simulations (117) aiming to increase the accuracy of droplet size and distribution. For this application a conventional model was used that has been proven to work well with large 2-stroke marine engines.

The injected fuel is distributed into zones according to the injection rate and for each zone the fuel is divided into groups of droplets that have the same Sauter mean diameter. The formula used for the distribution of droplet diameters in the packages is given by (105,107):

$$\frac{dV}{V} = 13.5\left(\frac{D_d}{D_{SM}}\right)^3 \exp\left[-3\left(\frac{D_d}{D_{SM}}\right)\right] d\left(\frac{D_d}{D_{SM}}\right) \tag{3.25}$$

While a conventional approach, the use of the above relation gives a quite accurate prediction of the fuel-air equivalence ratio distribution inside the jet, (which is important for the present analysis) and the SMD packages approach is used in detailed analyses (with some variations to improve accuracy) that employ advanced flow simulations such as (118).

The Sauter mean diameter D_{SM} is obtained by the use of semi-empirical correlations derived by analysis of experimental data and is given as:

$$D_{SM,1} = 0.38 Re_{inj}^{0.25} We_{inj}^{-0.32} \left(\frac{v_l}{v_a}\right)^{0.37} \left(\frac{\rho_l}{\rho_a}\right)^{-0.47} d_{inj} \tag{3.26}$$

$$D_{SM,2} = 4.12 Re_{inj}^{0.12} We_{inj}^{-0.75} \left(\frac{v_l}{v_a}\right)^{0.54} \left(\frac{\rho_l}{\rho_a}\right)^{0.18} d_{inj} \tag{3.27}$$

where the 1 and 2 subscripts are used to refer to complete and incomplete sprays respectively. The required for calculations Reynolds and Weber number are given by:

$$Re_{inj} = \frac{u_{inj} d_{inj}}{v_l} \tag{3.28}$$

$$We_{inj} = \frac{u_{inj}^2 d_{inj} \rho_l}{\sigma} \tag{3.29}$$

The Sauter mean diameter is taken as the maximum of the two values received from equation 3.26 and 3.27.

For evaporation, similarly multiple modes are available (105,110,119) with one used in for the current model being the one of (120). The rate of droplet mass change according to the model selected is given by:

$$\frac{dm}{dt} = -\frac{2\pi r D_v P}{R_{fv} T_m} \ln\left(\frac{P}{P - P_v}\right) Sh \tag{3.30}$$

The Sherwood number Sh is calculated as:

$$Sh = 2 + 0.6 Re^{0.5} Sc^{1/3} \tag{3.31}$$

In the above eq. 3.30 D_v is the mass transfer diffusivity for the fuel air mixture, T_m the mean temperature of the fuel-air mixture and P_v the partial pressure of the fuel vapor at the liquid surface. To obtain the temperature of the droplets the energy balance equation given below is integrated.

$$m_l c_{pl} \frac{dT_l}{dt} = 2\pi r \kappa_m (T_a - T_l) \left[\frac{z}{e^z - 1}\right] Nu + L_f \frac{dm}{dt} \tag{3.32}$$

The Nusselt number included in eq. 3.32 is given by:

$$Nu = 2 + 0.6Re^{0.5}Pr^{1/3} \tag{3.33}$$

and the z exponent is a dimensionless correction factor for heat transfer that includes the effect of the mass transfer in its formulation given in:

$$z = -c_{pf}\frac{dm}{dt}\frac{1}{2\pi r\kappa_m Nu} \tag{3.34}$$

In the last equation of this series, 3.34, κ_m is the thermal conductivity of the mixture and L_f is the fuel's latent heat of vaporization. The integration of equations 3.25 and 3.27, 3.28 provides the history of each droplet group inside the zones.

3.2.8 Combustion Model

For each zone the internal mixing rate is controlled by turbulent diffusion. The evaporated fuel and the entrained air mass of each zone are divided into two portions, macromixed one a micromixed one, (102). The corresponding mass rates are given by:

$$\dot{m}_{fmic} = D_t(u)(m_{fmac} - m_{fmic}) \tag{3.35}$$

$$\dot{m}_{amic} = D_t(m_{amac} - m_{amic}) \tag{3.36}$$

$$D_t(u) = a_{mix}u \tag{3.37}$$

with a_{mix} a constant and u the relative velocity of the burning zone element with respect to the surrounding air. The a_{mix} constant is used to control the overall intensity of the heat release rate and affects the estimated engine power. For this reason, it is used as a calibration constant to match the desired engine power output. The process of calibration is conducted as in (102).

The fuel ignition delay can be determined by the correlation of (121):

$$S_{pr} = \int_0^t \frac{1}{a_{del}P_g^{-2.5}\Phi_{eq}^{-1.04}\exp(5000/T_g)}dt = 1 \tag{1.38}$$

In eq. 1.38, Φ_{eq} is the local equivalence ratio of the fuel air mixture inside the zone. The a_{del} is a constant calculated from the constants determination procedure of (115) and the ignition quality of the fuel i.e., a function of its cetane number.

The combustion rate depends strongly on local temperature and on the concentration of O_2 and evaporated fuel. The local fuel combustion rate is modelled using an Arrhenius type equation (107):

$$\begin{aligned} m_{fb} &= K_b\frac{(m_{fmic}-m_{fb})}{T^{0.5}}e^{\frac{-E_c}{T}}P_{O_2}, \quad \text{for (AFR)} > (\text{AFR})_{st} \\ m_{fb} &= K_b\frac{(m_{fmic}-m_{fb})}{(\text{AFR})_{ST}T^{0.5}}e^{\frac{-E_c}{T}}P_{O_2}, \quad \text{for (AFR)} < (\text{AFR})_{st} \end{aligned} \tag{3.39}$$

In the above K_b is a constant, E_c is the reduced activation energy, AFR the fuel air ratio and P_{O2} the partial pressure of oxygen in the zone. By using this approach, the effect of the EGR and also of the oxygen rich biofuels on the combustion rate are taken into account.

3.2.9 Fuel Injection System

A simple fuel injection model is used which considers for the following control volumes: high pressure pump chamber, delivery valve chamber, delivery pipe from pump to injector, and injector.

The fuel is considered to be compressible, its compressibility defined by the following function,

$$K_f = -V_j \frac{dP_j}{dV_j} \tag{3.40}$$

The simulation of each control volume is accomplished by considering the previous equation and the incoming and outgoing volume flow rates, obtaining thus the following relation,

$$\frac{dP_j}{dt} = \frac{K_f}{V_j}\left(\frac{dV_j}{dt} - \dot{Q}_{tj}\right) \tag{3.41}$$

where $\dot{Q}_{tj}$ is the total net volume flow rate into the control volume and dV_j/dt is the rate of its volume change. The volumetric flow rate through orifices, various openings or ports is given by the formula,

$$\dot{Q}_j = A_j C_{dj}\left(\frac{2\Delta P_j}{\rho_j}\right)^{0.5} \tag{3.42}$$

and "j" is the corresponding volume. The delivery valve is modelled as a check valve allowing fuel flow only from the delivery chamber to the fuel pipe. The injector is modelled in a similar way, as a check valve, allowing fuel to flow towards the combustion chamber only when the pressure exceeds its opening pressure.

The pressure estimation in the control volumes is achieved by solving the unsteady flow equations inside the tube using the two basic principles of mass continuity and momentum conservation. The corresponding differential equations are solved using the method of characteristics, (122).

The injection profile is determined from the simple fuel injection simulation model using the actual fuel cam geometry. The model allows the use of this approach or the use of a predefined injection profile. A comparative analysis was performed using the simulated injection rate and a mean injection rate defined from the fuel consumption and injection duration at each operating condition to evaluate its effect on predicted values. The last was defined from the point of injection initiation and the peak combustion rate after significant analysis. As revealed, the qualitative results remained valid and only minor effect was observed for absolute performance and emission data.

3.2.10 Gas Exchange System

For the simulation of the inlet and exhaust manifolds the method of filling and emptying technique is used, (107), (115). This allows the calculation of gas exchange rate between them and the engine cylinder. Good

results have been found in other applications for large 2-stroke marine engines, (123). The model also includes the air cooler, EGR cooler, and turbocharger operation, (115).

Turbocharger:

As known from practice, characteristic charts for the compressor and the turbine are usually not available. For this reason the method of operation similarity (124,125) is used from which the charts are reproduced using existing experimental data. The method is efficient for engine loads in the range of 40% to 100% and is as follows:

Using the least squares method, a set of constants is calculated for the polynomial curves that fit the following functions,

$$\eta_{is_C} = f_1(\varphi) \tag{3.43}$$

$$\eta_{is_T} = f_2(\varphi) \tag{3.44}$$

$$k_{is} = f_3(\varphi) = \Delta h_{is}/U^2 \tag{3.45}$$

where $\phi = m/(\rho AU)$ is the flow coefficient.

The data required for the calculation of the turbine and compressor characteristic maps in the previous form are:

- Pressure before and after the compressor.
- Pressure before and after the turbine.
- Air temperature before and after the compressor.
- Exhaust gas temperature before and after the turbine.
- Rotational speed of the turbocharger.

In the present application these data were obtained from the official engine shop tests.

Air-Cooler:

The air cooler is modelled using a simple approach that is based on the processing of shop test data. The pressure drop and the effectiveness are expressed as functions of the mass flow rate through it (126,127) as follows,

$$\varepsilon = 1 - b\dot{m}^2 \tag{3.46}$$

$$\Delta P_{ac} = a_{ac}\dot{m}^2 \tag{3.47}$$

where "ε" is the effectiveness defined as,

$$\varepsilon = \frac{T_{a,in} - T_{a,out}}{T_{a,in} - T_{c,in}} \tag{3.48}$$

where subscripts "a, c, in, out" denote respectively: air, cooling medium, inlet and outlet from the air cooler. The mass flow rate of air is calculated from the engine simulation model using the measured data mentioned above. The same approach is applied for the simulation of the EGR cooler.

Exhaust Duct:

The exhaust backpressure after the turbine at the exhaust duct is expressed in a way similar to the pressure drop at the air cooler as follows,

$$\Delta P_{exh} = a_{exh}\dot{m}^2 \quad (3.49)$$

Constant a_{exh} is estimated using the engine shop test data and the mass flow rate estimated from the simulation model.

3.2.11 Scavenging Model

Scavenging is of significant importance for 2-stroke engine operation and emission formation. It affects, beyond others, the temperature level inside the combustion chamber and the fuel jet and O_2 availability and thus NO_x formation. A two-zone model was used for simulating the scavenging process. One zone consists of the inlet charge mix of fresh air and recirculated gases and the second of the combustion products from the last combustion cycle. A description of the model is provided in (102). The scavenging model employs two zones so that for the gas exchange process the cylinder contents are divided in two parts, one for the fresh entrained air and the second for a mix for fresh air and combustion products of the previous engine cycle. During the scavenging process part of the intake air escapes directly to the exhaust manifold, which lower the temperature of the exhaust gas. The total amount of air entering the cylinder at a certain time step is divided in the part that enters the fresh air zone and the part that joins the combustion products zone. These amounts are given by the following equations:

$$dm_{a,fz} = dm_{a,inl}(1 - C_{1scav}) \quad (3.50)$$

$$dm_{a,cz} = dm_{g,exh}(1 - C_{2scav}) \quad (3.51)$$

The total amount of exhausted mass to exhaust manifold comprises of part of the fresh air zone and the combustion product zone as established above. The gas masses of the two zones are calculated by:

$$dm_{g,fz} = dm_{g,exh}C_{2scav} \quad (3.52)$$

$$dm_{g,cz} = dm_{g,exh}(1 - C_{2cav}) \quad (3.53)$$

In the above two equations the C_{iscav} are the constants of the scavenging model. At the end of scavenging perfect mixing between the two zones is assumed that results to a single zone comprised of fresh air and combustion products from the previous cycle.

3.2.12 Nitric Oxide Formation Modeling

The formation of nitric oxides is calculated using a chemical equilibrium scheme for each zone. Due to the very high temperatures inside the zones, chemical dissociation takes place. The contents of each zone are initially assumed to contain air and ideal combustion products, (123). Eleven chemical species are assumed in the complete chemical equilibrium scheme; O_2, N_2, CO_2, H_2O, H, H_2, N, NO, O, OH, CO.

The chemical reactions describing the species formation are:

$$\frac{1}{2}H_2 \leftrightarrow H,\ \frac{1}{2}O_2 \leftrightarrow O,\ \frac{1}{2}N_2 \leftrightarrow N,\ \frac{1}{2}H_2 \leftrightarrow H,\ 2H_2O \leftrightarrow 2H_2 + O_2 \tag{3.54}$$

$$H_2O \leftrightarrow OH + \frac{1}{2}H_2, H_2 + CO_2 \leftrightarrow H_2O + CO \tag{3.55}$$

$$H_2O + \frac{1}{2}N_2 \leftrightarrow H_2 + NO \tag{3.56}$$

Including the above equilibrium equations and the equations for the atom balance of C, H, N and O a system of eleven available equations is formed. The solution of these non-linear equations provides the concentration of the subject species in each zone.

The formation of NO_x is chemical kinetics controlled and for the present calculations the extended Zeldovich mechanism is applied, (128) that involves the below reactions:

$$O + N_2 \overset{k_{1f}}{\leftrightarrow} NO + N,\quad k_{1f} = 1.6 \cdot 10^{10} \tag{3.57}$$

$$N + O_2 \overset{k_{2f}}{\leftrightarrow} NO + O,\quad k_{2f} = 6.4 \cdot 10^{6} \cdot T \cdot \exp\left(\frac{-3125}{T}\right) \tag{3.58}$$

$$N + OH \overset{k_{3f}}{\leftrightarrow} NO + H,\ k_{3f} = 4.2 \cdot 10^{10} \tag{3.59}$$

with k_{if} the corresponding forward reaction rate constants.

Inside each zone the change of NO concentration is given by eq. 3.60:

$$\frac{1}{V} \cdot \frac{d([NO])V}{dt} = \frac{2(1-\beta^2)R_1}{1 + \beta \cdot \frac{R_1}{R_2 + R_3}} \tag{3.60}$$

In eq. 3.60 $R_1 = k_{1f}[N]_e[NO]_e$, $R_2 = k_{2f}[N]_e[O_2]_e$, $R_3 = k_{3f}[N]_e[OH]_e$ and $\beta = \frac{[NO]}{[NO]_e}$. The "e" index denotes equilibrium. The NO concentration in each zone is obtained by the integration of eq. 3.60, as in (123).

Chapter 4 Liquified Natural Gas Dual Fuel Engines

LNG has been used in the maritime industry for considerable time with the first trials taking place in 1970 and the first low-speed engine entering the market in 1972, (129). However, the fuel until recently was exclusively used in engines of LNG containerships utilizing their cargo boiloff gas, (130). The modern iterations of 2-stroke low-speed marine engines burning natural gas are based on two different principles of operation. Regardless of type, all such engines operate on a dual-fuel basis, with natural gas injected first in the cylinder and another easily ignitable fuel, MGO or HFO, injected to initiate combustion. The primary difference between them is the method used for natural gas injection. Both methods were introduced by the two major marine engine manufacturers in the early 2010s, (129,131,132). The conditions for market adoption were highly favourable at the time with the cost of natural gas at record low levels compared to the previous decade, and the impending ban of high sulphur fuels requiring the use of expensive LSFO/VLSFO or scrubber exhaust gas cleaning devices, (133,134).

In this chapter performance analysis is conducted on two dual fuel high-pressure gas injection engines, based on measured cylinder pressure traces at both diesel-only and gas modes. Similar analysis for the low-pressure variants was not feasible due to lack of measurement points to conduct cylinder pressure measurements. The removal of the traditional on-cylinder indicators was attributed to security concerns of the engine designer regarding the possibility of gas leakage in the engine room, due to the low-pressure gas admission concept.

2-Stroke Low Pressure Natural Gas Engines

The 2-stroke low-pressure gas injection gas engine operation resembles the premixed Otto cycle when using a lean burn approach, (135). Natural gas is admitted early in the compression phase following scavenging. The early admission allows adequate time for the fuel gas and air to be well mixed. Ignition is achieved near TDC by the injection of a small amount of pilot diesel fuel, which is highly ignitable. The air/fuel ratio is by design relatively high in these engines and the amount of diesel pilot is very low, roughly 1% of the full load total fuel consumption. The combination of fuel lean mixture and a premixed cylinder charge leads to lower combustion temperature compared to the mainly diffusion controlled combustion process normally occurring on diesel engines. In this way these engines can achieve up to 90% reduction in NO_x emissions compared to diesel only and high-pressure natural gas ones, (135,136). This allows to achieve the Tier-III emissions standard without the use of additional installations such as SCR and EGR systems. The downside of this approach is that limitations are introduced regarding operational characteristics to avoid the possibility of knocking (137). As the air and gas fuel mix during the compression stroke the risk of a misfire or pre-ignition increases. This is enhanced when the gas fuel is mixed into the total swept volume of the engine. Due to this possibility the power output is limited compared to diesel engines and the engine operating window is narrowed down to a safe region, as shown in the schematic of Figure 4-2. The operating region satisfying the safety and stability criteria requires lower compression ratio and mean effective pressure, thus peak compression and combustion pressure values are reduced. The previous result in overall lower thermodynamic

efficiency compared to engines operating at the Diesel cycle. Part of the efficiency penalty is compensated by the aforementioned significantly lower NO_x emissions that can achieve Tier-III standard without use of additional techniques, as all abatement techniques for this pollutant currently used in maritime increase fuel consumption. Another significant issue with the low-pressure admission implementation is methane slip, (138). The global warming potential of methane is 28 times higher than CO_2 over a 100 period and 86 times higher when evaluating on a 20 year horizon, (139). In low-pressure DF engines any amount of unburnt natural gas is classified as methane slip due to its high methane content. The main mechanisms of methane slip are valve overlap, which does not apply in 2-stroke engines, quenching through walls and crevices and incomplete combustion. The latter is mainly the result of high air-fuel ratio. When the mixture becomes too lean, the speed of the flame initiated by the pilot fuel ignition is reduced and is not sufficient to cover the chamber volume before expansion starts and decreases temperature below the conditions required for complete combustion of all species. On the other hand, by decreasing air fuel ratio (AFR) the overall cylinder temperature rises promoting NO_x formation. It is expected that as early as 2027 the IMO will introduce regulations regarding methane emissions from vessels, (140,141), while the EU will start methane emissions regulation in 2025 with the fuelEU Maritime initiative, (142). Due to the impending limitations marine engine manufacturers have recently introduced a new type of low-pressure DF engine that operates on the Otto principle and also utilizes an EGR system to limit methane slip to the environment, (137). The development of this solution started just in 2017 with the first full scale demonstration taking place in 2021. The use of the EGR system allows for greater flexibility regarding engine tuning as it suppresses pre–ignition and limits excessive combustion rate that can occur on engines operating on premixed air – fuel concept. The gas admission strategy and other factors such as compression ratio can be adjusted to a wider range improving efficiency. The main benefit of EGR use, however, is that methane slip is reduced by around 50%. The number of current orders for this engine type is high for all manufacturers, thus good levels of market penetration can be expected in the near future, (143). Despite that, the introduction of EGR installation in low-pressure DF engines removes one of the two main benefits of this implementation compared to the high-pressure approach, the ability to use this engine without a Tier-III NO_x reduction solution.

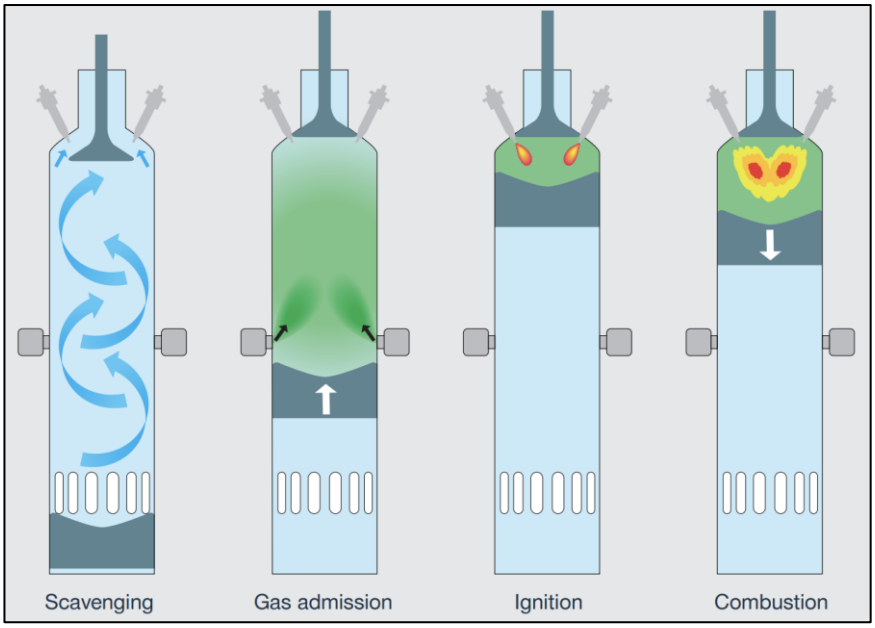

Figure 4-1 Dual Fuel, Low-Pressure gas admission operating principle, (137)

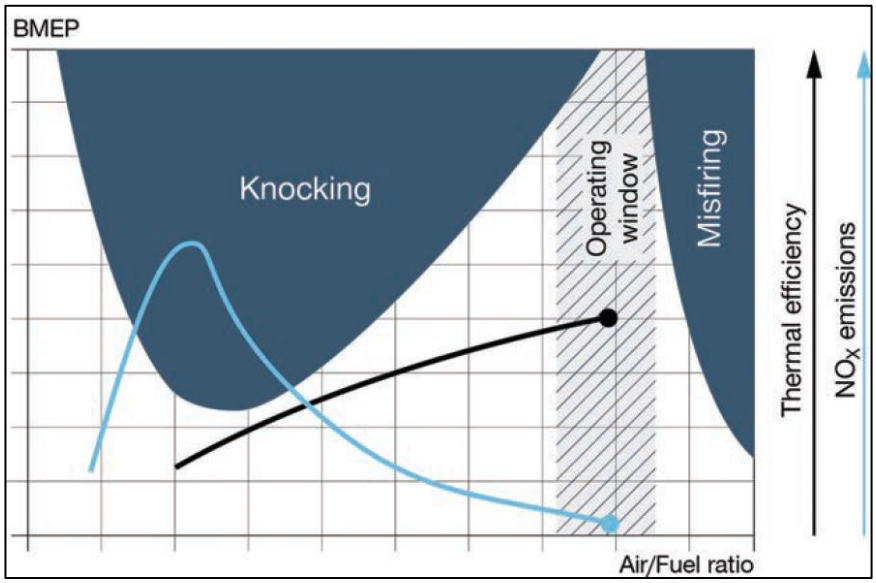

Figure 4-2 Low-pressure natural gas marine engine operating region, (137)

2-Stroke High Pressure Natural Gas Engines

The high-pressure 2-stroke DF engine solution, which is examined in detail in the present thesis, in its present form entered commercial operation at roughly the same period as the low-pressure approach, (132). High-pressure gas injection engines operate on the Diesel cycle with the natural gas injected near top dead center (TDC) mostly slightly earlier than the diesel pilot fuel, (131). As with the low-pressure approach, combustion start is achieved by the auto-ignition of the pilot fuel. The injection of both gaseous and liquid fuel close to TDC, shortly before ignition, means that combustion is primarily diffusion controlled. The main advantage of this approach is that the compressed cylinder charge is air, thus there is no danger of pre-ignition and misfire allowing higher compression ratio and overall peak pressure values, increasing efficiency. In addition, by

injecting the natural gas (NG) close to TDC methane slip due to crevices and wall quenching is non-existent and the higher temperature diffusion combustion that ensues leaves significantly lower amounts of unburnt fuel, thus methane concentration at exhaust is minimal in this implementation. In addition, the improved combustion increases fuel efficiency. The downside is considerable increase of NO_x emissions so these engines cannot satisfy the Tier-III standard without the use of EGR or an SCR system increasing cost and complexity compared to low-pressure DF engines. The main challenge of the high-pressure solution is the requirement to inject NG at a pressure above the peak in-cylinder combustion pressure. This typically translates to injection pressure up to 300 bar for maximum load, that requires special infrastructure to achieve for a gaseous fuel. The cryogenic installation used for injection of NG at this pressure level is very complex and can raise CAPEX significantly for the larger engine variants, (20). In addition, power consumption of the various auxiliary systems supporting the high-pressure gas injection system will raise operating costs. Beyond expenses, an overall highly complicated installation is usually undesirable for ocean going vessels due to potential negative impact on vessel downtime and the difficulties of maintenance procedures conducted during sailing. With the upcoming introduction of EGR use also in low-pressure DF engines part of the simplicity and lower CAPEX advantages has been lost, while the high-pressure engines retain their superior fuel efficiency and very low methane emissions and have achieved significant market penetration with a high number of active orders.

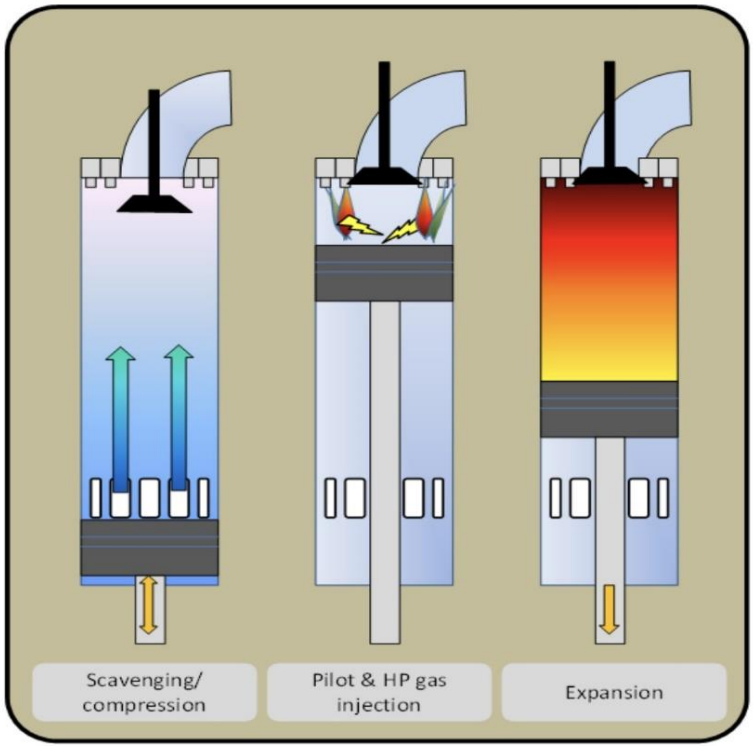

Figure 4-3 Dual Fuel, High-Pressure gas injection operating principle, (129)

4.1 Operating Characteristics of High-Pressure Gas Injection Dual-Fuel Engines

The operation of 2-stroke high-pressure natural gas injection dual-fuel engines is analysed in this section. Comparison is conducted for two engines, for which different tuning approaches were selected by the manufacturers. In the case of “Engine-1” tuning choices to achieve very high grade of similarity between diesel and gas mode was followed, while for “Engine-2” fuel efficiency was improved by the engine manufacturer with considerable differences in overall performance and especially combustion as a result of tuning and component revisions.

The objective of the study is to evaluate the differences in overall performance between the diesel and DF mode of two engines that belong to the same overall type but are of two consecutive generations, with the newer one being the most advanced version currently available. The general engine behavior is examined, and focus is directed towards comparing the differences in the combustion process due to the use of LNG and pilot diesel fuel injection for ignition. A direct comparison of the two modes utilizing actual measurement data from this engine type in a controlled environment and without the use of a simulator is challenging due to significant constraints in the measurement procedure. The constraints result mainly from the sheer size, fuel consumption and power output of the engines, which prohibits testing in a laboratory environment, and the limited availability of vessels’ schedule to allow for lengthy measurement procedures along with the various challenges of conducting on-board tests. Thus, at the time of this study, comparisons of the two-stroke high-pressure gas injection engines using experimental data are scarce in the literature, especially when considering data for both diesel and gas modes under various loads. Most of the available information is based on simulation results, and commonly refer to four-stroke or low-pressure gas injection engines, as detailed below. The majority of research works employ the use of computational methods.

One approach is the use of computational fluid dynamics (CFD) simulation of fuel and gas injection and combustion, as in the case of (144,145). Both works confirm the expectation of a fast and intense fuel burn rate of methane, which is visible in the fuel burn rate diagrams. Additionally, in (144), the influence of the pilot injection and ignition angle is evaluated regarding its effect on combustion intensity, which generally increases with pilot injection delay. Investigations based on the utilization of experimental data from direct gas injection engines are provided in (146), but no information is available for two-stroke marine engines. The use of experimental data and analysis with simulation software is utilized in (147) to investigate the combustion characteristics of diesel and gas modes. An intense combustion of NG is found, with most of the gas fuel burning during the rapid combustion phase, resulting in an overall lower combustion duration, which is partly in agreement with the general findings of the present thesis. Further results based on experimental data are reported in a review of various types of marine dual fuel engines in (148). In these investigations, a significant effect of the dual fuel combustion mechanism on the heat release rate mechanism is revealed. The effect is similar to the one predicted by the aforementioned CFD simulation works, which reveals their

usefulness. For low-pressure gas induction, marine dual fuel engines are examined in the studies of (149,150) which are also mainly computational. The results are not comparable to the high-pressure direct gas injection variant, as fuel-air mixing and, consequently, the combustion process, differ significantly.

For the present study, acquisition of the experimental data under both diesel and gas modes from full scale testing was achieved by conducting the measurement procedure alongside the process of the engine's factory acceptance tests at the engine manufacturer's facility. This provided a controlled environment with high-quality instrumentation and the same conditions for the testing of both modes, diesel and DF. With this approach, high-quality experimental data were acquired and used to conduct a full comparative investigation of the two modes using the actual engine under normal operation, providing insight into the studied subject using measurement data, which were hitherto limited in peer-reviewed work. In addition to the recorded data, engine settings were determined using an analysis conducted with the aid of a specialized methodology described in (151). This step is important, as tuning between single and dual fuel mode differs for these engines by design. The two modes' individual tuning settings are compared, and their effect on engine performance is examined in tandem with the fuel effect achieved. The acquired cylinder pressure traces were processed to derive the heat release rate, which was used to conduct an analysis of the combustion process. The estimated heat release rate was used to determine the effect of natural gas use on combustion progression, intensity and combustion duration in comparison to the corresponding values of the diesel mode, which are the areas expected to be most affected based on the available literature detailed above.

4.1.1 Measurement Procedure

The measurement installation is provided in the following simplified schematic, Figure 4-4 which applies to both engines tested. The tested engines and used fuels most important properties are given in Table 4-3 - Table 4-4. In this and all further cases only the basic data of the engines are provided to the degree allowed by the manufacturers and shipowners. Because of this no detailed information is provided, even though available, for nozzle geometry, designs, etc. The specifications of the measurement equipment involved are provided in

Table 4-5 along with the error level associated with each measured value.

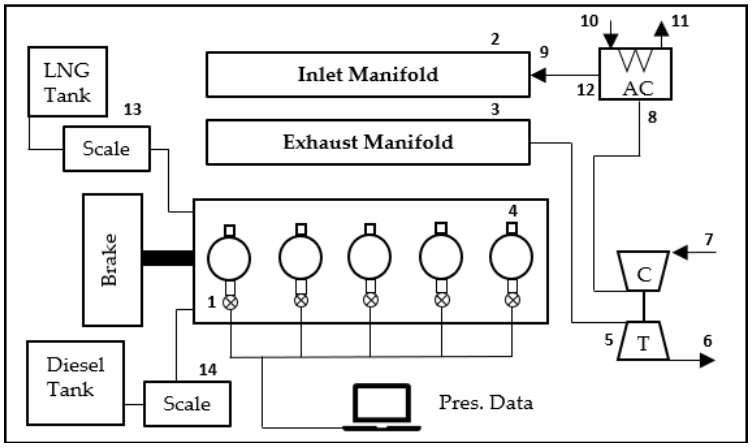

1. Cylinder Pressure Trace	8. Air Temp. before Cooler
2. Scavenging Pressure	9. Air Temp. after Cooler
3. Exhaust Pressure	10. A/C Water Temp. In
4. Cylinder Exhaust Gas Temp.	11. A/C Water Temp. Out
5. Turbine Inlet Temp.	12. A/C Pressure Drop
6. Turbine Outlet Temp.	13. NG Consumption
7. Compressor Air Inlet Temp.	14. Diesel Consumption

Figure 4-4 Measurement Setup for the dual fuel engines, Schematic View

Table 4-1 Particulars of Engine 1

5G70ME-C9.5GI	**Units**	**Value**
Type	-	Two-stroke
Electronic Control	-	Yes
Cylinder No.	-	5
Bore	mm	700
Stroke	mm	3256
Nominal Speed	rpm	68.1
Nominal Power	kW	11,975

Table 4-2 Particulars of Engine 2

6G70ME-C10.5GI	**Units**	**Value**
Type	-	Two-stroke
Electronic Control	-	Yes
Cylinder No.	-	6
Bore	mm	700
Stroke	mm	3256
Nominal Speed	rpm	71.0
Nominal Power	kW	15,081

Table 4-3 Diesel fuel and natural gas properties, Engine 1.

Diesel Fuel Properties	**Units**	**Value**
Density at 15 °C	kg/m^3	879
Lower Calorific Value	kcal/kg	10,116
Viscosity at 40 °C	cSt	5.98
Sulfur (m/m)	%	0.16
Carbon (m/m)	%	86.70
Natural Gas Properties	**Units**	**Value**
Methane (CH_4)	% mol	86.60
Ethane (C_2H_6)	% mol	9.89
Lower Heating Value	kcal/kg	11,762
Total Carbon (m/m)	%	76.30

Table 4-4 Diesel fuel and natural gas properties, Engine 2.

Diesel Fuel Properties	**Units**	**Value**
Density at 15 °C	kg/m^3	825.60
Lower Calorific Value	kcal/kg	10,274.60
Viscosity at 40 °C	cSt	4.56
Sulfur (m/m)	%	0.12
Carbon (m/m)	%	85.38
Natural Gas Properties	**Units**	**Value**
Methane (CH_4)	% mol	87.63
Ethane (C_2H_6)	% mol	6.24
Lower Heating Value	kcal/kg	11,545.89
Total Carbon (m/m)	%	74.81

Table 4-5 Characteristics of instrumentation for engine performance monitoring.

Instrument	**Measured Parameter**	**Range**	**Accuracy**
Hydraulic Brake	Torque		<0.5%
	Speed	0–250 rpm	0.1 rpm
Diesel Fuel Scale	Diesel Fuel Consumption	0–10,000 kg	0.2%
Gaseous Fuel Scale	Gas Fuel Consumption	0–10,000 kg	0.3%
MBS 3000	Scavenging Air Pressure	0–10 bar	0.5%
Air Temperature Sensors	Scavenging Air Temperature	−10–80 °C	0.2 °C
Exhaust Gas Temperature Sensors	Exhaust Gas Temperature	−10–700 °C	0.5 °C
Cooling Water Temperature Sensors	Cooling Water Temperature	0–180 °C	0.2 °C
Kistler 6613CG2	In-Cylinder Pressure	0–250 bar	±0.5 bar

4.1.2 Processing of Measured Cylinder Pressure Data

The most valuable source of information for the evaluation of dual fuel performance and comparison with a typical diesel mode is the cylinder pressure trace. The cylinder pressure trace used for all cases examined is the mean value of all engine cylinders in order to have a representation of overall engine performance. For each cylinder the mean value of 40 cycles is used. Before using the mean cylinder pressure trace, uniformity

between all cylinders was verified regarding pressure values and power output. This was possible since, as mentioned, in the following measurements at each load were repeated 3-4 times. Using the cylinder pressure data recorded, the following information was derived using an advanced diagnostic technique described in detail in (102,152).

- Engine brake power: Estimated from the indicated power using the mechanical efficiency map of the engine defined during the shop test procedure. The power is compared against the one measured using the hydraulic brake to evaluate the quality and accuracy of the measured pressure data.
- Combustion rate of fuel: Estimated by applying the heat release rate analysis methodology described below.
- Start of combustion (SOC): The ignition angle was estimated from the cumulative heat release from the point where 3% of total energy was released. For verification of the derived values, a second methodology was used based on the second derivative of cylinder pressure to crank angle.
- Start of injection (SOI): Estimated from the ignition angle and the correlation used to derive the ignition delay, (153). The value was cross-referenced with the engine control system (ECS) indication. Furthermore, the methodology was verified using data from common rail engines where a signal for the injection angle of diesel is provided.
- Exhaust valve opening (EVO): This value is directly provided by the ECS and is secondarily estimated for verification from the measured cylinder pressure trace using a technique described in, (102,152). The latter is based on the simulation of cylinder expansion stroke after combustion using the closed cycle assumption.
- Exhaust valve closing (EVC) angle: This value is provided indirectly by the exhaust valve actuator signal, which is available in the ECS. The value is verified using an engine simulation model to match the measured P_{comp}/P_{scav} value, as described in (102,152). Furthermore, it is estimated for the comparison of the actual and the simulated compression curve corresponding to close cycle compression.

It is noted that the exhaust valve and injection angle timings vary due to engine design (electronic engines) while an additional variation is added due to auto tuning which for all cases examined was “ON”.

4.1.3 Estimation of Combustion Rate

The burn rate of fuel provides information on the combustion process, which is of major interest for dual fuel operation. It allows a study of ignition, combustion progression and duration, which are expected to differ when using a high-ignitability pilot fuel and a low-ignitability main fuel injected in parallel inside the combustion chamber. The fuel burn rate is derived by conducting a heat release rate analysis of the measured cylinder pressure traces. The process to estimate the net heat release rate is based on the first thermodynamic law, (107):

$$\frac{dQ_{net}}{d\varphi} = \frac{C_v}{R}\left(P\frac{dV}{d\varphi} + V\frac{dP}{d\varphi} - \frac{PV}{m}\frac{dm}{d\varphi}\right) + P\frac{dV}{d\varphi} \quad (4.1)$$

In the above equation, the following assumptions are made:

- The cylinder contents are assumed to behave as an ideal gas, which is close to reality.
- The cylinder mass is considered constant, which does not present an accuracy reduction due to the extremely low blow-by rate of the tested engine, as revealed in the performance analysis.
- Uniform distribution of the thermodynamic properties inside the combustion chamber.

The composition of cylinder content charge variability is estimated using the initial mass after EVC and the amount of fuel burnt from the heat release rate analysis and the measured fuel consumption. For this purpose, an iterative procedure is used until the convergence of the total estimated fuels amount with the measured ones using the known heating value of the fuels, (152).

For the estimation of engine fuel consumption and the actual fuel combustion rate, it is necessary to use the gross heat release rate. This is provided in, (107):

$$\frac{dQ_{gross}}{d\varphi} = \frac{dQ_{net}}{d\varphi} - \frac{dQ_w}{d\varphi} \quad (4.2)$$

The heat loss rate $\frac{dQ_w}{d\varphi}$ is estimated using the heat transfer model of Annand, (154), which has been found accurate in multiple similar applications for this engine type.

$$\frac{dQ_w}{d\varphi} = A\left(a_c\frac{\kappa}{D}Re^b\left(T_w - T_g\right) + c_r\left(T_w^4 - T_g^4\right)\right) \quad (4.3)$$

The heat transfer model is calibrated using the shop test data for which the measured cylinder pressure traces under 25%, 50%, 75% and 100% load along with accurate fuel consumption (FC) data are available. For the heat release rate analysis, the mean cylinder gas temperature is used, calculated using the ideal gas law assumption:

$$T_g = \frac{PV}{mR} \quad (4.4)$$

The initial charge mass after EVC is estimated using the simulation model e utilizing an open cycle approach and the filling–emptying technique for mass exchange, (152). The accuracy of the methodology is validated using the exhaust gas and air mass flow rates, which are determined using the carbon balance methodology and are available in the official NO_x file documentation of the engine.

4.2 General Performance Values

The overall performance differences between diesel and DF modes are presented herein for the two engines examined. In this first subsection the direct measurement results are presented. The mean compression pressure (P_{comp}) and peak combustion pressure (P_{max}) during dual-fuel and diesel operation are compared in Figure 4-5a, b and Figure 4-6a, b, respectively for the two engines. In Figure 4-7a, b and Figure 4-8a, b pressure increase due to combustion (ΔP) and cylinder exhaust gas temperature for natural gas and diesel mode are compared. Initially, significant differences could be expected due to the use of pilot diesel injection for ignition and the properties of the natural gas fuel, mainly the energy content, which is significantly above that of conventional marine diesel.

As revealed by the analysis, this expectation was not verified by the results for "Engine 1". The differences are minimal for combustion pressure and exhaust gas temperature. Thus, no effect is expected on exhaust system components and the turbocharger during dual fuel mode operation. Regarding maximum pressure, the highly similar values reveal an effort by the engine manufacturer to maintain these values steady between the two modes via engine tuning (Figure 4-5a). Differences are observed for the compression pressure (Figure 4-5b) which are mainly the result of scavenging pressure (P_{scav}) values. The specific engine type features variable exhaust valve timing, thus, the P_{comp} differences are also attributed to slight closing angle variation, as shown below in section 4.2.1. The engine settings that affect the main operating parameters, namely the start of injection, exhaust valve opening/closing angle and air mass flow, can also have a significant effect on exhaust gas temperature. As seen in Figure 4-7a, these values were the same between the diesel and DF mode for "Engine 1". The compression pressure differences are reflected in the pressure rise due to combustion between the two modes, Figure 4-7b, as the peak combustion pressure values are almost identical. For both modes, a steep decrease in pressure rise is observed as the load increases. Differences between the two modes are observed at 90% load and above, affected by the compression pressure values.

For "Engine 2" the differences between diesel and DF mode are high revealing different overall tuning and considerable variations in the combustion process between the two modes. Compression and peak combustion pressure are higher during DF operation, Figure 4-6a, b, with P_{comp} increased due to earlier EVC. Despite that exhaust gas temperature was decreased during DF mode operation, Figure 4-8a. ΔP is also increased during DF operation, Figure 4-8b, but the difference is lesser compared to the P_{comp} and P_{max} values indicating to earlier gas fuel ignition.

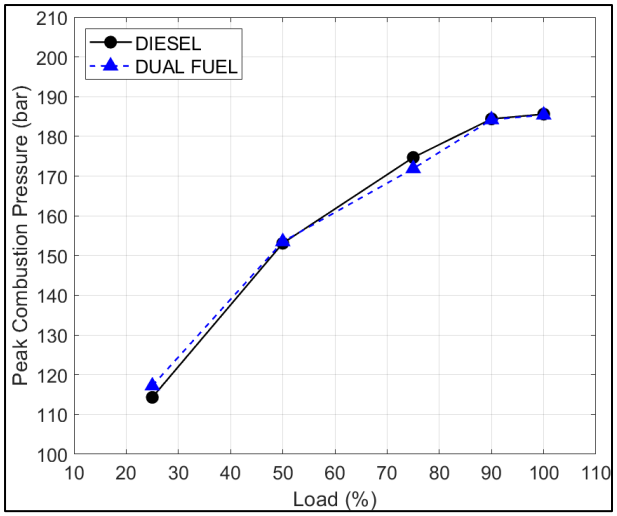

(a)

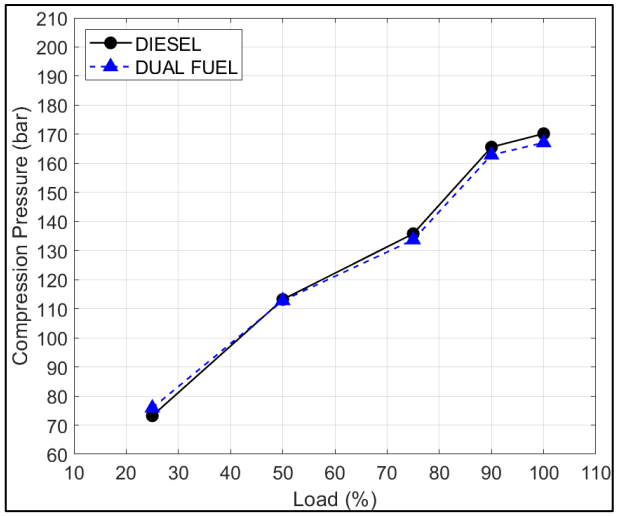

(b)

Figure 4-5 (a) Mean peak combustion pressure, diesel, DF modes; (b) Mean peak compression pressure, diesel, DF modes; Engine 1.

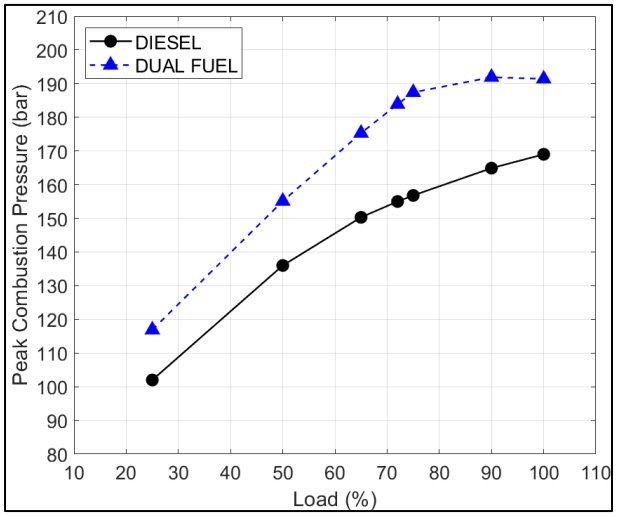

(a)

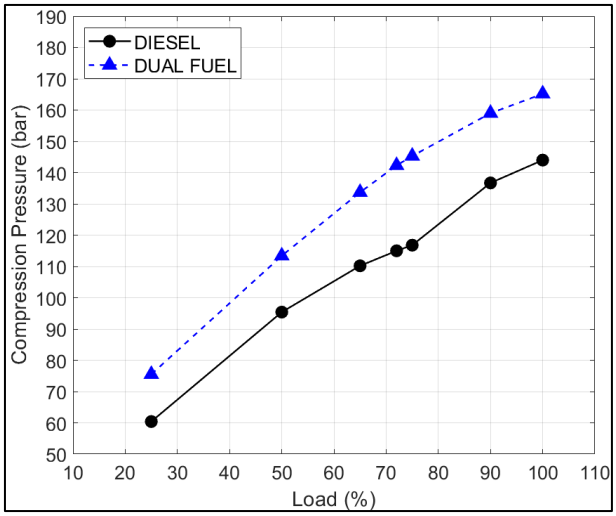

(b)

Figure 4-6 (a) Mean peak combustion pressure, diesel, DF modes; (b) Mean peak compression pressure, diesel, DF modes; Engine 2.

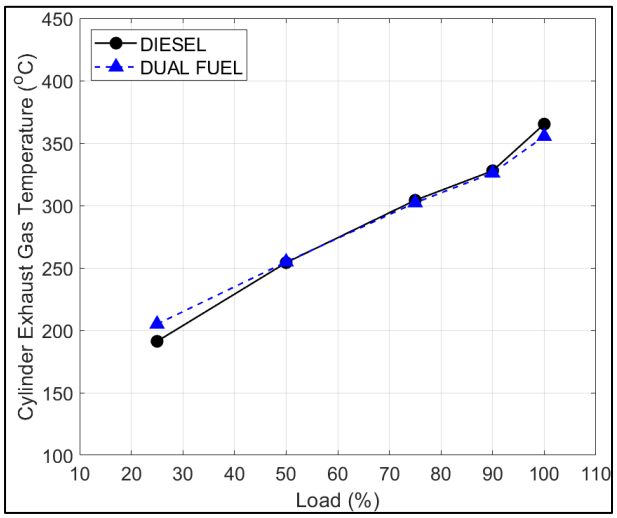

(a)

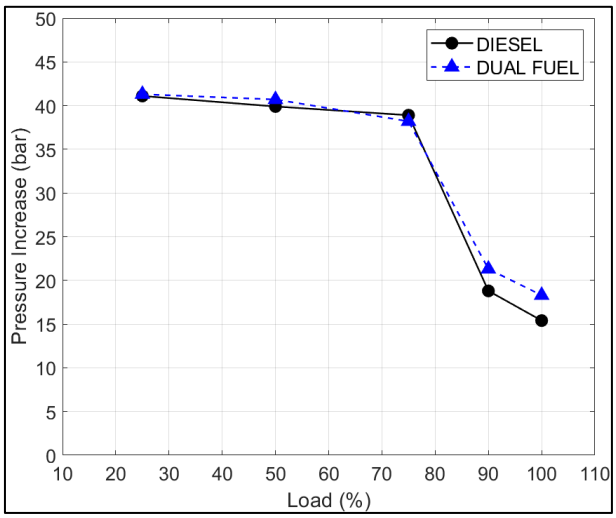

(b)

Figure 4-7 (a) Mean cylinder exhaust gas temperature, diesel and DF modes; (b) Pressure rise due to combustion, diesel and DF modes; Engine 1.

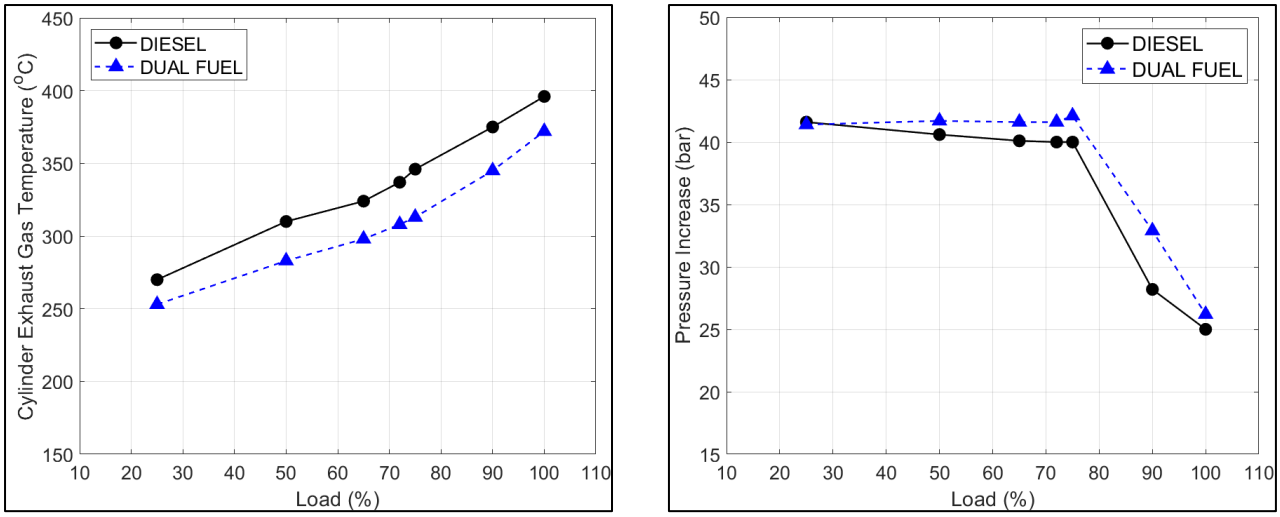

(a) (b)

Figure 4-8 (a) Mean cylinder exhaust gas temperature, diesel and DF modes; (b) Pressure rise due to combustion, diesel and DF modes; Engine 2.

The diesel and natural gas consumptions are provided in Figure 4-9a, b in kg/h for "Engine 1". The total hourly fuel mass flow rate is higher for the diesel mode. On average, 12.9% more total fuel mass is consumed in the diesel mode, and this difference remains mostly steady with engine load. The diesel to natural gas mass ratio under DF mode operation is provided in Figure 4-9c. The peak value is 14.53% under 25% load, and it gradually decreases to 5.16% at 100% load. The previous ratios expressed in energy content result in 12.48% and 4.43%, respectively. According to the manufacturer, higher percentages are expected for very low load operation, up to the threshold for switchover to the diesel mode, (151). In Figure 4-9d, e, the ISO corrected BSFC for the two modes is shown. For the DF mode, the BSFC of the diesel pilot decreases steadily, with the minimum value observed under maximum load, and the reverse is found for natural gas. For the diesel mode, the minimum BSFC value is observed for 50% load operation. The highest value is observed for the lowest load tested, 25%, which is normal under low load due to deterioration of the mechanical efficiency. The most important parameter for long-term engine operation, also considering its size and CO_2 emissions, is specific fuel consumption. Due to the difference in LCV, the evaluation between the two modes in terms of efficiency cannot be based on the comparison of specific fuel consumption without LCV correction. For this reason, for the comparison of the two operating modes, the use of the total heat rate (THR) of both fuels consumed in (kJ/kWh) is preferred. The total heat rate was calculated as follows:

$$THR = SPC_{iso} * LCV_{diesel} + SGC_{iso} * LCV_{gas}, \quad (4.5)$$

where SPC is the specific pilot fuel consumption and SGC the specific gas consumption. Based on Figure 4-9f, the overall efficiency of the diesel mode is found to be higher, with lower total heat rate required for the same power output; however, the average difference is small. The efficiency gains under diesel mode are mainly found in the region of 50% load and under maximum load. The average increase was estimated at 1.15%. In contrast, advantage in efficiency for the DF mode is observed under low load operation (25% load)

at 1.82%. The accuracy of the previous calculation is the same as the accuracy of the fuel consumption values measured in the factory acceptance tests, which is higher than the level of difference observed and is thus reliable. Considering the mean values, only a small reduction in efficiency is observed for the DF mode, which is in the range of 1%. Further study of the performance under lower loads, below 25%, would be of interest, as the pilot fuel energy fraction increases significantly (151); this was not feasible during the factory acceptance tests procedure, as in all cases, the load point tests begin at 25%. The findings of other studies regarding fuel consumption efficiency for marine high-pressure LNG engines are summarized in (148). Different results can be found depending on the engine type and tuning, such as (155,156). Overall, modern dual fuel high-pressure engines are capable of similar efficiency as diesel engines under selected load regions. Using the values of total gas and liquid fuel mass consumed and the carbon content of the fuels, as provided in Table 4-3, the specific CO_2 emissions of both modes can be estimated. This results in an almost steady 22.6% improvement under DF mode, which is considerable.

"Engine 2" fuel consumption values show significant improvement in overall fuel efficiency between the diesel and DF mode, Figure 4-10. In addition, improvement is found compared to the "Engine 1" data for both diesel and DF mode when comparing BSFC and specific total heat rate. Another improvement is the reduction of diesel to gas mass ratio from low to full load; this comparison however must also take into account the energy content of the fuels used. It was found that this improvement was also present when conducting comparison of the diesel to gas energy content ratio. The ratio reduction was most pronounced for medium and high load which also affected the overall diesel fuel consumption vs load trend, considering the graphs of Figure 4-9a ("Engine 1") and Figure 4-10a ("Engine 2").

These initial observations are analysed along with the engine settings and operating conditions in the following section. Review of the specific consumption of both fuels, Figure 4-9e and Figure 4-10e shows that "Engine 2" is optimized for medium load operation. The reduction of specific total heat rate during DF mode for "Engine 2" was found to reach 4.8% for 75% load. The total specific heat rate shows slightly lower thermal efficiency for low load and significant gains for both medium and full load operation for DF mode operation. Efficiency gains of "Engine 2" compared to "Engine 1" are also present for diesel mode, but to a lower degree, specifically an overall energy efficiency improvement of 3.5% was found for DF operation in favour of "Engine 2", and for diesel operation the improvement was 2.1%. Thus, after one generation the high-pressure dual fuel engine presented very high improvement regarding fuel efficiency and DF mode capability regarding diesel fuel percentage requirements. This improvement results to further reduction of tailpipe CO_2 emissions by 6.9%, increasing the potential benefits of this technology.

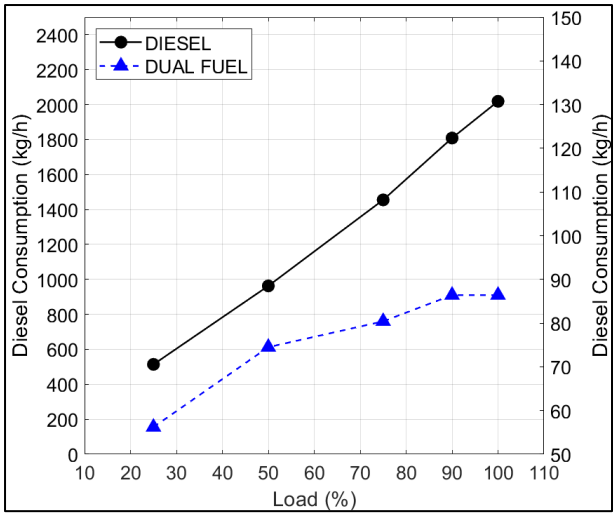

(a)

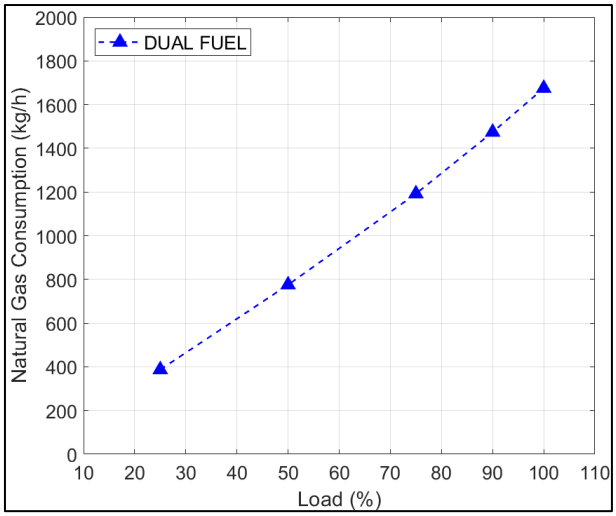

(b)

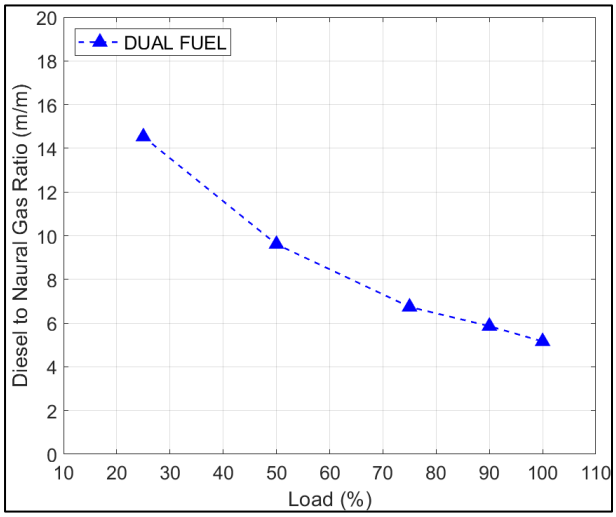

(c)

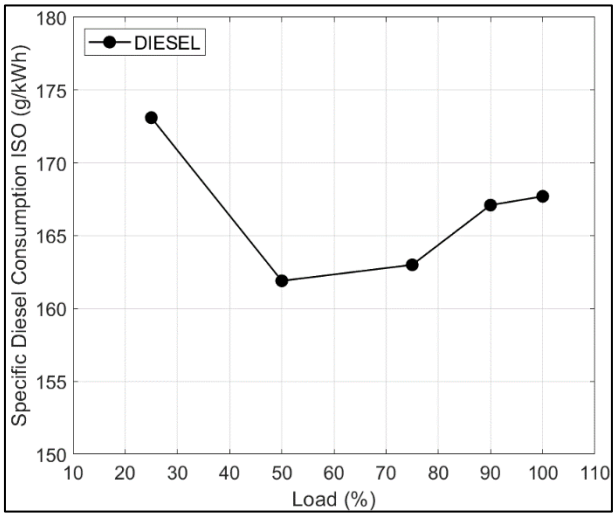

(d)

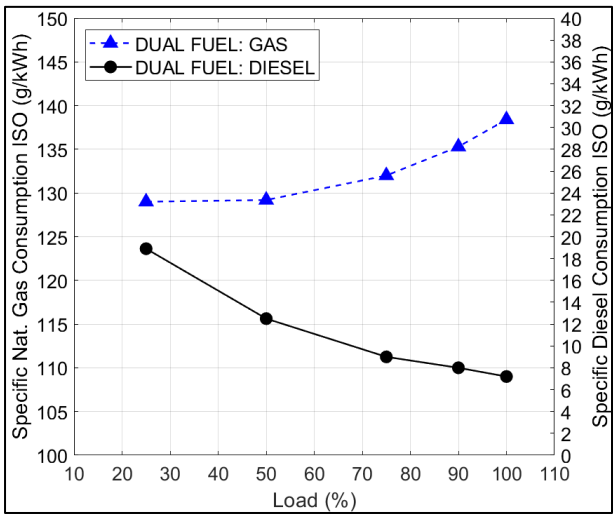

(e)

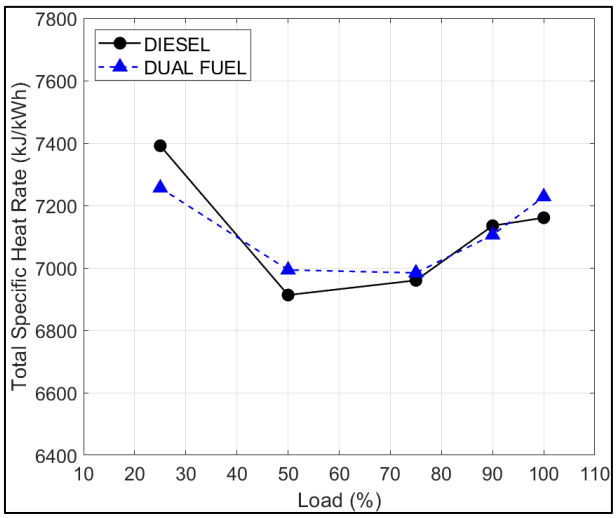

(f)

Figure 4-9 (a) Diesel consumption, diesel and DF modes; (b) Natural gas consumption, DF mode; (c) Mass ratio of diesel to natural gas; (d) Specific fuel consumption ISO, diesel mode; (e) Specific natural gas and diesel consumption ISO, DF mode; (f) Cumulative specific heat rate, diesel and DF modes; Engine 1.

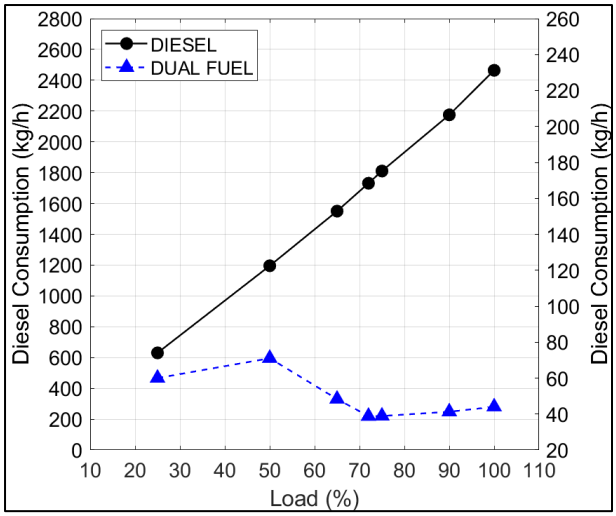

(a)

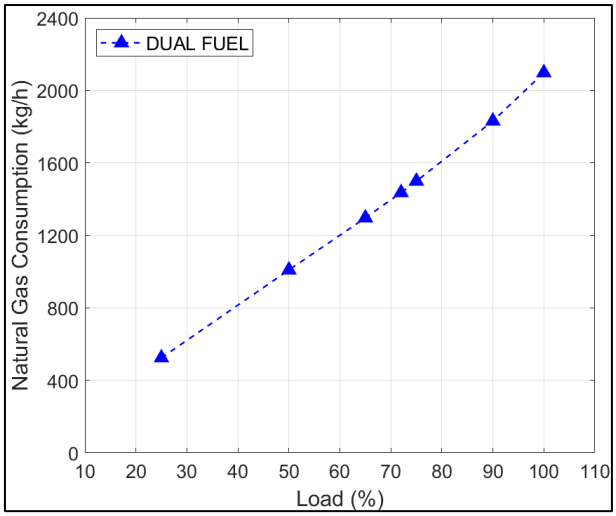

(b)

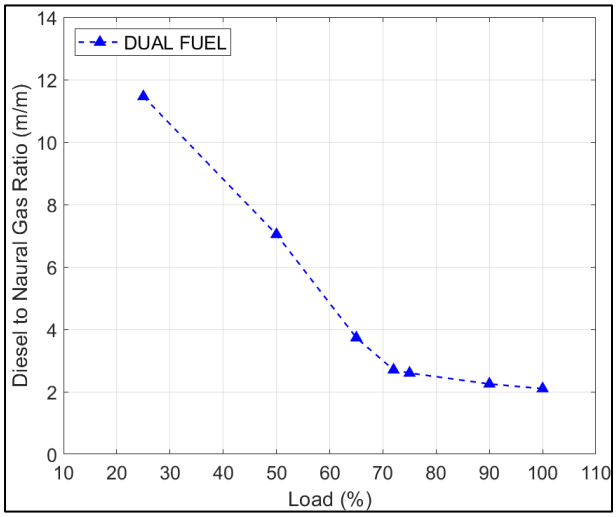

(c)

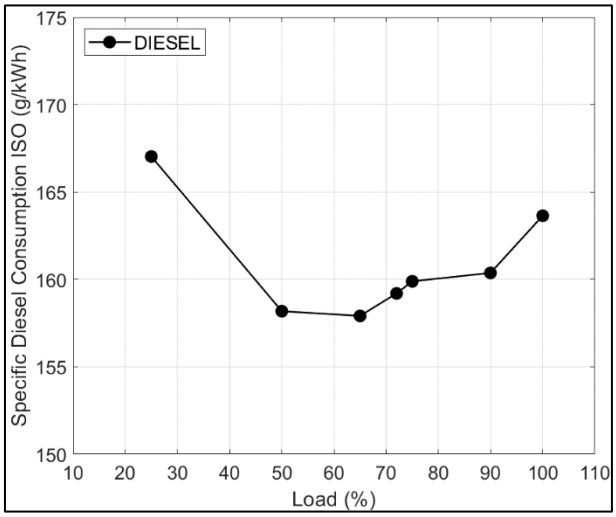

(d)

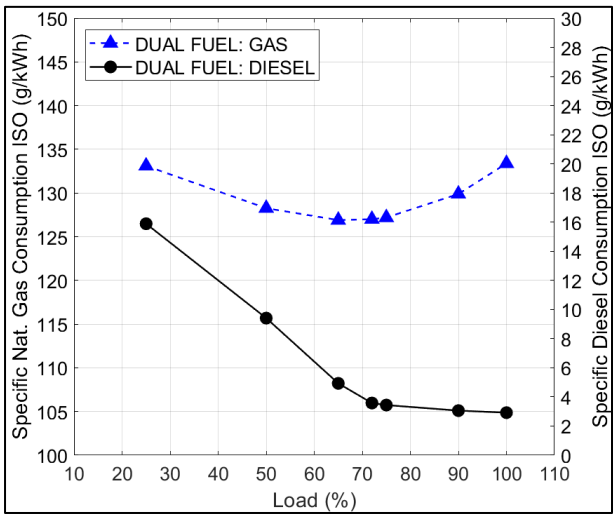

(e)

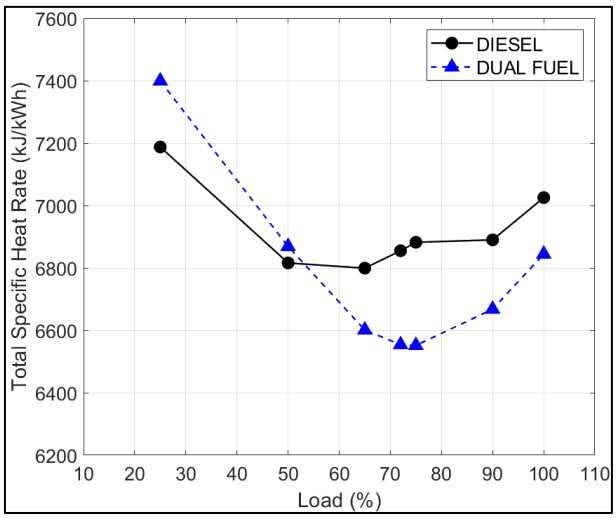

(f)

Figure 4-10 (a) Diesel consumption, diesel and DF modes; (b) Natural gas consumption, DF mode; (c) Mass ratio of diesel to natural gas; (d) Specific fuel consumption ISO, diesel mode; (e) Specific natural gas and diesel consumption ISO, DF mode; (f) Cumulative specific heat rate, diesel and DF modes; Engine 2.

4.2.1 Comparative Evaluation of Engine Settings

In the present section, the engine settings are presented and compared for diesel and DF modes. The injection timing of diesel fuel and exhaust valve opening/closing angles, as well as the resulting pressure ratio (P_{comp}/P_{scav}), are examined for the two engines at both modes. These values were estimated from the processing of the cylinder pressure data as described above and cross-referenced with the ECS indications. For "Engine 1" the exhaust valve opening angle variation with load was found to be the same and generally very small for both modes. The absolute values are shown in Figure 4-11a, revealing the identical tuning. This is important, as it confirms that exhaust gas temperatures, also found to be nearly identical, were not affected by the valve timing. The exhaust valve closing angle variation affects the pressure ratio, with earlier EVC resulting to increase and retarded EVC to decrease. The EVC variation with load is intense for both modes, as revealed by the change of the pressure ratio, Figure 4-11b. This is in contrast with the mostly steady EVO angle timing. This analysis revealed only minimal differences in EVC angle timing between the DF and diesel mode. The valve closing angle is slightly delayed under DF mode operating at 50% load and below; for higher loads, the values are identical up to 100% load, and finally, the closing angle is advanced at 110% load for both modes. The EVC timings do not result in significant differences in P_{comp} values (Figure 4-5b). P_{comp} control is used to regulate peak combustion pressure in the DF mode and not to exceed the maximum permissible value. The alternative solution would be to delay fuel injection, but this would have a negative impact on engine efficiency (BSFC).

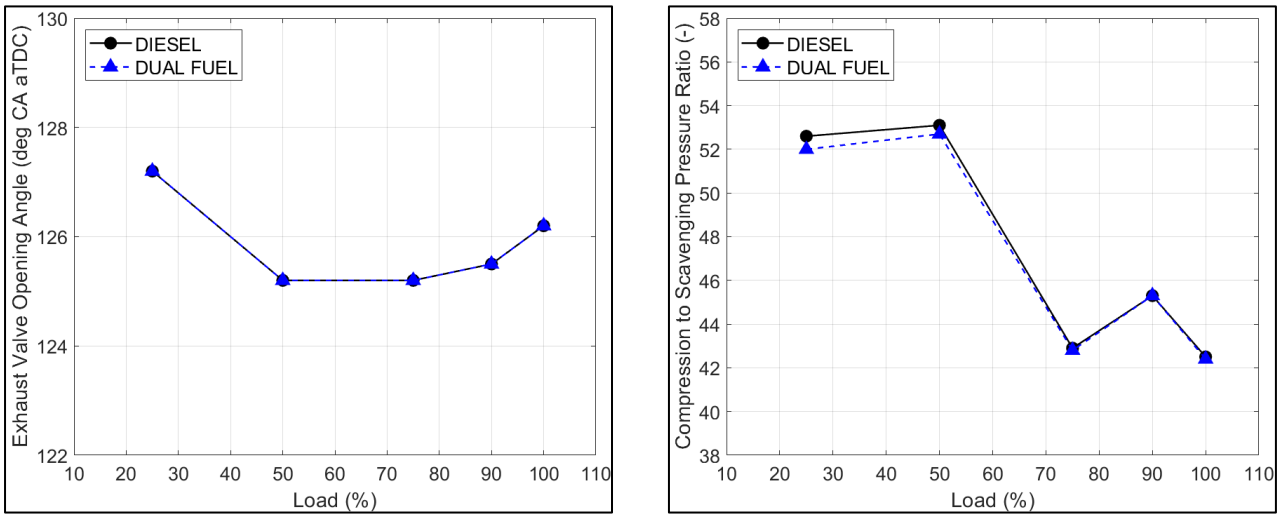

(a) (b)

Figure 4-11 (a) Exhaust valve opening angle, diesel and DF modes; (b) Effective compression ratio (P_{comp}/P_{scav}), diesel and DF modes; Engine 1.

For "Engine 2" the respective values are provided in Figure 4-12a, b, and confirm the expectation of high engine tuning differences between diesel and DF mode. In addition, the tuning approach of the engine manufacturer considerably deviates from that of "Engine 1" for both modes. EVO presents again small variations with load and rather similar values between the two engines. As in the case of "Engine 1" the mostly minimal differences between diesel and DF mode are not expected to affect the cylinder exhaust gas

temperature values. EVC angle is well advanced for all loads during DF mode operation of “Engine 2”, especially in between 62% and 75% load. This region coincides with the highest thermal efficiency improvements between the two operating modes.

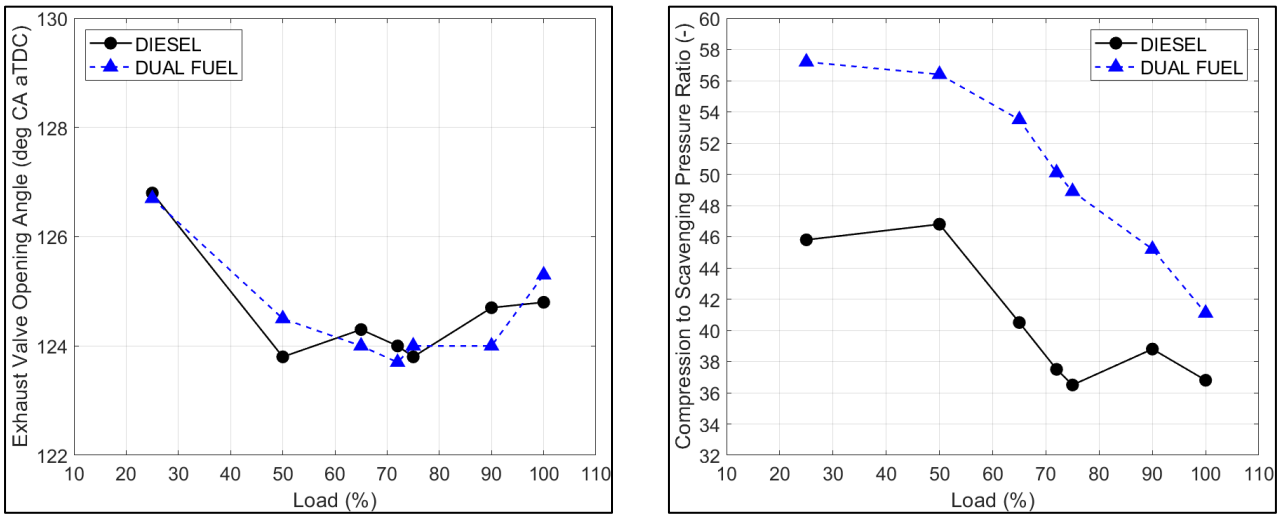

(a) (b)

Figure 4-12 (a) Exhaust valve opening angle, diesel and DF modes; (b) Effective compression ratio (P_{comp}/P_{scav}), diesel and DF modes; Engine 2.

The main difference observed in engine settings and the resulting performance for diesel and DF modes is injection, and consequently, ignition timing. The liquid fuel injection timing, which is the ignition source, was estimated using the diagnostic software utilized for two-stroke diesel engine applications. The ignition angle was estimated using two techniques for confidence, one based on the cumulative heat release diagram and a second based on the second derivative of cylinder pressure. Both methods provided essentially the same ignition angle in all examined cases, increasing the validity of the derived result. The point of combustion initiation was deemed to coincide with the ignition point of the diesel fuel. This assumption is valid and has been proven by various investigations, such as (144,157–160).

In Figure 4-13a,b, the diesel (diesel mode) and diesel pilot (DF mode) injection angle and ignition angle are provided for all load tests of “Engine 1”. The difference between the two figures is small due to the low value of diesel ignition delay. Fuel injection is advanced (before TDC) in diesel mode up to 75% load. Above that, the injection angle is retarded and remains almost steady. Advanced SOI has been found to provide efficiency advantages (161), while retarded SOI commonly results in lower NO_x emissions and limits P_{max} values (162). These are the main factors that affect engine tuning choices in this type of marine engine, and indeed, as shown in Figure 4-9b and Figure 4-9f, the fuel efficiency and pressure increase are affected by SOI in the mid and high load regions. On the other hand, in the DF mode, pilot injection is retarded (after TDC) under all loads. Despite the retarded SOI, the pressure rise due to combustion is comparable to or slightly higher than the diesel mode. This is the first indication of significantly more intense combustion in the DF mode, at least in the early (premixed) stage. For the 90% and 100% loads, the ignition angle is slightly advanced compared to the lower loads of this mode and is similar to the injection timing estimated for the diesel mode. The overall

variation in liquid fuel injection timing is small, in the range of ±1° CA across all loads. For both modes, the injection timing of liquid fuel is generally retarded, close to or after TDC, to control the peak combustion pressure. Despite the difference in diesel fuel SOI timing, the peak combustion pressures were found nearly identical for all loads, as already shown in Figure 4-5a. This was attributed to the engine maker defining the SOI timing curves to have the same values of P_{max} for both modes and achieve similar performance. This is further elaborated in the combustion rate analysis section below and is mainly a result of the difference in the peak value of heat release between the two operating modes, as well as the premixed combustion rate difference.

In Figure 4-14a, b the fuel injection and ignition angles for "Engine 2" are provided, revealing also small diesel fuel ignition delay as found for "Engine 1". This was expected based on the higher pressure ratio of "Engine 2" that resulted to in-cylinder conditions more favourable towards diesel auto-ignition. The pilot fuel injection angle is well advanced compared to diesel mode injection timing, and as could be expected, the highest degree of SOI advance was found for the loads with the biggest efficiency advantage compared to diesel mode operation. This comes in contrast to the tuning choices of "Engine 1" that revealed SOI delay during DF mode. The SOI and ignition angle advance of "Engine 2" compared to "Engine 1" for both modes is in agreement with the lower BSFC values and the increased P_{max} at each load.

The comparison of the EVC and SOI settings between the diesel and DF mode for the two engines tested provides valuable insight into the effect of tuning on overall operation, even for units of the same main type. Furthermore, it is estimated that the approach followed for the older generation dual-fuel engine was to match DF to diesel mode performance as close as possible, which proved feasible while retaining similar fuel efficiency capabilities. For the newer (current) generation engine increase of pressure values to higher levels, more than 20 bar on average, even at maximum continuous rating (MCR), during DF mode allowed for considerable fuel consumption reduction to be achieved. Last, it is noted that the ΔP values are also increased compared to "Engine 1" operation by a considerable degree (roughly 10 bar at each tested load).

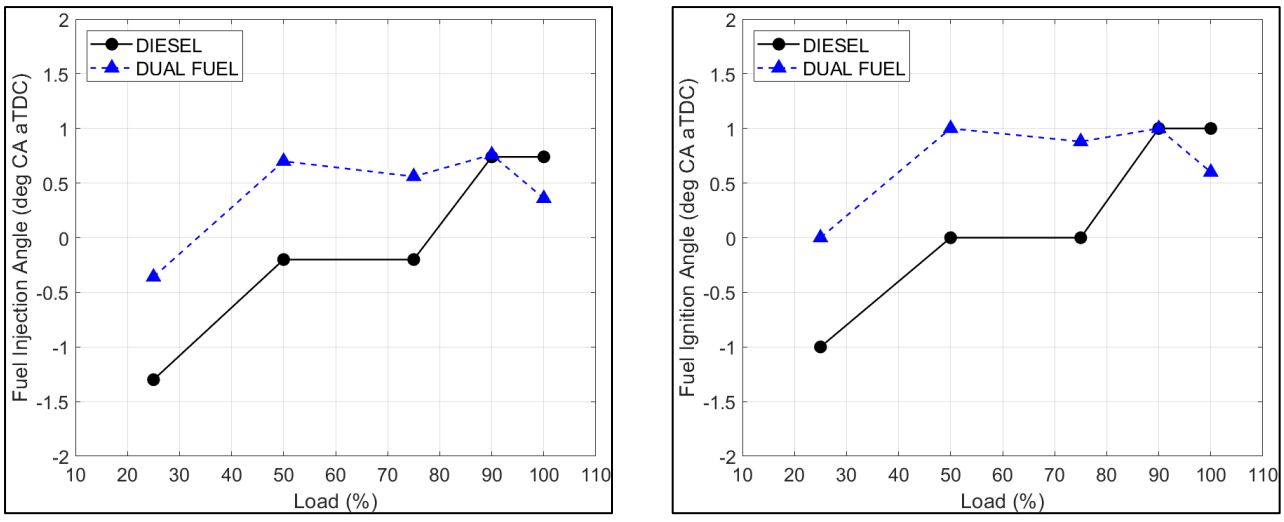

(a) (b)

Figure 4-13 (a) Diesel SOI angle, diesel and DF modes; (b) Diesel ignition angle, diesel and DF modes; Engine 1.

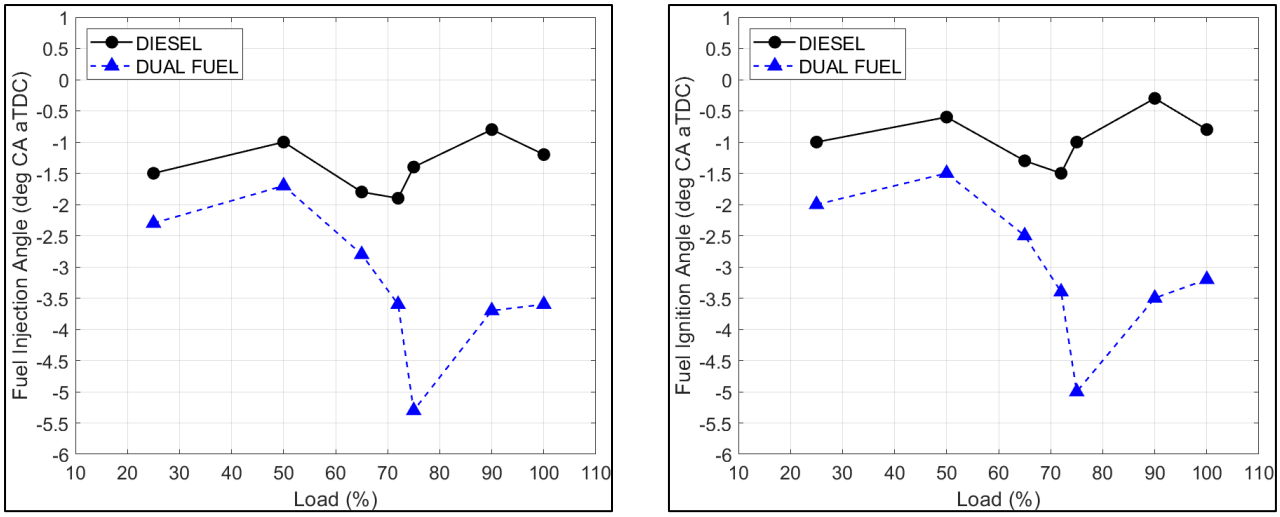

(a) (b)

Figure 4-14 (a) Diesel SOI angle, diesel and DF modes; (**b**) Diesel ignition angle, diesel and DF modes; Engine 2.

4.2.2 Measured Cylinder Pressure Traces and Combustion Rate Analysis

The measured cylinder pressure traces are shown in Figure 4-15 for "Engine 1" and are compared between the diesel and DF modes for four of the six measured load points: 25%, 50%, 75% and 100%. In Figure 4-16 the respective data are shown for "Engine 2". Based on the analysis of the pressure traces, the net heat release rate diagrams were estimated and are provided for comparison. The calculated heat release rate diagrams Figure 4-17 ("Engine 1") and Figure 4-18("Engine 2") provide information on the evolution of the combustion process inside the combustion chamber. They are used for the estimation of the ignition angle, peak heat release rate, initial combustion slope and combustion duration. Utilizing this information, the overall combustion process can be comparatively evaluated from the early to the late stage.

In Figure 4-15a-d, the mean cylinder pressure traces for the diesel and DF modes are provided for 25% up to 100% loads for "Engine 1". The overall differences are limited, as detailed in the previous section; differences are observed for the peak compression and combustion pressure and ignition angle. This is in line with the similarity in engine settings, apart from the fuel injection timing. The specific engine is ME-type technology, equipped with the auto-tuning system, which enables dynamic control of both P_{comp} and P_{max} on each cylinder, triggered by the measured cylinder pressure signal. After reviewing the cylinder pressure traces in the corresponding graphs, the tuning of the engine with the goal of achieving the same variation of P_{max} to load for both modes is made evident. This confirms that the specific DF marine engine design can provide similar performance under both DF and diesel modes, which is not the case for all engine types when DF operation is tested (163). This is an important finding in the present investigation. For the "Engine 2" tests, in Figure 4-16a-d are provided the measured pressure data, that better display the high change in engine operation after the switch to DF mode. The most notable observation from Figure 4-16a-d is the very high maximum pressure values during DF operation. From these graphs the difference in compression between the two modes for

"Engine 2" is noticeable, and specifically the higher compression and peak combustion pressure for DF mode, as result of earlier EVC and, to a lower degree, the increase in ΔP during combustion.

As a general comment, the initial concern of manufacturers for tuning of engines using high energy content gaseous fuels relying on secondary means of ignition were knock and the danger of extreme pressure buildup in the cylinder. Such events could result in the compromise of engine integrity and reliability after the accumulation of operating hours which probably led to the rather conservative engine tuning regarding the overall cylinder pressure values and SOI timing of "Engine 1". The previous is clearly shown in the next section containing the analysis of the fuels' combustion process.

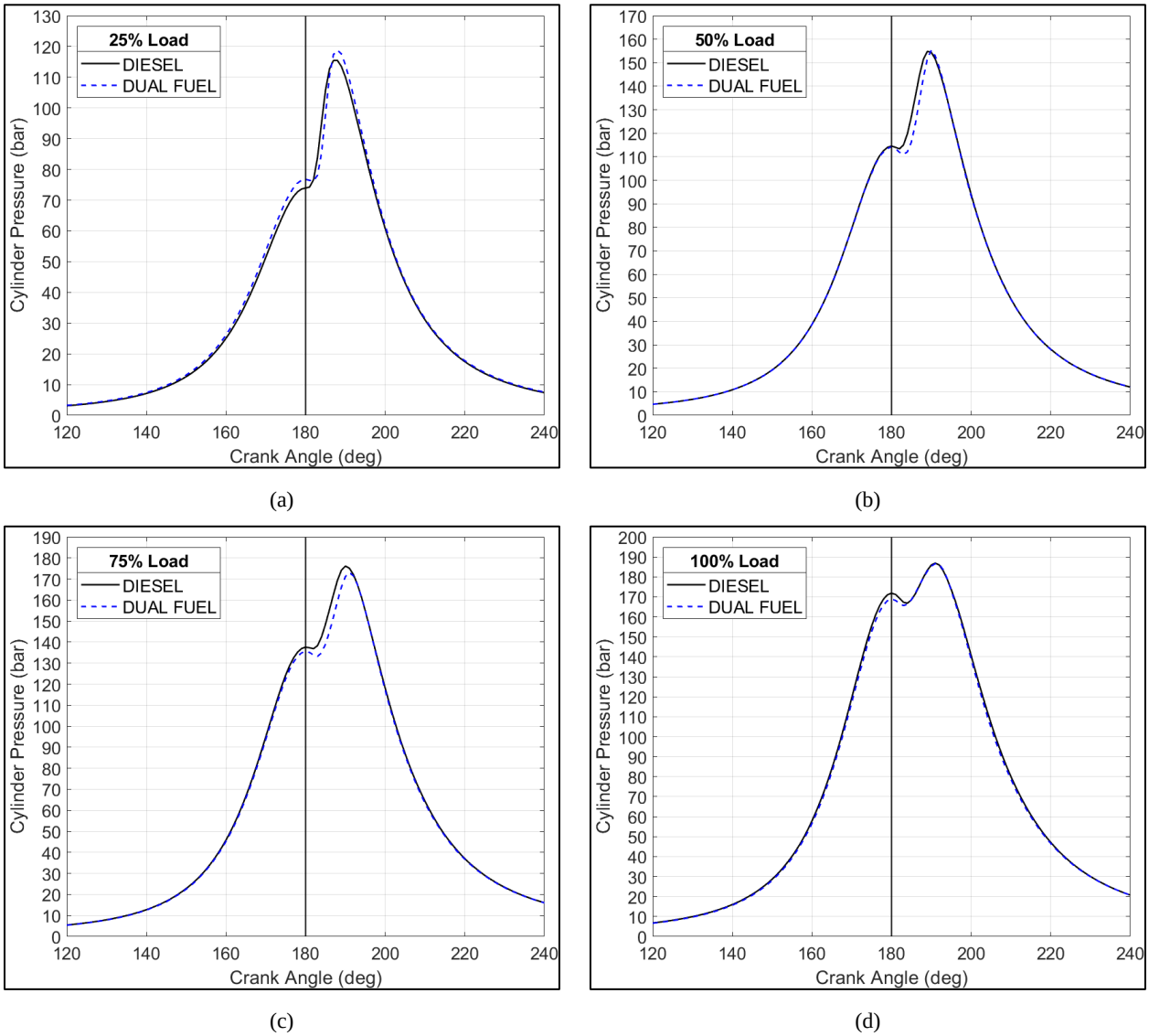

Figure 4-15 (a) Mean cylinder pressure traces at 25% load; (b) Mean cylinder pressure traces at 50% load; (c) Mean cylinder pressure traces at 75% load; (d) Mean cylinder pressure traces at 100% load, at diesel & DF modes, Engine 1.

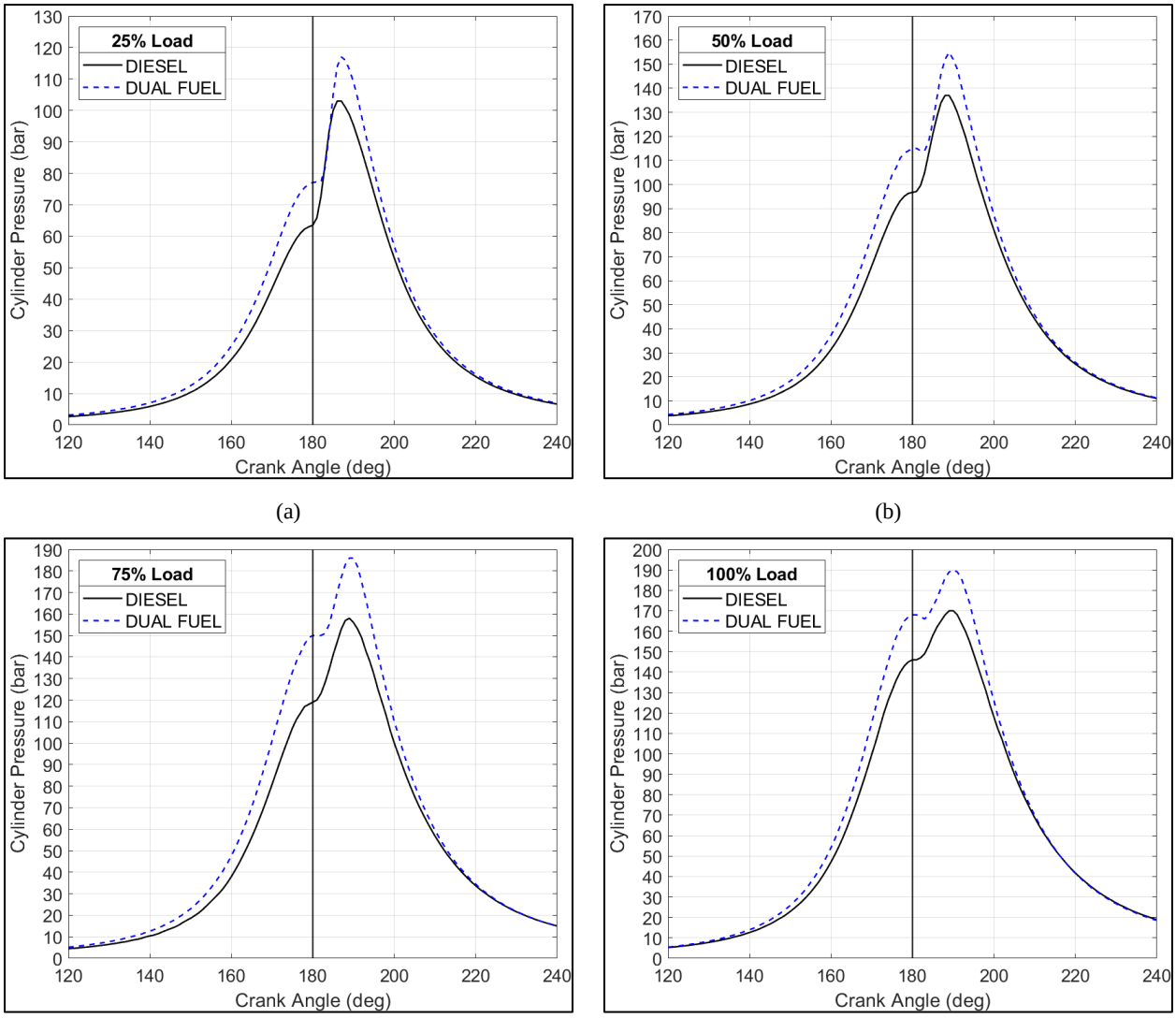

Figure 4-16 (a) Mean cylinder pressure traces at 25% load; (b) Mean cylinder pressure traces at 50% load; (c) Mean cylinder pressure traces at 75% load; (d) Mean cylinder pressure traces at 100% load; at diesel & DF modes, Engine 2.

In Figure 4-17a–d, the net heat release rate estimated from the mean cylinder pressure traces is presented for 25% up to 100% load of "Engine 1". In contrast to the cylinder pressure traces of Figure 4-15, the differences between diesel and DF modes are now clear, especially in the low and medium load regions. This is an advantage of heat release rate analysis for engine performance and combustion investigation. From 25% to 75% load, ignition occurs later for DF mode operation, as expected, since both diesel fuel (main and pilot) SOI timing and ignition delay are similar for both modes, Figure 4-13a, b. The peak value of heat release rate is considerably higher for the DF mode, with a maximum increase of 17.4% under 50% load. This is in general agreement with similar studies of natural gas DF engines, such as (156). However, the reverse may also be encountered (145), mainly depending on the pilot ignition angle and the amount of diesel fuel injected (161). The peak heat release rate (HRR) difference, however, does not lead to a higher value of pressure rise due to combustion, which is about the same for both modes, Figure 4-7. Thus, the effect of the faster heat release rate for the DF mode is offset by the retarded ignition angle. In the case of the same ignition angle, the

pressure rise due to combustion would be significantly higher, and P_{max} would be expected to increase. The faster heat release rate is mostly attributed to fast mixing of the NG fuel (gaseous fuel) and to its 16.3% higher heating value which results to a faster energy input. For a 90% load and above, the differences are minimized between the two operating modes, and the fuel ignition angle is similar. The same is observed for the peak value of heat release rate. This, again, reveals the ability of the injection system to supply fuel at the required rate even at full load. The physical properties of natural gas could potentially limit fuel mass delivery in the cylinder. However, this engine type and other modern NG engines inject natural gas at a low temperature and high pressure (in the range of 40^o C and 300 bar), hence enabling a relatively high mass injection rate, (131,164). The relevant temperature and pressure values were measured at the site of tests, confirming previous findings. Despite similarities in the combustion rate for 100% load, Figure 4-17d, the pressure rise due to combustion was higher for DF mode operation, Figure 4-7b. For all tested loads, except 100%, late combustion was found to progress at a slightly slower rate under DF operation, despite later ignition in most cases. This conflicts with the findings reported in (163), where a better behaviour of DF combustion in the late stages was observed. Regarding natural gas fuel injection duration, the injection end can be estimated from Figure 4-17, as it occurs roughly at the angle of the peak HRR value (observed from the analysis of a significant number of engines were injection duration was provided from the engine control system i.e., two stroke engine with common rail fuel injection system). Figure 4-17 indicates that, for high load, the injection duration is similar to that of diesel fuel. In addition to the differences in the progression rate of early stages, variations in diffusion-controlled and late-stage combustion can be observed. The observed differences in the HRR in DF mode under low and mid loads of 25 to 75%, Figure 4-17a–c, lead to the assumption that the combustion process in DF mode deviates further from the typical diesel mechanism when the ignition angle of pilot fuel is retarded, and the ratio of diesel/gas is high. It can be anticipated that these conditions could influence the premixed over the diffusion burn processes.

In Figure 4-18 the net HRR values estimated for “Engine 2” are presented. The HRR diagrams show significant difference between diesel and DF mode, with the early ignition of the diesel pilot easily identifiable for all loads, especially at 75%, Figure 4-18c. A brief intermediate stage can be observed in all loads with the combustion rate slightly increasing before the main combustion event, which is attributed to the difference in timing of liquid pilot fuel and gas fuel injection. The peak combustion rate is considerably higher during DF mode, with increased initial rate following the ignition of the injected natural gas. The premixed stage combustion is more intense for DF mode operation for all loads, as most of the fuel is burnt within the first 10^o to 15^o CA after ignition. Following that, the late-stage combustion is quite slow during DF mode compared to diesel only. This behaviour is attributed to a different strategy regarding the injection the diesel pilot and the main gas fuel. Overall, the specific combustion rate favours efficiency since combustion is fast and slightly after TDC. For “Engine 2” the diesel pilot is injected well before TDC compared to “Engine-1” and generally to modern engine standards. The ignition of the two fuels is staged with a clear time difference between diesel and NG. This difference is the result of slight staging of the diesel pilot injection and the

timing of NG. For this to be achieved, the liquid fuel injector was redesigned for the new generation engines, with adjustable nozzle injection bores able to accommodate both the low volume diesel pilot injection and the MCR fuel supply requirements of diesel mode, (165). In addition, a different profile was implemented for the pilot injection. Comparison between the two studied engines shows that peak HRR during DF is considerably enhanced for “Engine 2”, and that this is present for all loads, even MCR, which was the load with the lowest difference between diesel and DF mode for “Engine 1”. It is noted that the overall lower HRR values for “Engine 2” compared to “Engine 1” are due to its similar power output per cylinder but lower total fuel consumption and the practically no delay between diesel and NG ignition for “Engine 1”. The last is the result of the reduction of the difference between the two injection events, pilot and gaseous fuel.

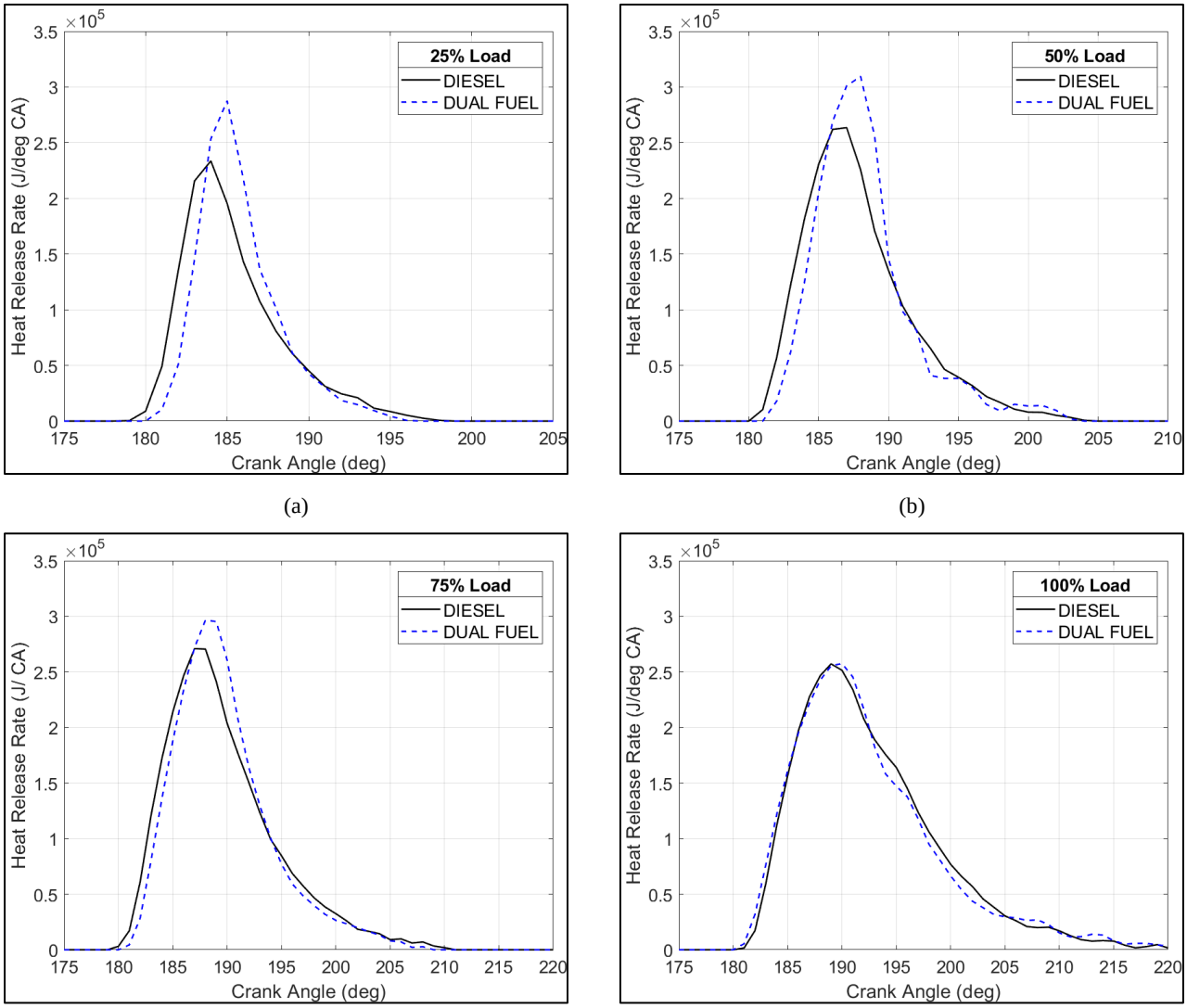

Figure 4-17 (a) Net mean heat release rate at 25% load; (b) Net mean heat release rate at 50% load; (c) Net mean heat release rate at 75% load; (d) Net mean heat release rate at 100% load, at diesel and DF modes; Engine 1.

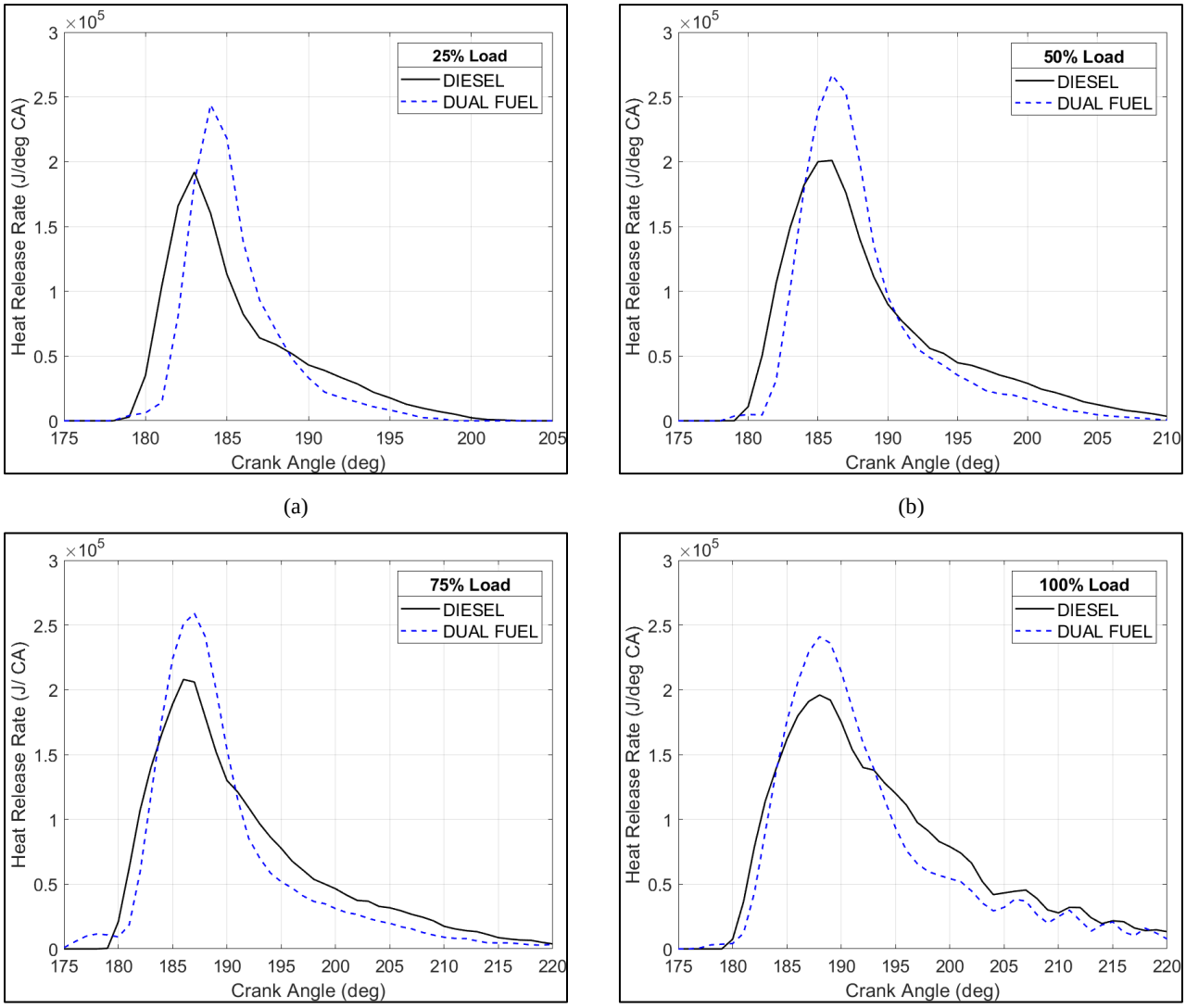

Figure 4-18 (a) Net mean heat release rate at 25% load; (b) Net mean heat release rate at 50% load; (c) Net mean heat release rate at 75% load; (d) Net mean heat release rate at 100% load, at diesel and DF modes; Engine 2.

The combustion duration for 50% and 95% of total diesel and natural gas fuel mass fraction burnt was calculated using the cumulative heat release, which is the integral of Figure 4-17 and Figure 4-18 diagrams' values. The results are provided in Figure 4-19 and Figure 4-20 for the two engines. In the case of "Engine 1" for 25% up to 75% load and for both 50% and 90% of total fuel mass fraction burnt, early combustion progresses at a notably higher rate in DF mode operation, indicated by the 6–8% shorter combustion duration. Due to the longer premixed combustion duration and comparable diffusion stage burn rate, the difference increases further for 95% fuel combustion duration. The shorter total combustion duration in DF mode was also reported in (147). Usually, a shorter combustion duration results in efficiency benefits, as thermal losses are also limited. In the present case, this is observed at 25% load. The SOI delay of the pilot diesel fuel in DF mode is possibly the major reason for the small efficiency loss of 1% for "Engine 1". The near maximum load premixed phase combustion rate is similar for both modes. The late combustion stage progresses at a lower rate in DF mode, which contrasts with the expectations based on (160) which is, however, based only on

simulation results of a marine four-stroke propulsion engine. This highlights the importance of experimental data use on actual scale engines of the two-stroke variant. The slower late combustion under full load affects combustion duration, which is equal to or slightly longer than that of the diesel mode, in contrast to the shorter duration observed under lower loads. This is found by examining both the 50% and 95% total fuel burnt. The difference in the total heat release between the two modes that can be observed in some cases is attributed to the slight load differences and variation in heat losses.

Relatively similar behaviour regarding total combustion duration is observed for “Engine 2” with shorter total combustion length for DF mode, except near the MCR load region. For the 50% fuel burnt time the opposite trend is found for “Engine 2” with shorter duration during diesel operation for all loads. This is mostly affected by the late NG ignition which is more pronounced at 75% load. The very high combustion rate of the NG during the premixed stage and its longer duration (after the main ignition event) makes up for this difference and total combustion duration is not negatively impacted. Slightly higher values compared to “Engine 1” are mainly due to the prolonged combustion of only the diesel pilot, while for “Engine 1” the ignition angle of gas was practically simultaneous to that of diesel (it is noted that engine speed was roughly the same between the two engines).

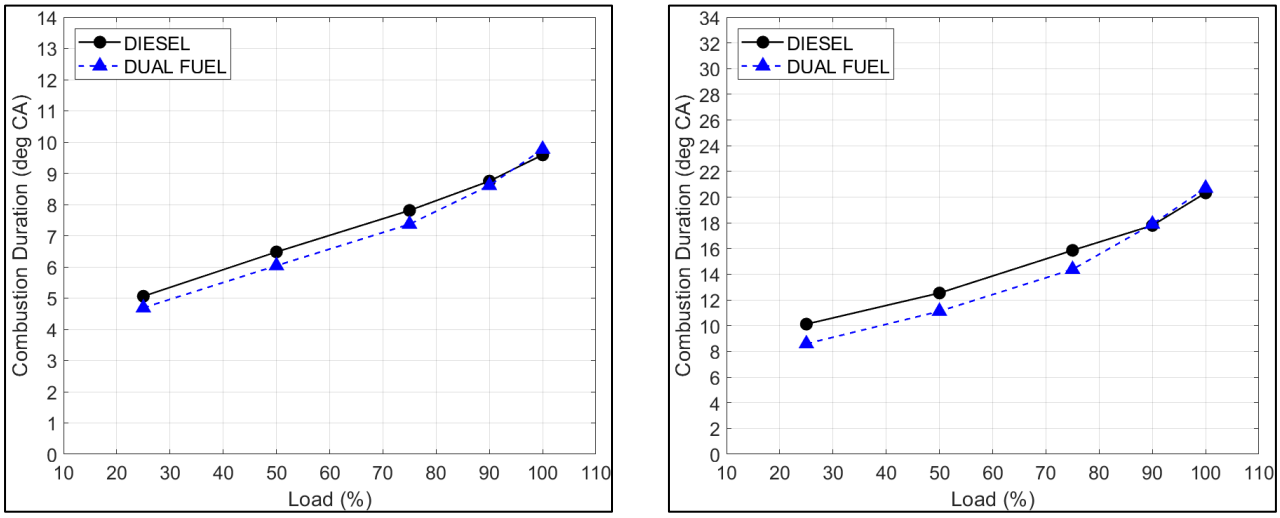

(a) (b)

Figure 4-19 (a) Combustion duration for 50% fuel mass fraction burnt, diesel and DF modes; (b) Combustion duration for 95% fuel mass fraction burnt, diesel and DF modes; Engine 1.

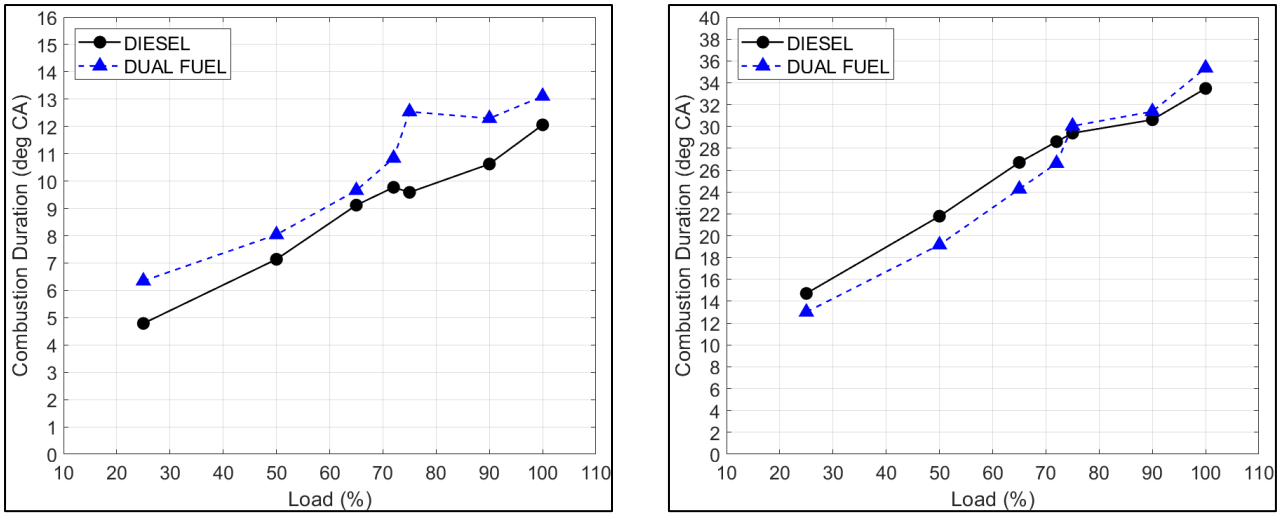

(a) (b)

Figure 4-20 (a) Combustion duration for 50% fuel mass fraction burnt, diesel and DF modes; (b) Combustion duration for 95% fuel mass fraction burnt, diesel and DF modes; Engine 2.

4.2.3 NO_x Emissions, Diesel & DF Mode

The high differences in the combustion process between diesel and DF mode, observed mainly for "Engine 2" equipped with the redesigned liquid fuel injection nozzles, could potentially affect NO_x emissions. The NO_x emissions of "Engine 1" are extensively reviewed in Chapter 6 for Tier-II and Tier-III mode as this engine is equipped with an EGR system ("Engine 2" is outfitted with an SCR system). In this brief section a short comparison is made between NO_x emissions at Tier-II operation in diesel and DF mode for the two engines to examine if any effect on emissions can be expected. As the principles of the Diesel cycle are retained in the high-pressure approach it is expected that emissions, especially for "Engine 1" that presented similar performance for DF and diesel only modes, should be at Tier-II NO_x emissions levels. Due to the exhaust gas mass flow not being the same between the two operating modes, specific NO_x emissions are used for the comparison instead of measured concentrations. The specific values, non-ISO corrected, are given in Figure 4-21a for "Engine 1" and Figure 4-21b for "Engine 2". As seen, emissions were affected by the transition to DF mode. The general trend appears to be similar for both engines with higher values at lower loads and lower values at high load. For "Engine 2" the transition point between lower and higher NO_x emissions takes place at a higher load. This is the result of its tuning which focuses on BSFC reduction. At low load, for both engines the combustion rate of fuel for the DF mode is more intense, especially for "Engine 2", resulting to higher NO_x emissions. Examination of the HRR diagrams provided, reveals that NO_x emissions for DF mode are decreased compared to diesel mode values when the diffusion combustion stage becomes shorter and less intense. This occurs at elevated load especially for "Engine 2". NO_x emissions are also affected from the pressure increase due to combustion and possibly by the mass ratio of pilot diesel to gaseous fuel that is known to have an impact on NO_x emissions, (166) and last by the lower flame temperature of methane that comprises a large portion of the injected NG especially at higher loads. NO_x emissions decrease compared to

diesel mode operation was also observed in (167), where similarly to the present case the high effect of pilot and main injection timing was significant.

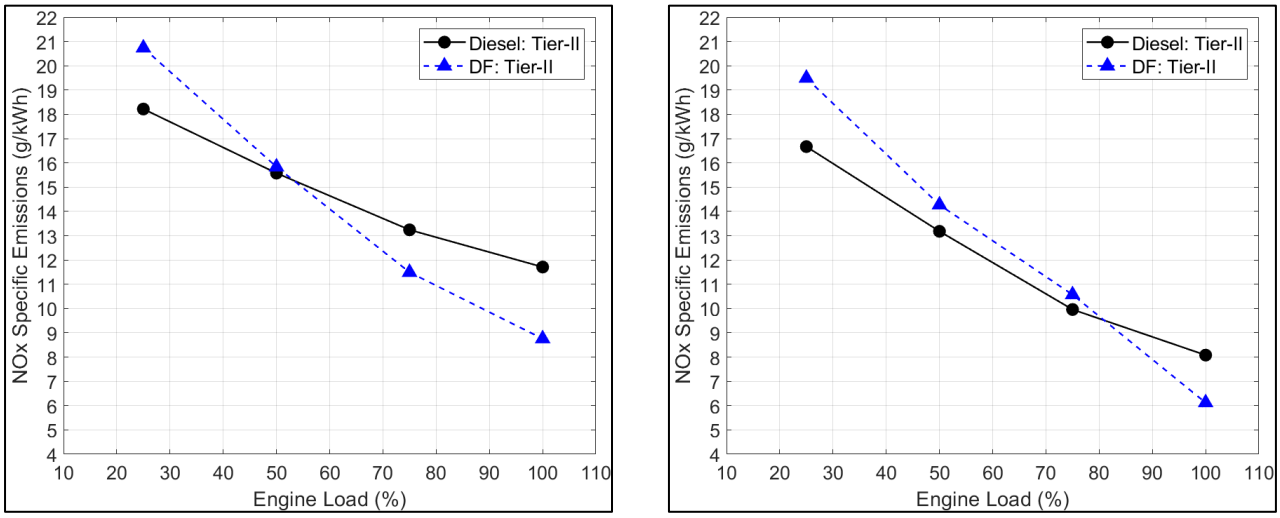

(a) (b)

Figure 4-21 Specific NO_x Emissions non-ISO corrected for Diesel and DF Tier-II mode; a) “Engine 1”, b) “Engine 2”.

4.3 Summary and Conclusions

In this chapter of the thesis, the performance of two 2-stroke marine diesel engines operating under the high-pressure natural gas injection principle was examined for DF and diesel modes. The two engines belonged in the same model category but were of different generations with the latest being the current one, recently introduced in the market. The two engines presented considerably different behaviour between them and in their tuning when switching to DF operation from diesel only mode.

For the older generation "Engine 1", the comparative evaluation revealed that, overall, limited differences existed between the two modes for the specific engine design. The engine settings regarding exhaust valve timing were found to be nearly identical for the opening angle, with differences observed only for the closing angle at low and high loads. For the diesel injection (pilot in the case of DF operating mode) and, consequently, ignition angle, differences up to 1° crank angle for low and mid loads, with retarded injection timing for the DF mode, were observed. This is an important finding, since multiple studies have shown that the injection angle has a major effect on pressure rise and on the overall evolution of the combustion process (144,163,168). The main performance data were found to be similar between diesel and DF mode for "Engine 1", and the only difference of note was observed in the pressure increase due to combustion influenced by the SOI angle and combustion intensity under DF mode due to the NG high LCV.

For the new generation "Engine 2", the switch to DF mode resulted in considerable performance changes. The peak pressure values for DF operation were increased well above the values of the diesel mode and also the values measured for "Engine 1" in either mode. The increase was partly attributed to the increased compression pressure as the result of earlier EVC angle. Settings were altered considerably with the only restrained difference found in EVO timings, which were quite similar for both modes. EVC angles were advanced and resulted to substantial increase of the cylinders' effective compression ratio. Diesel pilot (DF mode) and main (diesel mode) SOI angles were before TDC for all loads at both modes, with higher injection timing advance at DF mode.

The combustion process analysis revealed differences between diesel and DF mode mainly for low and medium loads for "Engine 1". The combustion rate was more intense in DF operation and presented a higher peak rate, similar to the findings of (156), (161) for which SOI timing under DF mode was also retarded. Increased combustion intensity was attributed to the higher LCV of injected natural gas and the better mixing of gas and air until the diesel pilot ignition. The same was observed for part of the diffusion-controlled combustion process, attributed to the fast ignition (144) of NG inside the combustion chamber. A prerequisite for the former was the ability of the NG fuel supply system to inject a high mass of gaseous fuel in the combustion chamber at a rate comparable to diesel operation. This was confirmed by the HRR diagrams, as the time from ignition to peak HRR, where injection is approximately considered to terminate, was similar or lower in the DF mode. Late-stage combustion also progressed slightly faster in the DF operation. The faster burn rate resulted in lower combustion duration under the DF mode for these loads for both 50% and 90% fuel mass fraction burnt. The aforementioned differences were not observed under high loads, with the HRR being

mostly identical. Based on these differences, it can be estimated that the combustion process in DF mode deviates from the typical diesel mechanism when the ignition angle of pilot fuel is retarded, and the ratio of diesel to natural gas is high, by affecting the intensity of premixed and diffusion burn processes and the ratio of fuel burn between them.

For “Engine 2” the HRR analysis revealed a significantly different combustion process during DF mode operation. The main similarity to the “Engine 1” findings was the increase in peak HRR. The increase in maximum combustion rate value, relative to the diesel mode. was considerably above that of the previous generation engine. The most significant finding of the “Engine 2” combustion analysis was staged combustion of the diesel pilot fuel and the main NG mass injected. Following a small energy release from the combustion of the pilot fuel and a brief intermediate stage, very rapid premixed combustion of the NG followed. The diffusion combustion stage was mostly below the one of diesel fuel with a markedly slower mid and late stage. The slow early diesel pilot and late-stage NG combustion did not negatively impact the total combustion duration that was similar to or shorter in most cases than for diesel mode operation. Unlike “Engine 1” the overall combustion process did not present notable differences between load, with the only observed variation being in the case of 75% load due to the high SOI advance of the pilot and rather retarded NG injection allowing for longer combustion of the diesel before NG ignition and subsequently very rapid NG burn. The improvements by the manufacturer regarding the injector nozzle design and pilot injection profile resulted in the decrease of the total diesel mass required for engine stable operation compared to the previous generation.

In the case of “Engine 1” BSFC of diesel mode was lower overall when expressed in terms of the total heat rate provided by the supplied fuel, signifying better overall thermal efficiency. The difference between the two modes was very low in the range of 1–2%. This is promising, considering the known positive effect of dual fuel operation on CO_2 emissions, (36). Regarding CO_2 emissions, the overall effect was a 22.6% improvement despite the efficiency reduction, as the carbon content of natural gas was 12% lower than diesel while also providing 16.3% higher energy content, which resulted in lower total fuel mass consumed.

For “Engine 2” the aforementioned differences and other refinements in the overall engine design resulted in fuel efficiency improvement over the previous generation for both modes. The most important change, however, was the degree of engine thermal efficiency improvement of DF mode over the diesel one. Except for an efficiency penalty at 25% and minor deficiency at 50% load, the total specific heat rate was lowered up to the engine MCR, with the maximum improvement close to 5% at 75% load. The actual consumption was also lower in terms of total fuel mass burnt in DF mode. In terms of GHG emissions the advances in the efficiency of both modes (diesel and DF) resulted in a similar reduction of carbon emissions with “Engine 1” namely 22.8% on average. Comparison between the two engines showed a gen-on-gen improvement of 6.9% regarding specific carbon emissions due to the improvement of both diesel pilot and gas fuel efficiency.

Overall, the analysis of the two engines showed that the use of a high-pressure system for natural gas injection allows operation and efficiency very close to that of a typical diesel cycle without the need for extensive setting changes that could be expected due to the dual fuel aspect, mainly regarding injection timing. The

major performance values can be maintained almost identical, excluding some limited differences in fuel efficiency, as in the case of the older “Engine 1” that was optimized for low–medium load operation at DF mode and its efficiency was lower but sufficiently close to that of the diesel mode for the other (higher) loads. The current generation “Engine 2” showed that with some component improvements allowing extended control capabilities and higher level of tuning variation, engines of this type can operate at efficiency significantly superior to that of the diesel mode, at least in a large part of their load range. For “Engine 2” the combustion process was found altered and more akin to what would be theoretically expected to be observed for a DF engine with pilot fuel ignition, such as staged combustion events and high pressure increase values. The overall evaluation and analysis reveal that modern marine two-stroke high-pressure DF engine performance can be very close to, or above the standards of diesel-only operation, while providing concrete environmental benefits in terms of CO_2 emissions. Considering the quite substantial improvements between the two consecutive generations studied, these benefits might further increase in the future. This makes natural gas or other low-carbon gaseous dual fuel engines a very attractive option until zero-carbon solutions become possible for large marine vessels.

Chapter 5 Marine Type Biofuels-Impact on Performance and Emissions

Use of biofuels based on biodiesel from non-edible biomass is lately gaining traction in the marine sector. The aim is to use blends of biodiesel and VLSFO as a drop-in fuel that can improve the GHG footprint of existing vessels without resorting to extensive retrofit projects that may not be financially viable for operators, especially in the case of older vessels, (169,170). The subject of biofuel use in IC diesel engines has been extensively studied in the automotive sector and currently automotive use diesel comprises of biodiesel at a 5% ratio in the United States, (171) and is also contained at 7% in fuels distributed in Europe (172). Biofuels are separated into four generations with only the first two having entered commercial use (173–175). The first-generation biofuels are the product of edible crops such as grains, sugar cane and vegetable oils, (176). The requirement for land use that would normally be used for food production has caused concerns regarding food security, (177). In addition, the potential of this biofuel type for GHG emissions reduction is rather limited, (176,178). The 2nd generation biofuels are the product of non-edible biomass such as wastes of edible plants or municipal wastes such as cooking oil and disposed food, (179). Especially the case of used cooking oils is quite promising as currently their primary disposal path is the sewage system, (180). This makes the cost of raw materials used very low, but the production process is costly making 2nd generation biodiesel pricier than traditional fuels.

The third and fourth generation biofuels are still at the research and development stage and are both algae based, (175,181,182). The 3rd generation biofuels based on microalgae are a promising technology as they offer distinctive advantages compared to the two previous generations. The land use requirements are considerably lower and the harvesting cycle of grown biomass is also shorter, (183–185). A further benefit is found in the quality of the produced biomass, which is closer to the final product, biodiesel or bioethanol, compared to previous generations. There are still challenges to be overcome until the commercial use of this production method, with the main one being cost, as 3rd generation biofuels are currently not financially viable. The 4th generation biofuels are an advanced approach to the 3rd generation aiming to utilize genetically modified algal organisms to enhance biomass production capabilities and improve cultivation efficiency, (181–183). Several concerns exist currently regarding costs and also environmental hazards that could result from releasing genetically modified microorganisms to the environment, making this technology not viable as a mid-term solution.

Thus, at present, marine use biodiesel is mostly produced via the 2nd generation approach, with most variants being fatty acid methyl ester (FAME) based and sourced from used oil. The production process of biodiesel from used cooking oils is transesterification, (186,187). This process is based on the reaction of the triglycerides in the waste oils with low-carbon alcohols in the presence of a catalyst to produce esters and glycerol. A benefit of using this process is that the boiling point of the alcohols used, mostly methanol or ethanol, is low and the reaction does not require high temperature to proceed. The conversion of the used oils

to alkyl-esters decreases the molecular weight, viscosity, pour point and flash point values of the cooking oils, while increasing the volatility value. This allows for the produced biodiesel to be used as is, or in blends with normal diesel without the need for engine modifications. Biodiesel production comprises of four stages, pretreatment, two step esterification and refining. The pretreatment stage comprises of gravity settling of the various solid impurities that are removed with centrifugation along with water and water-soluble compounds. The first step of esterification involves the use of acids to remove free fatty acids as they can lead to soap formation if they remain in the next production stages. A typical method for their removal is use of an acid catalyst such as sulfuric acid in the process of excess methanol in a continuous plug-flow reactor. The second stage is transesterification which involves the mixing of the oil and alcohol or methanol in the presence of homogeneous or heterogeneous catalyst. The reaction is alkaline-, acidic-, or enzymatic-catalyzed with fatty acid methyl esters as the main product and also glycerol. For large scale applications homogeneous alkali catalysts are used due to cost effectiveness compared to other options. The most common catalyst used for the reaction of oil and alcohol is potassium hydroxide or in recent years potassium methoxide which allows for increased biodiesel production. The final stage of the biodiesel production process is refining to achieve purification according to the standards allowing in-engine use. In this step, water, CH_3OH and any remaining catalyst amounts from the previous processes are removed along with heavy composites and possible traces of sulphur.

The environmental benefit of biodiesel towards GHG emissions relies mostly on its well-to-wake emissions, (188). For a biofuel to result to actual carbon emissions reduction a net benefit must be verified. Newer research has shown that 2nd generation biofuels have higher benefit on carbon emissions reduction than 1st generation ones, with the exception of sugarcane based fuels, (177,189–191). It must be stated, however, that the degree of expected environmental benefit differs considerably between studies, mainly due to the various assumptions made and different conditions examined, (187,192). Studies have shown almost 90% lower GHG emissions for vegetable oil based biodiesel compared to typical low-sulfur diesel, (173,192–194). In the marine industry the currently available biofuels are blends of biodiesel, mostly sourced by waste oil, and VLSFO. The most common blends contain 20% (B20) or 30% (B30) FAME with 50% (B50) variants also under evaluation. Despite the moderate amount of biodiesel used, studies estimate that high GHG emissions reduction can be achieved for 30% FAME blends, in the range of 25%, (176). This percentage was confirmed by the analysis provided by biofuel suppliers for the variants studied in this thesis. Thus, for a vessel operator, use of B30 allows to reduce the carbon intensity index of existing vessels considerably without resorting to any type of modification to equipment or sailing capabilities. The use of biodiesel in the form of blends with typical fuels provides multiple benefits. The most immediate is cost, which is significantly reduced compared to pure 2nd generation biodiesel that is considerably more expensive than VLSFO due to the energy and infrastructure requirements of the transesterification process, (195). Recent studies that take into account current fuel prices and updated trends, estimate that FAME based fuels will remain more expensive than HFO and VLSFO but become competitive in the coming years with competitiveness further increasing if penalties to conventional fuel use become stricter, (20,196–198). Blending with conventional fuel also contributes to

increasing availability of biofuel, which is important in the marine industry. Data from 2019 shows that international shipping activities consume about 300 Mt of fuel, almost in total diesel residuals or distillates, (1). With the production capacity of biodiesel being limited to 47429 ML per year (58) in 2022 according to the International energy Agency (IEA), (6,41), use of blends is the only viable approach. Another major issue that forces the use of blended biodiesel is the impact of FAME fuel products on an IC engine performance and emissions. Biodiesel differs from fossil fuels in physical and chemical properties, (199,200). Density, viscosity, bulk modulus, energy content, cetane index are some of the primary values that are changed considerably for biodiesel and can affect the engine and its fuel supply system, (201). Density and viscosity values can have a negative effect on the operation of fuel pumps and injectors, (202). In addition, bulk modulus affects performance of the fuel supply circuit and can alter dynamic fuel injection timing by changing the speed of pressure buildup in the piping between the pumps and injectors, (201). The difference in cetane index value, which is further increased for FAME compared to other biofuel types, leads to reduced ignition delay, (203). The ignition point is a major parameter for engine operation as it affects the rate and total value of pressure increase in-cylinder, and combustion efficiency, hence fuel consumption and emissions. The lower calorific content of biodiesel results in increased consumption requirements to achieve the same power output from the engine, (204). Further potential issues regarding use in engines can result by the elevated oxygen content of biodiesel that alter properties such as bulk modulus and NO_x emissions formation.
The main aspects currently under investigation for biofuel use in marine engines are the effect on fuel consumption, storage and supply system and most importantly on NO_x emissions.
Due to the low data available for marine engines and mainly large low-speed 2-stroke ones, a series of tests were conducted between 2020 and 2022 to investigate emissions and performance with various biofuel blends, mainly of 30% FAME content. The main reason for the testing requirement is that the end effect of biodiesel use on NO_x emissions of different engines cannot be predicted as it depends on multiple parameters. The main mechanism enhancing NO_x emissions has been proven, by various researchers, to be increased oxygen content, (205,206). Oxygen contained in a fuel enhances its concentration in the most crucial position in the cylinder, the flame region. Combustion is enhanced as high oxygen availability increases the rate of reactions, (207). This results in higher peak localized temperature that increases exponentially NO_x formation according to the Zeldovich mechanism, (99). In addition, the increased presence of O_2 itself results in more Nitrogen reacting with the oxidizing element due to its abundance. Another common finding of studies is that the increased O_2 concentration in the used fuel enhances NO_x formation to a higher degree than an oxygen rich cylinder charge, (208). This again highlights that NO_x formation is heavily influenced by localized in-cylinder conditions. Other factors affecting NO_x formation are LCV and ignition delay, the latter dependent on cetane index. Review of multiple studies shows that the lower ignition delay can have variable effect on NO_x formation, (209,210). Earlier ignition can result in higher peak cylinder pressure and temperature. In addition, for cases of ignition prior to TDC, maximum combustion and consequently temperature may occur before cylinder expansion which can mitigate the mean temperature increase. On the other hand, very low ignition delay inhibits the fuel – air mixing. This results in lower rate and intensity of premixed combustion and lower

peak pressure and temperature in the cylinder. A further change in NO_x emissions may depend on the LCV of the biofuel, that is typically lower than conventional diesel and low quality fuel, such as HFO. Blending with conventional fuel can mitigate the LCV reduction to a degree. A lower LCV value can lead to lower peak combustion pressure and decreased NO_x formation but at the cost of total fuel efficiency. Research specifically aimed at marine engines is currently at the initial stage with a low volume of published works on 2-stroke engines, (194). Furthermore, very limited information is available for the actual impact of biofuels on engine performance, cylinder pressure and the combustion rate. Especially for 2-stroke engines due to difficulties in testing very limited information exists.

For 4-stroke generators more published studies are available, however only in small part of them the current generation of marine use biofuels is evaluated as most blends tested use biofuel and distilled high quality diesel/MGO, such as (211). Also, in these cases very limited information exists for the actual effect of biofuels on engine performance and cylinder pressure. As of mid-2023 studies for 2-stroke marine propulsion engines are limited to the part of the present thesis' content published separately, one peer-reviewed study using a B50 type biofuel examining effect only on emissions, (194) and the published results of a marine classification society in collaboration with vessel operators (53). The latest development, June 2022, on the issue of biofuel use is the exception granted to vessel operators for use of fuel blends containing up to 30%v/v biofuel, (212). Despite this, operators still have concerns for the actual effect of biofuel on engine performance which motivated the investigation conducted under the present thesis. Since the biofuels were classified as RM-grade, as for conventional fuels, up to 10% NO_x emissions over the applicable limit can be allowed for results of on-board measurements.

5.1 Literature Review of Biofuel Use on Marine Engines

The subject of biodiesel's effect on engine performance has been extensively studied for fuels of various sources and in blends of different percentages for engines used in land transport. In the field of marine engines, information is limited compared to other sectors, especially in the case of large two-stroke propulsion engines (194) as most peer-reviewed works refer to medium-speed four-stroke units mainly used for auxiliary power generation. In this section, findings of relative research are presented mainly for marine engines and are complemented with studies conducted on heavy-duty CI (compression ignition) engines used for land transport and power generation. The findings focus on the mechanisms of NOx formation, the corresponding biofuel effect, on techniques used to control NOx emissions, and new generations of biofuel. As stated above information for the impact on performance, cylinder pressure and combustion is very limited.

One of the few currently available sources regarding two-stroke engines is the work of (194). It reports on an experimental investigation about the NOx emissions of a large two-stroke marine engine using B50, 50% FAME (Fatty Acid Methyl Ester) content, a second-generation biofuel, against typical MGO. NOx emissions were decreased compared to the typical marine diesel. The average fuel consumption was found to be lower

for B50. This contrasts with expectations based on biofuels tests on other diesel engines that all showed increase regardless of type, as is summarized below. For four-stroke heavy-duty engines including marine variants, a significant volume of research work is available. In (211) various percentages of biodiesel sourced from waste cooking oil were tested, and fuel consumption was found to increase with biofuel percentage mostly due to its low energy content. The same was observed in multiple other studies (213–215) that cover various engine types and biofuels of a wide source range. The main factor affecting FC was the lower calorific value of pure and blended biofuels. In (211,213,215–218), the effect of biodiesel on ignition and combustion was investigated. In most cases, the difference in the combustion process was clear even for tests with only 10% biodiesel content. The main findings were lower ignition delay, also reported in (203), which is expected due to higher cetane index, and faster combustion but with a lower peak heat release value, which is to be expected due to the lower ignition delay and heating value of the biofuel blend. In some outlier cases, however, the initial burn rate was found to be slower when the biofuel content in the tested blends increased (217). The main factors affecting combustion according to these researchers were LCV (lower calorific value), ignition characteristics, and O2 content of each fuel blend.

In all studies, NOx emissions were affected by biofuel even when examining blends of low percentage; both increase (190,191) and decrease (203,221) were observed. A common conclusion of experimental and computational investigations (215,217,222) that is also mentioned in the extensive review of (223) is that the effect of biofuel use on NOx emissions cannot be predetermined due to a number of mechanisms influencing formation. This is also the conclusion of (205), in which the decisive factor is considered to be how close to stoichiometric the air–gas mixture is at ignition and in the standing premixed autoignition zone near the flame lift-off length. The combination of multiple factors affecting the final NOx emissions is also mentioned in the review conducted by (224,225), where on average, NOx emission increase was confirmed, despite the variation between study findings. As mentioned in Section 1, the increased presence of O_2 in the flame region due to its relatively high concentration in biofuels has a greater effect than elevated O_2 concentration in the cylinder charge (208,226). This is considered one of the main factors of NO_x emissions increase when using biofuels (219,227). In (211), NOx emissions were found to increase with biofuel percentage despite the lower peak combustion rate, which is expected to lead to NO_x formation reduction. The increase, despite the unfavorable conditions for higher emissions, was attributed to the fuel elevated O_2 content. In (224) both pure biodiesel and blends with normal diesel were tested with very high NO_x emission increase for the pure biofuel and marginal reduction for the blended fuel. Other factors can affect NO_x formation such as lower heating value, cetane number, and physical properties, mainly bulk modulus, and viscosity. Studies using multiple biofuel blend percentages and comparing them to typical diesel fuel revealed a correlation between O_2 content, cetane number (CN), and NO_x emissions (219,222). Biofuels with a higher CN than typical diesel presented similar NOx emissions to diesel fuel tests, while for cases with a similar CN number and, consequently, ignition delay, emissions during biofuel use were increased (222). Further effects can stem from physical properties that can affect the injection system performance, pump, and injector, as the increased bulk modulus and viscosity of biofuels can lead to advanced actual injection event when the same static timing is

used. This can result in increased NO_x emissions (201). In the case of engines supplied with preheated fuel, which is the case for marine engines due to their design for crude oil use, these effects are mostly eliminated (201). The only concern when applying such measures is the possibility of biofuels' oxidization, which can alter the fuels' physical and chemical properties (227) and lead to different fuel treatment requirements, such as heating to a higher temperature. In the extensive study of (219), biofuel blends from various sources were compared. It was found that for fuels sourced by waste oil, LCV values were on par with diesel. This is in agreement with (197). Additionally, an increased tendency for higher NO_x formation due to elevated oxygen content was reported. These fuels' CN number was increased compared to typical diesel but lower than the other biodiesel variants which further contribute to higher NO_x emissions compared to the other biodiesel types tested in the study. Utilizing such findings, combustion analysis, and NO_x formation models, researchers propose optimal strategies for minimizing biofuel effect. In (224), 20% biodiesel blends were found optimal and EGR (exhaust gas recirculation) use was tested to control tailpipe emissions with good results, as is also reported in the experimental work of (228). Another emission control method currently studied by researchers is hydrogenation of biofuels, which is found to result in lower NOx formation (228,229). Recently published works examine the use of new-generation algae-based biofuel blends in CI engines. Since this is a state-of-the-art biofuel, these tests are mostly constrained in automotive-sector engines, such as in (230), with promising results regarding NOx and soot formation. De-spite the promising results, at its current state, the technology is facing scaling issues regarding production considering both scaling capabilities and regulatory concerns (183), especially in the case of the fourth-generation biodiesel produced by genetically modified algae strains (181). In addition, production costs make commercial use of both third- and fourth-generation biodiesel prohibitive compared to the previous two bio-diesel generations (175) that are sourced from feedstock biomass. Thus, the use of such fuels in the marine industry is not expected in the foreseeable future.
In the past two years, experimental campaigns were conducted by shipowners in cooperation with institutional bodies (53) to study biodiesel's effect on marine engine NOx emissions. The consensus was that a tendency for increased but not excessive NOx emissions exists, confirming prior expectations (198) based on other applications. The level of emission increase, however, was heavily dependent on engine type again for this study. Performance in these tests was usually not evaluated beyond fuel consumption, which was found to increase with biofuel use. Biofuels with up to 30% FAME content have been recently granted permission for use in marine vessels (212), making B30 the most common variant commercially available.

5.2 On-Board Measurement Procedure

The evaluation of the biofuels blends newly introduced in the marine industry required a series of on-board measurements. Multiple engine types were tested, both 2-stroke propulsion and 4-stroke auxiliary ones, the typical configuration for most commercial cargo vessels. The 2-stroke engines tested were of the newer generation featuring electronic control for their operation. As verified by the official IMO guidelines for NO_x

emissions evaluation, results of on-board measurements are expected to differ from the ones conducted during certification for the NO_x file registration and use approval, with the difference expected to be higher when using RM-grade heavy fuel variants. For this reason, the measurement campaigns conducted and included in this thesis primarily aimed to provide a comparative evaluation of emissions and performance with conventional fuels and biofuel blends. For all tests the blends used were of roughly 30% v/v FAME content, produced by recycled waste oils sourced within the EU. The conventional fuels used for comparative analysis were MGO, HFO and VLSFO. The emissions measurement process was performed according to the guidelines of the direct measurement and monitoring method of the 2008 NTC, (27), providing results that met official specifications. The testing process was conducted for three or two separate loads in each case. The selection of load points and number was approved by each vessel's classification society and was according to the E3 cycle for all main engines as they operated on the propeller law and the D2 cycle for the steady speed auxiliary generators. The weighting factors, provided in chapter 2 Table 2-1 and Table 2-2 for emissions of each load were modified accordingly to the number of tested loads in each case. The equipment used for emissions measurements was the Testo 350 Maritime V1 and V2 flue gas analyzer, (231). Both instruments have acquired type approval by MARPOL for use in marine engines on-board measurements of NO_x and other emissions and have nearly identical specifications, provided in Table 5-1. The sampling point was selected according to the NTC requirements, at least ten pipe diameters after engine outlet, turbine or exhaust after treatment device and at least 0.5m or three pipe diameters upstream of the funnel. In addition, gas sampling was performed prior to any secondary devices such as boilers that could affect measurement accuracy by lowering exhaust gas temperature. The measurement procedure was conducted for a series of ten-minute intervals in each case at a 1Hz sampling rate. The final average value was used for all calculations. The measurement of the other data required was mostly performed using the on-board instrumentation of each vessel. Since equipment specifications were not identical for all tested vessels a sample is provided in Table 5-1; in general, the values contained are representative for all vessels. In the process of the measurement procedure arrangement, the respective on-board instruments were calibrated and tested to the degree feasible for on-board instrumentation. Performance measurements included detailed cylinder pressure and temperature data for the cylinders, turbocharger and air-cooler operation. The main source of information for cylinder performance was cylinder pressure trace measurements conducted in parallel to the emission measurement procedure. The pressure traces were acquired by a piezoelectric pressure sensor outfitted on each cylinder's indicator cock. The instrument's specifications are provided in Table 5-2 along with the other measurement devices used. For each load tested, a minimum of 30-minute steady sailing was conducted. A schematic of the engine room installation to conduct the measurement procedure is provided in Figure 5-1. Vessel speed and course were kept steady; the allowed deviation in engine speed was kept between ±5% of the specified load, otherwise the test run was repeated as is required by the "Direct measuring and monitoring method" of the NTC. Logging of all aforementioned values was performed in regular intervals during each run with continuous monitoring of the main engine power output. Fuel consumption from the installed flowmeters (usually of the coriolis type) was logged for a 30 minute period to estimate the hourly consumption value.

Power output and fuel consumption were also estimated using the cylinder pressure traces, following analysis according to a specialized and proven methodology. For auxiliary generators the measurement process was more versatile as maintaining constant power was simpler by splitting auxiliary power generation between the three or four installed generators of each vessel and having the tested one maintain steady electrical power output. The main challenge encountered for the auxiliary generator tests was the fuel supply line in certain vessels that did not allow fuel consumption measurements per unit. In these cases, the values estimated by the cylinder pressure traces analysis was used. The NO_x emissions limits and the values registered in the official engine certification documentation are specific values in g/kWh. The flue gas analyzers measure in all cases concentration on a volume basis for all species in the exhaust gas. Calculation of mass flow for NO and NO_2 requires the estimation of total exhaust mass flow, that cannot be measured directly with the required accuracy. The proposed approach by the regulations is the carbon balance method described in the next paragraph. The calculations involved require CO_2 concentration in the exhaust gas, fuel oil consumption and carbon content of the used fuel. Each value must be measured with high accuracy, as any error is directly transferred to the NO_x emissions calculation. The same applies to the value of engine power when calculating the specific emissions value. The process of calculations is described in the following section.

A summary of the specifications of the used engines and fuels is provided in Table 5-3 through Table 5-5.

Table 5-1 Flue gas analyser Specifications

Instrument	Measured Parameter	Range	Accuracy
	CO_2	0–25 %vol	±0.3%vol
	O_2	0–25 %vol	±0.3% vol
Testo 350 Maritime	NO_x	<100–1999 ppm	±5%
	CO	0–10,000 ppm	±5%
	SO_2	0–5000 ppm	±5%
	Ambient pressure, absolute	600–1150 hPa	±10 hPa
Humidity Meter	Ambient Humidity	0–100 %RH	±2%

Table 5-2 Measuring Instrument Specifications

Instrument	Measured Parameter	Range	Accuracy
Torquemeter	Torque		<0.5%
	Speed	0–250 rpm	0.1 rpm
Power Meter	Electrical Power		0.1 kW
Coriolis Mass Flowmeter	Fuel Consumption	0–10,000 kg/h	0.30%
Volumetric Flowmeter	Fuel Consumption	0–2500 L/min	1.50%
Cylinder Pressure Sensor	Cylinder Pressure	0–250 Bar	0.50%
Scavenge Pressure Sensor	Scavenging air Pressure	0–10 Bar	0.10%
Scavenge Temperature Sensor	Scavenging air Temperature	−10–80 °C	0.2 °C
Exhaust Temperature Sensor	Exhaust Gas Temperature	−10–600 °C	0.5 °C

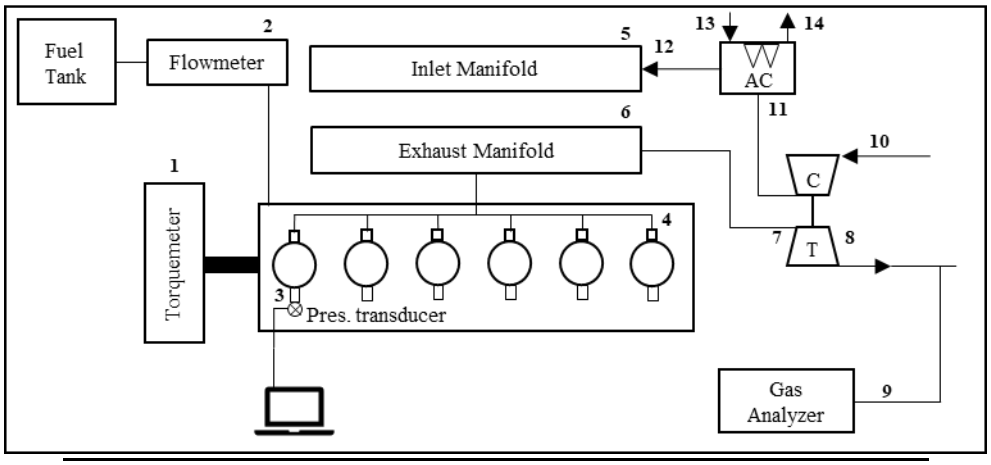

1: Engine Power	8: Turbine Outlet Temperature
2: Fuel Consumption	9: Exhaust Gas Composition
3: Cylinder Pressure	10: Compressor Air Inlet Temperature
4: Cylinder Exhaust Temperature	11: Air Temperature Before Cooler
5: Scavenge Air Pressure	12: Air Temperature After Cooler
6: Exhaust Pressure	13: Air Cooler Water Inlet Temperature
7: Turbine Inlet Temperature	14: Air Cooler Water Outlet Temperature

Figure 5-1 Measurement Setup Schematic View

Table 5-3 Tested 2-stroke engines particulars

Engine No.	**1**	**2**	**3**	**4**	**5**
Cylinder No.	6	6	6	6	6
Rated Speed (rpm)	75	77	85.5	89	89
Rated Power (kW)	15,748	10,215	16,780	9660	9660
Bore (mm)	700	600	700	600	600
Stroke (mm)	3256	2790	2800	2400	2400
Electronic Control	Yes	Yes	Yes	Yes	Yes
Fuels Tested	B30, HFO, MGO	B30, VLSFO, MGO	B30, VLSFO	B30, VLSFO	B30

Table 5-4 Tested 4-stroke engines particulars

Engine No.	**1**	**2**	**3**	**4**	**5**
Cylinder No.	6	6	6	6	6
Rated Speed (rpm)	900	900	900	900	900
Rated Power (kW)	970	970	1710	610	610
Bore (mm)	220	220	210	185	185
Stroke (mm)	320	320	320	280	280
Fuels Tested	B30, HFO, MGO	B30, HFO, MGO	B30, VLSFO	B30	B30
Units Tested (#)	1	1, 3	2, 3	1	1

Table 5-5 Tested fuels particulars

Vessel No.	**1**			**2**			**3**		**4**	**5**	
Fuel Type	B30	HFO	MGO	B30	VLSFO	MGO	B30	VLSFO	B30	VLSFO	B30
LCV (kcal/kg)	9575.23	9548.95	10,172.49	9563.3	9864.3	10,122.3	9608.27	9790.24	9981.37	9904.92	9981.37
Density @ 15 °C (kg/m^3)	930	989.7	863.1	930.2	970	880.2	929.5	979.6	939.6	956.1	934.9
Viscosity @ 50 °C (cSt)	38.66	357.8	3.591	38.37	154.7	3.812	37.7	37.7	6.7	194.8	44.7
Sulfur (% m/m)	0.35	3.23	0.078	36	0.45	0.069	0.36	0.47	0.34	0.47	0.48
CCAI	820	851	-	821	841	-	818	870	867	824	823
Cetane No.	-	-	47	-	-	41	-	-	-	-	-
Carbon (%m/m)	83.7	84.3	87.6	84.4	86.9	87.4	81.9	86.9	82.1	85.8	80.5
Hydrogen (%m/m)	11.8	10.3	12.1	11.9	11.1	12.6	12.2	11.1	10.6	12.1	10.8
Nitrogen (%m/m)	0.48	0.41	<0.10	0.2	0.4	0.11	0.5	0.4	0.2	0.45	0.2
Oxygen (%m/m)	3.67	1.76	0.22	3.22	<0.2	<0.2	4.69	0.2	1.6	<0.2	3.1
FAME (%V/V)	29.7	<0.10	0.2	28.31	<0.1	<0.1	34.15	<0.10	25	<0.10	28.54

5.2.1 Exhaust gas mass flow calculations

Following review of the measured and estimated data, the exhaust mass flow rate q_{mew}, on a wet basis, was calculated following the NTC official guidelines for marine engines, (26,27):

$$q_{mew} = q_{mf} \cdot \left(\left(\frac{\frac{1.4 \cdot (w_{BET} \cdot w_{BET})}{\left(\frac{1.4 + w_{BET}}{f_c} + (w_{ALF} \cdot 0.08936) - 1\right) \cdot \frac{1}{1.293} + f_{fd}}}{f_c \cdot f_c} + (w_{ALF} \cdot 0.08936) - 1 \right) \cdot \left(1 + \frac{H_a}{1000}\right) + 1 \right) \quad (5.1)$$

With q_{mf} the fuel mass flow rate, H_a the absolute humidity measured at the compressor intake, w_{ALF}, w_{BET} the H and C mass percentage content of fuel, f_{fd} a fuel specific constant calculated from its elemental composition and f_c the fuel carbon factor.

The fuel specific constant f_{fd} is calculated according to equation:

$$f_{fd} = -0.055593 \cdot w_{ALF} + 0.008002 \cdot w_{DEL} + 0.0070046 \cdot w_{EPS} \quad (5.2)$$

with w_{EPS} the oxygen content of the fuel.

The fuel carbon factor f_c was calculated according to equation:

$$f_c = (c_{CO2d} - c_{CO2ad}) \cdot 0.5441 + \frac{c_{COd}}{18522} + \frac{c_{HCw}}{17355} \quad (5.3)$$

based on dry CO_2 concentration in the exhaust gas c_{CO2d}, the ambient air c_{CO2ad} and the CO and HC concentration in the exhaust gas c_{cod}, c_{HCw}. The last was neglected due to the extremely low concentration.

Following the above the NO_x mass flow rate q_{mNOx} is calculated as:

$$q_{mNOx} = u_{NOx} \cdot c_{NOx} \cdot q_{mew} \cdot k_{hd} \quad (5.4)$$

with u_{NOx} the density ratio between NO_x and exhaust gas, c_{NOx} the measured NO_x concentration and k_{hd} the NO_x humidity correction factor, according to the NTC guidelines. The k_{hd} correction factor is calculated using the following equation:

$$k_{hd} = \frac{1}{1 - 0.012 \cdot (H_a - 10.71) - 0.00275 \cdot (T_a - 298) + 0.00285 \cdot (T_{SC} - T_{SCRef})} \quad (5.5)$$

which applies to engines equipped with an intermediate aircooler. In eq. 5.5 T_{SC} is the scavenge air temperature and T_{SCRef} the reference scavenge air temperature that corresponds to seawater temperature of 25ºC and is specified by the engine manufacturer in the official engine NO_x file.

Following the calculation of the mass flow rate and the required correction factors the specific emissions are calculated as the ratio of NO_x mass flow to engine power. For all cases examined, the exhaust mass flow calculation of eq. 4.1 was also performed using O_2 mass balance to ensure that both CO_2 and O_2 measurement device sensors were working properly during the measurements. Additionally, a dedicated version engine model was used to estimate expected exhaust gas flow rate values and was utilized on the spot as a

verification that external air entrainment in the measurement line during measurement did not occur, as this would affect the recorded NO_x concentration.

5.2.1.1 Cylinder pressure traces analysis methodology

Extensive degree of analysis of measured cylinder pressure traces was conducted for all applications studied in this thesis. For all topics investigated the pressure traces were used to estimate engine effective brake power, fuel consumption and the fuel burn rate by conducting combustion analysis. The cylinder pressure traces, as measured, were used in tandem with the fuel burn rate results to derive engine settings, specifically exhaust valve opening and closing angles and fuel ignition angle. The calculated ignition angle was used to estimate the dynamic fuel injection timing with the use of experimentally derived correlations that provide fuel ignition delay. The analysis was similar to the one described in section 4.1.2.

5.3 Biofuel Effect on Engine Performance and the Combustion Process, 2-Stroke Propulsion Engines

In this section, the effect of biofuel on engine performance is presented by comparison of the major engine performance metrics during operation with B30 biodiesel blend and conventional fuels, including the results of the official engine certification tests. For 2-stroke main propulsion engines a total of five units was tested. Some characteristic results are separately provided for MGO, HFO and VLSFO use, and a statistical summary is included, presenting the overall performance differentiation between the fuels used. Emphasis is placed in fuel consumption following ISO correction to examine the effect of individual fuel properties on combustion, hence engine efficiency. Performance is further evaluated using measured cylinder pressure traces between the tests conducted using B30 and conventional distilled and crude oils as well as the reference data. The last and most important part of performance analysis is evaluation of fuel combustion rate and the characteristics of combustion in the cylinders. For all the above, the mean cylinder values are used. Prior to the use of average values, performance uniformity between all cylinders was confirmed for each engine examined. At the end of section 5.4 the tabulated summary of all the results is provided for the tested 2-stroke engine for performance and emissions in Table 5-6.

5.3.1 2-Stroke Engine Performance during B30, HFO, VLSFO & MGO Operation

The first parameter evaluated was brake specific fuel consumption before and after ISO correction. Both values are important in this aspect as non-corrected BSFC values are used to assess the biofuel's impact on operational costs of the engine, while the ISO corrected values reveal how the different physical and chemical properties affect combustion efficiency. In Figure 5-2a and Figure 5-2b BSFC results from tests conducted with MGO, HFO and B30 from the first engine "Engine 1" tested are provided as measured, and after ISO

correction. For the second engine “Engine 2” presented, tests were conducted with B30, MGO and VLSFO; only the ISO corrected results are given in Figure 5-3. Due to vessel schedule constraints and logistical challenges of storing four different fuels in the vessels’ storage tanks a single test with all the above fuels on the same vessels was not possible. For both engines consumption values during MGO operation were similar to the reference data, as MGO is the fuel typically used during a certification procedure. Due to the high similarity of MGO consumption values for measured and reference operation, the assumption is made that both engines were at very good condition at the time of the on-board tests. The ISO corrected BSFC values for B30, HFO and VLSFO were all above MGO tests and reference values, as is normally expected due to overall lower fuel quality and the obvious LCV difference. The ISO corrected BSFC increase during crude oil operation is about 2.5% compared to MGO. HFO and B30 BSFC values prior to ISO correction are identical. For ISO corrected values, the difference between B30 and HFO/VLSFO is marginal, roughly 1% higher for B30 in some cases.

In Figure 5-4 a statistical summary of all results, 5 engines in total, is included. The medial and mean values of ISO-corrected BSFC differences were mostly similar for all engines. On average, B30 use was found to increase ISO BSFC by 1–2% when comparing against the reference, and a similar increase was found when comparing to the trials conducted using MGO. The increase and variation between the tested engines were small, which is attributed to their electronic control. The highest deviations were observed for the comparisons against reference data, as is seen by the maximum and minimum values in Figure 5-4. This is most probably the result of the current engine operational parameters’ difference compared to the time of reference tests. For one case, Engine 5, ISO BSFC values for all tested fuels were below the reference, which is uncommon. This difference was confirmed to result from the use of a low-quality fuel during certification tests after review of the refence performance data. The comparison of ISO-corrected BSFC for B30 against that of crude oil revealed minimal difference and, in some cases, mainly at the higher load tested, a small improvement during B30 operation. Comparison cannot be made against other studies regarding this finding as all researchers used only high-quality diesel as the benchmark for “normal” engine operation. The very low level of variance seen in Figure 5-4 indicates that ISO-corrected BSFC of B30 should be practically identical to crude oil. Total actual fuel consumption, however, will be slightly higher for B30 due to its LCV, which is in most cases below that of crude oil (especially when comparing to VLSFO), as seen in Table 5-5 containing data for the fuels used.

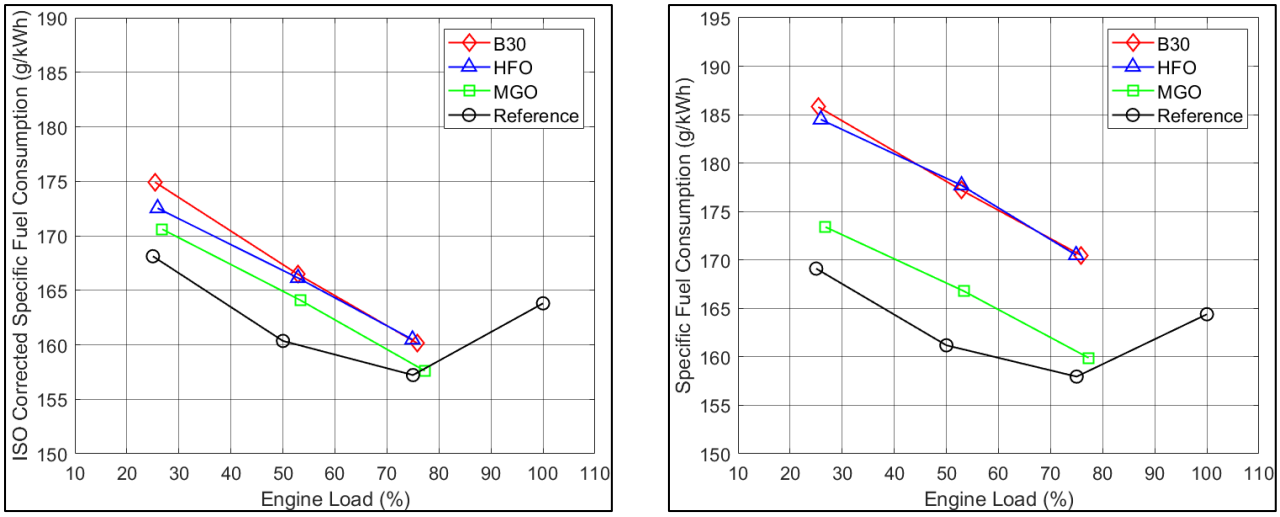

(a) (b)

Figure 5-2 Specific Fuel Oil Consumption vs load for B30, HFO, MGO, reference; a) ISO corrected, b) as measured; Engine 1

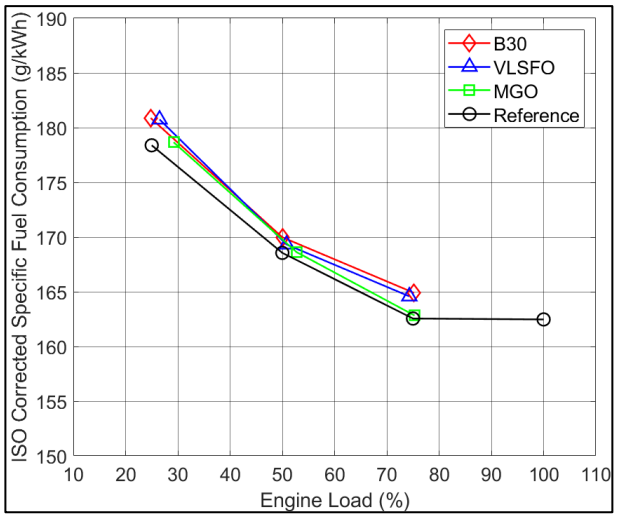

Figure 5-3 Specific Fuel Oil Consumption vs load for B30, VLSFO, MGO, reference, ISO corrected; Engine 2

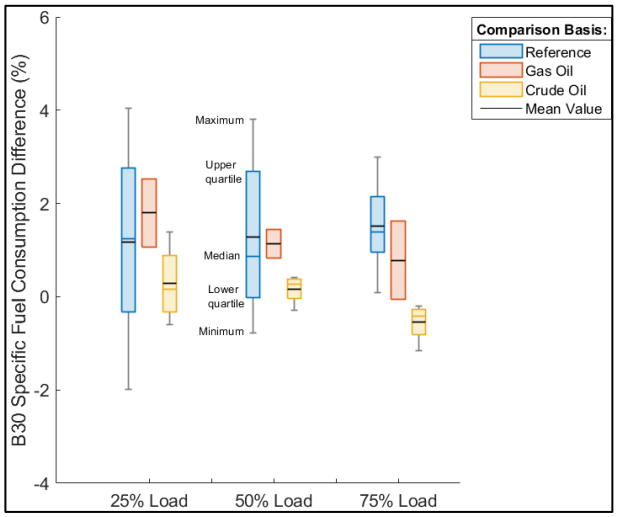

Figure 5-4 ISO Specific Fuel Consumption Comparison, B30 – Reference, Gas Oil, Crude Oil, all 2-stroke Engines

The other major parameters commonly used for marine engine performance evaluation are peak combustion pressure P_{max}, compression pressure P_{comp}, pressure increase due to combustion ΔP, and exhaust gas temperature values at cylinder outlet. All of the aforementioned are affected by both fuel quality and engine settings during testing, such as exhaust valve opening and closing angle, fuel injection timing, both static (command) and dynamic (actual event) and ignition delay. The use of any form of RM-grade fuel most commonly results in reduction of the peak combustion pressure, due to lower calorific content that curbs heat release rate and, as a result, pressure increase during the combustion process. The same is expected for the case of marine biofuel blends as they are 70% VLSFO fuel and biodiesel LCV tends to be even lower, even though for FAME variants from waste oil LCV is rather close to RM fuel oil. As briefly mentioned in the introduction the peak pressure due to combustion also depends on the fuel ignition delay, which affects how close before TDC combustion initiates and on the ignition delay that determines fuel air mixing time prior to ignition, thus premixed combustion intensity. The same two engines are used as characteristic examples, in Figure 5-5 - Figure 5-9 the P_{comp}, P_{max}, ΔP, ignition angle and ignition delay are provided for MGO, HFO, VLSFO and B30 for engines “1” and “2”.

Regarding pressure values, for “Engine 1” performance was identical for all tests conducted. Minute differences that were present for P_{comp} and slightly impacted other related parameters were due to the variation of ambient conditions and inlet air properties during testing, which is normal as the duration of each test was rather long. Pressure increase did not change to a considerable degree with fuel type, despite the differences in LCV between the three fuels. For all tested loads, pressure increase due to combustion was lower for MGO. Reviewing the ignition angle and ignition delay values in Figure 5-8 and Figure 5-9, consistently lower ignition delay, hence earlier start of combustion, is found for B30, followed by MGO and finally HFO, in line with their measured CN content/aromatic index values. The combination of ignition angle, ignition delay and fuel energy content did not result in performance variations beyond typically allowed or expected margins. The mean exhaust gas temperature values measured at cylinder outlet are provided in Figure 5-10 for indicative purposes only, as NO_x formation occurs at peak values and is highly localized as examined in the multizone model section after the measurement results analysis and is mostly affected by the increase to air fuel ratio and less due to temperature increase. Exhaust gas temperature did not present variations between the fuels, indicating similar exhaust valve opening angle and possibly similar combustion duration.

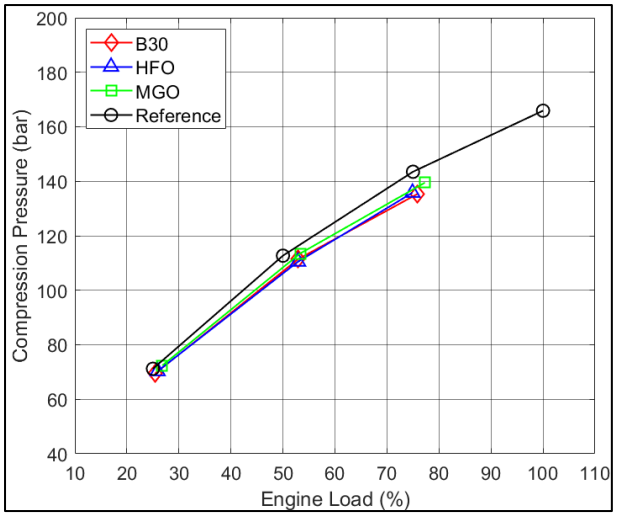

Figure 5-5 Compression Pressure vs load for B30, HFO, MGO, reference; Engine 1

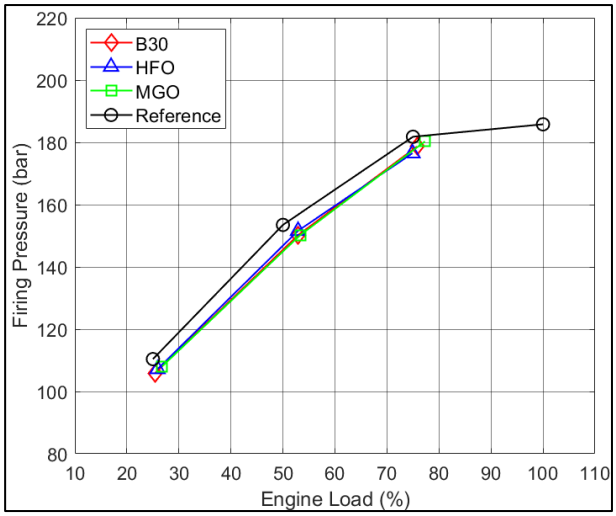

Figure 5-6 Peak Combustion Pressure vs load for B30, HFO, MGO, reference; Engine 1

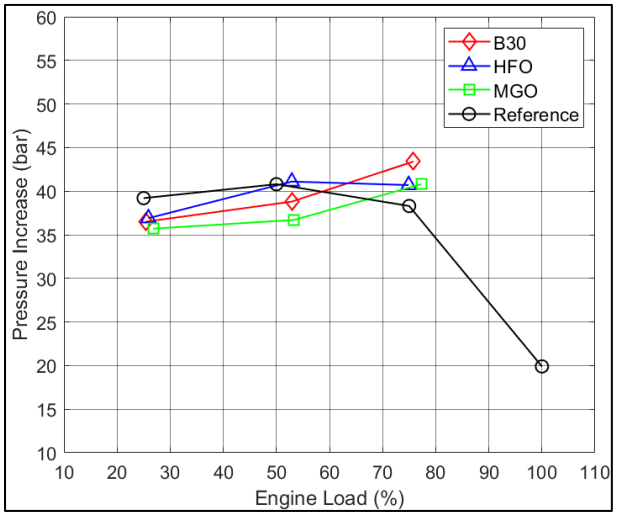

Figure 5-7 Pressure Increase due to Combustion vs load for B30, HFO, MGO, reference; Engine 1

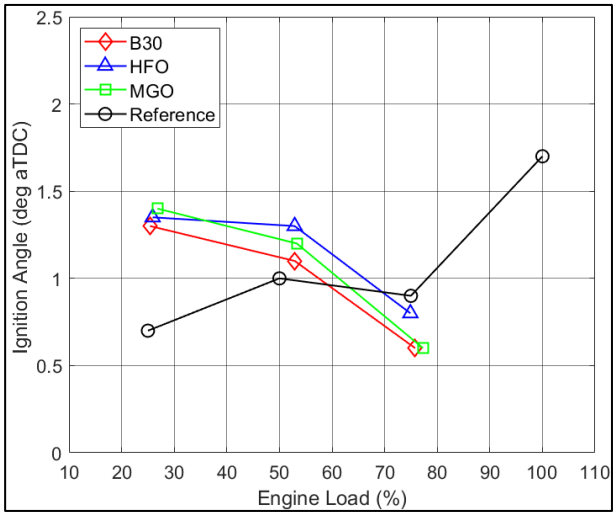

Figure 5-8 Fuel Ignition Angle (aTDC) vs load for B30, HFO, MGO, reference; Engine 1

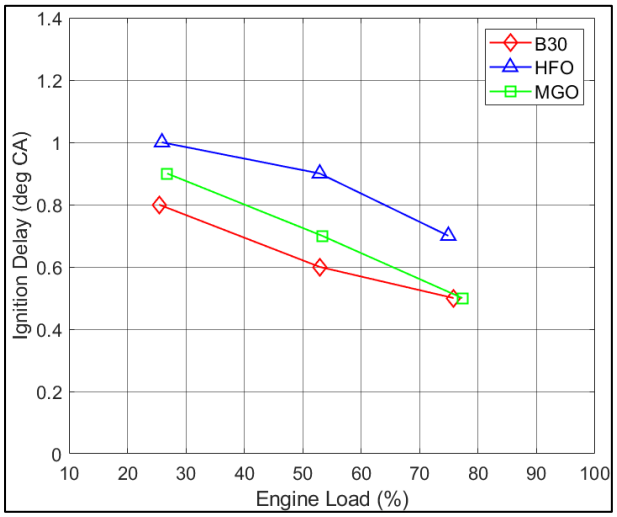

Figure 5-9 Fuel Ignition Delay vs load for B30, HFO, MGO; Engine 1

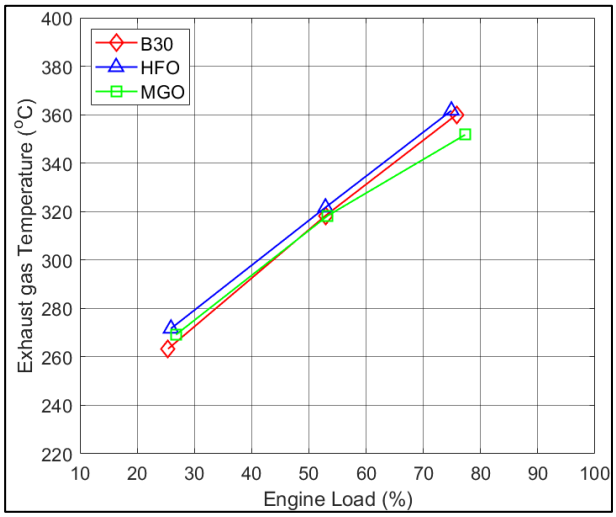

Figure 5-10 Measured cylinder exhaust gas temperature vs load for B30, HFO, MGO; Engine 1

For “Engine 2”, the values of P_{max}, ΔP, fuel ignition angle and fuel ignition delay are presented in Figure 5-11 - Figure 5-14. The cylinder exhaust gas temperature was not recorded with proper accuracy due to issues with the measuring equipment and is not provided in this comparative analysis. Peak pressure values for all fuels are close to the reference data as is expected from an electronic engine with automated pressure control enabled. The differences observed are attributed to small differences in compression pressure and operating conditions which are not compensated from the engine control system even though autotuning was enabled during the tests. The pressure rise presents small differences and is increased for MGO, while VLSFO and B30 values are the same with the exception of 50% load. The ignition angle and ignition delay values show nearly identical start of combustion for VLSFO and B30, and generally earlier ignition for MGO. The previous are affected by SOI timing and the ignition delay of each fuel. The differences are less pronounced compared to “Engine 1” examined above, for which HFO ignition angle was considerably delayed compared to the other two fuels. Due to the addition of biodiesel the B30 ignitability is found slightly enhanced compared to pure VLSFO. The ΔP and P_{max} differences are the result of the ignition angle variation and the LCV differences of the three fuels, with MGO’s being the highest and B30’s the lowest.

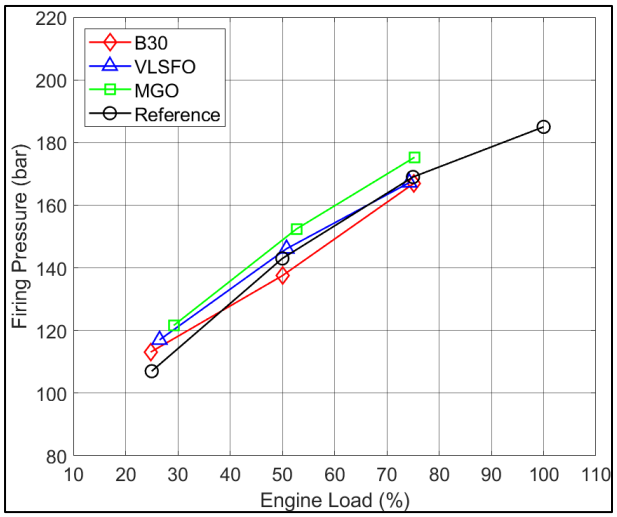

Figure 5-11 Peak Combustion Pressure vs load for B30, VLSFO, MGO, reference; Engine 2

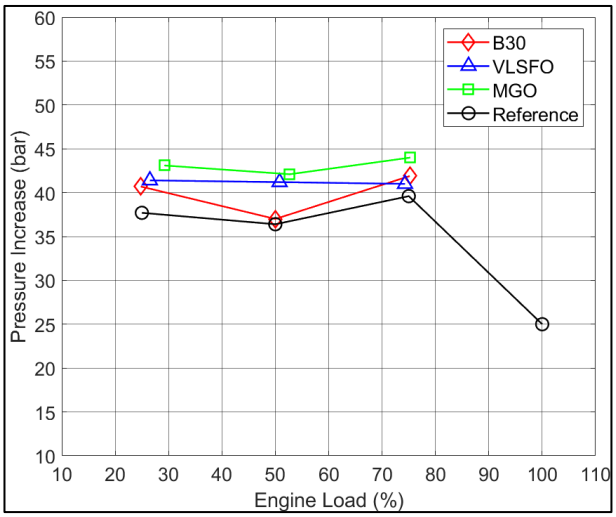

Figure 5-12 Pressure Increase due to Combustion vs load for B30, VLSFO, MGO, reference; Engine 2

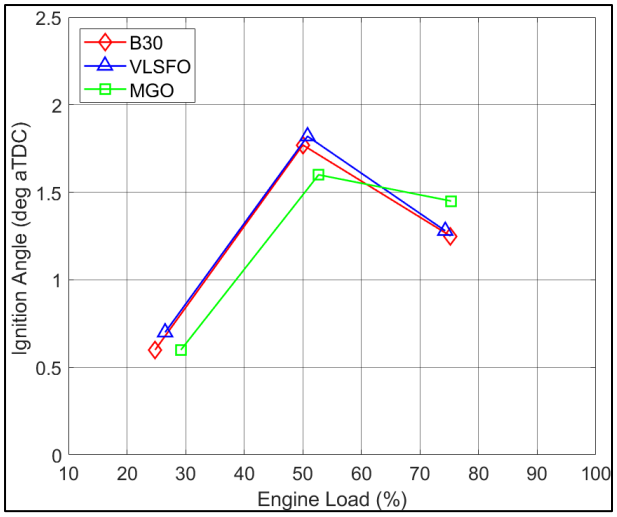

Figure 5-13 Fuel Ignition Angle (aTDC) vs load for B30, VLSFO, MGO; Engine 2

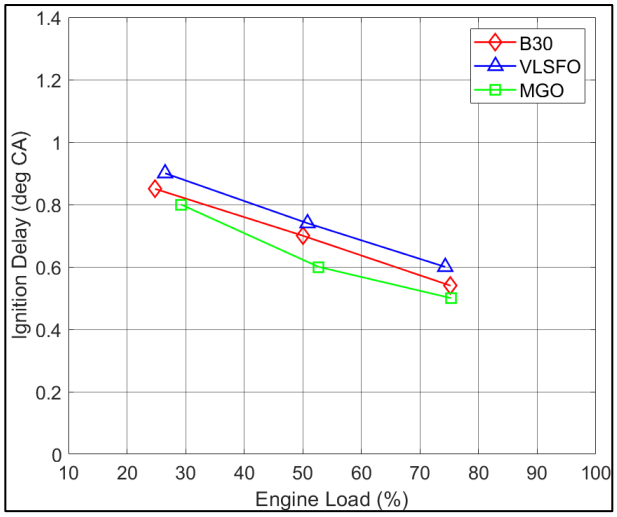

Figure 5-14 Fuel Ignition Delay vs load for B30, VLSFO, MGO; Engine 2

Last the statistical summary graphs of all 2-stroke engines tested are provided, in Figure 5-15 and Figure 5-16 for peak pressure and pressure rise respectively. The effect of the biofuel on engine performance presented significant deviations between the engines regarding both P_{max} and ΔP. A clear tendency for P_{max} decrease is revealed when using B30, as seen from the mean values, but results vary considerably between the tested engines. The highest reduction of P_{max} when using B30 was observed when comparing against reference and the trials conducted with MGO. Compared to crude oil, P_{max} values were the least affected. As far as ΔP is concerned, Figure 5-16 shows significantly lower variance and the tendency for reduction during B30 operation remains present for 25% and 50% load. The decrease in ΔP is low for B30 use, as in most cases both the average and median values were at or below 2 bar for most comparisons. The main reason for the lower scatter of ΔP values compared to P_{max}, is that variation in cylinder pressure at fuel ignition point was present between the tests, especially when comparing against reference data. Since the absolute P_{max} values affect maximum in-cylinder temperature, they can be used when reviewing performance and NO_x emissions in tandem, but only in conjunction with ΔP. Both P_{max} and ΔP are affected by a fuel's properties, typically increasing with higher LCV. The other factors affecting P_{max} and ΔP are injection angle and fuel ignition delay. The former might be affected by physical properties such as viscosity and the bulk modulus and the latter differs due to the tested fuels' CN number, Table 5-5. The rather low decrease of ΔP for B30 compared to MGO, which has roughly 6% higher LCV shows that the slight ignition advance makes up for the lower LCV in regards of pressure increase. The biofuel ignition point effect making up for other deficiencies compared to conventional fuels was reported in multiple studies and was the conclusion of an extensive review on the subject (35). Last, B30 and crude oil results were quite similar, especially viewed against the other two comparisons. The effect of biodiesel on engine performance and emissions results from the combination of LCV, ignition delay, premixed combustion intensity and total combustion duration. The variation in P_{max}, ΔP and BSFC is an indication of the degree that these vary between engines and fuels evaluated, and their results are evident regarding NO_x formation as shown in section 5.4.

Based on performance parameters the effect of B30 on engine operation was found to be minimal. It is possible that longer testing may reveal impact on the fuel supply system operation, especially in cases where poor handling and storage affect the biofuel quality due to oxidation, or the engine condition is sub-optimal. Such cases were observed during the early period of VLSFO use that replaced HFO in vessels not equipped with SO_x scrubbers following the change in allowed fuel sulphur content starting in 2020, (202).

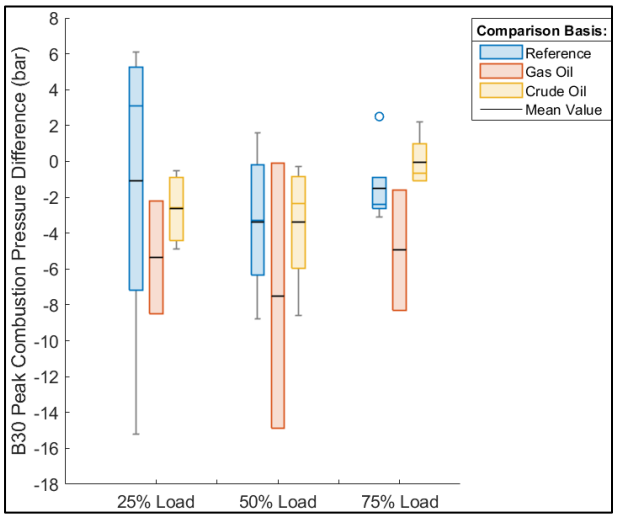

Figure 5-15 Peak Combustion Pressure Comparison, B30 – Reference, Gas Oil, Crude Oil, Main Engines

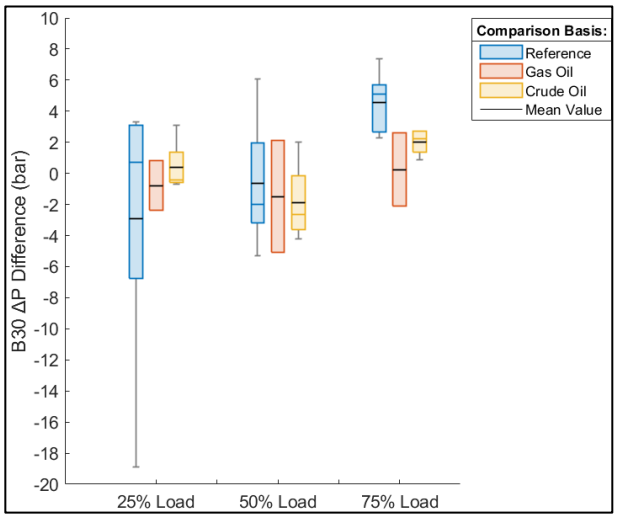

Figure 5-16 Pressure Rise due to Combustion Comparison, B30 – Reference, Gas Oil, Crude Oil, Main Engines

5.3.2 2-Stroke Engine Combustion Characteristics during B30, HFO, VLSFO & MGO Operation, Experimental Data

In this subsection the effect of biofuel use on the combustion characteristics of 2-stroke marine engines is investigated using measurement data to estimate fuel combustion rate with the method described in section 4.1.2. The diagrams presented were measured from “Engine 1” and “2” of the previous section. As the overall form of the diagrams is assessed to estimate combustion quality, this comparison is qualitative in nature and a statistical summary for all five tested engines is not provided. For the other engines, where cylinder pressure measurement for multiple fuels was possible, the differences were found similar to the two characteristic examples provided. In Figure 5-17a to Figure 5-17c the estimated combustion rates using MGO, B30 and HFO for 25%, 50% and 75% load are compared for “Engine 1”. Results from the engine FAT measurements were available and are included. The comparative evaluation of the combustion rates is focused on peak value, initial- and late-stage rate of combustion and combustion duration. In general, peak combustion rate is mostly affected from the lower calorific value of the fuel, the injection rate and the percentage of premixed combustion. For cases with small difference in ignition delay and comparable injection timing, thus similar amounts of premixed fuel, a higher peak burn rate should be observed for MGO, followed by HFO and B30. This is the pattern found for all loads examined. It is noted, however, that the difference is low except for the case of 75% load, Figure 5-17c. Combustion rate, up to the peak value, is similar for all fuels examined, with only minor differences. Further to the initial stage, late-stage combustion rate is similar for all cases, with a

slight indication of longer combustion duration when operating the engine on MGO at 50% and 75% load. The overall shape of the combustion rate of the tested fuels is close to that of the reference FAT measurements revealing relatively similar combustion progress. The only notable difference compared to the FAT results is attributed to changes in injection timing and consequently ignition angle. The similarity of the present combustion rate shape compared to FAT results confirms the very good condition and performance of the engine's fuel pumps and injectors at the time of testing. The similar combustion rate during the B30 fuel use compared to the other two fuels, reveals that its use does not affect the performance of the injection system, at least on a short-term basis. The fuel supply system performance could be a concern due to the varying physical properties of the fuels tested, as this has been found to have a measurable effect on fuel injection equipment in studies regarding VLSFO operation.

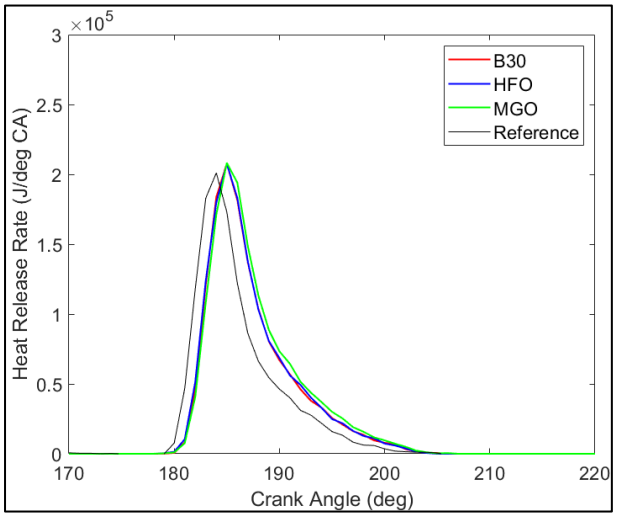

(a)

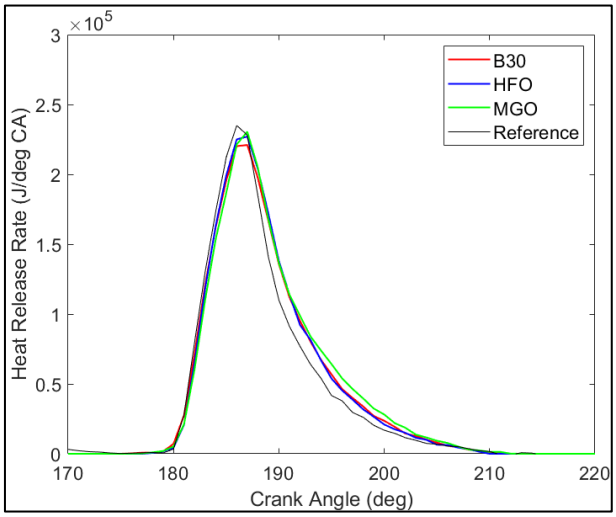

(b)

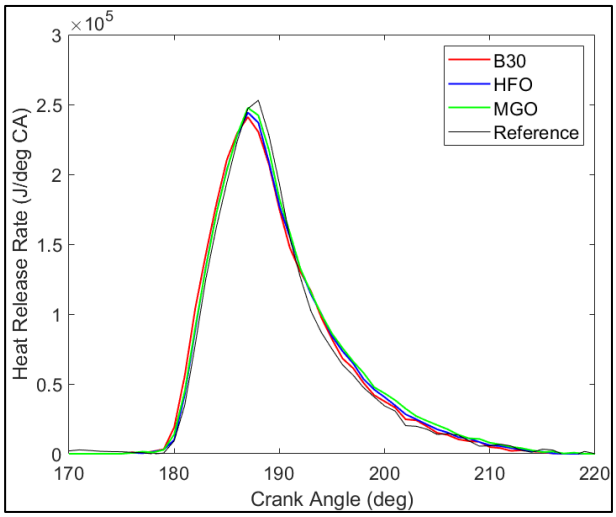

(c)

Figure 5-17 Net heat release rate for B30, HFO, MGO, Reference; a) 25% Load, b) 50% Load, c) 75% Load; Engine 1

Another important criterion for evaluation of the biofuel effect on the combustion mechanism is combustion duration. For its expression, the crank angle period required for the combustion of 50% and 95% of the total

burnt fuel is commonly used. The results for combustion duration are provided in Figures Figure 5-18a and Figure 5-18b. Combustion duration for 50% fuel burnt increases with engine load. The differences between the three fuels are very small. The results for 95% burnt fuel amount are similar. The only noticeable difference is for HFO which presents a trend for slightly lower combustion duration compared to MGO. This is possibly attributed to its physical properties (higher density and viscosity) resulting to higher fuel injection rate. The previous are an important finding as they confirm that the use of B30 does not affect combustion duration. Combustion process and duration findings are in line with the BSFC results and the cylinder exhaust gas temperature readings which were similar, Figure 5-10. Longer combustion duration, especially when coupled with high rate at the late stage, under similar operating conditions and same engine tuning, would result in higher cylinder exhaust gas temperature and reduced efficiency.

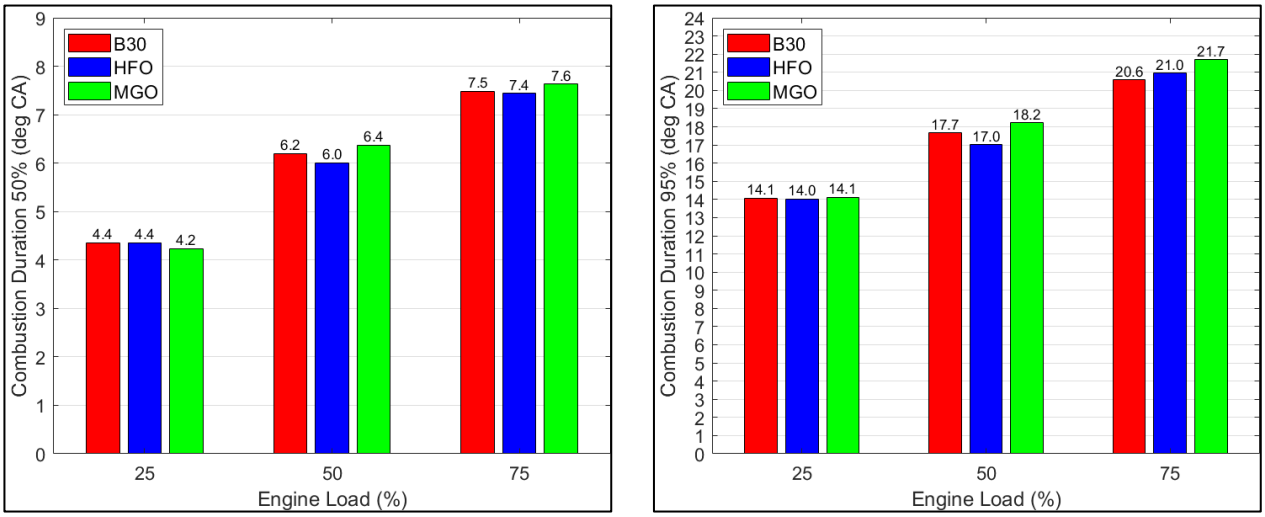

(a) (b)

Figure 5-18 Combustion duration vs load for B30, HFO, MGO; a) 50% of fuel burnt, b) 95% of fuel burnt; Engine 1

The respective results from the "Engine 2" trials are given in Figure 5-19a - Figure 5-19c for combustion rate diagrams at 25%, 50% and 75% and in Figure 5-20a and Figure 5-20b for combustion duration. Combustion rate presents small variation between the three fuels as was the case for "Engine 1". The peak HRR occurs for all loads during MGO operation and initial burn rate shows minimal difference except for 50% load, where slightly slower initial combustion progression is identified for B30. This resulted to the lower ΔP shown in Figure 5-12. Combustion duration was very similar between the fuels with slightly faster initial rate (50% fuel burnt) for B30. While the differences are very low, the B30 values for 95% fuel burn were closer to the MGO ones compared to VLSFO. This is attributed to the slightly faster combustion of biodiesel confirmed by Figure 5-20a depicting duration for 50% fuel burnt. The values between the two engines were almost identical, however the engine operating speed should also be considered, which was higher by 2.5 rpm on average in the case of "Engine 2". This translates to a reduction of 8% at 25% load and of 5% at 75% load in terms of actual burn time for "Engine 2". In terms of engine performance, however, the comparison is more important regarding actual CA of combustion start and end. The actual time duration of the combustion is of interest when considering the effect of heat losses.

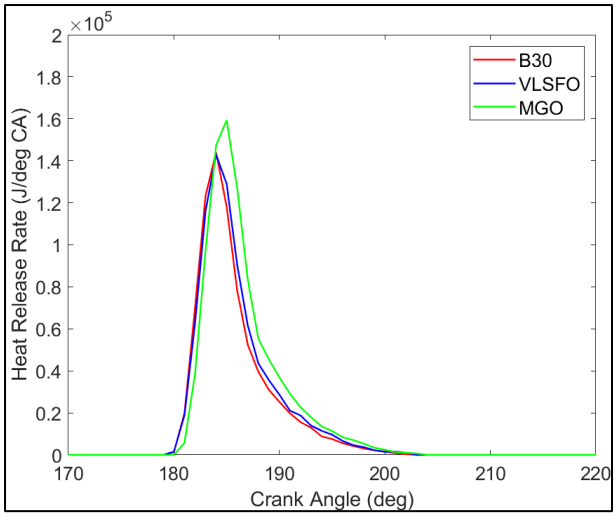

(a)

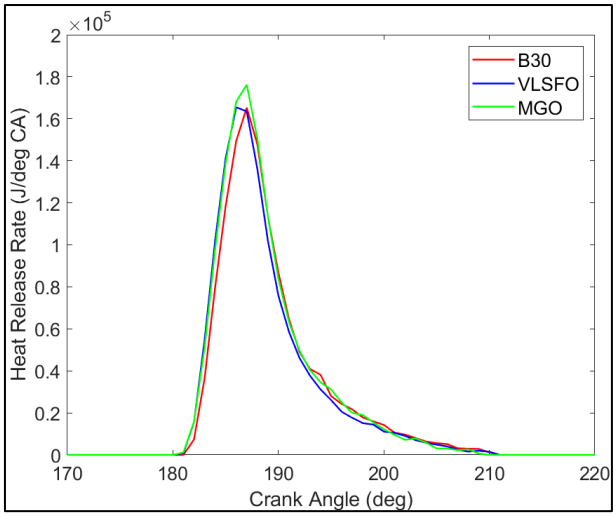

(b)

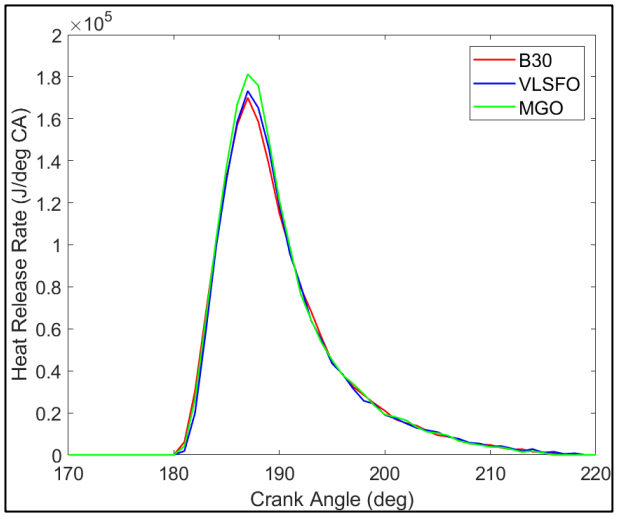

(c)

Figure 5-19 Net heat release rate for B30, VLSFO, MGO, Reference; a) 25% Load, b) 50% Load, c) 75% Load; Engine 2

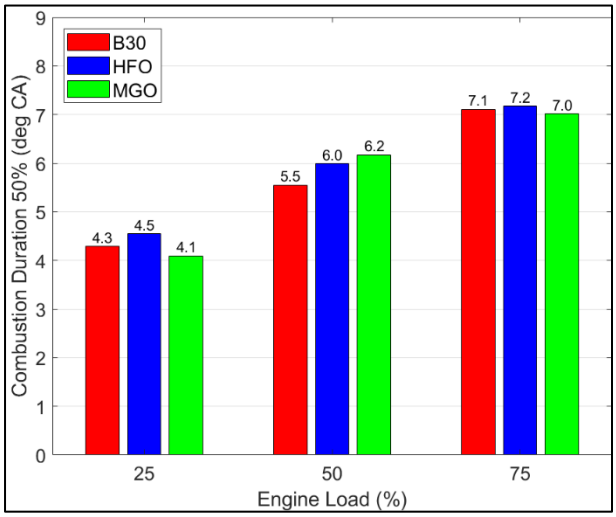

(a)

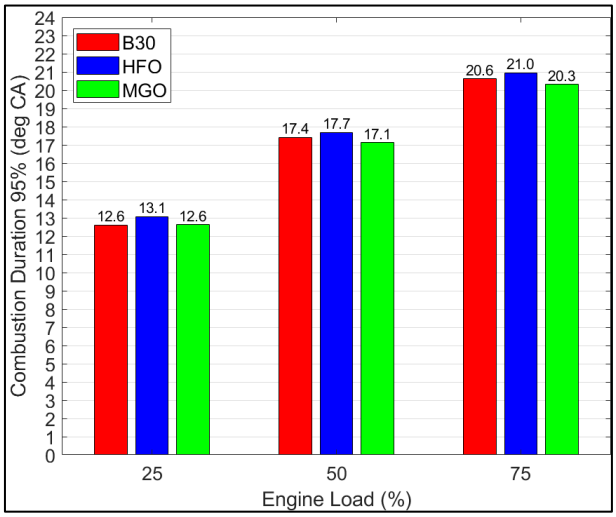

(b)

Figure 5-20 Combustion duration vs Load for B30, HFO, MGO; a) 50% of fuel burnt, b) 95% of fuel burnt; Engine 2

5.4 Biofuel Effect on Exhaust Emissions, 2-Stroke Propulsion Engines

The present section focuses on NO_x emissions which is a regulated pollutant for marine engines and its values are a major concern regarding biofuel use. CO_2 emissions are also presented to provide an indication for the effect of the fuels' carbon content on tank-to-wake emissions. As stated above, NO_x emissions in the marine sector are evaluated using their specific values, the estimation of which requires the exhaust gas mass flow rate. The estimated exhaust gas mass flow rate as derived from the application of the carbon balance method (27) is provided in Figure 5-21 for "Engine 1" and Figure 5-22 for "Engine 2". In the case of "Engine 1", exhaust mass flow rate is similar for all tested fuels with minor differences, which resulted from the variation in ambient conditions and P_{scav} during the tests. For "Engine 2" considerable difference was found between MGO and the other two fuels. This was due to the P_{scav} and ambient air values which differed considerably during the time of the MGO trials. For B30 and VLSO no difference is found as conditions were the same. As mentioned in section 5.2.1, further to the standard carbon balance method, oxygen mass balance calculations were performed with similar results verifying measurement accuracy.

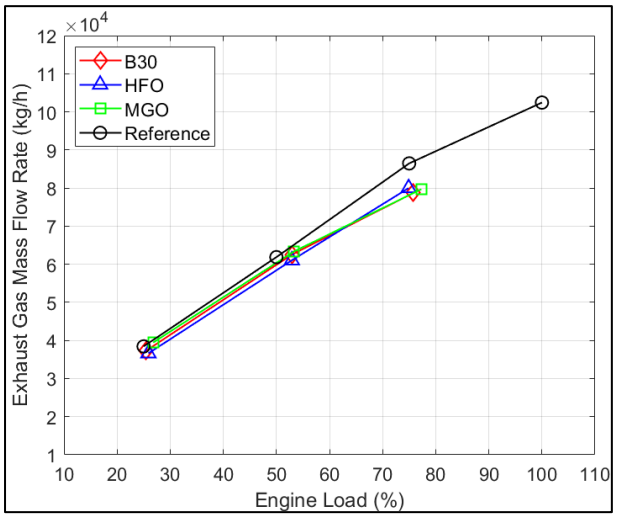

Figure 5-21 Exhaust gas mass flow rate vs load for B30, HFO, MGO, reference; Engine 1

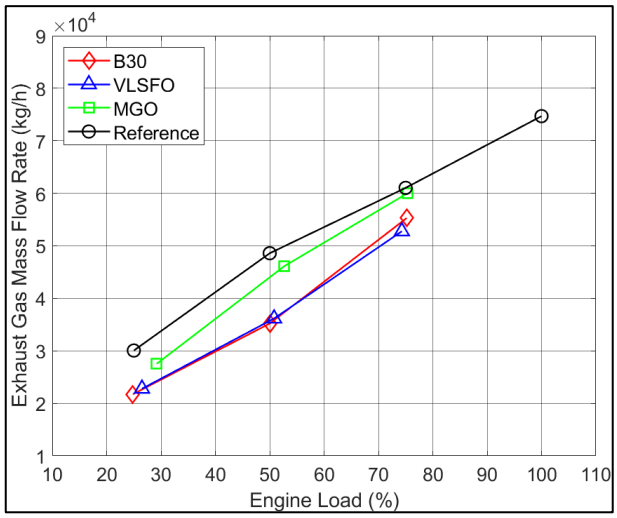

Figure 5-22 Exhaust gas mass flow rate vs load for B30, VLSFO, MGO, reference; Engine 2

5.4.1 Biofuel On-site CO_2 Emissions, 2-Stroke Engines

CO_2 emissions of a fuel are the result of its carbon content and the engine's consumption. For "Engine 1" the B30 blend carbon content (83.7%) was lower than the one of MGO (87.6%) and HFO (84.3%), which leads to lower CO_2 emissions on-site, however, this was partially offset by the difference in LCV value and overall fuel quality negatively affecting fuel consumption. In Figure 5-23 are presented the specific CO_2 emissions expressed in g/kWh. The CO_2 specific emission values are lower for MGO, followed by B30 and HFO. In Figure 5-24 the values for "Engine 2" using VLSFO instead of HFO are presented. Unlike the case of "Engine 1" practically no benefit is found for B30 when compared to VLSFO. In both cases the use of MGO was the only one to provide clear benefit regarding carbon emissions. An improvement is observed using B30

compared to HFO, but overall, the effect of the carbon content was minimal for all fuels examined. For this reason, the GHG reduction benefit of moderate FAME content blends will result mainly from the well-to-tank cycle. The benefit is expected to be around 25% based on extrapolation from data for marine use 2nd generation biofuels of 100% and 50% FAME content, (193), (194) and the data provided by the suppliers of the biofuels used in the tests.

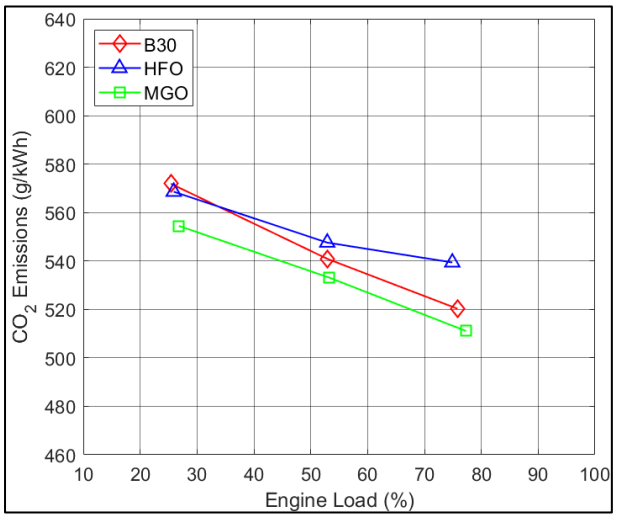

Figure 5-23 Specific CO_2 Emissions vs Load for B30, HFO, MGO; Engine 1

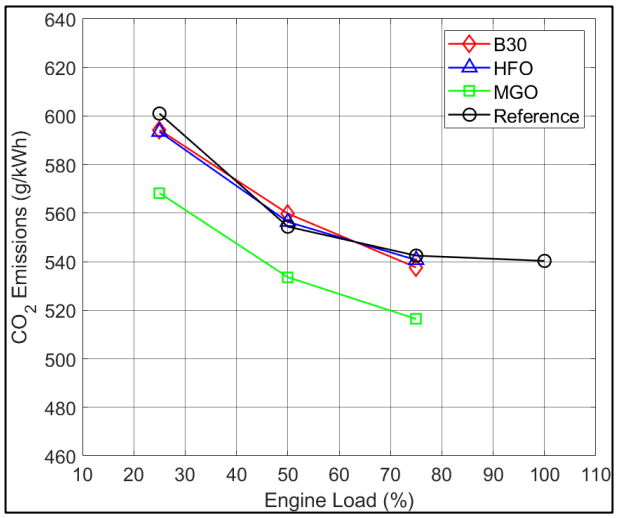

Figure 5-24 Specific CO_2 Emissions vs Load for B30, VLSFO, MGO; Engine 2

5.4.2 Biofuel NO_x Emissions, 2-Stroke Engines

Specific NO_x emissions were calculated using the measured exhaust gas NO_x concentration, engine power, exhaust gas mass flow rate and the ambient and charge air properties after applying the corrections required by the NTC, (27). Since all 2-stroke engines tested are Tier-II emission certified, the E3 cycle total weighted value was calculated using the values from the three load points to verify emission compliance.

The measured NO_x emissions concentration at wet conditions is provided in Figure 5-25 for “Engine 1” and Figure 5-26 for “Engine 2”. For both engines it follows a similar trend for all fuels that is close to the one of the reference emissions data. The measured NO_x concentration peak value is observed at 50% load with a subsequent decrease at 75% load regardless of fuel type. For “Engine 1” HFO and B30 measured NO_x values are similar for all load points, the average value being slightly higher for B30. MGO NO_x values are lower and except for the 75% load measurement close to reference. For “Engine 2” different results are found with the highest NO_x concentration measured during the MGO tests. The concentration measured during the HFO trials was similar to the MGO tests, and for B30 considerably lower NO_x values were measured that were below reference for 75% load. The specific NO_x emissions are provided in Figure 5-27 and Figure 5-28 for the two engines, including the values from their emissions certification procedure. In the case of “Engine 1” the emissions trend across engine load is generally retained, especially for the MGO results, which are very close to reference, as was expected by the engine performance results. Specific NO_x emissions are higher for B30, followed by HFO and MGO. On average NO_x emissions for B30 are increased by 7% compared to MGO and

3.5% compared to HFO. Considering the similar results from the performance and combustion rate analysis, the increase of NO_x emissions for B30 is attributed to its properties and primarily to the increased O_2 content (207) and to a lower degree the molecular structure of its carbon content, which has been found to increase NO_x formation, (199). The consistent increase of specific NO_x emissions for B30 compared to the other fuels verifies the concerns expressed regarding the possible impact of oxygenated fuel use.

These findings were not repeated for the "Engine 2" specific NO_x emissions, Figure 5-28. For this engine specific NO_x emissions are the highest during MGO operation and quite similar between the B30 and VLSFO trials, with the exception of 25% load. It is noted that for MGO specific emissions are above the NO_x file reference values, while for B30 and VLSFO operation specific emissions are below the reference data. The only difference between VLSFO and B30 is found at 25% load, with significantly higher specific emissions during B30 operation.

Considering the total weighted emissions values of "Engine 1", Figure 5-29, which is used to test for compliance against the official limit, the overall impact for B30 is approximately 7.1% increase compared to MGO and 2.6% against HFO. The increase found for the total weighted NO_x emissions falls within the range, (0% - 6%) of the results reported in (53) conducted by vessel operators for similar type engines, when comparing B30 to crude oil emissions. Concerning the tested engine "1", sufficient margin exists between the total weighted emissions value calculated during the tests and the applicable regulation limit, Tier-II. The borderline criterion for evaluation of B30 NO_x emissions are the guidelines of the NTC, which, as mentioned, allow an additional 10% increase above the applicable limit for on-board measurements (27). This margin further increases by a flat 5% when testing crude oil grade fuels, (27).

For "Engine 2" the total weighted NO_x emissions value during MGO operation was found above the Tier-II limit, however, still within the 10% margin allowed for on-board measurements, Figure 5-30. The B30 and VLSFO values were practically identical and similar to the respective results of "Engine 1". The high variation between the tested fuels found for the second engine is attributed to performance and ambient conditions differences. Specifically, P_{max} and ΔP differences were present between the different tests, with these values well above reference during the MGO tests. In combination with the difference in ambient and air inlet conditions the NO_x mass flow was considerably increased during the MGO tests. The previous findings make clear the importance of overall engine performance and ambient conditions on the final NO_x emissions to the environment, as in the case of the "Engine 2" the emissions limit was not met when using the supposedly most favorable fuel but was within limits for the other two fuels that tend to result in higher emissions. Despite the results of the MGO tests, for "Engine 2" the minimal effect of B30 on NO_x emissions compared to VLSFO was demonstrated.

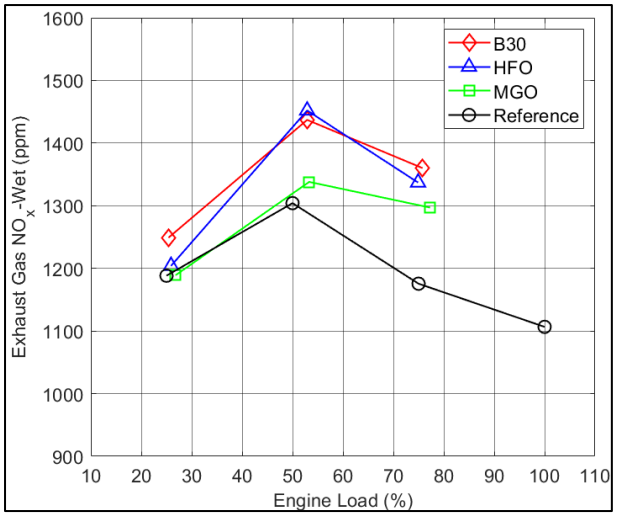

Figure 5-25 Measured exhaust gas NO_x concentration (ppm wet) vs Load for B30, HFO, MGO, reference; Engine 1

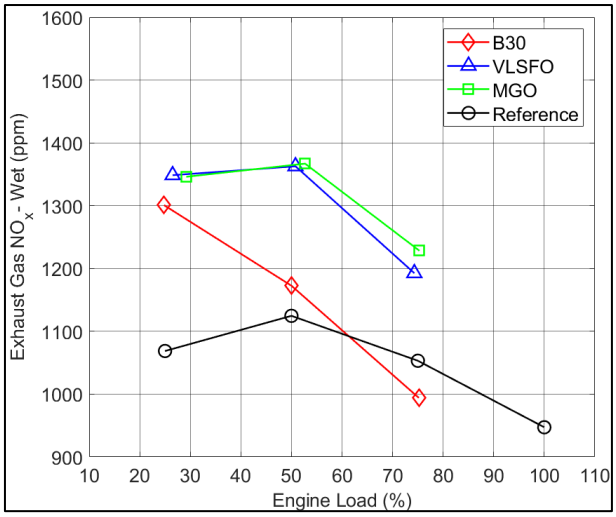

Figure 5-26 Measured exhaust gas NO_x concentration (ppm wet) vs Load for B30, VLSFO, MGO, reference; Engine 2

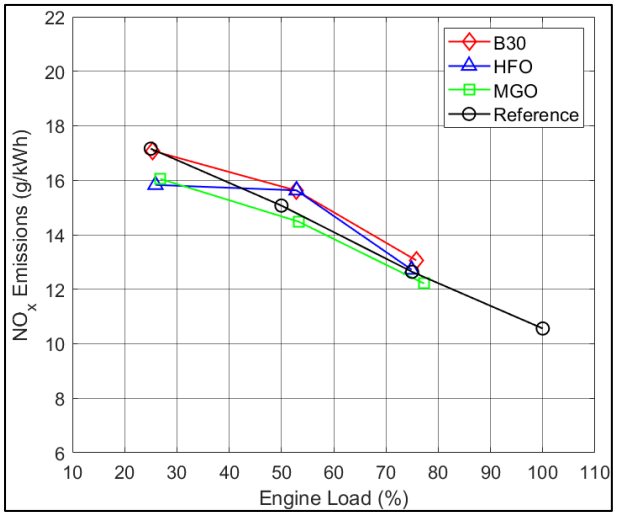

Figure 5-27 Specific NO_x (g/kWh) emissions vs Load for B30, HFO, MGO, reference; Engine 1

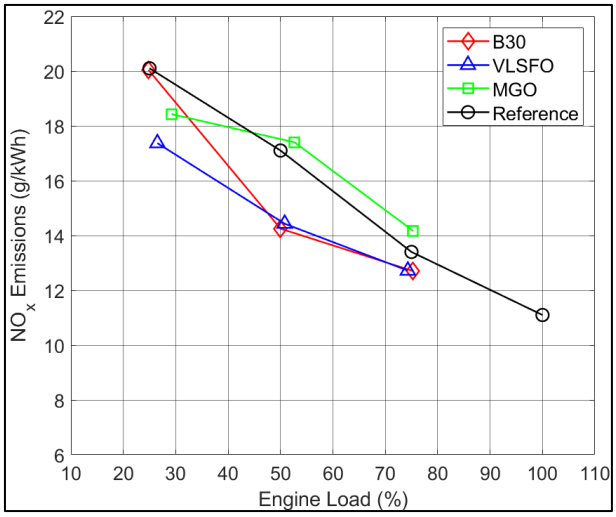

Figure 5-28 Specific NO_x (g/kWh) emissions vs Load for B30, VLSFO, MGO, reference; Engine 2

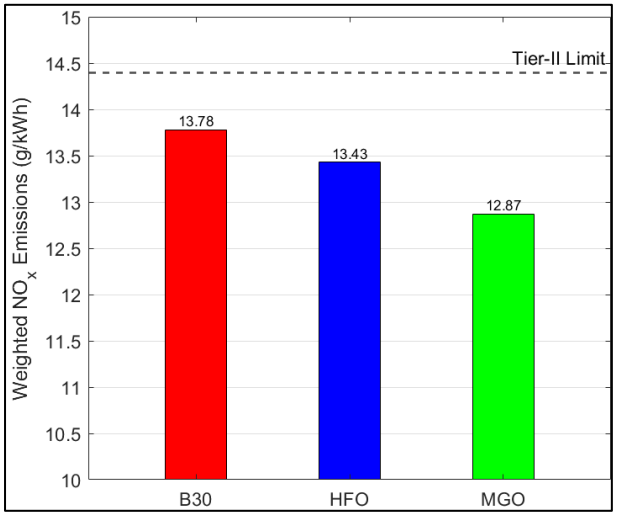

Figure 5-29 NTC E3 Cycle weighted total NO_x value, B30, HFO, MGO; Engine 1

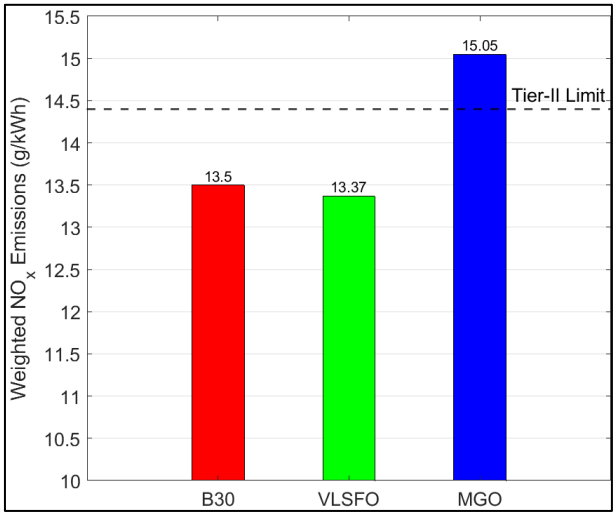

Figure 5-30 NTC E3 Cycle weighted total NO_x value, B30, VLSFO, MGO; Engine 2

The last aspect to be investigated is in-cylinder temperature due to its relation with NO_x formation. The mean temperature of the cylinder charge, estimated as described in 4.2.2, is provided in Figure 5-31a - c for "Engine 1". Even though this is significantly lower than the temperature inside the fuel jet where NO_x is formed (102), (103), its value can be used as an index for the tendency for NO_x formation. The highest peak temperature difference is observed for the B30 measurement at 25% load. This coincides with the highest NO_x emissions increase compared to the other fuels and the reference. For the remaining loads temperature values are nearly identical for all fuels. It was estimated that the temperatures inside the fuel jet will show higher differences, especially for B30 operation due to its oxygen content which promotes combustion. This was investigated and is presented in the section of the simulation model results. The previous estimation was not confirmed. While the burnt zone temperature was significantly higher than the cylinder average, it was found that the factor promoting NO_x formation was primarily related to air fuel ratio increase. The model showed that NO_x emissions increase during B30 use is mostly attributed to its increased O_2 content and not necessarily more intense combustion and local temperature. This agrees with (102), in which biofuel combustion NO_x emission increase was attributed to the O_2 available inside the combustion zones of fuel driving NO_x formation.

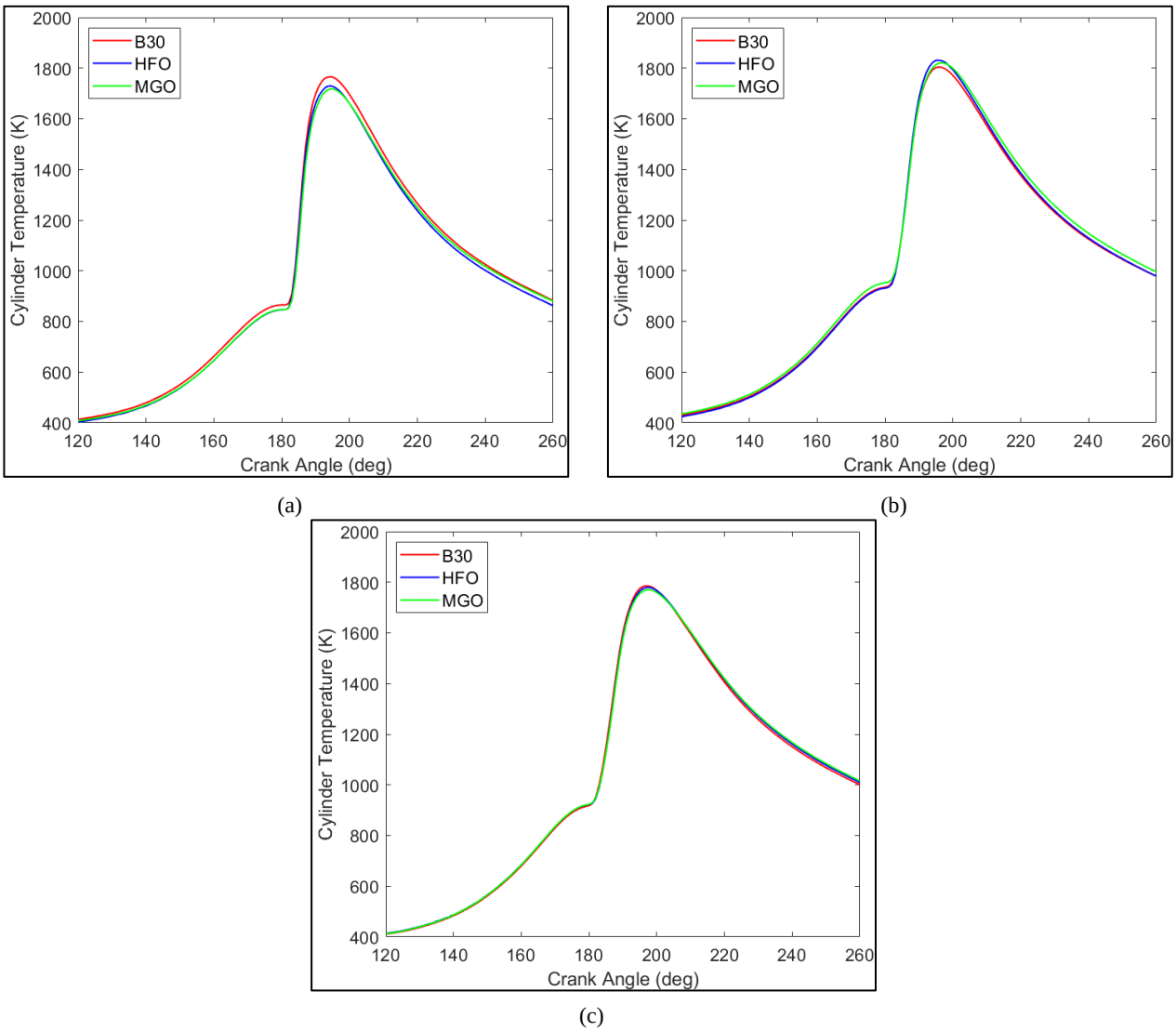

Figure 5-31 Cylinder mean charge temperature for B30, HFO, MGO; a) 25% Load, b) 50% Load, c) 75% Load; Engine 1

Further to the detailed comparison provided above in Figure 5-29 and Figure 5-30, the deviation of the weighted NO_x emissions during B30 operation compared to reference and other fuels tested is provided for all 2-stroke engines tested, Figure 5-32. An important finding was that for all cases the total weighted NO_x emissions were above the reference value regardless of tested fuel. In most cases the total weighted NO_x emissions for B30 were increased compared to reference and to crude oil trials, as is shown by the median values. This has been the finding of most 2-stroke engines studied by vessel operators in (53). Variation was observed which was expected, as it is mentioned in studies such as (224) and extended reviews (225). These works referred to engines of different type than the ones tested, however the mechanism of NO_x formation and factors affecting combustion are common in CI engines. It must be stated, however, that the degree of effect will differ. For one application, "Engine 2" above, consistent NOx emissions decrease was observed for B30 operation with the MGO NO_x emissions being considerably higher. This coincided with the highest measured decrease in P_{max} as identified in Table 5-6 and is similar to the results reported in (194), albeit with a higher FAME content fuel. Due to the high difference between the results of the two engines tested with MGO, Figure 5-15 and Figure 5-16, no estimate is made regarding the difference between MGO and B30 emissions on a wider basis. However, these results clearly show the degree that NO_x emissions using any fuel type can be engine specific. The variation for each load point differed with the highest range of differences observed at 25% load. Review of the results on a load basis, also makes clear that emissions at low load are the most affected, as was found for most of the engines tested in (53). This again coincides with the high degree of difference in P_{max} values, Figure 5-15. The mean increase in total weighted emissions for B30 compared to reference values was 10%. Considering the fact that the IMO provides allowance for 10% emission increase over the official limit for tests conducted on board vessels (27), this result is promising. Trials comparing B30 and MGO showed almost equal difference upwards and downwards for B30 NO_x emissions with the results being highly engine dependent, as was also found in the previous section. Compared to crude oil, for B30 the increase of NO_x emissions was low, with the increase in total emissions values normal range between 1% – 8%. The average value was 4% and the median slightly lower. Considering that similar performance was observed for tests using B30 and crude oil, the NO_x emissions increase is attributed to the higher O_2 content of the biofuel, which has been established to enhance NO_x formation in multiple studies such as (207). The O_2 concentration was similar for most B30 variants evaluated, except for Engine-3, on which higher O_2 content biofuel was used. The increase did not result in higher NO_x emissions than for other applications, thus it was not possible to correlate between fuel O_2 content and NO_x emissions increase. Overall, for NO_x emissions, B30 use was found to result in elevated pollutant formation in most cases, on average 10% compared to reference and 4% compared to crude oil, thus its effect is considered moderate, especially considering that these engines usually operate using crude oil.

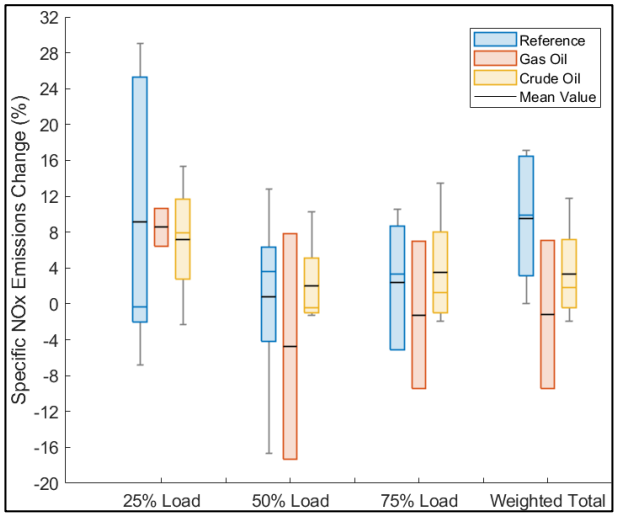

Figure 5-32 Specific NO_x Emissions Comparison, B30 – Reference, Gas Oil, Crude Oil, Main Engines

Table 5-6 Main Engine B30 Comparison Summary

	Engine 1				**Engine 2**			
Spec. Emissions (%)	25% Load	50% Load	75% Load	Total Weighted	25% Load	50% Load	75% Load	Total Weighted
Reference	-0.47	3.65	3.22	9.89	-6.85	12.85	-5.06	4.20
Gas Oil	6.42	7.87	6.96	7.07	-	-	-	-
Crude Oil	7.90	-0.06	2.67	2.61	-2.30	-0.79	-1.96	-1.90
Pmax (bar)								
Reference	-4.50	-3.30	-3.10		5.00	1.60	2.50	
Gas Oil	-2.20	-0.10	-1.60		-	-	-	
Crude Oil	-1.30	-1.40	2.20		-0.50	-0.30	-1.10	
ΔP (bar)								
Reference	-2.70	-2.00	5.10		3.30	-2.50	5.10	
Gas Oil	0.80	2.10	2.60		-	-	-	
Crude Oil	-0.40	-2.30	2.70		-0.50	-3.00	1.80	
	Engine 3				**Engine 4**			
Spec. Emissions (%)	25% Load	50% Load	75% Load	Total Weighted	25% Load	50% Load	75% Load	Total Weighted
Reference	29.05	4.14	8.10	16.27	24.09	-0.07	10.53	17.09
Crude Oil	7.90	10.25	13.45	11.77	-	-	-	-
Pmax (bar)								
Refrence	3.10	-8.80	-2.50		-15.20	-0.80	-2.40	
Crude Oil	-4.90	-3.30	-1.10		-	-	-	
ΔP (bar)								
Reference	0.70	6.10	7.40		-18.90	-5.30	2.80	
Gas Oil	3.10	2.00	2.70		-	-	-	
	Engine 5							
Spec. Emissions (%)	25% Load	50% Load	75% Load	Total Weighted				
Reference	-0.30	-16.67	-5.15	-0.14				
Gas Oil	10.66	-17.34	-9.47	-9.40				
Crude Oil	15.37	-1.25	-0.08	0.97				
Pmax (bar)								
Reference	6.10	-5.50	-2.00					
Gas Oil	-8.50	-14.90	-8.30					
Crude Oil	-3.90	-8.60	-0.20					
ΔP (bar)								
Reference	3.00	0.60	2.30					
Gas Oil	-2.40	-5.10	-2.10					
Crude Oil	-0.70	-4.20	0.90					

5.5 Biofuel Effect on Engine Performance and the Combustion Process, 4-Stroke Auxiliaries

In this section, the effect of biofuel on 4-stroke auxiliary generators performance is presented by comparison of the major engine performance metrics during operation with B30 biodiesel blend and conventional fuels, including the results of the official engine certification tests. The detailed measurement results for the 4-stroke units tested are given in Table 5-7 at the end of the section.

5.5.1 Performance for B30, HFO & MGO Operation, 4-Stroke Auxiliary Units

Similar to the 2-stroke engines analysis above, the first parameter examined is the biofuel effect on total consumption. Due to the smaller size of the auxiliary engines their fuel efficiency does not affect the overall vessel fuel consumption to a significant degree, as the average consumption of one auxiliary unit will usually be less than a tenth of the main engine hourly fuel requirements. Thus, for the auxiliary units this comparison is mostly conducted to estimate the overall effect of the biofuel on the 4-stroke engine performance. The ISO corrected, hence also LCV normalized, BSFC values are provided in Figure 5-33 for a 4-stroke auxiliary unit tested on MGO, HFO and B30. The unit belongs to the same vessel as the 2-stroke "Engine 1" examined in detail in the above section, and was tested at the same time so conditions and fuels used are identical. In this vessel the fuel line was shared between the installed three auxiliary generators and a single flowmeter was installed, so accurate fuel consumption measurements were not feasible because more than one unit had to be in operation at all times. However, an estimate was derived by sharing the total fuel consumption between all operating units using their power and reference BSFC to load curves and was compared with the results of the computational estimation. The BSFC values reported on Figure 5-33 are based on a thermodynamic estimation performed using the measured cylinder pressure traces as described in 4.2.2. Any other approach would not attain the required accuracy level to identify differences between the fuels, beyond the obvious variation created by the LCVs. The ISO corrected BSFC values for B30, are between the HFO and MGO ones, with low variation between the fuels. In addition, the difference remains practically identical for all loads.

In Figure 5-34 the statistical review of findings from multiple 4-stroke auxiliary units tested is presented for ISO corrected BSFC compared against the reference value and any additional trials conducted with MGO and crude oil. ISO BSFC was found to be higher for most engines, with few marginal outliers having similar consumption values, hence making the engine of Figure 5-33 an outlier. The increase of ISO corrected BSFC for B30 operation compared to reference was on average 2.5%. Compared to MGO values, a 3% increase was found at the present state, which remained almost steady with engine load. As in the case of the 2-stroke engines, crude oil BSFC values were close to B30, with a slight increase of 1% found for all loads. Thus, for 4-stroke auxiliary generators a clearer effect of B30 on BSFC compared to 2-stroke engines is observed when

considering all fuels tested. The level of difference remains within acceptable limits regarding fuel economy concerns, even after factoring in the LCV value.

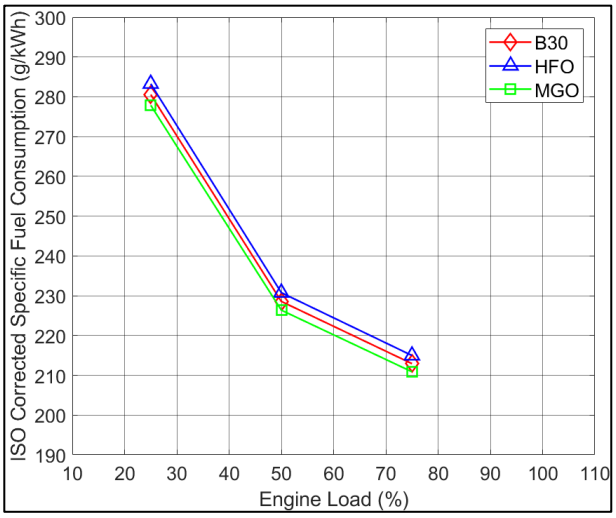

Figure 5-33 Specific Fuel Oil Consumption vs load for B30, HFO, MGO; ISO corrected; Auxiliary Generator 1

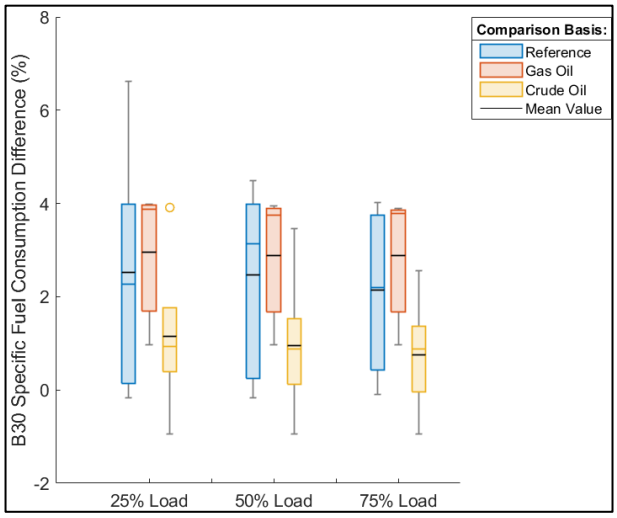

Figure 5-34 ISO Specific Fuel Consumption Comparison, B30 – Reference, Gas Oil, Crude Oil, Auxiliary Generators

Following BSFC the peak combustion/firing pressure P_{max} and pressure increase due to combustion values are comparatively evaluated. Unlike modern 2-stroke main engines the auxiliary units do not feature variable engine settings for their inlet and exhaust valve timings or fuel injection timing as all are cam driven even for state of the art models. Thus, no effect will be found regarding P_{comp} due to the fuel change effect on overall operation and this comparison, along with valve timings is omitted. For the 2-stroke engines examined in the previous section, the use of biofuel did affect to a degree the peak combustion values due to altering pressure increase during combustion. The same is expected for the 4-stroke engines to a higher degree due to their considerably higher (roughly x10) operating speed. In Figure 5-35 and Figure 5-36 the P_{max} and ΔP values of the same auxiliary unit are compared. With the exception of 25% load, the peak combustion and pressure increase values are increased during B30 operation. Since the ambient conditions were similar between the tests and engine settings are steady for engines of this type, the alteration found is attributed mostly to the effect of the biofuel, and to a lower extent the result of slight variation of P_{scav} as it was decreased during the MGO tests. The outlier behavior during the 25% load HFO test was attributed to very high fuel ignition delay during the specific measurement that is confirmed in the next section with the HRR analysis. In Figure 5-37 and Figure 5-38 the fuel ignition angle and ignition delay values are given. The injection angle timing was roughly the same for all fuels, with some minor variations due to the physical properties (viscosity and bulk modulus) affecting the pressure increase speed in the fuel line. It is noted that all ignition delay values are considerably above those reported in the 2-stroke engine section as they are expressed in degrees CA and engine rotational speed is significantly higher. For HFO ignition delay, values were considerably above those of the other two fuels as expected. For MGO and B30 results were similar. As can be seen from the differences between ignition angle and ignition delay, the B30 physical properties did result to a rather consistent slightly advanced actual start of injection in the cylinder, especially clear at 50% load. Comparison

of HFO and B30 regarding the dynamic start of injection shows high variation between loads and is not conclusive.

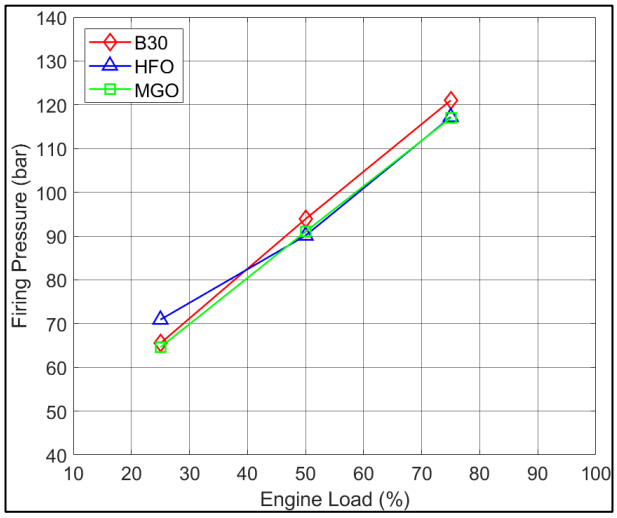

Figure 5-35 Peak Combustion Pressure vs load for B30, HFO, MGO; Auxiliary Generator

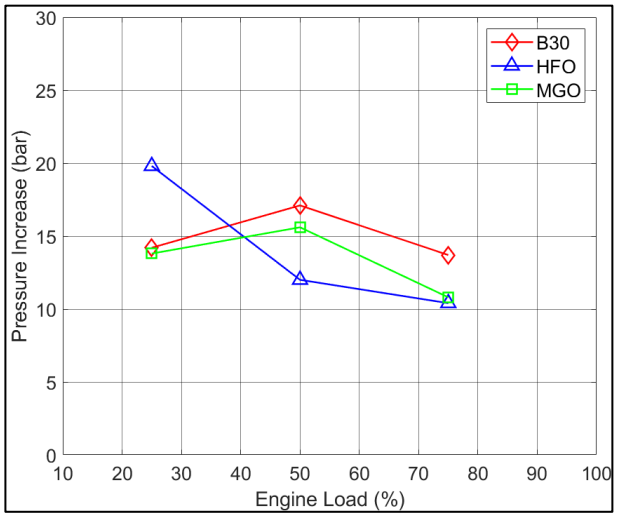

Figure 5-36 Pressure Increase due to Combustion vs load for B30, HFO, MGO; Auxiliary Generator

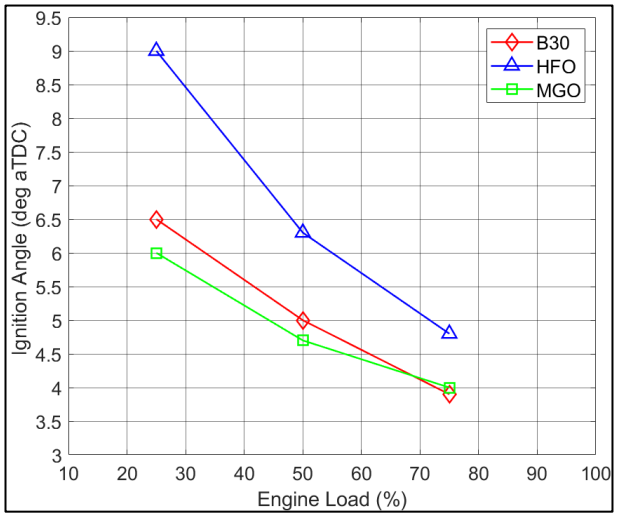

Figure 5-37 Fuel Ignition Angle (aTDC) vs load for B30, HFO, MGO; Auxiliary Generator 1

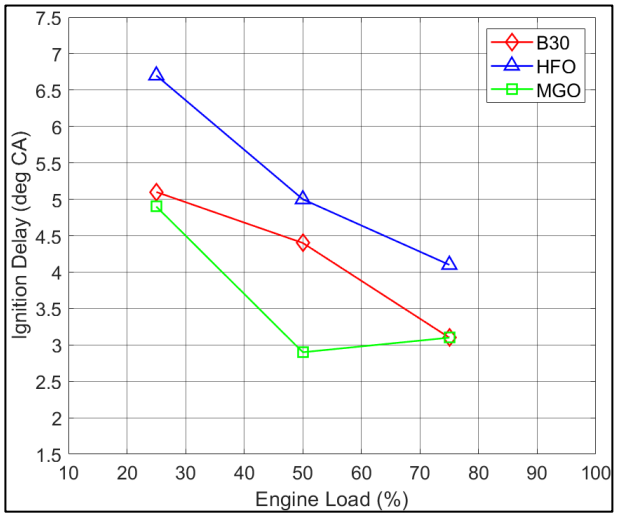

Figure 5-38 Fuel Ignition Delay vs load for B30, HFO, MGO; Auxiliary Generator 1

In Figure 5-39 and Figure 5-40 the statistical summaries of all tests conducted on auxiliary units for P_{max} and ΔP are presented compared to their respective reference. Both values were found to significantly differ from reference for all fuels examined. The values for B30 were similar to the other fuels, and both considerably lower and higher compared to reference. The similarity between the different fuel trials' P_{max} and ΔP values revealed that the differences compared to reference were the result of engine tuning and not the fuel used. The previous also shows that for 4-stroke auxiliary units engine tuning can vary considerably compared to reference state due to the lack of electronic control. The sample of MGO measurements was small, only for one engine, for which lower P_{max} and ΔP compared to B30 were measured. The difference in P_{max} was within 2 – 6 bar, and the difference in ΔP was below 4 bar. Thus, as in the case of the 2-stroke engines the higher ignitability of B30 made up for the difference in LCV between the two fuels. Comparison to measurements

using crude oil, shows increase and decrease for both parameters depending on the engine tested. The median values show that the general tendency is lower P_{max} and ΔP for B30 operation. Based on the results with MGO and the findings of other works discussed above, this trend is attributed to the degree of fuel and air mixing before fuel ignition that can result in more intense premixed early combustion enhancing pressure rise to the maximum value.

Based on the results presented in Figure 5-39 and Figure 5-40, the performance differences for B30 in the case of 4-stroke generators were overall higher than 2-stroke engines. For this reason, when considering the variation compared to reference, wider range of effects on NO_x formation should be expected.

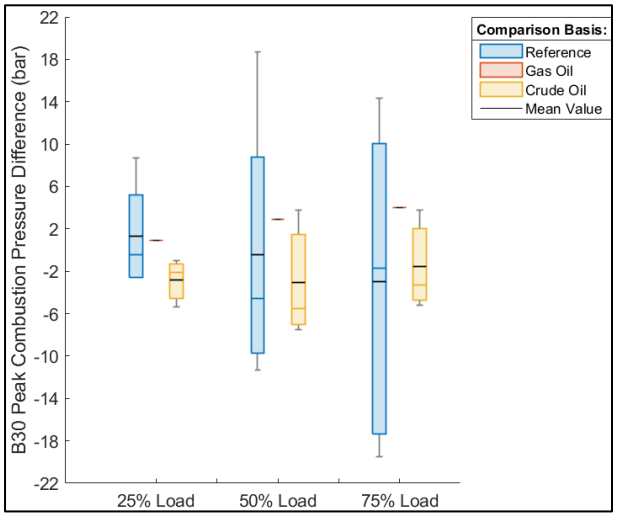

Figure 5-39 Peak Combustion Pressure Comparison, B30 – Reference, Gas Oil, Crude Oil, Auxiliary Generators

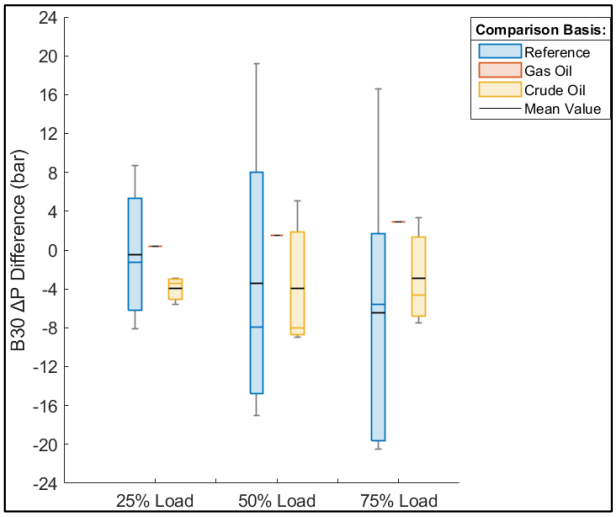

Figure 5-40 Pressure Rise due to Combustion Comparison, B30 – Reference, Gas Oil, Crude Oil, Auxiliary Generators

5.5.2 Combustion Characteristics during B30, HFO & MGO Operation, 4-Stroke Auxiliaries

In this subsection the effect of biofuel use on the combustion characteristics of 4-stroke marine engines is investigated using measurement data to estimate fuel combustion rate as detailed in section 4.2.2. The diagrams presented correspond to the same auxiliary unit as the one presented separately in the above section. As a short note for all the below diagrams a secondary combustion event is observed. This is not actual and is the result of dynamic flow phenomena affecting cylinder pressure measurement. These occur due to the small diameter and relatively long length of the indicator cocks that the pressure sensor is mounted on in conjunction with the high engine rotational speed. This has been investigated in detail using a special layout which allows the mounting of two pressure sensors, one flush mounted and second at the end of the indicator cock. Reference to this issue has also been made by engine makers. Despite this the derived combustion rate provides reliable information for the initial combustion rate, its peak and combustion duration.

In Figure 5-41-a to Figure 5-41-c the estimated combustion rates using MGO, B30 and HFO for 25%, 50% and 75% load are compared. Results from the engine FAT measurements are not included because in the case of auxiliary units the complete cylinder pressure traces are not measured during the factory tests, and only the peak pressure value is recorded with a max pressure meter. As detailed above, peak combustion rate is mostly affected from the LCV of the fuel, the injection rate and the percentage of premixed combustion. For cases with small difference in ignition delay and comparable injection timing, thus similar amounts of premixed fuel, a higher peak burn rate should be observed for MGO, followed by HFO and B30 as was the case in the 2-stroke engines. Higher variation is to be expected due to the 4-stroke engines high rotational speed which affects fuel ignition angle proximity to the TDC. From the HRR traces retarded fuel ignition angle in the case of HFO is observed. The highest difference is found at 25% load, where the HFO ignition delay was very high. This allowed more time for the fuel and air to mix, resulting to intense premixed combustion. This led to significantly higher peak combustion rate value compared to the other two fuels and even the higher loads, as it also surpassed the peak HRR values estimated for 75% load of any fuel. This resulted to high pressure increase due to combustion as shown in Figure 5-36 above and highlights the degree that fuel properties can affect engine operation. Further to the peak HRR values for all loads, the initial fuel burn rate was faster in the case of HFO as shown by the slope of the HRR curve up to peak value. Difference between B30 and MGO combustion progress was rather low, with slightly faster combustion progression in the case of B30 and marginally higher peak burn rate. This contrasts with the 2-stroke engines results that showed almost identical combustion process for all fuels. Studies on the fuel effect show that 4-stroke auxiliary units are sensitive to the effect of different fuel properties mainly due to their fuel injection system behaviour. The fuel supply system performance could be a concern as VSLFO use, as already mentioned, has been found to have a measurable effect on fuel injection equipment of such units.

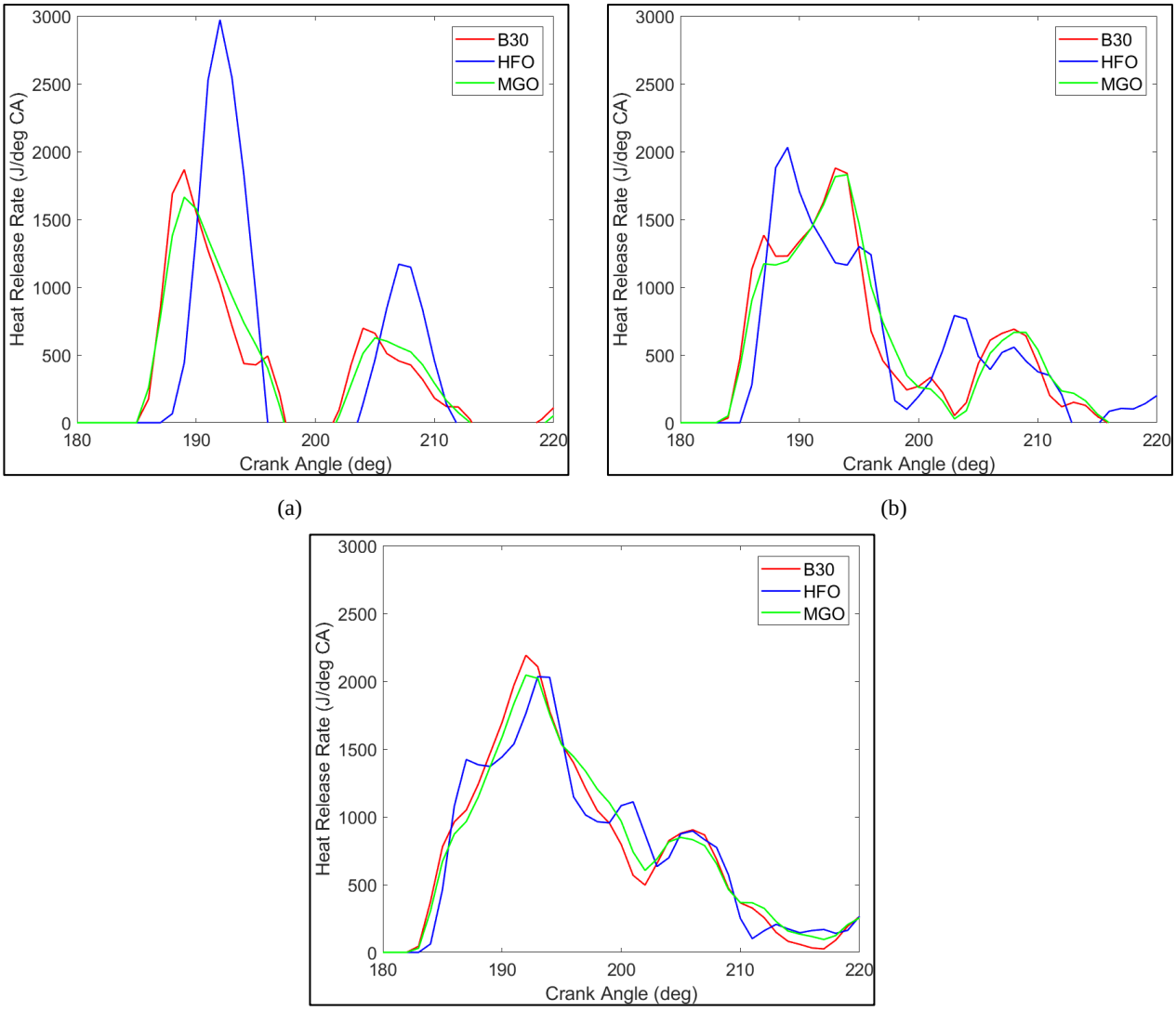

Figure 5-41 Net heat release rate for B30, HFO, MGO; a) 25% Load, b) 50% Load, c) 75% Load

The results for combustion duration are provided in Figure 5-42a and Figure 5-42b. As for the ignition delay these values differ considerably than the corresponding results of the 2-stroke engine section due to the difference in engine speed. Combustion duration for 50% fuel burnt increases with engine load for all fuels. The differences between MGO and B30 are small. For HFO 50% combustion duration was found markedly lower, as expected by the HRR diagrams, attributed to the fuel's higher ignition delay promoting premixed combustion from the point of ignition. A common finding with the 2-stroke engines is that B30 combustion progresses faster than that of MGO while injection angle, ignition delay and ignition angle present minimal differences. The results for 95% burnt fuel amount follow the same trend, however the difference of HFO combustion speed lessens as diffusion-controlled combustion is the primary mechanism when considering total combustion duration and the benefits from the initial (premixed) combustion stage are lessened. The combustion duration findings are important since they confirm that B30 use does not have any significant effect on the progress of the combustion mechanism that could impact efficiency or promote pollutant

formation. Combustion process and combustion duration findings are in line with the BSFC results which were similar.

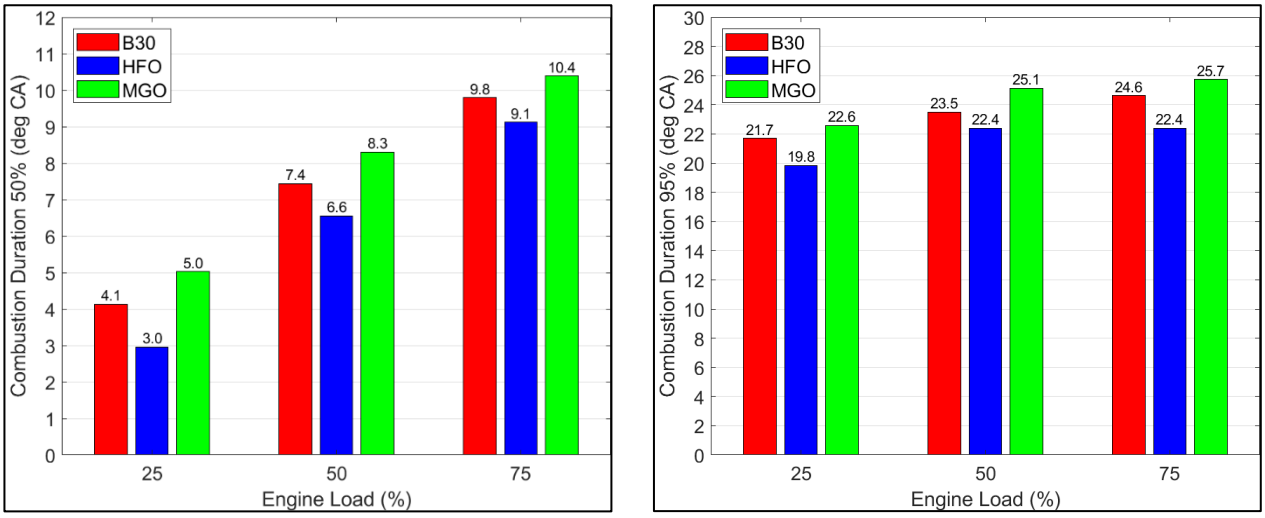

(a) (b)

Figure 5-42 Combustion duration vs Load for B30, HFO, MGO; a) 50% of fuel burnt, b) 95% of fuel burnt; Auxiliary Generator

5.6 Biofuel Effect on NO_x Emissions, 4-Stroke Engines

Specific NO_x emissions were estimated using the measured exhaust gas NO_x concentration, engine power, exhaust gas mass flow rate (from the carbon balance) and the ambient and charge air properties after applying the corrections required by the NTC, (27). Since the engine is Tier-II emission certified operating at steady rpm and used for power generation the D2 cycle total weighted value was calculated using the values from the three load points to verify emission compliance.

The measured NO_x emissions concentration, as measured (dry conditions) is provided in Figure 5-43. It follows a similar trend for MGO and B30 fuels and slightly different for HFO. For the first two a sharp increase is observed from 25% to 50% load and lower increase from 50% to 75% load, while for HFO the NO_x concentration in exhaust gas follows a linear trend. For all cases the peak value is observed at 75% load. HFO NO_x concentration values are the lowest for all loads with the highest difference found at 50% load. For B30 NO_x concentration is the highest, especially at 75% load. Contrary to the 2-stroke engines, for 4-stroke auxiliaries the highest weighting factor values for NO_x emissions are not at 75% load, but at 25% and 50% load. For these load points MGO and B30 NO_x measured emissions are very close. An interesting finding is that NO_x concentration in the case of 25% load HFO test is the lowest, while the very high peak HRR and ΔP values pointed at considerable increase of NO_x formation. However, the later ignition angle is noted. The specific NO_x emissions are provided in Figure 5-44 for all cases. The emissions trend across engine load differs for all fuels due to variation of the exhaust gas flow and the ambient and engine conditions to a lesser extent, as specific values are ISO corrected. The lowest specific NO_x emissions are, as expected by the measured concentration, found in the case of HFO and the highest for B30. The more significant deviation from the two conventional fuels is observed for 75% load. The measured performance data and HRR analysis do show a slight tendency for NO_x increase due to more intense early combustion process and significantly higher pressure increase. On average NO_x emissions for B30 are increased by 6% compared to MGO and by 13.5% compared to HFO. Considering the results from the performance and combustion rate analysis, the increase of NO_x emissions for B30 is partly attributed to its effect on the combustion process that is faster compared to MGO. The most important parameter is its properties and specifically the increased O_2 content (207) and the molecular structure of its carbon content, which has been found to increase NO_x formation, (199). Since NO_x production rate is highly reliant on temperature, the mean temperature of the cylinder charge estimated is provided in Figure 5-45a – Figure 5-45b. Even though this is significantly lower than the local temperature inside the resulting fuel jet where NO_x is formed, (102), (103) its value can be used as an index for the tendency for NO_x formation. The highest peak mean temperature difference is observed for the HFO measurement at 25% load, followed by a steep decline as combustion initiated well after the TDC and consequently during cylinder volume expansion. Despite this peak, the measured NO_x concentration was not adversely affected compared to the other two fuels. For 50% and 75% load, the mean cylinder temperature was highest for B30 or at the same level as for MGO, and the temperature values of the HFO tests were the lowest. Considering this the mean cylinder temperature value, analysis did not provide conclusive information

regarding NO_x formation. However, it provides an indication that for B30 O_2 content is the controlling parameter resulting to NO_x emission increase. Similar to the 2-stroke engines, it is estimated that localized hot spots at the periphery of the fuel where AFR is close to stoichiometric will be the cause for most of the NO_x formation. For the case of B30 these spots will increase in number due to the added oxygen supply which is directly available for NO_x formation. This comment is supported from the results of the theoretical investigation using the muti-zone combustion analysis presented later on.

Considering the total weighted emissions value, Figure 5-46, which is used to test for compliance against the official limit, the overall emissions impact for B30 is approximately 7% increase compared to MGO and 14% against HFO. The increase found for the total weighted NO_x emissions when comparing B30 to crude oil emissions falls within the range of the results conducted by vessel operators and reported in (53) for similar type engines. Overall, the effect on emissions was found more pronounced for the auxiliary unit compared to the 2-stroke engines.

For the tested engine, sufficient margin exists between the total weighted emissions value calculated during the tests and the applicable regulation limit, Tier-II. The borderline criterion for evaluation of B30 NO_x emissions are the guidelines of the NTC, which, as mentioned, allow an additional 10% increase above the applicable limit for on-board measurements (27). This margin further increases by a flat 5% when testing crude oil grade fuels, (27). Considering the findings of this study and the findings published by vessel operators (53), B30 and similar blends can be safely used in similar engine designs without increased risk provided that engine operation is normal.

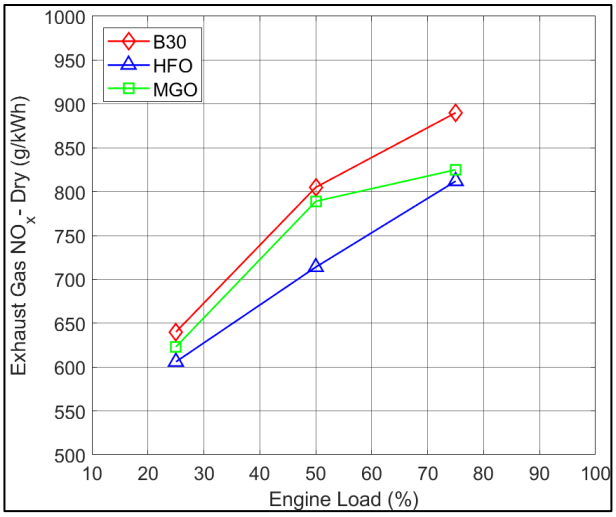

Figure 5-43 Measured exhaust gas NO_x concentration (ppm) vs Load for B30, HFO, MGO; dry conditions; Auxiliary Generator

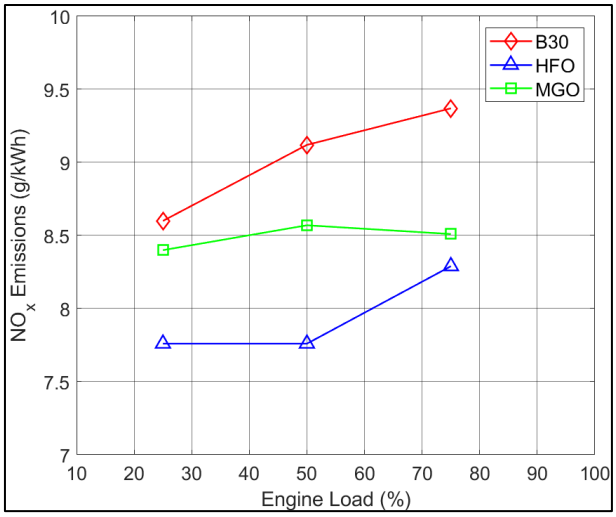

Figure 5-44 Specific NO_x (g/kWh) emissions vs Load for B30, HFO, MGO, reference; Auxiliary Generator

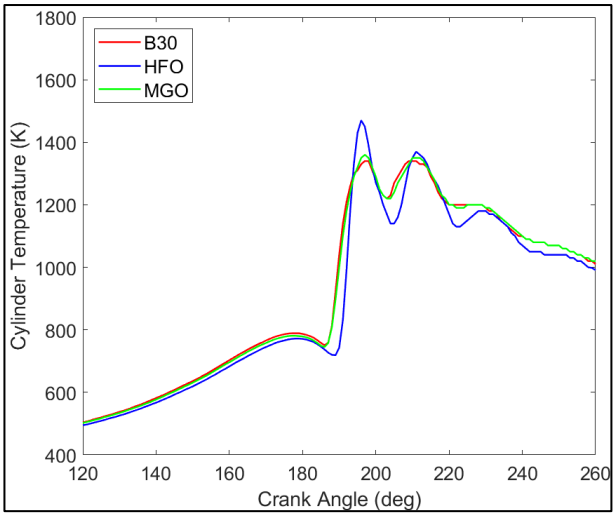

(a)

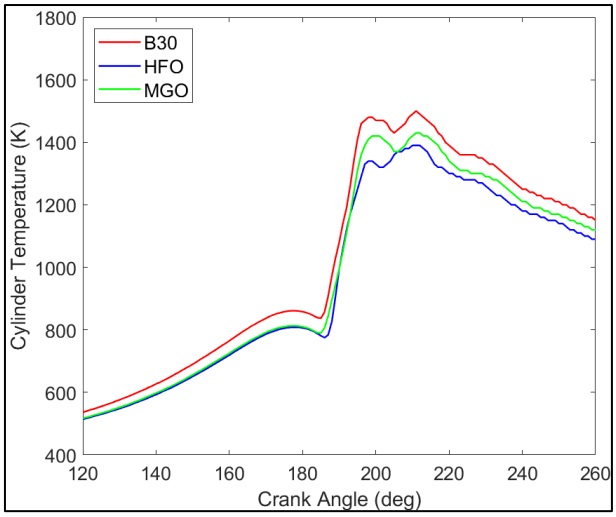

(b)

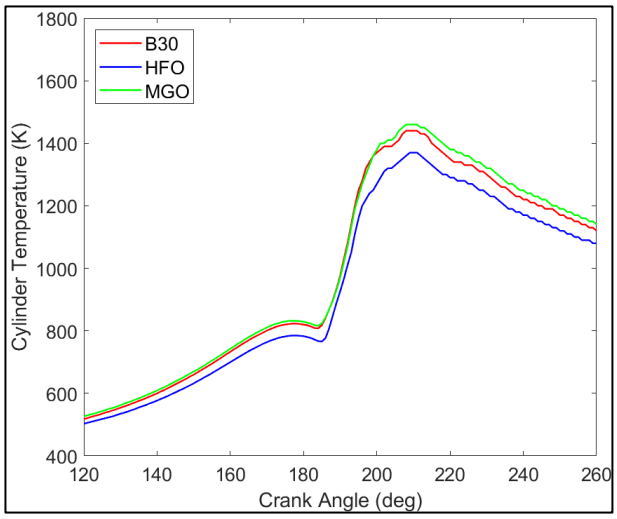

(c)

Figure 5-45 Cylinder mean charge temperature for B30, HFO, MGO; a) 25% Load, b) 50% Load, c) 75% Load; Auxiliary Generator

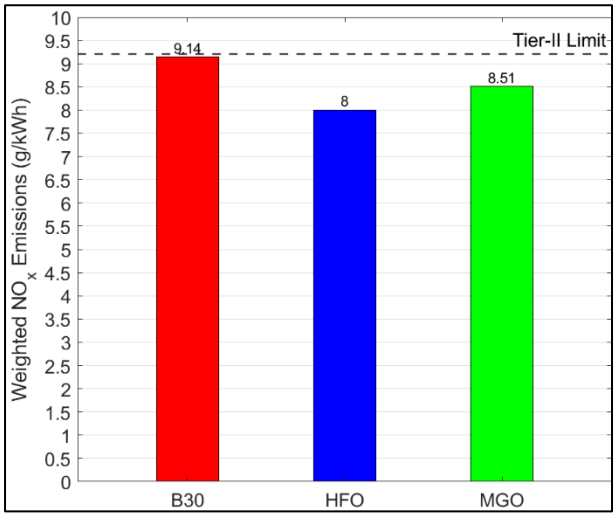

Figure 5-46 NTC E3 Cycle weighted total NO_x value, B30, HFO, MGO; Auxiliary Generator

Regarding the total number of auxiliary units tested, performance analysis results revealed NO_x emissions both below and above reference, as P_{max} and ΔP, which are major contributors to NO_x formations, varied significantly against reference. In Figure 5-47 the NO_x emissions comparison statistical summary is provided. Lower specific NOx emissions values were found compared to reference for most of the engines examined. In contrast, comparison with trials using MGO and crude oil showed higher NO_x emissions for B30 operation. The total weighted emission value was on average 5% lower than reference for B30 tests. The median was close to 0%, showing that for most generators NO_x emissions using B30 were similar to reference. The variation between median and average was mostly the result of the lower and minimum values of Figure 5-47. Examining Table 5-7 these coincide with the engines that reported some of the lowest P_{max} values depicted in Figure 5-39. This finding makes clear the importance of engine tuning regarding NO_x emissions, which can be more important than fuel effect as is also established in (205). Tests at present conditions, however, showed that for B30 total NO_x emissions were increased by 6% – 15%, on average 10%, compared to MGO and were mainly affected by the high NO_x formation at 75% load. This increase is above the findings of the 2-stroke engine tests and is close to values reported in other studies for these engines (175,197). Comparison to the crude oil tests presented rather even distribution of B30's effect, with the mean and median values being practically identical except for 25% load. The average total NO_x emissions increase for B30 was 2.4% compared to crude oil operation, albeit with high variance as values in the range of ±10% were recorded. The upper values of NO_x increase were generally higher than those for 2-stroke engines. Overall, a tendency for increased NO_x formation during B30 use was confirmed despite the P_{max} and ΔP values being generally lower. The enhanced NO_x formation is consequently attributed to the higher O_2 content of the biofuels used. Considering the results of this and other experimental works' results, especially (53) that focuses on marine engines, for auxiliary 4-stroke generators B30 use will only moderately affect NO_x emissions, allowing compliance with emission limits. In addition, it is confirmed that engine tuning can be used to further decrease impact, possibly allowing use of even higher percentages of biodiesel.

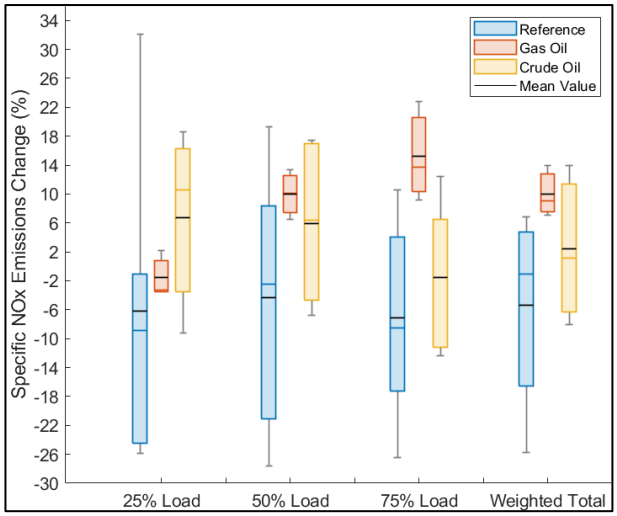

Figure 5-47 Specific NO_x Emissions Comparison, B30 – Reference, Gas Oil, Crude Oil, Auxiliary Generators

Table 5-7 Auxiliary Generators B30 Comparison Summary

	Auxiliary Generator 1				**Auxiliary Generator 2**			
Spec. Emissions (%)	25% Load	50% Load	75% Load	Total Weighted	25% Load	50% Load	75% Load	Total Weighted
Reference	-13.12	1.45	10.59	3.86	-1.06	-6.30	-8.54	-6.34
Gas Oil	2.15	6.55	9.18	7.03	-	-	-	-
Crude Oil	10.62	17.40	12.44	13.97	-9.23	-3.99	-10.80	-8.11
Pmax								
Reference	-2.50	-8.10	-19.50		-2.60	-11.30	-16.60	
Gas Oil	0.90	2.90	4.00		-	-	-	
Crude Oil	-5.40	3.80	3.80		-2.10	-7.50	-5.20	
ΔP								
Reference	1.90	-3.20	-5.60		-4.40	-12.60	-19.40	
Gas Oil	0.40	1.50	2.90					
Crude Oil	-5.60	5.10	3.30		-3.40	-8.00	-4.60	
	Auxiliary Generator 3				**Auxiliary Generator 4**			
Spec. Emissions (%)	25% Load	50% Load	75% Load	Total Weighted	25% Load	50% Load	75% Load	Total Weighted
Reference	32.13	8.37	-1.49	6.82	-4.52	-	5.87	5.11
Crude Oil	18.60	-6.76	-12.33	-5.69	-	-	-	-
Pmax (bar)								
Reference	1.70	-1.10	-1.70		8.70	-	14.30	
Crude Oil	-1.00	-5.50	-3.30		-	-	-	
ΔP (bar)								
Reference	-8.10	-17.00	-20.50		8.70	-	16.30	
Crude Oil	-2.90	-9.00	-7.50		-	-	-	
	Auxiliary Generator 5							
Spec. Emissions (%)	25% Load	50% Load	75% Load	Total Weighted				
Reference	-	19.35	-10.41	-1.90				
Pmax (bar)								
Reference	-	18.70	8.60					
ΔP (bar)								
Reference	-	19.20	-3.30					
	Auxiliary Generator 6				**Auxiliary Generator 7**			
Spec. Emissions (%)	25% Load	50% Load	75% Load	Total Weighted	25% Load	50% Load	75% Load	Total Weighted
Reference	-24.45	-21.11	-19.50	-19.98	-25.83	-27.57	-26.40	-25.75
Gas Oil	-3.52	10.08	13.70	9.08	-3.29	13.36	22.84	12.97
Crude Oil	-1.64	6.34	-1.58	1.12	15.56	16.75	4.43	10.58

5.7 Theoretical Analysis for B30 Effect on 2-Stroke Engine Performance and Emissions Using a Multizone Combustion Model

As noted in the introduction, the investigation of biofuels use is of major importance for 2-stroke engines. The reason is that for these engines exists limited information in the literature. In the present section the results derived from the application of the multizone model described above are presented to provide further context on the biofuel's effect on engine performance and mostly on the combustion process and NO_x formation. For this purpose, the multizone model was modified to consider for the effect of fuel properties (density, heating value and composition) and mainly oxygen content. The engine selected for the computational investigation was "Engine 1" of the experimental findings section.

Before applying the specific model for the biofuel effect analysis, it is necessary to validate its predictive ability regarding global engine performance, cylinder pressure and NO_x emissions. In addition, it was necessary to calibrate the simulation model and then apply it for all cases examined without any modification of its constants in order to have actual "predictions". For the calibration and validation, it was decided to use the available shop test data that include engine performance, cylinder pressure and other data from the official engine NO_x file which also provides data for air and exhaust gas mass flow rate.

Following this, simulation results are generated and presented in detail for engine performance. Information is provided for the effect of fuel properties on temperature and O_2 concentration inside the fuel jet and its evolution with crank angle. Furthermore, information is also provided for the NO_x formation history.

5.7.1 Model Validation: Conventional fuel results

As the first part of the numerical investigation with the multizone model the engine performance during reference operation, was replicated. All loads available in the official FAT tests were considered, 25%, 50%, 75 and 100%. This followed multizone combustion model calibration which involved the following parameters:

1. Air entrainment correction coefficient which affects the peak pressure values.
2. Estimation of EVC variation to match the measured P_{comp} values.
3. Turbine effective flow to match the measured exhaust manifold pressure.
4. Scavenging model calibration to match exhaust manifold mean exhaust gas temperature and measured mass flow rate.
5. Estimation of SOI and EVO settings at all loads corresponding.
6. NO_x scaling factor.

Following this, model constants were retained the same, and most importantly for constants 1, 4 and 6 the values were maintained the same regardless of engine load. After completion of the calibration procedure for which was used a newly developed automated process, the FAT results were reproduced, and the predicted

values were compared with measured data. In the following part, for the sake of space, detailed results are provided for 25% and 75% load.

The pressure trace results provided in Figure 5-48 and Figure 5-49 below are for MGO reference operation, at 25% and 75% load. As shown, the calculated pressure traces provide a close match to the measured ones. The same was found for the other load results. For further validation the measured and calculated power were compared and the same was conducted for the BSFC. The comparison findings are given in Figure 5-50 and Figure 5-51 with very good agreement for brake power and good overall coincidence of calculated and measured values for specific fuel consumption. The NO_x emissions were calculated for the Shop Test measurement data and good agreement was found as shown in Figure 5-52 with acceptable deviation at 50% and 100% load. Most importantly, the trend of the values with load is properly predicted. Due to its importance in the overall calculations the model estimation of the exhaust gas mass flow rate is compared to the results of the carbon balance method using measured CO_2 concentration in the exhaust gases. As shown in Figure 5-53 minimal level of error is found between measured and calculated values.

The simulation model provides information for the combustion rate of fuel through the net heat release rate. The estimated net heat release rate is given in Figure 5-54 for all loads examined. As observed, the more intense initial increase occurs at 25% load, while the peak increases with engine load at a lower rate.

Following comparison of the calculated and measured pressure data the NO_x emissions formation history is examined. In Figure 5-55 is provided the NOx in-cylinder formation. NOx is shown to slightly decrease after its peak and then freeze revealing that its formation is kinetically controlled. As revealed, NO_x formation takes place in the early stages after ignition. In Figure 5-56 is provided additional information for NO_x formation with the percentage contribution of each zone package (their total number is equal to the fuel injection duration considering a 1^o CA time step) to the total NO_x formed. The number of zones depend on the injection event duration and increases for higher loads and fuel amount. As observed, according to the model calculations the highest percentage of NO_x is formed in the first zones. This is considerably increased for lower loads, which is normal as fewer zones are considered due to much shorter injection duration. For longer injection duration, after the first few zones the contribution to total NO formed shows a tendency for stabilization.

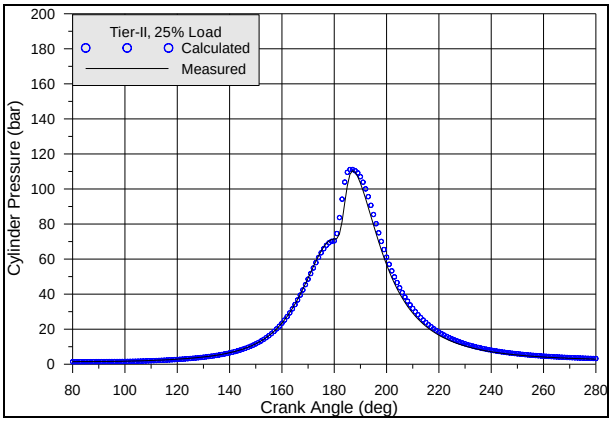

Figure 5-48 Comparison between measured and calculated pressure traces, Reference Measurement 25% Load

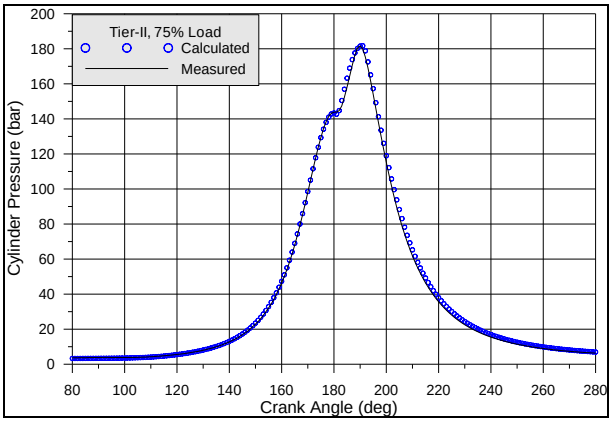

Figure 5-49 Comparison between measured and calculated pressure traces, Reference Measurement 75% Load

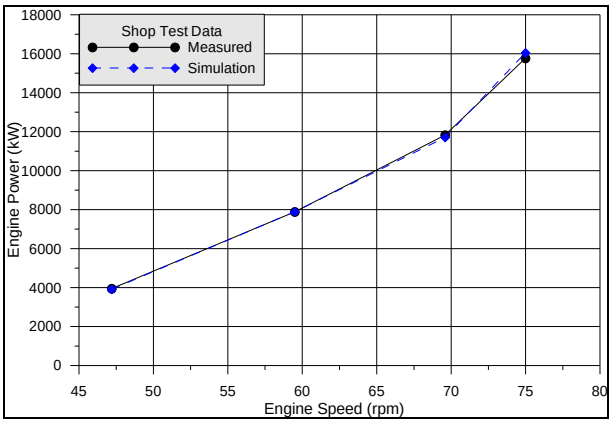

Figure 5-50 Calculated and measured power comparison, reference measurements

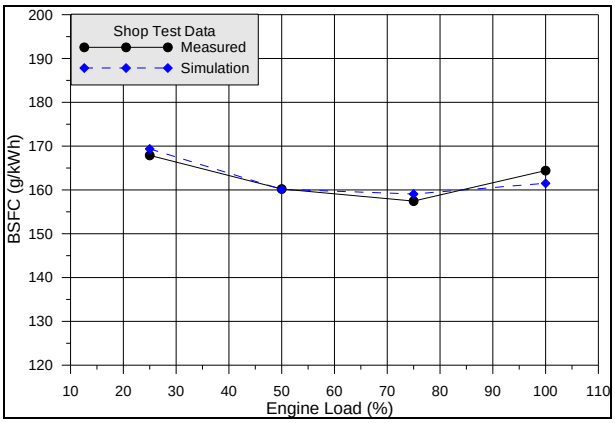

Figure 5-51 Calculated and measured bsfc comparison, reference measurements

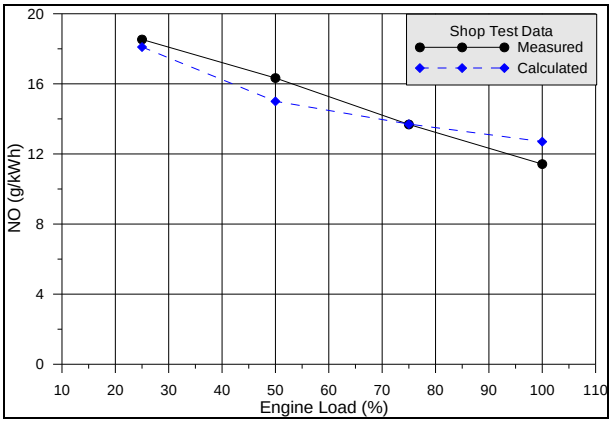

Figure 5-52 Calculated and measured NO_x specific emissions comparison, reference measurements

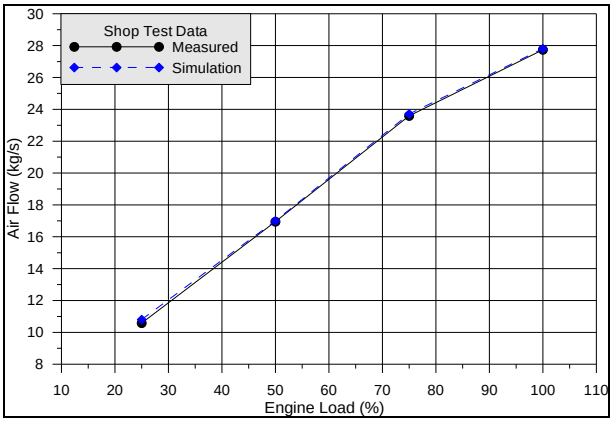

Figure 5-53 Calculated and measured exhaust gas flow rate, reference measurements

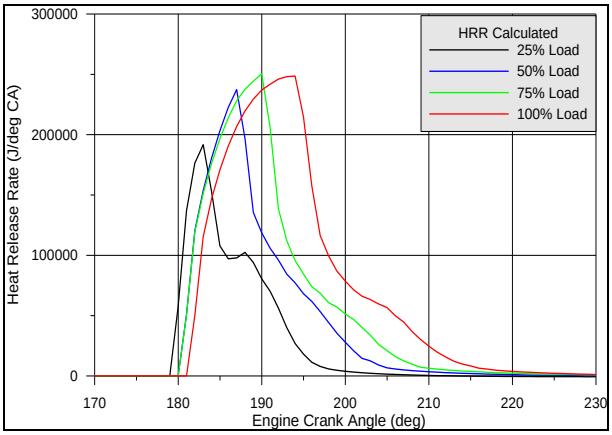

Figure 5-54 Calculated net heat release rate, all loads reference measurements

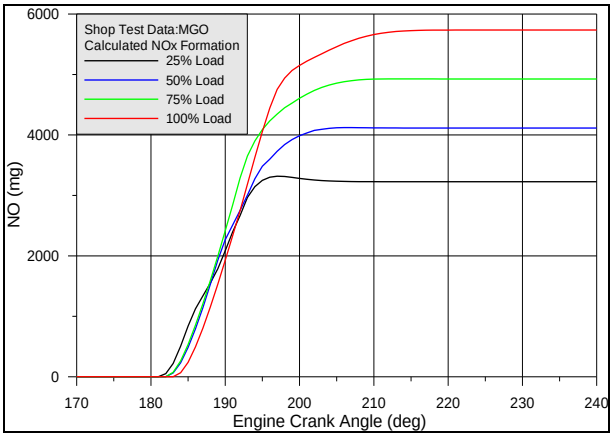

Figure 5-55 Calculated NO formation history, all loads reference measurements

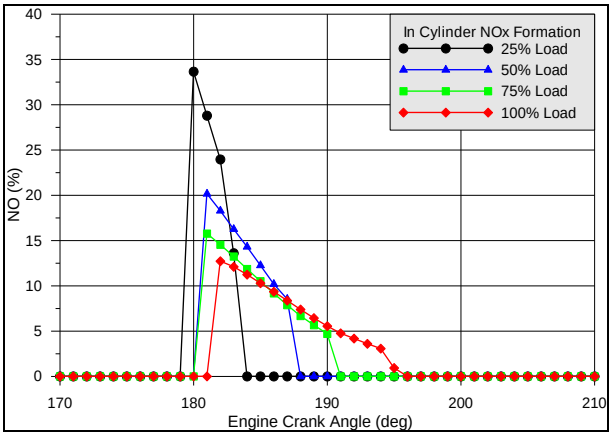

Figure 5-56 Estimated zone group contribution to NO emissions, all loads reference measurements

5.7.2 Computational results for Biofuel Operation

In the present section are compared model predictions against measurements for the trials conducted using HFO and B30. Results were generated also for MGO but are omitted due to space constraints. In Figure 5-57 and Figure 5-58 is provided the comparison of the measured and calculated cylinder pressure traces for the on-board HFO testing for 25% and 75% load. It is noted that no additional model calibration or constant tuning was applied following initial calibration. The calculated results are very close to the actual measurements. This revels the ability of the model to consider for the effect of B30 on the combustion mechanism and reveals that the results for the in-cylinder NO_x formation and temperature history are reliable and trustworthy. The same is found for the B30 calculations, Figure 5-59 and Figure 5-60 at the same loads.

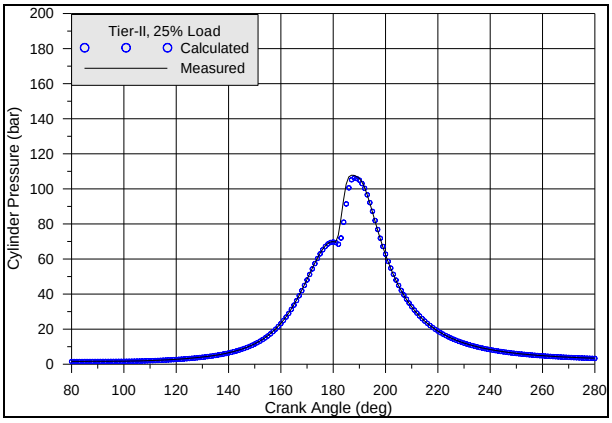

Figure 5-57 Comparison between measured and calculated pressure traces, On-board HFO Measurement 25% Load

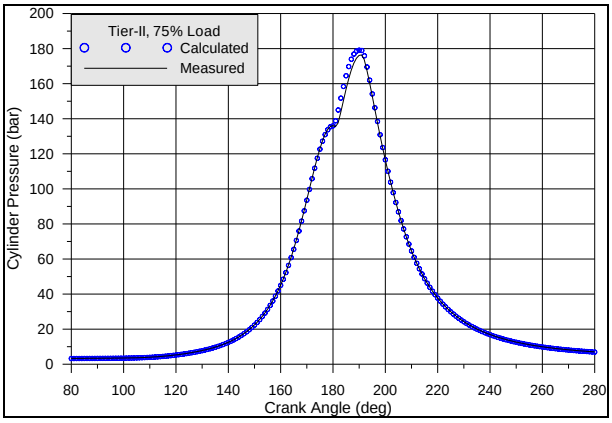

Figure 5-58 Comparison between measured and calculated pressure traces, On-board HFO Measurement 75% Load

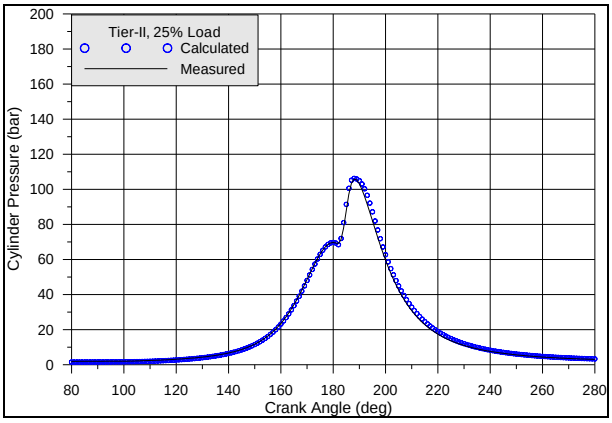

Figure 5-59 Comparison between measured and calculated pressure traces, On-board B30 Measurement 25% Load

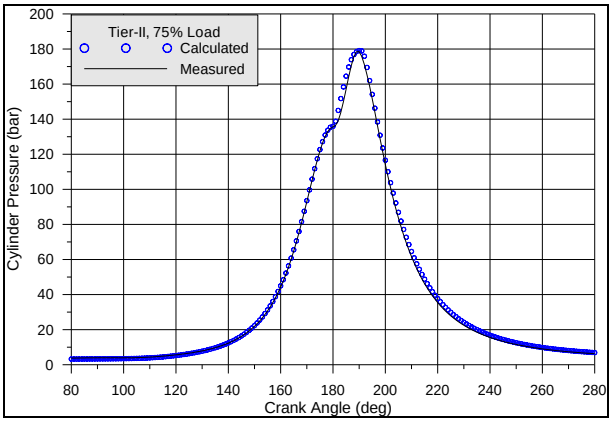

Figure 5-60 Comparison between measured and calculated pressure traces, On-board B30 Measurement 75% Load

Of significant importance is the model's ability to predict the effect of B30 on NO_x emissions. In the following are presented results for total specific NO_x emissions, as well as for their in-cylinder formation history for both HFO and B30 in. The specific NO_x values for each load calculated for HFO and B30 operation are given in Figure 5-61 with the values of B30 being moderately increased compared to HFO operation. The highest increase is observed at 25% load, which coincides with the trend observed in the measurement data. The corresponding NO formation history is provided in Figure 5-62 for both fuels, HFO

and B30. As observed, for both fuels NO_x freezes later with increasing load while the slope of NO_x formation remains fairly the same and the B30 emissions are higher.

The corresponding result for the zone contribution to final NOx formation is provided in Figure 5-63 for all three loads (25%, 50%, 75%) for HFO and B30. A new group of zones (in the circumferential direction) is formed for every computational time step. The total number of zones is defined from the injection duration and is variable. The percentage contribution of each package of fuel to the final NO formed is used to understand which part of the injected fuel contributed most to NO_x formation. Small differences are observed, with the most interesting being lower contribution values for all zones during B30 calculations. The difference in the X-Axis (engine crank angle) is attributed to the differences in SOI. This shows that in the case of B30 the contribution of all zones is more even than in the case of HFO and that the contribution of the late formed zones is higher. From the analysis of the jet history, O_2 and temperature distribution inside the fuel jet, it appears that this is the result of the oxygen contained in the biofuels that improves the fuel air ratio in the burning zone at the stages when the combustion products have reached significant concentration decreasing O_2 availability. The net HRR calculated by the model is given in Figure 5-64 that shows minimal differences between the two fuels for all loads, as should be the case considering the combustion analysis results from the measured cylinder pressure traces. The average fuel jet temperature (mean burnt zones temperature) is compared between the B30 and HFO tests in Figure 5-65 for 25% load and in Figure 5-66 for 75% load. As can be observed the mean burn zone temperature is lower for B30 in both cases indicating to lower tendency for NO_x formation. This reveals that the increase of NO_x emissions observed for B30 is attributed to the presence of O_2 inside the combustion zones that is directly available for combustion and reaction with local N_2 resulting to the increased NO_x formation, and not to temperature increase by more intense combustion. As already established from Figure 5-63 depicting zonal contribution to NO_x formation, the effect of the O_2 in the fuel can be quite prevalent after high combustion product concentration is reached and the entrained O_2 is consumed for combustion. In the case of a low oxygen fuel these conditions would lead to a very low air fuel ratio and drastically inhibit NO_x formation. The average percentage of oxygen available in the fuel jet should also be compared. Because operating conditions, settings and heating value are not the same for the tested fuels, a separate analysis is conducted using biofuel and an a theoretical HFO fuel variant with the same properties, except minimal O_2 content, as the 1.8% content of the use HFO was rather high. This allows to better demonstrate the difference of biofuel's O_2 content. The results for the O_2 concentration inside the fuel jet are given in Figure 5-67 and Figure 5-68 for the same loads, 25% and 75%. Following 5^o CA after ignition, the oxygen trapped in the fuel has been consumed and the entrained air O_2 content remains higher in the case of B30 but NO_x formation is still on-going and enhanced by the higher O_2 availability. Last, in Figure 5-69 to Figure 5-74 the distribution of fuel-air equivalence ratio, temperature and NO inside the fuel jet is provided for B30 and the low oxygen HFO fuel for 50% load simulated operation at the same conditions and 5^o CA after injection. Clear and significant reduction of the fuel-air ratio is found inside the fuel jet for the B30 calculations due to its O_2 content. As mentioned, O_2 presence should be quite limited in the inner jet areas and this is indeed observed for the HFO calculations. The increase of O_2 availability led to higher localized

temperature values inside the jet in this case as it drives combustion. The difference compared to Figure 5-65 and Figure 5-66 (lower temperature for B30) is due to the use of same conditions in this second set of calculations and also setting a lower O_2 content for HFO, as the 1.8% actual content of the tested fuel was rather high. The use of the simulation model allows to examine the actual effect of the O_2 content on combustion rate and NO_x formation since it is possible to isolate for the previous differences, engine settings and O_2 content of HFO. From the NO_x concentration in Figure 5-73 and Figure 5-74, it is shown that the increased O_2 availability and also temperature led to the much higher NO values. As expected, the higher NO_x values are formed in the jet periphery where fuel air equivalence ratio is close to stoichiometry being slightly fuel lean.

Considering the previous the rather mild increase of NO_x emissions with B30 is explained and is attributed to the combined effect of temperature and O2 availability. Specifically, the trend for NO increase due to increased fuel O_2 content is partially counteracted by the temperature decrease that results from fuel reduced heating value.

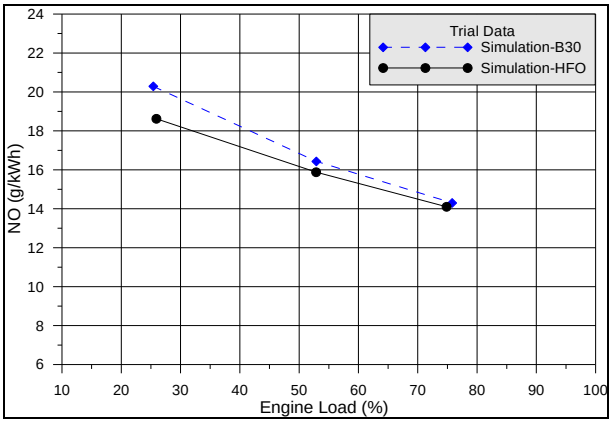

Figure 5-61 Comparison of calculated NO emissions, all loads on-board HFO and B30 operation

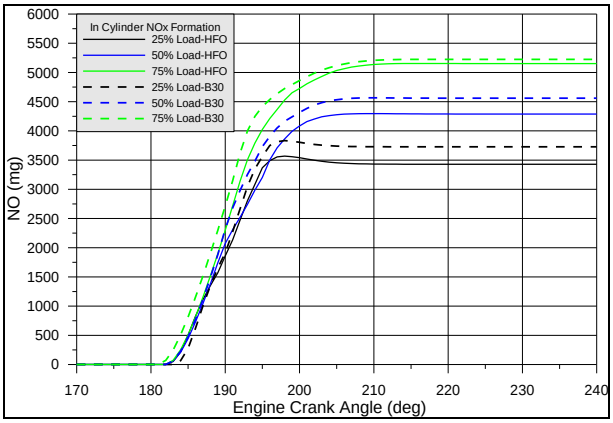

Figure 5-62 Calculated NO formation history, all loads, HFO and B30 operation

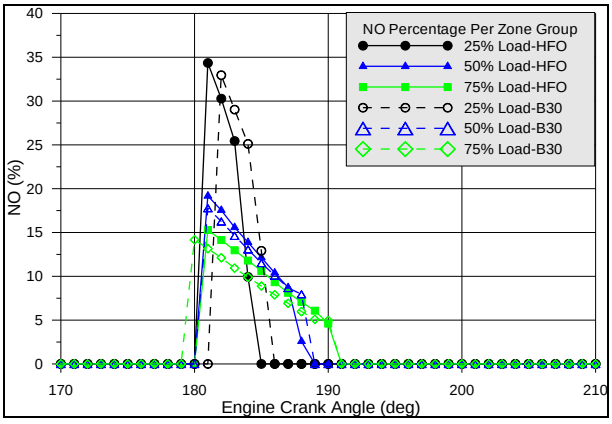

Figure 5-63 Calculated zone contribution to NO emissions, all loads on-board HFO and B30 operation

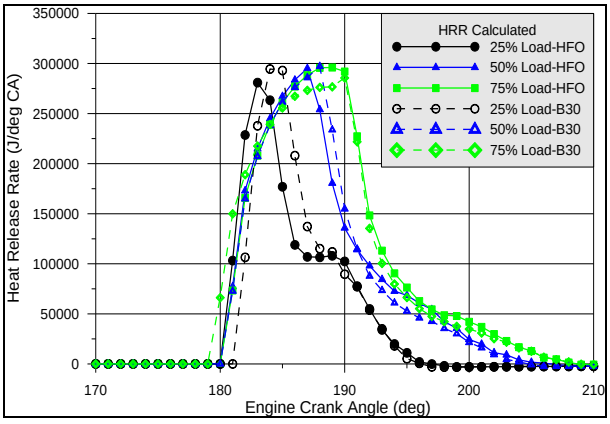

Figure 5-64 Calculated net heat release rate, all loads on-board HFO and B30 operation

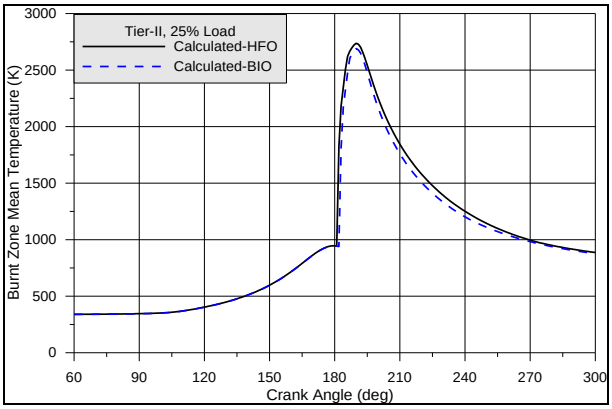

Figure 5-65 Calculated burn zone mean temperature, 25% Load on-board HFO and B30 measurements

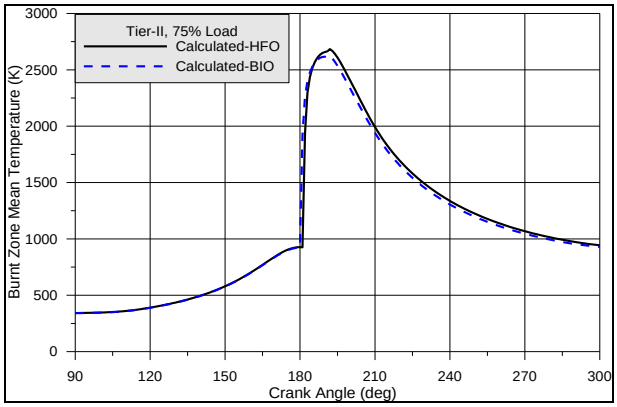

Figure 5-66 Calculated burn zone mean temperature, 75% Load on-board HFO and B30 measurements

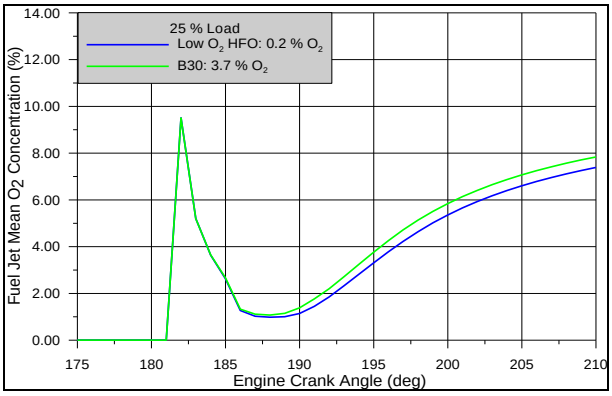

Figure 5-67 Mean oxygen concentration in fuel spray for HFO & B30 operation, same conditions & LCV; 25% load

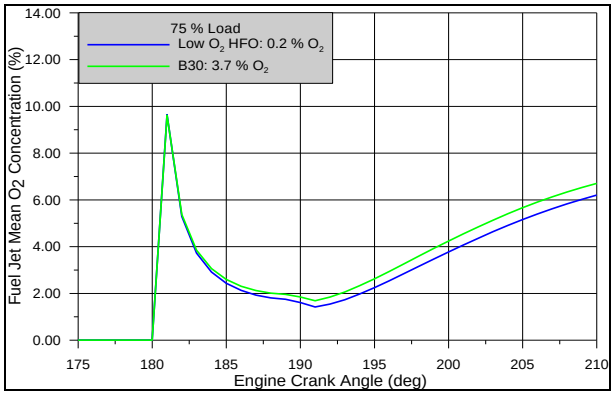

Figure 5-68 Mean oxygen concentration in fuel spray for HFO & B30 operation, same conditions & LCV; 75% load

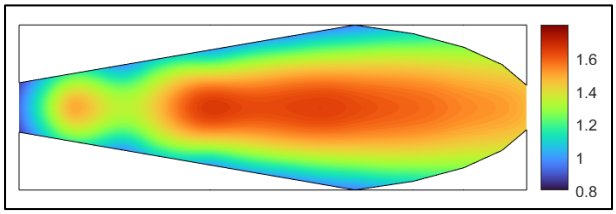

Figure 5-69 Fuel-Air Equivalence ratio distribution in the jet area 5deg CA after injection, 50% load, B30

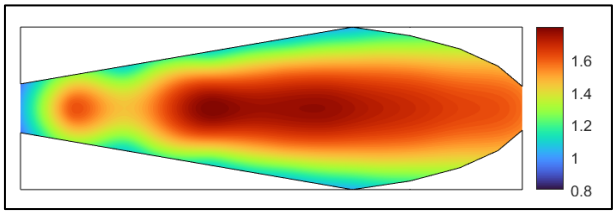

Figure 5-70 Fuel-Air Equivalence ratio distribution in the jet area 5deg CA after injection, Low O_2 HFO

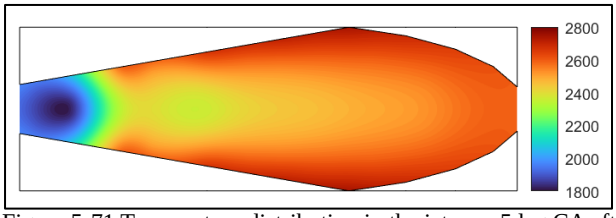

Figure 5-71 Temperature distribution in the jet area 5deg CA after injection, 50% load, B30

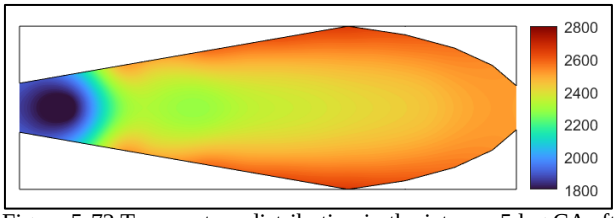

Figure 5-72 Temperature distribution in the jet area 5deg CA after injection, Low O_2 HFO

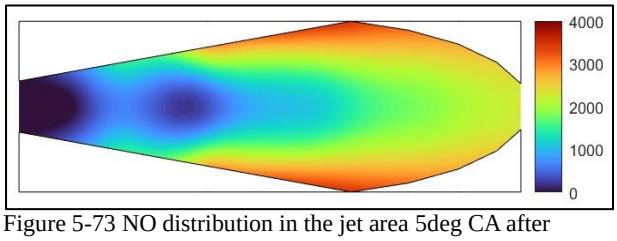

Figure 5-73 NO distribution in the jet area 5deg CA after injection, 50% load, B30

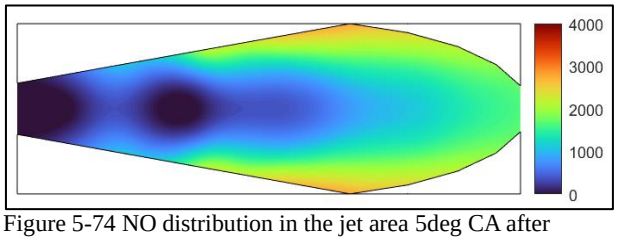

Figure 5-74 NO distribution in the jet area 5deg CA after injection, 50% load, Low O_2 HFO

5.8 Summary and Conclusions

The effect of biofuel blends on marine 2-stroke propulsion and 4-stroke auxiliary power generation engines was reviewed using results of various available studies and an extended experimental campaign conducted aboard marine vessels using B30. For certain units detailed analysis was performed examining the combustion process for each tested fuel, B30, MGO and HFO or VLSFO. The literature review revealed that for 2-stroke low-speed propulsion engines, limited experimental data are available from full-scale applications. Specifically, (194) from early 2022 states to be the only peer-reviewed study to contain such information at the time of writing. Following this (53) containing results of tests conducted by various vessel operators was published that contained data for both 2-stroke and 4-stroke marine engines. The literature review survey revealed that other available results are mainly from lab tests conducted for heady-duty diesel engines used for automotive applications. Furthermore, in most evaluations the basis for comparison was distillate diesel fuel while in the marine sector crude oil variants such as HFO and VLSFO are commonly used. Common findings of published studies were increased fuel consumption, attributed to the biodiesel blends lower LCV, decreased fuel ignition delay and less intense premixed combustion because of the earlier ignition. These resulted to either increased or decreased NO_x emissions during biofuel use on a case-by-case basis, with the end effect being the result of several factors. A common conclusion was that O_2 content of biofuels enhances NO_x formation and the combination of injection angle, ignition delay and fuel LCV, either contribute to or work against this increase. The extended experimental review conducted using measurements on-board five maritime vessels provided important information in the scarcely studied subject of the 2-stroke engines and additional important data for the performance and emissions of marine 4-stroke generators for biofuel, marine diesel (gas oil) and typical crude oil operation.

The experimental review showed that B30 use had measurable impact on tested engines performance. ISO corrected BSFC was increased when using B30 for both the 2-stroke and the 4-stroke engines when comparing to the trials conducted with MGO and crude oil at the present engine state. For the 2-stroke engines the average efficiency penalty was slightly over 1% compared to MGO while no increase was found compared to crude oil. The respective differences for 4-stroke engines were 3% and 1% revealing slightly higher biofuel effect. For the performance data high variance was found when conducting comparisons of B30 operation against reference, especially in the case of P_{max} and ΔP, as the reference tests were not conducted under same conditions and probably engine state. For the trials conducted with B30 and crude oil or MGO at the present state variance was significantly lower. Overall, a tendency for lower P_{max} and ΔP values when using B30 was found for both the 2-stroke and the 4-stoke engines. The cases of detailed analysis also presented further insight on the effect of each fuel type on engine performance and the combustion process. For the two 2-stroke engines and 4-stroke generator examined in detail lower ignition delay for B30 was confirmed, as expected by the available literature and the CN/CAAI numbers measured. This is important for minimization of its effect on cylinder pressure and NO_x formation. The HRR analysis of the 2-stroke engines' measurements showed mostly similar initial fuel combustion rate for MGO, HFO, VLSFO and B30 for the 2-

stroke propulsion engines. The peak burn rate of B30 was found consistently slightly lower due to the decrease in LCV caused by the addition of biodiesel. Further to the result of the fuel's lower energy content this is also attributed to the shorter ignition delay. Combustion duration was found slightly prolonged for MGO. Values for B30 and VLSFO were almost identical, and the lowest combustion duration was measured in the case of HFO.

In the case of the 4-stroke auxiliary unit the effect of fuel type on combustion was more pronounced than for the 2-stroke engines. B30 combustion was similar to the MGO data, while for HFO high ignition delay resulted to considerably faster early (premixed) combustion especially for 25% load. The highest peak combustion rate was observed for HFO followed by B30 despite its lower LCV compared to MGO. Combustion duration was, as observed for the 2-stroke engines, longer for MGO operation and shorter for HFO operation. The HFO values were the only ones to present considerable difference. As the combustion process was found very close to that of conventional fuels the main contributor to NO_x emissions is the added O_2. This promotes NO_x formation by increasing oxygen availability at localized hot spots inside the combustion chamber and in some cases also affecting the local temperature.

To further investigate and understand the mechanisms related to B30 effect on performance, combustion and NO_x emissions a multizone model was utilized to study a 2-stroke low-speed main propulsion engine which is the most important contributor for both CO_2 and NO_x emissions. Further motivation for selecting the 2-stroke engine was the fact that very limited information exists for the actual B30 effect on these engines. The measured data during operation on HFO, MGO and B30 was replicated in the model with very good accuracy. The comparison concentrates on B30 and HFO, but similar results were obtained for MGO. Review of the results obtained for the distribution of properties, mainly temperature, and species, predominantly O_2, in the burnt zone confirmed that the main factor driving NO_x formation increase during B30 operation was the increase of local AFR. The difference compared to low oxygen content fuel was more prevalent in the mid and late stages of combustion and in spots closer to the inner volume of the burn zone where oxygen concentration tends to decrease considerably. In addition, the specific CO_2 emissions for B30 were examined. These were slightly lower compared to HFO due to its lower carbon content but higher compared to MGO. Based on the B30 fuel carbon content, up to 4.5% lower specific CO_2 emissions would be expected compared to MGO. However, the beneficial effect of the biofuel's carbon content was offset by its lower calorific value and thus the increased consumption. Based on this the GHG reduction benefits of the B30 use will be restricted to the well-to-tank part.

The emission measurements revealed NO_x increase for B30 compared to MGO and crude oil for most engines. This applied to both 2-stroke and 4-stroke engines. For the 2-stroke engines B30 total NO_x emissions compared to crude oil and MGO are increased, mostly in the range of 1% – 8%, with a 4% average value. Comparison between MGO and crude oil could not be safely made as only two engines were tested using MGO and provided significantly varied results and are thus treated only as indications. In the case of the 4-stroke engines the total B30 emissions were considerably higher compared to MGO and only slightly increased compared to crude oil, the average values being 10% and 2.4% respectively. In addition, for the 4-

stroke engines tests with B30 and crude oil also resulted to one case with emissions reduction close to 8.1% in favour of the biofuel. The detailed analysis for the two 2-stroke engines and the auxiliary unit allowed to estimate the effect of combustion characteristics to the NO_x emissions and better assess the effect of the biodiesel increased oxygen and different carbon structure.

It is noted that the differences found compared to the MGO tests were also partly the result of the crude oil used in the B30 blending, as high difference was also observed between the MGO and crude oil tests.

Considering published studies (53,194) for 2-stroke propulsion marine engines the reported results all fall within the range of values produced by the current experimental campaign. This also applies for the high NOx emissions increase at 25% load for most engines which is also reported in some of the applications studied in these works. However, due to the high variance between tested engines safe conclusions regarding biofuel effect and load cannot be made with the published dataset. The 4-stroke generator tests also showed considerable deviation between units tested even for same type engines, when comparing against reference. The values were in the range of those reported in the other major study of marine auxiliary generators (53). It was also verified that the cases presenting the highest change in emissions showed similarly high deviation in terms of peak pressure and pressure increase. This proved that engine performance is of outmost importance for emissions.

Overall, regarding biofuel effect, the multiple engines studied along with other investigations published provide sufficient support to conclude that in cases of similar operation the particularities of biofuel, mainly the O_2 content, tend to enhance NO_x formation. The level of NO_x increase for normally operating marine 2-stroke engines when using B30 is 2 - 4% compared to commonly used crude oil and the increase is slightly higher for 4-stroke auxiliary units. Thus, only a small to moderate NOx increase should be expected when using B30.

The analysis highlighted aspects to be considered for further research especially when factoring in the need for wider biofuel adoption, and possibly at higher percentages of FAME content. It is noted that such studies would require a substantial level of preparation and co-operation with ship owners if to be conducted on board. The process would be easier in the case of auxiliary generators that can also be found on land installations and are easier to test during normal vessel operation. The need for further research is more prevalent for 2-stroke engines, for which biofuel studies are limited. Minimal data are also available for older engine designs that lack electronic control systems so the level of variance in performance and emissions should be investigated. Another important aspect for future research is the long-term effect of biofuel blends on engine components and especially the engine injection system.

Chapter 6 In-Cylinder NOx Emissions Reduction Technologies: Exhaust Gas Recirculation

6.1 Exhaust Gas Recirculation in Marine Engines

EGR is one of the most widespread solutions for NO_x emission reduction in IC engines and is well established in the automotive industry. Its operating principle targets both temperature and oxygen availability in the cylinder, (232). A portion of the exhaust gases is collected and circulated back into the scavenge air receiver following a cooling and cleaning process. The ratio of recirculated gas to total mass flow varies and can surpass 50% in some applications, (233). The replacement reduces O_2 concentration in the cylinder charge. The lower O_2 availability impedes nitrogen oxidation lowering NO_x formation. An additional effect is that the species contained in the recirculated gases are mostly not combustible and have higher heat capacity then air, (234). This results to lower combustion temperatures further decreasing NO_x formation, via thermal NO_x reduction. Dissociation of recirculated combustion products i.e., CO_2 and H_2O also contributes towards this direction. Despite the benefit regarding NO_x emissions, the use of EGR also introduces some negative effects. Soot formation may increase (235), as high recirculation ratios tend to increase soot formation, due to the limited O_2 available for soot oxidation. Another adverse effect is that combustion rate decreases, lowering the engine operating efficiency and increasing fuel consumption, (236). These effects can become even further pronounced in cases where EGR use is coupled with retarded fuel injection timing, (237). An example of the various effects expected by EGR use at various recirculation rates is given in Figure 6-1 below for IC engines in general.

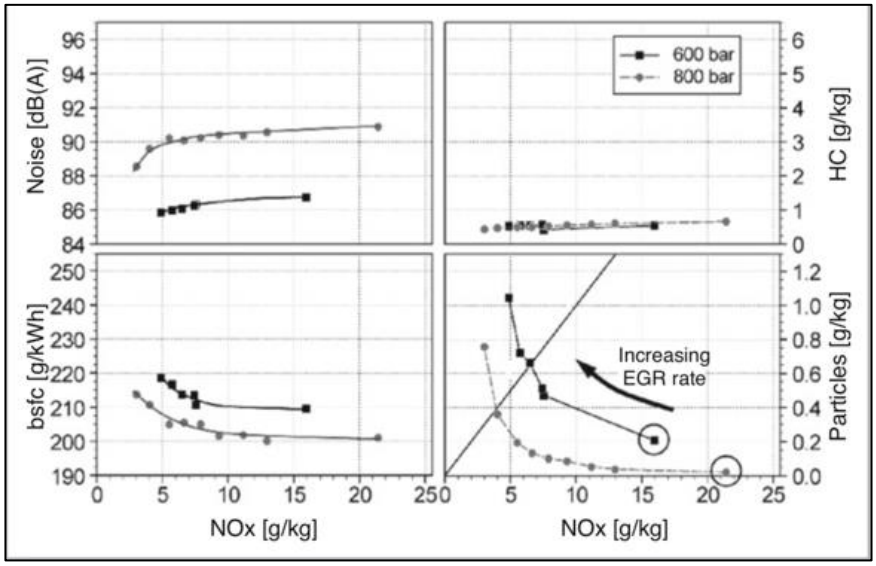

Figure 6-1 Effect of EGR rate on NOx, Particulates, uHC, BSFC & Noise, (206)

In the marine engines field, there are two types of EGR system implementation that depend on engine cylinder size, the turbocharger bypass for engines equipped with one turbocharger and the turbocharger cut-out for

engines of high power output that use two turbochargers at Tier-II mode, (233). The use of EGR is, as briefly explained in Chapter 4, a solution that can be applied to both conventional diesel engines and the state-of-the-art dual-fuels ones. For the dual-fuel engines, the recirculation of exhaust gasses is not only used for the reduction of NO_x emissions, when required, but also to limit the methane slip to the environment, (137). Thus, EGR implementation is found in both high-pressure gas injection engines that have similar NO_x emissions to conventional diesel ones, but also in low-pressure gas admission engines that are Tier-III limit compliant by design but have higher methane slip values.

In this chapter the effect of EGR use on large marine 2-stroke low-speed engines will be evaluated using measurement data from a diesel and a dual-fuel one. Following the experimental results analysis, an engine simulation multizone model is utilized to investigate in detail the mechanism related to EGR effect on engine performance, combustion mechanism and NO_x formation. Furthermore, the simulation is used to examine on a theoretical basis the potential for BSFC penalty reduction when using EGR via modified engine tuning and use of increased EGR rates to also retain similar NO_x emissions values.

6.1.1 Description of Turbocharger Bypass EGR System

For engines with a bore size of 700 mm or below the system is configured for the use of one turbocharger that includes a main and bypass string for the exhaust gasses. The complete configuration is given in the schematic of Figure 6-2. Compared to the usual marine engine layout two strings are used to supply the scavenge air receiver. These are the main string, that has the capacity to supply all scavenge air through the inlet and turbocharger system, and the EGR string with the capacity to lead up to a certain mass flow of exhaust gas, usually 40% of the mass at MCR, through the EGR unit up to a mixing point at the scavenge receiver, (233). The turbocharger bypass has two modes for this implementation, one used during Tier-II operation with the EGR system inactive for low-load tuning purposes, and the other during operation at Tier-III mode. In Tier-II mode the exhaust gas bypass (EGB) is fully open at high loads and partially open at lower loads to balance the turbocharger and optimize performance at low loads. This way the turbocharger can be optimized for the entire operating range of the engine.

At Tier-III mode the EGB valve is permanently closed. During this mode the cylinder bypass valve (CBV) is used to increase scavenge air pressure as a method to improve engine efficiency. This valve provides fresh air directly to the exhaust manifold assisting turbine operation resulting to increased Pscav. An overview of the various settings for this engine size implementation is provided in Figure 6-3.

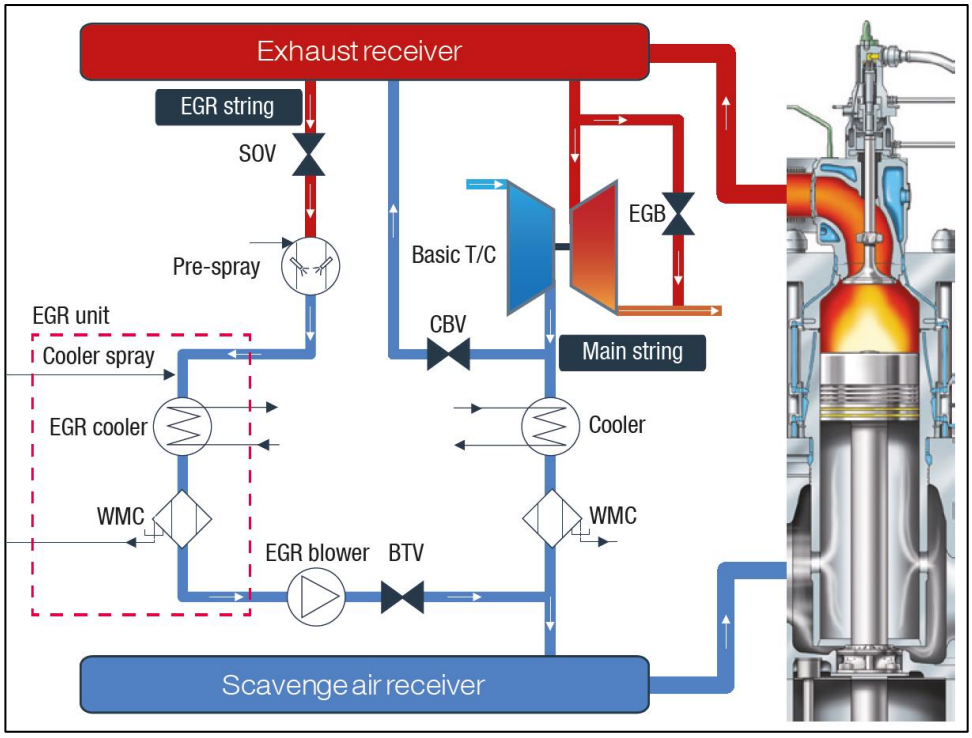

Figure 6-2 Schematic of 2-stroke marine engine equipped with EGR by-pass, (233)

Bypass matching - 45 ≤ Bore ≤ 70

	Tier II mode			Tier III mode		
	SOV BTV	CBV	EGB	SOV BTV	CBV	EGB
100	Closed	Closed	Open	Open	Open	Closed
75			Partly Open			
65						
50						
25					Closed	

Bypass Matching - Bore ≤ 40

	Tier II mode			Tier III mode		
	SOV BTV	CBV	EGB	SOB BTV	CBV	EGB
100	Open	Closed	Closed	Open	Open	Closed
90	Closed		Partly Open			
75		Closed				
65						
50						
25					Closed	

Figure 6-3 EGR-BP system valves control, (233)

6.1.2 Description of Turbocharger Cut-out EGR System

For engine with bore size above 700 mm, the use of two turbochargers is the adopted solution by manufacturers, with a basic and a cut-out turbine used, (233). During Tier-II operation, both the main and the cut-out string are active, with around 60% of the scavenge air passing through the main string. At Tier-III operation the cut-out string is isolated via the turbine cut-out valve (TCV). The CBV is used as in the previous implementation to increase scavenging pressure, in an effort to compensate for the efficiency impact caused by the EGR system. A schematic of the implementation is given in Figure 6-4 and of the various control specifics at Tier-II and Tier-III mode in Figure 6-5.

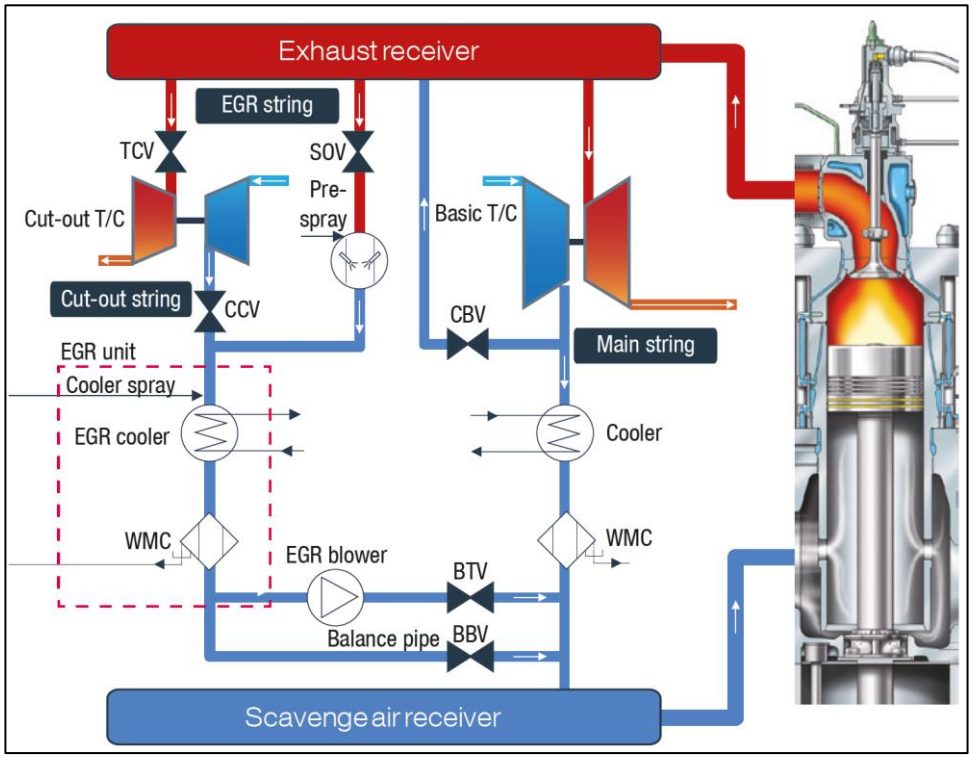

Figure 6-4 Schematic of 2-stroke marine engine equipped with EGR T/C cut-out, (233)

TC cut-out matching - Bore ≥ 80

	Tier II mode			Tier II mode – TC cut-out			Tier III mode		
	SOV BTV	CBV	TCV CCV BBV	SOV BTV	CBV	TCV CCV BBV	SOV BTV	CBV	TCV CCV BBV
100	Closed	Closed	Open	Not applicable			Open	Closed	Closed
75				Closed	Closed	Closed		Partly Open	
65									
50									
25								Closed	

Figure 6-5 EGR-TC cut-out system valves control, (233)

6.1.3 EGR System Layout-Detailed Description

The EGR system is integrated in the engine and in all implementations contains a water mist catcher, the exhaust gas cooler system, the EGR blower and a water treatment (WTS) system, (233,238). The differences between the two implementations described above refer to the integration of the EGR system in regards to the connection to the inlet and exhaust manifold. The turbocharger cut-out is more complex due to the use of two turbochargers and multiple strings for air and exhaust gas. The rest of the layout is mostly the same for the two systems. The rate of gas recirculation is controlled in all cases by the EGR blowers by varying their speed. The reference and control value for the overall system is the percentage of O_2 measured in the scavenge receiver. This has been selected by the manufacturers because thermal NO_x formation in the engine has been shown to correlate well with the partial pressure of O_2 in the cylinder charge, (239).

The exhaust gases must be cleaned and cooled before returning to the engine scavenger receiver. The cleaning process initiates with a water pre-spray and an EGR cooler spray using recirculated freshwater. The previous process is required to remove sulphur and particles that may damage the engine. The cleaned gases are then cooled in the EGR cooler before entering the scavenge air receiver. To prevent high accumulation of particles and sulphuric acid form the recirculated water a water handling system is installed. The latter requires the use of caustic soda (NaOH). Its major components are the caustic soda tank and supply pump, the receiving tank and circulating pump, the buffer tank and circulated water supply pump and last the water treatment unit. The control of all subsystems including the various valves mentioned, blower speed and the WTS is performed by the emission reduction control system (ERCS) and a separate control system for the WTS.

6.2 Tested Engines – Experimental Investigation Details

In this chapter the effect of the recirculated gases on the overall performance, combustion and emissions of two marine engines is analysed using measured data acquired during the official FAT tests. It is noted that similar data were acquired during the official sea trials of various vessels but are not included herein since the former are of superior accuracy since they correspond to controlled conditions. The engines considered are equipped with EGR-BP systems due to their bore size of 700mm. The first engine is a modern 2-stoke diesel only engine and the second one the dual-fuel engine designated as “Engine 1” in Chapter 2 LNG section. The engines belong to the same generation with respect to their type and are commercially available currently, with their next generation entering the market at the time of writing.

The particulars of the tested engines are provided in this subsection along with the properties of the fuels used and the measurement equipment utilized.

Table 6-1 Particulars of Engine 1

6G60ME-C9.5EGRBP	Units	Value
Type	-	Two-Stroke
Electronic Control	-	Yes
Cylinder No.	-	6
Bore	mm	600
Stroke	mm	2790
Nominal Speed	rpm	86.0
Nominal Power	kW	13,000
NO_x Certification	-	Tier-III
EGR Type	-	Turbocharger Bypass

Table 6-2 Particulars of Engine 2

5G70ME-C9.5GI	Units	Value
Type	-	Two-stroke
Electronic Control	-	Yes
Cylinder No.	-	5
Bore	mm	700
Stroke	mm	3256
Nominal Speed	rpm	68.1
Nominal Power	kW	11,975
NO_x Certification	-	Tier-III
EGR Type	-	Turbocharger Bypass

Table 6-3 Measurement Instrument Particulars, Engine 1

Instrument	Measured Parameter	Range	Accuracy
Hydraulic Brake	Torque		<0.5%
	Speed	0–250 rpm	0.1 rpm
Diesel Fuel Scale	Diesel Fuel Consumption	0–10,000 kg	0.2%
Gaseous Fuel Scale	Gas Fuel Consumption	0–10,000 kg	0.3%
MBS 3000	Scavenging Air Pressure	0–10 bar	0.5%
Air Temperature Sensors	Scavenging Air Temperature	−10–80 °C	0.2 °C
Exhaust Gas Temperature Sensors	Exhaust Gas Temperature	−10–700 °C	0.5 °C
Cooling Water Temperature Sensors	Cooling Water Temperature	0–180 °C	0.2 °C
Horiba CLA-750A	NO_x (Dry)	0 – 2000 ppm	±0.5%
Horiba MPA-720	O_2 (Dry)	0 – 25 %	±0.5%

Table 6-4 Measurement Instrument Particulars, Engine 2

Instrument	Measured Parameter	Range	Accuracy
Torquemeter	Torque	0 - 250 rpm	<0.5%

	Speed		0.1 rpm
Diesel Fuel Scale	Diesel Fuel Consumption	0 - 10000 kg	0.2%
Scavenge Pressure Sensor	Scavenging air Pressure	0 - 10 Bar	0.1%
Air Temperature Sensors	Scavenging air Temperature	-10 - 80 ^{o}C	0.2^{o}C
Exhaust Gas Temperature Sensors	Exhaust Gas Temperature	-10 – 700 ^{o}C	0.5^{o}C
Horiba CLA-750A	NO_x (Dry)	0 – 2000 ppm	±0.5%
Horiba MPA-720	O_2 (Dry)	0 – 25 %	±0.5%

6.3 Analysis of EGR Impact on Engine Performance

6.3.1 EGR Effect on Overall Engine Performance

In the first part of the EGR effect on engine performance analysis the findings of the experimental procedures are presented. For both engines tested performance is compared for Tier-II and Tier-III operation. It is noted that for “Engine 2” comparisons are provided for the DF mode operation and also comparison of Tier-III diesel and Tier-III DF mode is made. First the most important global performance values are compared, specifically, the variations in peak pressure values and fuel oil consumption. In the following part variation of engine settings and alterations in the combustion mechanism are examined following the switch to Tier-III mode.

For the diesel engine “1” considerable differences are found in compression pressure values, Figure 6-6 between the two modes. This is the result of altered engine tuning and air inlet system operation as detailed in the following section containing engine tuning per mode of operation. P_{comp} is increased for Tier-III except for 25% load, due to lower P_{scav} values at this load shown below. Peak combustion pressure, Figure 6-7, is decreased for all loads except 100% at Tier-III mode with the decrease being higher for 25% and 50% load. The decrease of maximum pressure values was also reported in various experimental and numeric investigations such as (240) and (241) for large diesel engines during EGR use. P_{comp} and P_{max} comparisons for the DF engine at Tier-II and Tier-III gas mode operation are provided in Figure 6-7 and Figure 6-8, and show a similar trend in changes during the use of EGR with elevated P_{comp} and decreased P_{max}.

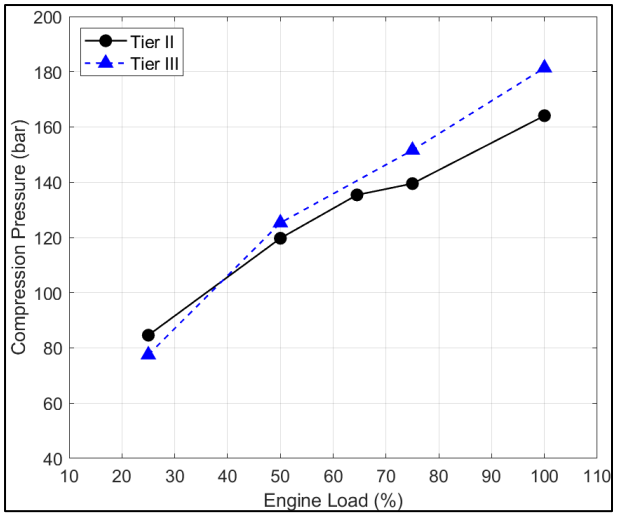

Figure 6-6 Compression pressure, Tier-II & Tier-III; Engine 1

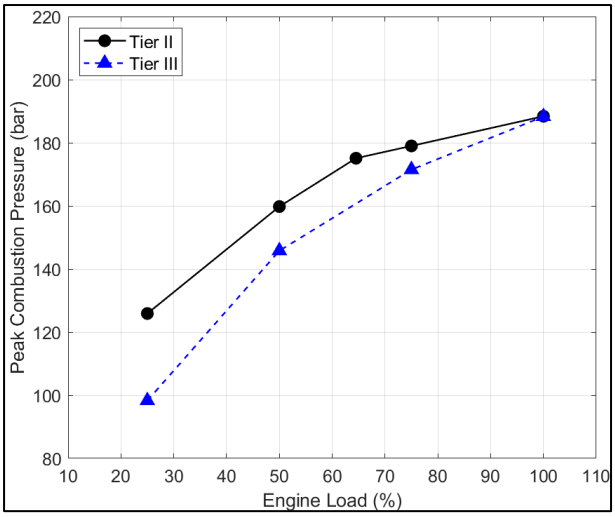

Figure 6-7 Peak Firing Pressure, Tier-II & Tier-III; Engine 1

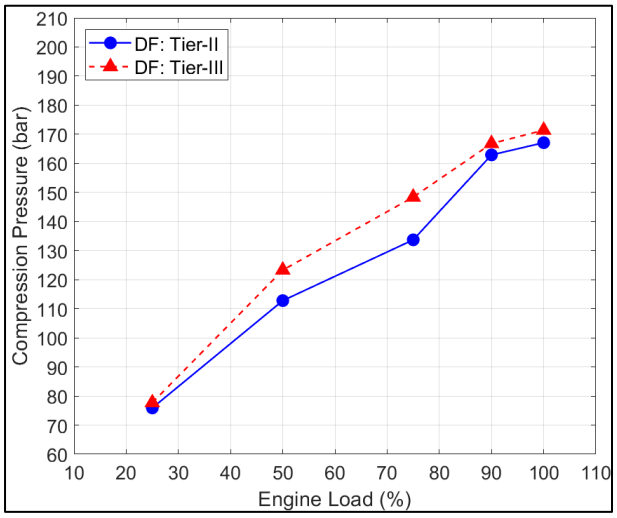

Figure 6-8 Compression pressure, Tier-II & Tier-III; Engine 2 Gas Mode

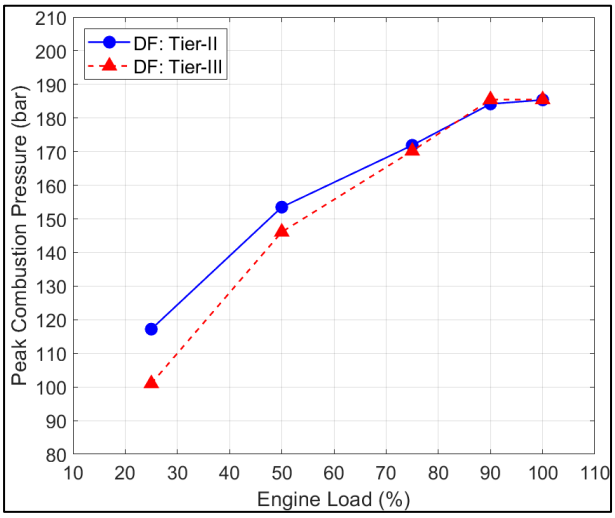

Figure 6-9 Peak Firing Pressure, Tier-II & Tier-III; Engine 2 Gas Mode

In Figure 6-10 and Figure 6-11 the P_{scav} and effective compression ratio values are presented for "Engine 1". P_{scav} values are considerably lower at Tier-III. To compensate for the lower inlet pressure, the engine pressure ratio is increased via EVC timing advance and this results to P_{comp} values similar or even higher than during Tier-II mode operation as seen above. The EVC angle advance is observed for all loads, including MCR, where inlet pressure is the same for both modes. This is in contrast with expectations set by considerable part of available literature regarding EGR implementation in diesel engines, in which utilization of the Miller Cycle is suggested to limit the fuel consumption penalty and aid in NO_x formation reduction, (237), (242), (243). However, the advanced EVC angle observed in this application is the opposite approach from the Miller cycle, (244). Pressure increase due to combustion is lower for Tier-III mode, with the difference being mostly steady across load at about 20 bar, Figure 6-12. The lower pressure increase during combustion is solely the effect of the recirculated gases but is also partly attributed to injection angle retard, Figure 6-13, which affects pressure rise considerably (237). Combustion characteristics also contribute to lower pressure

rise and are reviewed in the heat release rate analysis results. It is noted that SOI retard is an in-engine measure employed by engine manufacturers to reduce NO_x emissions (245). Thus, the timing change during Tier-III mode operation is possibly aimed towards lowering NO_x formation to achieve compliance with legislation while also reducing the recirculated gas ratio required. Some computational studies for 2-stroke marine and heavy duty diesel engines have shown that the combination of EGR at a high rate and injection retard can have a cumulative high effect on soot emissions, (236,246,247). In the first study (236) the effect of EGR on soot became exponential above a certain percentage, thus it is assumed that SOI retard was used to aid in NO_x formation reduction so that the EGR percentage required was limited and soot formation was kept within acceptable values. In the case of "Engine 2" the respective values are provided in the same format in Figure 6-14 - Figure 6-17. As with the compression and maximum pressure values above, the tuning changes after the switch to Tier-III mode are quite similar to the observations of "Engine 1". P_{scav} is reduced and EVC is advanced for all loads to increase the effective compression ratio of the cylinders. ΔP due to combustion is considerably decreased, with the exception of 90% and 100%, due to the sharp drop of these values also at Tier-II mode. SOI timing of the diesel pilot is retarded up to 75% load but advanced at 90% and 100% load. Despite the SOI timing advance (and earlier gas ignition as shown in the next section) the ΔP values remained lower than Tier-II operation, which is fully attributed to the effect of the recirculated gasses in the combustion chamber and the difference in the total mass trapped in the cylinder during Tier-III operation.

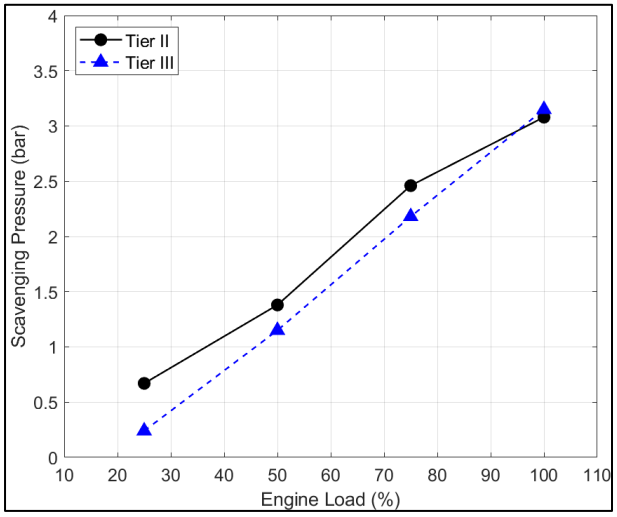

Figure 6-10 Scavenging Pressure, Tier-II & Tier-III; Engine 1

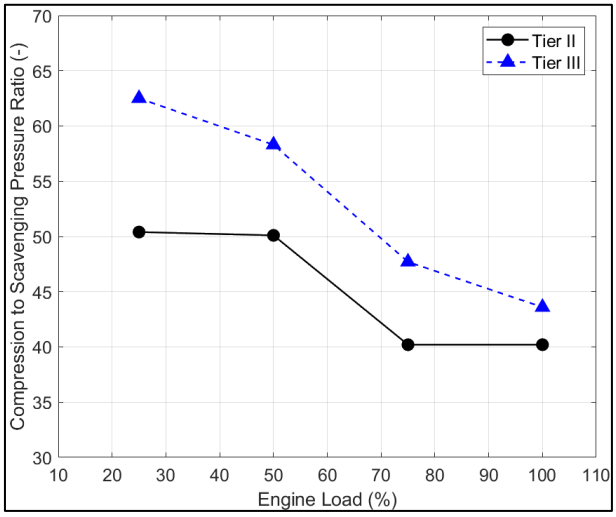

Figure 6-11 Pressure Ratio, Tier-II & Tier-III; Engine 1

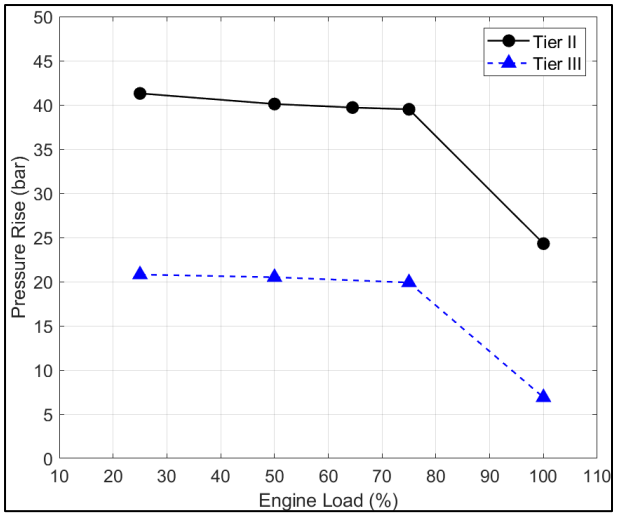

Figure 6-12 Pressure Rise due to Combustion, Tier-II & Tier-III; Engine 1

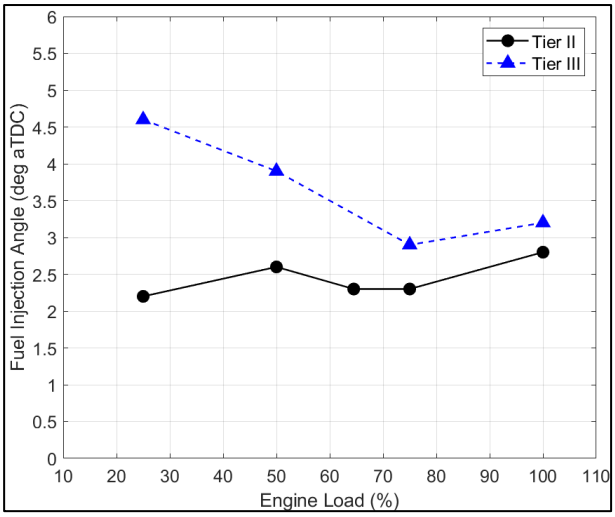

Figure 6-13 Fuel Injection Angle, Tier-II & Tier-III; Engine 1

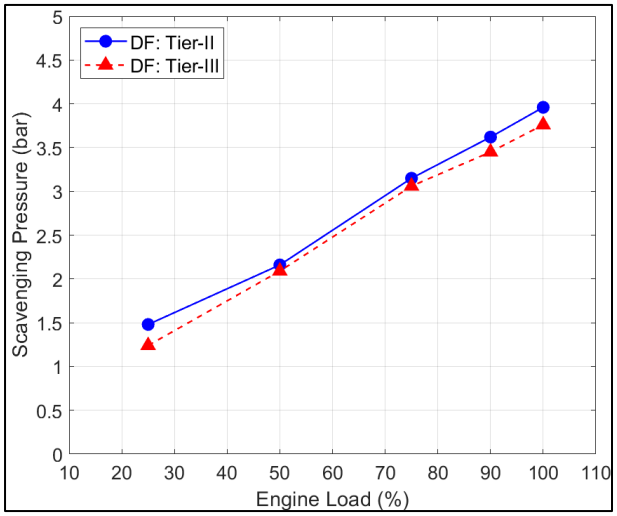

Figure 6-14 Scavenging Pressure, Tier-II & Tier-III; Engine 2Gas Mode

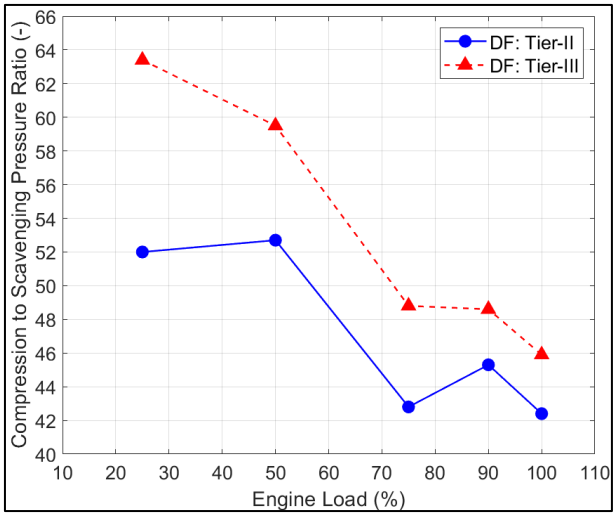

Figure 6-15 Pressure Ratio, Tier-II & Tier-III; Engine 2 Gas Mode

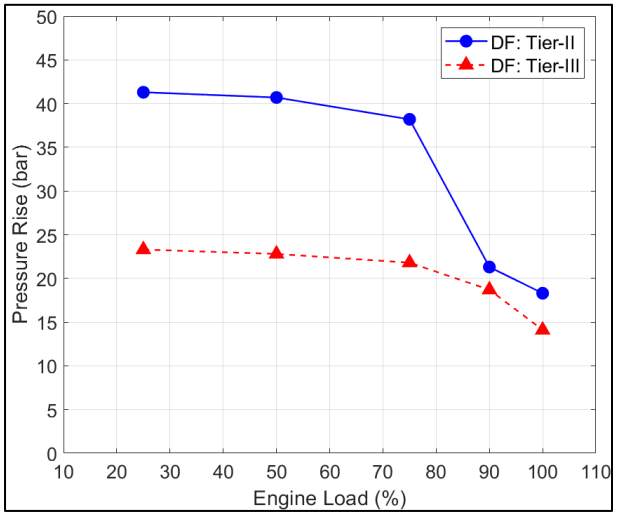

Figure 6-16 Pressure Rise due to Combustion, Tier-II & Tier-III; Engine 2 Gas Mode

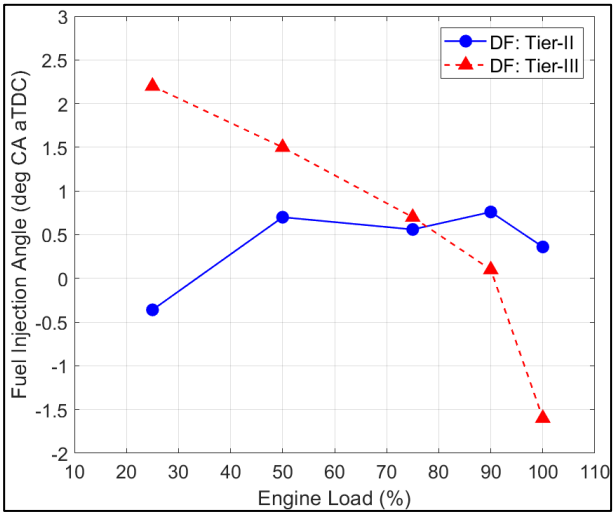

Figure 6-17 Fuel Injection Angle, Tier-II & Tier-III; Engine 2 Gas Mode

For both engines fuel oil consumption is negatively impacted by the exhaust gas recirculation and settings changes, especially the high SOI retard. For “Engine 1” increase in BSFC is found across the whole operating region, with the highest penalty between 50% and 75% load, Figure 6-18. The mean BSFC increase is 3.5% with 5.1% maximum increase at 50% load. For “Engine 2” the total specific heat rates are compared due to the dual-fuel operation, Figure 6-19, and similar levels of fuel efficiency penalty are observed, on average 2.6%, with the higher consumption increase at 25% and 50% load. The impact on engine efficiency is a known major downside of EGR, (248), (249). The considerable fuel consumption increase at usual operating load regions introduces operational costs to the EGR system that should be considered.

Closing this subsection, the differences between diesel only and DF operation at Tier-III (EGR enabled) mode of “Engine 2” are given. As with the Tier-II performance of the two modes, DF and diesel, in Chapter 4 minimal differences are observed. Global performance values, and engine settings show minimal variation, Figure 6-20 - Figure 6-22, with the exception of the SOI advance near and at MCR during DF mode, Figure 6-23. The fuel efficiency advantage of DF over diesel mode at low load is retained and further increased, Figure 6-24. The previous shows that the use of EGR has roughly the same overall effect on engine operation and efficiency regardless of single or dual fuel operation. This can be expected to a degree as the same operating principle (Diesel cycle) is used for both modes due to the high-pressure gas injection.

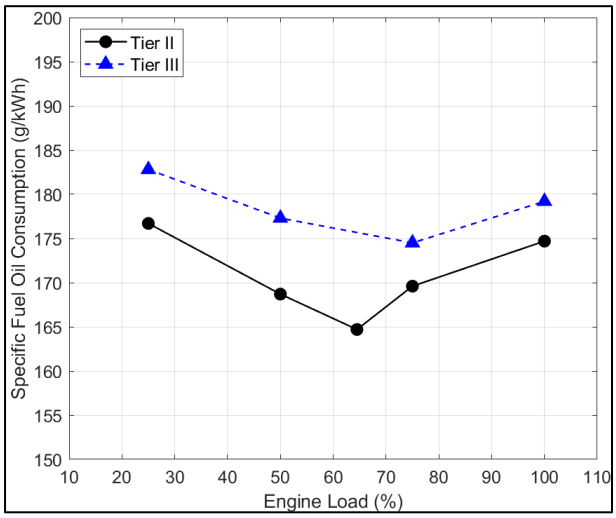

Figure 6-18 Specific fuel consumption, Tier-II & Tier-III; Engine 1

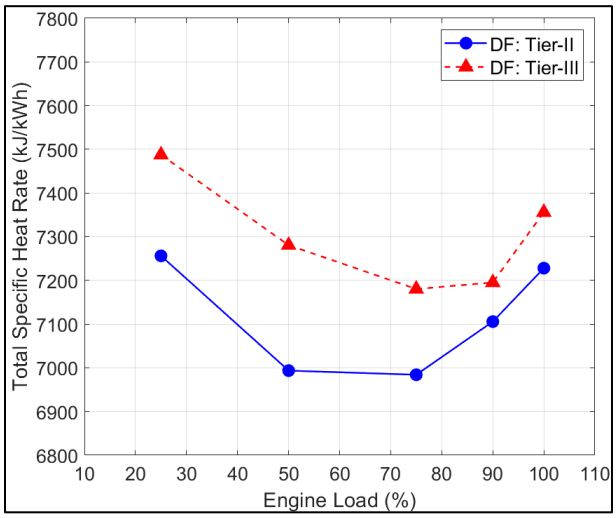

Figure 6-19 Specific total heat rate, Tier-II & Tier-III; Engine 2 Gas Mode

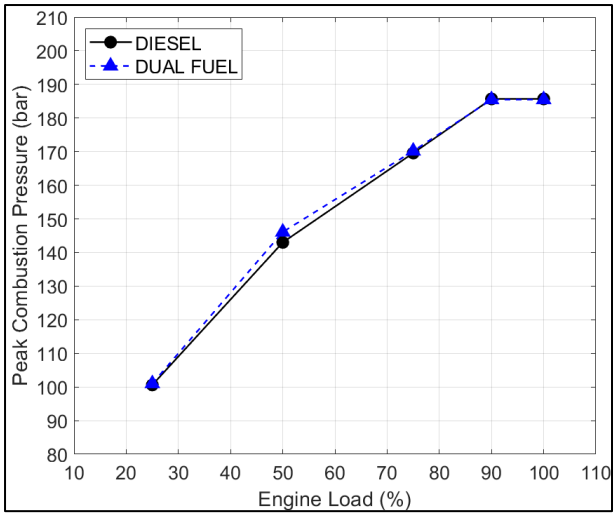

Figure 6-20 Peak Firing Pressure, Diesel & Gas Mode; Tier-III, Engine 2

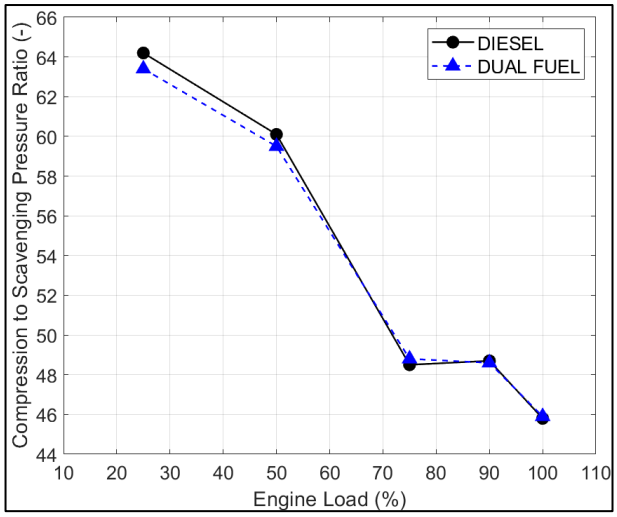

Figure 6-21 Pressure Ratio, Diesel & Gas Mode; Tier-III, Engine 2

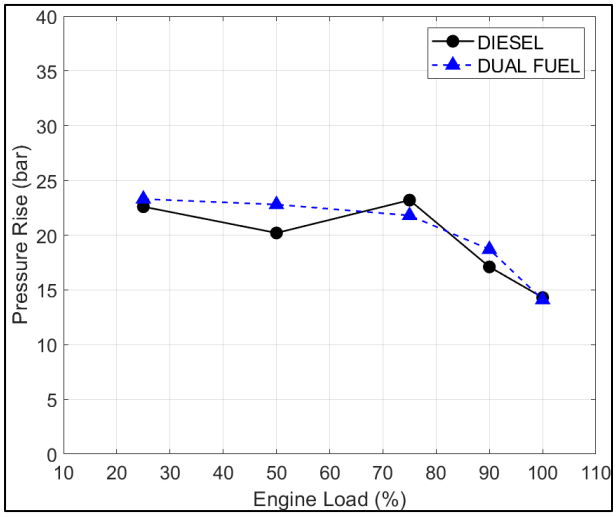

Figure 6-22 Pressure Rise due to Combustion, Diesel & Gas Mode; Tier-III, Engine 2

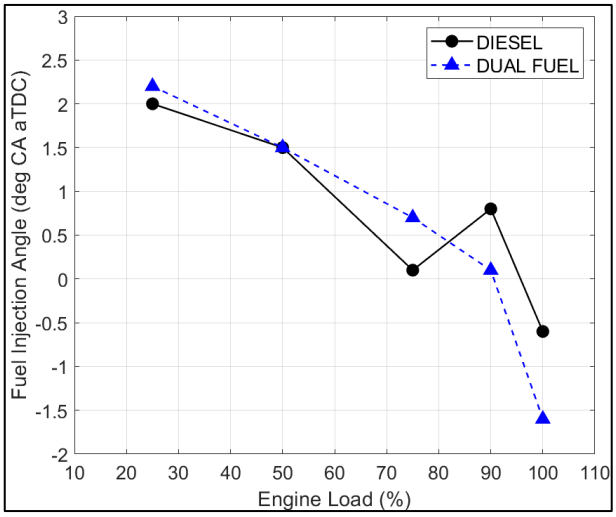

Figure 6-23 Fuel Injection Angle, Diesel & Gas Mode; Tier-III, Engine 2

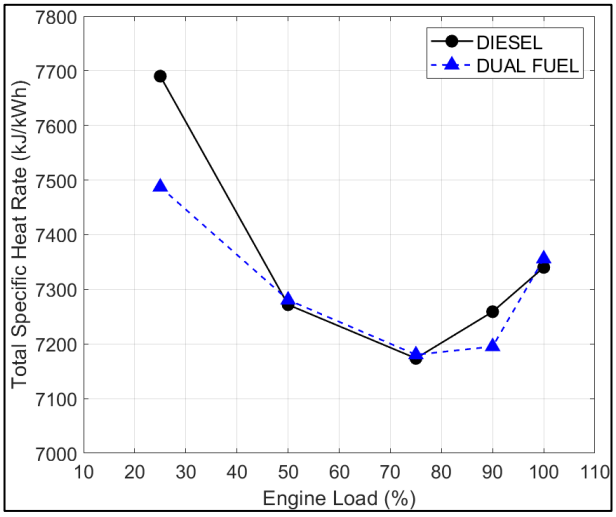

Figure 6-24 Specific total heat rate, Diesel & Gas Mode; Tier-III, Engine 2

6.3.2 Cylinder Pressure Traces comparison for Tier-II and Tier-III Mode with EGR use

In Figure 6-25a-d the measured cylinder pressure traces of "Engine 1" for Tier-II and Tier-III mode are compared for 25% - 100% with the same comparisons for "Engine 2" provided in Figure 6-26a-d for DF operation. Due to the aforementioned differences in engine settings and air inlet system operation, pressure traces are altered considerably for both engines when EGR is used. The effects of P_{scav}, EVC timing and SOI angle are easily identified with steeper compression and retarded fuel ignition. Indications of slower fuel burn rate are present, especially near maximum load, despite the retard of injection timing compared to Tier-II operation being the lowest for this load, below 0.5 deg CA retard for "Engine 1" and advance in the case of "Engine 2". Despite that, for both engines the peak combustion pressure is matched between Tier-II and Tier-III modes at higher loads. Overall, engine operation during Tier-III mode differs significantly. To quantify the effect of the combustion mechanism changes, the net fuel burn rate diagrams are compared next, estimated by heat release rate analysis as described in Chapter 4.

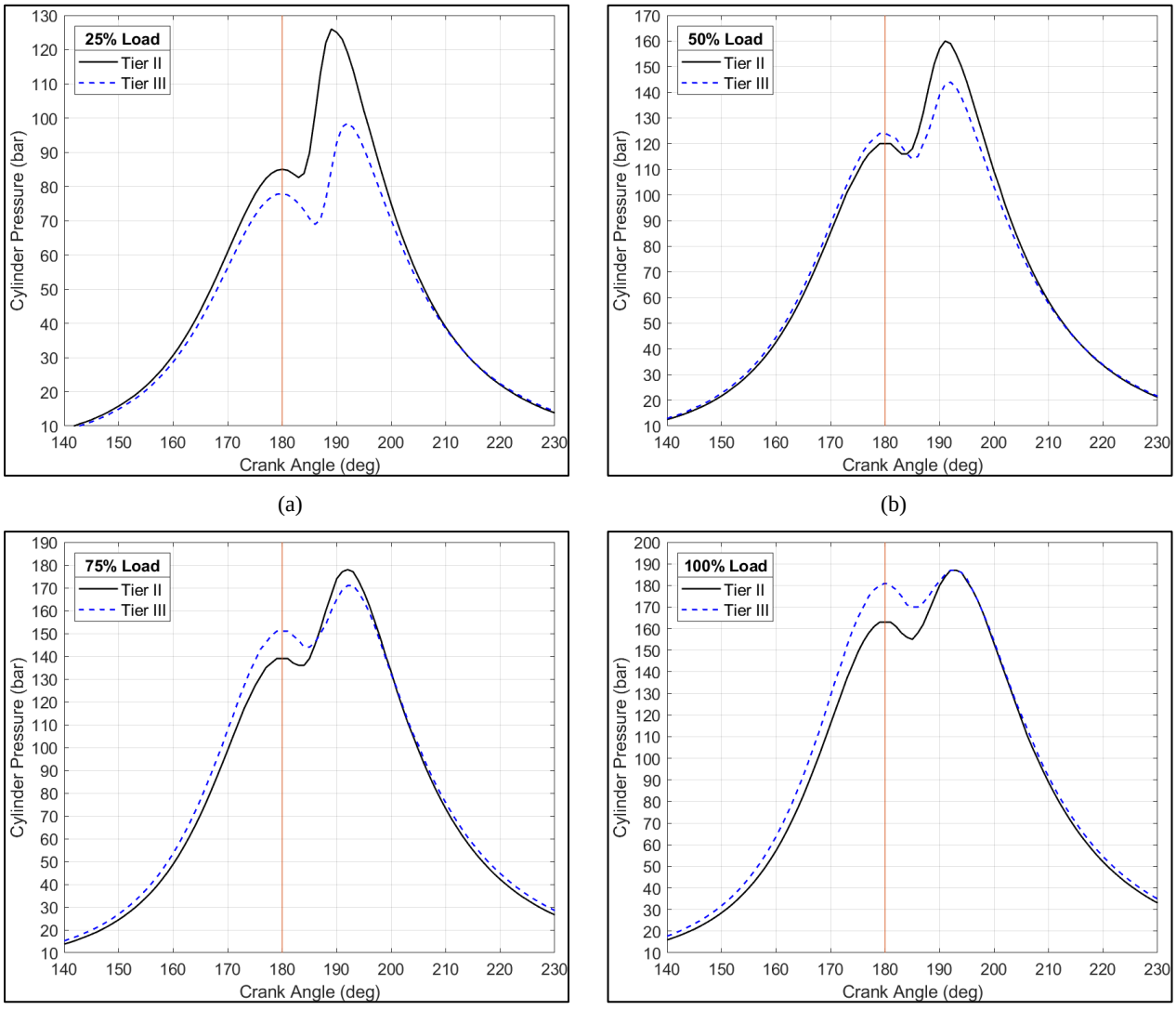

(a) (b)

(c) (d)

Figure 6-25 Measured Cylinder Pressure Traces, Tier-II & Tier-III; a) 25%, b) 50%, c) 75%, d) 100% Load; Engine-1

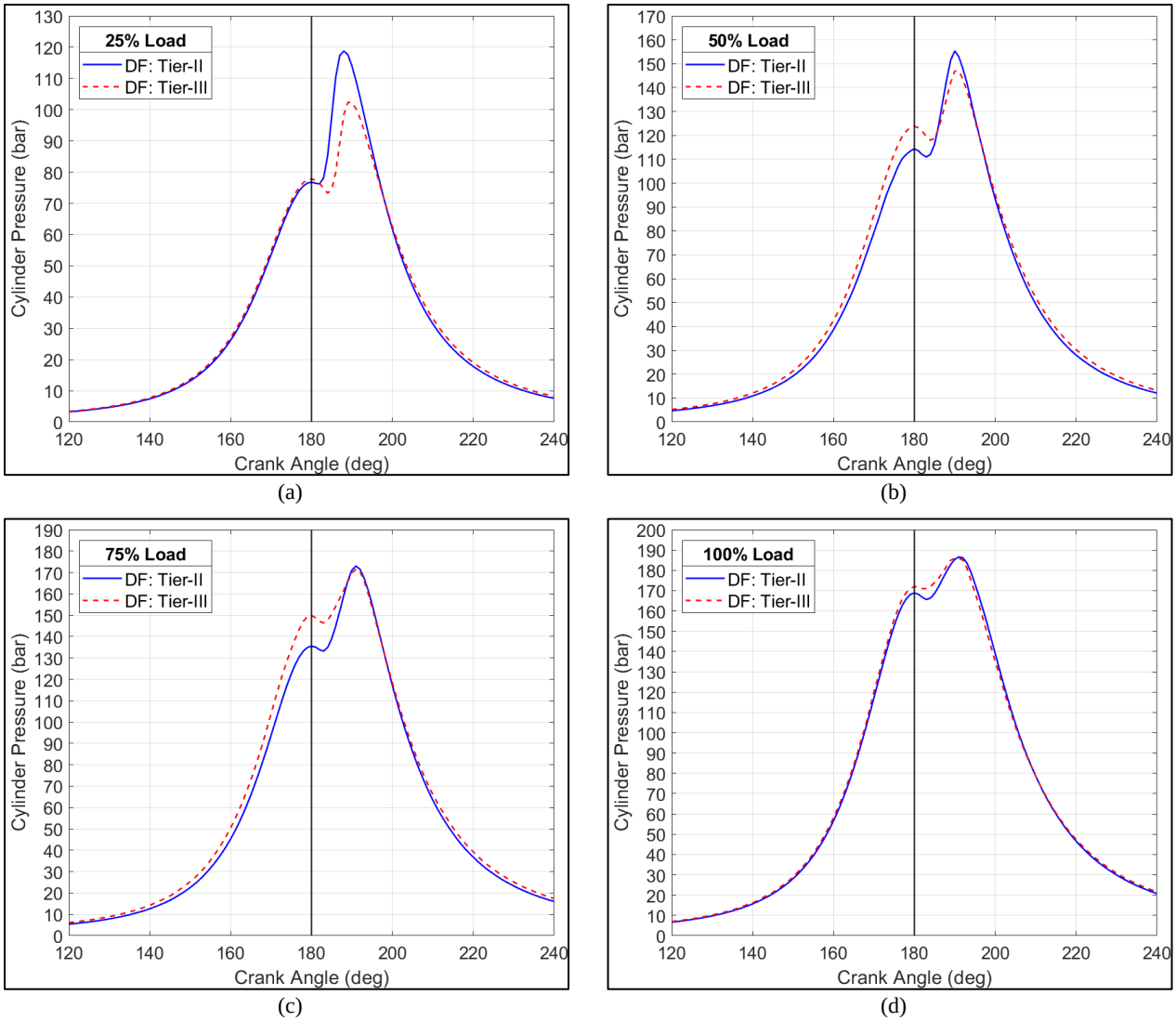

Figure 6-26 Measured Cylinder Pressure Traces at Gas Mode, Tier-II & Tier-III; a) 25%, b) 50%, c) 75%, d) 100% Load; Engine 2

6.3.3 Effect of EGR on the Combustion Rate: Diesel and Dual Fuel Engine

The effect of recirculated gases on the combustion process is examined using heat release rate analysis of the measured cylinder pressure traces. In Figure 6-27a - Figure 6-27d is provided the comparison of the combustion rates at the tested loads for Tier-II and Tier-III for “Engine 1”. For all loads fuel ignition is retarded at Tier-III mode. This is the result of fuel injection angle and the recirculated gases effect resulting to ignition delay increase, (250) and (251), due to the decrease of cylinder charge temperature. However, the increased compression ratio at Tier-III partly offsets the previous, thus the main contributor to late ignition angle in this case is injection timing. Initial fuel burn rate is decreased at Tier-III operation with visibly lower slope and peak value, which is in-line with other studies (250), (252), (253). By limiting fuel combustion intensity, the pressure and temperature rise in the cylinder are reduced, resulting in NO_x formation reduction. Lower peak burn rate limits the maximum mean and localized in-cylinder temperature contributing significantly to emissions decrease, as NO_x formation is exponential to temperature (251). Fuel burn rate at the late diffusion stage is considerably higher than for Tier-II operation. While this negatively affects

efficiency, as confirmed by the BSFC increase, the effect on NO_x formation is minimal, as at this stage pressure and temperature in the cylinder are rapidly decreasing due to expansion. The overall shifting of the combustion process towards expansion results in faster cooling of the combustion gases limiting NO_x formation, (251). In Figure 6-28a - Figure 6-28d the "Engine 2" estimates for HRR are provided for Tier-II and Tier-III DF operation. The effect of the recirculated gases is practically the same as for the diesel-only "Engine 1" but more intense. The reduction of gaseous fuel combustion intensity is more pronounced, especially at 75% and 100%, with staggered combustion rate roughly 5^o CA after gas ignition. The peak HRR and late-stage combustion intensity are negatively affected as found for "Engine 2". For both engines, the presence of the recirculated gas and decrease of oxygen availability and cylinder charge temperature inhibits diffusion combustion, while the premixed early-stage is less affected at least in initial stage. The nearly equivalent initial intensity of the premixed combustion is most probably the result of the higher ignition delay values during Tier-III operation, (250). For both engines all net HRR diagrams show overall lower values for Tier-III operation. Considering that the total supplied energy is higher by up to 5% during this mode, equivalent to the BSFC increase, heat losses are significantly higher due to the EGR use. This is attributed to the lower pressure values that decrease engine efficiency and in some cases to prolonged combustion duration, especially in the high-rate peak temperature region with the piston position still close to the TDC.

Combustion duration for 50% and 95% of total fuel burnt is provided in Figure 6-29 and Figure 6-30 for engines "1" and "2". Due to the difference in early combustion intensity, 50% fuel burn duration is higher at Tier-III mode for both engines in most loads. For the DF engine "2", 50% fuel burn duration is not affected by the EGR and is equivalent to Tier-II operation. For both engines the difference further increases for 95% combustion duration because of the prolonged late stage combustion. The increase in combustion duration does not present significant change with load, with an average value of 3.5^o CA for "Engine 1" and 7.6^o CA for the dual-fuel "Engine 2" as DF late-stage combustion was affected to a higher degree. The prolonged combustion duration both considering 50% and 95% of total fuel mass burnt (or supplied energy content for the DF engine) makes clear the efficiency penalty from the combination of EGR and engine settings used in Tier-III mode, which significantly affects thermal efficiency and consequently fuel consumption, (254).

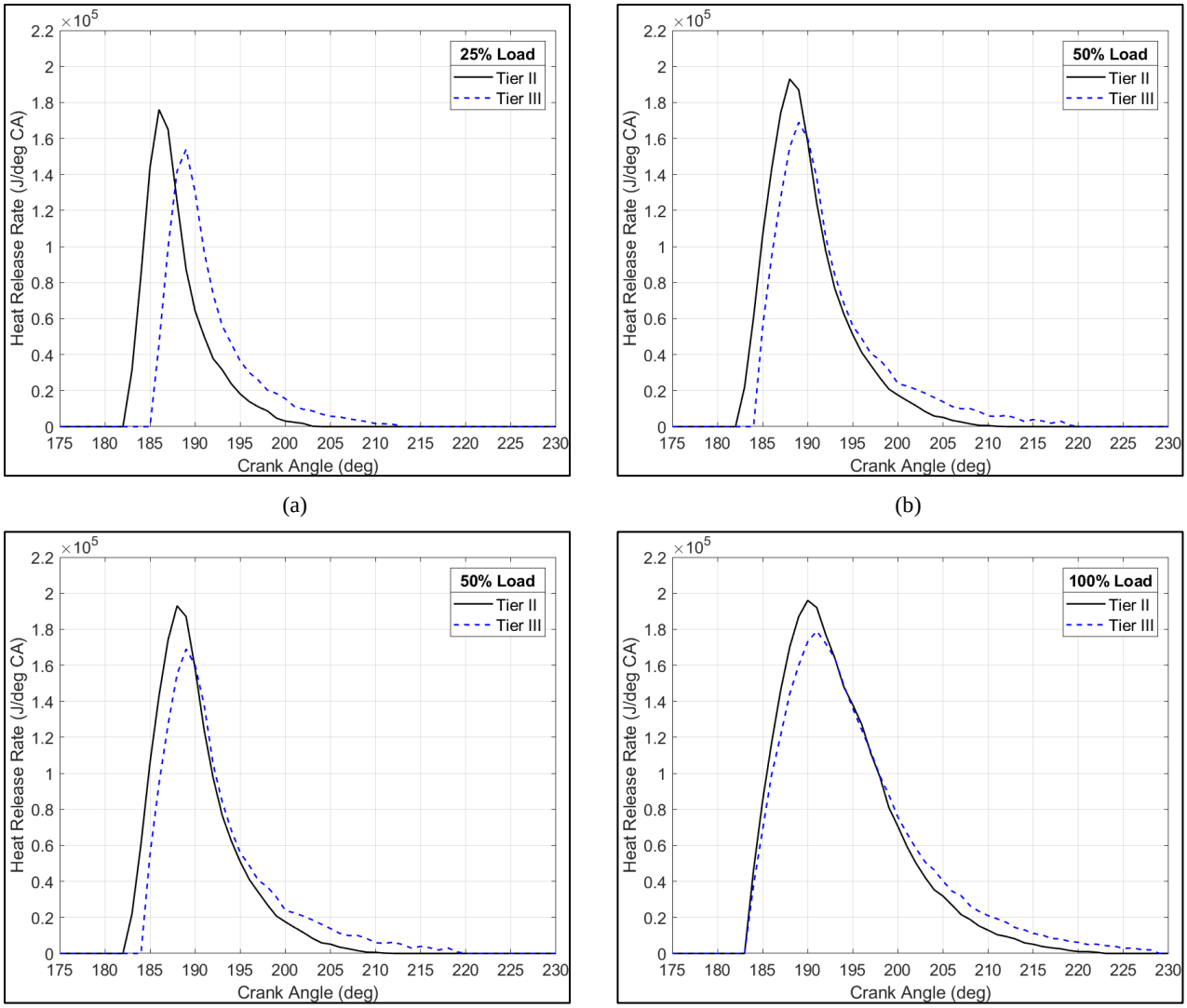

(a) (b)

(c) (d)

Figure 6-27 Net Heat release rate from fuel combustion, Tier-II & Tier-III; a) 25%, b) 50%, c) 75%, d) 100% Load; Engine 1

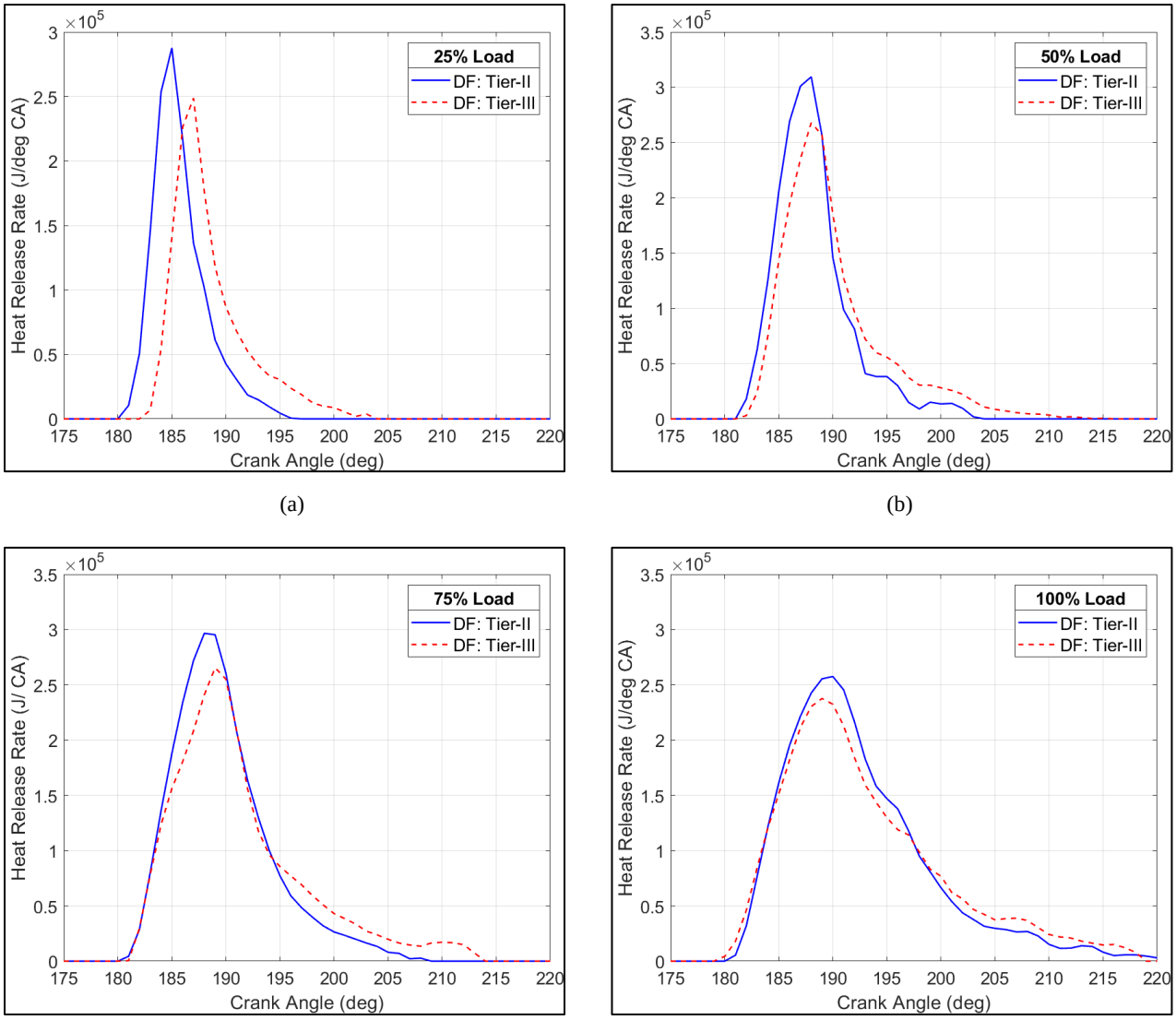

Figure 6-28 Net Heat release rate from fuel combustion at Gas Mode, Tier-II & Tier-III; a) 25%, b) 50%, c) 75%, d) 100% Load; Engine 2

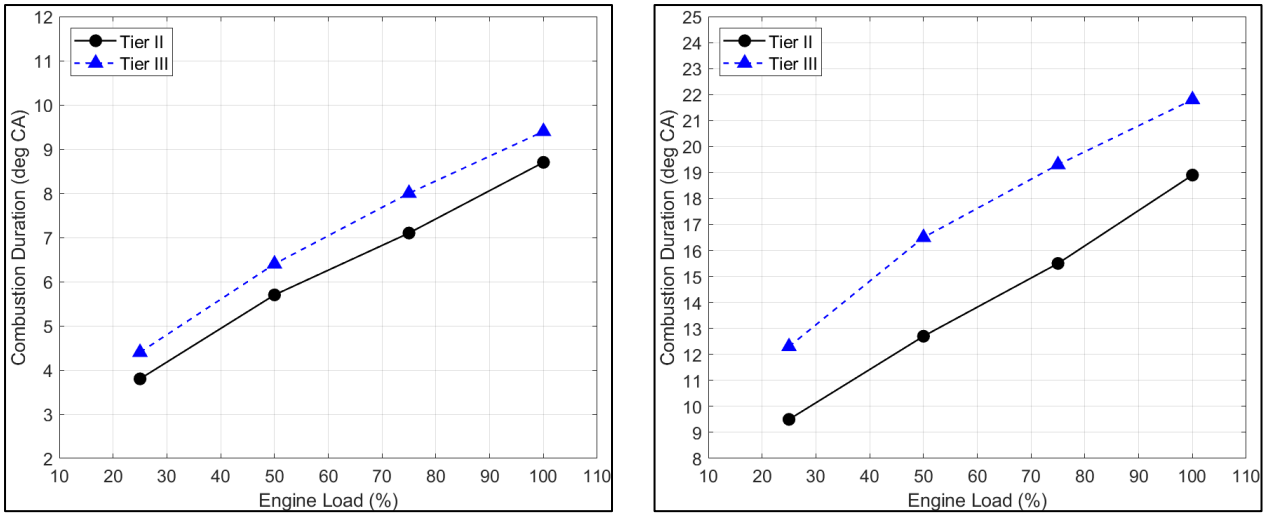

(a) (b)

Figure 6-29 Combustion duration for Tier-II & Tier-III operation; a) 50% of total fuel burnt, b) 95% of total fuel burnt; Engine 1

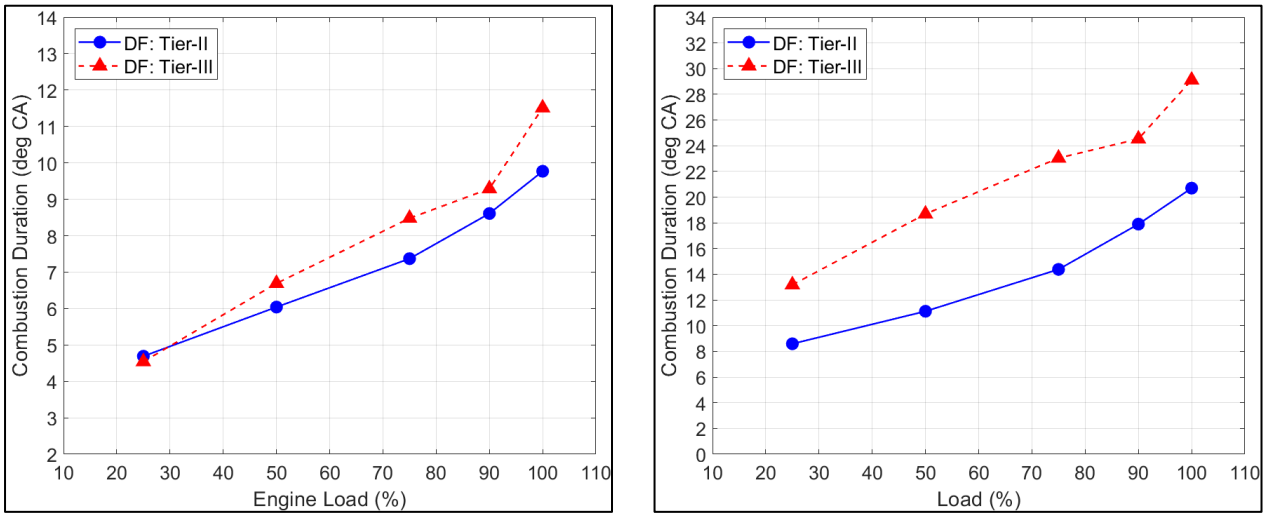

(a) (b)

Figure 6-30 Combustion duration at Gas Mode for Tier-II & Tier-III operation; a) 50% of total fuel burnt, b) 95% of total fuel burnt; Engine 2

6.3.4 EGR Effect on NO_x Formation

NO_x emissions were measured for Tier-II and Tier-III mode for the two engines, and for engine "2" at both diesel and DF operation. The NO_x emission concentration in the exhaust gases is provided in Figure 6-31 for "Engine 1", with the corresponding reduction during Tier-III operation in Figure 6-32. In Tier-II mode the highest NO_x emissions were recorded at 50% load, while in Tier-III at 25% load. Emissions reduction is high for all loads with the peak value at 75% load. "Engine 2" NO_x emissions data during the DF tests are given in Figure 6-33 and Figure 6-34 showing similar values of NO_x emissions to "Engine 1" but better NO_x reduction capabilities of the EGR in this case. It is noted that for "Engine 1" no data were available for the EGR ratio and for this reason it was estimated by the multi-zone combustion model described above. A direct estimation utilizing in-engine or scavenge air receiver mass balance was not feasible when the CBV was open (all loads

except 25%). For “Engine 2” the EGR rate was available since exhaust gas and air concentration data were provided at the engine inlet and exhaust. The estimated values were also available in the FAT tests and the values calculated were verified. The EGR rate per load point for the two engines is given in Figure 6-35 and Figure 6-36 for engine “1” and “2” respectively. The values are mostly between 40% - 50% with higher ratio of recirculated gases for “Engine 2” for all loads. This is in line with the measured NO_x emissions reduction at Tier-III mode and also the seemingly higher effect of EGR on the “Engine 2” combustion process. For both engines EGR ratio is reduced below 40% at MCR as this is the maximum capacity of exhaust mass flow that the recirculation system’s cooling and cleaning components can accommodate. While there is direct correlation of the EGR percentage with NO_x emissions reduction for both engines, emissions decrease is not directly proportional to EGR rate. It is expected that NO_x reduction should be almost linear to the EGR rate, (233), which is actually valid for both engines up to 75% load with deviation at MCR.

The emission reduction in the present applications is also attributed to engine tuning and performance which differ considerably between the Tier-II and Tier-III mode and affect NO_x formation, further to the EGR use. Retarded injection timing and lower cylinder pressure increase reduce NO_x emissions, (254). These are altered for Tier-III mode as established above. Thus, the actual effect of EGR on NO_x formation is slightly lower. This is observed in the case of 100% load, where EGR percentage is lower, but NO_x formation reduction is not significantly impacted, especially in the case of “Engine 1”. It is estimated that the main contributing factor to the previous is the very low pressure rise at this load, influenced by fuel ignition well after TDC. However, examining “Engine 2” the same results are observed, while engine tuning is set to SOI (and actual ignition) advance, but low ΔP is also achieved and HRR is considerably affected (Figure 6-27d, Figure 6-28d). Thus, it is estimated that despite the lower ratio of EGR the total mass value of exhaust gases in the cylinder at MCR affects combustion significantly creating multiple localized high A/F ratio reductions. Another contributing factor could be an increased O_2 percentage in the recirculated gases at MCR, however the difference was minimal for all loads, except 25%, where significantly higher concentration was measured.

Summarizing, for both the diesel and the dual-fuel engine, high NO_x emission reduction is achieved at the requirement of high EGR rate. This last requirement is a concern as EGR systems are known to be faced with issues regarding fouling in the recirculated gases system mainly the cooler, (255–257). The high mass flow through this system could exaggerate this effect in this engine type, however as stated operational experience is still rather limited. In addition, substantial alteration of engine settings was required with the switch to Tier-III mode, mostly required by the change of air mass inlet requirements and turbocharger altered operation due to the EGB being closed and reduced P_{scav}. The change in settings also affected NO_x emissions to a degree, but the major contributor to the emissions reduction was the presence of the recirculated exhaust gases lowering the A/F ratio and the mean in-cylinder temperature. Further investigation is conducted in the following section with the utilization of a multi-zone model for detailed analysis of the operation of “Engine 1” at Tier-III mode.

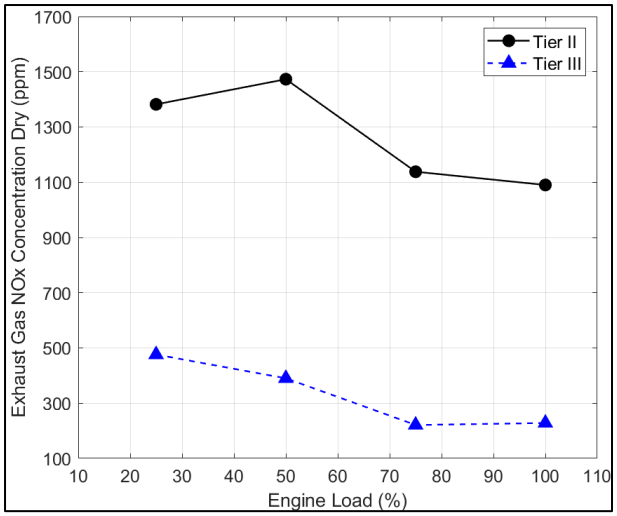

Figure 6-31 NO_x Concentration on exhaust gas, dry; Engine-1

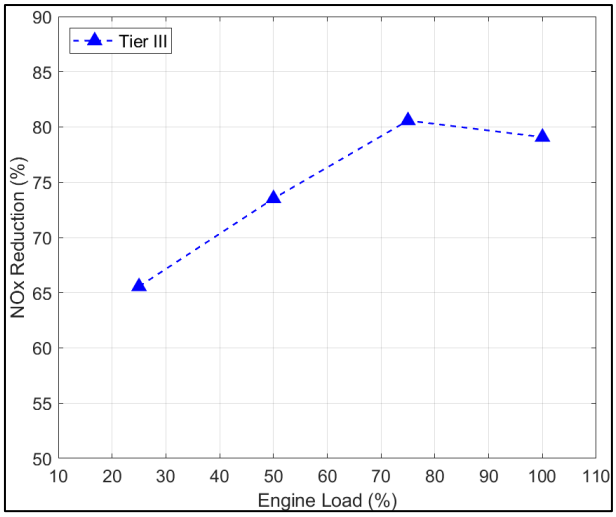

Figure 6-32 NO_x Concentration Reduction at Tier-III Mode; Engine-2

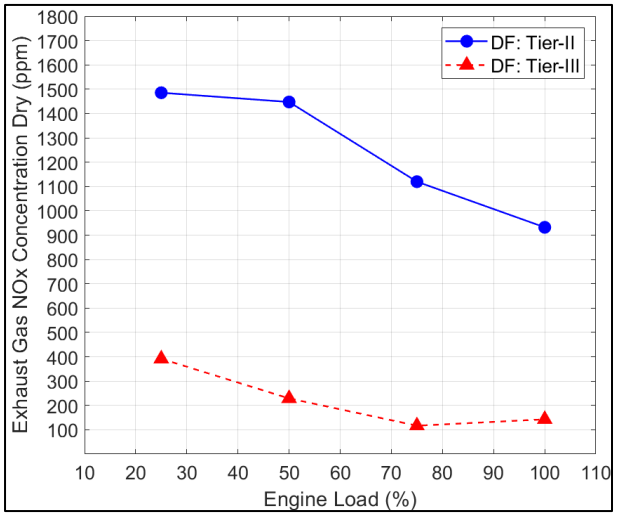

Figure 6-33 NO_x Concentration on exhaust gas, dry; DF Engine

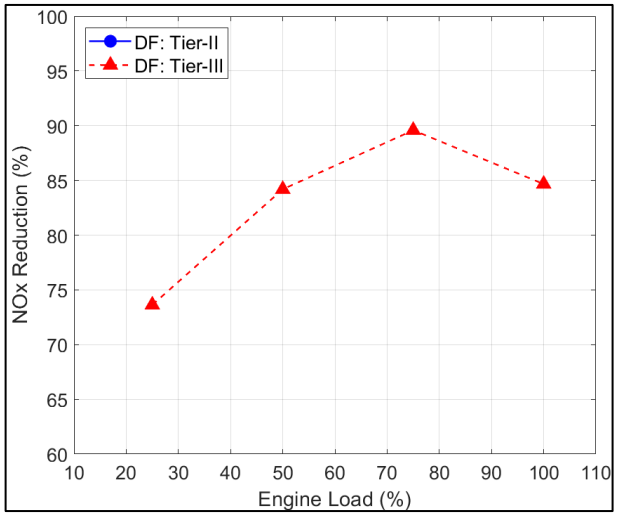

Figure 6-34 NO_x Concentration Reduction at Tier-III Mode; DF engine

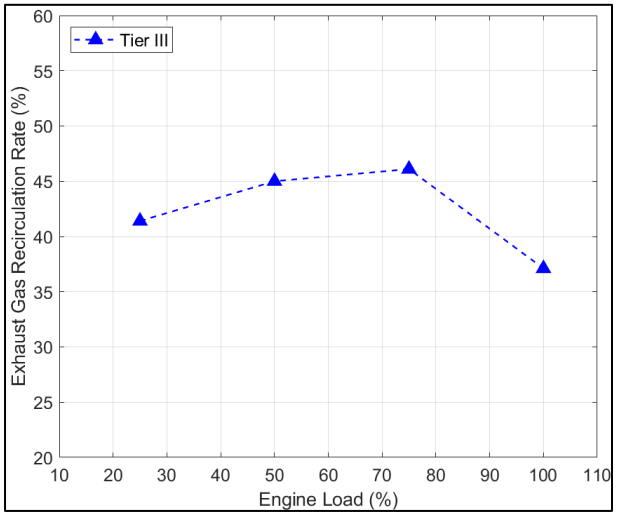

Figure 6-35 Exhaust Gas Recirculation Rate; Engine-1

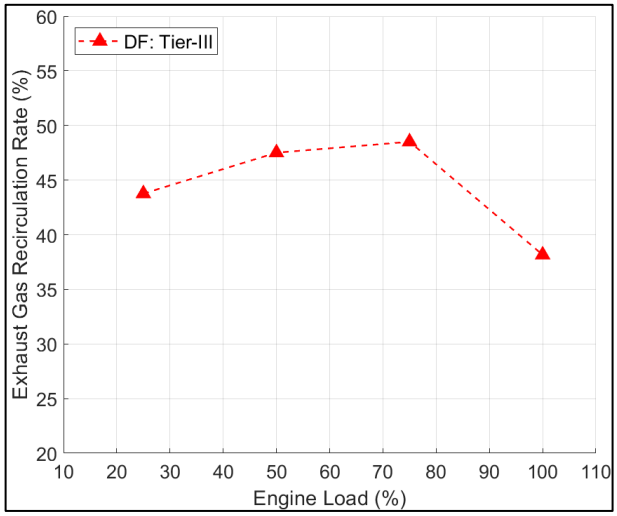

Figure 6-36 Exhaust Gas Recirculation Rate; Engine-2 DF mode

6.4 Computational Investigation for EGR Effect on 2-stroke Engines Equipped with EGR

6.4.1 Multizone Model Modifications for EGR Emulation

As detailed in the above sections, the EGR implementation on marine 2-stroke engines introduces certain modifications that have to be taken into account by the multizone combustion model for proper analysis and results. The modifications conducted include the following:

- Use of EGR during the open cycle analysis.
- EGR cooler.
- Incorporation of cylinder bypass valve (CBV) in the engine.
- Incorporation of exhaust gas bypass (EGB) valve at the turbine.
- Development of computation procedure to estimate EGR and CBV valve mass flow rates.

The selected approach to their incorporation in the model is detailed below.

6.4.1.1 Modelling of EGB and CBV Valve

The modeling of the EGB and CBV valves is based on the estimation of the mass flow rate (exhaust gas and air) assuming isentropic compressible flow. The opening of both valves refers to the angle and from this and the orifice diameter the geometric flow is calculated. The effective flow is estimated form the following relations:

$$A_{CBV} = A_{max}\left(1 - \cos(\varphi)\right) \tag{6.1}$$

$$A_{CBV,eff} = A_{CBV}C_d \tag{6.2}$$

Where "ϕ" is the valve position. The same approach is considered for the EGB valve.

For practical applications the discharge coefficient is considered to be constant with load and is integrated into the geometrical flow area. The estimation of both the EGB and CBV opening and mass flow rates is achieved using a newly developed iterative procedure. This allows to estimate the EGR rate when the CBV valve is open. With reference to below Figure 6-37 it is noted that for Tier-III operation with EGR use the EGB valve remains closed for all loads.

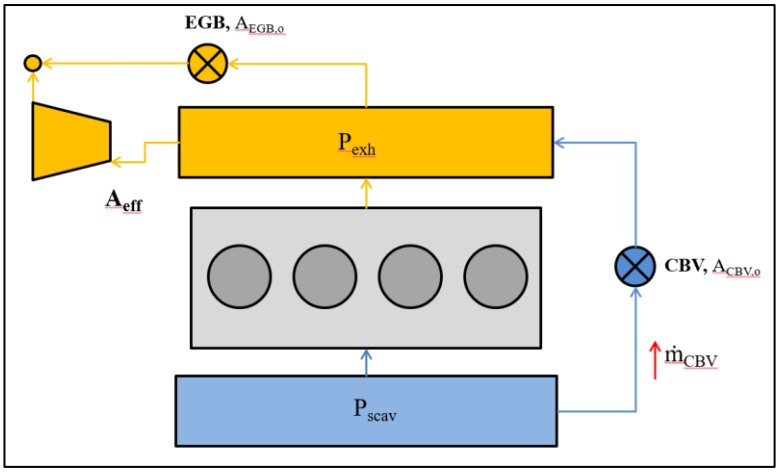

Figure 6-37 Schematic of air & exhaust gas flow lines with use of CBV & EGB

an iterative procedure is used to estimate the A_{CBV} and A_{EGB} opening area for each case while A_{eff} is the effective turbine flow area. The flow through each restriction is simulated using the typical equation for isentropic compressible flow. The effective turbine flow area is determined for Tier-II operation when both A_{CBV} and A_{EGB} valves are closed. The criteria for this is to match the measured mean exhaust manifold pressure, P_{exh}. The EGB valve area is estimated using the shop test data for the cases when it is opened using as criteria the exhaust manifold pressure and the temperature at the turbine outlet.

Having determined the EGB characteristics when the CBV valve is open the flow area is estimated to match the calculated pressure at the exhaust manifold with the measured one as follows:

$$P_{exh,cal} = P_{exh,meas}$$

For all the above an automated iterative procedure has been developed and implemented into the modified model. The gas exchange system and turbocharger simulation are further used to provide information for the rate of EGR and mainly the amount of air bypassed directly to the exhaust receiver due to the CBV opening. For the latter the pressure balance in the exhaust manifold is used along with exhaust gas temperature balance between the cylinder exhaust and turbine inlet.

6.4.1.2 EGR Rate Estimation

The requirement for EGR operation modeling introduced several additions to the above model. The basis for estimating the EGR percentage at each load was the measured O_2 concentration after the mixing tank of scavenge air and recirculated gas and O_2 concentration measured after the exhaust gas receiver. Part of the process followed was based on the EGR system description and approaches followed in (239,250,258). Using these values mass balance of oxygen can be performed to directly calculate the recirculated gas percentage by eq. (6.3) when the CBV is closed.

$$\dot{m}_{EGR} = \dot{m}_{a,in} \frac{X_{O2,atm} - X_{O2,scav}}{X_{O2,scav} - X_{O2,exh}} \quad (6.3)$$

For operating regions with the CBV open the previous equation is not valid since oxygen measurements at engine exhaust were performed downstream of the turbine. Eq. (6.3) is replaced by eq. (6.4) containing the bypassed air mass which is not known and varies due to different CBV opening at each load.

$$\dot{m}_{EGR} = \frac{\dot{m}_{a,in}\left(X_{O2,atm} - X_{O2,scav}\right) + \dot{m}_{CBV}\left(X_{O2,scav} - X_{O2,atm}\right)}{X_{O2,scav} - X_{O2,exh}} \tag{6.4}$$

The mass flow through the CBV is modelled as a compressible turbulent restriction. The formulation of the model in a generic form, considering that flow is subsonic is written as:

$$\dot{m} = \frac{A_{CBVe} P_{in}}{\sqrt{R_i T_{in}}} \sqrt{\frac{2\gamma_i}{\gamma_i - 1}\left(\Pi^{\frac{2}{\gamma_i}} - \Pi^{\frac{\gamma_i+1}{\gamma_i}}\right)} \tag{6.5}$$

for the above A_{CBVe} is the effective area of the CBV, Π is the pressure ratio and γ and R the heat capacity ratio and gas constant of air respectively. The CBV effective area is variable by its opening, which differs with load. The effective area is calculated as:

$$A_{CBVe} = A_{max}\left(1 - \cos\left(n_{CBV}\frac{\pi}{2}\right)\right) \tag{6.6}$$

with A_{max} the maximum area of the restriction and n_{CBV} a tuning parameter which is a function of the orifice area. For the EGB valve a similar approach is adopted.

An iterative procedure was employed using the multizone model to determine the bypassed air mass and recalculate the actual EGR rate. The initial EGR percentage value for each load was calculated by the measured oxygen concentrations assuming that the CBV is closed; this will coincide with the minimum EGR rate. The criteria for the estimation of $\dot{m}_{egr}$ and $\dot{m}_{cbv}$ is the following:

- X_{O2} at the engine inlet
- P_{exh} the exhaust manifold mean pressure
- T_{exh} when EGB is open

The previous is possible during Tier-III operation since the EGB valve is closed.

Last the EGR percentage is estimated from eq. (6.7), as in (259).

$$\Phi_{EGR} = \frac{\dot{m}_{EGR}}{\dot{m}_{EGR} + \dot{m}_{TC,in} - \dot{m}_{CB}} \tag{6.7}$$

6.4.2 Validation and Analysis of Tier-II Engine Calculated Performance and Emissions

In this section the results of the multizone model will be presented and analysed. As conducted in the biofuels section, first a short validation segment is provided since this is a different engine design. The engine simulated is the diesel "Engine 1" of the experimental results part. Using the Tier-II FAT data the simulation was calibrated, and following this was applied for the prediction of both Tier-II and Tier-III performance and emissions without additional tuning of the related constants. In order to validate the model predictive ability in the following part the comparison between measured and calculated performance and emission data is provided. In Figure 6-38 and Figure 6-39 the results of the comparison between computational and measurement data are provided for 25% and 75% load. Almost exact agreement is achieved for the cylinder pressure traces. The power output and BSFC calculations are also compared to the measured data in Figure 6-40 and Figure 6-41 respectively. Overall, good agreement between the computational and experimental data is seen, especially for higher load. The exhaust gas flow rate estimated by the model is compared to the values calculated using carbon balance from the exhaust gas composition measured during the tests in Figure 6-42 with minimal error between the two values. Last, in Figure 6-43 the calculated value of exhaust manifold mean exhaust gas temperature is compared to the measured one for all loads with very good agreement. It is noted that since the specific engine has a constant pressure turbocharger system the variation of the exhaust manifold temperature is significantly reduced and fairly constant.

For evaluation of NO_x formation prediction capability, the specific NO_x emissions data, as calculated by the model, and by the measurement data are given in Figure 6-44. Actually, the model predicts NO and the conversion to NO_x is included in the overall scaling factor derived from the calibration procedure. The emissions estimation using the model is close to the measured values, with the highest deviation at 25% load. For the other loads agreement is very good with low error. The higher difference at 25% is partially attributed to the overall lower mass flow rate values that increase the error level when fractions/composition is calculated as a percentage. Most important is the fact that the simulation predicts adequately NO_x variation with engine load. In order to have an insight of the NO_x formation its formation history is provided in Figure 6-45 where again it is revealed (as in chapter 6) that NO_x formation is kinetically controlled. The percentage contribution of each zone group is given in Figure 6-46. The results show that for low loads the highest contribution to NO emissions is from the fuel injected at the first stages. This is expected as combustion initiates at the tip of the fuel jet and proceeds inwards. In addition, the highest percentage of NO_x formation should occur, as established in multiple works such as (102), in areas that are relatively fuel lean close to stoichiometric and where local temperature is also high. It is noted that the zone percentage contribution is quite different than the one of the engine studied in chapter 6 with the multizone model. The difference is attributed to the overall tuning of the two engines and their respective fuel injection systems. The zones studied by this model that are better suited to satisfy this criterion are again the ones injected earlier that have achieved higher penetration and are also most probably more affected by in-cylinder swirl.

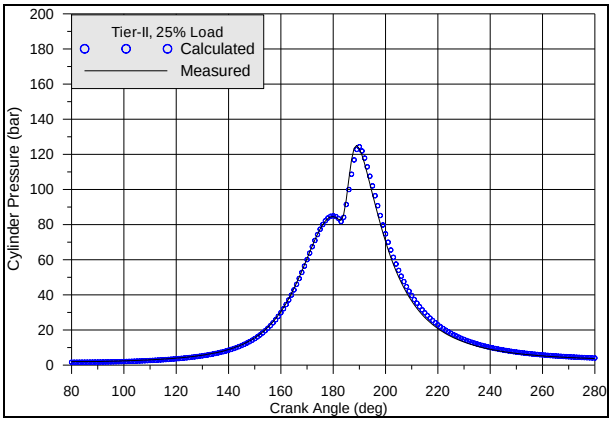

Figure 6-38 Comparison of calculated and measured cylinder pressure traces, 25% load, Tier-II

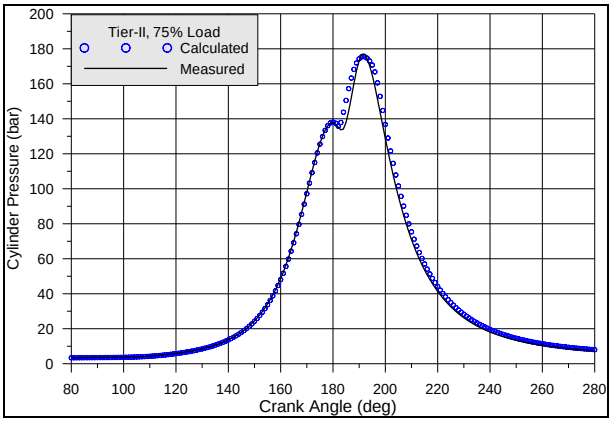

Figure 6-39 Comparison of calculated and measured cylinder pressure traces, 75% load, Tier-II

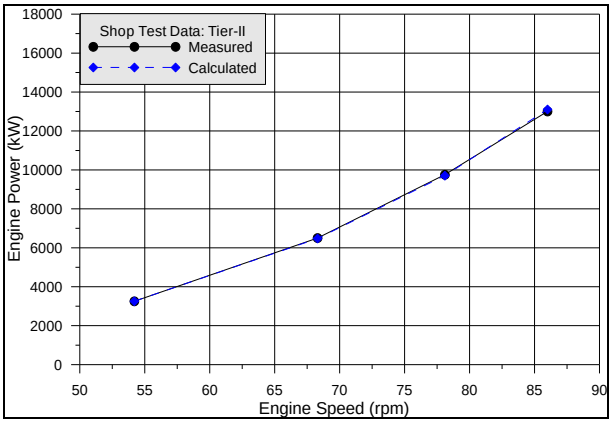

Figure 6-40 Comparison of calculated and measured engine power, all loads, Tier-II

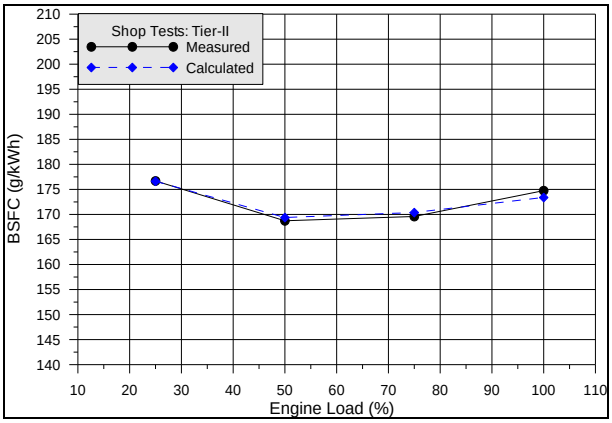

Figure 6-41 Comparison of calculated and measured engine bsfc, all loads, Tier-II

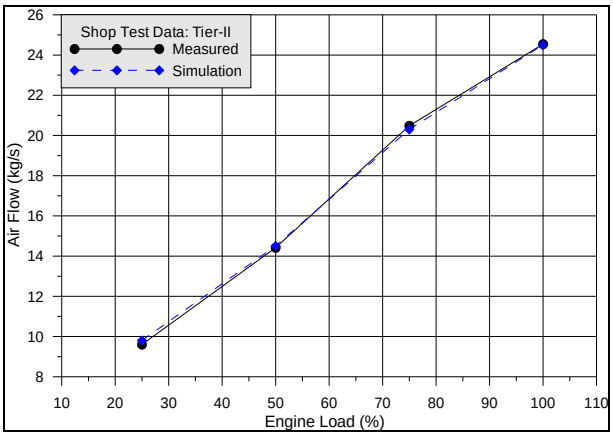

Figure 6-42 Comparison of calculated and measured exhaust gas flow rate, all loads, Tier-II

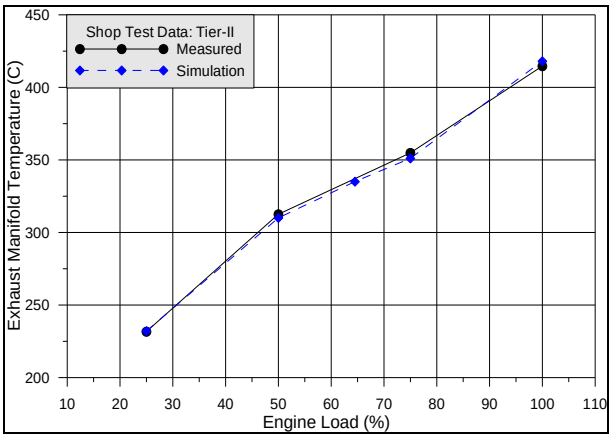

Figure 6-43 Comparison of calculated and measured exhaust manifold temperature, all loads, Tier-II

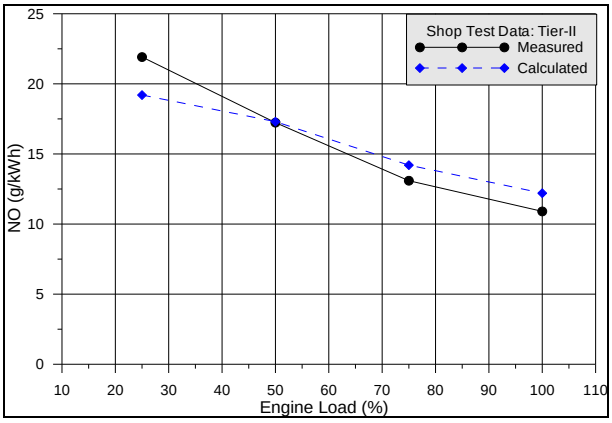

Figure 6-44 Comparison of calculated and measured specific NO emissions, all loads Tier-II

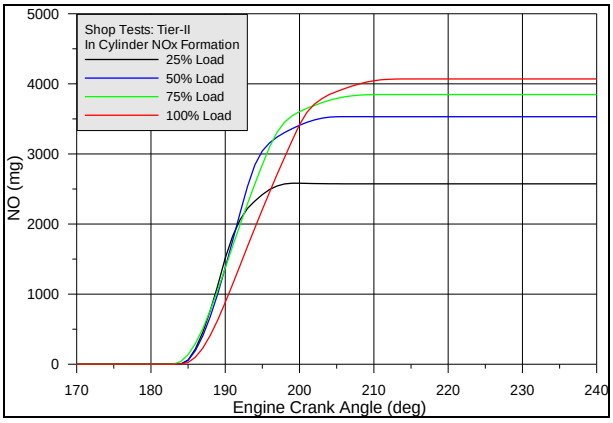

Figure 6-45 Calculated NO_x formation history, Tier-II, all loads

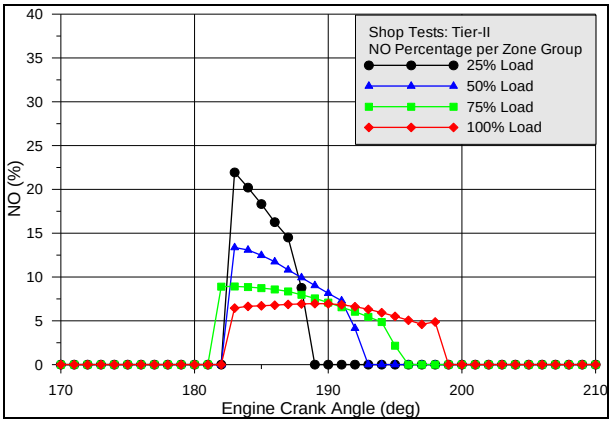

Figure 6-46 Calculated zone contribution to total NO formation, all loads Tier-II

6.4.3 Computational Results Analysis for EGR Enabled Tier-III Engine Performance and Emissions

Following the Tier-II analysis of the engine performance with the use of the multi-zone mode, the Tier-III operation was replicated using the multi-zone combustion model but without application of additional tuning or any constants modification. For this case the operation of both EGR and CBV valves was enabled as described above. The first part of results presented is, as above, comparison of the measured and calculated cylinder pressure traces. This comparison is of high interest since, as established by the measured data, the pressure traces should present considerable differences due to both tuning changes and the recirculated gases presence in the cylinder during Tier-III operation of the engine. In Figure 6-47 to Figure 6-50 the calculated pressure traces comparison with the measured values is provided for all tested loads, 25% - 100%. The agreement remains good but is of slightly lower accuracy compared to the Tier-II results above and is adequate for the present analysis. Some uncertainty exists mainly in the fuel ignition angle but the difference is relatively small. This also results to small differences in the early expansion stage affected by the different start of combustion. Despite the differences the match is adequate and promising especially considering the two factors affecting the cylinder charge mass and composition, namely CBV and EGR. In Figure 6-51 and Figure 6-52 the comparison of calculated and measured engine power output and BSFC is provided with also

relatively good agreement between actual and calculated values. As in the case of the other comparisons, accuracy is slightly lower than the one confirmed for Tier-II operation, which is normal.

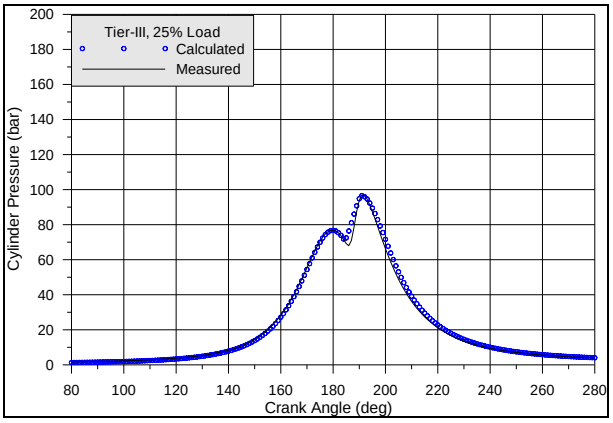

Figure 6-47 Comparison of calculated and measured cylinder pressure traces, 25% load, Tier-III

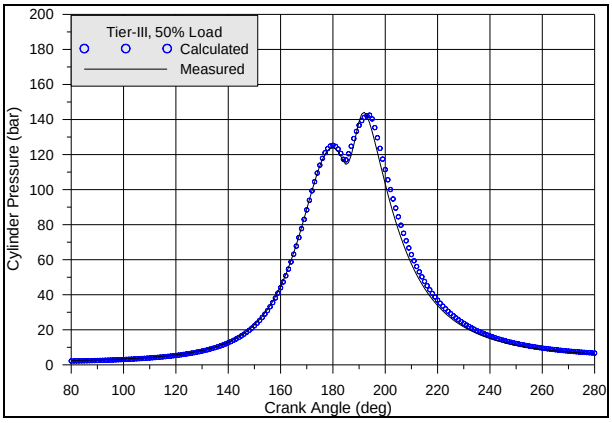

Figure 6-48 Comparison of calculated and measured cylinder pressure traces, 50% load, Tier-III

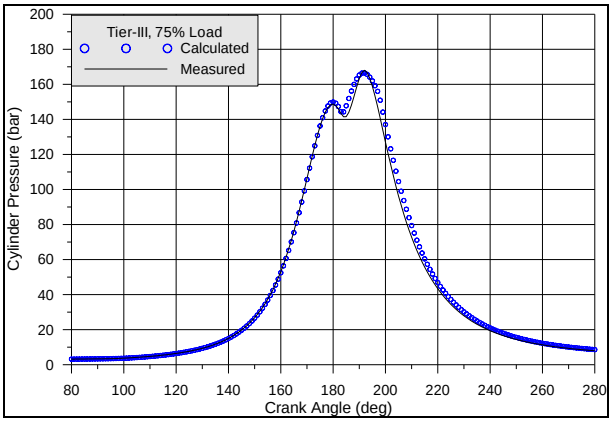

Figure 6-49 Comparison of calculated and measured cylinder pressure traces, 75% load, Tier-III

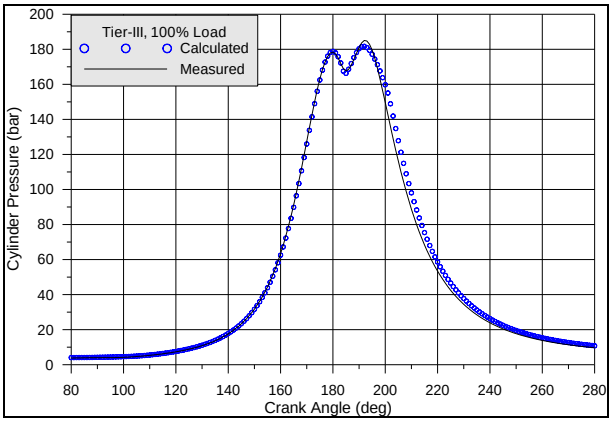

Figure 6-50 Comparison of calculated and measured cylinder pressure traces, 100% load, Tier-III

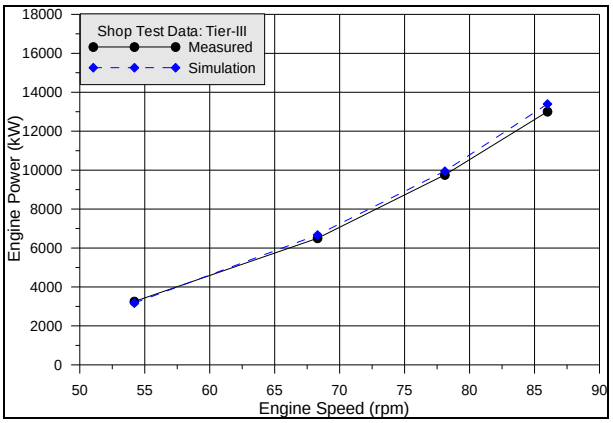

Figure 6-51 Comparison of calculated and measured engine power, all loads, Tier-III

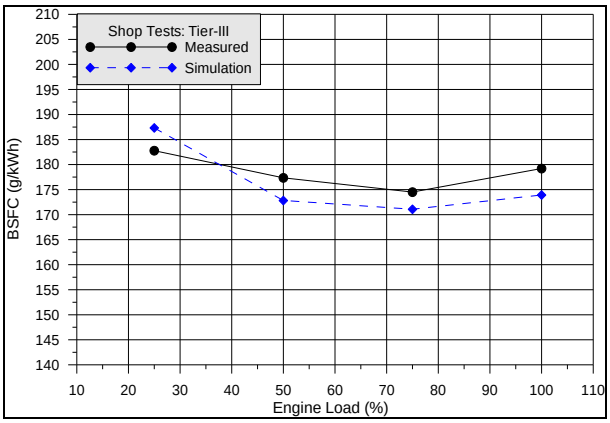

Figure 6-52 Comparison of calculated and measured bsfc, all loads, Tier-III

In order to better understand and analyse the effect of EGR on engine performance and emissions it was decided to utilize the results of the purely theoretical analysis using the multizone model. The comparison conducted below contains only calculated data and is more informative since the differences between measured and calculated data are overcome. Furthermore, this approach allows to distinguish from the direct

comparison of measured data and determine the actual effect of EGR on engine performance and emissions. The comparison focuses mainly on the combustion rate mechanism, NO_x formation, in-cylinder temperature history, air-fuel equivalence ratio and conditions in the exhaust gas manifold from which the recirculated exhaust gas is extracted.

Following the initial comparisons, the effect of the recirculated gases on the burnt zone temperature is investigated using the simulation results. The mean temperature of the burnt zone averaged from the time step used to 1º CA is compared between Tier-II and Tier-III operation. This comparison allows to assess the contribution of EGR to the in-cylinder temperature change and potentially to NO_x reduction. The comparisons are given in Figure 6-53 to Figure 6-56 for all tested loads. The anticipated temperature reduction is clearly confirmed by the model results at all loads examined. Reviewing the difference for each load, the temperature reduction is higher for 25% and 100% load and lower for 75% and 100%. In addition, it is found that temperature is decreased for the first stages of combustion and then gradually increases becoming in higher than Tier-II levels. The last is attributed to engine tuning leading to late combustion and the slower combustion rate of fuel caused by EGR. The late combustion is verified from the experimental findings and is the result of the main combustion event being moved later in the engine cycle and also of the longer combustion duration during Tier-III operation. Regarding NO_x formation this stage has lower effect as the temperatures are rather low and the air fuel ratio is further decreased due to the products of the fuel combustion further to the recirculated gases already present in the cylinder. Since the Zeldovich mechanism shows exponential increase of NO formation with temperature the peak value decrease achieved by the EGR will be of substantial contribution to the pollutant's reduction.

In Figure 6-57 the measured and estimated oxygen percentage in the scavenge receiver is compared. The model estimation is very close to the measured concentration, with lower but still good agreement at 25% load. Overall, minimal levels of error are found with relative difference of predicted O_2 concentration being below 1% which is close to the actual measurement's accuracy. The measured and estimated specific NO_x emissions are given in Figure 6-58. The model estimation of the EGR effect resulted in very good prediction of the NO_x formation in the cylinder. This allows the use of further findings regarding in-cylinder conditions to be used for investigation of the EGR effects. In Figure 6-59 the model calculated specific NO_x emissions are given for both Tier-II and Tier-III mode. The corresponding reduction in emissions due to the use of EGR is provided in Figure 6-60 with inclusion of the measurement results for comparison. A slight tendency to overestimate NO_x reduction is observed at low load, which is partially due to the underestimation of O_2 concentration by the model as seen above in Figure 6-57. The EGR percentage used in the simulation is shown in Figure 6-61. In order to assess the replication of the CBV effect the exhaust manifold pressure comparison of measured and calculated values is given in Figure 6-62. The agreement is very good for all loads that confirms to the degree possible that the effect of the CBV was correctly replicated. Last, in Figure 6-63, the effect of the EGR on the air-fuel equivalence ratio for all loads examined is presented. Two values are provided for each operating mode, Tier-II and Tier-III, one corresponding to the open cycle which represents the overall air-fuel equivalence ratio (scavenge air included) and a second corresponding to the

close cycle which is the actual air-fuel equivalence for combustion. The latter is obviously lower. The effect of the recirculated gases is clear as both values are affected with the later values lower for both non-EGR and EGR operation. The very high λ reduction because of EGR is observed at 25% due to decrease in exhaust mass flow, that as established is half of the Tier-II during Tier-III mode. In addition, the 100% load λ values along with the temperature comparison, Figure 6-56, confirm the expectation form the measurement data analysis stage that the decrease in NO formation is also affected by the engine tuning at this load point, as EGR percentage is decreased and the difference between Tier-II and Tier-III temperature and λ values is the lowest at this point. The decreased λ values in conjunction with the reduced temperature result in the decrease of NO_x formation predicted by the model and actually measured. Overall, the previous findings are a promising result for the model's ability to replicate the multiple changes occurring during Tier-III mode operation and their effect on emissions. Furthermore, a deeper insight is provided that allows the understanding of the NO_x reduction mechanism resulting from the use of EGR.

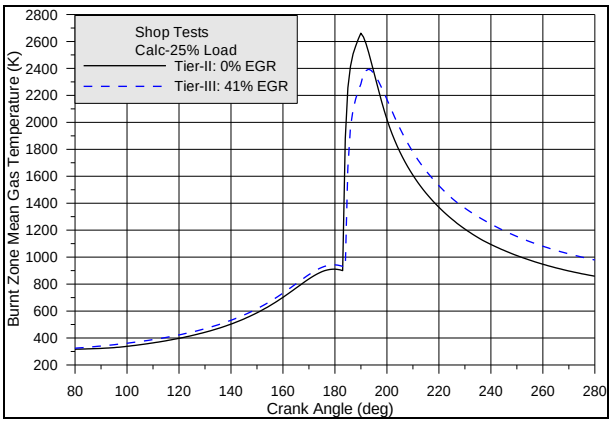

Figure 6-53 Calculated mean burnt zone temperature comparison, Tier-II to Tier-III, 25% load

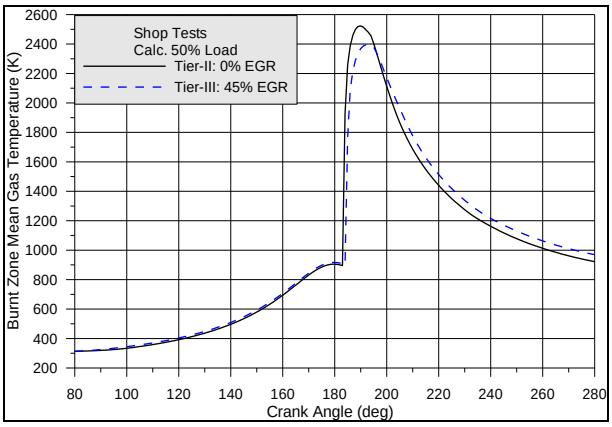

Figure 6-54 Calculated mean burnt zone temperature comparison, Tier-II to Tier-III, 50% load

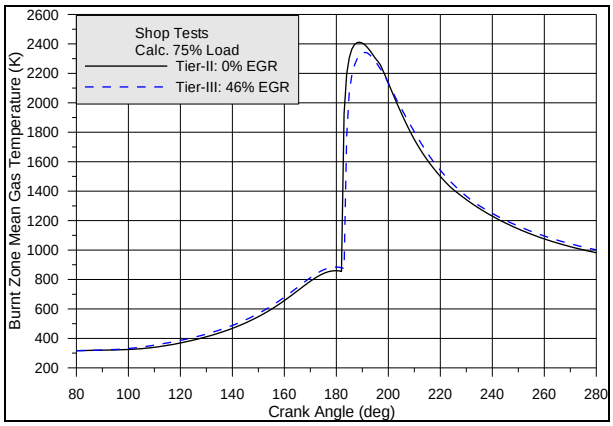

Figure 6-55 Calculated mean burnt zone temperature comparison, Tier-II to Tier-III, 75% load

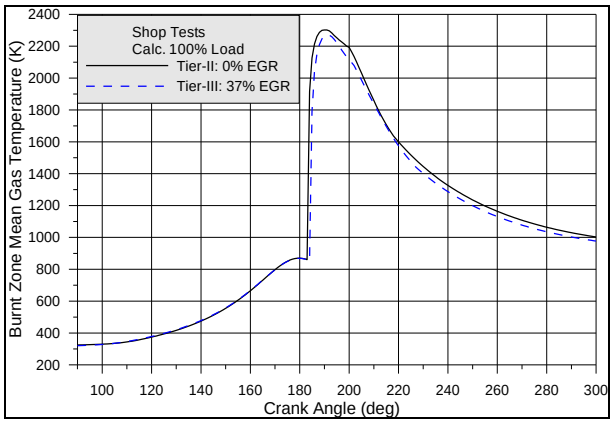

Figure 6-56 Calculated mean burnt zone temperature comparison, Tier-II to Tier-III, 100% load

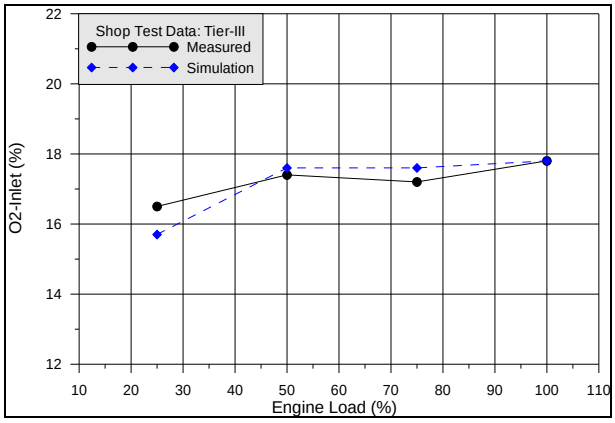

Figure 6-57 Comparison of calculated and measured O2 concentration in the scavenging air receiver, Tier-III

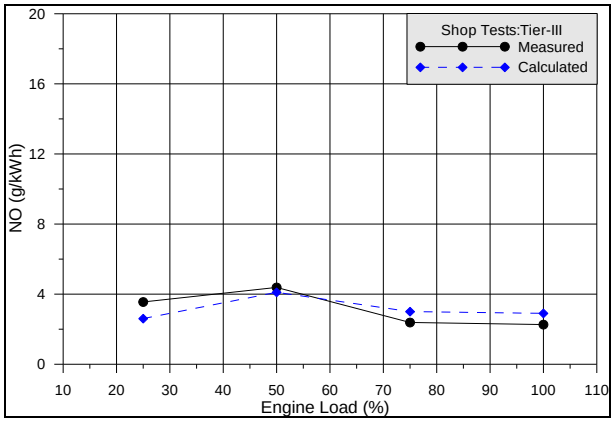

Figure 6-58 Comparison of calculated and measured specific NO emissions, Tier-III, all loads

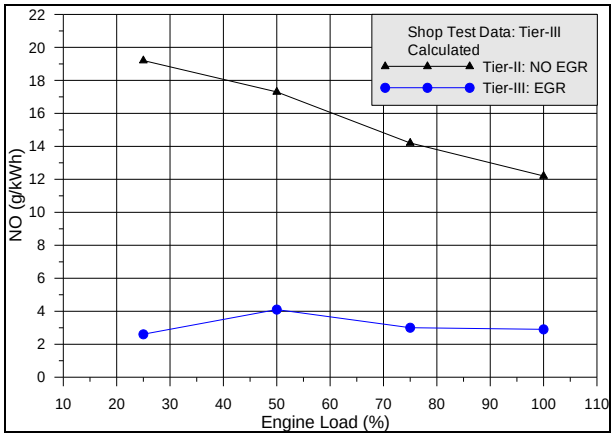

Figure 6-59 Calculated specific NO emissions, Tier-II and Tier-III, all loads

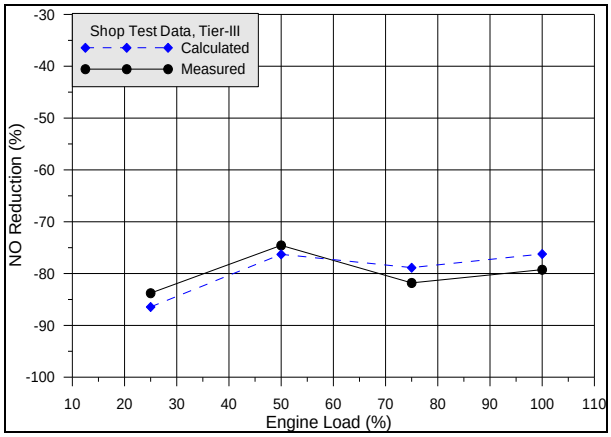

Figure 6-60 Comparison of calculated and measured NO emission reduction due to EGR, Tier-III

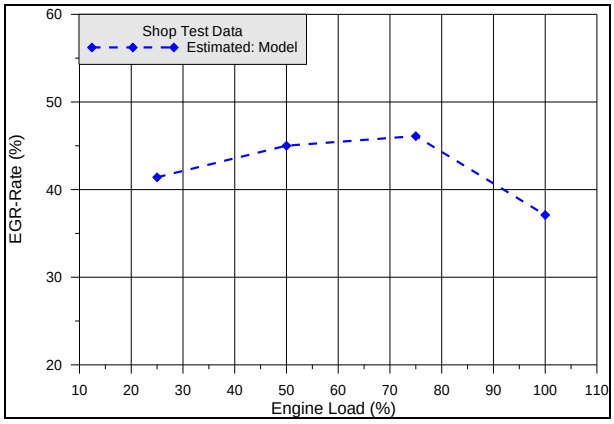

Figure 6-61 EGR rate vs Load estimated by Tier-III simulation

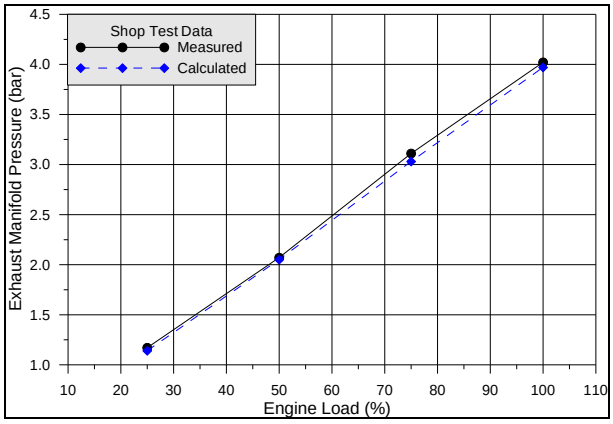

Figure 6-62 Comparison of calculated and measured exhaust manifold pressure, Tier-III, all loads

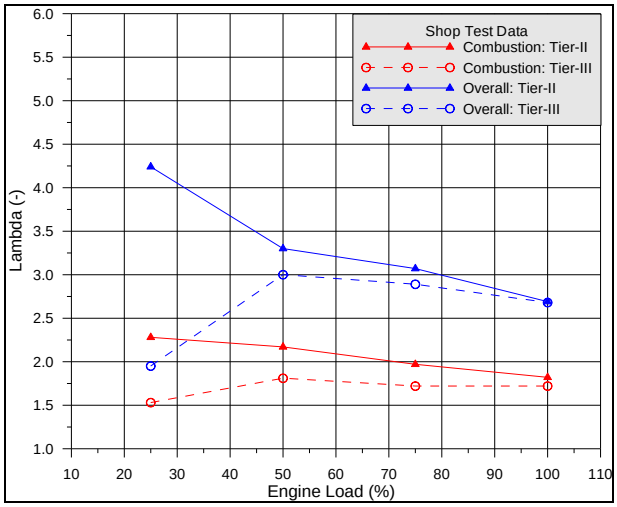

Figure 6-63 Calculated mean air-fuel equivalence ratio overall and during combustion, Tier-II & Tier-III

To further investigate the effect of EGR use on emissions the zone contribution on total emissions is examined. In Figure 6-64 the contribution of the fuel packets of each formed zone during Tier-III operation is given and in Figure 6-65 the comparison of zone contribution between the calculated values for Tier-II and Tier-III mode. From Figure 6-64 and Figure 6-65 less even distribution of NO_x formation is found between the zones, with markedly higher contribution for the fuel packets introduced first in the cylinder and rather steep drop for fuel packets in the zones formed at the end of the injection event. This is normal as the zones formed first will achieve first higher penetration in the combustion chamber and as a result entrainment of the cylinder charge will be higher in them. For the other zones that are formed late during the injection process the combination of the fresh combustion products and the recirculated gases will lead to low λ values and inhibit NO_x formation. Considering the results of the chapter 6 biofuel analysis, the previous acts in a reverse method than the oxygen enriched fuel effect that allowed higher NO_x formation in the zones that should have very low contribution due to lack of oxygen. In Figure 6-66 the NO_x formation history for Tier-III operation is presented. The rate is notably slower for 25% load and highest for 50% and 75% load. This behaviour does not correlate with the change in EGR percentage with load, but rather close match can be found when comparing to the estimated net HRR diagrams of Figure 6-67 peak burn rate regions. It is also noted that the CO_2 percentage is quite higher at 25% load (and O_2 concentration markedly lower), and this also contributes to the overall effect, despite the lower EGR percentage. The comparison of the HRR for Tier-II and Tier-III operation is given for 25% and 75% load in Figure 6-68 and Figure 6-69 respectively. Last, in Figure 6-70 to Figure 6-75 the distribution of fuel-air equivalence ratio, temperature and NO inside the jet is provided for EGR use and “conventional” operation at 75% load 5º CA after injection. The effect of EGR is quite clear, with high reduction of oxygen availability in the fuel jet, especially in the jet inner region, as expected. Significant reduction is also found in the jet periphery. This was also detected by the zone contribution to NO_x formation examined in Figure 6-64 and Figure 6-65. The corresponding temperature distribution reveals lower values compared to non-EGR operation, with the highest reduction, as expected located in the inner jet area.

Thus, NO_x formation is significantly reduced by the combined effect of the lower temperature and O_2 content. Values are higher in the jet's periphery.

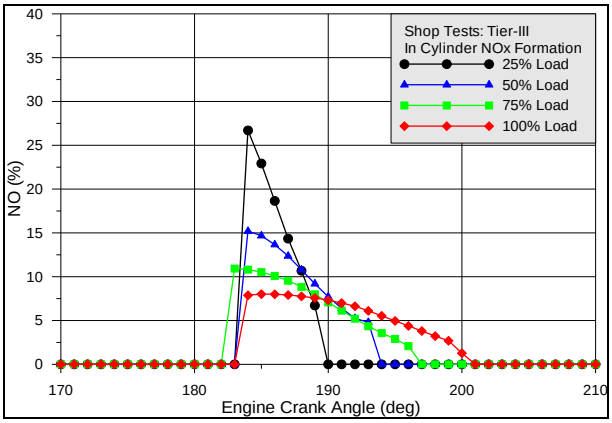

Figure 6-64 Calculated contribution of zones to total NO formation, Tier-III, all loads

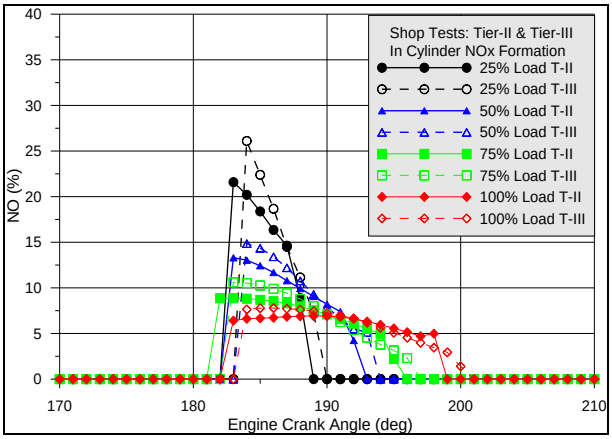

Figure 6-65 Comparison of calculated contribution of zones to total NO formation, Tier-III to Tier-II, all loads

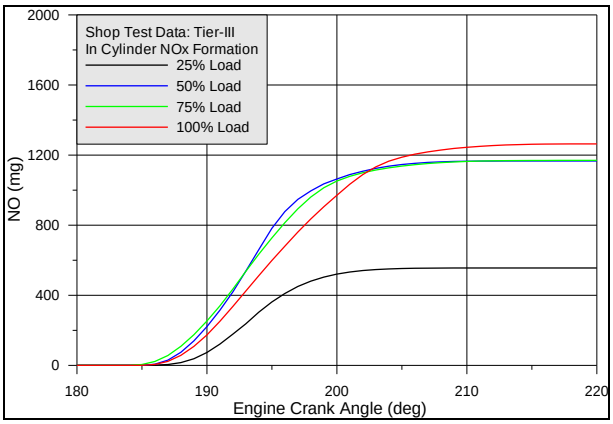

Figure 6-66 Calculated cumulative NO formation, Tier-III all loads

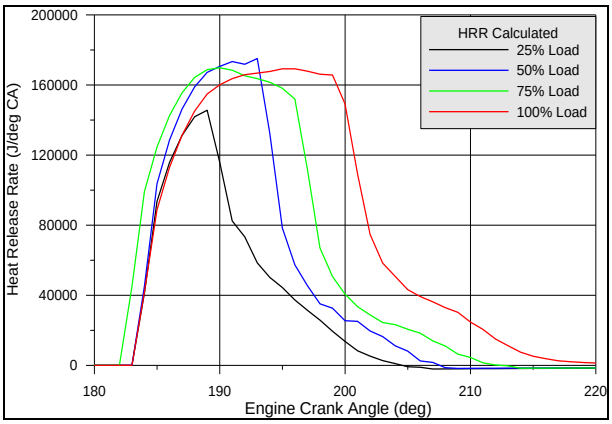

Figure 6-67 Calculated net heat release rate, Tier-III all loads

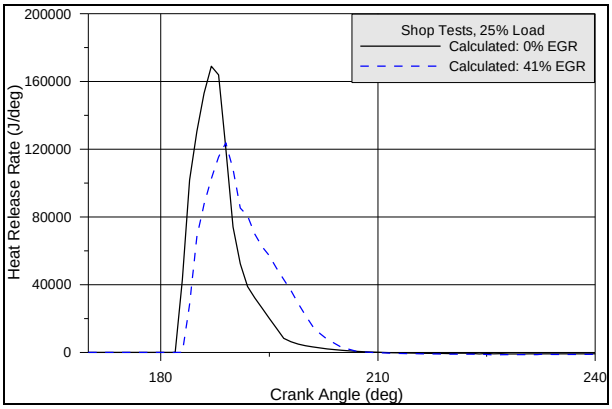

Figure 6-68 Calculated heat release rate, 25% load, Tier-II & Tier-III

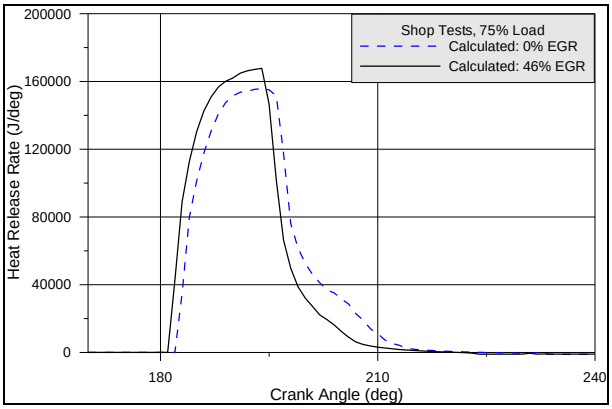

Figure 6-69 Calculated heat release rate, 75% load, Tier-II & Tier-III

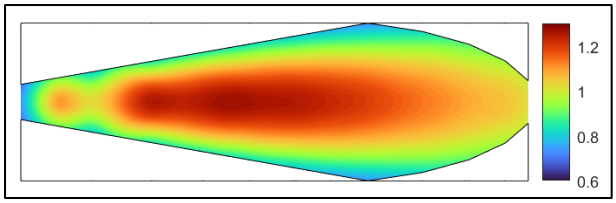

Figure 6-70 Fuel-Air equivalence ratio distribution in the jet area 5deg CA after injection, 75% load EGR

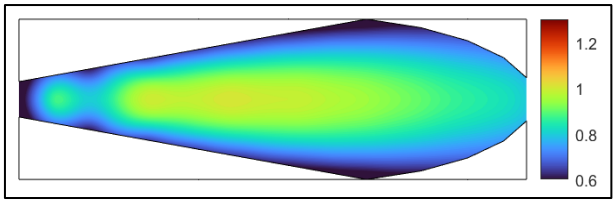

Figure 6-71 Fuel-Air equivalence ratio distribution in the jet area 5deg CA after injection, 75% load no EGR

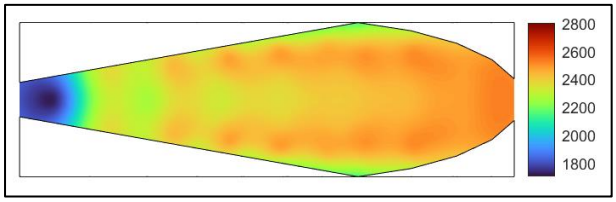

Figure 6-72 Temperature distribution in the jet area 5deg CA after injection, 75% load EGR

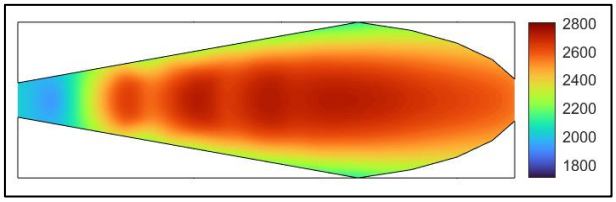

Figure 6-73 Temperature distribution in the jet area 5deg CA after injection, 75% load no EGR

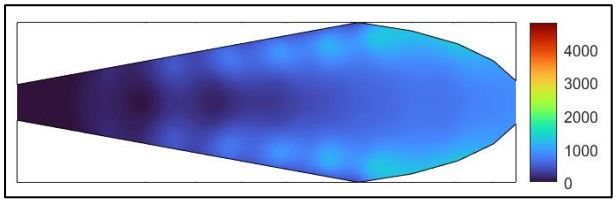

Figure 6-74 NO distribution in the jet area 5deg CA after injection, 75% load EGR

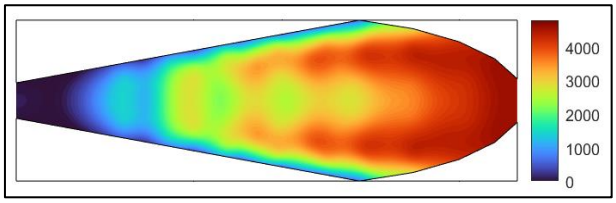

Figure 6-75 NO in the jet area 5deg CA after injection, 75% load no EGR

6.4.4 Computational Investigation to Minimize the BSFC Penalty from the Use of EGR

In this section a parametric analysis is conducted for Tier-III operation to examine the potential for BSFC penalty reduction via engine tuning changes. The investigation is conducted using the multi-zone combustion model using the following criteria:

- Same NO_x emission values which result to the same NO_x reduction. This requires increase of the EGR rate which is to be maintained below 55%.
- Minimization of the BSFC penalty.
- Maintenance of peak combustion pressure at acceptable levels.

For the analysis and based on similar studies conducted for 2-stroke engines the engine setting parameter investigated is SOI timing as it has considerable effect on combustion and fuel efficiency. Furthermore, it is the easiest parameter to adjust in modern marine engines.

In Figure 6-76 the achieved BSFC reduction is presented and compared to the values of Tier-III reference setting operation and the Tier-II values. It is noted that all values depicted are the result of the calculations. As observed the BSFC was significantly reduced for all loads. For 25% the BSFC penalty was reduced by more than 50%. The required change in SOI timing is given in Figure 6-77. An up to 4^o CA SOI advance was required for the required levels of BSFC reduction. Further increase at 25% load would lead to P_{max} values that are too high but would result to no additional BSFC benefit, while increasing at the same time NO_x emissions. The required SOI retard decreases with the increase of engine load and is limited by the corresponding increase of peak cylinder pressure P_{max}. The available range for timing changes was also found to decrease with load, due to the effect on P_{max} and also due to diminishing results in terms of fuel efficiency gains as increase in the gas recirculation rate was also required to contain NO_x formation that had the opposite effect on combustion efficiency. The required increase of EGR ratio to maintain NO_x emissions at the same level, as calculated by the model is shown in Figure 6-78. On average the SOI advanced tuning will require 5% EGR ratio increase on average, that for some loads translates to above 50% recirculation ratio, which is very high. The effect of SOI advance on P_{max} values mentioned earlier is presented in Figure 6-79. The pressure increase compared to reference, both Tier-II and Tier-III values is considerable especially at low load. The specific investigation reveals that there exists a potential for BSFC improvement. However, careful consideration due to the estimated high EGR rates is required due to the limitations of the total mass of recirculated gasses that can be treated in the gas cleaning system.

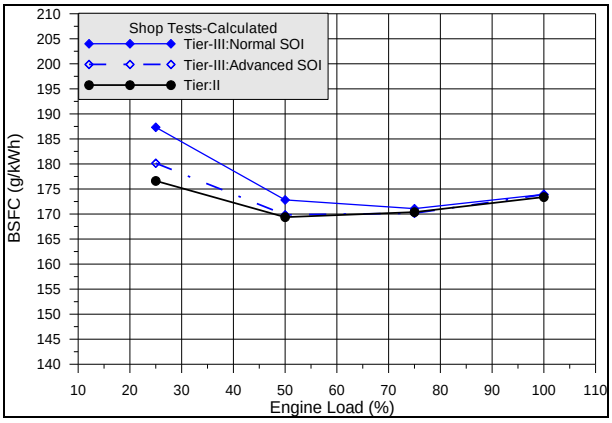

Figure 6-76 BSFC after SOI advance comparison to reference SOI timing Tier-III & Tier-II values; model calculation results

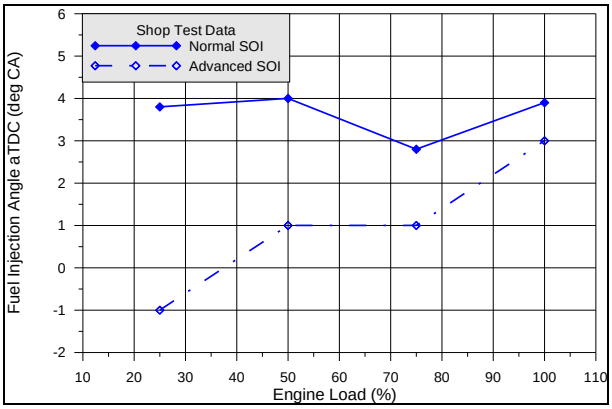

Figure 6-77 SOI advance estimated for Tier-III BSFC optimization

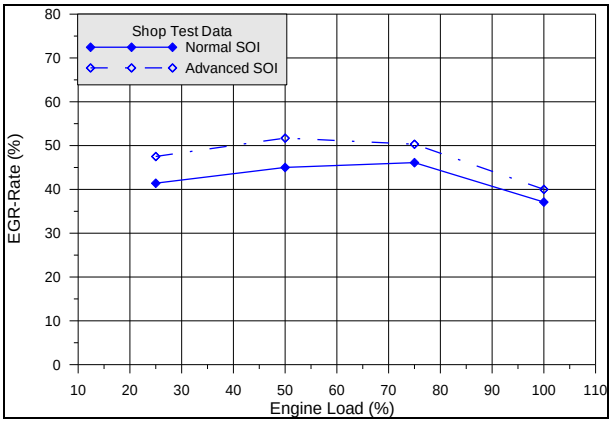

Figure 6-78 EGR rate estimated for Tier-III BSFC optimization via SOI advance

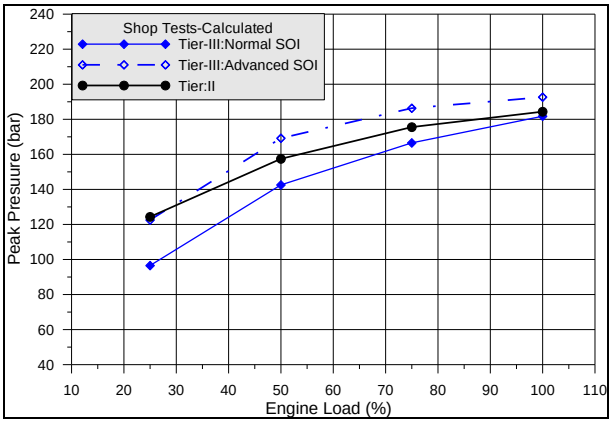

Figure 6-79 Calculated effect of SOI advance on P_{max}, comparison to reference tuning Tier-III & Tier-II values; calculation results

Following review of the global values below are provided the calculated values for cylinder pressure and heat release rate in comparison the ones prior to SOI adjustment. The results are presented for two characteristic cases, 25% and 100% load. The calculated Tier-III operation cylinder pressure traces are compared using the reference and advanced fuel injection angles in Figure 6-80 and Figure 6-81; the calculated HRR diagrams comparison is provided in Figure 6-82 and Figure 6-83. The effect of the SOI advance on cylinder pressure is clear in terms of ΔP at 25% load, while the effect is much lower at 100% load. The HRR diagrams show small differences and appear only to be shifted earlier relative to TDC. As revealed from the simulation this is the result of the increased EGR rate which affects the combustion mechanism. Peak burn rate is estimated at roughly the same value and the overall combustion process follows similar rate at all stages. The effect of the SOI advance and increase EGR percentage on the burn zone temperature is of interest as it affects NO_x formation. The changes found were very low, as only an offset of the temperatures history in the cylinder cycle was found due to the earlier fuel ignition. The rate of temperature increase, peak values and duration of peak value region were mostly unaffected as the increased EGR ratio was able to limit the close to TDC combustion effects on temperature (and pressure) rise, Figure 6-84 and Figure 6-85. This is in accordance with the similar NO_x values for both cases, of advanced and retorted timing. The injection timing change and

increased EGR ratio affected both fuel-air equivalence values, combustion and overall, only slightly. The effect was twofold as the EGR percentage increased, but the total fuel mass injected in the cylinder was decreased. The combined change was minimal as the overall equivalence ratio values pre- and after the revised tuning are almost the same, Figure 6-86, which is required when aiming to similar NO_x formation levels.

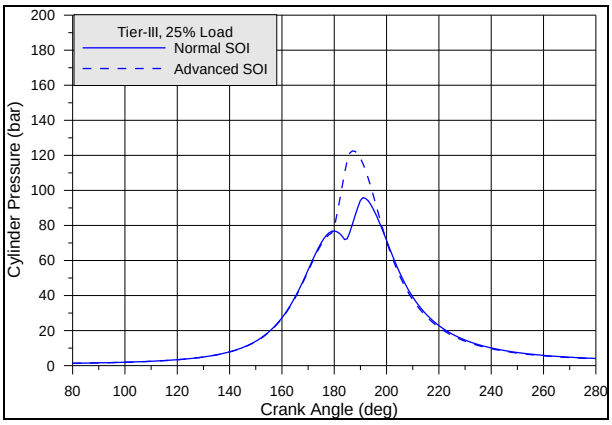

Figure 6-80 Estimated effect of Tier-III SOI advance on cylinder pressure traces; 25% Load

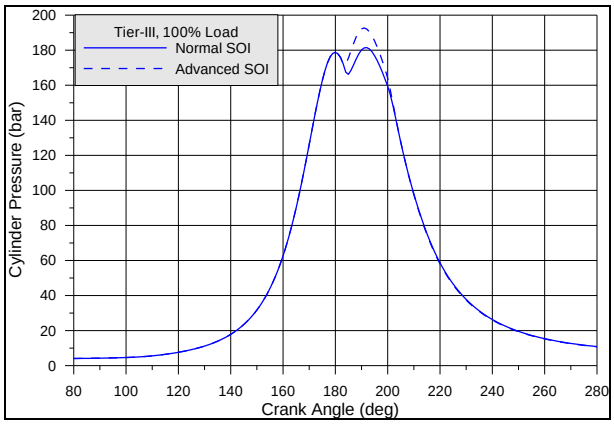

Figure 6-81 Estimated effect of Tier-III SOI advance on cylinder pressure traces; 100% Load

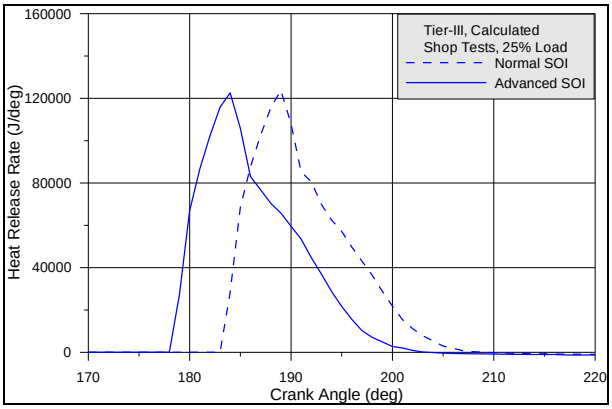

Figure 6-82 Estimated effect of Tier-III SOI advance on heat release rate; 25% Load

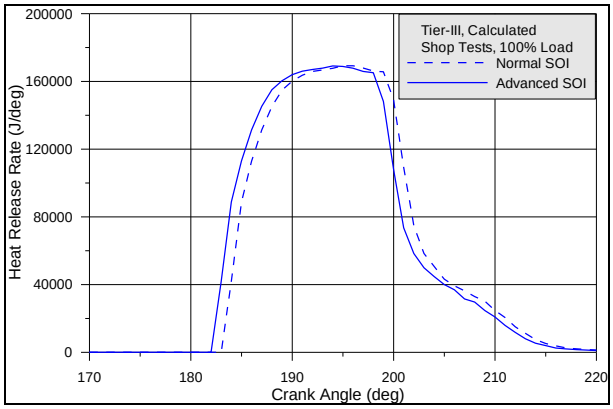

Figure 6-83 Estimated effect of Tier-III SOI advance on heat release rate; 100% Load

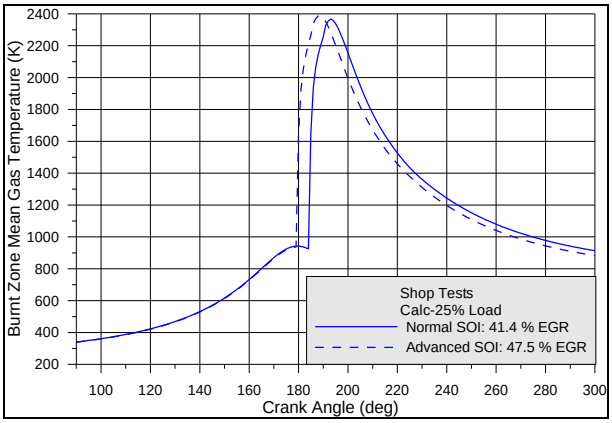

Figure 6-84 Estimated effect of Tier-III SOI advance on burnt zone average temperature; 25% Load

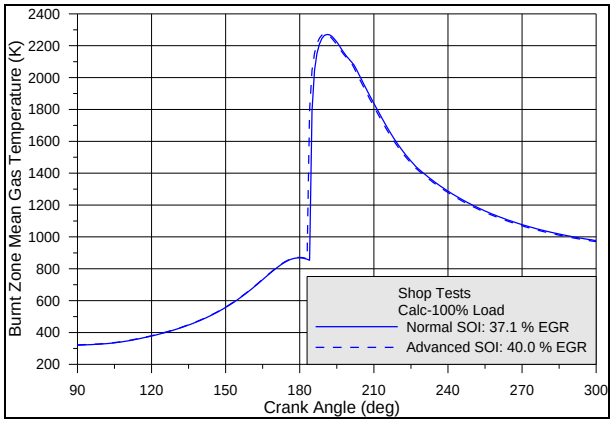

Figure 6-85 Estimated effect of Tier-III SOI advance on burnt zone average temperature; 100% Load

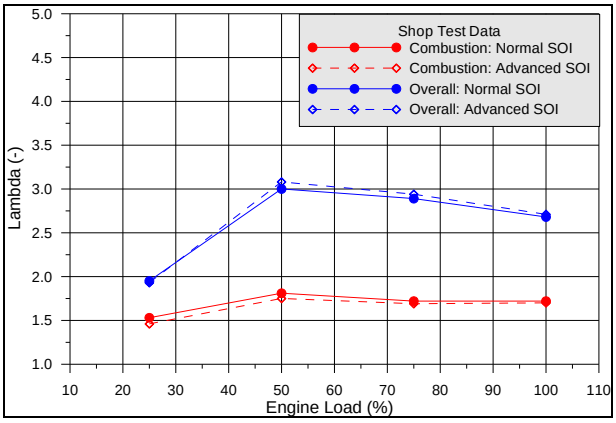

Figure 6-86 Estimated effect of Tier-III SOI advance on overall and burnt zone air-fuel equivalence ratio

6.5 EGR Analysis Summary

In this chapter the effect of EGR use for NO_x formation reduction was investigated for two large 2-stroke engines, one operating with diesel and one operating with LNG at high-pressure injection.

The effects on performance and tuning requirements were investigated by comparison of operation with and without EGR. The main findings were decreased peak pressure values, advanced EVC and SOI timing retard. The use of EGR in combination with the retarded injection timing resulted in reduced ΔP due to combustion, which aided in reducing NO_x formation. The combustion analysis showed reduced rate of fuel burn in the cylinder at all stages and prolonged combustion duration. The "slower" combustion and SOI retard had a negative impact on thermal efficiency and BSFC was increased, especially at low and medium load, with up to 5% higher BSFC compared to operation without EGR. This will significantly increase OPEX when EGR is in use. The results were similar for the diesel only and dual-fuel engine.

The use of EGR proved potent at reducing NO_x formation, but it was found that high EGR percentage is required for this level of NO_x reduction, in most cases over 40%. Linear relation of EGR rate and NO_x reduction was found for most loads.

The theoretical analysis revealed in greater detail the effect of EGR use on O_2 availability. The air-fuel equivalence ratio, λ, was reduced overall and in the fuel jet region especially its inner parts. The contribution of the fuel mass injected at the last stages of injection was considerably decreased due to the combined effect of recirculated gases and new combustion products. Temperature reduction was verified mostly for the peak values that have the highest impact on NO_x formation.

A parametric study was conducted to review the potential of using SOI advance to reduce the BSFC penalty of EGR use. It was found that BSFC can be considerably improved but in order to retain low NO_x emissions higher EGR rate must be used, which might not be feasible in actual conditions due to the recirculated gases handling system limitations. In addition, despite the higher EGR percentage P_{max} values were increase above Tier-II levels.

Chapter 7 Exhaust Gas After-Treatment Measures for NO_x Emissions Reduction: Selective Catalytic Reduction

In this chapter, SCR, the second major technology used to achieve Tier-III emissions limits of marine engines is examined and evaluated.

The SCR system utilizes a NO_x reduction catalyst to remove the pollutant from the engine exhaust gases without intervening directly on engine operation. Currently the SCR system is the most common technological solution used in the marine industry to achieve Tier-III emission limits, (238). The SCR system is based on using mainly ammonia (NH_3) as a reductant, typically stored in a 40% urea solution, or less commonly used directly, and a catalyst reactor. The catalyst internal design and materials used may differ between vendors, with most marine applications containing primarily vanadium based chemical components due to its increased resistance to sulfur poisoning, (33). For safety reasons, because of the enclosed environment of a marine vessel engine room the reducing agent is in most applications added to the system in the 40% aqueous urea solution form mentioned, (260) commonly known as AUS-40. Inside the vaporiser part of the SCR installation, AUS-40 decomposes into ammonia and carbon dioxide following the reactions below.

$$(NH_2)_2CO_{(aq)} \rightarrow (NH_2)_2CO_{(s)} + xH_2O_{(g)} \quad (7.1)$$

$$(NH_2)_2CO_{(s)} \rightarrow NH_{3(g)} + NHCO_{(g)} \quad (7.2)$$

$$NHCO_{(g)} + H_2O_{(g)} \rightarrow NH_{3(g)} + CO_{2(g)} \quad (7.3)$$

The nitrous oxides in the exhaust gas are reduced to N_2 in the catalytic converter where chemical reactions take place on its elements. The common reaction path is provided in the below equations:

$$4NO + 4NH_3 + O_2 \rightarrow 4N_2 + 6H_2O \quad (7.4)$$

$$2NO + 2NO_2 + 4NH_3 \rightarrow 4N_2 + 6H_2O \quad (7.5)$$

$$2NO_2 + 4NH_3 + O_2 \rightarrow 3N_2 + 6H_2O \quad (7.6)$$

The above reactions occur on the surface of the reactors' elements comprised of heavy metals, such as vanadium. The internal layout of the catalyst consists of various blocks with a large number of channels to increase the surface area on which the catalytic process takes place, (261). The above reactions require a certain temperature window to proceed with the required path and with high rate in the catalyst environment. The typically desired reaction temperature is a minimum of 300ºC, (233). The reaction rate, and consequently SCR system efficiency generally improves with temperature, (234). However, in cases of extreme exhaust gas temperature values the ammonia added may burn leading to lower overall system efficiency and possible degradation of the catalytic elements, (262). In addition, temperature lower than 450ºC should be maintained to avoid the possibility of SO_3 formation as it can react with ammonia to create ammonium sulfate, which is corrosive and create depositions on the catalytic elements' surface reducing the efficiency of the catalyst, (262). For temperatures that are too low, the sulphur oxides react with ammonia to create ammonium

bisulfate, a form of salt that similarly creates depositions and causes catalyst efficiency degradation by reducing its effective surface, (263).

The reliance of the SCR systems on urea use is the main negative of its implementation in marine engines which require, as demonstrated below with the use of measured data, considerable amounts of reductant for operation. The price of urea is provided in Figure 7-1 in comparison to crude oil provided by the source suggested by the ICTT in their analysis of the SCR system in a marine environment, (264). Excluding the maximum and minimum values of both commodities it is established that for the last five years prices were roughly equivalent between urea and HFO. The pricing of the AUS 40 has similar high variations in price as is lately the case for the AdBlue equivalent solution for automotive SCR applications, (265). Some studies of SCR OPEX viability for large marine engines estimate roughly equivalent AUS 40 to the solid urea prices, while in others the solution's price is estimated based on the 40% mass content of urea (238) and (266–269).

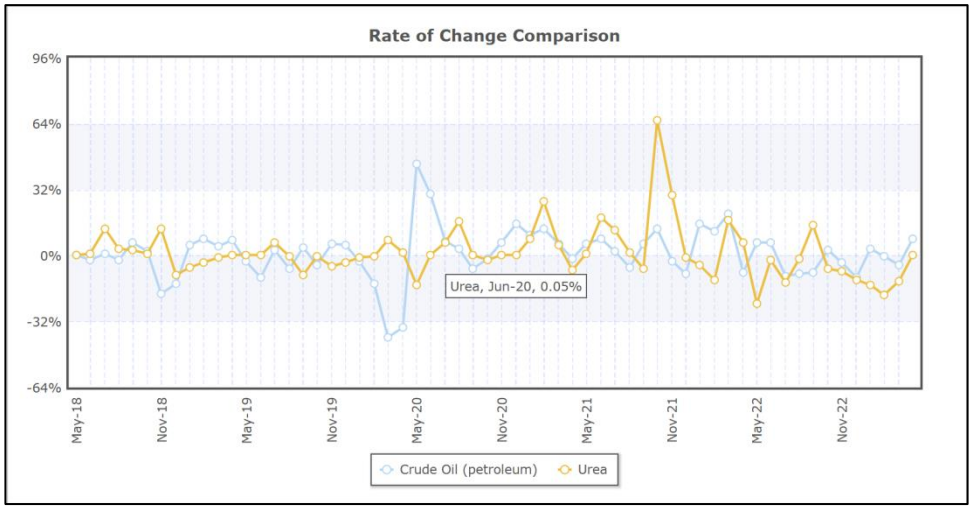

Figure 7-1 Historical trend of urea vs crude oil price, 2018 – 2023, (270)

7.1 SCR System Implementation in Marine Engines

There are two forms of SCR system installation in marine engines depending on the catalyst placement; before or after the turbocharger, (233). Arrangements after the turbine are designated low-pressure (LP-SCR) systems, while implementations before the turbine are designated high-pressure (HP-SCR) systems. For both implementations the denitrification efficiency is high and can reach up to 90%. The main difference between them is the minimum exhaust gas temperature and maximum fuel sulphur content that can be supported, (261). The HP-SCR systems can operate with fuels of higher sulphur content such as HFO, even though such applications are relatively uncommon due to catalyst fouling concerns. The HP systems are recommended for large 2-stroke engines that commonly have low exhaust gas temperatures due to their scavenging process and low fuel-air ratio, (263). The working pressure of HP-SCR systems is commonly 1.0 ~ 4.5 times the atmospheric pressure and the operating temperature around 50 ~ 175^{o}C above the temperature after the

turbine, (261,263). Despite the previous, for low loads the exhaust gas temperature can be lower than ideal. For this reason, the engines outfitted with HP-SCR systems are usually equipped with a cylinder bypass valve (CBV), (233). The CBV allows to control the amount of air entering the cylinder while keeping scavenging pressure steady. By opening of the CBV, part of the inlet air is bypassed to the exhaust manifold lowering air mass in the cylinder and resulting in temperature increase of the exhaust gases. At the same time turbine operation is assisted due to the increased exhaust manifold pressure. The main drawback of HP systems is that by their placement they have an impact on engine operation by the induced additional exhaust back-pressure, and turbine efficiency is also decreased, as the presence of the catalyst disturbs gas flow, (260,271). The previous negatively affect the engine fuel efficiency. The fuel penalty is mostly negligible for higher load, as found in other studies, (233,260), even though pressure drop in the catalyst increases with exhaust gas flow, hence also load. Other issues are an overall more complex layout that requires changes in the typical engine inlet and outlet systems, (233,260) and high space requirements for installation in the engine room. Sizeable thermal inertia of the reactor can affect transient conditions performance, especially when enabling the system from Tier-II mode, (272).

The LP-SCR implementation is more suitable to 4-stroke auxiliary generators as their exhaust gas temperature is considerably higher than that of 2-stroke engines, (263). The system's operating pressure is the same or slightly above the atmospheric pressure. The impact on fuel efficiency is minimal due to the previous. For 4-stroke auxiliary generators the LP-SCR system can operate on both low and high sulphur content fuel, (263). This implementation is also used in 2-stroke main engines due to the lack of an efficiency penalty, however certain requirements must be met. The system requires the use of very low sulphur fuel, typically 0.1% and below, and changes to engine tuning, especially at low load, to raise exhaust gas temperature, (233). Apart from the tuning itself, common techniques used are cylinder air bypass and exhaust gas bypass to raise gas temperature at reactor inlet, (233,260). Other methods that can be used are heating of the exhaust gas using a secondary electric device or fuel injection in the exhaust pipe for re-ignition, with the latter being the preferred method by engine manufacturers if such an approach is followed, (260). The use of the heating systems can have a negative impact on fuel consumption that is more pronounced at low load when heating requirements are higher. The same applies for the use of exhaust gas by-pass via an EGB. The penalty will be further pronounced in cases that the exhaust gas temperature is close to the required minimum threshold for safe catalyst operation, (233).

The estimated specific fuel consumption penalty values for the HP implementation are between 0.5 – 2.0 g/kWh and for the LP systems between 1.0 – 2.0 g/kWh compared to a low load EGB tuning engine, (233). The urea solution consumption is expected to range around the 17.9 g/kWh value, (233). This, however, will depend on the catalyst geometrical design and size, as well as the exhaust gas temperature values, which affect the efficiency of the NO_x reduction reactions. The previous shows that the BSFC benefit of the LP-SCR system compared to the HP one is mainly expected for 4-stroke engines that do not require additional measures to increase exhaust gas temperature. This does not mean that LP-SCR systems do not provide

benefits in the case of 2-stroke engines, as the overall installation is much simpler compared to the HP implementation.

7.1.1 SCR System Layout

The components and layout of the SCR system are mostly common for both HP and LP implementations. The main parts of the system are the reactor, urea tank, vaporiser assembly of the mixer and the urea supply system, soot blowing system and the SCR valves. The LP system additionally requires a burner and blower system, (260). An example schematic for each implementation is provided in Figure 7-2 and Figure 7-3. The urea solution flows into a vaporiser unit, is heated by the flowing exhaust gas and quickly decomposes into ammonia. The ammonia mixes with the exhaust gasses, aided by compressed air or fresh water injection and enters the reactor where the denitrification reactions take place, (262,273). The mixer is usually a static assembly with a geometry specifically designed to affect gas flow and enhance mixing speed and uniformity of urea concentration in the mix entering the SCR reactor, (262). The soot blowing system is required to avoid clogging of the reactor elements from depositions by particles in the exhaust gas, ash and soot and is activated routinely via an automatic process, (233).

The specifications of the SCR system can be modelled using known correlations as is performed in (269) and are the function of exhaust gas quantity and space velocity. The number and density of the catalytic material layers inside the catalyst is estimated using the exhaust gas flow, its velocity, catalyst calculated size and the desired NO_x reduction efficiency. Then, the required urea consumption can be calculated using the expected NO concentration in the exhaust gas entering the catalyst. For more accurate predictions an allowed percentage of ammonia slip can be set along with the expected catalyst effectiveness, (274). The total size of the SCR catalyst will affect the capital investment cost. Due to its size being proportional to exhaust gas flow rate this will scale with engine power output. The same will occur with the special requirements in the engine room to accommodate the reactor system, especially for HP systems due to the higher exhaust gas space velocity compared to the LP system that is placed after the turbine. This is one of the major drawbacks of an SCR system installation as it can require extensive modifications to the main engine room layout, (233).

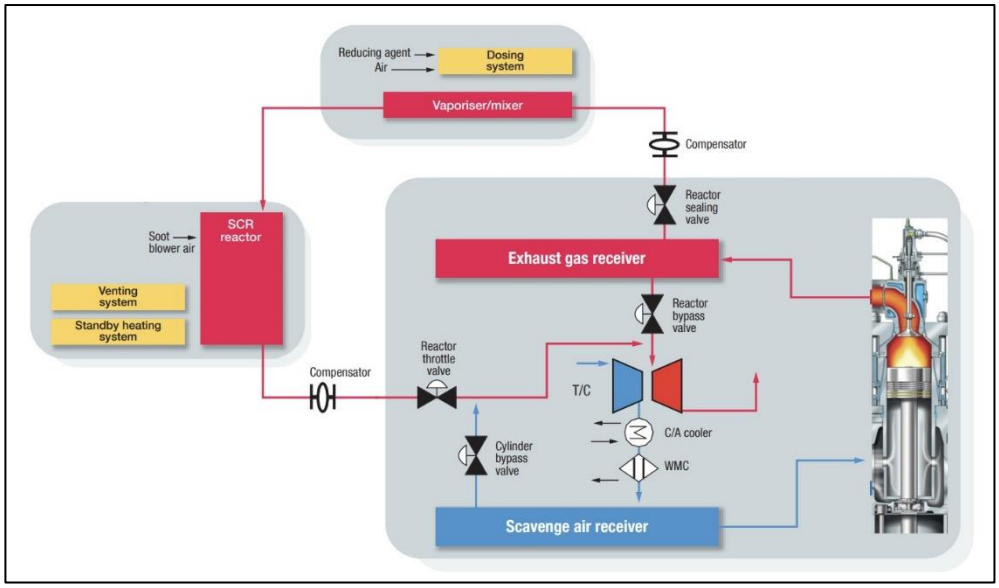

Figure 7-2 Schematic of 2-stroke marine engine High Pressure SCR system, MAN Energy Solutions, (233)

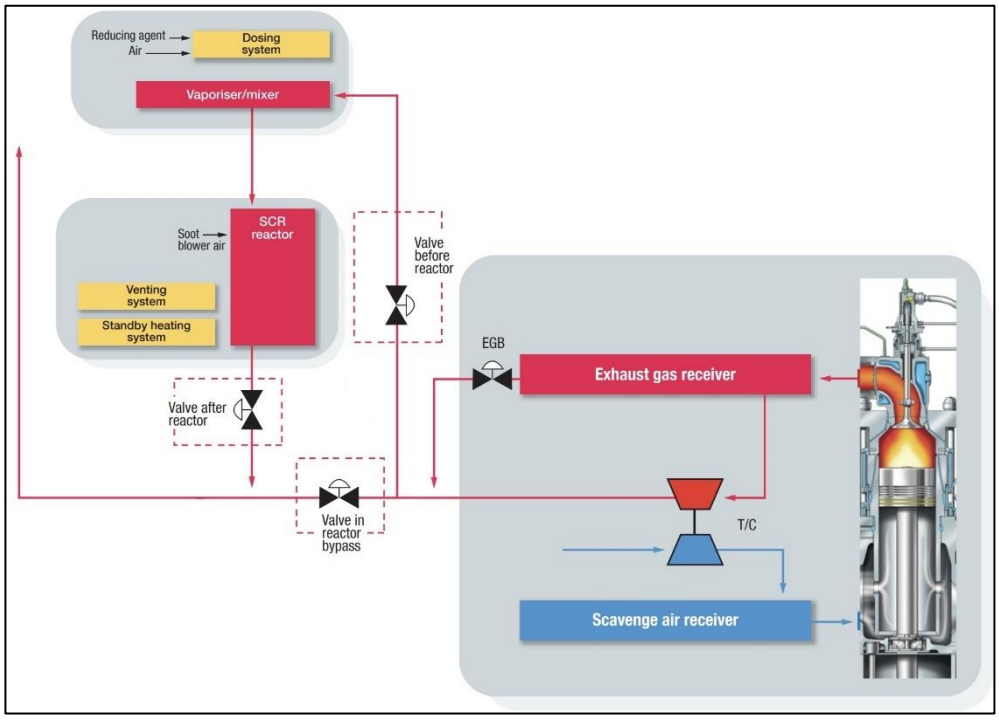

Figure 7-3 Schematic of 2-stroke marine engine Low Pressure SCR system, MAN Energy Solutions, (233)

7.2 Evaluation of Low Pressure SCR System on Engine Performance & Emissions

In the present section the impact of utilizing a low-pressure SCR system to achieve Tier-III NO_x emissions certification on a 2-stroke large marine engine is examined. In addition to the SCR system the tuning choices of the manufacturer for the Tier-II and Tier-III modes are examined. The data used for the analysis were

acquired both during the engine NO_x certification process and during the official Sea Trials after the engine's installation on the vessel.

7.2.1 Engine Performance & Combustion process Comparison Tier-II – Tier-III, LP SCR System

Since the SCR is an exhaust gas after treatment device, the expected effect on engine operation is minimal. Penalties will result by the added pressure drop in the catalyst and any other accompanying device inhibiting gas flow, and work loss in the turbine due to EGB opening. Further impact may occur from efforts of the engine manufacturer to increase exhaust gas temperature at cylinder outlet by alternating the effective compression ratio via EVC timing or using early EVO angles. Another possible approach is increasing SOI retard well after the TDC. This will provide the added benefit of lowering NO_x concentration in the exhaust gasses that will decrease the catalyst reduction efficiency requirements and further potentially result in higher exhaust gas temperature during the expansion cycle. In the examined engine, its particulars provided in Table 7-1 below, the exhaust gas temperature control is achieved using an EGB valve that allows the exhaust gas to bypass the turbine and to mix again with the exhaust gas to increase mean temperature at the catalyst inlet. The fuel used in these engine's tests was typical MGO grade with minimal sulfur content. This is the type of marine fuel recommended for use in the LP-SCR system of a large 2-stroke low-speed engine.

Table 7-1 SCR-LP engine particulars

7G80ME-C9.5	**Units**	**Value**
Type	-	Two-stroke
Electronic Control	-	Yes
Cylinder No.	-	7
Bore	mm	800
Stroke	mm	3720
Nominal Speed	rpm	72.0
Nominal Power	kW	26,890
NO_x Certification	-	Tier-III
SCR Type	-	Low-Pressure with TC EGB

7.2.2 LP-SCR Engine Performance Analysis

In Figure 7-4 the peak combustion pressure is compared between Tier-II and Tier-III operation, and the pressure increase due to combustion is provided in Figure 7-5. The P_{max} values are nearly identical for all loads with minor differences. The ΔP result of the combustion process shows minimal differences with only the 75% load lower value being of note. As the 75% load point is the most crucial for achieving a low total weighted NO_x emissions value due to its high W_f, the ΔP decrease (which commonly lowers NO_x formation) may be conducted by the engine manufacturer to further decrease NO_x emissions even before the SCR catalyst. Review of the engine settings affecting P_{max} and ΔP, specifically fuel injection and ignition angle, Figure 7-6, and pressure ratio (P_{comp}/P_{scav}), Figure 7-7, show considerable differences in engine tuning between the Tier-II and Tier-III modes. A very slight ignition, hence also injection angle, advance is found for Tier-III

operation. The difference is between 0.2º – 0.5º C.A. which is low but not negligible due to the engine low rotational speed. A minor benefit in BSFC can be expected by the small SOI advance, however the parameter controlling injection timing is the P_{max} value that has the same setting for Tier-II and Tier-III mode in the engine control system and SOI is automatically modified accordingly. High difference is found regarding effective compression ratio, hence EVC angle timing. A considerable advance of the EVC angle during Tier-III operation was required, due to lower P_{scav} value to retain P_{comp} values at Tier-II levels. For Tier-III mode the operation region of the turbocharger was altered to reduce the exhaust gas mass flow rate, Figure 7-8. The lower in-cylinder mass and similar high pressure values lead to increased temperature allowing efficient and most importantly safe catalyst operation. In combination with the effect of the exhaust gas bypassing the turbine and being directed to the low-pressure side via the EGB the previous effect is further enhanced. The temperature after the turbine for the two modes is given in Figure 7-9. A considerable exhaust gas temperature increase is achieved, especially at low load. The lower temperature values at MCR are due to only partial EGB opening at this load, while for all lower loads the valve was fully open according to the engine control system indications. It is noted that the exhaust gas temperature at cylinder outlet was also increased during Tier-III mode, Figure 7-10. This is the result of the lower mass trapped in the cylinder at similar pressure values. At MCR the exhaust gas temperature at the cylinder outlet was roughly the same for both modes as equivalent in-cylinder mass was trapped. The increase of the in-cylinder gas temperature allows to achieve the after-turbine required temperature with lower percentage of the exhaust gas circumventing the turbine and limiting work loss. The NO_x emissions will be slightly affected, however as found in the previous chapters the highest levels of NO_x formation are localized. In addition, the potential of catalytic reduction systems to eliminate NO_x emissions is very high and only limited by the AUS-40 injection system metering capacity and the catalyst ability to accommodate higher dosing rates without excessive ammonia slip, (234). Measurement of the NO_x emissions before the catalyst was not performed during the tests to experimentally assess the impact of the previous. The exhaust gas mass of Tier-III operation approaches the Tier-II values with load increase, as the exhaust gas temperature is also increased and safety margin above the minimum temperature for the catalyst operation is achieved so no tuning actions that impact efficiency are required.

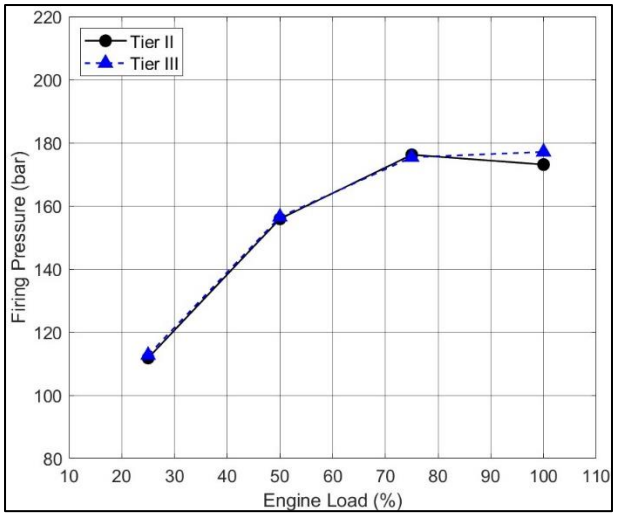

Figure 7-4 Peak combustion pressure comparison, Tier-II vs Tier-III; LP-SCR System

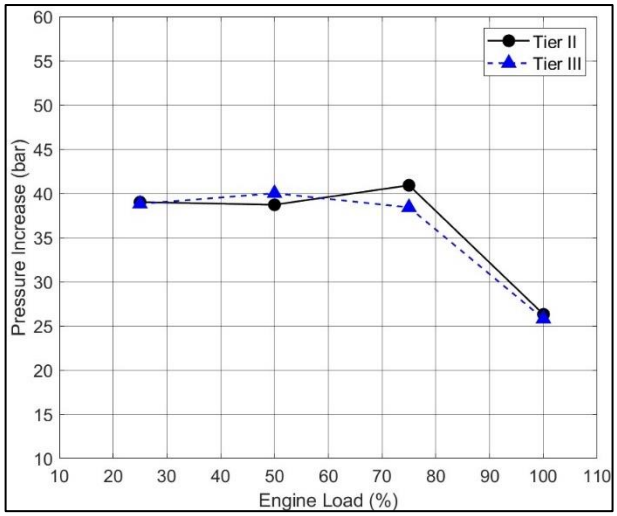

Figure 7-5 Pressure increase due to combustion comparison, Tier-II vs Tier-III; LP-SCR System

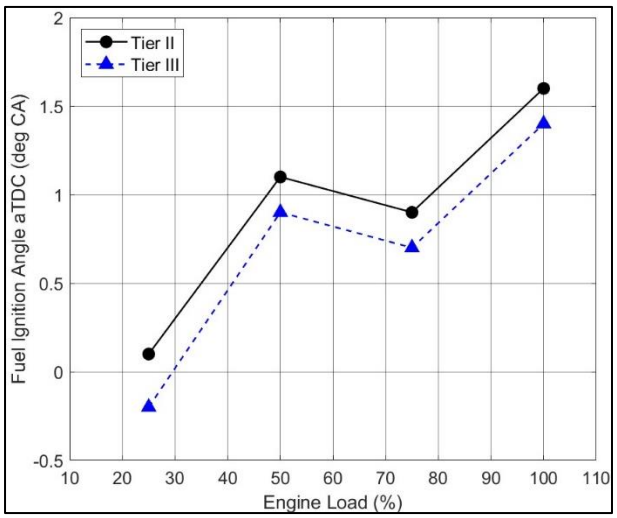

Figure 7-6 Fuel ignition angle aTDC, Tier-II vs Tier-III; LP-SCR System

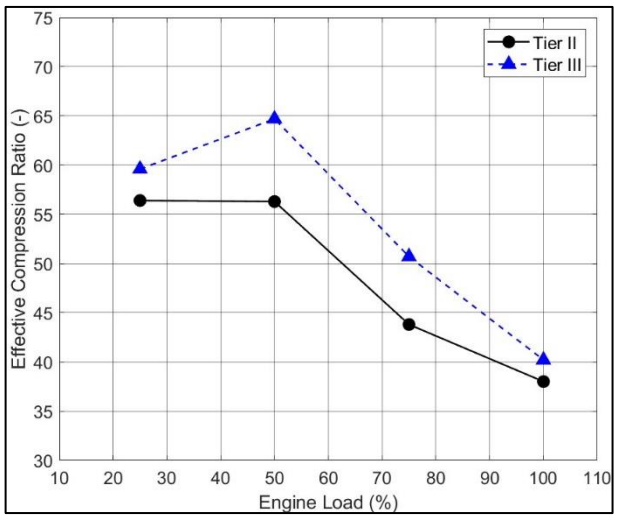

Figure 7-7 Effective compression ratio (P_{comp}/P_{scav}) Tier-II vs Tier-III; LP-SCR System

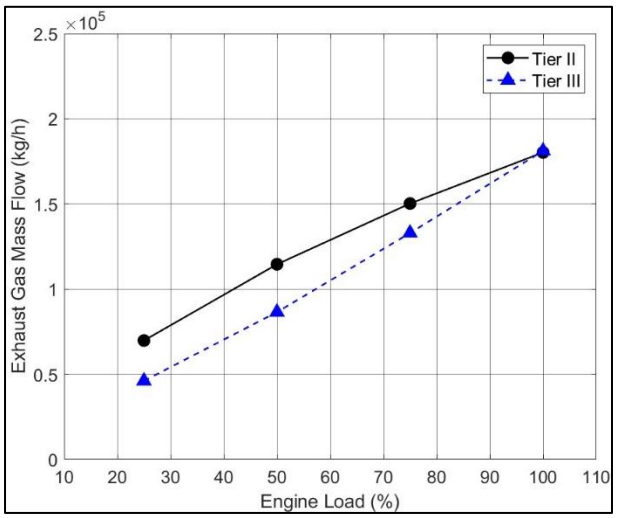

Figure 7-8 Exhaust gas mass flow rate, Tier-II vs Tier-III; LP-SCR System

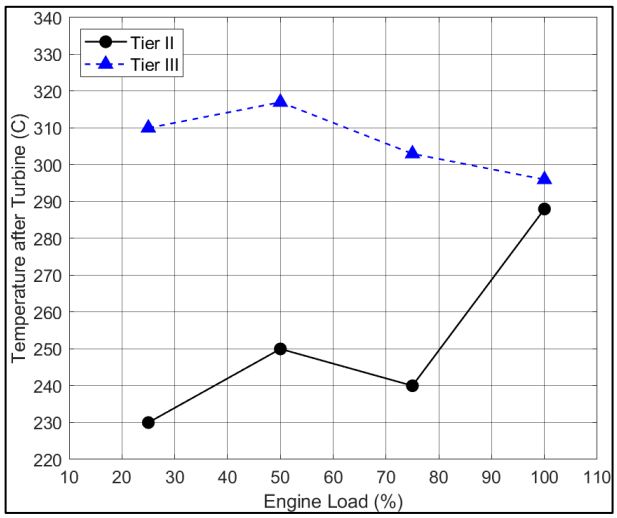

Figure 7-9 Exhaust Gas temperature after turbine, Tier-III mode; LP-SCR System

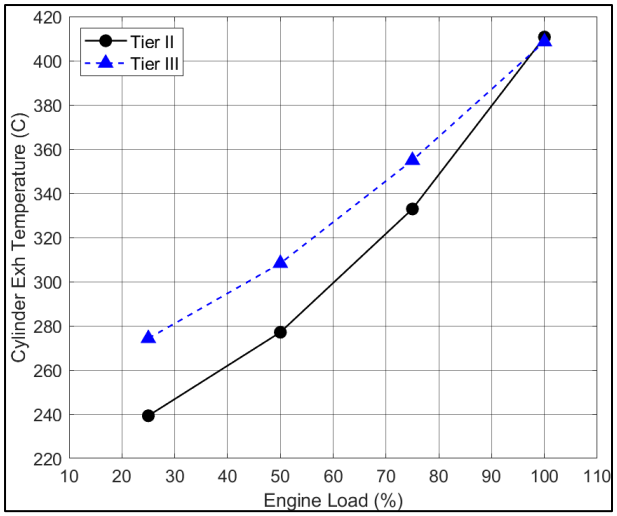

Figure 7-10 Cylinder Exhaust Gas temperature after turbine, Tier-III mode; LP-SCR System

The above alterations are expected to affect the overall engine efficiency and emissions. The effect on engine efficiency can be assessed by the change in specific fuel consumption after normalization to the same LCV. In Figure 7-11 the comparison between BSFC values during Tier-II and Tier-III operation are provided. Efficiency penalty is found during Tier-III operation, that increases with load. This is in contrast with the expectations set by the manufacturer regarding fuel penalty that should be higher at low load as the EGB is fully open up to 75% and partially closed for 100% load. However, with higher exhaust mass flow, Figure 7-8, the impact of the catalyst pressure drop also increases, Figure 7-12, which also results to engine net work loss. At 100% load the pressure drop in the SCR catalyst approached 300mmW, the upper limit for such applications according to official documentation. Last, with the exception of 100% load the BSFC penalty is within the expected range, 1.0 – 2.0 g/kWh, (233). Since it is highly unlikely that a vessel will operate near maximum sailing speed, inside ECA areas, that would require operation close to MCR, for Tier-III mode tuning was prioritized for optimal low and medium load operation.

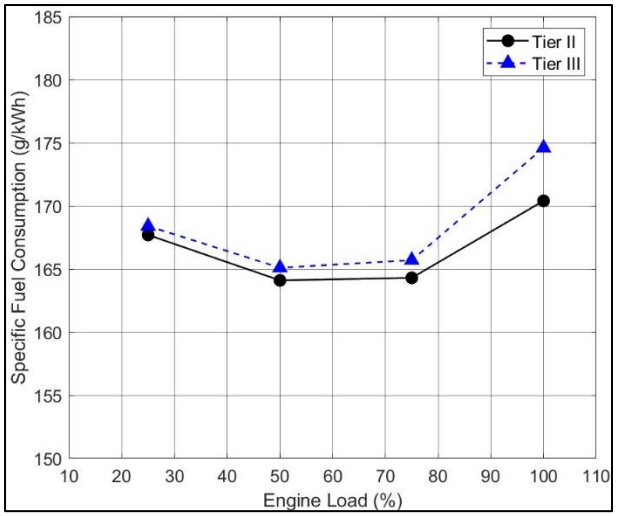

Figure 7-11 Specific Fuel Consumption, Tier-II vs Tier-III; LP-SCR System

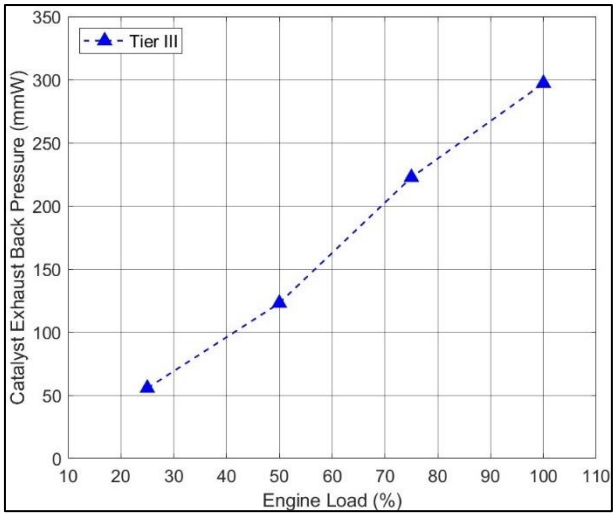

Figure 7-12 SCR Catalyst added back-pressure at Tier-III mode; LP-SCR System

To investigate the impact on the combustion mechanism the comparison of HRR for Tier-II and Tier-III operation is provided. The comparison is given for 25% load and 75% load in Figure 7-13 and Figure 7-14. Heat release rate diagrams present minimal variation with almost identical fuel burn rate, combustion duration and peak combustion values. This verifies that the LP-SCR system has a very low effect on engine performance while requiring some tuning alterations for safe and efficient operation. This analysis verified its expected main benefit compared to the EGR NO_x reduction methodology.

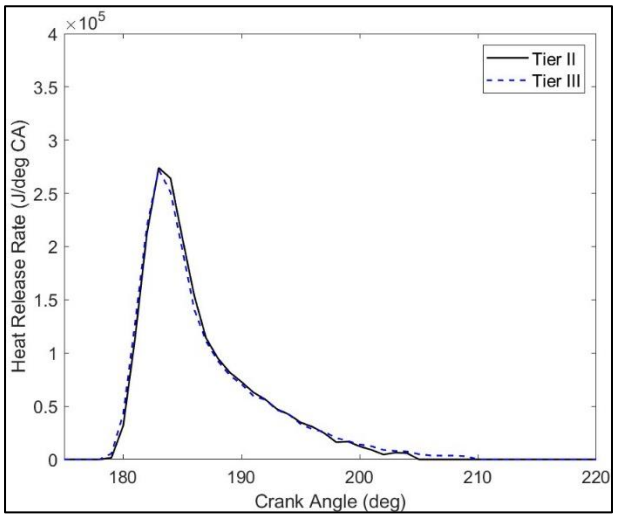

Figure 7-13 Net HRR comparison, Tier-II & Tier-III at 25% load; LP-SCR

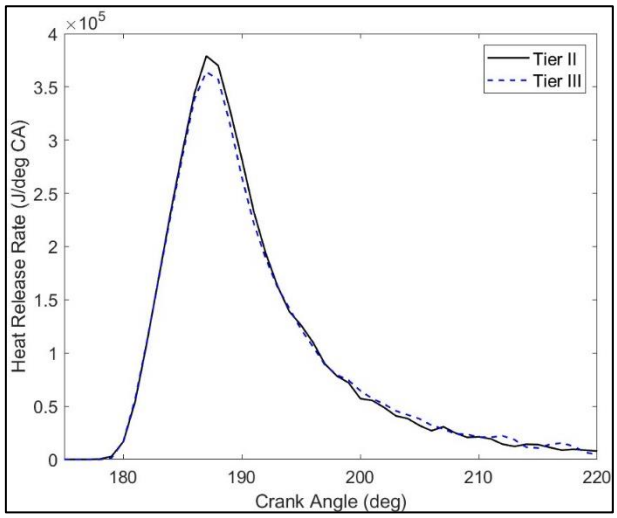

Figure 7-14 Net HRR comparison, Tier-II & Tier-III at 75% load; LP-SCR

7.2.3 LP-SCR System NOx Emissions Evaluation

Due to the quite strict Tier-III NO_x emission limits compared to Tier-II, an SCR system should achieve high emissions reduction efficiency. The performance and emission measurements were acquired during the official certification process of the engine for NO_x emissions, as this was the parent engine of the group specifically tested for NO_x compliance. The NO_x concentration in the exhaust gases measured during Tier-II and Tier-III mode is provided on a wet basis in Figure 7-15. The correction to wet basis (measured values are dry) was selected to better display the actual concentration of NO_x in the gas flow through the catalyst reactor. The specific NO_x emissions are given in Figure 7-16 calculated using the NTC methodology. Using the values of the Tier-II and Tier-III mode the reduction efficiency of the catalyst is given in Figure 7-17, calculated as the difference of Tier-II to Tier-III values. The level of NO_x reduction ranges between 68% to 80%, with the highest values at the 75% load point, as is required to satisfy the total weighted value threshold more easily. For 25% and 50% load the specific NO_x emission values are slightly above the Tier-III limit, however for 75% and 100% values are lower with the total emissions value of the engine ending up well below the Tier-III limit. The previous is affected by the exhaust gas temperature, exhaust gas flow rate and urea solution that can be safely metered at 25% and 50% load. This highlights the challenges of using a LP-SCR system on a large 2-stroke marine engine.

As already noted, an important aspect of the SCR implementation on engines of large size, hence also gas flow, is the required urea solution consumption, as its price historically can range between equal that of crude oil or roughly half, as detailed in section 7.1. In addition its production is rather energy intensive, so its use increases the carbon footprint of the vessel further to OPEX. In Figure 7-18 and Figure 7-19 the total and specific urea consumption is given, as measured during testing. The total urea consumption increases with load up to 75% load, where the peak consumption is required to achieve a better NO_x reduction efficiency. Notably, urea consumption is lower at MCR compared to 75% load, which results in lower catalyst efficiency. The specific urea consumption ranges between 10-24 g/kWh depending on engine load.

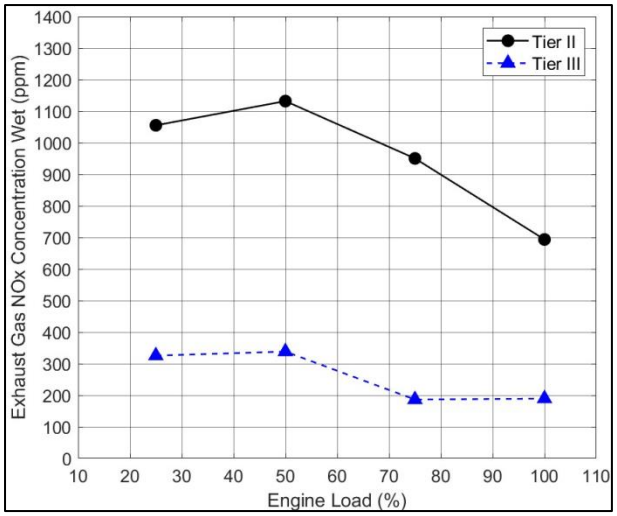

Figure 7-15 Exhaust gas NO_x concentration, Tier-II vs Tier-III; LP-SCR System

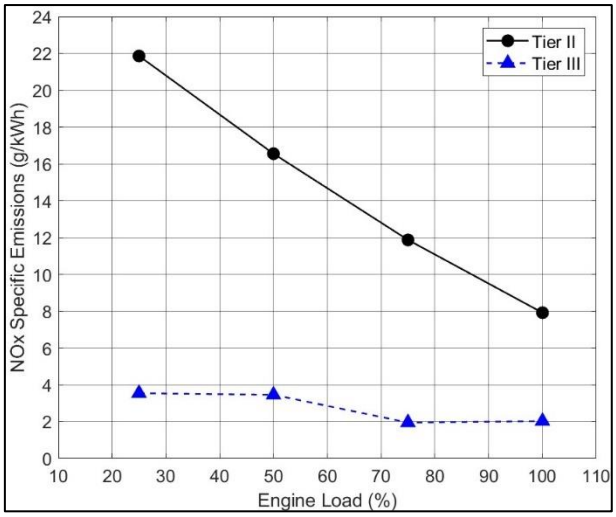

Figure 7-16 Specific NO_x emissions, Tier-II vs Tier-III; LP-SCR System

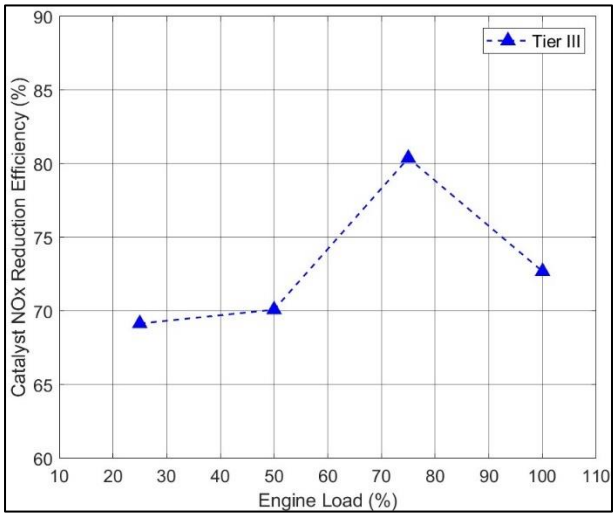

Figure 7-17 Catalyst NO_x reduction efficiency Tier-II vs Tier-III; LP-SCR System

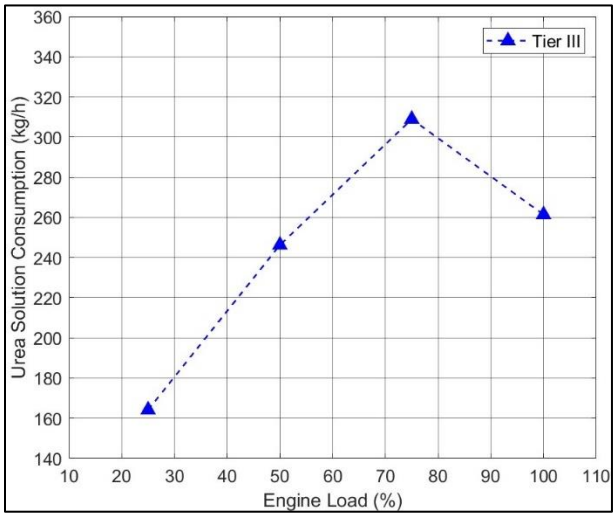

Figure 7-18 Total urea consumption at Tier-III mode; LP-SCR System

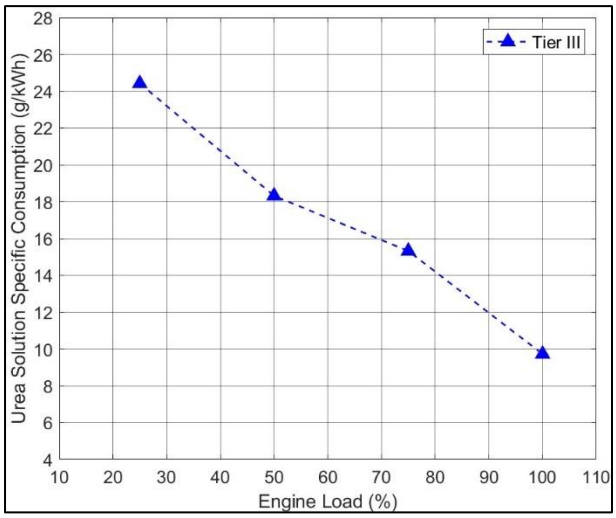

Figure 7-19 Specific urea consumption at Tier-III mode; LP-SCR System

7.3 High Pressure SCR Engine Performance & Emissions

In this section is evaluated the impact of a HP-SCR system on 2-stroke engine performance and emissions using measured data. As mentioned, the HP-SCR system is located between the engine exhaust manifold and the turbine and is overall a more complex implementation than the LP-SCR. Its presence will increase the engine back pressure and impact fuel efficiency. In addition, theoretical studies have shown that the presence of the SCR catalyst affects the flow of the exhaust gases making the overall flow unsmooth while also consuming part of the gas energy lowering turbine effectiveness, (261). These effects will lead to a small turbine exhaust back pressure decrease which would appear beneficial but due to the flow increased turbulence levels, result in a fuel efficiency penalty. Despite the considerably higher temperature of the exhaust gas entering the catalyst compared to the LP-SCR system the safety and good reaction efficiency

thresholds will likely not be met at low engine load, (263). To increase exhaust gas temperature, engines with HP-SCR systems are equipped with a cylinder by-pass valve (CBV), to lower the air volume trapped in the cylinder, while also retaining P_{scav} levels as required. This is akin to the effect observed for the LP-SCR above when the EGB was open but operates on a different principle as the air compressed in the turbocharger circumvents the engine cylinders and directly ends at the turbine inlet. This increases exhaust manifold pressure and improves turbine operation. Depending on the temperature increase requirements for catalyst operation, the CBV opening will increase and an impact on BSFC will be introduced. Further efficiency impact may occur by efforts of the engine manufacturer to increase exhaust gas temperature at the cylinder outlet by alternating the exhaust valve opening and closing angle timings or SOI angle.

For the HP-SCR system study, multiple engines were tested during both FAT tests and official on-board trials. The particulars of the engines examined equipped with an HP-SCR system, are given in Table 7-2. Three engines were examined in total, the first two equipped with catalysts that required the use of very low sulfur fuel and were tested during the FATs and official sea trials with MGO operation.

The third engine tested was equipped with a different type of catalyst capable for operation with high sulfur HFO, of up to 3.2% content. Tests with HFO use were conducted during the official sea trials, while during its FATs MGO was used as usual. For the first system detailed analysis on its effect on engine performance is provided below. For the other two systems only the results of catalyst NO_x reduction efficiency and urea consumption are provided due to space constraints, at section 7.3.2. Their impact on the engine performance was mostly the same as the one of the "HP-SCR 1" engine detailed below.

Table 7-2 HP-SCR Engines particulars

HP_SCR System	**1**	**2**	**3**
Engine Model	6G70ME-C9.5	6G60ME-C9.5	7WFX82B
Type	Two-stroke	Two-stroke	Two-stroke
Electronic Control	Yes	Yes	Yes
Cylinder No.	6	6	7
Bore (mm)	700	600	820
Stroke (mm)	3256	2790	3375
Nominal Speed (rpm)	75.0	77.0	66.1
Nominal Power (kW)	18,300	15,745	24,500
NO_x Certification	Tier-III	Tier-III	Tier-III
SCR Type	High-Pressure low sulfur	High-Pressure low sulfur	High-Pressure high sulfur

7.3.1 Impact of HP-SCR System on Engine Performance

In Figure 7-20 the peak combustion pressure is compared between Tier-II and Tier-III operation, with the pressure increase due to combustion provided in Figure 7-21. The P_{max} values are increased during Tier-III operation for all loads; the observed difference is low, on average 3.5 bar and decreases with load. The ΔP values are practically identical as the difference in P_{max} is the result of the P_{comp} differences between the two modes. The fuel ignition angles derived by the HRR analysis reveal very similar tuning for the two modes

with the only variation close to 0.5º CA at 25% load, Figure 7-22. Similarly, the EVC angles appear identical with minor difference between the P_{comp}/P_{scav} ratio for Tier-III operation compared to Tier-II, Figure 7-23. The exhaust gas flow rate also is about the same for both modes, Figure 7-24, showing similar operation of the turbocharger. While this engine is also equipped with an EGB valve like the LP-SCR one, its use is for tuning purposes for low and high load operation. According to the engine control system indications the EGB at both Tier-II and Tier-III mode was open only at 100% load. A lower in-cylinder mass and similar high pressure values will considerably increase temperature allowing efficient and safe catalyst operation and this is achieved by opening of the CBV valve. It is noted that the CBV valve effect on exhaust mass flow cannot be identified by the values of Figure 7-24 due to the measurement position used for CO_2 and carbon balance calculations. In the present case not enough data were available to proceed to a safe estimation either using measurement results or an engine simulator model. The total exhaust gas mass of Tier-III operation is lower than the Tier-II values only at 100% load. The catalyst inlet temperature values at Tier-II (an installed sensor displays potential inlet temperature also at Tier-II mode) and Tier-III modes is given in Figure 7-25. For 25% load exhaust gas temperature is considerably increased due to the CBV partial opening. The CBV is slightly open at 50% load and closed for 75% and 100% load as temperature is within the desired range for catalytic reduction reactions at high rate. Notably, compared to the catalyst inlet temperature data for the LP-SCR system, the lowest inlet temperature for the HP catalyst is slightly above the maximum measured for the LP system.

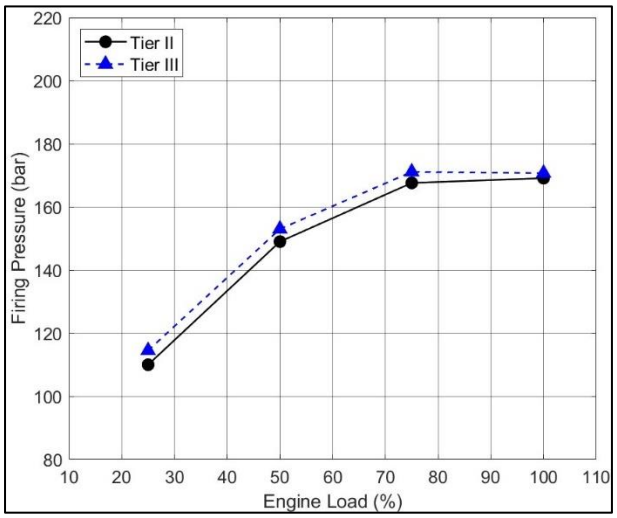

Figure 7-20 Peak combustion pressure comparison, Tier-II vs Tier-III; HP SCR System

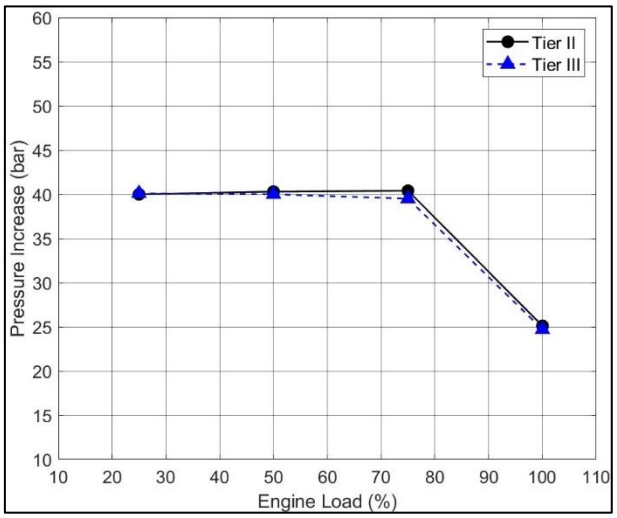

Figure 7-21 Pressure increase due to combustion comparison, Tier-II vs Tier-III; HP SCR System

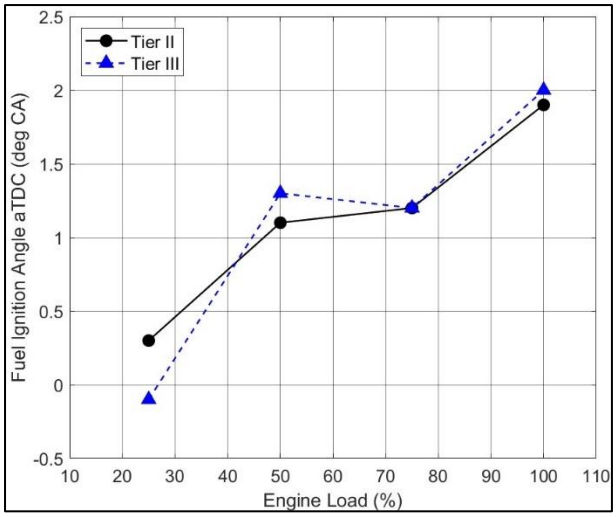

Figure 7-22 Fuel ignition angle aTDC, Tier-II vs Tier-III; HP SCR System

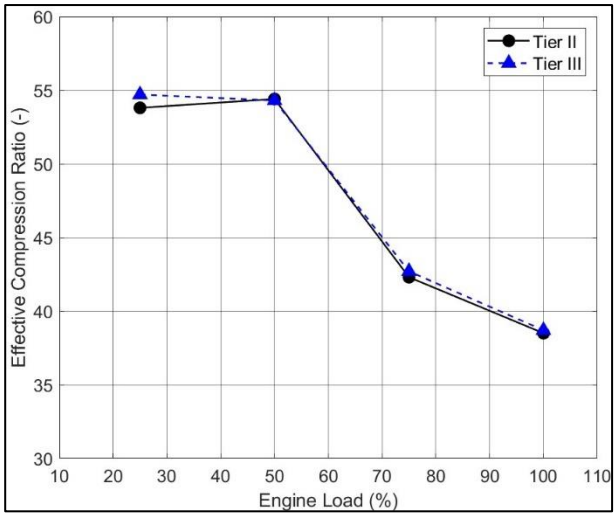

Figure 7-23 Effective compression ratio (P_{comp}/P_{scav}) Tier-II vs Tier-III; HP SCR System

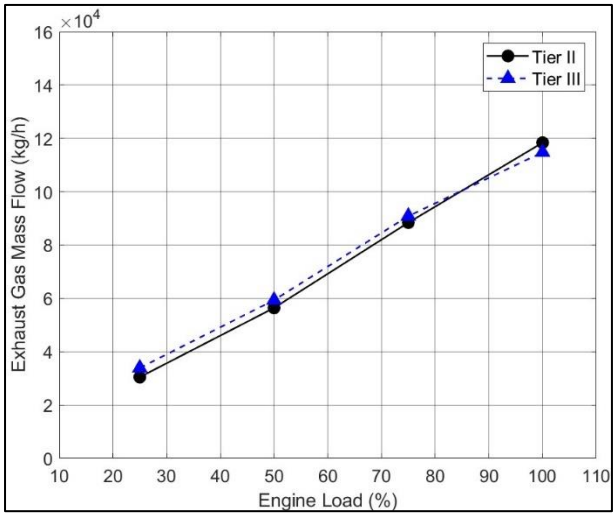

Figure 7-24 Exhaust gas mass flow rate, Tier-II vs Tier-III; HP SCR System

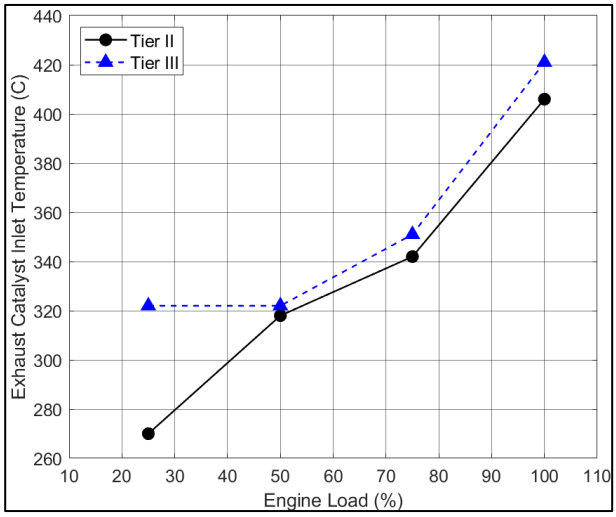

Figure 7-25 Catalyst exhaust gas inlet temperature, Tier-III mode; HP SCR System

Considering the above comparisons, the HP-SCR engine operation for Tier-II and Tier-III mode was nearly identical. As a result, the effect on fuel consumption during Tier-III mode will result from the increase in engine back-pressure due to the pressure drop in the catalyst, and for 25% load also due to the effect of the CBV, with the latter expected to be rather low. The effect on engine efficiency can be assessed by the change in specific fuel consumption as was done for the LP-SCR engine. In Figure 7-26 the comparison between BSFC values during Tier-II and Tier-III operation is provided. An efficiency penalty is found during Tier-III operation that is higher for low load as the effect of the CBV opening is also added. For the LP-SCR system, Figure 7-11, the reverse was found with higher BSFC penalty at high load due to very high increase in exhaust gas flow (due to the EGB closing at MCR) and consequently due to the added back-pressure after the turbine and EGB induced turbine work loss. As the exhaust mass flow increases with load, Figure 7-24, the impact of the catalyst pressure drop also increases, Figure 7-27, which results to engine work loss. This effect was much more pronounced in the LP-SCR system partly due to the high difference in mass flow rate with load increase.

For the HP-SCR engine, the highest efficiency penalty is found at 25% and 50% load when the CBV is also open. For all cases the BSFC penalty is very close to the manufacturers expected range i.e., 0.5 – 2.0 g/kWh, (233,260). The BSFC penalty at low load for the HP-SCR is close to double that of the LP-SCR system, but considerably lower fuel penalty is found at high load operation. The difference at high load could provide measurable benefit in total fuel consumption even for differences marginally over 1.5 g/kWh over time, improving OPEX of the system. However, based on data from multiple operating vessels, the vast majority of the engine operation will remain in the 25% - 50% load range and rarely approach or exceed 75% in any area and especially near coastal areas and ECAs. This is in agreement with some sailing scenarios estimated by the engine designer, (233). Thus, from an operational point of view the LP-SCR system will most probably prove superior to the HP-SCR in terms of fuel economy, with the total OPEX comparison requiring also review of the urea consumption requirements of each approach.

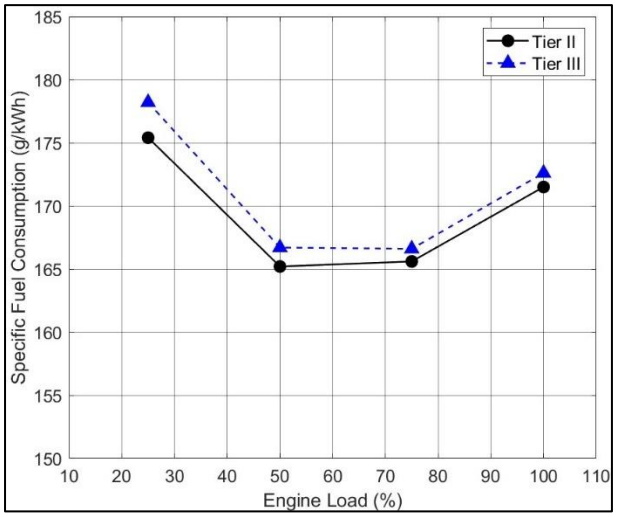

Figure 7-26 Specific Fuel Consumption, Tier-II vs Tier-III; HP SCR System

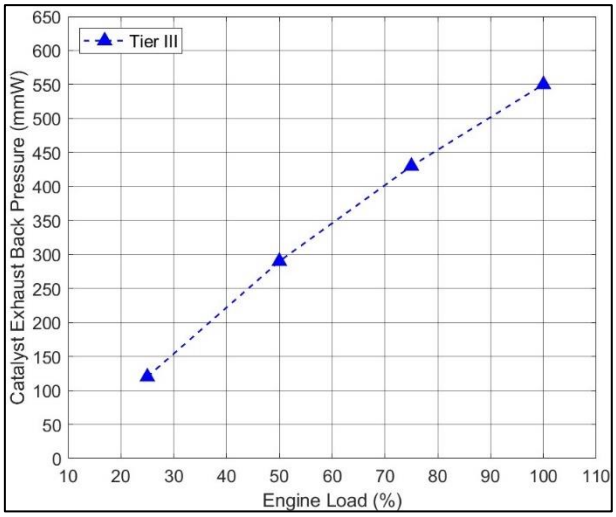

Figure 7-27 SCR Catalyst added back-pressure at Tier-III mode; HP SCR System

The impact of the HP SCR on combustion is evaluated by the comparison of HRR for Tier-II and Tier-III operation. As in the case of the LP-SCR engine, the HRR diagrams at 25% and 75% load are compared for context in Figure 7-28 and Figure 7-29 respectively. The diagrams comparison shows a slight variation in the case of 25% load due to earlier fuel ignition angle. All other parameters such as fuel burn rate, combustion duration and peak combustion values are identical between Tier-II and Tier-III modes. For 75% load the fuel combustion process presents no difference while the SCR system is in use. In conclusion, as in the case of the LP system the HP-SCR has minimal effect on engine operation, with the only measurable impact being an average 1.5 g/kWh added BSFC at low load and practically no effect for 75% load and above.

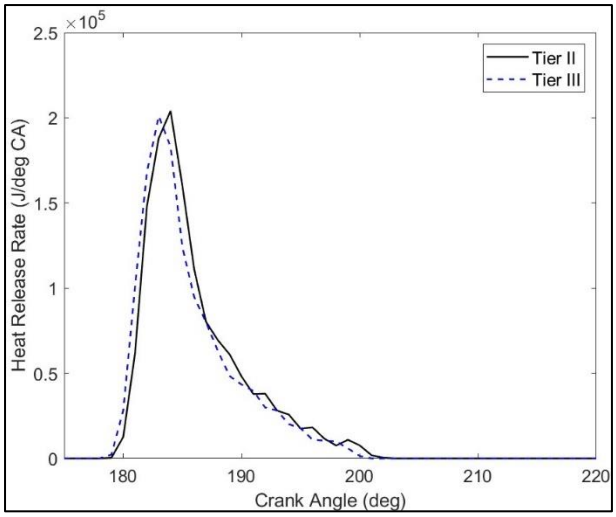

Figure 7-28 Net HRR comparison, Tier-II & Tier-III at 25% load; HP SCR System

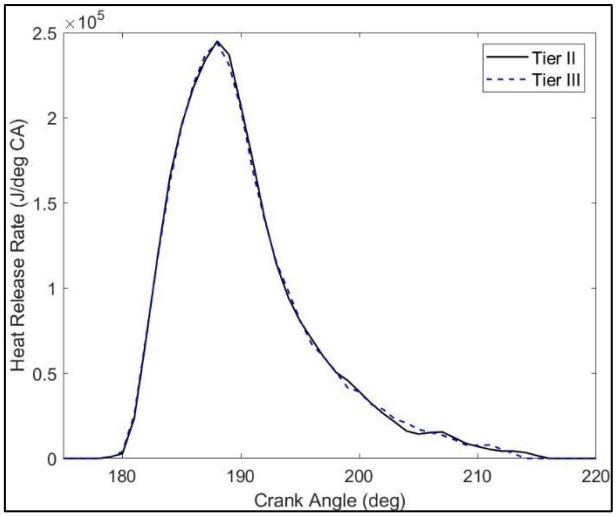

Figure 7-29 Net HRR comparison, Tier-II & Tier-III at 75% load; HP SCR System

7.3.2 HP SCR System Impact on NO_x Emissions for Tier-II and Tier-III operation

The effectiveness of the HP-SCR system regarding NO_x emissions reduction is expected to be higher than that of the LP one due to the higher exhaust gas temperature increasing the catalytic reaction chain speed. The NO_x concentration in the exhaust gases measured during Tier-II and Tier-III mode is provided on a wet basis in Figure 7-30 and the estimated specific NO_x emissions are given in Figure 7-31. The reduction efficiency of the catalyst is given in Figure 7-32. The lowest level of NO_x concentration in the exhaust gasses is found for 100% load, while for specific emissions the lowest value is as in most cases at 75% load. The level of NO_x reduction ranges between 75% to 88%, with the highest decrease at the 75% load point as required to satisfy the total weighted value threshold more easily. The level of NO_x reduction is improved compared to the LP-SCR tests, Figure 7-17 and the EGR equipped engine results. A high initial reduction efficiency will prove important as the SCR catalyst effectiveness is projected to degrade with use. In Figure 7-33 and Figure 7-34 the total and specific urea consumption is given. Despite the increased temperature the urea consumption does not present improvements compared to the LP-SCR system. The total consumption of the HP-SCR system is lower, (Figure 7-18 LP-SCR), but this is attributed to the smaller engine size and exhaust gas mass flow rate, as specific urea consumption values are slightly higher in the case of the HP-SCR system, Figure 7-19 LP-SCR) and Figure 7-34. In Figure 7-35 values of specific urea consumption from the other tested engines equipped with HP-SCR systems are included for added context. In the case of the LP-SCR system more data could not be collected as the HP installation is much more widely adopted for 2-stroke engines. Based on the data of Figure 7-35, the urea consumption for all engines presented low deviation for 25% and 100% load. In the case of 50% and 75% load considerable variation is observed with the higher values found for “HP-SCR 1” which is the system examined in detail. Despite the markedly higher specific urea consumption for the “HP-SCR 1” system, NO_x reduction efficiency did not present notable improvement compared to the data of the other engines. Due to the difference in the size and type of the three engines analysis of the previous finding is difficult, but it is probably related to the catalyst design based on a comparison between “HP-SCR

1" and "HP-SCR 2". The "HP-SCR 2" implementation was installed on an engine of the same main type, but smaller size, as "HP-SCR 1" and the catalyst inlet temperature data were nearly identical between the systems. The same applied to the specific NO_x emission values except for 100% load. The difference between the two systems' effectiveness and urea requirements is then attributed to the total gas flow and mainly the catalyst design, that was different and featured an added layer of elements in the case of "HP-SCR 2". The average urea requirement of the tested HP systems did not significantly differ from the LP one, with the same observed for the BSFC penalty to the engine, so no tangible difference regarding OPEX should be expected between the HP and LP system. A potential difference in recurring cost could prove to be the lifetime of the LP reactor systems compared to the HP ones, due to the lower temperature values of the entry gas. This could increase fouling and clogging of the reactor cells at a higher rate and require earlier replacement. The average lifetime expected by manufacturers and classification societies is three to five years, (233,238,260). A clear benefit of the HP-SCR systems is the capability of operation on higher sulfur content fuels such as HFO, which are considerably lower in price compared to the MGO fuel requirement for an LP catalyst. The added cost of a scrubber system operation should however be factored in this case, (275). As stated, the "HP-SCR 3" system specifications allow for HFO operation of up to 3.2% sulfur content. The data presented in Figure 7-36 refer to the tests conducted with MGO during the certification procedure to be consistent with the other two SCR systems included in the graph. SCR tests with HFO were conducted during the official sea trials and were among the first for HFO capable systems. Data from Sea Trials operation was acquired for all three HP catalysts. In Figure 7-37 the catalyst efficiency using HFO is provided, which was found decreased compared to the MGO tests. The effectiveness of the other HP-SCR systems tested during Sea Trials with MGO is provided in Figure 7-38. Similar to the HFO capable catalyst tests, a general tendency for lower efficiency during Sea Trials testing is found especially at 100% engine load for all tested units. For all applications it was confirmed that the drop in NO_x reduction capacity was not the result of lower exhaust gas temperature at the catalyst inlet or lower urea supply to the system. The difference is attributed primarily to the environmental and engine operating conditions during the tests and the accuracy of the measurement process which presents inherent issues in on-board applications as detailed in Chapter 2. Catalyst fowling at this point is not probable due to minimal operation hours of the systems.

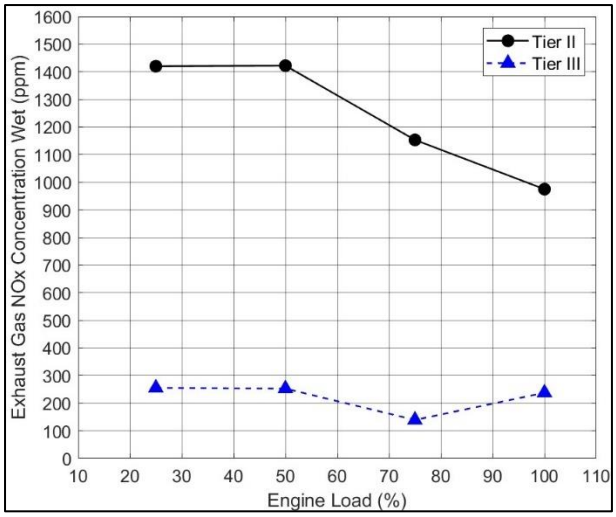

Figure 7-30 Exhaust gas NO_x concentration, Tier-II vs Tier-III; HP SCR System

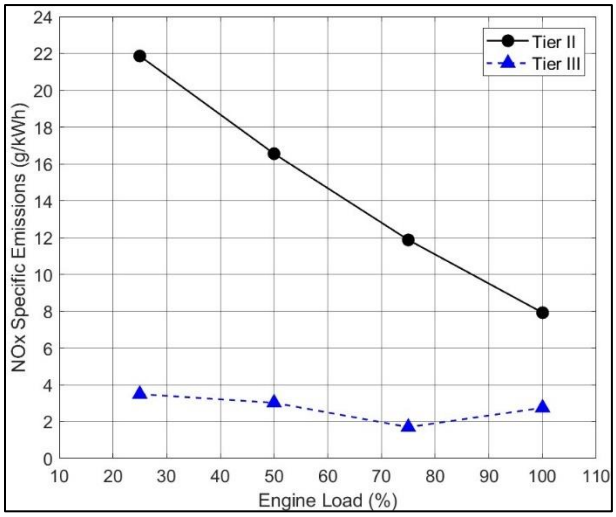

Figure 7-31 Specific NO_x emissions, Tier-II vs Tier-III; HP SCR System

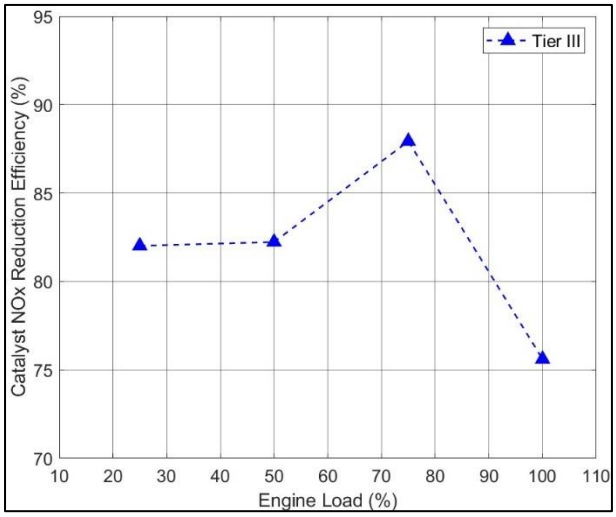

Figure 7-32 Catalyst NO_x reduction efficiency Tier-II vs Tier-III; HP SCR System

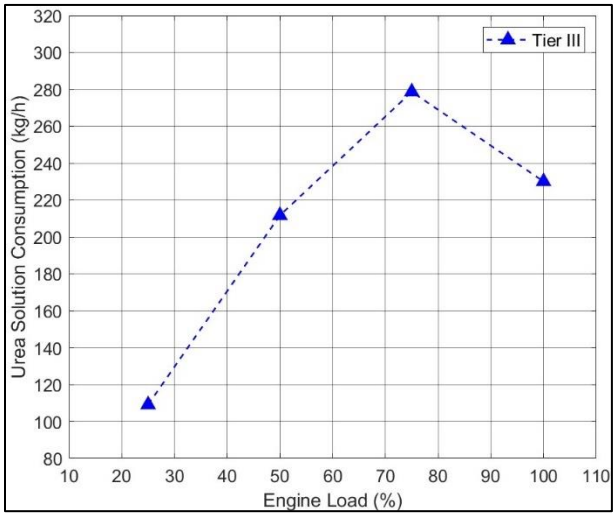

Figure 7-33 Total urea consumption at Tier-III mode; HP SCR System

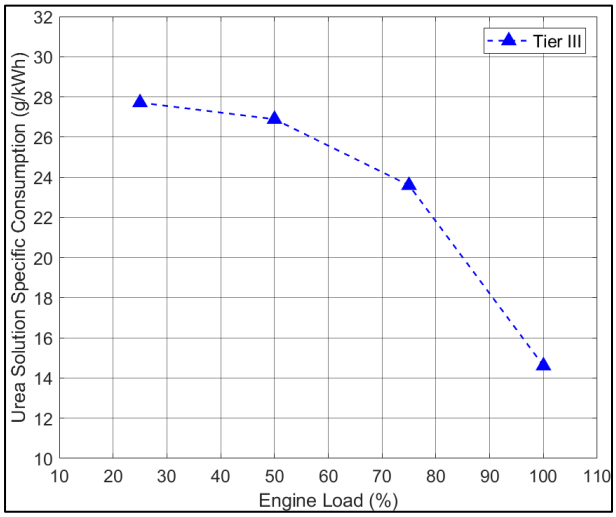

Figure 7-34 Specific urea consumption at Tier-III mode; HP SCR System

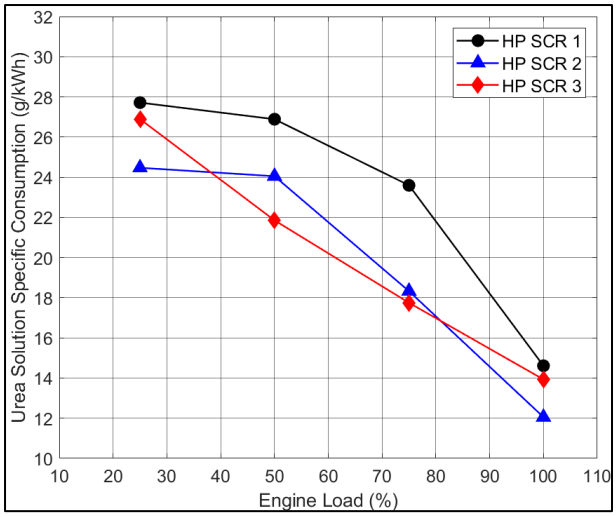

Figure 7-35 Specific urea consumption at Tier-III mode for all tested vessels; HP SCR System

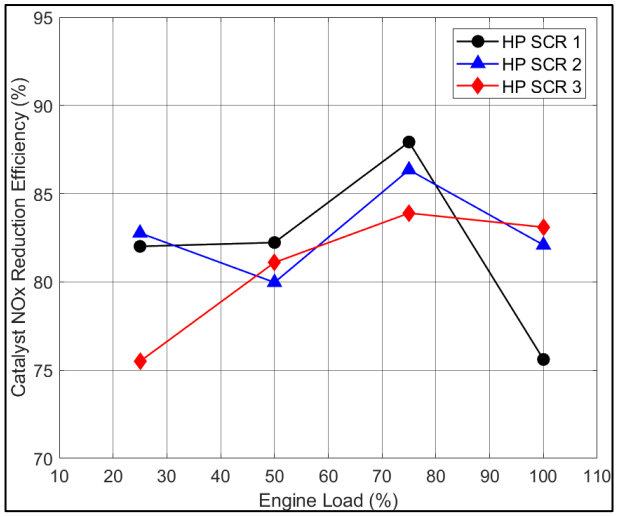

Figure 7-36 Catalyst NO_x reduction efficiency for all tested vessels; HP SCR System

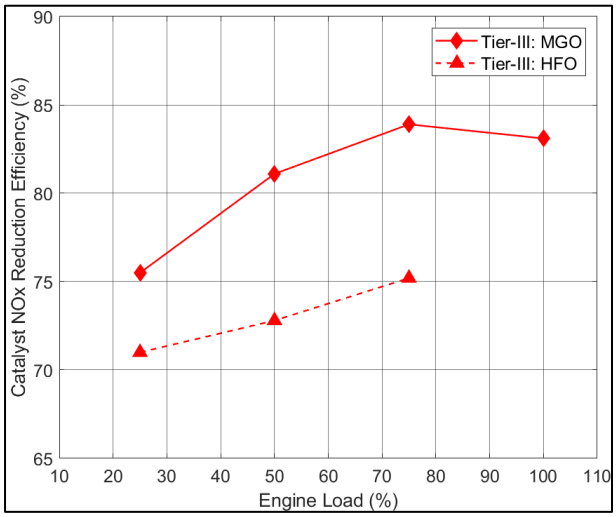

Figure 7-37 Catalyst effectiveness during Shop Test MGO tests and Sea Trials HFO Tests; HP SCR System

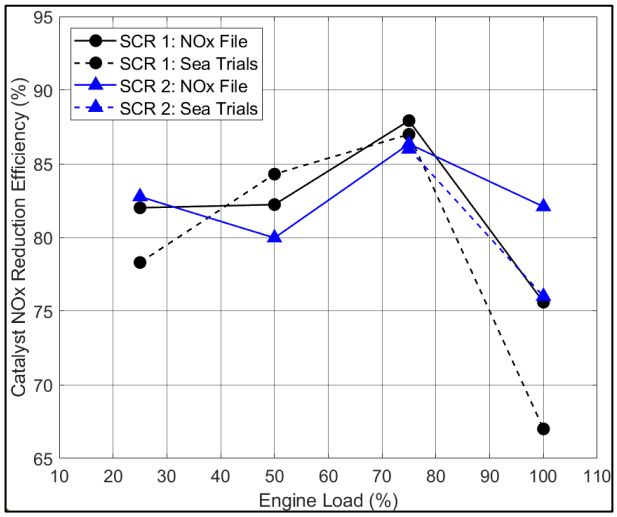

Figure 7-38 Catalyst effectiveness during Shop Test MGO tests and Sea Trials MGO Tests; HP SCR Systems

7.3.3 LP- and HP-SCR analysis summary

Considering the results for the two types of SCR implementation regarding engine performance, no clear advantage for either type is found when considering all parameters, engine performance, catalyst efficiency and OPEX. For both systems rather low impact was found for engine performance. The effect on fuel efficiency was low and very close to the manufacturer estimates, confirmed using the measured data for both HP and LP-SCR implementations. In most cases the difference between the two systems was up to or below 1.0 g/kWh. The higher impact of the LP-SCR system occurred at full engine load and is not considered significant as Tier-III operation at this load is highly unlikely for any extended time period. In contrast the HP-SCR system had no impact on fuel consumption at high load but had bigger impact than the LP-SCR system at low load, which will mostly be used during ECA areas sailing, as they are close to land and cover congested shipping routes. The difference in specific urea consumption was also low in most cases. Thus, the

main advantage of the LP system is its reduced complexity, as the typical engine installation in the engine room is more easily retained and only minimal changes need to be performed to the engine inlet and outlet systems and piping and slightly better fuel efficiency at low load. For the HP-SCR system, the major advantage and the main reason for its widespread adoption is overall better operation of the catalyst with increased efficiency and improved safety margins for its operation due to higher exhaust gas temperature that can be achieved without any change to engine operation for 50% load and above. For the HP-SCR systems catalyst inlet temperature even at low load was well above the minimum safe operating temperate of 200^{o}C guaranteeing better efficiency of NO_x reduction and longer lifespan of the inner catalyst cells. The SCR systems are set to undergo regular inspections regarding both their state (pressure drop) and performance (NO_x reduction efficiency) that can result to catalyst inner parts replacement should the previous factors not meet specifications. The added reliability of the HP-SCR system overcomes the simplicity advantages of the LP implementation and the minimal benefit in OPEX.

As for the HP-SCR system with utilization of HFO capability, analysis showed adequate capability for NO_x reduction. It is noted that catalyst effectiveness measured during the HFO tests was lower, but that may be due to comparing FAT test measurements to on-board ones. The use of HFO, or preferably LSFO/VLSFO to lessen concerns on the catalyst's longevity will lower costs to a degree and make up for the urea requirement. However, the potential cost increase by the use of a scrubber system must be also considered in this case, (275), especially for areas where the use of open loop systems is forbidden, and close loop scrubber systems are required, (276,277). The close loop scrubber systems require the use of NaOH and contribute to operational cost, (278).

7.4 Engine Performance & Economical Considerations for SCR & EGR NOx Control Solutions

Following the analysis of the SCR and EGR systems, which are the only NO_x reduction technologies that can satisfy Tier-III NO_x emissions compliance for marine engines, with the exception of low-pressure dual-fuel engines, a comparison is made between the two solutions regarding their effect on engine performance and the impact on a vessel's APEX and OPEX.

Regarding complexity and the degree of alterations to the design of an engine inlet and outlet system the SCR approach, especially the LP installation, is considerably simpler than an EGR unit. This is due to the requirement of an: EGR cooler, exhaust gas cleaner and a treatment system for the water used in exhaust gas cleaning as it cannot be immediately disposed to open sea.

In addition, the overall installation of the EGR system requires extensive modifications on the side of the scavenging air receiver and the turbocharger. Some of the modifications are similar for the two systems with EGB and CBV valves used in both to control air/gas mass flow in the system to accommodate the recirculated gasses or increase cylinder charge or turbine outlet gas temperature for the SCR system. Despite the number

of modifications since the EGR is integrated in the engine, it results in a much more compact overall installation, while the SCR systems have high engine room space requirements.

The effect on engine operation was low for the SCR system with slight variation in engine performance for the LP-SCR, while for the HP-SCR a mild effect existed for loads below 50% load. A slight BSFC increase was measured that ranged between 0.5 – 2.0 g/kWh, which is low. For the EGR equipped engines the presence of the recirculated gasses and the different tuning required had significant impact on overall performance, the combustion mechanism and efficiency, with a final high penalty on BSFC. For both the diesel and the DF engine the recorded BSFC increased during EGR Tier-III operation ranged, depending on load, from 8.6 to 4.5 g/kWh, with the increase at 25% and 50% load being 6.1 and 8.6 g/kWh respectively, amounting to 3.5% and 5.1% higher fuel consumption that Tier-II operation. For the dual-fuel engine, the increase in energy content supplied in total was 3.2% and 4.1% at the same loads. Impact was lower for higher loads but engine operation at Tier-III mode at sailing scenarios requiring higher engine power is unlikely for any substantial amount of time annually. The application of the CII and requirements for vessel consumption reporting will soon constitute high load operation hours, even shorter (279) than today's already low standards, (280,281). Comparing the BSFC penalty between the EGR and SCR operation shows that for EGR engine consumption will be increased at a minimum by 4g/kWh for low load and will range between 7 - 8g/kWh at medium load, which is a high penalty. While both systems introduce secondary consumptions in the form of NaOH for EGR bleed-off water cleaning and urea for the SCR operation, the former is rather irrelevant in terms of OPEX impact for low sulfur fuel operation as the NaOH consumption is minimal. For reference the hourly urea consumption of 16.4MW engine will range between 1.7 to 4.1 litres from low to maximum load. The NaOH price is usually close to $550 per ton, so costs will be substantial for higher consumption values. On the other hand, the cost of urea and its consumption are both rather high. Due to the high volatility of urea prices in the last years, estimation of operating costs is very difficult, (282).

The expected average 40% urea solution specific consumption will be close to 17.9 g/kWh based on manufacturer estimates (233). Using the measurement data from all four SCR systems tested, the actual specific AUS-40 consumption at 25% load is expected on average at 25g/kWh and slightly below 24g/kWh at 50% load. The cost of marine use AUS-40, as mentioned above, can range between 100% or slightly above 40% of the HFO price, but the pricing slowly normalizes towards the latter, following the coronavirus induced shortage issues. Since the EGR and SCR systems predominantly operate on MGO the aforementioned values must be corrected to MGO pricing; the price ratio of HFO to MGO is about 65% as a global average, (283). The result of the previous calculations is that the cost of the specific urea consumption values is equivalent to about 16.5 g/kWh in the, now unlikely, worst-case scenario or to 7g/kWh increase in BSFC for normal pricing, same to HFO. Factoring in the 1.5g/kWh increase in BSFC caused by the engine efficiency reduction, the urea and fuel consumption OPEX increase can be expected between 18.0g/kWh to 8.5g/kWh for low and medium load. These values are double or roughly equivalent to the highest added cost expected by the EGR system, assuming only low and medium load sailing. The other major factor for SCR recurring costs is the requirement of catalyst elements renewal every three to five years due to its deterioration, (238,260). The

replacement cost is proportional to the catalyst size and number of catalytic elements and is estimated by various sources to amount to roughly $150,000 for each one required, (238,260). The last parameter to be considered is the electrical power requirement for the systems. The EGR unit will require auxiliary electrical power for the operation of the blowers and the water treatment system, while for the SCR unit, power requirements are from the urea injection and soot blowing system. These will depend on engine size and load and will be provided on a case-by-case basis from the engine manufacturer, (233,269). Overall, the estimate of the two major engine manufacturers is that the electrical requirements of the EGR system will be substantially higher, (233,260).

Several cost analysis studies have been published for SCR marine use in large 2-stroke engine, without any distinction between LP and HP installations. The estimated OPEX costs in the studies are high due to the urea price and its substantial consumption during Tier-III operation. One of the earlier available studies by (267), in 2013, contains a detailed analysis for a 10 MW engine and estimated that 1500h (62 full days) sailing in ECA would introduce urea consumption costs of $38,000, with the 2013 urea prices comparable to mid-2023, (284) after the normalization of the coronavirus extreme price hike. These data were also used by the ICCT in its feasibility study of SCR implementation in marine vessels in the cost analysis part, (285). A recent study published in 2021, (286), considers all potential costs including catalyst deterioration, electrical power requirements, system maintenance with labor costs factored in, and even depreciation of the overall installation. As with the previous study the major cost factor is urea consumption and price, that was estimated to amount to about 62% of total operating expenses of the SCR installation per annum, in three different cases, ranging from engine power of 7MW to 11MW. In addition, this study concluded that while short annual SCR system use will significantly reduce operating expenses it will create an unfavorable ratio of indirect to total operating costs due to system depreciation. The studies also include the CAPEX required for the SCR system installation. This will vary with engine size and specifically the exhaust mass flow and the concentration of NO_x in the exhaust gases, (267,286).

The expenses required for an SCR system installation are also mentioned in official IMO documentation, (287). The organization estimates that the required CAPEX amount will typically be $40 - $135 per kW of engine power. The equivalent amount for an EGR system is estimated by the IMO at $55 - $82/kW. In the previous two studies the CAPEX requirement was set at $50/kW in (267) and $29/kW in (286) where more recent data were used.

The EGR total installation and operational expenses are not extensively documented for marine engine use but are estimated to be above SCR for smaller engines and lower for larger engines. In the study of (288) comparison is made between EGR and SCR for an 11.6MW engine. The initial investment cost will scale rather linearly with engine power for both systems. For lower power output engines, the EGR cost will be higher, while SCR will require higher monetary investment for bigger engines, as also mentioned in (238). After conducting multiple comparisons, the researchers concluded that in a scenario of continuous high fuel prices the cost between the two systems will be roughly equal, while for lower fuel prices a 5% - 7% margin will result in favor of the EGR installation. Marine classification societies, such as DNV, have also provided

comparative estimates regarding CAPEX and OPEX of the two systems. In their study, (289) the CAPEX costs were estimated to range $1.26m to $3.86m for the SCR and $1.3m to $2.91m for the EGR system on engines ranging from 13.4MW to 78MW confirming that EGR initial investment cost becomes considerably more favorable for large and very large engines (and vessels).

The same price range for in previously mentioned analyses was used for urea powder, and the cost of AUS-40 solution was based on this price range. The price range used is low by today's standards. The vessel used for annual cost calculation was larger than the other studies, a VLCC with a 25.9MW engine and the time annually in ECA areas requiring the SCR use was set to 20 days. This amounted to AUS-40 costs between $65,000 and $25,000 depending on urea price. The amount of urea injected was estimated to 10% of the fuel consumption. This value is close to the average of the measurement data from the four SCR units tested in the present investigation, however, it is noted that AUS-40 specific consumption will increase if only low load sailing is assumed. The cost of EGR for the same conditions was estimated at $25,000 for a 4% fuel penalty, relatively close to the average actual BSFC increase measured but again lower than only low and medium operation levels. The study of the classification society (289), resulted to an SCR OPEX that will be similar to that of EGR or more than double depending on urea and fuel prices, with both fuels used being MGO. In the present analysis the same estimates were reached with using the current ratios of urea to fuel prices, and higher specific urea consumption due to assuming mainly low load sailing. Other engine manufacturers estimate that for normal urea prices (260) the OPEX costs of SCR and EGR will be almost the same when also including the electric power requirements, however this estimate is probably based on high fuel prices, as found in (288), though no relevant information is provided. Even in the best-case scenario of urea and fuel pricing and sailing conditions, the requirement of catalyst element renewal every 3 to 5 years will considerably increase costs for the SCR system with a further $50,000 to $30,000 expense per year; the previous practically double the OPEX of SCR use. The use of higher sulfur fuel to reduce overall costs is possible as demonstrated by the tests conducted on the HP-SCR catalyst using 3.2% S content fuel. Attention, however, must be made regarding scrubber requirements for NaOH that will add further costs. For some EGR systems operation on HFO below 3.5% S content is possible for certain designs. This will considerably increase electrical power requirements and NaOH consumption and sludge production, thus careful consideration is needed, (278) as also in this case use of a scrubber system will be required.

When considering use of MGO or VLSFO, based on economic terms the EGR system will prove consistently more favourable. The main reason for the SCR dominance in the market is its earlier commercial entry and the fact that limited operational experience for EGR installations exists in the marine field. It is expected that as the EGR equipped engines become more widely available and prove to operate without serious issues their market adoption for new vessels will readily surpass SCR.

Chapter 8 Summary, Conclusions and Perspectives

It this thesis four state-of-the-art technological solutions for the control of marine engine emissions were investigated using newly acquired experimental data. The investigation was supported from a computational analysis using a multizone combustion model. The subject emissions are CO_2 and NO_x, which are officially controlled by the International Maritime Organization, along with SO_2. The CO_2 reduction technologies for the maritime industry examined thoroughly in the present thesis are biofuels and LNG used in dual-fuel high-pressure engines. The NO_x abatement technologies investigated are EGR and SCR, used to achieve the strict Tier-III emissions standard.

By conducting an extended number of on-site measurements, either on-board vessels or during FAT tests and in collaboration with shipowners for data acquisition via telemetry, substantial volume of operational and emission data from the use of the above technical solutions was gathered.

For each application thorough literature research was conducted prior to the whole procedure. This revealed low number of published works containing detailed analysis of the effect of these technologies on engine performance in general and relative to conventional marine engine operation. The subset of studies that contained measured data from large 2-stroke main propulsion engines was found even lower, with the many of the data being the product of theoretical investigations on past engine designs. The most characteristic case is biofuels as they were just introduced in the field, and no relevant detailed information was available for 2-stroke engines when research on this subject commenced. For the high-pressure 2-stroke LNG engines information from full-scale applications' analysis was also limited. Most published works on the subject, experimental or computational, considered smaller engines of different type than those included in this thesis. Available data from marine applications mostly referred to low-pressure gas admission engines. Literature coverage of EGR equipped marine engines was improved compared to the aforementioned technologies, but focus was primarily on effect on NO_x emissions only and was based on older engine designs. In addition, the impact of EGR on fuel efficiency was mostly estimated by manufacturer claims or simulation results and not actual measurements. The subject of SCR use in 2-stroke large marine engines was more sufficiently covered, but the available studies did not provide details for urea consumption requirements, and technical difficulties, especially at low load. In addition, the information for the impact on engine performance was limited. Thus, the measurement campaign and analysis conducted for the current thesis fills a substantial gap of data availability and full-scale implementation analysis.

8.1 Summary: CO_2 Reduction Technologies - Use of LNG and Biofuels

The analysis conducted provided significant findings for both studied technologies. Two consecutive generations of high-pressure gas injection LNG engines were tested for performance and emissions, with the newer generation engine only recently available in active vessels. The analysis revealed different approach in

dual fuel mode operation between the two engine generations. For the previous generation engine, the major performance values were nearly identical between diesel and DF mode. No tuning changes were found between the two operating modes, with the only difference being the pilot diesel retarded SOI timing compared to the diesel mode timing. The HRR analysis revealed faster premixed combustion for DF mode and higher peak rate. For most loads the diffusion-controlled combustion stage progressed at a considerably slower rate. This was reflected in the combustion duration estimated for 50% and 95% of the total injected fuel mass to burn. The retarded ignition angle resulted in similar values of pressure increase despite the stronger premixed combustion. The increased combustion intensity was attributed to the higher LCV of injected natural gas and the better mixing of gas and air until the pilot fuel ignition. The overall effect in efficiency was minimal, with nearly the same total heat rate for diesel and DF mode. The new generation engine presented different tuning, with earlier EVC angle timings for DF mode and advanced pilot fuel injection. This resulted to substantial changes in overall operation compared to diesel mode, and considerable increase of cylinder peak pressure values, to 10 bar higher for DF mode at all loads. HRR analysis revealed staged combustion of the pilot fuel. It is noted that for the older engine the pilot fuel combustion was not discernible from the gaseous' fuel, even though more diesel mass was injected in total, and the pilot/gas mass ratio was higher. Following the diesel pilot combustion for roughly 3^o – 4^o CA, the main ignition event occurred for the natural gas. Very high intensity combustion ensued after a short intermediate stage and a high reduction of fuel burn rate at the diffusion stage, but initial diffusion-controlled combustion speed was considerably above that of the older engine. This led to higher pressure increase despite retarded start of the main combustion event, which combined with higher compression pressure, led to further increase of maximum in-cylinder pressure. In terms of fuel efficiency both engines showed lower total fuel mass requirements for the same power output in DF mode. The specific total heat rate was roughly the same for the older engine and considerably lower for the current generation one, with the exception of low load operation. Overall, thermal efficiency of both engines was very good in DF mode, 1% lower for the older design engine and 3.5% higher for the revised one compared to diesel only operation. The fuel consumption values measured showed a 23% potential for carbon emissions reduction, due to the lower fuel mass required, a result of the high NG LCV, and due to its lower carbon content. The pilot fuel mass required decreased gen-on-gen with lower mass ratio compared to gas; the decrease was very high for maximum load, with the newer engine's diesel to gas ratio being half of the older one's. This required substantial improvements in the fuel injector nozzles that also allowed for the different pilot fuel injection and combustion approach revealed by the HRR analysis. NO_x emissions were at Tier-II levels. Overall, the analysis showed that dual-fuel LNG high-pressure gas injection engines are a maturing technology that can operate on-par with conventional diesel engines when required and provide concrete CO_2 reduction benefits. It was also established that tangible improvements are possible as operational experience accumulates and higher tuning flexibility becomes available via improvements in components and control devices. Furthermore, it is revealed that engine settings are of major importance for DF engine operation.

The biofuel testing procedure was extensive and involved five 2-stroke large propulsion engines and seven 4-stroke auxiliary generators. Comparison of engine performance and combustion process in the cylinder for operation on B30 and conventional fuels, MGO, HFO, VLSO, showed only minimal impact. For the 2-stroke engines a slight fuel consumption penalty was confirmed, 1% on average compared to MGO, and minimal increase compared to crude oil. The fuel consumption penalty was increased to 3% compared to MGO and 1% compared to crude oil for the auxiliary generators. The effect on combustion was low and a combination of its lower LCV resulting to slightly slower heat release, and its higher CN leading to earlier ignition. No significant deviation was confirmed after the considerable number of tests conducted. Clear effect was confirmed for NO_x emissions during B30 operation, with tendency for increase. Due to the minimal effect of the biofuels on the combustion process, the higher emissions were attributed to the increased oxygen content of the biofuels. The multizone model provided further insight and confirmed the contribution of the added oxygen on the flame region to NO_x formation increase. The main factor driving formation was confirmed to be localised increase of λ in the burn zone, that increased NO formation both in areas of lower and higher air-fuel ratio. The highest difference was found for zones in the inner parts of the fuel jet where normally oxygen concentration would be quite poor and despite the high temperatures NO_x formation would be limited. It was also found that the added O_2 presence tends to increase temperature locally by enhancing the combustion intensity. The level of impact on NO_x formation differed between the 2-stroke and 4-stroke engines. For the 2-stroke engines B30 NO_x emissions compared to crude oil and MGO are increased by 4% on average. In the case of the 4-stroke engines the B30 emissions were higher compared to MGO and only slightly increased compared to crude oil, the average values being 10% and 2.4% respectively. Through the multiple tests it was also verified that engine tuning is of vital importance along with the individual fuel properties, as all emission value outliers were accompanied by high differences in performance values.

The tank-to-wake carbon emissions of biofuels were slightly decreased compared to HFO but still below MGO. The benefit of the lower B30 carbon content was offset by higher total consumption. Considering well-to-wake emissions the expected benefit for CO_2 emissions is close to 25%. The conclusion of the testing procedure in a total of 12 marine engines was that biofuel has no effect on engine and subsystems performance, at least based on short term operation observations. Fuel consumption impact is manageable, however, B30 prices remain above HFO and VLSFO. For a normally operating marine engine biofuel use should not result in NO_x emission limits violation, thus biofuels should be into consideration by vessel owners that require a fast and manageable solution to improving carbon footprint of their vessels.

8.2 Summary: NO_X Reduction Technologies-SCR and EGR

Two engines outfitted with an EGR system were tested, a diesel one and the older generation dual-fuel engine mentioned above. The testing procedure of the latter involved mainly dual-fuel operation. It was confirmed that for both engines high rate of gas recirculation is required. This is due to the scavenging process and high

excess air mass, characteristic to large 2-stroke low-speed engines. The EGR rate was estimated with the assistance of a multizone model, since recorded data were not adequate to describe the operation of the CBV valve. For both engines the EGR rate ranged between 37% - 47% with the rate at MCR dropping below 40% as this was the peak capacity of the gas treatment system for cleaning and cooling. The NO_x reduction capabilities of the EGR solution were proven potent and exceeded 80% in some cases. Except for 100% load, for both engines an almost linear relation to EGR percentage and NO_x reduction capacity was found. The variation at 100% load was attributed to engine tuning that would limit NO_x formation regardless of EGR use. This allowed the use of lower EGR percentage at MCR required by the peak mass flow rate limitations of the recirculated gas handling system. The effect of EGR on NO_x emissions was verified by the computational analysis that confirmed both significant decrease of air-fuel equivalence ratio and in-cylinder temperature in the total volume and in the fuel jet area. EGR impact on the engines' performance was significant, more than any other solution examined in the thesis. Different exhaust valve tuning was required due to cylinder total inlet mass decrease when the recirculation system was active; at 25% load air mass flow was reduced at half of the Tier-II value. The SOI timings were also mostly retarded, and increased delay of fuel ignition was found. Pressure increase due to combustion was inhibited and the HRR analysis showed considerably slower combustion when using EGR with a prolonged diffusion-controlled stage which should be expected when lowering air-fuel ratio. The previous were also produced by the multizone model simulation which provided detailed information for the corresponding mechanisms. An overall interesting finding was that for higher loads a sudden reduction in combustion rate occurred when roughly 50% of the peak HRR value was reached, and this was more intense for the dual-fuel engine. This was attributed to the low air-fuel ratio slowing down the mixing rate of fuel and air; the higher intensity of this phenomenon in the dual-fuel engine was attributed to its slightly higher EGR percentage and the mixing rate of the diesel pilot and gas in the cylinder compared to that of diesel only operation. The fuel consumption penalty was high due to the poorer combustion quality and increased thermal losses, almost 4% on average for the diesel engine and close to 3% for the dual fuel engine. An important observation was that this is further increased in the of 25% - 50% load; this is not considered by many studies investigating OPEX of the system as an average fuel consumption penalty is used regardless of load. This constitutes a significant omission since ECA area sailing is mostly at lower speeds and engine power.

Overall, the EGR system was found to perform well in terms of engine stability and NO_x decrease, but with a high impact on engine fuel efficiency. No significant difference between the diesel only and DF engine was found beyond earlier injection timing of the pilot compared to the highly retarded diesel main injection of the single fuel engine. The pilot fuel SOI advance was probably required due to the EGR impact on combustion delay, combustion "speed" and temperature increase, the latter required for the gas ignition. The computational investigation conducted using the multizone combustion model revealed that, at least on theoretical basis, it is possible to minimize the BSFC penalty due to the introduction of EGR, while maintaining similar NO_x reduction, by using advanced SOI and approximately 5% higher (in absolute change) EGR rates. Concern remains regarding the performance of the exhaust gas handling system due to the high

recirculation rate and the long-term impact of the EGR use in engine components. Based on experience from various new technology applications, issues will probably be revealed to some degree after real world operational hours accumulate for these engines.

Regarding SCR use for NO_x control, its impact on engine operation is mostly straightforward and stems from increasing backpressure after the turbine in low-pressure catalyst installations, or engine exhaust back pressure in the high-pressure installations. In addition, measures used to increase exhaust gas temperature, such as the use of CBV and EGB were found to also impact efficiency by a measurable degree. Overall, the average consumption impact was low, close to 1.5g/kWh at mid load for both systems. For the HP-SCR the BSFC penalty was slightly higher at low load and negligible above 50% load. In contrast, practically no fuel consumption change was found at low load for the LP-SCR, but at MCR BSFC was increased by 5g/kWh, which is practically of no impact as Tier-III operation at full load is highly unlikely. No further change was found on engine operation for either application. Despite that, analysis revealed the necessity for specific tuning requirements for the LP system to achieve a minimum threshold of catalyst inlet temperature for the exhaust gas. The main approach was bypassing a portion of the exhaust gas from the turbine to the exhaust and catalyst inlet. In addition, the amount of inlet air was reduced, and compression ratio was increased by earlier EVC to further increase temperature values. The HP system involved the use of CBV opening only at low load, where the only tangible BSFC penalty of this implementation was measured. The NO_x reduction capabilities of the SCR systems were confirmed, for both LP and HP implementation. High NO_x reduction percentages were calculated approaching 90% in certain cases, with a baseline of roughly 75%. In addition, the capability of an HP system to operate on HFO was verified. Adequate performance was measured, albeit with some concerns for the rate of the catalyst elements deterioration due to the sulfur presence. For a catalyst of these specifications, operation using LSFO/VLSFO should not present any issue regarding its efficiency reduction. In general, the SCR system was found to have minimal effect on overall engine operation and consumption, relatively low complexity (especially the LP-SCR), though at the cost of volume requirements, and very good NO_x reduction potential. The major drawback of the system was the urea solution consumption that could range between 24 to 18g/kWh in the load range of interest (25% to 50% engine load). These values were the average results from tests on four different engines both during FATs and official sea trials. Urea price is high, traditionally close to that of HFO, and is known to be highly volatile due to shortages appearing rather frequently, so despite the dilution AUS-40 is a significance expense. This placed the OPEX costs of the SCR system above those of EGR equipped engines, even in the best-case scenario when including the added fuel consumption cost of the SCR's impact on the engine. Assuming a worst-case urea price scenario and MGO operation for both EGR and SCR equipped engines the SCR OPEX for fuel and urea could be double that of EGR. For some combinations of urea and fuel pricing SCR OPEX could be below that of EGR. However, further to the urea expenses, every three to five years replacement of the catalyst elements is required that further increases costs by a considerable margin. It must be considered that up to now EGR maintenance costs are unknown and multiple issues may appear in the future that could introduce regular replacements for certain components. The SCR systems benefits should not be neglected until further testing

of EGR systems is conducted in vessels frequently sailing in ECA areas and operating on Tier-III mode under various conditions.

8.3 Conclusions: Overall Findings and Thesis Contribution

The current and immediate future capabilities of the marine industry for reducing the two most important combustion emissions, CO_2 and NO_x, were examined, aiming at technical solutions at a level of maturity that allows use during commercial operation of vessels. Concrete assessment was provided for their effect on engine performance, tuning requirements, combustion and emissions.

The data collected allowed for the analysis to be conducted on a basis of actual data and not rely on assumptions or estimations from models. This was an extremely demanding campaign and closed the existing gap regarding available experimental data for technology evaluation and for support of computational studies. CO_2 reduction capabilities were confirmed for the relevant technologies, biofuels and LNG use on high-pressure gas injection dual-fuel engines. Analysis of performance showed that LNG use in maritime is a mature technology at the moment that allows safe operation on par with the conventional diesel engine, while having further potential for improvement. Biofuels were found to allow safe engine operation and have only moderate effect on NO_x emissions despite initial concerns In contrast to initial expectations no noticeable effect was observed on peak combustion pressure and performance in general. The computational study provided further insight on their effect regarding the NO_x formation mechanism, specifically the impact of higher O_2 content and lower LCV. The last was made possible from the simulation where a fuel with similar heating value and different O_2 content was examined and its effect on performance and emissions was defined. Overall, their proposition as a ready to use drop-in fuel was confirmed.

The NO_x emissions reduction technologies review and analysis revealed advantages and disadvantages for both EGR and SCR systems. The main highlight was the level of impact of recirculated gases on 2-stroke large engines' performance and efficiency. A detailed computational analysis was performed for the use of EGR to examine required gas recirculation rate and potential tuning options to reduce the efficiency penalty introduced from its use. With the use of modelling, it was made possible to determine the actual EGR percentages in the engines examined since available data were not adequate for direct estimation. For the SCR system the challenges of retaining exhaust gas temperature at levels that allow the catalyst reactor operations and the specific urea consumption at low load operation were another important finding. A detailed evaluation of HP against LP SCR systems was made for the first time. The same is the case for an HP-SCR system operating with HFO. For all SCR systems examined a small degradation of the catalyst efficiency was detected from shop tests to sea trials which creates some concerns regarding catalyst reactors aging. The NO_x reduction potential was confirmed for both solutions, but with the aforementioned concerns for the level of EGR percentage and amount of urea solution in the SCR catalyst required to achieve these values as these lead to operational and economical concerns respectively.

Further to the above, the findings and the research methodology involved amount to a substantial contribution to the information available for the studied technologies in the marine field, as the number of published works of this type on the subject are limited.

8.4 Elements of "Innovation"

Considering the previous, the elements of innovation of the specific Thesis can be summarized as:

- Modification of a multi-zone model to:
  - ✓ Consider for fuel composition effect on performance and emissions.
  - ✓ Simulate 2-stroke engine operation using EGR with consideration for EGB, EGR and CBV valve.
  - ✓ Improve the fuel-air mixing model and avoid constant tuning to account for engine operating conditions.
- Investigation for the effect of fuel "MGO, HFO and B30" on 2-stroke marine engine performance and emissions at same conditions for various loads.
- Detailed investigation for biofuel effect on performance and the combustion mechanism of 2-stroke engines. Definition of the contribution of O_2 content and LCV.
- Generation of detailed measurement database from various 2-stroke engines at actual operating conditions using biofuels.
- Detailed comparison of 2-stroke dual-fuel engine performance, combustion and emissions for "Diesel" and "DF mode" from processing of test bed data.
- Effect of designs and settings in dual-fuel engine performance and emissions.
- Detailed analysis using measured data for EGR effect on 2-stroke engines' performance, combustion and NO_x emissions. Determination of BSFC penalty.
- Estimation of required EGR rate to achieve Tier-III emission limits using measured data and a new iterative approach introduced into the multi-zone model.
- Application of the multi-zone model to investigate the possibility to minimize BSFC penalty due to EGR use in 2-stroke engines.
- Detailed comparative evaluation of LP and HP-SCR system effect on engine performance.
- Investigation of the limitations for application of LP and HP-SCR for NO_x control on 2-stroke engines.
- Evaluation of a new application of HP-SCR using HFO.
- Comparative evaluation in terms of OPEX for NO_x reduction technologies using actual operational data.

8.5 Considerations for Future Work

The research conducted in the above subjects resulted to considerations for future work and investigations.

Theoretical analysis is considered on the subject of the dual-fuel LNG engines with the development of a detailed model (two-zone and multi-zone) for combustion with versatility regarding the fuel pilot injection characteristics. The model will also allow to investigate the use of low-carbon fuels (CH_3OH) and carbon neutral fuels (NH_3). To assist model development, a process is currently underway to collect actual operating data two LNG dual fuel engines at actual operating conditions.

Biofuels tests showed very promising results in terms of engine performance and emissions. However, these tests were only conducted on short term and further research is recommended. In addition, the use of higher percentage biodiesel blends may also produce good results, as indicated by a sample analysis conducted, but not included due to size considerations. As a next step trials with biofuel blends of higher FAME percentage and tests on older engines for longer periods are planned to assess the viability of B50 for use and examine potential issues on engine fuel injection system and fuel handling system of the vessels (purifiers, tanks, etc.).

Data from EGR operating engines are also being collected during on-board operation. The long-term performance and potential issues regarding the system have already been highlighted above. As of now the systems in vessels accessible for information have very short operating period due to rarely sailing within ECA zones. Further to the previous studies regarding newer versions of EGR equipped engines is planned to review potential tuning changes and other improvements as in the case of the LNG engines. A subject not reviewed in the thesis is soot formation that is normally influenced by the use of EGR. Soot is not currently controlled for marine engines and was not included in the present measurement campaign. For the same reason minimal information is available on published peer-reviewed works. As soot formation can also be linked to EGR cooler longevity this is an interesting subject for future work.

Last, regarding SCR systems an on-going campaign is underway to review catalyst reactor longevity and behaviour under different fuels, where possible. As most vessels studied have less than four years in operation as of the time of writing the SCR reactor systems are only now approaching their expected end-of-life status.

References

1. Fridell E. Emissions and Fuel Use in the Shipping Sector. Green Ports: Inland and Seaside Sustainable Transportation Strategies. 2019 Jan 1;19–33.
2. European Commission. Climate Action Committee. 2016 [cited 2023 Mar 20]. p. 6–8 Reducing emissions from the shipping sector. Available from: https://climate.ec.europa.eu/eu-action/transport-emissions/reducing-emissions-shipping-sector_en
3. Boningari T, Smirniotis PG. Impact of nitrogen oxides on the environment and human health: Mn-based materials for the NOx abatement. Curr Opin Chem Eng. 2016 Aug 1;13:133–41.
4. IMO. International Maritime Organization. 2022 [cited 2023 Mar 20]. Initial IMO GHG Strategy. Available from: https://www.imo.org/en/MediaCentre/HotTopics/Pages/Reducing-greenhouse-gas-emissions-from-ships.aspx
5. Dos Santos VA, da Silva PP, Serrano LMV. The Maritime Sector and Its Problematic Decarbonization: A Systematic Review of the Contribution of Alternative Fuels. Energies 2022, Vol 15, Page 3571 [Internet]. 2022 May 13 [cited 2023 May 24];15(10):3571. Available from: https://www.mdpi.com/1996-1073/15/10/3571/htm
6. CO2 Emissions in 2022 – Analysis - IEA [Internet]. [cited 2023 Jul 2]. Available from: https://www.iea.org/reports/co2-emissions-in-2022
7. ICCT. Vision 2050 - International Council on Clean Transportation [Internet]. 2021 [cited 2023 Jul 2]. Available from: https://theicct.org/vision-2050/
8. Global Warming of 1.5 ºC — [Internet]. [cited 2023 Jul 2]. Available from: https://www.ipcc.ch/sr15/
9. Mercer JH. West Antarctic ice sheet and CO2 greenhouse effect: a threat of disaster. Nature 1978 271:5643 [Internet]. 1978 Jan 1 [cited 2023 May 16];271(5643):321–5. Available from: https://www.nature.com/articles/271321a0
10. Menne MJ, Williams CN, Gleason BE, Jared Rennie J, Lawrimore JH. The Global Historical Climatology Network Monthly Temperature Dataset, Version 4. J Clim. 2018 Dec 1;31(24):9835–54.
11. NASA SVS | Global Temperature Anomalies from 1880 to 2019 [Internet]. [cited 2023 Jul 2]. Available from: https://svs.gsfc.nasa.gov/4787
12. Heat Records Broken Across Earth - The New York Times [Internet]. [cited 2023 Jul 10]. Available from: https://www.nytimes.com/2023/07/06/climate/climate-change-record-heat.html
13. Global Carbon Dioxide: 2020-2021 – Climate Change: Vital Signs of the Planet [Internet]. [cited 2023 Jul 2]. Available from: https://climate.nasa.gov/climate_resources/296/global-carbon-dioxide-2020-2021/
14. Nitrous oxide emissions, 2021 [Internet]. [cited 2023 Jul 2]. Available from: https://ourworldindata.org/grapher/nitrous-oxide-emissions
15. Deng J, Wang X, Wei Z, Wang L, Wang C, Chen Z. A review of NOx and SOx emission reduction technologies for marine diesel engines and the potential evaluation of liquefied natural gas fuelled vessels. Science of The Total Environment. 2021 Apr 20;766:144319.
16. IMO 2020 – cutting sulphur oxide emissions [Internet]. [cited 2022 Nov 14]. Available from: https://www.imo.org/en/MediaCentre/HotTopics/Pages/Sulphur-2020.aspx
17. International Maritime Organization. IMO 2020 : consistent implementation of MARPOL Annex VI. OMi [Internet]. 2020 [cited 2023 Jul 2];2019–20. Available from: https://imopublicsite.azurewebsites.net/en/MediaCentre/PressBriefings/pages/34-IMO-2020-sulphur-limit-.aspx
18. Sulfur Dioxide Basics | US EPA [Internet]. [cited 2023 Jul 2]. Available from: https://www.epa.gov/so2-pollution/sulfur-dioxide-basics
19. DNV GL. Energy Transition Outlook 2020 - A global and regional forecast to 2050. Dnv Gl Energy Transition Outlook [Internet]. 2021;306. Available from: https://eto.dnvgl.com/2020/index.html
20. Alternative fuels: the options - DNV [Internet]. [cited 2023 Jul 1]. Available from: https://www.dnv.com/expert-story/maritime-impact/alternative-fuels.html
21. Deniz C, Zincir B. Environmental and economical assessment of alternative marine fuels. J Clean Prod. 2016 Feb 1;113:438–49.
22. Kumar J, Memon AA, Kumpulainen L, Kauhaniemi K, Palizban O. Design and analysis of new harbour grid models to facilitate multiple scenarios of battery charging and onshore supply for modern vessels. Energies (Basel). 2019;12(12).
23. Brief History of IMO [Internet]. [cited 2023 Jul 2]. Available from: https://www.imo.org/en/About/HistoryOfIMO/Pages/Default.aspx
24. International Maritime Organization. Fourth IMO GHG Study 2020 [Internet]. London; 2021. Available from: https://wwwcdn.imo.org/localresources/en/OurWork/Environment/Documents/Fourth IMO GHG Study 2020 - Full report and annexes.pdf
25. Zannis TC, Katsanis JS, Christopoulos GP, Yfantis EA, Papagiannakis RG, Pariotis EG, et al. Marine Exhaust Gas Treatment Systems for Compliance with the IMO 2020 Global Sulfur Cap and Tier III NOx Limits: A Review. Energies 2022, Vol 15, Page 3638 [Internet]. 2022 May 16 [cited 2023 Mar 13];15(10):3638. Available from: https://www.mdpi.com/1996-1073/15/10/3638/htm
26. International Maritime Organization. Amendments to the Technical Code on Control of Emission of Nitrogen Oxides from Marine Diesel Engines (NOx Technical Code 2008). 2010;
27. International Maritime Organization. NOx Technical Code 2008, Technical Code on Control of Emission of Nitrogen Oxides from Marine Diesel Engines. 2008.
28. IMO. 2020 IMO global 0.50 percent fuel sulphur regulation WinGD operation guideline. 2019.
29. Ivanova G. Analysis of the Specifics in Calculating the Index of Existing Marine Energy Efficiency EEXI in Force since 2023. In: 2021 13th Electrical Engineering Faculty Conference (BulEF) [Internet]. IEEE; 2021 [cited 2023 Mar 20]. p. 1–4. Available from: https://ieeexplore.ieee.org/document/9690805/

30. Lloyd's Register. IMO GHG Strategy – What does it mean ? [Internet]. 2018 [cited 2023 Mar 20]. Available from: https://www.lr.org/en/insights/articles/imo-ghg-strategy-what-does-it-mean/
31. IMO. IMO. 2022 [cited 2023 Mar 20]. Rules on ship carbon intensity and rating system enter into force. Available from: https://www.imo.org/en/MediaCentre/PressBriefings/pages/CII-and-EEXI-entry-into-force.aspx
32. Emission Standards: IMO Marine Engine Regulations [Internet]. [cited 2023 Jul 15]. Available from: https://dieselnet.com/standards/inter/imo.php
33. Marine SCR System for Compliance with IMO NOx Tier 3 Regulations｜YANMAR Technical Review｜Technology｜About YANMAR｜YANMAR [Internet]. [cited 2023 Jun 28]. Available from: https://www.yanmar.com/global/about/technology/technical_review/2018/0413_2.html
34. Platts Market Data | S&P Global Platts [Internet]. [cited 2023 Jul 22]. Available from: https://commodityinsights.spglobal.com/ss-platts-market-data.html
35. Roadmap to Zero Emission from International Shipping Ministry of Land, Infrastructure, Transport and Tourism. 2020;
36. DNV. Maritime Forecast To 2050 - Energy Transition Outlook 2021. Dnv [Internet]. 2021;118. Available from: https://www.naucher.com/wp-content/uploads/2021/09/DNV_Maritime_Forecast_2050_2021-Web.pdf
37. Global update on scrubber bans and restrictions - International Council on Clean Transportation [Internet]. [cited 2023 Jul 1]. Available from: https://theicct.org/publication/marine-scrubber-bans-and-restrictions-jun23/
38. Dual-fuel conversion for two-stroke engines [Internet]. [cited 2023 Jul 3]. Available from: https://www.man-es.com/services/new-service-solutions/retrofit-upgrade/dual-fuel-conversion
39. Masson-Delmotte V, Zhai P, Pörtner HO, Roberts D, Skea J, Shukla PR, et al. Global warming of 1.5°C An IPCC Special Report.
40. UNCTAD. Review of Maritime Transport 2021. New York; 2021 Nov. (Review of Maritime Transport).
41. IEA. International Shipping – Analysis [Internet]. 2022 [cited 2023 Mar 20]. Available from: https://www.iea.org/reports/international-shipping
42. DNV-GL. Low carbon shipping towards 2050 [Internet]. 2021. Available from: https://www.dnv.com/Publications/low-carbon-shipping-towards-2050-93579
43. Moradi MH, Brutsche M, Wenig M, Wagner U, Koch T. Marine route optimization using reinforcement learning approach to reduce fuel consumption and consequently minimize CO2 emissions. Ocean Engineering. 2022 Sep 1;259:111882.
44. Fagerholt K, Laporte G, Norstad I. Reducing fuel emissions by optimizing speed on shipping routes. https://doi.org/101057/jors200977 [Internet]. 2017 [cited 2023 Jul 2];61(3):523–9. Available from: https://www.tandfonline.com/doi/abs/10.1057/jors.2009.77
45. Relating short-term measures to IMO's minimum 2050 emissions reduction target - International Council on Clean Transportation [Internet]. [cited 2023 Mar 20]. Available from: https://theicct.org/publication/relating-short-term-measures-to-imos-minimum-2050-emissions-reduction-target/
46. Schroer M, Panagakos G, Barfod MB. An evidence-based assessment of IMO's short-term measures for decarbonizing container shipping. J Clean Prod. 2022 Aug 20;363:132441.
47. Ampah JD, Yusuf AA, Afrane S, Jin C, Liu H. Reviewing two decades of cleaner alternative marine fuels: Towards IMO's decarbonization of the maritime transport sector. J Clean Prod. 2021 Oct 20;320:128871.
48. DNV AS. Energy Transition Outlook 2023 TRANSPORT IN TRANSITION. Norway; 2023.
49. Balcombe P, Brierley J, Lewis C, Speirs J, Hawkes A, Staffell I. How to decarbonise international shipping: Options for fuels, technologies and policies. 2018 [cited 2023 Jul 2]; Available from: https://doi.org/10.1016/j.enconman.2018.12.080
50. World LNG Report 2022 | IGU [Internet]. [cited 2023 May 17]. Available from: https://www.igu.org/resources/world-lng-report-2022/
51. Huan T, Hongjun F, Wei L, Guoqiang Z. Options and Evaluations on Propulsion Systems of LNG Carriers. In: Serpi A, Porru M, editors. Propulsion Systems [Internet]. Rijeka: IntechOpen; 2019. Available from: https://doi.org/10.5772/intechopen.82154
52. Biofuels | ClassNK - English [Internet]. [cited 2023 Mar 20]. Available from: https://www.classnk.or.jp/hp/en/info_service/bio/
53. Lloyd's Register. NOx from marine diesel engines using biofuels NOx from marine diesel engines using biofuels [Internet]. 2022 [cited 2023 Mar 20]. Available from: https://www.lr.org/en/reports/nox-from-marine-diesel-engines-using-biofuels/
54. Li K, Wu M, Gu X, Yuen KF, Xiao Y. Determinants of ship operators' options for compliance with IMO 2020. Transp Res D Transp Environ. 2020 Sep 1;86:102459.
55. Sou WS, Goh T, Lee XN, Ng SH, Chai KH. Reducing the carbon intensity of international shipping – The impact of energy efficiency measures. Energy Policy. 2022 Nov 1;170:113239.
56. Chuah LF, Mokhtar K, Mhd Ruslan SM, Bakar AA, Abdullah MA, Osman NH, et al. Implementation of the energy efficiency existing ship index and carbon intensity indicator on domestic ship for marine environmental protection. Environ Res. 2023 Apr 1;222:115348.
57. Comer B, Chen C, Rutherford D. Relating short-term measures to IMO ' s minimum 2050 emissions reduction target [Internet]. ICCT Working Paper 2018-13. 2018 [cited 2023 Mar 20]. Available from: https://theicct.org/wp-content/uploads/2021/06/IMO_Short_term_potential_20181011.pdf%0Ahttps://www.theicct.org/sites/default/files/publications/IMO_Short_term_potential_20181011.pdf
58. IEA. Transport biofuels – Renewables 2022 – Analysis [Internet]. [cited 2023 May 24]. Available from: https://www.iea.org/reports/renewables-2022/transport-biofuels
59. Panoutsou C, Germer S, Karka P, Papadokostantakis S, Kroyan Y, Wojcieszyk M, et al. Advanced biofuels to decarbonise European transport by 2030: Markets, challenges, and policies that impact their successful market uptake. Energy Strategy Reviews. 2021 Mar 1;34:100633.
60. Hansson J, Månsson S, Brynolf S, Grahn M. Alternative marine fuels: Prospects based on multi-criteria decision analysis involving Swedish stakeholders. Biomass Bioenergy. 2019 Jul 1;126:159–73.

61. Mukherjee A, Bruijnincx P, Junginger M. Techno-economic competitiveness of renewable fuel alternatives in the marine sector. Renewable and Sustainable Energy Reviews. 2023 Mar 1;174:113127.
62. Law LC, Foscoli B, Mastorakos E, Evans S. A comparison of alternative fuels for shipping in terms of lifecycle energy and cost. Energies (Basel). 2021;14(24).
63. Harnessing ammonia as ship fuel - DNV [Internet]. [cited 2023 Jul 1]. Available from: https://www.dnv.com/expert-story/maritime-impact/Harnessing-ammonia-as-ship-fuel.html
64. The Nordic Green Ammonia Powered Ships (NoGAPS) | Nordic Innovation [Internet]. [cited 2023 Jul 1]. Available from: https://www.nordicinnovation.org/programs/nordic-green-ammonia-powered-ships-nogaps
65. Machaj K, Kupecki J, Malecha Z, Morawski AW, Skrzypkiewicz M, Stanclik M, et al. Ammonia as a potential marine fuel: A review. Energy Strategy Reviews. 2022 Nov 1;44:100926.
66. Imhoff TB, Gkantonas S, Mastorakos E. Analysing the performance of ammonia powertrains in the marine environment. Energies (Basel) [Internet]. 2021 Nov 8 [cited 2023 Apr 10];14(21):7447. Available from: https://www.mdpi.com/1996-1073/14/21/7447/htm
67. Yang M, Lam JSL. Operational and economic evaluation of ammonia bunkering – Bunkering supply chain perspective. Transp Res D Transp Environ. 2023 Apr 1;117:103666.
68. IEA. Ammonia Technology Roadmap [Internet]. Paris; [cited 2023 Jul 5]. Available from: https://www.iea.org/reports/ammonia-technology-roadmap
69. DNV. Handbook for Hydrogen-fuelled Vessels [Internet]. 2021 [cited 2023 Jul 2]. Available from: https://www.dnv.com/maritime/publications/handbook-for-hydrogen-fuelled-vessels-download.html
70. Van Hoecke L, Laffineur L, Campe R, Perreault P, Verbruggen SW, Lenaerts S. Challenges in the use of hydrogen for maritime applications. Energy Environ Sci [Internet]. 2021 Feb 23 [cited 2023 Jul 2];14(2):815–43. Available from: https://pubs.rsc.org/en/content/articlehtml/2021/ee/d0ee01545h
71. Sürer MG, Arat HT. Advancements and current technologies on hydrogen fuel cell applications for marine vehicles. Int J Hydrogen Energy. 2022 May 26;47(45):19865–75.
72. Atilhan S, Park S, El-Halwagi MM, Atilhan M, Moore M, Nielsen RB. Green hydrogen as an alternative fuel for the shipping industry. Curr Opin Chem Eng. 2021 Mar 1;31:100668.
73. Bicer Y, Dincer I. Clean fuel options with hydrogen for sea transportation: A life cycle approach. Int J Hydrogen Energy. 2018 Jan 11;43(2):1179–93.
74. MAN B&W ME-LGIP [Internet]. [cited 2023 Jul 2]. Available from: https://www.man-es.com/marine/products/two-stroke-engines/lgip
75. Yeo SJ, Kim J, Lee WJ. Potential economic and environmental advantages of liquid petroleum gas as a marine fuel through analysis of registered ships in South Korea. J Clean Prod. 2022 Jan 1;330:129955.
76. Wang Y, Cao Q, Liu L, Wu Y, Liu H, Gu Z, et al. A review of low and zero carbon fuel technologies: Achieving ship carbon reduction targets. Sustainable Energy Technologies and Assessments. 2022 Dec 1;54:102762.
77. MAN Energy Solutions. Methanol Future fuels [Internet]. [cited 2023 Jul 2]. Available from: https://www.man-es.com/marine/strategic-expertise/future-fuels/methanol
78. Brynolf S, Fridell E, Andersson K. Environmental assessment of marine fuels: liquefied natural gas, liquefied biogas, methanol and bio-methanol. J Clean Prod. 2014 Jul 1;74:86–95.
79. Zincir B, Deniz C. Methanol as a Fuel for Marine Diesel Engines. Energy, Environment, and Sustainability [Internet]. 2021 [cited 2023 Jul 2];45–85. Available from: https://link.springer.com/chapter/10.1007/978-981-16-0931-2_4
80. Wartzila. THE WÄRTSILÄ 32 METHANOL ENGINE. 2023.
81. Zincir B, Deniz C, Tunér M. Investigation of environmental, operational and economic performance of methanol partially premixed combustion at slow speed operation of a marine engine. J Clean Prod. 2019 Oct 20;235:1006–19.
82. Fridell E, Salberg H, Salo K. Measurements of Emissions to Air from a Marine Engine Fueled by Methanol. Journal of Marine Science and Application [Internet]. 2021 Mar 1 [cited 2023 Jul 2];20(1):138–43. Available from: https://link.springer.com/article/10.1007/s11804-020-00150-6
83. Wei L, Yao C, Wang Q, Pan W, Han G. Combustion and emission characteristics of a turbocharged diesel engine using high premixed ratio of methanol and diesel fuel. Fuel. 2015 Jan 15;140:156–63.
84. Pan W, Yao C, Han G, Wei H, Wang Q. The impact of intake air temperature on performance and exhaust emissions of a diesel methanol dual fuel engine. Fuel. 2015 Dec 15;162:101–10.
85. Gong C, Peng L, Chen Y, Liu J, Liu F, Han Y. Computational study of intake temperature effects on mixture formation, combustion and unregulated emissions of a DISI methanol engine during cold start. Fuel. 2018 Dec 15;234:1269–77.
86. The Methanol-fuelled MAN B&W LGIM Engine Application, service experience and latest development of the ME-LGIM engine MAN Energy Solutions The methanol-fuelled MAN B&W LGIM engine 2 Future in the making 3.
87. MAN Energy Solutions. Methanol in shipping Marine Four-Stroke. 2021.
88. MAN Energy Solutions. Methanol: Future fuels [Internet]. [cited 2023 Jul 2]. Available from: https://www.man-es.com/marine/strategic-expertise/future-fuels/methanol
89. Wang H, Zhou P, Wang Z. Reviews on current carbon emission reduction technologies and projects and their feasibilities on ships. Journal of Marine Science and Application [Internet]. 2017 Jun 1 [cited 2023 Jul 2];16(2):129–36. Available from: https://link.springer.com/article/10.1007/s11804-017-1413-y
90. Bouman EA, Lindstad E, Rialland AI, Strømman AH. State-of-the-art technologies, measures, and potential for reducing GHG emissions from shipping-A review. Technology (Singap World Sci) [Internet]. [cited 2023 Jul 2]; Available from: http://dx.doi.org/10.1016/j.trd.2017.03.022
91. Joung TH, Kang SG, Lee JK, Ahn J. The IMO initial strategy for reducing Greenhouse Gas(GHG) emissions, and its follow-up actions towards 2050. Journal of International Maritime Safety, Environmental Affairs, and Shipping [Internet]. 2020 [cited 2023 Jul 2];4(1):1–7. Available from: https://www.tandfonline.com/action/journalInformation?journalCode=tsea20

92. Zhou P, Wang H. Carbon capture and storage—Solidification and storage of carbon dioxide captured on ships. Ocean Engineering. 2014 Nov 15;91:172–80.
93. Long NVD, Lee DY, Kwag C, Lee YM, Lee SW, Hessel V, et al. Improvement of marine carbon capture onboard diesel fueled ships. Chemical Engineering and Processing - Process Intensification. 2021 Nov 1;168:108535.
94. Lichtschlag A, Pearce CR, Suominen M, Blackford J, Borisov SM, Bull JM, et al. Suitability analysis and revised strategies for marine environmental carbon capture and storage (CCS) monitoring. International Journal of Greenhouse Gas Control. 2021 Dec 1;112:103510.
95. Zhou S, Ren J, Xi H, Lu S, Shreka M, Zhu Y, et al. Experimental study on carbon capture characteristics of marine engine exhaust gas by activated potassium carbonate absorbent. Environmental Science and Pollution Research [Internet]. 2023 Jun 10 [cited 2023 Jul 2];1–16. Available from: https://link.springer.com/article/10.1007/s11356-023-28054-2
96. ABS. Carbon Capture for marine and offshore industries.
97. Al Baroudi H, Awoyomi A, Patchigolla K, Jonnalagadda K, Anthony EJ. A review of large-scale CO 2 shipping and marine emissions management for carbon capture, utilisation and storage. 2021 [cited 2023 Jul 2]; Available from: http://creativecommons.org/licenses/by/4.0/
98. A. M.K. P. Taylor and A. Costall. ME4 Vehicle Propulsion Technology. Imperial College London; 2017.
99. Zeldovich J. The oxidation of nitrogen in combustion and explosions. European Physical Journal A Hadrons and Nuclei [Internet]. 1946;21:577–628. Available from: https://heronet.epa.gov/heronet/index.cfm/reference/download/reference_id/34215
100. Helmut MKT. Handbook of Diesel Engines. Mollenhauer K, Tschöke H, editors. Berlin, Heidelberg: Springer Berlin Heidelberg; 2010.
101. Hountalas DT, Kouremenos DA, Binder KB, Schwarz V, Mavropoulos GC. Effect of injection pressure on the performance and exhaust emissions of a heavy duty di diesel engine. In: SAE Technical Papers. SAE International; 2003.
102. Kouremenos DA, Rakopoulos CD, Hountalas DT. Multi-zone combustion modelling for the prediction of pollutants emissions and performance of di diesel engines. SAE Technical Papers. 1997;
103. Hountalas DT, Zovanos GN, Sakellarakis D, Antonopoulos AK. Validation of multi-zone combustion model ability to predict two stroke diesel engine performance and nox emissions using on board measurements. In: Proceedings of the Spring Technical Conference of the ASME Internal Combustion Engine Division [Internet]. American Society of Mechanical Engineers Digital Collection; 2012 [cited 2023 Jan 31]. p. 47–60. Available from: /ICES/proceedings-abstract/ICES2012/44663/47/239919
104. Willis DA, Meyer WE, Birnie C. Mapping of Airflow Patterns in Engines with Induction Swirl. SAE Transactions [Internet]. 1967;75:416–26. Available from: http://www.jstor.org/stable/44563649
105. Ramos JI (Juan I. Internal Combustion Engine Modeling. In: Internal Combustion Engine Modeling. Hemisphere Pub. Corp; 1989. p. 422.
106. Dent JC, Derham JA. Air Motion in a Four-Stroke Direct Injection Diesel Engine. http://dx.doi.org/101243/PIME_PROC_1974_188_030_02 [Internet]. 2006 Feb 3 [cited 2023 Mar 10];188(21):269–80. Available from: https://journals.sagepub.com/doi/10.1243/PIME_PROC_1974_188_030_02
107. Heywood JB. Internal Combustion Engine Fundamentals. 2nd ed. McGraw-Hill Education; 2018. 1056 p.
108. Amsden AA, Butler TD, O'Rourke PJ, Ramshaw JD. KIVA-A comprehensive model for 2-D and 3-D engine simulations. SAE Technical Papers. 1985;
109. Nishida K, Hiroyasu H. Simplified three-dimensional modeling of mixture formation and combustion in a D.I. diesel engine. SAE Technical Papers. 1989;
110. Baumgarten Carsten. Mixture Formation in Internal Combustion Engine [Internet]. Mixture Formation in Internal Combustion Engine. Springer Berlin Heidelberg; 2006 [cited 2023 Jul 1]. (Heat, Mass Transfer). Available from: http://link.springer.com/10.1007/3-540-30836-9
111. Williams TJ. Parameters for Correlation of Penetration Results for Diesel Fuel Sprays. Proceedings of the Institution of Mechanical Engineers [Internet]. 1973 Jun 1;187(1):771–4. Available from: https://doi.org/10.1243/PIME_PROC_1973_187_073_02
112. Glauert MB. The wall jet. J Fluid Mech [Internet]. 2006/03/28. 1956;1(6):625–43. Available from: https://www.cambridge.org/core/article/wall-jet/A40D1EDA1B0E730382560086D5AD5CA6
113. Kumar S, Kumar Chauhan M, Varun. Numerical modeling of compression ignition engine: A review. Renewable and Sustainable Energy Reviews. 2013 Mar 1;19:517–30.
114. Jung D, Assanis DN. Multi-Zone DI Diesel Spray Combustion Model for Cycle Simulation Studies of Engine Performance and Emissions. SAE Transactions [Internet]. 2001;110:1510–32. Available from: http://www.jstor.org/stable/44724414
115. Kouremenos DA, Hountalas DT KP. Computer simulation of turbocharged marine diesel engines and its application for engine and turbocharger diagnosis. In: Proceedings of 5th international conference on turbocharging and turbochargers. London: Institution of Mechanical Engineers; 1994. p. 13–20.
116. Turner MR, Sazhin SS, Healey JJ, Crua C, Martynov SB. A breakup model for transient Diesel fuel sprays. Fuel. 2012 Jul 1;97:288–305.
117. Karimi M, Andersson R. Stochastic simulation of droplet breakup in turbulence. Chemical Engineering Journal. 2020 Jan 15;380:122502.
118. Lettieri Claudio. Large Eddy Simulation of Two-phase Reacting Flows. [London]: Imperial College London; 2010.
119. Günter P. Merker, Christian Schwarz, Gunnar Stiesch FO. Simulating Combustion [Internet]. 1st ed. Berlin/Heidelberg: Springer-Verlag; 2006. 402 p. Available from: http://link.springer.com/10.1007/3-540-30626-9
120. Borman GL, Johnson JH. Unsteady vaporization histories and trajectories of fuel drops injected into swirling air. SAE Technical Papers. 1962;
121. KADOTA T, HIROYASU H, OYA H. Spontaneous Ignition Delay of a Fuel Droplet in High Pressure and High Temperature Gaseous Environments. Bulletin of JSME. 1976;19(130):437–45.

122. Kouremenos D, Rakopoulos C, Hountalas D, Kotsiopoulos P. A Simulation technique for the fuel injection system of diesel engines. In: ASME-WA Meeting Atlanta. 1991. p. 91–102.
123. Raptotasios SI, Sakellaridis NF, Papagiannakis RG, Hountalas DT. Application of a multi-zone combustion model to investigate the NOx reduction potential of two-stroke marine diesel engines using EGR. Appl Energy. 2015 Nov 1;157:814–23.
124. Vavra MH. Aero-thermodynamics and flow in turbomachines. In 1960.
125. Kouremenos DA, Hountalas DT, Kotsiopoulos PN. Development of a Thermodynamic Method for Diagnosis and Tuning of Diesel Engines And its Application on Marine Engines. Proceedings of the Institution of Mechanical Engineers, Part A: Journal of Power and Energy [Internet]. 1995 May 1;209(2):125–39. Available from: https://doi.org/10.1243/PIME_PROC_1995_209_023_02
126. Hountalas DT, Kouremenos AD. Development and application of a fully automatic troubleshooting method for large marine diesel engines. Appl Therm Eng. 1999 Mar 1;19(3):299–324.
127. Watson N, Janota MS. Turbocharging the Internal Combustion Engine. Turbocharging the Internal Combustion Engine. Macmillan Education UK; 1982.
128. Lavole GA, Heywood JB, Keck JC. Experimental and Theoretical Study of Nitric Oxide Formation in Internal Combustion Engines. http://dx.doi.org/101080/00102206908952211 [Internet]. 2007 Feb 1 [cited 2023 Mar 15];1(4):313–26. Available from: https://www.tandfonline.com/doi/abs/10.1080/00102206908952211
129. WinGD - WinGD Engine History [Internet]. [cited 2023 Jul 2]. Available from: https://www.wingd.com/en/engines/our-engine-history/
130. Pavlenko N, Comer B, Zhou Y, Clark N, Rutherford D. The climate implications of using LNG as a marine fuel. 2020 [cited 2023 Jul 1]; Available from: www.theicct.org
131. MAN Diesel & turbo. MAN B&W ME-GI Dual-fuel, low-speed engine [Internet]. Copenhagen: MAN Diesel & Turbo; 2016 [cited 2022 Dec 5]. Available from: https://mandieselturbo.com/docs/default-source/shopwaredocuments/man-b-w-me-giee40ba7d787543c688da0d9c11628006.pdf?sfvrsn=3
132. Doosan Delivers World's First ME-GI Engine [Internet]. [cited 2023 May 18]. Available from: https://www.maritime-executive.com/corporate/Doosan-Delivers-Worlds-First-MEGI-Engine-2014-06-23
133. Sea/LNG Ltd. LNG as a marine fuel- The investment opportunity. 2019;17. Available from: https://sea-lng.org/independent-study-reveals-compelling-investment-case-for-lng-as-a-marine-fuel/
134. Der Noske Veritas. LNG as ship fuel: The future - today. 2014;(01):1–60.
135. Ott M (Winterthur G& D, Ingemar Nylund IA, Roland Alder WG& DLtd, Takayuki Hirose IC, Yoshiyuki Umemoto DULtd, Takeshi Yamada IC. The 2-stroke Low-Pressure Dual-Fuel Technology: From Concept to Reality. In Helsinki: CIMAC; 2016 [cited 2022 Dec 7]. p. 46–50. Available from: www.tcpdf.org
136. Sharafian A, Blomerus P, Mérida W, Mérida W. Natural Gas as a Ship Fuel: Assessment of Greenhouse Gas and Air Pollutant Reduction Potential.
137. MAN B&W ME-GA The latest dual-fuel MAN B&W two-stroke engine MAN Energy Solutions MAN B&W ME-GA-The latest dual-fuel MAN B&W two-stroke engine 2 Future in the making 3.
138. Rochussen J, Jaeger NSB, Penner H, Khan A, Kirchen P. Development and demonstration of strategies for GHG and methane slip reduction from dual-fuel natural gas coastal vessels. Fuel. 2023 Oct 1;349:128433.
139. Understanding Global Warming Potentials | US EPA [Internet]. [cited 2023 Jul 2]. Available from: https://www.epa.gov/ghgemissions/understanding-global-warming-potentials
140. UN agency pushes forward on shipping emissions reduction [Internet]. [cited 2023 Jul 2]. Available from: https://www.imo.org/en/MediaCentre/PressBriefings/Pages/11-MEPC-74-GHG.aspx
141. Comer B, Lead MP. Methane slip: LNG's Achilles heel. [cited 2023 May 19]; Available from: https://www.imo.org/en/OurWork/Environment/Pages/Fourth-IMO-Greenhouse-Gas-Study-2020.aspx.
142. FuelEU Maritime | European Economic and Social Committee [Internet]. [cited 2023 Jul 2]. Available from: https://www.eesc.europa.eu/en/our-work/opinions-information-reports/opinions/fueleu-maritime
143. Press release Surge of Orders for ME-GA. [cited 2023 Jul 2]; Available from: www.man-es.com
144. Nemati A, Ong JC, Pang KM, Mayer S, Walther JH. A numerical study of the influence of pilot fuel injection timing on combustion and emission formation under two-stroke dual-fuel marine engine-like conditions. Fuel. 2022 Mar 15;312.
145. Yang R, Theotokatos G, Vassalos D. CFD modelling and numerical investigation of a large marine two-stroke dual fuel direct injection engine. Ships and Offshore Structures. 2022;17(5):1062–74.
146. Hountalas DT, Papagiannakis R. Theoretical and Experimental Investigation of a Direct Injection Dual Fuel Diesel-Natural Gas Engine. 2002.
147. Yu H, Wang W, Sheng D, Li H, Duan S. Performance of combustion process on marine low speed two-stroke dual fuel engine at different fuel conditions: Full diesel/diesel ignited natural gas. Fuel. 2022 Feb 15;310:122370.
148. Arefin MA, Nabi MN, Akram MW, Islam MT, Chowdhury MW. A review on liquefied natural gas as fuels for dual fuel engines: Opportunities, challenges and responses. Energies (Basel). 2020;13(22).
149. Figari M, Theotokatos G, Coraddu A, Stoumpos S, Mondella T. Parametric investigation and optimal selection of the hybrid turbocharger system for a large marine four-stroke dual-fuel engine. Appl Therm Eng [Internet]. 2022;208(February):117991. Available from: https://doi.org/10.1016/j.applthermaleng.2021.117991
150. Stoumpos S, Theotokatos G. A novel methodology for marine dual fuel engines sensors diagnostics and health management. International Journal of Engine Research. 2022;23(6):974–94.
151. Hountalas DT, Papagiannakis RG. Development of a simulation model for direct injection dual fuel diesel-natural gas engines. In: SAE Technical Papers [Internet]. 2000 [cited 2022 Dec 11]. Available from: https://www.jstor.org/stable/44634226

152. Papagiannakis RG, Hountalas DT. Combustion and exhaust emission characteristics of a dual fuel compression ignition engine operated with pilot Diesel fuel and natural gas. Energy Convers Manag [Internet]. 2004 Nov 1 [cited 2019 Dec 5];45(18–19):2971–87. Available from: https://www.sciencedirect.com/science/article/pii/S0196890404000330
153. Hardenberg HO, Hase FW. An Empirical Formula for Computing the Pressure Rise Delay of a Fuel from Its Cetane Number and from the Relevant Parameters of Direct-Injection Diesel Engines. SAE Transactions [Internet]. 1979 Oct 6;88:1823–34. Available from: http://www.jstor.org/stable/44658184
154. Thermodynamics, Group FM, Annand WJD. Heat Transfer in the Cylinders of Reciprocating Internal Combustion Engines. Proceedings of the Institution of Mechanical Engineers [Internet]. 1963;177(1):973–96. Available from: https://doi.org/10.1243/PIME_PROC_1963_177_069_02
155. Yu H, Duan S, Sun P. Comparative analysis between natural gas/diesel (dual fuel) and pure diesel on the marine diesel engine. Journal of Engineering Research. 2015;3(4):111–25.
156. Lounici MS, Loubar K, Tarabet L, Balistrou M, Niculescu DC, Tazerout M. Towards improvement of natural gas-diesel dual fuel mode: An experimental investigation on performance and exhaust emissions. Energy. 2014 Jan 1;64:200–11.
157. Xu S, Anderson D, Hoffman M, Prucka R, Filipi Z. A phenomenological combustion analysis of a dual-fuel natural-gas diesel engine. Proceedings of the Institution of Mechanical Engineers, Part D: Journal of Automobile Engineering. 2017;231(1):66–83.
158. Larson CR. Injection study of a diesel engine fueled with pilot-ignited, directly-injected natural gas [Internet]. 2003. Available from: https://open.library.ubc.ca/collections/831/items/1.0080985
159. Naber JD, Siebers DL, Di Julio SS, Westbrook CK. Effects of natural gas composition on ignition delay under diesel conditions. Combust Flame [Internet]. 1994;99(2):192–200. Available from: https://www.sciencedirect.com/science/article/pii/0010218094901228
160. Liu H, Li J, Wang J, Wu C, Liu B, Dong J, et al. Effects of injection strategies on low-speed marine engines using the dual fuel of high-pressure direct-injection natural gas and diesel. Energy Sci Eng [Internet]. 2019;7(5):1994–2010. Available from: https://onlinelibrary.wiley.com/doi/abs/10.1002/ese3.406
161. Li M, Zhang Q, Li G, Shao S. Experimental investigation on performance and heat release analysis of a pilot ignited direct injection natural gas engine. Energy. 2015 Oct 1;90:1251–60.
162. Guo H, Zhou S, Zou J, Shreka M. A Numerical Study on the Pilot Injection Conditions of a Marine 2-Stroke Lean-Burn Dual Fuel Engine. Processes [Internet]. 2020 [cited 2023 Apr 8];8(11). Available from: www.mdpi.com/journal/processes
163. Pham VC, Choi JH, Rho BS, Kim JS, Park K, Park SK, et al. A numerical study on the combustion process and emission characteristics of a natural gas-diesel dual-fuel marine engine at full load. Energies (Basel) [Internet]. 2021 Mar 1 [cited 2023 Apr 7];14(5):1342. Available from: https://www.mdpi.com/1996-1073/14/5/1342/htm
164. Boretti A. Advances in Diesel-LNG Internal Combustion Engines. Applied Sciences [Internet]. 2020;10(4). Available from: https://www.mdpi.com/2076-3417/10/4/1296
165. MAN Energy Solutions. LNGC-optimised designs of ME-GI engines and fuel gas supply systems. Denmark; 2020.
166. Theotokatos G, Stoumpos S, Bolbot V, Boulougouris E. Simulation-based investigation of a marine dual-fuel engine. https://doi.org/101080/2046417720201717266 [Internet]. 2020 Jan 3 [cited 2023 Jul 4];19(sup1):5–16. Available from: https://www.tandfonline.com/doi/abs/10.1080/20464177.2020.1717266
167. Ma C, Yao C, Song EZ, Ding SL. Prediction and optimization of dual-fuel marine engine emissions and performance using combined ANN with PSO algorithms. https://doi.org/101177/1468087421990476 [Internet]. 2021 Feb 7 [cited 2023 Jul 4];23(4):560–76. Available from: https://journals.sagepub.com/doi/10.1177/1468087421990476
168. Sun L, Liu Y, Zeng K, Yang R, Hang Z. Combustion performance and stability of a dual-fuel diesel-natural-gas engine. Proceedings of the Institution of Mechanical Engineers, Part D: Journal of Automobile Engineering [Internet]. 2015 Jul 1 [cited 2023 Apr 8];229(2):235–46. Available from: https://journals.sagepub.com/doi/abs/10.1177/0954407014537814?journalCode=pidb
169. Herdzik J. Decarbonization of Marine Fuels—The Future of Shipping. Energies 2021, Vol 14, Page 4311 [Internet]. 2021 Jul 17 [cited 2023 Jul 2];14(14):4311. Available from: https://www.mdpi.com/1996-1073/14/14/4311/htm
170. Woon KS, Phuang ZX, Taler J, Varbanov PS, Chong CT, Klemeš JJ, et al. Recent advances in urban green energy development towards carbon emissions neutrality. Energy [Internet]. 2023;267:126502. Available from: https://www.sciencedirect.com/science/article/pii/S0360544222033886
171. Biofuels explained - use and supply - U.S. Energy Information Administration (EIA) [Internet]. [cited 2023 Jul 2]. Available from: https://www.eia.gov/energyexplained/biofuels/biodiesel-rd-other-use-supply.php
172. Puricelli S, Cardellini G, Casadei S, Faedo D, van den Oever AEM, Grosso M. A review on biofuels for light-duty vehicles in Europe. Renewable and Sustainable Energy Reviews. 2021 Mar 1;137:110398.
173. Hsieh CWC, Felby C. Biofuels for the marine shipping sector: An overview and analysis of sector infrastructure, fuel technologies and regulations [Internet]. 2017 [cited 2023 Apr 27]. Available from: https://www.ieabioenergy.com/wp-content/uploads/2018/02/Marine-biofuel-report-final-Oct-2017.pdf
174. Zhou Y, Pavlenko N, Rutherford D, Osipova L, Comer B. The potential of liquid biofuels in reducing ship emissions. International Council on Clean Transportation [Internet]. 2020 [cited 2022 Dec 14];1(September):31. Available from: www.theicct.org
175. International Energy Agency. State of Technology Review-Algae Bioenergy An IEA Bioenergy Inter-Task Strategic Project. 2017.
176. Naik SN, Goud V V., Rout PK, Dalai AK. Production of first and second generation biofuels: A comprehensive review. Renewable and Sustainable Energy Reviews. 2010 Feb 1;14(2):578–97.
177. Jeswani HK, Chilvers A, Azapagic A. Environmental sustainability of biofuels: a review.
178. Mohr A, Raman S. Lessons from first generation biofuels and implications for the sustainability appraisal of second generation biofuels. Efficiency and Sustainability in Biofuel Production: Environmental and Land-Use Research [Internet]. 2015;63:281–310. Available from: http://dx.doi.org/10.1016/j.enpol.2013.08.033

179. Sims REH, Mabee W, Saddler JN, Taylor M. An overview of second generation biofuel technologies. Bioresour Technol [Internet]. 2010 Mar 1 [cited 2023 Jan 26];101(6):1570–80. Available from: https://linkinghub.elsevier.com/retrieve/pii/S0960852409015508
180. Hosseinzadeh-Bandbafha H, Nizami AS, Kalogirou SA, Kumar Gupta V, Park YK, Fallahi A, et al. Environmental life cycle assessment of biodiesel production from waste cooking oil: A systematic review. Renewable and Sustainable Energy Reviews [Internet]. 2022 [cited 2023 May 20];161:112411. Available from: https://doi.org/10.1016/j.rser.2022.112411
181. Moravvej Z, Makarem MA, Rahimpour MR. The fourth generation of biofuel. In: Second and Third Generation of Feedstocks [Internet]. Elsevier; 2019 [cited 2023 May 22]. p. 557–97. Available from: https://linkinghub.elsevier.com/retrieve/pii/B9780128151624000203
182. Abdullah B, Syed Muhammad SAF, Shokravi Z, Ismail S, Kassim KA, Mahmood AN, et al. Fourth generation biofuel: A review on risks and mitigation strategies. Renewable and Sustainable Energy Reviews [Internet]. 2019;107:37–50. Available from: https://www.sciencedirect.com/science/article/pii/S136403211930111X
183. Aro EM. From first generation biofuels to advanced solar biofuels. Ambio [Internet]. 2016 Jan 1 [cited 2023 May 20];45(1):24–31. Available from: https://link.springer.com/article/10.1007/s13280-015-0730-0
184. Alalwan HA, Alminshid AH, Aljaafari HAS. Promising evolution of biofuel generations. Subject review. Renewable Energy Focus [Internet]. 2019 Mar 1 [cited 2023 Mar 20];28:127–39. Available from: https://linkinghub.elsevier.com/retrieve/pii/S1755008418303259
185. Rulli MC, Bellomi D, Cazzoli A, De Carolis G, D'Odorico P. The water-land-food nexus of first-generation biofuels. Scientific Reports 2016 6:1 [Internet]. 2016 Mar 3 [cited 2023 May 20];6(1):1–10. Available from: https://www.nature.com/articles/srep22521
186. Foteinis S, Chatzisymeon E, Litinas A, Tsoutsos T. Used-cooking-oil biodiesel: Life cycle assessment and comparison with first- and third-generation biofuel. Renew Energy [Internet]. 2020 Jun 1 [cited 2023 May 20];153:588–600. Available from: https://linkinghub.elsevier.com/retrieve/pii/S0960148120302081
187. Ben-Iwo J, Manovic V, Longhurst P. Biomass resources and biofuels potential for the production of transportation fuels in Nigeria. Renewable and Sustainable Energy Reviews. 2016 Sep 1;63:172–92.
188. van der Kroft DFA, Pruyn JFJ. A study into the availability, costs and GHG reduction in drop-in biofuels for shipping under different regimes between 2020 and 2050. Sustainability (Switzerland). 2021;13(17).
189. Hoekman SK. Biofuels in the U.S.-Challenges and Opportunities. 2008;
190. Cho HJ, Kim JK, Ahmed F, Yeo YK. Life-cycle greenhouse gas emissions and energy balances of a biodiesel production from palm fatty acid distillate (PFAD). Appl Energy. 2013 Nov 1;111:479–88.
191. Dufour J, Iribarren D. Life cycle assessment of biodiesel production from free fatty acid-rich wastes. Renew Energy. 2012 Feb 1;38(1):155–62.
192. Lechon Y, Cabal H, Sáez R. Life cycle greenhouse gas emissions impacts of the adoption of the EU Directive on biofuels in Spain. Effect of the import of raw materials and land use changes. Biomass Bioenergy. 2011 Jun 1;35(6):2374–84.
193. Zhou Y, Pavlenko N, Rutherford D, Osipova L, Comer B. The potential of liquid biofuels in reducing ship emissions. International Council on Clean Transportation. Report. [Internet]. Vol. 1, International Council on Clean Transportation. 2020 [cited 2022 Oct 4]. Available from: https://theicct.org/publication/the-potential-of-liquid-biofuels-in-reducing-ship-emissions/
194. Maria Stathatou P, Scott Bergeron, Christopher Fee, Paul Jeffrey, Michael Triantafyllou, Neil Gershenfeld. Towards decarbonization of shipping: direct emissions & life cycle impacts from a biofuel trial aboard an ocean-going dry bulk vessel. Sustain Energy Fuels [Internet]. 2022 Mar 29 [cited 2022 Apr 6];6(7):1687–97. Available from: https://pubs.rsc.org/en/content/articlehtml/2022/se/d1se01495a
195. Li S, Tan ECD, Dutta A, Snowden-Swan LJ, Thorson MR, Ramasamy KK, et al. Techno-economic Analysis of Sustainable Biofuels for Marine Transportation. Environ Sci Technol [Internet]. 2022 Dec 6 [cited 2023 Jul 2];56(23):17206–14. Available from: https://pubs.acs.org/doi/full/10.1021/acs.est.2c03960
196. Paulauskiene T, Bucas M, Laukinaite A. Alternative fuels for marine applications: Biomethanol-biodiesel-diesel blends. Fuel. 2019 Jul 15;248:161–7.
197. Mohd Noor CW, Noor MM, Mamat R. Biodiesel as alternative fuel for marine diesel engine applications: A review. Vol. 94, Renewable and Sustainable Energy Reviews. Pergamon; 2018. p. 127–42.
198. Mohd Noor CW, Noor MM, Mamat R. Biodiesel as alternative fuel for marine diesel engine applications: A review. Renewable and Sustainable Energy Reviews. 2018;94(October):127–42.
199. Graboski MS, Mccormick RL, Alleman TL, Herring AM. The Effect of Biodiesel Composition on Engine Emissions from a DDC Series 60 Diesel Engine: Final Report; Report 2 in a Series of 6. 2003 [cited 2022 Apr 12]; Available from: http://www.osti.gov/bridge
200. CIMAC. Fuel Quality Guide-Ignition and Combustion, 2011. 2011;
201. Pandey RK, Rehman A, Sarviya RM. Impact of alternative fuel properties on fuel spray behavior and atomization. Vol. 16, Renewable and Sustainable Energy Reviews. Pergamon; 2012. p. 1762–78.
202. Chountalas T, Founti M. Effect of Low-Sulfur Fuel on Auxiliary Engine Combustion and Performance. In: SNAME 7th International Symposium on Ship Operations, Management and Economics, SOME 2021 [Internet]. OnePetro; 2021 [cited 2023 Jan 28]. Available from: /SNAMESOME/proceedings-abstract/SOME21/2-SOME21/461284
203. Kalligeros S, Zannikos F, Stournas S, Lois E, Anastopoulos G, Teas C, et al. An investigation of using biodiesel/marine diesel blends on the performance of a stationary diesel engine. Biomass Bioenergy. 2003 Feb 1;24(2):141–9.
204. Yang Y Bin, Ryu C, Khor A, Yates NE, Sharifi VN, Swithenbank J. Effect of fuel properties on biomass combustion. Part II. Modelling approach - Identification of the controlling factors. Fuel [Internet]. 2005 [cited 2023 Jan 31];84(16):2116–30. Available from: www.fuelfirst.com
205. Mueller CJ, Boehman AL, Martin GC. An Experimental Investigation of the Origin of Increased NO_x Emissions When Fueling a Heavy-Duty Compression-Ignition Engine with Soy Biodiesel. SAE Int J Fuels Lubr [Internet]. 2009 Apr 27;2(1):789–816. Available from: http://www.jstor.org/stable/26273427

206. Lin CY. Effects of biodiesel blend on marine fuel characteristics for marine vessels. Energies (Basel) [Internet]. 2013 Sep 24 [cited 2023 Mar 20];6(9):4945–55. Available from: https://www.mdpi.com/1996-1073/6/9/4945/htm
207. Rakopoulos CD, Hountalas DT, Zannis TC, Levendis YA. Operational and Environmental Evaluation of Diesel Engines Burning Oxygen-Enriched Intake Air or Oxygen-Enriched Fuels: A Review. SAE Transactions [Internet]. 2004 Jan 31;113:1723–43. Available from: http://www.jstor.org/stable/44740884
208. Aydin H, Bayindir H. Performance and emission analysis of cottonseed oil methyl ester in a diesel engine. Renew Energy. 2010 Mar 1;35(3):588–92.
209. Weigand A, Atzler F, Kastner O, Rotondi R, Schwarte A. The effect of closely coupled pilot injections on diesel engine emissions. Institution of Mechanical Engineers - Internal Combustion Engines: Improving Performance, Fuel Economy and Emissions. 2011 Jan 1;111–24.
210. Suryawanshi JG, Deshpande N V. Effect of Injection Timing Retard on Emissions and Performance of a Pongamia Oil Methyl Ester Fuelled CI Engine. SAE Technical Papers [Internet]. 2005 Oct 24 [cited 2023 Jul 2]; Available from: https://www.sae.org/publications/technical-papers/content/2005-01-3677/
211. Wei L, Cheng R, Mao H, Geng P, Zhang Y, You K. Combustion process and NOx emissions of a marine auxiliary diesel engine fuelled with waste cooking oil biodiesel blends. Energy [Internet]. 2018;144:73–80. Available from: https://www.sciencedirect.com/science/article/pii/S0360544217320315
212. IMO. MEPC.1/Circular.795 Rev.6 – Unified Interpretations to MARPOL Annex VI – (10 June 2022).
213. Aydın S. Comprehensive analysis of combustion, performance and emissions of power generator diesel engine fueled with different source of biodiesel blends. Energy [Internet]. 2020 Aug 15 [cited 2023 Jan 31];205:118074. Available from: https://linkinghub.elsevier.com/retrieve/pii/S0360544220311816
214. Wu G, Jiang G, Yang Z, Huang Z. Emission characteristics for waste cooking oil biodiesel blend in a marine diesel propulsion engine. Pol J Environ Stud [Internet]. 2019 Apr 9 [cited 2023 Mar 20];28(4):2911–21. Available from: http://www.pjoes.com/Emission-Characteristics-for-Waste-Cooking-Oil-nBiodiesel-Blend-in-a-Marine-Diesel,92704,0,2.html
215. Boubahri C, Ridha E, Rachid S, Jamel B. Experimental study of a diesel engine performance running on waste vegetable oil biodiesel blend. Journal of Energy Resources Technology, Transactions of the ASME [Internet]. 2012 Sep 1 [cited 2023 Mar 21];134(3). Available from: https://asmedigitalcollection.asme.org/energyresources/article/134/3/032202/465055/Experimental-Study-of-a-Diesel-Engine-Performance
216. Love ND, Parthasarathy RN, Gollahalli SR. Rapid characterization of radiation and pollutant emissions of biodiesel and hydrocarbon liquid fuels. Journal of Energy Resources Technology, Transactions of the ASME [Internet]. 2009 Mar 1 [cited 2023 Mar 21];131(1):0122021–9. Available from: https://asmedigitalcollection.asme.org/energyresources/article/131/1/012202/455601/Rapid-Characterization-of-Radiation-and-Pollutant
217. Puškár M, Kopas M, Sabadka D, Kliment M, Šoltésová M. Reduction of the gaseous emissions in the marine diesel engine using biodiesel mixtures. J Mar Sci Eng [Internet]. 2020 May 8 [cited 2023 Mar 21];8(5):330. Available from: https://www.mdpi.com/2077-1312/8/5/330/htm
218. Nishio S, Fukuda T, Fathallah AZM, Setiapraja H. Influence of Palm Biofuel for Marine Diesel Engine on Combustion and Exhaust Emission Characteristics. Marine Engineering. 2018 May 1;53(3):441–6.
219. Wu F, Wang J, Chen W, Shuai S. A study on emission performance of a diesel engine fueled with five typical methyl ester biodiesels. Atmos Environ. 2009 Mar 1;43(7):1481–5.
220. Mofijur M, Rasul M, Hassan NMS, Uddin MN. Investigation of exhaust emissions from a stationary diesel engine fuelled with biodiesel. In: Energy Procedia. Elsevier; 2019. p. 791–7.
221. Sagin S, Karianskyi S, Madey V, Sagin A, Stoliaryk T, Tkachenko I. Impact of Biofuel on the Environmental and Economic Performance of Marine Diesel Engines. J Mar Sci Eng [Internet]. 2023 Jan 5 [cited 2023 Mar 20];11(1):120. Available from: https://www.mdpi.com/2077-1312/11/1/120/htm
222. Zheng M, Mulenga MC, Reader GT, Wang M, Ting DSK, Tjong J. Biodiesel engine performance and emissions in low temperature combustion. Fuel. 2008 May;87(6):714–22.
223. Varatharajan K, Cheralathan M. Influence of fuel properties and composition on NO x emissions from biodiesel powered diesel engines: A review. Vol. 16, Renewable and Sustainable Energy Reviews. Pergamon; 2012. p. 3702–10.
224. Sun J, Caton JA, Jacobs TJ. Oxides of nitrogen emissions from biodiesel-fuelled diesel engines. Prog Energy Combust Sci [Internet]. 2010;36(6):677–95. Available from: https://www.sciencedirect.com/science/article/pii/S0360128510000237
225. Hoekman SK, Robbins C. Review of the effects of biodiesel on NOx emissions. Fuel Processing Technology [Internet]. 2012;96:237–49. Available from: https://www.sciencedirect.com/science/article/pii/S0378382012000021
226. Rickeard DJ, Thompson ND. A review of the potential for bio-fuels as transportation fuels. In: SAE Technical Papers [Internet]. SAE International; 1993 [cited 2023 Mar 23]. Available from: https://www.sae.org/publications/technical-papers/content/932778/
227. Monyem A, Van Gerpen JH, Canakci M. The effect of timing and oxidation on emissions from biodiesel-fueled engines. Transactions of the American Society of Agricultural Engineers [Internet]. 2001 [cited 2023 Mar 22];44(1):35–42. Available from: https://elibrary.asabe.org/azdez.asp?JID=3&AID=2301&CID=t2001&v=44&i=1&T=1
228. Agarwal D, Sinha S, Agarwal AK. Experimental investigation of control of NOx emissions in biodiesel-fueled compression ignition engine. Renew Energy [Internet]. 2006;31(14):2356–69. Available from: https://www.sciencedirect.com/science/article/pii/S0960148105003587
229. Rajkumar S, Thangaraja J. Effect of biodiesel, biodiesel binary blends, hydrogenated biodiesel and injection parameters on NOx and soot emissions in a turbocharged diesel engine. Fuel [Internet]. 2019;240:101–18. Available from: https://www.sciencedirect.com/science/article/pii/S0016236118320350
230. Rajak U, Nashine P, Dasore A, Balijepalli R, Chaurasiya PK, Verma TN. Numerical analysis of performance and emission behavior of CI engine fueled with microalgae biodiesel blend. In: Materials Today: Proceedings. Elsevier; 2021. p. 301–6.

231. Testo Inc. Testo 350 Flue Gas Analyzer: Instruction Manual. 2020.
232. Zheng M, Reader GT, Hawley JG. Diesel engine exhaust gas recirculation—a review on advanced and novel concepts. Energy Convers Manag. 2004 Apr 1;45(6):883–900.
233. MAN Energy Solutions. Emission Project Guide. Copenhagen; 2019.
234. Klaus Mollenhauer HT. Handbook of Diesel Engines [Internet]. 1st ed. Mollenhauer K, Tschöke H, editors. Berlin, Heidelberg: Springer Berlin Heidelberg; 2010. 636 p. Available from: http://link.springer.com/10.1007/978-3-540-89083-6
235. Idicheria CA, Pickett LM. Soot Formation in Diesel Combustion under High-EGR Conditions. SAE Transactions [Internet]. 2005;114:1559–74. Available from: http://www.jstor.org/stable/44721068
236. Sun X, Liang X, Shu G, Lin J, Wang Y, Wang Y. Numerical investigation of two-stroke marine diesel engine emissions using exhaust gas recirculation at different injection time. Ocean Engineering. 2017 Nov 1;144:90–7.
237. Sun X, Liang X, Shu G, Lin J, Wang Y, Wang Y. Numerical investigation of two-stroke marine diesel engine emissions using exhaust gas recirculation at different injection time. Ocean Engineering. 2017 Nov 1;144:90–7.
238. American Burau of Shipping (ABS). ABS Advisory on NOx Tier III Compliance. 2020.
239. Vodder Nielsen K. Exhaust Recirculation Control for Reduction of NOx from Large Two-Stroke Diesel Engines. Technical University of Denmark; 2016.
240. Wang Z, Zhou S, Feng Y, Zhu Y. Research of NOx reduction on a low-speed two-stroke marine diesel engine by using EGR (exhaust gas recirculation)–CB (cylinder bypass) and EGB (exhaust gas bypass). Int J Hydrogen Energy. 2017 Jul 27;42(30):19337–45.
241. Wang Z, Zhou S, Feng Y, Zhu Y. Investigation of EGR With EGB (Exhaust Gas Bypass) on Low Speed Marine Diesel Engine Performance and Emission Characteristics. In American Society of Mechanical Engineers Digital Collection; 2017 [cited 2023 Mar 13]. Available from: /OMAE/proceedings-abstract/OMAE2017/57748/281550
242. Sun X, Liang X, Zhou P, Yu H, Cao X. Computational study of NOx reduction on a marine diesel engine by application of different technologies. Energy Procedia. 2019 Feb 1;158:4447–52.
243. Wang D, Shi L, Zhu S, Liu B, Qian Y, Deng K. Numerical and thermodynamic study on effects of high and low pressure exhaust gas recirculation on turbocharged marine low-speed engine. Appl Energy. 2020 Mar 1;261:114346.
244. Cui Y, Hu Z, Deng K, Wang Q. Miller-Cycle regulatable, two-stage turbocharging system design for marine diesel engines. J Eng Gas Turbine Power [Internet]. 2014 Feb 1 [cited 2023 Mar 14];136(2). Available from: https://asmedigitalcollection.asme.org/gasturbinespower/article/136/2/022201/373463/Miller-Cycle-Regulatable-Two-Stage-Turbocharging
245. Lamas MI, Rodríguez CG. Emissions from marine engines and NOx reduction methods. Journal of Maritime Research [Internet]. 2012 [cited 2023 Mar 14];9(1):77–82. Available from: https://www.jmr.unican.es/index.php/jmr/article/view/172
246. Wang C, Wang T, Sun K, Lu Z, Gui Y. Effects of EGR and Injection Strategies on the Performance and Emissions of a Two-Stroke Marine Diesel Engine. In: SAE Technical Papers [Internet]. SAE International; 2017 [cited 2023 Mar 13]. Available from: https://www.sae.org/content/2017-01-2249/
247. Yin X, Li W, Zhang W, Lv X, Yang B, Wang Y, et al. Experimental analysis of the EGR rate and temperature impact on combustion and emissions characteristics in a heavy-duty NG engine. Fuel [Internet]. 2022 Feb 15 [cited 2023 May 19];310:122394. Available from: https://linkinghub.elsevier.com/retrieve/pii/S0016236121022663
248. Agarwal AK, Srivastava DK, Dhar A, Maurya RK, Shukla PC, Singh AP. Effect of fuel injection timing and pressure on combustion, emissions and performance characteristics of a single cylinder diesel engine. Fuel. 2013 Sep 1;111:374–83.
249. Liang X, Zheng Z, Zhang H, Wang Y, Yu H. A Review of Early Injection Strategy in Premixed Combustion Engines. Applied Sciences [Internet]. 2019;9(18). Available from: https://www.mdpi.com/2076-3417/9/18/3737
250. Egnell R. The influence of EGR on heat release rate and NO formation in a di diesel engine. SAE Technical Papers. 2000;
251. Ladommatos N, Abdelhalim SM, Zhao H, Hu. Z. Effects of EGR on heat release in diesel combustion. SAE Technical Papers. 1998;
252. Abd-Alla GH. Using exhaust gas recirculation in internal combustion engines: A review. Energy Convers Manag [Internet]. 2002 [cited 2023 Mar 9];43(8):1027–42. Available from: www.elsevier.com/locate/enconman
253. Zheng M, Reader GT, Hawley JG. Diesel engine exhaust gas recirculation - A review on advanced and novel concepts. Energy Convers Manag. 2004;45(6):883–900.
254. Feng L, Tian J, Long W, Gong W, Du B, Li D, et al. Decreasing NOx of a low-speed two-stroke marine diesel engine by using in-cylinder emission control measures. Energies (Basel) [Internet]. 2016 Apr 21 [cited 2023 Mar 13];9(4):304. Available from: https://www.mdpi.com/1996-1073/9/4/304/htm
255. Hoard J, Abarham M, Styles D, Giuliano JM, Sluder CS, Storey JME. Diesel EGR cooler fouling. SAE Int J Engines [Internet]. 2009 Oct 6 [cited 2023 Mar 13];1(1):1234–50. Available from: https://www.sae.org/publications/technical-papers/content/2008-01-2475/
256. Kuan CK, Styles D, Bieniek M, Hoard J. An EGR Cooler Fouling Model: Experimental Correlation and Model Uses. SAE Int J Engines [Internet]. 2017 Mar 28 [cited 2023 Mar 13];10(2):541–9. Available from: https://www.sae.org/publications/technical-papers/content/2017-01-0535/
257. Park S, Lee KS, Park J. Parametric Study on EGR Cooler Fouling Mechanism Using Model Gas and Light-Duty Diesel Engine Exhaust Gas. Energies 2018, Vol 11, Page 3161 [Internet]. 2018 Nov 15 [cited 2023 Mar 13];11(11):3161. Available from: https://www.mdpi.com/1996-1073/11/11/3161/htm
258. Alegret G, Llamas X, Vejlgaard-Laursen M, Eriksson L. Modeling of a large marine two-stroke diesel engine with cylinder bypass valve and EGR system. IFAC-PapersOnLine. 2015 Oct 1;28(16):273–8.
259. Lu D, Theotokatos G, Zhang J, Zeng H, Cui K. Parametric investigation of a large marine two-stroke diesel engine equipped with exhaust gas recirculation and turbocharger cut out systems. Appl Therm Eng. 2022 Jan 5;200:117654.
260. Wintertur Gas & Diesel Ltd. Selective Catalytic Reduction FAQ. ; 2018.
261. Zhu Y, Zhang R, Zhou S, Huang C, Feng Y, Shreka M, et al. Performance Optimization of High-Pressure SCR System in a Marine Diesel Engine. Part I: Flow Optimization and Analysis. Top Catal. 2019 Feb 15;62(1–4):27–39.

262. Börnhorst M, Deutschmann O. Advances and challenges of ammonia delivery by urea-water sprays in SCR systems. Prog Energy Combust Sci. 2021 Nov 1;87:100949.
263. Zhang Y, Xia C, Liu D, Zhu Y, Feng Y. Experimental investigation of the high-pressure SCR reactor impact on a marine two-stroke diesel engine. Fuel. 2023 Mar 1;335:127064.
264. Azzara A, Rutherford D, Wang H. Feasibility of IMO Annex VI Tier III implementation using Selective Catalytic Reduction. 2014;
265. Fuel prices | IRU | World Road Transport Organisation [Internet]. [cited 2023 Jun 29]. Available from: https://www.iru.org/what-we-do/being-trusted-voice-mobility-and-logistics/fuel-prices
266. Bronsart R, Urbanski T, Shu ST. A Life Cycle Cost Analysis of Marine Scrubber Technologies Shih-Tung Shu "EMSHIP" Erasmus Mundus Master Course in "Integrated Advanced Ship Design" "EMSHIP" Erasmus Mundus Master Course, period of study. 2013;
267. IACCSEA. Marine SCR - Cost Benefit Analysis. 2013.
268. Lehtoranta K, Turunen R, Vesala H, nyyssönen sami, soikkeli niko, esselström lucas. Testing SCR in high sulphur application. In: CIMAC Congress [Internet]. Shanghai; 2013 [cited 2023 Jun 29]. Available from: https://www.researchgate.net/publication/316511059_Testing_SCR_in_high_sulphur_application
269. Zhang G, Yan H, Li T, Zhu Y, Zhou S, Feng Y, et al. Relation analysis on emission control and economic cost of SCR system for marine diesels. Science of The Total Environment [Internet]. 2021 Sep 20 [cited 2023 Jun 29];788:147856. Available from: https://linkinghub.elsevier.com/retrieve/pii/S0048969721029272
270. Urea vs Crude Oil (petroleum) - Price Rate of Change Comparison - IndexMundi [Internet]. [cited 2023 Jun 29]. Available from: https://www.indexmundi.com/commodities/?commodity=urea&months=60&commodity=crude-oil
271. Yang ZL, Zhang D, Caglayan O, Jenkinson ID, Bonsall S, Wang J, et al. Selection of techniques for reducing shipping NOx and SOx emissions. Transp Res D Transp Environ [Internet]. 2012 [cited 2023 Mar 9];17(6):478–86. Available from: http://dx.doi.org/10.1016/j.trd.2012.05.010
272. Xia C, Zhu Y, Zhou S, Peng H, Feng Y, Zhou W, et al. Simulation study on transient performance of a marine engine matched with high-pressure SCR system. International Journal of Engine Research [Internet]. 2022 Mar 7;24(4):1327–45. Available from: https://doi.org/10.1177/14680874221084052
273. Jang J, Na S, Roh H, Ahn S, Choi G. Spraying and Mixing Characteristics of Urea in a Static Mixer Applied Marine SCR System. Energies 2021, Vol 14, Page 5788 [Internet]. 2021 Sep 14 [cited 2023 Jun 7];14(18):5788. Available from: https://www.mdpi.com/1996-1073/14/18/5788/htm
274. Wang Z, Zhu Y, Zhou S, Feng Y. Reaction mechanism and chemical kinetics of NH3-NO/NO2-SCR system with vanadium-based catalyst under marine diesel exhaust conditions. Proceedings of the Institution of Mechanical Engineers, Part A: Journal of Power and Energy [Internet]. 2019 Jun 24;234(3):342–52. Available from: https://doi.org/10.1177/0957650919857618
275. Andersson K, Jeong B, Jang H. Life Cycle and Cost Assessment of a Marine Scrubber Installation. Journal of International Maritime Safety, Environmental Affairs, and Shipping [Internet]. 2020 Oct 1;4(4):162–76. Available from: https://doi.org/10.1080/25725084.2020.1861823
276. The trouble with scrubbers: shipping "solution" creates new pollution [Internet]. [cited 2023 Jul 15]. Available from: https://wwf.ca/stories/scrubbers-creates-new-pollution/
277. Turner DR, Edman M, Gallego-Urrea JA, Claremar B, Hassellöv IM, Omstedt A, et al. The potential future contribution of shipping to acidification of the Baltic Sea. Ambio. 2018 Apr 1;47(3):368–78.
278. Emission project guide MAN B&W Two-stroke marine engines. 2022 [cited 2023 Jul 6]; Available from: www.marine.man-es.com
279. Farkas A, Degiuli N, Martić I, Grlj CG. Is slow steaming a viable option to meet the novel energy efficiency requirements for containerships? J Clean Prod. 2022 Nov 10;374:133915.
280. Big Ship Slow Steaming: How Prevalent Is It? [Internet]. [cited 2023 Jun 29]. Available from: https://www.marinelink.com/news/prevalent-steaming-slow346554
281. Glujić D, Kralj P, Dujmović J. Considerations on the Effect of Slow-Steaming to Reduce Carbon Dioxide Emissions from Ships. Journal of Marine Science and Engineering 2022, Vol 10, Page 1277 [Internet]. 2022 Sep 9 [cited 2023 Jun 29];10(9):1277. Available from: https://www.mdpi.com/2077-1312/10/9/1277/htm
282. Kim SW, Brorsen BW. Forecasting urea prices. http://dx.doi.org/101080/0003684620171296554 [Internet]. 2017 Oct 21 [cited 2023 Jun 29];49(49):4970–81. Available from: https://www.tandfonline.com/doi/abs/10.1080/00036846.2017.1296554
283. World Bunker Prices - Ship & Bunker [Internet]. [cited 2023 Jun 29]. Available from: https://shipandbunker.com/prices
284. Urea - Monthly Price - Commodity Prices - Price Charts, Data, and News - IndexMundi [Internet]. [cited 2023 Jun 30]. Available from: https://www.indexmundi.com/commodities/?commodity=urea&months=180
285. Azzara A, Rutherford D, Wang H. Feasibility of IMO Annex VI Tier III implementation using Selective Catalytic Reduction. 2014;
286. Zhang G, Yan H, Li T, Zhu Y, Zhou S, Feng Y, et al. Relation analysis on emission control and economic cost of SCR system for marine diesels. 2021 [cited 2023 Jun 29]; Available from: https://doi.org/10.1016/j.scitotenv.2021.147856
287. Marine Environment Protection Committee (MEPC), 66th session, 31 March to 4 April 2014 [Internet]. [cited 2023 Jun 30]. Available from: https://www.imo.org/en/MediaCentre/MeetingSummaries/Pages/MEPC66.aspx
288. Zhao Y, Fan Y, Fagerholt K, Zhou J. Reducing sulfur and nitrogen emissions in shipping economically. Transp Res D Transp Environ [Internet]. 2021 Jan 1 [cited 2023 Jun 29];90:102641. Available from: https://linkinghub.elsevier.com/retrieve/pii/S1361920920308269
289. DNV GL NOx TIER III Update - DNV [Internet]. [cited 2023 Jun 30]. Available from: https://www.dnv.com/maritime/publications/NOx-TIER-3-Update-download.html

ΕΘΝΙΚΟ ΜΕΤΣΟΒΙΟ ΠΟΛΥΤΕΧΝΕΙΟ

Σχολή Μηχανολόγων Μηχανικών
Εργαστήριο Ετερογενών Μιγμάτων και Συστημάτων Καύσης

Διδακτορική Διατριβή
(Εκτεταμένη Περίληψη)

Διερεύνηση νέων τεχνικών μείωσης εκπομπών για τον περιορισμό των περιβαλλοντικών επιπτώσεων κινητήρων πλοίων χρήσης υγρών ή αερίων καυσίμων

Θεοφάνης Χουντάλας
Εθνικό Μετσόβιο Πολυτεχνείο

Επιβλέπων Καθηγητής: Μαρία Φούντη

Αθήνα, Ιούλιος 2023

Ευχαριστίες

Καταρχάς, θα ήθελα να ευχαριστήσω την επιβλέπουσα της διδακτορικής μου διατριβής Καθ. Μαρία Φούντη για την αμέριστη υποστήριξή της σε αυτό το εγχείρημα. Η βαθιά γνώση της, η υποστήριξή της, η καθοδήγηση και η θετική της στάση ήταν καθοριστικής σημασίας για την έρευνα και την ολοκλήρωσή της. Θα ήθελα επίσης να εκφράσω τις ευχαριστίες μου προς τα άλλα μέλη της επιτροπής τον Καθ. Ευάγγελο Γιακουμή και τον Καθ. Λάμπρο Καϊκτσή για τα εύστοχα σχόλια και παρατηρήσεις τους.

Στην συνέχεια, θα ήθελα να εκφράσω την αμέριστη ευγνωμοσύνη μου στην οικογένειά μου και κυρίως στον πατέρα μου. Η βαθιά του γνώση, η διαρκής υποστήριξη και η θέση του στον χώρο της ελληνικής ναυτιλίας ήταν μια ουσιαστική συμβολή στην έρευνα που έγινε η οποία δεν θα ήταν δυνατή, τουλάχιστον σε αυτή τη μορφή, διαφορετικά. Ευχαριστώ ιδιαίτερα τους φίλους και τη σύντροφό μου για την υποστήριξή τους και την υπομονή τους στις δυσκολίες που αντιμετώπισα στα χρόνια της διεξαγωγής αυτής της έρευνας.

Τέλος, θα ήθελα να εκφράσω τις ευχαριστίες μου προς τα τεχνικά τμήματα των ναυτιλιακών εταιρειών που παρείχαν αυτήν την πολύτιμη ευκαιρία για διεξαγωγή πειραμάτων στα πλοία τους. Θα ήθελα να ευχαριστήσω ιδιαίτερα τα πληρώματα των σκαφών και τους επόπτες μηχανικούς που παρευρέθηκαν στις διάφορες δοκιμές, με καλωσόρισαν στο πλοίο και ήταν διαθέσιμοι για βοήθεια ακόμα και αρκετά μετά το τέλος της βάρδιας τους. Η βοήθειά τους στις διαδικασίες μέτρησης ήταν καθοριστική για την ολοκλήρωση των πολυάριθμων δοκιμών που κατέληξαν στην παρούσα διατριβή.

Περιεχόμενα

1. Εισαγωγή

1.1 Αντικείμενο και Σκοπός

Η προστασία του περιβάλλοντος και βελτίωση της ποιότητας του ατμοσφαιρικού αέρα είναι από τις σημαντικότερες τεχνολογικές προκλήσεις για το άμεσο μέλλον και αναμένεται να οδηγήσει σε ραγδαίες αλλαγές σε όλους τους τομείς ανθρώπινης δραστηριότητας με εξάρτηση στα ορυκτά καύσιμα και τις μηχανές εσωτερικής καύσης. Εκτιμάται πως η ναυτιλιακή δραστηριότητα ευθύνεται για το 15% των ανθρωπογενών εκπομπών NO_x παγκοσμίως και 16.5% της έκθεσης του πληθυσμού της Ευρωπαϊκής Ένωσης σε αυτό τον ρύπο (1,2), ενώ παράλληλα καταγράφονται σταθερά αυξητικές τάσεις (2). Ο έλεγχος των εκπομπών NO_x είναι μεγάλης σημασίας λόγω των σοβαρών αρνητικών επιπτώσεών του στην ανθρώπινη υγεία και το περιβάλλον, (3). Οι εκπομπές CO_2 από ναυτικά σκάφη αποτελούν το 3.3% των συνολικών εκπομπών παγκοσμίως και προβλέπεται σημαντική αύξησή τους στο άμεσο μέλλον εκτός και αν ληφθούν αυστηρά μέτρα (4,5). Ο περιορισμός απελευθέρωσης αερίων του θερμοκηπίου στο περιβάλλον, όπως το CO_2 είναι εξαιρετικής σημασίας και άμεσες δράσεις είναι αναγκαίες προκειμένου η άνοδος της μέσης παγκόσμιας θερμοκρασίας να μην ξεπεράσει τον 1.5^oC σε σχέση με τα επίπεδα προ της βιομηχανικής επανάστασης (6).

Πέραν των προηγούμενων, η ναυτική βιομηχανία έχει πολύ μεγάλη συμβολή στις εκπομπές SO_2 λόγω της χρήσης καυσίμων υψηλής περιεκτικότητας σε θείο.

Η χρήση μηχανών εσωτερικής καύσης είναι η βασική λύση αυτή τη στιγμή για πρόωση και ηλεκτροπαραγωγή στη ναυτική βιομηχανία και προβλέπεται να παραμείνει για τις επόμενες δεκαετίες, (7). Οι βασικοί λόγοι για την εξάρτηση της βιομηχανίας από αυτή την τεχνολογία είναι οι ιδιαίτερες απαιτήσεις των μεγάλων ποντοπόρων πλοίων σε συγκέντρωση ισχύος και τη δυνατότητα συνεχούς λειτουργίας για μεγάλες χρονικές περιόδους, κάτι που καθιστά άλλες επιλογές όπως η ηλεκτροκίνηση εξαιρετικά (8,9). Ο τύπος κινητήρα με την πλέον διαδεδομένη χρήση είναι ο μεγάλος αργόστροφος δίχρονος ντίζελ για πρόωση, και για την ηλεκτροπαραγωγή εντός πλοίων χρησιμοποιούνται κοινώς τετράχρονες ταχύστροφες γεννήτριες ντίζελ.

Αυτή τη στιγμή στο χώρο της ναυτιλίας οι ελεγχόμενοι ρύποι είναι CO_2, NO_2 και SO_2. Τα επιμέρους μέτρα είναι θεσπισμένα και ελέγχονται από τον Παγκόσμιο Οργανισμό Ναυτιλίας (IMO). Τα εν ισχύ μέτρα για τις εκπομπές NO_x τέθηκαν σε εφαρμογή το 2016 με τη θέσπιση ιδιαίτερα χαμηλών ορίων (Tier-III) σε ειδικά καθορισμένες περιοχές (ECA) ελέγχου ρύπων, (10). Για το SO_2 η πιο πρόσφατη μεταρρύθμιση έλαβε χώρα το 2020 επίσης με πολύ μεγάλη μείωση παγκοσμίως και ειδικά εντός ECA, (11). Μέτρα για το CO_2 καθιερώθηκαν μόλις το 2023, και ο σημερινός στόχος του IMO είναι με τα μέτρα αυτά και περαιτέρω μελλοντικές αλλαγές να επιτευχθεί μείωση στις εκπομπές αερίων θερμοκηπίου από το χώρο της ναυτιλίας κατά 40% έως το 2040, (4).

Λόγω των παραπάνω αλλαγών και των φιλόδοξων στόχων του IMO μεγάλες αλλαγές λαμβάνουν χώρα στη βιομηχανία. Οι τεχνικές λύσεις που θα υιοθετηθούν για την επίτευξη των παραπάνω στόχων δεν έχουν ακόμη διευκρινιστεί από τους διάφορους ρυθμιστικούς φορείς του χώρου, (12,13). Οι πλοιοκτήτες επίσης ερευνούν τις επιλογές τους προς διαμόρφωση ευέλικτων στόλων που θα έχουν λογικά κόστη λειτουργίας και παράλληλα θα μπορούν επαρκώς να καλύψουν τους σημερινούς και άμεσου μέλλοντος περιβαλλοντικούς κανονισμούς.

Σε αυτή τη διδακτορική διατριβή ερευνώνται σύγχρονες τεχνικές λύσεις για τη μείωση των εκπομπών CO_2 και NO_x. Οι τεχνολογίες αυτές είναι νέες στο χώρο, μερικές ακόμη εν μέρει στο στάδιο ελέγχου και αξιολόγησης, όμως με πραγματική εφαρμογή σε ναυτικά σκάφη σε κανονικές συνθήκες λειτουργίας. Η ανάλυση που ακολουθεί βασίζεται πρωτίστως σε μετρήσεις που έγιναν σε ναυτικούς κινητήρες εν πλω ή κατά τη διάρκεια εργοστασιακών δοκιμών. Σε περιπτώσεις που κατέστη αναγκαίο δεδομένα ελήφθησαν επίσης μέσω τηλεμετρίας. Η ανάλυση των πειραματικών δεδομένων συνοδεύτηκε με επιπλέον εις βάθος ανάλυση σε ορισμένες περιπτώσεις με τη χρήση ενός πολυζωνικού μοντέλου καύσης. Ο στόχος της διδακτορικής διατριβής είναι να παρέχει μια ολοκληρωμένη αξιολόγηση των σημαντικότερων τεχνολογιών μείωσης ρύπων που εισήχθησαν πρόσφατα στη ναυτιλιακή βιομηχανία, εστιάζοντας στην επίδρασή τους στην απόδοση του κινητήρα βασιζόμενη σε δεδομένα από μετρήσεις που πραγματοποιήθηκαν σε πραγματική κλίμακα. Δεδομένα αυτού του τύπου είναι περιορισμένα στη βιβλιογραφία λόγω του πολύ μεγάλου μεγέθους (και κατανάλωσης

καυσίμου) αυτών των μηχανών που εμποδίζουν την εκτέλεση πειραμάτων σε περιβάλλον εργαστηρίου, και των γενικών δυσκολιών προγραμματισμού δοκιμών εν πλω ή παράλληλα με εργοστασιακές δοκιμές. Για τις ανάγκες της παρούσας εκτεταμένης έρευνας σχεδιάστηκε μια απλουστευμένη διαδικασία για την απόκτηση λειτουργικών δεδομένων απόδοσης και εκπομπών με στόχο γρήγορες, αποτελεσματικές και κυρίως ακριβείς μετρήσεις που επιτρέπουν τη γρήγορη επαλήθευση της ποιότητας των δεδομένων που αποκτήθηκαν. Αυτό επέτρεψε την ανάλυση μεγάλου αριθμού κινητήρων, 19 συνολικά. Τα δεδομένα των μετρήσεων αναλυθήκαν για την αξιολόγηση της επίδρασης των εξεταζόμενων τεχνολογιών στη συνολική λειτουργία, την απόδοση και τις εκπομπές ρύπων. Σε ορισμένες περιπτώσεις, όπως τα βιοκαύσιμα, αυτά δεν είχαν καλυφθεί προηγουμένως στην υπάρχουσα βιβλιογραφία και τα περιεχόμενα αυτής της διατριβής παρέχουν την πρώτη ολοκληρωμένη επισκόπηση του θέματος. Μια ακόμη συμβολή της διατριβής είναι ότι δοκιμάστηκαν κινητήρες ειδικά σχεδιασμένοι για τη χρήση των τεχνολογιών που ερευνήθηκαν, ενώ οι περισσότερες προηγούμενες μελέτες εξέτασαν αλλαγές σε υπάρχοντα σχέδια κινητήρων και τεχνικές ρύθμισής τους με την ανάλυση να είναι επί το πλείστον θεωρητική. Οι κινητήρες που δοκιμάστηκαν και συμπεριλήφθηκαν στη διατριβή ήταν νέοι ή μόλις εισήχθησαν στην αγορά τη στιγμή που ξεκίνησε η ερευνητική διαδικασία. Η εκτεταμένη διαδικασία μέτρησης επέτρεψε η αξιολόγηση που διενεργήθηκε να βασίζεται σε πραγματικά δεδομένα και όχι σε εκτιμήσεις τρίτων. Όπως αναφέρθηκε, πραγματοποιήθηκε περαιτέρω λεπτομερής ανάλυση με τη χρήση πολυζωνικού μοντέλου καύσης. Το μοντέλο βασίστηκε σε προϋπάρχον κώδικα και τροποποιήθηκε κατάλληλα για τις ανάγκες της διατριβής. Συνολικά, παρασχέθηκε μια ουσιαστική συμβολή στο θέμα, συμπεριλαμβανομένων τόσο ποιοτικών όσο και ποσοτικών ευρημάτων, τα οποία μπορούν επίσης να χρησιμοποιηθούν ως κατευθυντήρια γραμμή για μελλοντικές αναλύσεις.

1.2 Εξεταζόμενες Τεχνολογίες Μείωσης Ρύπων

Οι τεχνολογίες που εξετάζονται στη διατριβή για τον περιορισμό εκπομπών CO_2 είναι η χρήση ναυτικού τύπου βιοκαυσίμων και υγροποιημένου φυσικού αερίου (LNG), το δεύτερο σε κινητήρες διπλού καυσίμου με ψεκασμό του αερίου σε υψηλή πίεση. Για τον έλεγχο εκπομπών NO_x οι εξεταζόμενες λύσεις είναι η ανακυκλοφορία καυσαερίου (EGR) και η εκλεκτική καταλυτική αναγωγή (SCR). Για κάθε τεχνολογία μελετάται η επίδραση στη λειτουργία του κινητήρα και το μηχανισμό της καύσης. Επίσης γίνεται λεπτομερής ανάλυση των απαιτούμενων αλλαγών στη ρύθμιση του κινητήρα. Έμφαση δίνεται στο μηχανισμό της καύσης που εκτιμάται με την ανάλυση των πειραματικών δεδομένων. Εκτενής αξιολόγηση πραγματοποιείται επίσης στην επίδραση των εκπομπών ρύπων.

Για τη μείωση των εκπομπών άνθρακα οι τεχνολογίες προς μελέτη επιλέχθηκαν με κριτήριο να είναι η πραγματική εφαρμογή τους στο χώρο. Τα βιοκαύσιμα έχουν ενδιαφέρον για χρήση ως καύσιμο έτοιμο προς χρήση που δεν απαιτεί τροποποιήσεις. Η χρήση LNG εξετάζεται κυρίως για νέα πλοία που θα ενταχθούν στον παγκόσμιο στόλο. Και τα δύο καύσιμα αναμένεται να έχουν θετική επίδραση στις τελικές εκπομπές άνθρακα, τα μεν βιοκαύσιμα λόγω οφελών που προέρχονται από το συνολικό κύκλο ζωής τους, (14–17) και το LNG λόγω της χαμηλής του περιεκτικότητας σε άνθρακα και ταυτόχρονα υψηλό ενεργειακό περιεχόμενο.

Διάφορες άλλες τεχνολογίες εξετάζονται για τη μείωση των εκπομπών CO_2 από ναυτικούς κινητήρες, με τις περισσότερες είτε να βρίσκονται ακόμα στο στάδιο της ανάπτυξης, είτε αντιμετωπίζουν σημαντικά προβλήματα παραγωγής και διάθεσης στην αγορά (8,12,18,19). Οι παραγγελίες σκαφών εξοπλισμένων με κινητήρες ικανούς να λειτουργούν με LNG αυξάνεται και έχει φτάσει σε σημαντικά επίπεδα, (20). Με μεγάλο αριθμό ενεργών παραγγελιών για πλοία εξοπλισμένα με κινητήρες έτοιμους για LNG, οι φορείς της βιομηχανίας αναμένουν ότι η χρήση του καυσίμου αυτού θα είναι η κύρια λύση στις μεσοπρόθεσμες προσπάθειες για απανθρακοποίηση.

Η ναυτική βιομηχανία ξεκίνησε πρόσφατα δοκιμές χρήσης βιοκαυσίμων. Τα καύσιμα που δοκιμάστηκαν ήταν μείξη 30% βιοντίζελ 2ης γενιάς και βαρέως πετρελαίου χαμηλού θείου (VLSFO). Οι δοκιμές διενεργήθηκαν από κατασκευαστές κινητήρων και πλοιοκτήτες σε συνεργασία με νηογνώμονες, (21,22). Μετά τα αρχικά αποτελέσματα δοκιμών, οι κανονισμοί ανανεώθηκαν στα μέσα του 2022 για να επιτραπεί τη λειτουργία με χρήση μειγμάτων καυσίμων που περιέχουν έως και 30% βιοντίζελ, (B30).

Οι κύριες μεθοδολογίες που εφαρμόζουν οι κατασκευαστές ναυτικών κινητήρων για τον περιορισμό των εκπομπών NO_x στα νεότερα πρότυπα Tier-III, είναι η επιλεκτική καταλυτική μείωση (SCR), ανακυκλοφορία καυσαερίων (EGR) και κινητήρες κύκλου Otto που λειτουργούν με αέριο καύσιμο που ψεκάζεται εντός κυλίνδρου με χαμηλή πίεση, (23). Οι τεχνολογίες είναι νέες στο ναυτικό χώρο και δεν έχουν καλυφθεί εκτενώς από τη βιβλιογραφία. Στη διατριβή αυτή οι εξεταζόμενες λύσεις είναι τα EGR και SCR. Το SCR αποτελεί την πλέον διαδεδομένη λύση αυτή τη στιγμή στο χώρο, και το EGR να είναι νεότερη προσθήκη για την οποία υπάρχει ακόμα χαμηλή επιχειρησιακή εμπειρία, (24).

1.3 Πειραματική διαδικασία και ανάλυση δεδομένων

Για τις δοκιμές με LNG μετρήσεις έγιναν παράλληλα με εργοστασιακές δοκιμές για δύο δίχρονους μεγάλους κινητήρες έγχυσης αερίου σε υψηλή πίεση, ιδίου τύπου και διαδοχικής γενιάς, με τον νεότερο να έχει μόλις εισαχθεί στο εμπόριο. Οι δοκιμές έγιναν σε λειτουργία μόνο με πετρέλαιο και σε λειτουργία με δύο καύσιμα, πετρέλαιο και φυσικό αέριο. Οι δοκιμές με βιοκαύσιμο πραγματοποιήθηκαν εν πλω και μετρήσεις πάρθηκαν από 5 δίχρονους και 7 τετράχρονους κινητήρες χρησιμοποιώντας βιοκαύσιμο B30 (30% βιοντήζελ και 70% VLSFO). Μετρήσεις έγιναν παράλληλα με συμβατικά ναυτικά καύσιμα. Οι μετρήσεις για την ανάλυση του EGR έγιναν σε δύο δίχρονους μεγάλους κινητήρες, έναν πετρελαίου και τον διπλού καυσίμου προηγούμενης γενιάς που αναφέρθηκε παραπάνω. Οι μετρήσεις έλαβαν χώρα κατά τις εργοστασιακές δοκιμές. Για τον κινητήρα πετρελαίου δεδομένα επίσης ελήφθησαν κατά τη διάρκεια δοκίμων εν πλω. Τέλος για τη μελέτη του SCR μετρήσεις έγιναν σε τέσσερις κινητήρες, έναν για σύστημα SCR χαμηλής πίεσης (LP) με τον καταλύτη μετά το στρόβιλο και σε τρεις για σύστημα υψηλής πίεσης (HP) με τον καταλύτη τοποθετημένο πριν το στρόβιλο. Οι μετρήσεις έγιναν κατά τις εργοστασιακές δοκιμές για το LP-SCR και HP-SCR, ενώ για τα HP-SCR συστήματα επαναλήφθηκαν εν πλω.

Το βασικότερο στοιχείο μέτρησης για την ανάλυση ήταν δυναμοδεικτικά διαγράμματα πίεσης των κυλίνδρων. Αυτά χρησιμοποιήθηκαν για να εκτιμηθούν βασικά στοιχεία λειτουργίας των κινητήρων και να εκτιμηθούν οι ρυθμίσεις τους. Τα δυναμοδεικτικά χρησιμοποιήθηκαν επίσης για ανάλυση ρυθμού καύσης (HRR). Με τα αποτελέσματα της ανάλυσης αξιολογήθηκε η επίδραση των τεχνολογιών στο μηχανισμό της καύσης και παράλληλα έγινε εκτίμηση της κατανάλωσης καυσίμου στις περιπτώσεις που απευθείας μέτρηση ακριβείας δεν ήταν εφικτή. Οι μετρήσεις σύστασης καυσαερίου λήφθηκαν με χρήση ειδικού εξοπλισμού και χρησιμοποιήθηκαν για την αξιολόγηση των εκπομπών και την επαλήθευση της συμμόρφωσης με τους κανονισμούς και αξιολόγηση του επίπεδο του αναμενόμενου οφέλους από τη χρήση κάθε τεχνολογίας.

2. Έλεγχος Εκπομπών CO_2 στη Ναυτιλία

2.1 Νομοθεσία

Επίσημη εφαρμογή μέτρων για τον περιορισμό εκπομπών άνθρακα από ναυτικές μηχανές ξεκίνησε μόλις τον Ιανουάριο του 2023, (4). Τα δύο πρώτα μέτρα είναι οι δείκτες απόδοσης λειτουργίας EEXI και CII. Ο δείκτης EEXI υπολογίζεται μία φορά στη ζωή του πλοίου εκτός και αν πραγματοποιηθούν σημαντικές παρεμβάσεις (4,25–28). Για κάθε τύπο πλοίου μια ελάχιστη τιμή αποδοτικότητας πρέπει να επιτευχθεί. Στην αντίθετη περίπτωση μέτρα όπως περιορισμός μέγιστης ισχύος μηχανών (EPL) και ταχύτητας πλεύσης πρέπει να εφαρμοστούν. Άλλες μέθοδοι για τη βελτίωση του δείκτη είναι μέθοδοι βελτιστοποίησης πρόωσης σκαφών, και μετατροπές στον κινητήρα που επιτρέπουν χρήση εναλλακτικών καυσίμων.
Ο δείκτης CII θα υπολογίζεται σε ετήσια βάση με αρχή συλλογής στοιχείων λειτουργίας για κάθε πλοίο το 2023 (29–31). Η χρήση του CII ισχύει για εμπορικά πλοία 5000 GT και άνω, ανεξάρτητα από τον τύπο πρόωσης. Ο δείκτης έχει πέντε κατηγορίες από A έως E. Για σκάφη που επιτυγχάνουν χαμηλές βαθμολογίες συστηματικά, θα πρέπει να γίνουν διορθωτικές παρεμβάσεις. Η βάση του υπολογισμού CII είναι οι εκπομπές CO_2 ανά μεταφορική ικανότητα φορτίου και ναυτικό μίλι. Μελέτες έχουν επαληθεύσει ότι η εφαρμογή περιορισμών ταχύτητας στα πλοία μπορεί να μειώσει σημαντικά τις εκπομπές, (32) και αυτή μαζί με τον περιορισμό ισχύος θα είναι η βασική λύση για βελτίωση του CII. Εναλλακτικά η χρήση βιοκαυσίμων ή άλλων καυσίμων χαμηλών εκπομπών άνθρακα μπορεί να προσφέρει σημαντική βελτίωση της αξιολόγησης. Τα πλοία που λειτουργούν με φυσικό αέριο που έχει χαμηλή περιεκτικότητα σε άνθρακα μπορούν εύκολα να επιτύχουν καλή αξιολόγηση.

2.2 Κινητήρες διπλού καυσίμου για χρήση LNG

Οι σύγχρονοι δίχρονοι ναυτικοί κινητήρες που χρησιμοποιούν φυσικό αέριο βασίζονται σε δύο διαφορετικές αρχές λειτουργίας. Ανεξάρτητα από τον τύπο, οι κινητήρες λειτουργούν σε βάση διπλού καυσίμου, συνήθως με φυσικό αέριο να εγχύεται πρώτα στον κύλινδρο και ένα άλλο εύκολα αναφλέξιμο καύσιμο, ναυτικό ντίζελ (MGO) ή βαρύ πετρέλαιο (HFO), να εγχύεται για την έναρξη της καύσης μέσω αυτανάφλεξής του. Η κύρια διαφορά μεταξύ των δύο αρχών λειτουργίας είναι η μέθοδος έγχυσης φυσικού αερίου. Οι μηχανές έγχυσης αερίου σε υψηλή πίεση ακολουθούν τον κύκλο Diesel, ενώ οι μηχανές με έγχυση αερίου σε χαμηλή πίεση νωρίς στη φάση συμπίεσης ομοιάζουν περισσότερο με τον κύκλο Otto.
Οι κινητήρες έγχυσης αερίου υψηλής πίεσης λειτουργούν στον κύκλο Diesel με το φυσικό αέριο να εγχύεται κοντά στο άνω νεκρό σημείο (TDC) επί το πλείστον ελαφρώς νωρίτερα από το πιλοτικό καύσιμο ντίζελ, (33). Η εκκίνηση της καύσης επιτυγχάνεται με την αυτανάφλεξη της πιλοτικής έγχυσης ντίζελ. Η έγχυση τόσο αερίου όσο και υγρού καυσίμου κοντά στο άνω νεκρό σημείο (TDC), λίγο πριν την ανάφλεξη, σημαίνει ότι επικρατεί κυρίως καύση διάχυσης. Το κύριο πλεονέκτημα της προσέγγισης είναι ότι το εργαζόμενο μέσο του κυλίνδρου είναι αέρας, επομένως δεν υπάρχει κίνδυνος προανάφλεξης, επιτρέποντας υψηλότερο λόγο συμπίεσης, και αυξάνοντας την απόδοση και παράλληλα περιορίζονται σε μεγάλο βαθμό οι διαφυγές μεθανίου στην ατμόσφαιρα το οποίο είναι σημαντικό πρόβλημα στις μηχανές έγχυσης αερίου με χαμηλή πίεση. Επιπλέον, η βελτιωμένη καύση αυξάνει την απόδοση και μειώνει την κατανάλωση καυσίμου. Το μειονέκτημα είναι η σημαντική αύξηση των εκπομπών NO_x, επομένως αυτοί οι κινητήρες δεν μπορούν να ικανοποιήσουν το αυστηρότερα πρότυπα Tier-III χωρίς τη χρήση EGR ή συστήματος SCR. Τέλος, η κρυογονική εγκατάσταση που χρησιμοποιείται για την έγχυση NG σε υψηλή πίεση είναι πολύ περίπλοκη και μπορεί να αυξήσει σημαντικά το κόστος, (8).

2.3 Μετρητική διάταξη, χαρακτηριστικά κινητήρων και καυσίμων που μελετήθηκαν

Ένα απλό σχεδιάγραμμα της μετρητικής διάταξης δίνεται στην Εικόνα 2-1 για τους κινητήρες που μελετήθηκαν. Η σχηματική αυτή διάταξη με την εξαίρεση του σημείου μέτρησης καταναλώσεων (για μετρήσεις εν πλω χρησιμοποιείται ροόμετρο) ισχύει και για τις υπόλοιπες εφαρμογές. Τα βασικά χαρακτηριστικά των κινητήρων δίνονται στον Πίνακας 2-1.

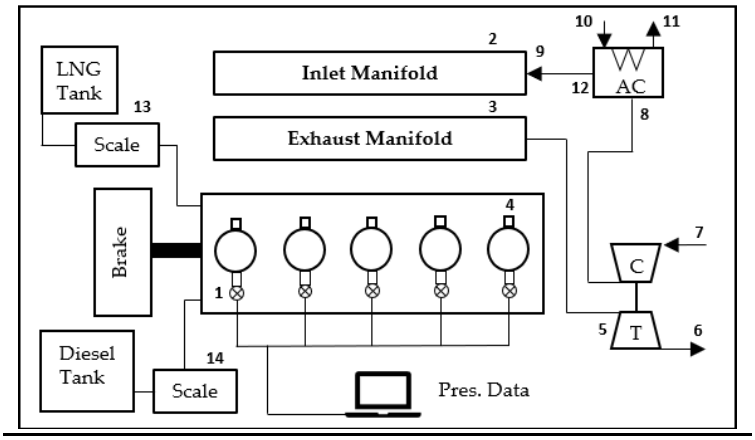

1. Δυναμοδεικτικά διαγράμματα	8. Θερμ. αέρα πριν το ψυγείο
2. Πίεση σάρωσης	9. Θερμ. αέρα μετά το ψυγείο
3. Πίεση εξαγωγής	10. Θερμ. εισ. νερού ψύξης
4. Θερμ. καυσαερίων κυλίνδρου	11. Θερμ. εξ. νερού ψύξης
5. Θερμ. εισ. στροβίλου	12. Πτώση πίεσης στο ψυγείο
6. Θερμ. εξ. στροβίλου	13. Παροχή ΦΑ
7. Θερμ. εισ. συμπιεστή	14. Παροχή ντίζελ

Εικόνα 2-1 Σχηματικό διάγραμμα διάταξης μέτρησης

Πίνακας 2-1 Χαρακτηριστικά κινητήρων 1 και 2

Κινητήρας 1	**Τιμή**	**Κινητήρας 2**	**Τιμή**
Μοντέλο	5G70ME-C9.5GI	Μοντέλο	6G70ME-C10.5GI
Τυπός	Δίχρονος	Τυπός	Δίχρονος
Αρ. Κυλίνδρων	5	Αρ. Κυλίνδρων	6
Διάμετρος	700	Διάμετρος	700
Διαδρομή	3256	Διαδρομή	3256
Ονομαστική Ταχύτητα	68.1	Ονομαστική Ταχύτητα	71.0
Ονομαστική Ισχύς	11,975	Ονομαστική Ισχύς	15,081

2.4 Βασικά λειτουργικά μεγέθη, λειτουργία με ένα και δύο καύσιμα

Παρουσιάζονται τα πιο σημαντικά ευρήματα σχετικά με τις διαφορές που προκύπτουν κατά τη λειτουργία με φυσικό αέριο (ΦΑ) σε σχέση με τη λειτουργία μόνο με MGO. Για τον κινητήρα "1", προηγούμενης γενιάς, οι διαφορές ήταν μικρές μεταξύ των δύο τρόπων λειτουργίας. Η μέγιστη πίεση καύσης (P_{max}), συμπίεσης (P_{comp}), θερμοκρασία καυσαερίου και αύξηση πίεσης κατά την καύση (ΔP) παρουσιάζουν σχετική ταύτιση μεταξύ λειτουργίας MGO και ΦΑ. Οι σημαντικότερες τιμές (P_{max} και ΔP) δίνονται στην Εικόνα 2-2α,β για τον κινητήρα "1". Για τον κινητήρα "2" τα σχετικά μεγέθη δίνονται στην Εικόνα 2-3α,β. Σημαντικές διαφορές εντοπίζονται σε αυτή την περίπτωση, με σημαντικά υψηλότερες P_{max}, P_{comp}, και ΔP. Τα παραπάνω υποδηλώνουν διαφορετική ρύθμιση του κινητήρα "2", ιδιαίτερα στην πιλοτική έγχυση καυσίμου.

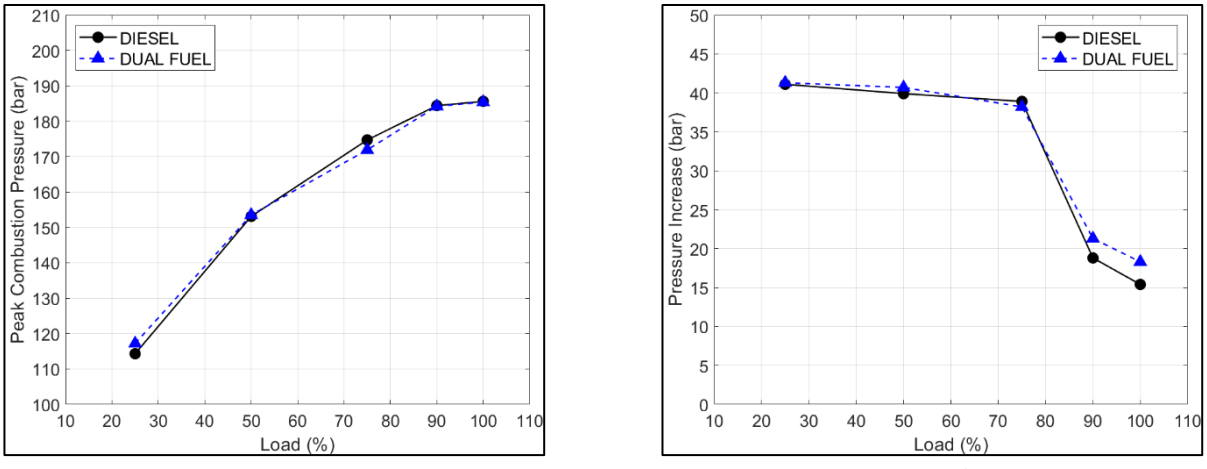

(α) (β)

Εικόνα 2-2 (α) Μέγιστη πίεση καύσης; (β) Άνοδος πίεσης κατά την καύση; λειτουργία με MGO & ΦΑ Κινητήρας 1.

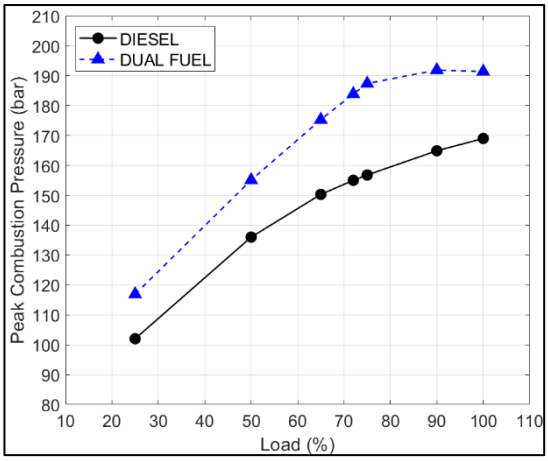

(α)

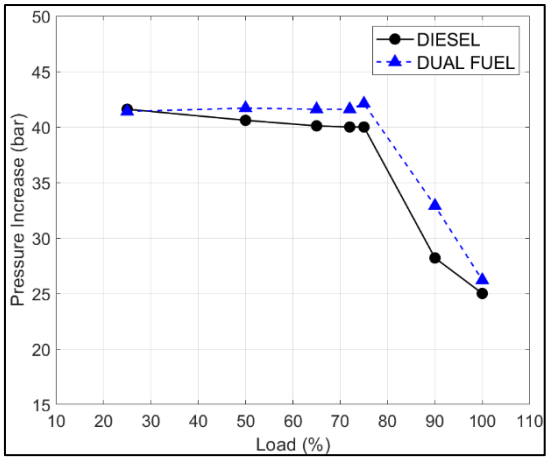

(β)

Εικόνα 2-3 (α) Μέγιστη πίεση καύσης; (β) Άνοδος πίεσης κατά την καύση; λειτουργία με MGO & ΦΑ, Κινητήρας 2.

Το σημαντικότερο μέτρο σύγκρισης απόδοσης των κινητήρων είναι η ειδική κατανάλωση καυσίμου. Επειδή χρησιμοποιούνται δύο διαφορετικά καύσιμα, η συνολική καθαρή απελευθέρωση θερμικής ενέργειας (THR) ανά μονάδα ισχύος μηχανής συγκρίνεται μεταξύ λειτουργίας MGO και ΦΑ, Εικόνα 2-4α. Επίσης στην Εικόνα 2-4b δίνεται η αναλογία μάζας MGO και ΦΑ για λειτουργία δύο καυσίμων. Διακρίνεται παρόμοια αποδοτικότητα της μηχανής κατά την καύση ΦΑ, με μία ελάχιστη μείωση της τάξης του 1% κατά μέσο όρο. Σημαντικό είναι επίσης ότι η αναλογία μάζας πιλοτικής έγχυσης προς ΦΑ είναι σχετικά χαμηλή. Η συνολική κατανάλωση μάζας καυσίμων είναι χαμηλότερη κατά τη λειτουργία ΦΑ. Σε συνδυασμό με το χαμηλό περιεχόμενο του ΦΑ σε άνθρακα η μείωση εκπομπων CO_2 υπολογίστηκε στο 22.6%. Τα παραπάνω μεγέθη δίνονται στην Εικόνα 2-5 για τον κινητήρα "2". Μεγάλη βελτίωση σε σχέση με τον "1" παρατηρείται και στους δύο τρόπους λειτουργίας, ειδικά για λειρουγία ΦΑ. Το ποσοστό απαιτούμενης μάζας πετρελαίου για σταθερή λειτουργία είναι μειωμένο σε όλα τα φορτία. Η THR είναι χαμηλότερη κατά τη λειτουργία δύο καυσίμων δείχνοντας αποδοτικότερη λειτουργία σε σχέση με αυτή μόνο με MGO, η μέση βελτίωση υπολογίστηκε σε 3.5%. Αυτό οδήγησε σε βελτίωση εκπομπών CO_2 σε σχέση με τον προηγούμενης γενιάς κινητήρα κατά σχεδόν 7%. Λόγω όμως των βελτιώσεων και στη λειτουργία με MGO για τον κινητήρα "2", η σχετική διαφορά εκπομπών CO_2 μεταξύ λειτουργίας MGO και ΦΑ παρέμεινε κοντά στο 23%.

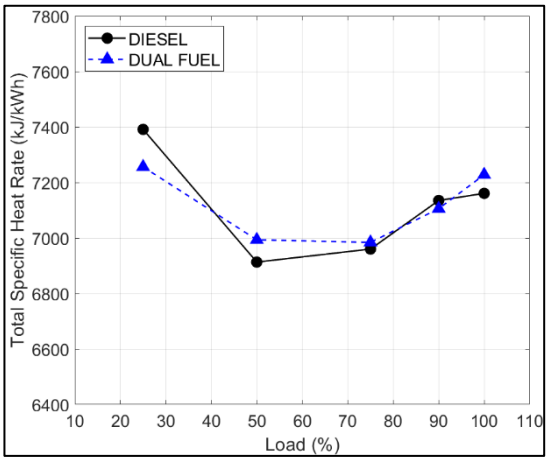

(α)

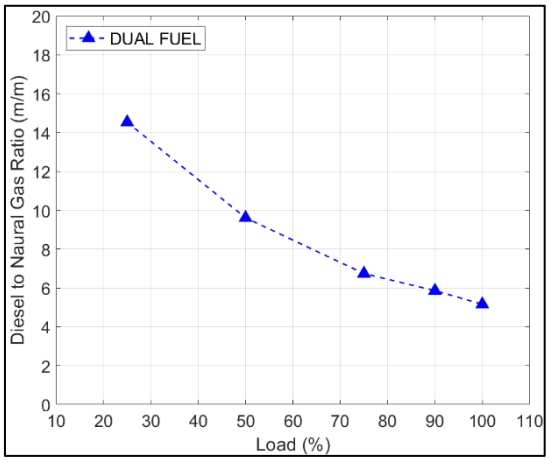

(β)

Εικόνα 2-4 (α) Ειδική παροχή ενέργειας; (β) Λόγος μάζας MGO ΦΑ; λειτουργία με MGO & ΦΑ, Κινητήρας 1.

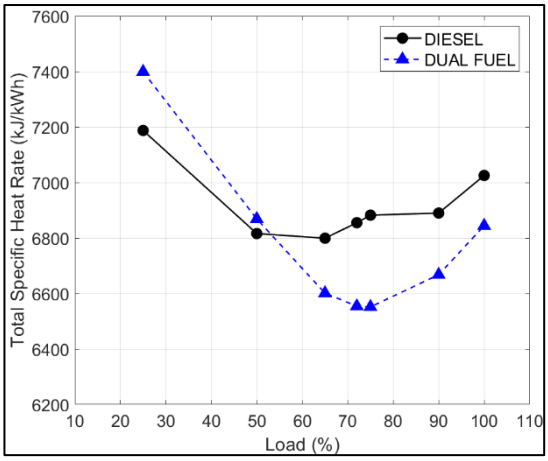

(α)

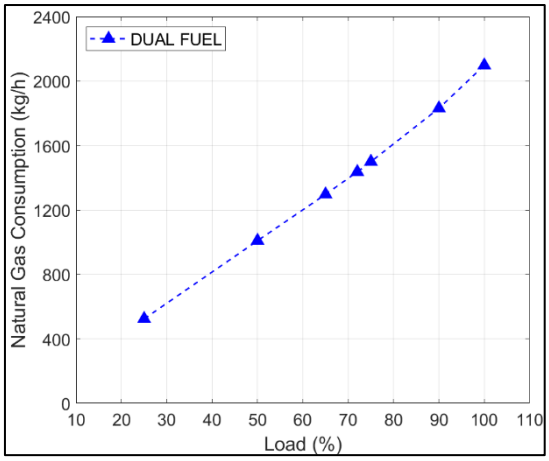

(β)

Εικόνα 2-5 (α) Ειδική παροχή ενέργειας; (β) Λόγος μάζας MGO ΦΑ; λειτουργία με MGO & ΦΑ, Κινητήρας 2.

2.4.1 Συγκριτική αξιολόγηση ρυθμίσεων

Τα μετρημένα δυναμοδεικτικά διαγράμματα χρησιμοποιήθηκαν για την εκτίμηση των ρυθμίσεων κάθε κινητήρα ανά φορτίο λειτουργίας. Οι τιμές που εξετάστηκαν ήταν το άνοιγμα και κλείσιμο της βαλβίδας εξαγωγής (EVO, EVC) και ο χρονισμός έγχυσης (SOI) του υγρού καυσίμου. Για τον κινητήρα "1" ελάχιστες διαφορές εντοπίστηκαν μεταξύ των δύο τρόπων λειτουργίας, ενώ ο κινητήρας "2" είχε σημαντικά διαφορετική ρύθμιση κατά τη λειτουργία ΦΑ. Και στις δύο περιπτώσεις η EVO δεν παρουσίασε σημαντική μεταβολή είτε μεταξύ τρόπου λειτουργίας, είτε μεταξύ των δύο κινητήρων. Για τον κινητήρα "1" δεν υπήρξε μεταβολή για τις τιμές EVC καθώς ο λόγος πίεσης (πίεση συμπίεσης/πίεση σάρωσης) παρέμεινε ο ίδιος. Για τον κινητήρα "2" σημαντική αύξηση του λόγου πιέσεων μετρήθηκε κατά τη λειτουργία ΦΑ, η οποία και επέφερε σημαντική αύξηση του P_{comp}. Η αλλαγή αυτή ήταν αποτέλεσμα αρκετά νωρίτερου EVC. Σύγκριση των αποτελεσμάτων για τους δύο κινητήρες για λειτουργία MGO και ΦΑ δίνεται στην Εικόνα 2-6α,β. Η αντίστοιχη σύγκριση για το χρονισμό έγχυσης δίνεται στην Εικόνα 2-7α,β. Η πιλοτική έγχυση γίνεται με βραδυπορεία στον κινητήρα "1" και σημαντική προπορεία στον κινητήρα "2". Η διαφορά αυτή επέφερε τις μεγάλες διαφορές στο ΔP και επηρέασε τις P_{max} εντός των κυλίνδρων. Επίσης αλλαγή επήλθε στη γωνία ανάφλεξης του αερίου καυσίμου. Η καθυστερημένη ανάφλεξη για τον κινητήρα "1" ευθύνεται σε μεγάλο βαθμό για τις μεγαλύτερες καταναλώσεις σε σχέση με τον "2".

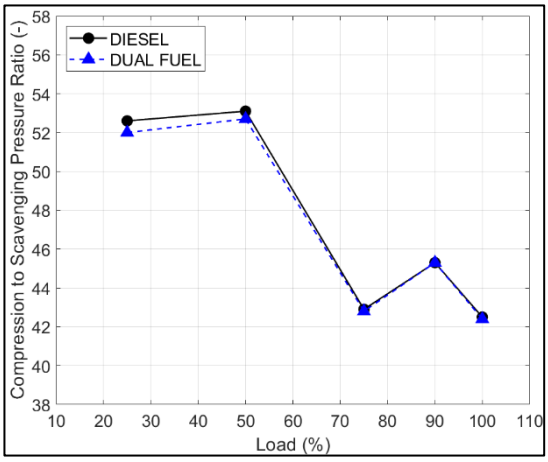

(α)

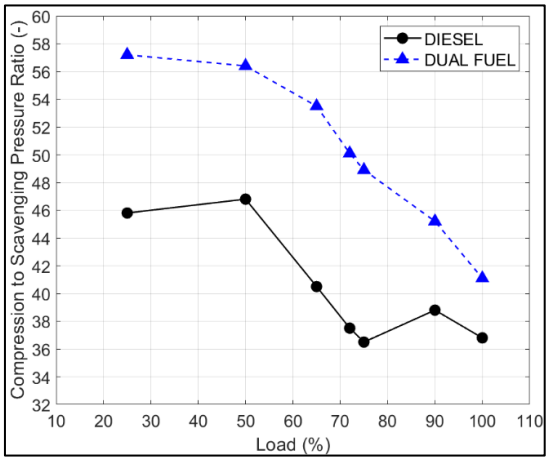

(β)

Εικόνα 2-6 (α) Κλείσιμο βαλβίδας εξαγωγής; (β) Λόγος πιέσεων; λειτουργία με MGO & ΦΑ Κινητήρες 1, 2.

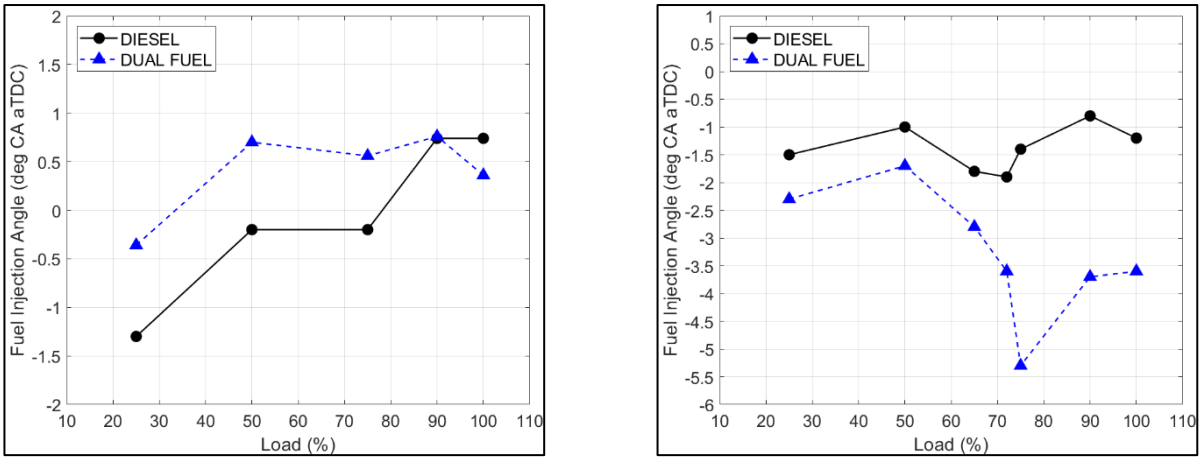

Εικόνα 2-7 Γωνία έγχυσης υγρού καυσίμου; λειτουργία με MGO & ΦΑ; (α) Κινητήρας 1; (β) Κινητήρας 2.

Τα δυναμοδεικτικά διαγράμματα που μετρήθηκαν χρησιμοποιήθηκαν για την εκτίμηση του ρυθμού καύσης με χρήση του 1ου θερμοδυναμικού νόμου. Και για τους δύο κινητήρες σημαντικές διαφορές παρουσιάζονται στη διαδικασία της καύσης λόγω της χρήσης ΦΑ, και της πιλοτικής έγχυσης MGO, Εικόνα 2-8. Και για τους δύο κινητήρες ο αρχικός ρυθμός καύσης μετά την κύρια έναυση (ΦΑ) ήταν υψηλότερος σε σχέση με τη λειτουργία μόνο με MGO όπως και ο μέγιστος ρυθμός καύσης, ειδικά για τον κινητήρα "2". Το αποτέλεσμα αυτό συμφωνεί και με άλλες μελέτες, (34). Τα προηγούμενα εξαρτώνται από τη γωνία ανάφλεξης της πιλοτικής έγχυσης και τη μάζα πετρελαίου, (35). Για τον κινητήρα "1" το ΔΡ δεν επηρεάστηκε σημαντικά, λόγω κυρίως της βραδυπορίας έγχυσης του πιλότου. Η εντονότερη καύση που ακολουθεί αποδίδεται στο διαθέσιμο χρόνο προανάμειξης ΦΑ αέρα και την υψηλότερη θερμογόνο του. Τα χαρακτηριστικά της καύσης επιβεβαιώνουν πως το σύστημα έγχυσης του ΦΑ είναι ικανό για υψηλή παροχή μάζας σε αυτές τις πιέσεις, το οποία έχει σημαντικό βαθμό τεχνικής δυσκολίας (33,36). Στα μεγάλα φορτία βραδύτερος ρυθμός καύσης του ΦΑ εντοπίστηκε στα τελικά στάδια. Οι διαφορές στο HRR σε λειτουργία ΦΑ υπό χαμηλά και μεσαία φορτία, οδηγούν στην υπόθεση ότι η διαδικασία καύσης αποκλίνει περαιτέρω από τον τυπικό μηχανισμό υγρού καυσίμου για καθυστέρηση στη γωνία ανάφλεξης του πιλότου, και υψηλή αναλογία MGO/ΦΑ. Εκτιμάται ότι αυτές οι συνθήκες επηρεάζουν τις διεργασίες καύσης προανάμειξης έναντι της διάχυσης. Ο κινητήρας "2" παρουσιάζει τα προηγούμενα σε εντονότερο βαθμό. Σε αντίθεση με τον "1", για τον κινητήρα "2" τα διαγράμματα HRR δείχνουν σημαντική διακύμανση μεταξύ λειτουργίας MGO και ΦΑ, με την πρόωρη ανάφλεξη του πιλότου να είναι εύκολα αναγνωρίσιμη για όλα τα φορτία, ειδικά στο 75%. Ένα σύντομο ενδιάμεσο στάδιο εντοπίζεται σε όλα τα φορτία με τον ρυθμό καύσης να αυξάνεται ελαφρώς πριν από την κύρια ανάφλεξη του ΦΑ. Η προαναμεμειγμένη καύση εξελίσσεται ταχύτερα και κατά τη λειτουργία ΦΑ για όλα τα φορτία, και το μεγαλύτερο μέρος του καυσίμου καίγεται εντός των πρώτων 10° έως 15° μετά την ανάφλεξη. Η καύση στο τελευταίο στάδιο είναι αρκετά αργή σε σύγκριση με τη λειτουργία MGO. Αυτή η συμπεριφορά αποδίδεται σε διαφορετική στρατηγική πιλοτικής έγχυσης. Ο πιλότος MGO ψεκάζεται πολύ πριν από το TDC σε σχέση με τα σύγχρονα πρότυπα λειτουργίας κινητήρων ενός καυσίμου. Η ανάφλεξη των δύο καυσίμων γίνεται με σαφή χρονική διαφορά, λόγω της σταδιακής πιλοτικής έγχυσης. Για να επιτευχθεί αυτό, το μπεκ ψεκασμού υγρού καυσίμου επανασχεδιάστηκε για τον κινητήρα νέας γενιάς, (37). Επιπλέον, εφαρμόστηκε ένα διαφορετικό προφίλ για την πιλοτική έγχυση. Η διάρκεια καύσης ερευνήθηκε για λειτουργία MGO και ΦΑ. Το αποτέλεσμα ήταν μικρότερη διάρκεια καύσης για τα αρχικά στάδια και ίδια συνολική διάρκεια για τον κινητήρα "1". Η συνολική διάρκεια παρέμεινε ίδια και για τον "2" με λίγο μεγαλύτερη διάρκεια καύσης στα αρχικά στάδια, που αποδίδεται στην αργή καύση της πιλοτικής έγχυσης μέχρι την ανάφλεξη της κύριας μάζας αερίου. Η διάρκεια καύσης είναι σημαντική καθώς επηρεάζει τις θερμικές απώλειες.

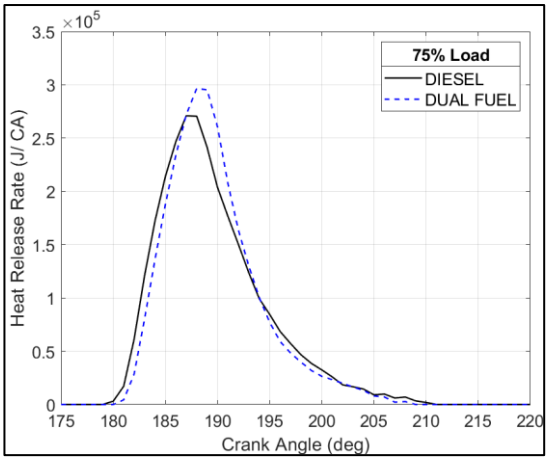

(α)

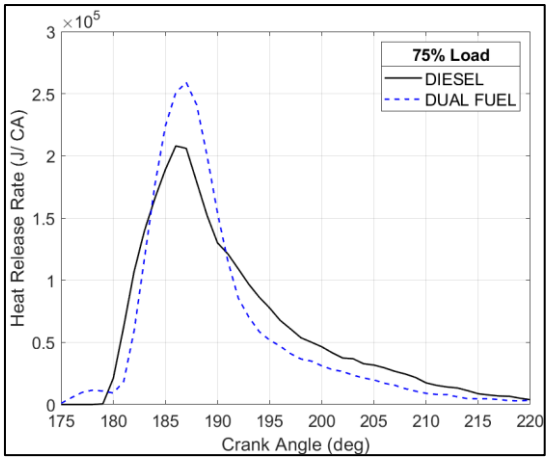

(β)

Εικόνα 2-8 Ρυθμός έκλυσης θερμότητας σε φορτίο 75%, λειτουργία με MGO & ΦΑ; (α) Κινητήρας 1; (β) Κινητήρας 2.

2.4.2 Εκπομπές NO_x σε λειτουργία διπλού καυσίμου

Λόγω της λειτουργίας σε κύκλο Diesel τα επίπεδα εκπομπών NO_x δεν άλλαξαν σημαντικά κατά τη χρήση ΦΑ. Στην Εικόνα 2-9 δίνονται οι τιμές ειδικών εκπομπών για τους κινητήρες για τους δύο τύπους λειτουργίας. Για τον "1" οι εκπομπές είναι μειωμένες σε υψηλό φορτίο και χαμηλότερες για υψηλό για λειτουργία ΦΑ. Στον "2" οι εκπομπές κατά την καύση ΦΑ είναι αυξημένες. Η διαφορά αυτή είναι το αποτέλεσμα της προπορείας πιλοτικής έγχυσης, της διαφοράς αναλογίας μάζας ντίζελ και ΦΑ και των γενικά υψηλών πιέσεων για τον κινητήρα "2". Ιδιαίτερη επιρροή εκτιμάται πως είχε ο έντονος ρυθμός καύσης για τη ΦΑ λειτουργία. Τέλος η καύση μεθανίου επιφέρει μείωση του σχηματισμού NO_x λόγω της μικρής θερμοκρασίας φλόγας.

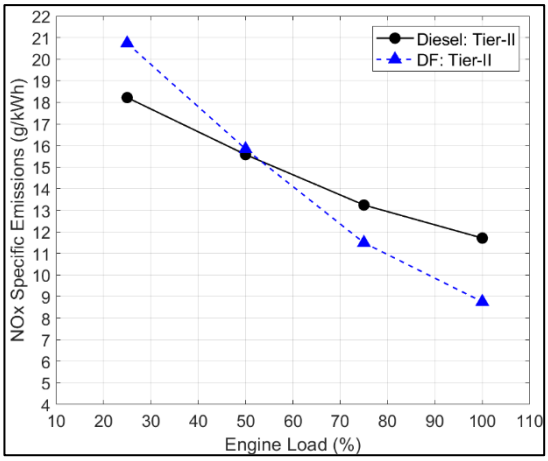

(α)

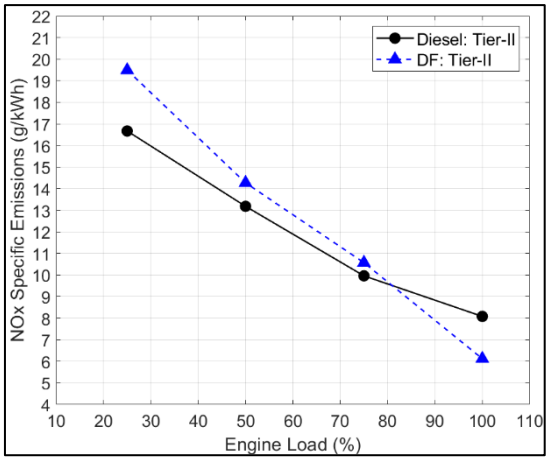

(β)

Εικόνα 2-9 Ειδικές εκπομπές NO_x, λειτουργία με MGO & ΦΑ; α) Κινητήρας 1, β) Κινητήρας 2.

3. Χρήση Βιοκαυσίμων στη Ναυτιλία

Η χρήση βιοκαυσίμων με βάση το βιοντίζελ παρουσιάζει τελευταία αυξημένο ενδιαφέρον στο χώρο της ναυτιλίας. Ο στόχος είναι να χρησιμοποιηθούν μείγματα βιοντίζελ και VLSFO για να βελτιωθεί το αποτύπωμα άνθρακα υφιστάμενων σκαφών χωρίς να πραγματοποιηθούν εκτεταμένες μετατροπές, (38,39). Επί του παρόντος, το βιοντίζελ για ναυτική χρήση είναι 2ης γενιάς, με τις περισσότερες παραλλαγές να βασίζονται σε μεθυλεστέρα λιπαρών οξέων (FAME). Τα βιοκαύσιμα 2ης γενιάς είναι προϊόν μη τροφικής βιομάζας, όπως απόβλητα βρώσιμων φυτών ή μαγειρικό λάδι, (40). Αυτό καθιστά το κόστος των πρώτων υλών χαμηλό, αλλά η διαδικασία παραγωγής είναι δαπανηρή, καθιστώντας το βιοντίζελ 2ης γενιάς ακριβότερο από τα παραδοσιακά καύσιμα. Τα ναυτικά βιοκαύσιμα είναι συνήθως μείγμα 30% βιοντίζελ και VLSFO (B30). Το περιβαλλοντικό όφελος του βιοντίζελ για τις εκπομπές άνθρακα στηρίζεται κυρίως στον συνολικό κύκλο ζωής του (41). Βάση

μελετών (42) και στοιχείων από τους προμηθευτές των καυσίμων που μελετήθηκαν, το όφελος εκτιμάται στο 25% για το B30, κάτι που θα βελτιώσει σημαντικά το δείκτη CII κατά τη χρήση του.
Οι βασικές ανησυχίες για τη χρήση βιοντίζελ είναι οι διαφορετικές φυσικές και χημικές του ιδιότητες σε σχέση με συμβατικά καύσιμα (43,44). Αυτές μπορεί να επηρεάσουν το σύστημα έγχυσης, το μηχανισμό της καύσης και τους παραγόμενους ρύπους, κυρίως NO_x, (45), (46), (47). Η κυριότερη επίδραση στο σχηματισμό τους αναμένεται να προέλθει από την αυξημένη περιεκτικότητα σε O_2 (48,49).

3.1 Λεπτομέρειες Μετρήσεων

Παρατίθενται παρακάτω τα στοιχεία των κινητήρων που μετρήθηκαν, Πίνακας 3-1, Πίνακας 3-2 και οι ιδιότητες των δοκιμασμένων καυσίμων, Πίνακας 3-3.

Πίνακας 3-1 Χαρακτηριστικά δίχρονων κινητήρων που μελετήθηκαν

Τύπος Κινητήρα	**1**	**2**	**3**	**4**	**5**
Αρ. Κυλίνδρων	6	6	6	6	6
Ον. Ταχύτητα (rpm)	75	77	85.5	89	89
Ον. Ισχύς (kW)	15,748	10,215	16,780	9660	9660
Διαδρομή (mm)	700	600	700	600	600
Διάμετρος (mm)	3256	2790	2800	2400	2400
Καύσιμα Δοκιμών	B30, HFO, MGO	B30, VLSFO, MGO	B30, VLSFO	B30, VLSFO	B30

Πίνακας 3-2 Χαρακτηριστικά τετράχρονων κινητήρων που μελετήθηκαν

Τύπος Κινητήρα	**1**	**2**	**3**	**4**	**5**
Αρ. Κυλίνδρων	6	6	6	6	6
Ον. Ταχύτητα (rpm)	900	900	900	900	900
Ον. Ισχύς (kW)	970	970	1710	610	610
Διαδρομή (mm)	220	220	210	185	185
Διάμετρος (mm)	320	320	320	280	280
Καύσιμα Δοκιμών	B30, HFO, MGO	B30, HFO, MGO	B30, VLSFO	B30	B30
Αρ. Μονάδων	1	1, 3	2, 3	1	1

Πίνακας 3-3 Χαρακτηριστικά καυσίμων που χρησιμοποιήθηκαν στις μετρήσεις

Αρ. Πλοίου	**1**			**2**			**3**		**4**		**5**
Τύπος Καυσίμου	B30	HFO	MGO	B30	VLSFO	MGO	B30	VLSFO	B30	VLSFO	B30
LCV (kcal/kg)	9575.23	9548.95	10,172.49	9563.3	9864.3	10,122.3	9608.27	9790.24	9981.37	9904.92	9981.37
Πυκνότητα 15C (kg/m^3)	930	989.7	863.1	930.2	970	880.2	929.5	979.6	939.6	956.1	934.9
Ιξώδες 50C (cSt)	38.66	357.8	3.591	38.37	154.7	3.812	37.7	37.7	6.7	194.8	44.7
S (%m/m)	0.35	3.23	0.078	36	0.45	0.069	0.36	0.47	0.34	0.47	0.48
CCAI	820	851	-	821	841	-	818	870	867	824	823
Αρ. Κετανίου	-	-	47	-	-	41	-	-	-	-	-
C (%m/m)	83.7	84.3	87.6	84.4	86.9	87.4	81.9	86.9	82.1	85.8	80.5
H (%m/m)	11.8	10.3	12.1	11.9	11.1	12.6	12.2	11.1	10.6	12.1	10.8
N (%m/m)	0.48	0.41	<0.10	0.2	0.4	0.11	0.5	0.4	0.2	0.45	0.2
O (%m/m)	3.67	1.76	0.22	3.22	<0.2	<0.2	4.69	0.2	1.6	<0.2	3.1
FAME (%V/V)	29.7	<0.10	0.2	28.31	<0.1	<0.1	34.15	<0.10	25	<0.10	28.54

3.2 Επίδραση βιοκαυσίμων στη λειτουργία ναυτικών κινητήρων

3.2.1 Κύριες λειτουργικές τιμές δίχρονων κινητήρων

Στην Εικόνα 3-1 δίνεται ένα γράφημα στατιστικής σύνοψης της επίδρασης χρήσης B30 σε πέντε δίχρονους ναυτικούς κινητήρες στην ειδική κατανάλωση καυσίμου (BSFC). Οι τιμές είναι διορθωμένες κατά ISO που περιλαμβάνει αναγωγή στην ίδια θερμογόνο (LCV). Η σύγκριση γίνεται σε σχέση με τις τιμές αναφοράς των εργοστασιακών δοκιμών και τις μετρημένες τιμές με MGO και βαρύ πετρέλαιο (HFO και VLSFO) που έγιναν εν πλω παράλληλα με του B30. Κατά μέσο όρο, η χρήση B30 βρέθηκε να αυξάνει το ISO BSFC κατά 1–2% σε σύγκριση με τις τιμές αναφοράς, και με τις δοκιμές MGO. Η διακύμανση μεταξύ των κινητήρων ήταν χαμηλή, γεγονός που αποδίδεται στον ηλεκτρονικό τους έλεγχο. Οι υψηλότερες αποκλίσεις παρατηρήθηκαν για τις συγκρίσεις έναντι των δεδομένων αναφοράς, Εικόνα 3-1. Αυτό είναι πιθανότατα το αποτέλεσμα της διαφοράς των τρεχουσών λειτουργικών παραμέτρων του κινητήρα σε σχέση με τις δοκιμές αναφοράς. Οι τιμές

λειτουργίας με B30 και αργού πετρελαίου αποκάλυψαν ελάχιστη διαφορά και, σε ορισμένες περιπτώσεις, μια μικρή βελτίωση κατά τη λειτουργία με B30. Η συνολική πραγματική κατανάλωση καυσίμου, ωστόσο, θα είναι ελαφρώς υψηλότερη για το B30 λόγω της χαμηλότερης LCV του.

Στη συνέχεια παρέχονται τα στατιστικά συνοπτικά γραφήματα των δίχρονων κινητήρων που δοκιμάστηκαν, για P_{max} και ΔP, Εικόνα 3-2 και Εικόνα 3-3. Η επίδραση του βιοκαυσίμου στη λειτουργία παρουσίασε σημαντικές αποκλίσεις μεταξύ των κινητήρων. Σαφής τάση για μείωση του P_{max} διακρίνεται κατά τη χρήση του B30, αλλά τα αποτελέσματα ποικίλλουν. Σε σύγκριση με το βαρύ πετρέλαιο, οι τιμές P_{max} επηρεάστηκαν λιγότερο. Όσον αφορά το ΔP, παρουσιάζεται μικρότερη διακύμανση και επίσης εντοπίζεται μία χαμηλή μείωση κατά τη χρήση B30. Ο κύριος λόγος για τη χαμηλότερη διασπορά των τιμών ΔP σε σύγκριση με το P_{max}, είναι ότι υπήρχε διαφορά της πίεσης του κυλίνδρου στο σημείο ανάφλεξης μεταξύ των δοκιμών. Τόσο το P_{max} όσο και το ΔP επηρεάζονται από τις ιδιότητες του καυσίμου, και συνήθως αυξάνονται με υψηλότερο LCV. Οι άλλοι παράγοντες που επηρεάζουν τα P_{max} και ΔP είναι η γωνία ψεκασμού και η καθυστέρηση ανάφλεξης. Το πρώτο μπορεί να επηρεαστεί από φυσικές ιδιότητες όπως το ιξώδες και το δεύτερο διαφέρει λόγω του αριθμού κετανίου (CN) των δοκιμασμένων καυσίμων. Η μάλλον χαμηλή μείωση της ΔP για το B30 σε σύγκριση με το MGO, το οποίο έχει περίπου 6% υψηλότερο LCV αποδίδεται σε νωρίτερη ανάφλεξη που αντισταθμίζει την επίδραση της LCV. Μία ενδεικτική διαφορά των τιμών καθυστέρησης ανάφλεξης μεταξύ των καυσίμων δίνεται στην Εικόνα 3-4. Τα αποτελέσματα B30 και αργού πετρελαίου ήταν αρκετά παρόμοια, σε σχέση με τις άλλες δύο συγκρίσεις.

Με βάση τις παραμέτρους απόδοσης, η επίδραση του B30 στη λειτουργία του κινητήρα βρέθηκε να είναι ελάχιστη. Είναι πιθανό μακροχρόνιες δοκιμές να αποκαλύψουν επιπτώσεις στη λειτουργία του συστήματος τροφοδοσίας καυσίμου, ειδικά σε περιπτώσεις όπου κακός χειρισμός και αποθήκευση επηρεάζουν την ποιότητα των βιοκαυσίμων λόγω οξείδωσης ή όταν η κατάσταση του κινητήρα δεν είναι καλή. Για κάθε περίπτωση έγινε μελέτη της επίδρασης της χρήσης του B30 στο μηχανισμό καύσης με εκτίμηση του HRR χρησιμοποιώντας τα μετρημένα διαγράμματα πίεσης. Τα αποτελέσματα ήταν ομοιόμορφα στις περισσότερες περιπτώσεις και η επίδραση του βιοκαυσίμου ήταν μικρή. Ο μέγιστος ρυθμός καύσης, και γενικά ο ρυθμός εξέλιξής της ήταν σχεδόν ίδια με των τυπικών καυσίμων που επίσης μελετήθηκαν. Αυτό επιβεβαίωσε πως το B30 είχε ελάχιστη έως μηδαμινή επίδραση και στην παροχή καυσίμου στον κύλινδρο, δηλαδή στο σύστημα έγχυσης. Αντίστοιχα πολύ χαμηλές ήταν και οι διαφορές στη διάρκεια της καύσης.

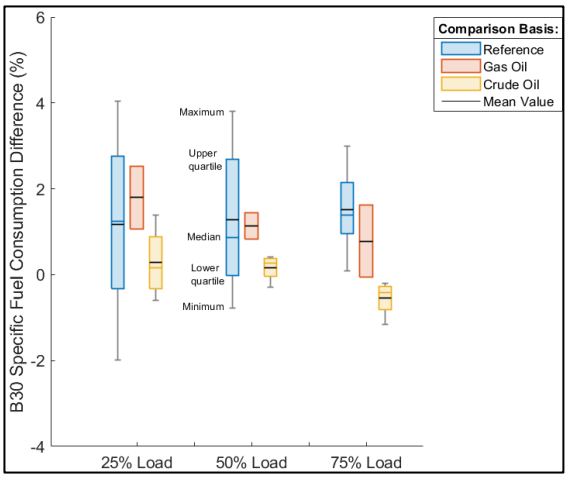

Εικόνα 3-1 Μεταβολή ειδικής κατανάλωσης κατά ISO, B30 σε σχέση με Εργοστασιακή τιμή, MGO, Βαρύ Πετρέλαιο; δίχρονοι κινητήρες

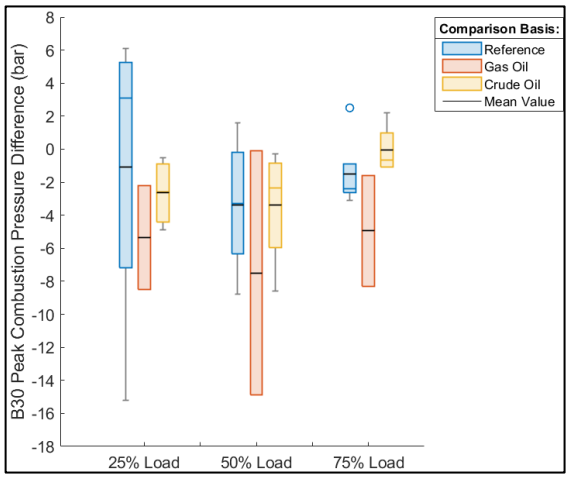

Εικόνα 3-2 Μεταβολή μεγ. πίεσης καύσης, B30 σε σχέση με Εργοστασιακή τιμή, MGO, Βαρύ Πετρέλαιο; δίχρονοι κινητήρες

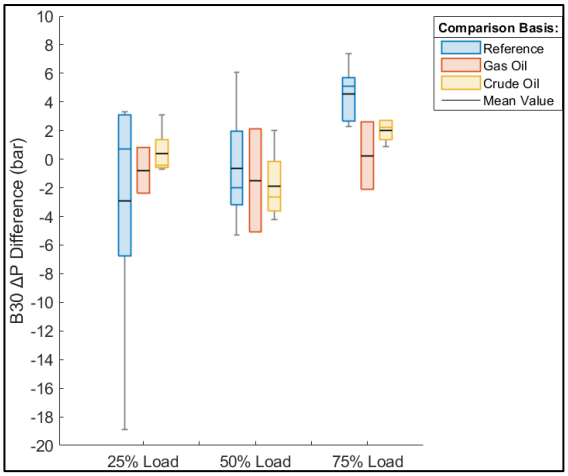

Εικόνα 3-3 Μεταβολή ανόδου πίεσης κατά την καύση, B30 σε σχέση με Εργοστασιακή τιμή, MGO, Βαρύ Πετρέλαιο; δίχρονοι κινητήρες

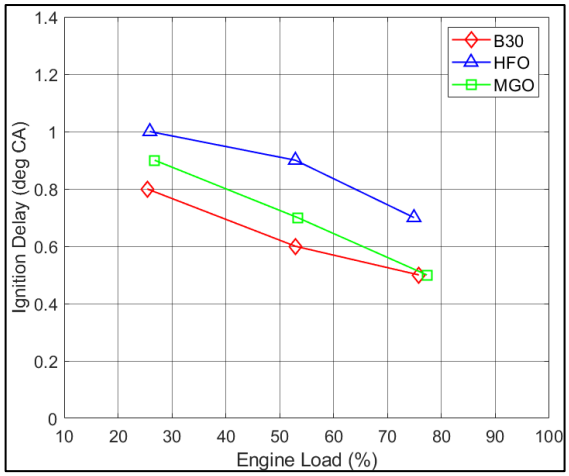

Εικόνα 3-4 Υπόδειγμα καθυστέρησης ανάφλεξης, B30, MGO, HFO; Δίχρονος κινητήρας

3.2.2 Επίδραση βιοκαυσίμου στην απόδοση τετράχρονων γεννητριών

Στις Εικόνα 3-5 - Εικόνα 3-7 η επίδραση της χρήση βιοκαυσίμου στην ειδική κατανάλωση, μέγιστη πίεση καύσης και άνοδο πίεσης κατά την καύση παρουσιάζεται για τις τετράχρονες γεννήτριες που εξετάστηκαν.

Το ISO BSFC λειτουργίας με B30 βρέθηκε να είναι υψηλότερο για τους περισσότερους κινητήρες, με λίγες περιπτώσεις να έχουν παρόμοιες τιμές κατανάλωσης. Η αύξηση του ISO BSFC για τη λειτουργία B30 σε σύγκριση με τις τιμές αναφοράς ήταν κατά μέσο όρο 2.5%. Σε σύγκριση με τις τιμές δοκιμών με MGO, διαπιστώθηκε αύξηση 3%. Όπως και στην περίπτωση των δίχρονων κινητήρων, οι τιμές BSFC του αργού πετρελαίου ήταν κοντά στο B30, με μια ελαφρά αύξηση 1% για όλα τα φορτία. Για τις τετράχρονες γεννήτριες παρατηρείται υψηλότερη επίδραση του B30 στο BSFC σε σύγκριση με τους δίχρονους κινητήρες. Η επίδραση στα P_{max} και ΔP βρέθηκε σημαντική σε σχέση με τις τιμές αναφοράς για όλα τα καύσιμα που εξετάστηκαν. Οι τιμές για το B30 ήταν παρόμοιες με τα άλλα καύσιμα. Η ομοιότητα μεταξύ των τιμών για όλες τις δοκιμές εν πλω αποκάλυψε ότι οι διαφορές σε σύγκριση με την αναφορά ήταν αποτέλεσμα ρύθμισης του κινητήρα και όχι του καυσίμου. Το προηγούμενο δείχνει ότι για τις τετράχρονες μονάδες η ρύθμιση και κατάσταση του κινητήρα μπορεί να ποικίλλει σημαντικά. Διαπιστώθηκε ότι η νωρίτερη ανάφλεξη του B30 αντιστάθμισε τη διαφορά του LCV μεταξύ B30 και MGO. Η σύγκριση με μετρήσεις αργού πετρελαίου δείχνει αύξηση αλλά και μείωση και για τις δύο παραμέτρους, ανάλογα με τον κινητήρα που δοκιμάστηκε. Οι διάμεσες τιμές δείχνουν ότι η γενική τάση είναι χαμηλότερη P_{max} και ΔP για τη λειτουργία με B30. Με βάση τα αποτελέσματα που παρουσιάζονται, οι διαφορές απόδοσης για το B30 στην περίπτωση των τετράχρονων γεννητριών ήταν συνολικά υψηλότερες από τους 2χρονους κινητήρες.

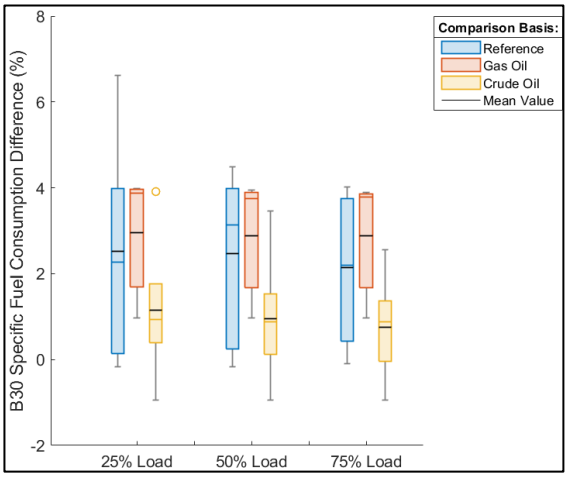

Εικόνα 3-5 Μεταβολή ειδικής κατανάλωσης κατά ISO, B30 σε σχέση με Εργοστασιακή τιμή, MGO, Βαρύ Πετρέλαιο; τετράχρονοι κινητήρες

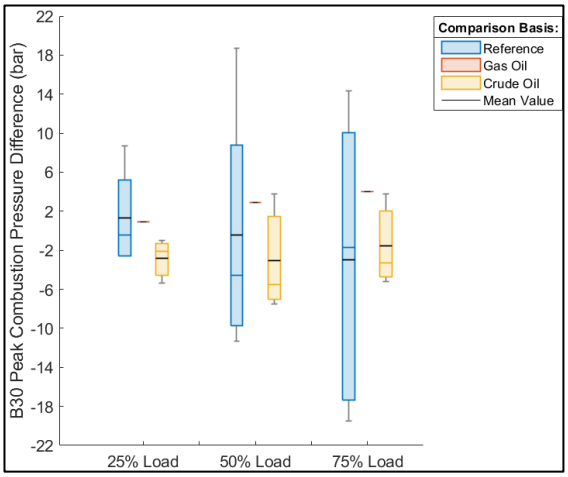

Εικόνα 3-6 Μεταβολή μεγ. πίεσης καύσης, B30 σε σχέση με Εργοστασιακή τιμή, MGO, Βαρύ Πετρέλαιο; τετράχρονοι κινητήρες

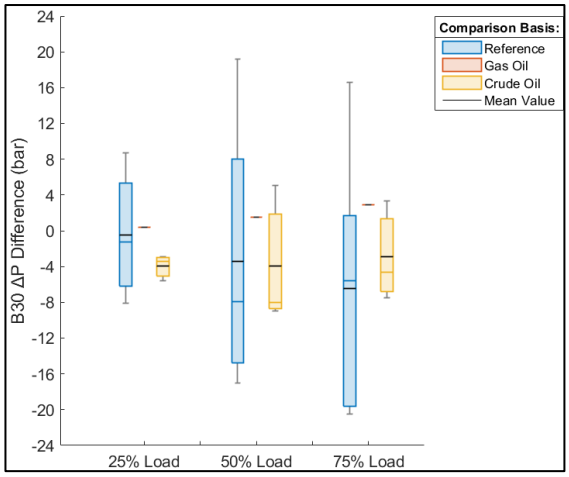

Εικόνα 3-7 Μεταβολή ανόδου πίεσης κατά την καύση, B30 σε σχέση με Εργοστασιακή τιμή, MGO, Βαρύ Πετρέλαιο; τετράχρονοι κινητήρες

3.2.3 Επίδραση χρήσης βιοκαυσίμου στις εκπομπές NO_x δίχρονων κινητήρων

Οι ειδικές εκπομπές NO_x υπολογίστηκαν με τη μετρημένη συγκέντρωση του ρύπου στα καυσαέρια, την εκτιμημένη ροή μάζας καυσαερίων με τη μέθοδο ισορροπίας μάζας άνθρακα, και τη μετρημένη ισχύ του κινητήρα σε κάθε περίπτωση. Στατιστική σύνοψη των αποτελεσμάτων δίνεται στην Εικόνα 3-8 για τους δίχρονους κινητήρες. Ένα σημαντικό εύρημα ήταν ότι για όλες τις περιπτώσεις οι συνολικές ειδικές εκπομπές NO_x ήταν πάνω από την τιμή αναφοράς, ανεξάρτητα από το καύσιμο που δοκιμάστηκε. Στις περισσότερες περιπτώσεις, οι τιμές εκπομπών NO_x για το B30 ήταν αυξημένες. Παρατηρήθηκε διακύμανση του βαθμού αύξησης η οποία ήταν αναμενόμενη, λόγω του μηχανισμού επίδρασης του βιοντίζελ στις μηχανές εσωτερικής καύσης (50), (51). Οι μεγαλύτερες διακυμάνσεις εκπομπών συνέπεσαν με τις υψηλότερες διακυμάνσεις στα δεδομένα απόδοσης των κινητήρων. Τα αποτελέσματα καθιστούν σαφές ότι οι εκπομπές σε χαμηλό φορτίο επηρεάζονται περισσότερο. Αυτό συμπίπτει με τον υψηλότερο βαθμό διαφοράς των τιμών P_{max} στο χαμηλό φορτίο. Η μέση αύξηση των συνολικών εκπομπών για το B30 σε σύγκριση με τις τιμές αναφοράς ήταν 10%. Λαμβάνοντας υπόψη το γεγονός ότι ο IMO παρέχει δικαίωμα για αύξηση των εκπομπών κατά 10% πάνω από το επίσημο όριο για δοκιμές που πραγματοποιούνται επί πλοίων, (52), αυτό το αποτέλεσμα είναι ενθαρρυντικό. Σε σύγκριση με το αργό πετρέλαιο, για το B30 η αύξηση των εκπομπών NO_x ήταν χαμηλή, με μέση τιμή 4%. Λαμβάνοντας υπόψη την παρόμοιά απόδοση των κινητήρων κατά τη χρήση B30 και αργού πετρελαίου, η αύξηση των εκπομπών αποδίδεται στην υψηλότερη περιεκτικότητα του βιοκαυσίμου σε O_2.

3.2.4 Επίδραση βιοκαυσίμου στις εκπομπές NO_x τετράχρονων γεννητριών

Στην Εικόνα 3-9 δίνεται η σύνοψη της επίδρασης του B30 στις εκπομπές NO_x για τις τετράχρονες γεννήτριες. Βρέθηκαν χαμηλότερες τιμές ειδικών εκπομπών NOx σε σύγκριση με τις τιμές αναφοράς για τους περισσότερους κινητήρες που εξετάστηκαν. Αντίθετα, η σύγκριση με δοκιμές με χρήση MGO και αργού πετρελαίου έδειξε υψηλότερες εκπομπές NO_x για τη λειτουργία με B30. Η συνολική σταθμισμένη τιμή εκπομπών ήταν κατά μέσο όρο 5% χαμηλότερη από την αναφορά για τις δοκιμές B30. Η διάμεση τιμή ήταν κοντά στο 0%, δείχνοντας ότι για τις περισσότερες γεννήτριες, οι εκπομπές NO_x με χρήση B30 ήταν παρόμοιες με αυτές της αναφοράς. Οι δοκιμές εν πλω, ωστόσο, έδειξαν ότι για το B30 οι συνολικές εκπομπές NO_x αυξήθηκαν μεταξύ 6% – 15%, κατά μέσο όρο 10%, σε σύγκριση με το ντίζελ. Αυτή η αύξηση είναι πάνω από τα ευρήματα των δοκιμών δίχρονου κινητήρα. Η σύγκριση με τις δοκιμές αργού πετρελαίου έδειξε μέση αύξηση των συνολικών εκπομπών NO_x για το B30 κατά 2,4% αλλά και μεγάλη διακύμανση καθώς καταγράφηκαν τιμές στην περιοχή ±10%. Συνολικά, επιβεβαιώθηκε τάση για αυξημένο σχηματισμό NO_x κατά τη χρήση του B30, παρά το γεγονός ότι οι τιμές P_{max} και ΔP ήταν γενικά χαμηλότερες. Ο ενισχυμένος σχηματισμός NOx αποδίδεται συνεπώς στην υψηλότερη περιεκτικότητα σε O_2 των βιοκαυσίμων. Λαμβάνοντας υπόψη τα αποτελέσματα, για τις τετράχρονες γεννήτριες η χρήση B30 θα επηρεάσει μέτρια τις εκπομπές NO_x, επιτρέποντας τη συμμόρφωση με τα όρια εκπομπών.

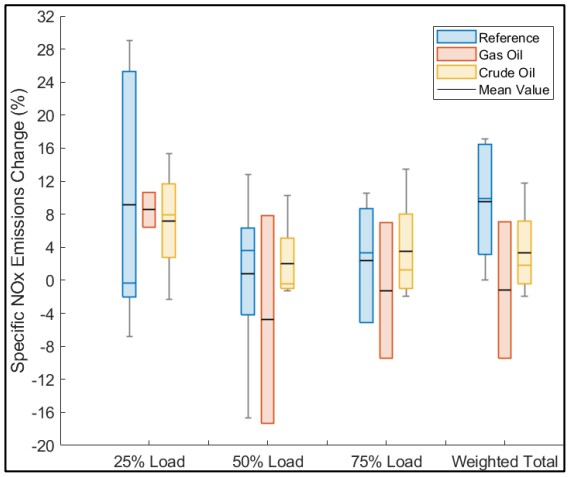

Εικόνα 3-8 Μεταβολή ειδικών εκπομπών NO_x, B30 σε σχέση με Εργοστασιακή τιμή, MGO, Βαρύ Πετρέλαιο; δίχρονοι κινητήρες

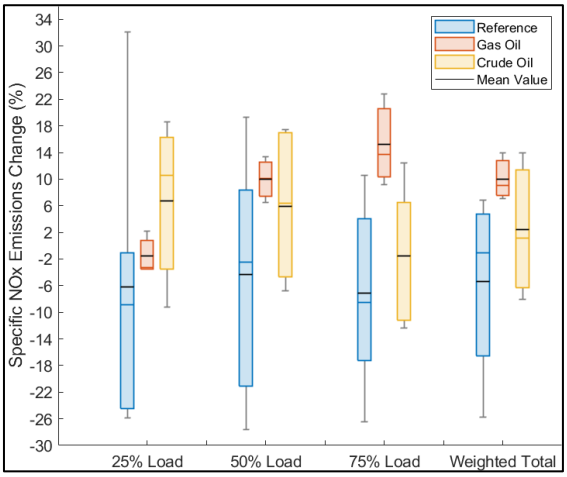

Εικόνα 3-9 Μεταβολή ειδικών εκπομπών NO_x, B30 σε σχέση με Εργοστασιακή τιμή, MGO, Βαρύ Πετρέλαιο; τετράχρονοι κινητήρες

3.2.5 Χρήση πολυζωνικού μοντέλου για μελέτη λειτουργίας δίχρονου κινητήρα με βιοκαύσιμο

Παρουσιάζονται τα αποτελέσματα της ανάλυσης του πολυζωνικού μοντέλου για την επίδραση του βιοκαυσίμου στη διαδικασία καύσης και στο σχηματισμό NO_x. Η πιστότητα του μοντέλου επιβεβαιώθηκε αναπαράγοντας τα αποτελέσματα των εργοστασιακών δοκιμών ενός εκ των μελετημένων δίχρονων κινητήρων με καλή πιστότητα. Στη συνέχεια ακολούθησε μελέτη της λειτουργίας εν πλω για τα τρία καύσιμα με επίσης καλή συμφωνία μεταξύ μετρημένων και υπολογισμένων μεγεθών για έναν δίχρονο κινητήρα.

Στην Εικόνα 3-10 δίνεται ο σχηματισμός NO_x σε κάθε ζώνη και για τα τρία φορτία (25%, 50%, 75%) για HFO και B30. Παρατηρούνται διαφορές, με την πιο ενδιαφέρουσα να είναι οι χαμηλότερες τιμές συνεισφοράς για όλες τις ζώνες κατά τους υπολογισμούς B30. Αυτό δείχνει ότι στην περίπτωση των βιοκαυσίμων η συνεισφορά όλων των ζωνών είναι πιο ομοιόμορφη από ό,τι στην περίπτωση του HFO και ότι η συμβολή των τελευταίων σχηματισμένων ζωνών είναι μεγαλύτερη. Αυτό είναι το αποτέλεσμα του οξυγόνου που περιέχεται στο B30 και βελτιώνει την αναλογία αέρα καυσίμου στη ζώνη καύσης. Ο ρυθμός καύσης που υπολογίζεται από το μοντέλο δίνεται στην Εικόνα 3-11 και δείχνει ελάχιστες διαφορές μεταξύ των δύο καυσίμων για όλα τα φορτία. Η μέση θερμοκρασία ζώνης καύσης συγκρίνεται μεταξύ των δοκιμών B30 και HFO στην Εικόνα 3-12 για φορτίο 75% Η μέση θερμοκρασία της ζώνης καύσης είναι υψηλότερη για το HFO και στις δύο περιπτώσεις. Αυτό δείχνει ότι η αύξηση των εκπομπών NO_x κατά τη χρήση βιοκαυσίμων οφείλεται πρωτίστως στην αύξηση της αναλογίας αέρα καυσίμου. Στην Εικόνα 3-13 δίνεται το αποτέλεσμα θεωρητικής μελέτης με δύο καύσιμα ίδιων χαρακτηριστικών αλλά διαφορετικό ποσοστό O_2. Φαίνεται καθαρά πως το επιπλέον O_2 επηρεάζει της περιεκτικότητα της δέσμης καυσίμου με τη διαφορά να γίνεται διακριτή αφού το O_2 του καυσίμου έχει καταναλωθεί ορισμένο χρόνο μετά την έναυση και το O_2 του εισερχόμενου αέρα στη δέσμη παραμένει με αποτέλεσμα η συγκέντρωση να αυξάνεται και να ευνοείται ο σχηματισμός NO_x. Οι διαφορά στο λόγο ισοδυναμίας καυσίμου αέρα, που προκύπτει από τη διαφορά περιεχομένου O_2 μεταξύ B30 και καυσίμου χαμηλής περιεκτικότητας O_2 δίνεται στην Εικόνα 3-14 και Εικόνα 3-15. Όπως φαίνεται μεγάλη διαφορά προκύπτει ειδικά στο εσωτερικό της δέσμης λόγω του O_2 στο B30. Αυτό ενισχύει σημαντικά την παραγωγή NO_x.

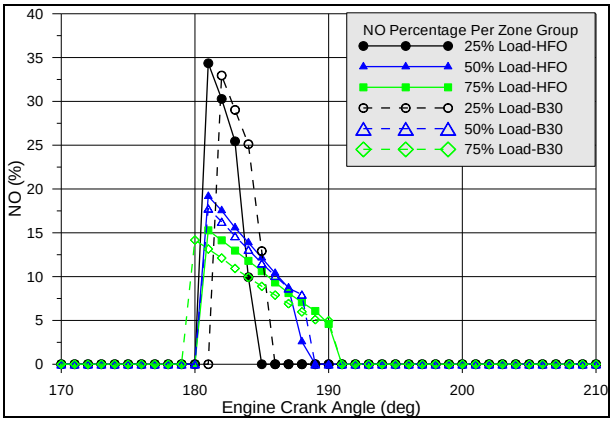

Εικόνα 3-10 Υπολογισμένη συμβολή ανά ζώνη στο σχηματισμό NO, λειτουργία με B30 και HFO

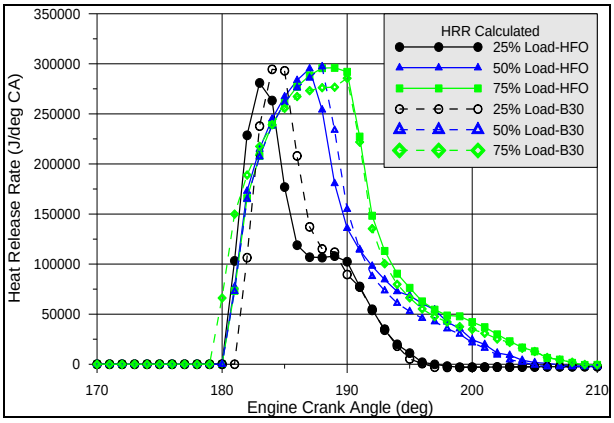

Εικόνα 3-11 Υπολογισμένος ρυθμός καύσης, λειτουργία με B30 και HFO

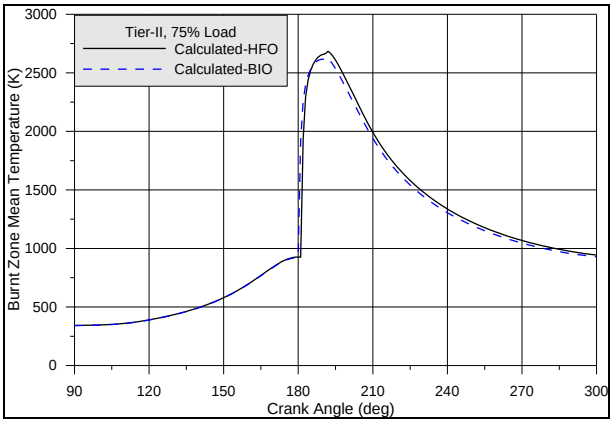

Εικόνα 3-12 Υπολογισμένη μέση θερμοκρασία ζώνης καύσης, 75% Φορτίο λειτουργία με B30 και HFO

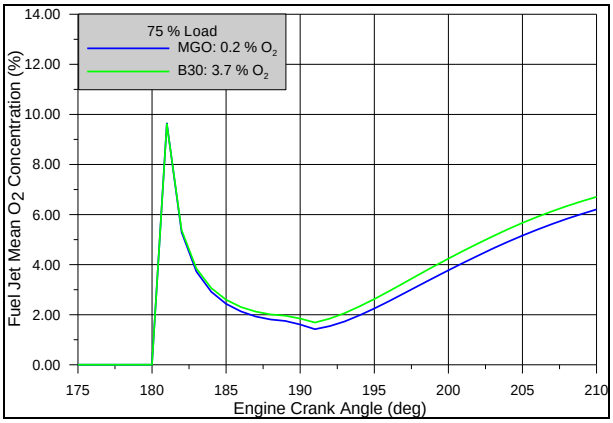

Εικόνα 3-13 Μέση συγκέντρωση O_2 στη δέσμη καυσίμου για κάυσιμο χαμηλού και υψηλού περιεχομένου O_2

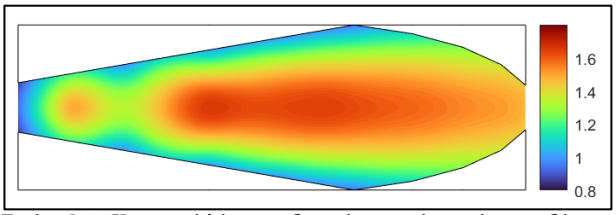

Εικόνα 3-14 Κατανομή λόγου ισοδυναμίας καυσίμου-αέρα στη δέσμη 5° μετά την έγχυση, 50% φορτίο, B30

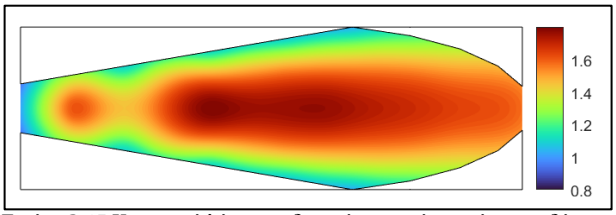

Εικόνα 3-15 Κατανομή λόγου ισοδυναμίας καυσίμου-αέρα στη δέσμη 5° μετά την έγχυση, 50% φορτίο, Low O_2 HFO

4. Χρήση ανακυκλοφορίας καυσαερίου για περιορισμό εκπομπών NO_x σε δίχρονους ναυτικούς κινητήρες

4.1 Βασική αρχή λειτουργίας

Η χρήση EGR γίνεται προκειμένου να μειωθεί η συγκέντρωση O_2 στο θάλαμο καύσης και παράλληλα να μειωθεί η μέση θερμοκρασία του (53). Τα δύο αυτά επιτυγχάνονται με την αντικατάσταση μέρους του αέρα σαν εργαζόμενο μέσον με ανακυκλοφορούντα καυσαέρια τα οποία είναι φτωχά σε οξειδωτικούς παράγοντες και παράλληλα έχουν υψηλή θερμοχωρητικότητα, (54).

4.2 Διάταξη συστήματος

Για κινητήρες με διάμετρο κυλίνδου 700 mm ή μικρότερη, το σύστημα EGR εφαρμόζεται με έναν στρόβιλο που διαθέτει βαλβίδα παράκαμψης καυσαεριών. Η διαμόρφωση δίνεται στην Εικόνα 4-1. Σε σύγκριση με τη συνηθισμένη διάταξη κινητήρα χρησιμοποιούνται δύο γραμμές προς τον οχετό αέρα σάρωσης. Αυτά είναι η κύρια γραμμή, που έχει την ικανότητα να τροφοδοτεί όλο τον αέρα σάρωσης μέσω του συστήματος εισαγωγής και του υπερσυμπιεστή, και η γραμμή EGR που οδηγεί μια ορισμένη ποσότητα καυσαερίων, έως το 40% της μάζας του μέγιστου φορτίου, μέσω της μονάδας EGR μέχρι το σημείο ανάμειξης στον οχετό εισαγωγής, (55). Η βαλβίδα παράκαμψης του στροβίλου (EGB) χρησιμοποιείται με το σύστημα EGR ανενεργό για βελτιστοποίηση απόδοσης σε χαμηλό φορτίο, και στη λειτουργία EGR η βαλβίδα είναι μόνιμα κλειστή. Κατά τη διάρκεια αυτής της λειτουργίας, η βαλβίδα παράκαμψης κυλίνδρου (CBV) χρησιμοποιείται για την αύξηση της πίεσης του αέρα σάρωσης ως μέθοδος βελτίωσης της απόδοσης του κινητήρα.
Τα χαρακτηριστικά των μελετούμενων κινητήρων δίνονται στον Πίνακας 4-1 για τον "1", ενώ ο κινητήρας "2" είναι ο ίδιος με τον κινητήρα "1" του κεφαλαίου 2 (Πίνακας 2-1).

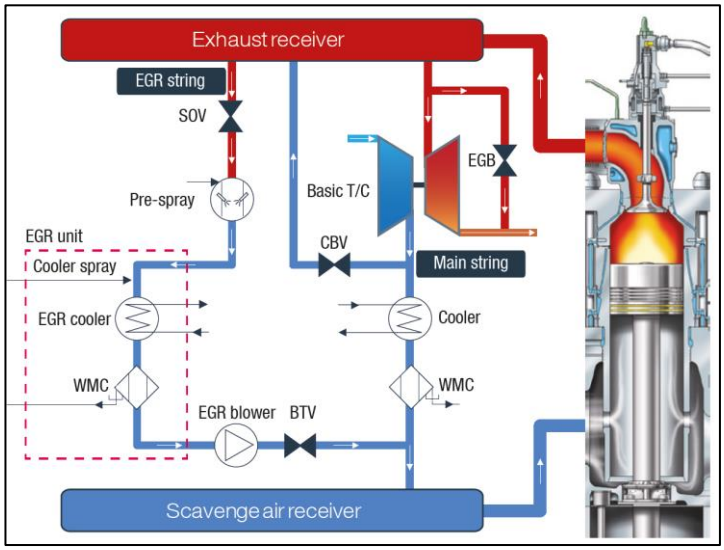

Εικόνα 4-1 Σχηματικό διάγραμμα δίχρονου ναυτικού κινητήρα εξοπλισμένου EGR και EGB, (55)

Πίνακας 4-1 Λειτουργικά χαρακτηριστικά μηχανής 1

6G60ME-C9.5EGRBP	Μονάδες	Τιμή
Τύπος	-	Δίχρονος
Αρ. Κυλίνδρων	-	6
Διάμετρος	mm	600
Διαδρομή	mm	2790
Ονομαστική Ταχύτητα	rpm	86.0
Ονομαστική Ισχύς	kW	13,000
Τύπος EGR	-	EGR-GB

4.3 Επίδραση EGR στα βασικά λειτουργικά μεγέθη των κινητήρων

Κατά τη λειτουργία με EGR (Tier-III) σημαντικές μεταβολές προέκυψαν στα βασικά λειτουργικά μεγέθη και για τους δύο κινητήρες σε σχέση με χωρίς EGR (Tier-II). Οι τιμές P_{comp} αυξήθηκαν, ενώ η P_{max} μειώθηκε, Εικόνα 4-2 - Εικόνα 4-5. Η αύξηση του P_{comp} επήλθε παρά τη μείωση της πίεσης σάρωσης, με αύξηση του λόγου πιέσεων που επιτεύχθηκε με νωρίτερο EVC, Εικόνα 4-6 και Εικόνα 4-7 για τους δύο κινητήρες αντίστοιχα. Η ΔP παρουσίασε σημαντική μείωση, Εικόνα 4-8 και Εικόνα 4-9, εν μέρει λόγω βραδυπορείας έγχυσης καυσίμου για την περίπτωση του κινητήρα "1", Εικόνα 4-10. Βραδυπορεία έγχυσης καυσίμου δεν παρατηρήθηκε για όλα τα φορτία στην περίπτωση του "2" Εικόνα 4-11, κυρίως λόγο της πιλοτικής έγχυσης πετρελαίου που δεν επιτρέπει μεγάλες καθυστερήσεις, αφού εκκρεμεί και η ανάφλεξη του φυσικού αερίου. Για τη γενική μείωση του ΔP ευθύνεται σε μεγάλο βαθμό το ανακυκλοφορόν καυσαέριο, όπως φαίνεται στη συνέχεια της ανάλυσης και είναι γνωστό από άλλες μελέτες (56). Η βραδυπορεία έγχυσης και ανάφλεξης έχει αρνητικό αντίκτυπο στην κατανάλωση καυσίμου. Με περαιτέρω ανάλυση χρησιμοποιώντας το πολυζωνικό μοντέλο, διαπιστώθηκε ότι η βραδυπορία χρησιμοποιήθηκε για να περιοριστεί το ποσοστό EGR ενώ περιορίζονται οι εκπομπές NO_x, όπως αναφέρεται και σε άλλες μελέτες (57–59).

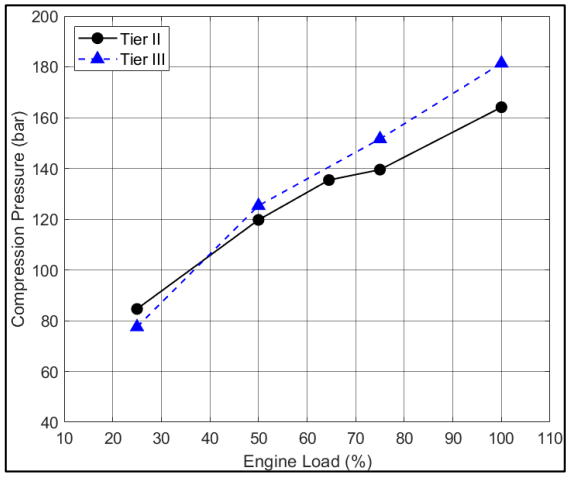

Εικόνα 4-2 Πίεση Συμπίεσης, Tier-II & Tier-III; Κινητήρας 1

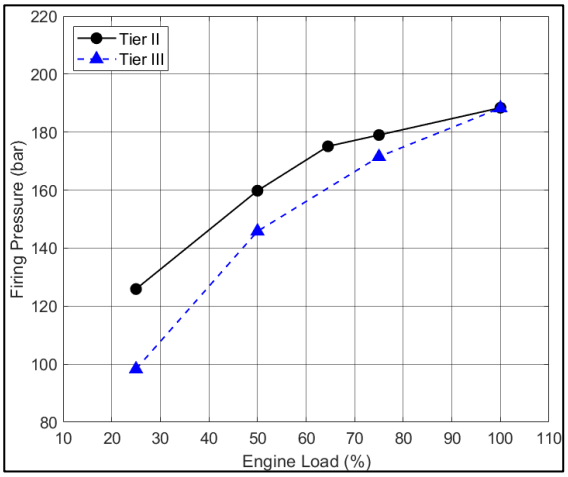

Εικόνα 4-3 Μέγιστη Πίεση Καύσης, Tier-II & Tier-III; Κινητήρας 1

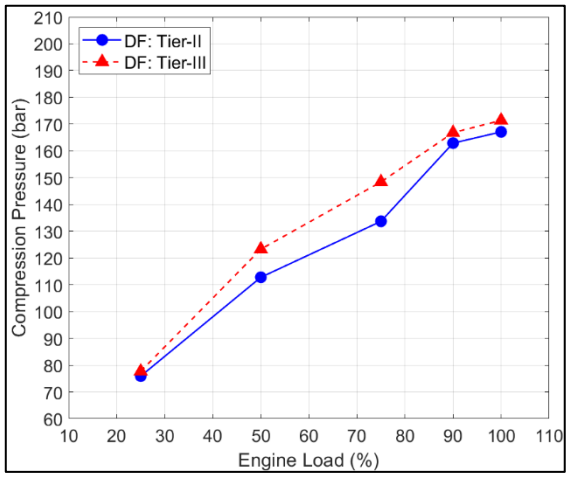

Εικόνα 4-4 Πίεση Συμπίεσης, Tier-II & Tier-III; ; Κινητήρας 2 ΦΑ

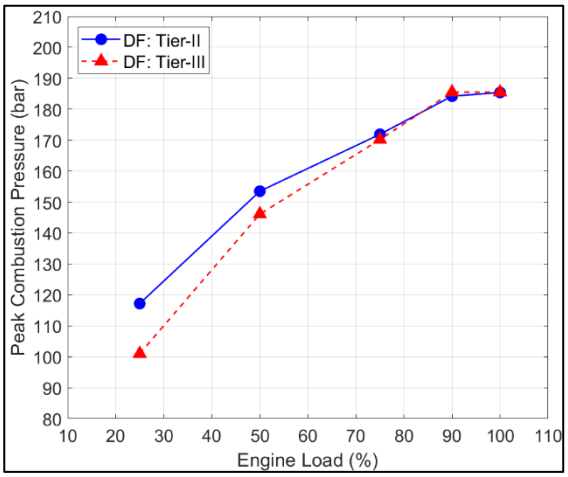

Εικόνα 4-5 Μέγιστη Πίεση Καύσης, Tier-II & Tier-III; Κινητήρας 2 ΦΑ

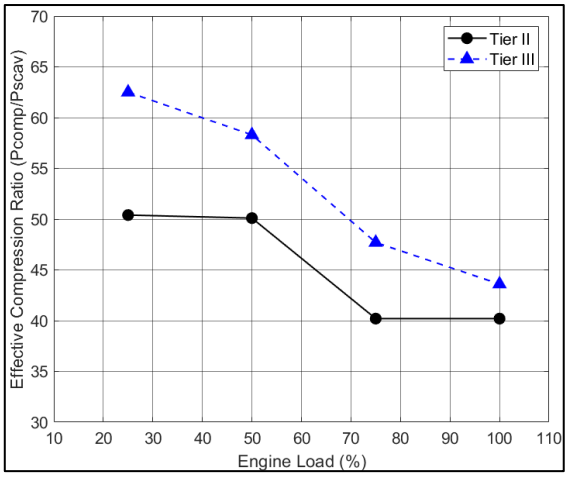

Εικόνα 4-6 Λόγος Πιέσεων, Tier-II & Tier-III; Κινητήρας 1

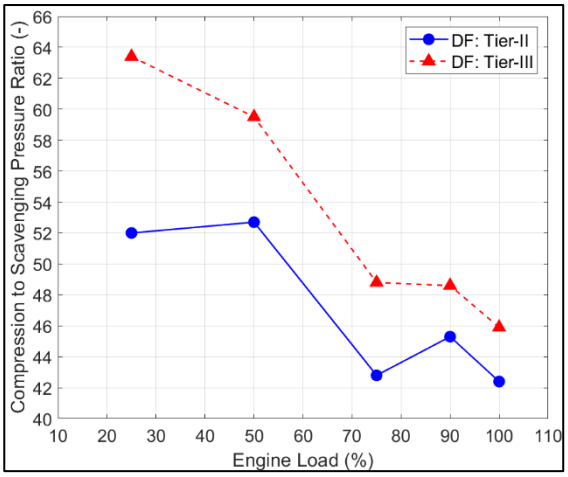

Εικόνα 4-7 Λόγος Πιέσεων, Tier-II & Tier-III; Κινητήρας 2 ΦΑ

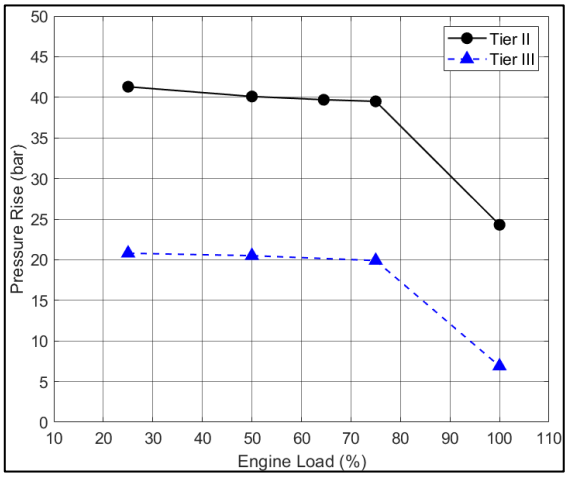

Εικόνα 4-8 Άνοδος πίεσης κατά την καύση, Tier-II & Tier-III; Κινητήρας 1

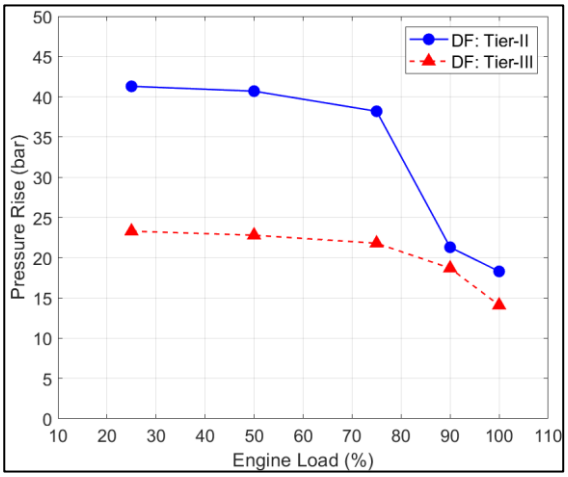

Εικόνα 4-9 Άνοδος πίεσης κατά την καύση, Tier-II & Tier-III; Κινητήρας 2 ΦΑ

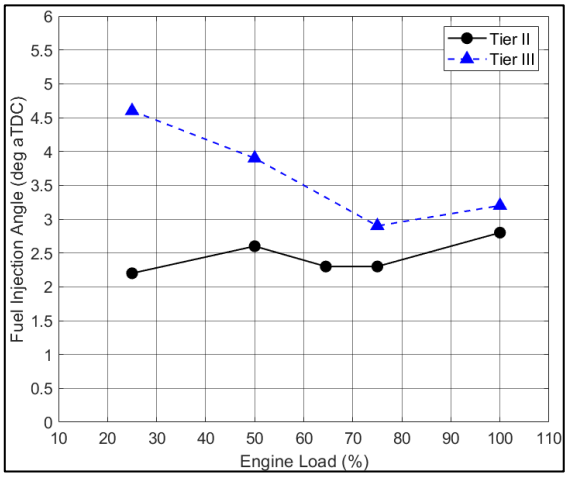

Εικόνα 4-10 Γωνία έγχυσης καυσίμου, Tier-II & Tier-III; Κινητήρας 1

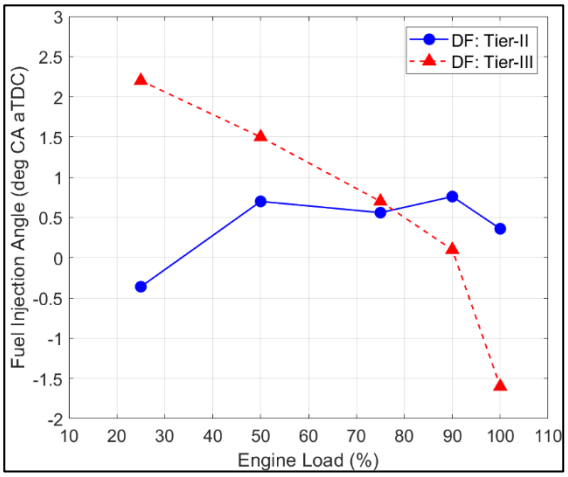

Εικόνα 4-11 Γωνία έγχυσης καυσίμου, Tier-II & Tier-III; Κινητήρας 2 ΦΑ

Και για τους δύο κινητήρες, η κατανάλωση καυσίμου επηρεάζεται αρνητικά από το EGR και τις αλλαγές στις ρυθμίσεις. Για τον κινητήρα "1" αύξηση του BSFC παρατηρείται σε ολόκληρη την περιοχή λειτουργίας, με την υψηλότερη άνοδο μεταξύ 25% και 50% φορτίου, Εικόνα 4-12. Η μέση αύξηση BSFC είναι 3.5% με μέγιστη αύξηση 5.1% στο φορτίο 50%. Για τον κινητήρα "2" συγκρίνεται το THR, Εικόνα 4-13, και παρατηρούνται παρόμοια επίπεδα αύξησης, κατά μέσο όρο 2,6%, με την υψηλότερη αύξηση στο 25% και 50% του φορτίου. Η

μείωση θερμικής απόδοσης είναι γνωστό μειονέκτημα της χρήσης EGR, (60), (61). Η αύξηση της κατανάλωσης καυσίμου στις συνήθεις περιοχές φορτίου αυξάνει το λειτουργικό κόστος του συστήματος EGR. Σημειώνεται πως η διαφορά στην αποδοτικότητα του κινητήρα "2" μεταξύ λειτουργίας MGO και ΦΑ με χρήση EGR ήταν χαμηλή. Αυτό δείχνει ότι η χρήση EGR έχει περίπου την ίδια επίδραση στην απόδοση του κινητήρα ανεξάρτητα από τη λειτουργία ενός ή διπλού καυσίμου.

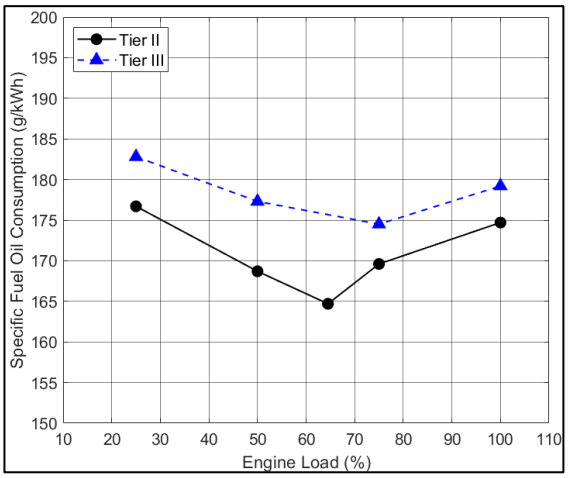

Εικόνα 4-12 Ειδική κατανάλωση καυσίμου, Tier-II & Tier-III; Κινητήρας 1

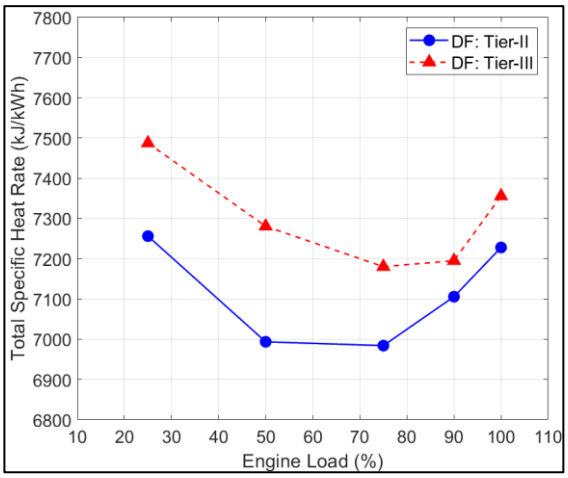

Εικόνα 4-13 Ειδική παροχή ενέργειας, Tier-II & Tier-III; Κινητήρας 2 ΦΑ

4.3.1 Επίδραση EGR στο μηχανισμό της καύσης

Η επίδραση του EGR στη διαδικασία καύσης εξετάζεται χρησιμοποιώντας την ανάλυση ρυθμού καύσης. Στην Εικόνα 4-14α,β παρέχεται η σύγκριση HRR σε φορτίο 75% για λειτουργία με και χωρίς EGR για τους δύο κινητήρες. Η ανάφλεξη του καυσίμου επιβραδύνεται στη λειτουργία με EGR. Αυτό είναι το αποτέλεσμα της βραδυπορείας έγχυσης και των ανακυκλωμένων καυσαερίων που αυξάνουν την καθυστέρηση ανάφλεξης, (62), (63), λόγω της μείωσης της θερμοκρασίας στον κύλινδρο. Ο αυξημένος λόγος συμπίεσης σε λειτουργία με EGR αντισταθμίζει εν μέρει τον προηγούμενο, επομένως ο κύριος παράγοντας για την καθυστερημένη ανάφλεξη είναι ο χρονισμός ψεκασμού. Ο αρχικός ρυθμός καύσης μειώνεται στη λειτουργία με EGR, όπως και η μέγιστη τιμή. Αυτό είναι σύμφωνο με άλλες μελέτες (62), (64), (65). Περιορίζοντας την ταχύτητα καύσης, η πίεση και η αύξηση της θερμοκρασίας στον κύλινδρο μειώνονται, με αποτέλεσμα τη μείωση του σχηματισμού NO_x. Ο ρυθμός καύσης στα τελευταία στάδια είναι υψηλότερος από ότι κατά τη συμβατική λειτουργία. Ενώ αυτό επηρεάζει αρνητικά την απόδοση, η επίδραση στον σχηματισμό NOx είναι ελάχιστη καθώς σε αυτό το στάδιο η πίεση και η θερμοκρασία στον κύλινδρο μειώνονται λόγω της εκτόνωσης. Τα παραπάνω εντοπίζονται σε μεγαλύτερο βαθμό στον κινητήρα "2". Και για τους δύο κινητήρες, η χρήση EGR οδηγεί σε μείωση της διαθεσιμότητας οξυγόνου και της θερμοκρασίας επιβραδύνοντας την καύση διάχυσης, ενώ το στάδιο προαναμεμιγμένης καύσης επηρεάζεται λιγότερο. Και για τους δύο κινητήρες, όλα τα διαγράμματα HRR έδειξαν συνολικά χαμηλότερες τιμές για τη λειτουργία με EGR. Λαμβάνοντας υπόψη ότι η συνολική παρεχόμενη ενέργεια είναι υψηλότερη έως και 5% κατά τη διάρκεια λειτουργίας με EGR, λόγω αύξησης του BSFC, εκτιμάται πως οι απώλειες θερμότητας είναι σημαντικά υψηλότερες λόγω της χρήσης EGR. Αυτό αποδίδεται κυρίως στην παρατεταμένη διάρκεια καύσης (66), ειδικά στην περιοχή της μέγιστης θερμοκρασίας με τη θέση του εμβόλου ακόμα κοντά στο TDC.

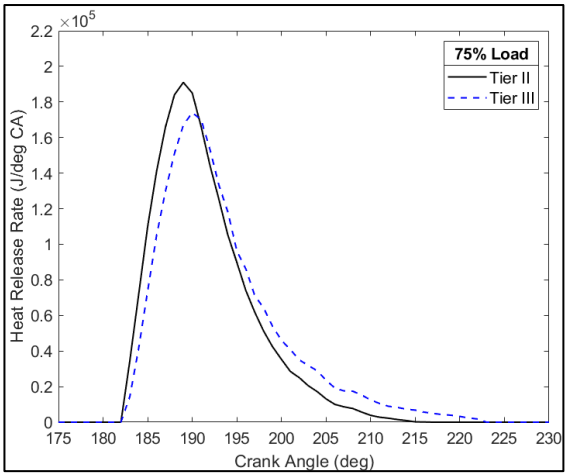

(α)

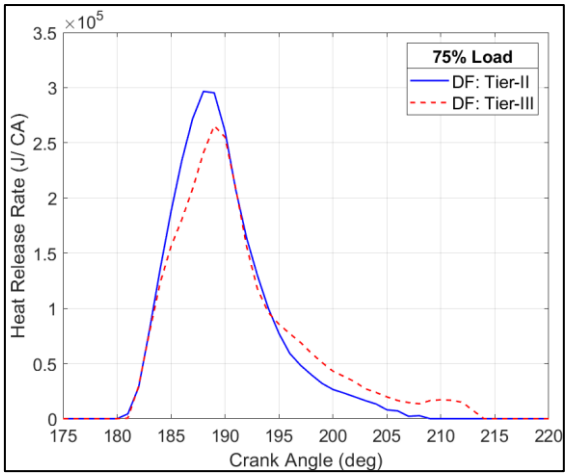

(β)

Εικόνα 4-14 Καθαρή έκλυση θερμότητας, Tier-II & Tier-III; (α) Κινητήρας 1; (β) Κινητήρας 2 ΦΑ

Η μείωση των εκπομπών NO_x στα καυσαέρια παρέχεται στην Εικόνα 4-15 και την Εικόνα 4-16 για τον κινητήρα "1" και "2" αντίστοιχα. Η μείωση είναι υψηλή για όλα τα φορτία με τη μέγιστη τιμή στο 75%. Για τον κινητήρα "2" παρατηρείται λίγο υψηλότερη μείωση εκπομπών. Τα απαιτούμενα ποσοστά ανακυκλοφορίας καυσαερίου δίνονται στις Εικόνα 4-17 και Εικόνα 4-18. Οι τιμές κυμαίνονται μεταξύ 38% - 47% με υψηλότερη αναλογία EGR για τον κινητήρα "2". Αυτό είναι σύμφωνο και με τη μετρούμενη μείωση των εκπομπών NO_x. Και για τους δύο κινητήρες ο λόγος EGR μειώνεται κάτω από 40% στο μέγιστο φορτίο, καθώς αυτή είναι η μέγιστη χωρητικότητα που μπορεί να διαχειριστεί το σύστημα. Με την εξαίρεση του μέγιστου φορτίου παρατηρείται γραμμική μείωση των NO_x με την αύξηση του λόγου ανακυκλοφορίας. Στο 100% του φορτίου η διαφορά προκύπτει από τη γενική λειτουργία του κινητήρα (τιμές πίεσης, χρονισμός έγχυσης, κλπ.). Επίσης, εκτιμάται ότι παρά τη χαμηλότερη αναλογία EGR στο μέγιστο φορτίο, η συνολική υψηλή τιμή μάζας των καυσαερίων στον κύλινδρο επηρεάζει σημαντικά την καύση δημιουργώντας τοπικές μειώσεις υψηλού λόγου ισοδυναμίας.

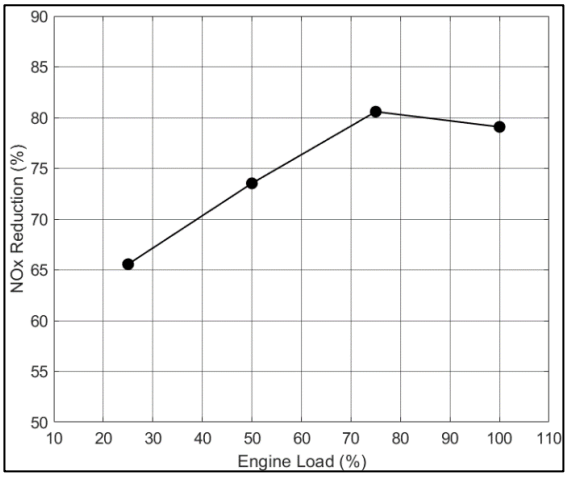

Εικόνα 4-15 Μείωση εκπομπών NO_x, Κινητήρας 1

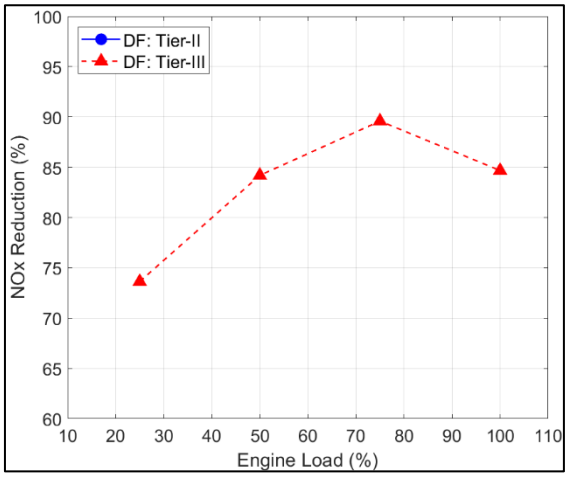

Εικόνα 4-16 Μείωση εκπομπών NO_x, Κινητήρας 2 ΦΑ

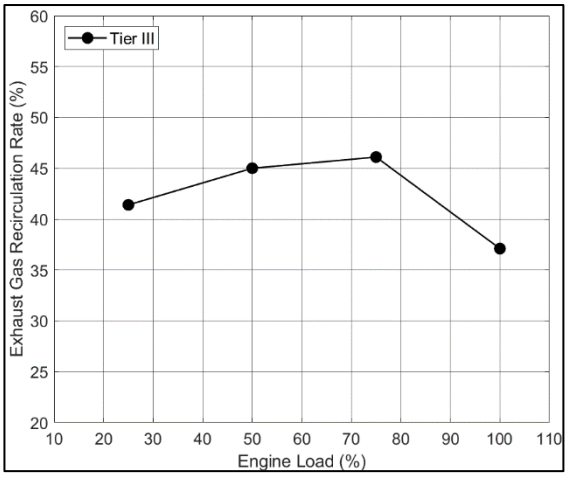

Εικόνα 4-17 Ποσοστό ανακυκλοφορίας καυσαερίων, Κινητήρας 1

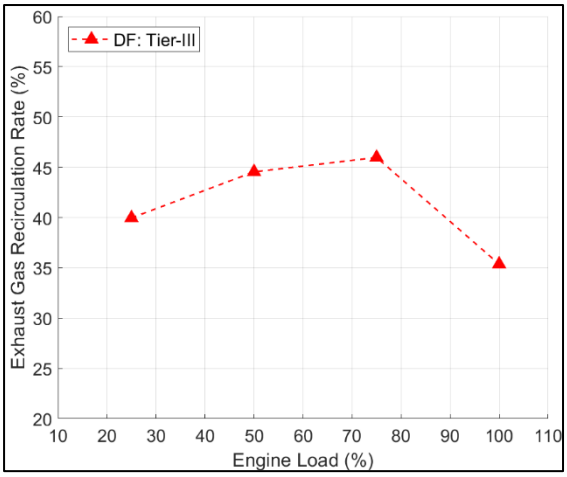

Εικόνα 4-18 Ποσοστό ανακυκλοφορίας καυσαερίων, Κινητήρας 2 ΦΑ

4.4 Χρήση του πολυζωνικού μοντέλου καύσης για διερεύνηση της επίδρασης του EGR

4.4.1 Θεωρητική ανάλυση της επίδρασης του EGR στο σχηματισμό NO_x

Το μοντέλο χρησιμοποιήθηκε για εκτίμηση της επίδρασης του EGR στη λειτουργία του κινητήρα και το σχηματισμό NO_x με αποτελέσματα καλής ακρίβειας. Η πιστότητα αναπαραγωγής των αποτελεσμάτων επιβεβαιώνει πως πέραν της επίδρασης των ανακυκλοφορούντων καυσαερίων το μοντέλο προέβλεψε με καλή ακρίβεια και την επίδραση του ανοίγματος της CBV.

Η υπολογισμένη μέση θερμοκρασία της καμένης ζώνης συγκρίνεται μεταξύ λειτουργίας με και χωρίς EGR . Οι συγκρίσεις δίνονται στην Εικόνα 4-19 και Εικόνα 4-20 για φορτίο 25% και 75%. Διαπιστώθηκε ότι μειώνεται κυρίως η μέγιστη θερμοκρασία και οι υπόλοιπες τιμές μπορεί να αυξηθούν σε ορισμένες περιπτώσεις παρά τη λειτουργία EGR. Αυτό είναι το αποτέλεσμα της μετακίνησης της καύσης αργότερα στον κύκλο του κινητήρα και της μεγαλύτερης διάρκειας καύσης κατά τη λειτουργία με EGR. Αυτό το στάδιο έχει μικρότερη επίδραση στο σχηματισμό NO_x καθώς οι θερμοκρασίες είναι χαμηλές και η αναλογία καυσίμου αέρα αυξάνεται περαιτέρω λόγω των προϊόντων της καύσης. Δεδομένου ότι ο σχηματισμός NO_x έχει εκθετική αύξηση με τη θερμοκρασία, η μείωση της μέγιστης τιμής που επιτυγχάνεται θα συμβάλει ουσιαστικά στη μείωση του ρύπου. Στην Εικόνα 4-21 παρουσιάζεται η επίδραση του EGR στον λόγο ισοδυναμίας αέρα-καυσίμου (λ) όπως υπολογίζεται από το μοντέλο για τον συνολικό μέσο όρο κύκλου και κατά την καύση, όταν συμβαίνει ο σχηματισμός NO_x. Η επίδραση είναι σαφής καθώς και οι δύο τιμές επηρεάζονται. Οι μειωμένες τιμές λ σε συνδυασμό με τη μειωμένη θερμοκρασία έχουν ως αποτέλεσμα τη μείωση του σχηματισμού NO_x. Συνολικά, τα προηγούμενα ευρήματα είναι ένα πολλά υποσχόμενο αποτέλεσμα για την ικανότητα του μοντέλου να αναπαράγει τις πολλαπλές αλλαγές που συμβαίνουν κατά τη λειτουργία με EGR και την επίδρασή τους στις εκπομπές. Επίσης, εξετάζεται η συμβολή κάθε ζώνης στις συνολικές εκπομπές. Στην Εικόνα 4-22 δίνεται η συνεισφορά των πακέτων καυσίμων κάθε διαμορφωμένης ζώνης κατά τη λειτουργία με και χωρίς EGR. Κατά τη λειτουργία με EGR λιγότερη ομοιόμορφη κατανομή του σχηματισμού NO_x εντοπίζεται μεταξύ των ζωνών, με αξιοσημείωτη μεγαλύτερη συμβολή για τα πακέτα καυσίμου που εισάγονται πρώτα στον κύλινδρο και απότομη πτώση για τα πακέτα καυσίμου στις ζώνες που σχηματίζονται στο τέλος. Αυτό είναι φυσιολογικό καθώς οι ζώνες που σχηματίζονται πρώτα θα επιτύχουν υψηλότερη διείσδυση στο θάλαμο καύσης και η εισχώρηση του μείγματος αέρα καυσαερίου στον κύλινδρο θα είναι μεγαλύτερη. Για τις υπόλοιπες ζώνες που βρίσκονται εντός του κύριου όγκου της ζώνης καύσης, ο συνδυασμός των φρέσκων προϊόντων καύσης και των ανακυκλοφορούντων αερίων θα οδηγήσει σε χαμηλές τιμές λ και θα εμποδίσει το σχηματισμό NO. Μία ενδεικτική απεικόνιση της κατανομής του λόγου ισοδυναμίας καυσίμου αέρα για λειτουργία με και χωρίς EGR 5^o μετά την έγχυση δίνεται στην Εικόνα 4-23 και Εικόνα 4-24.

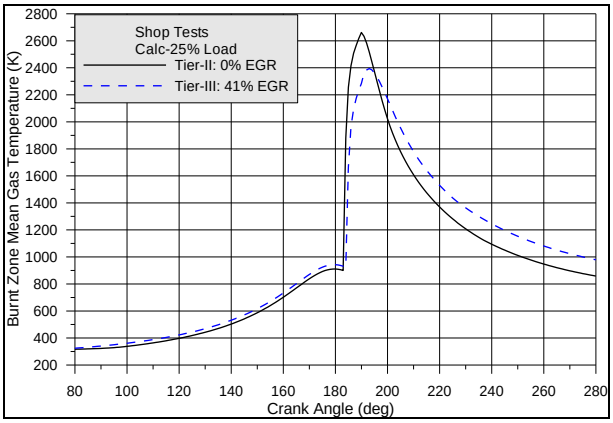

Εικόνα 4-19 Υπολογισμένη μέση θερμοκρασία ζώνης καύσης, Tier-II & Tier-III, 25% φορτίο

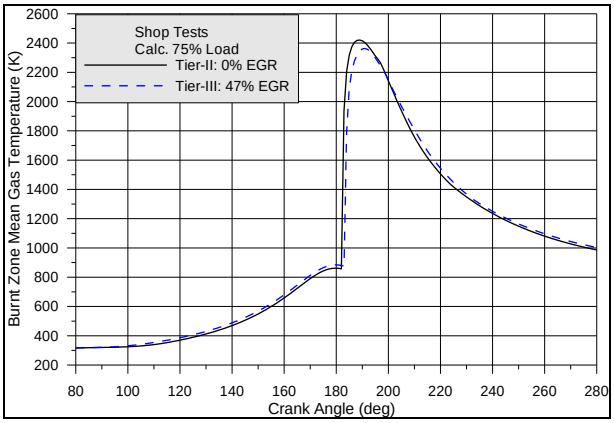

Εικόνα 4-20 Υπολογισμένη μέση θερμοκρασία ζώνης καύσης, Tier-II & Tier-III, 75% φορτίο

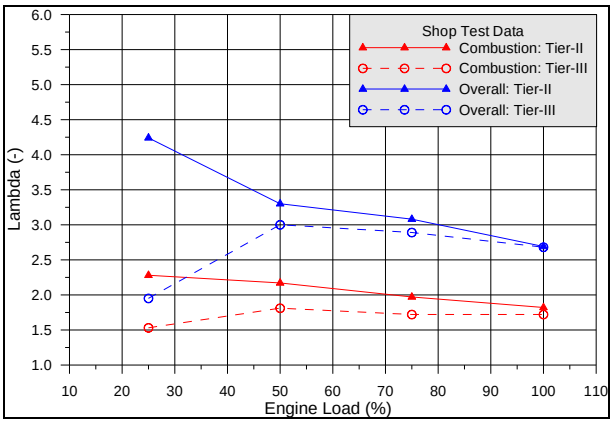

Εικόνα 4-21 Υπολογισμένος λόγος ισοδυναμίες, συνολικά και στη ζώνη καύσης, Tier-II & Tier-III

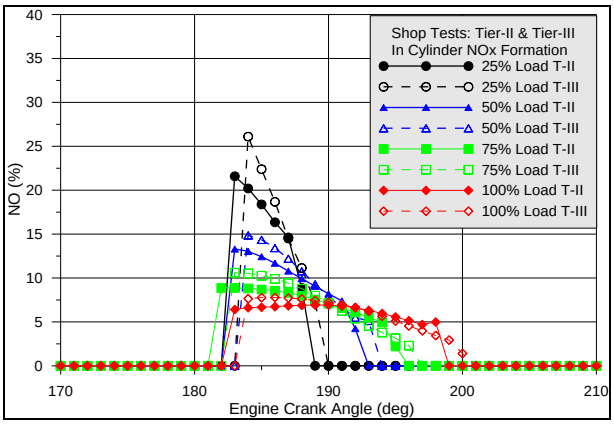

Εικόνα 4-22 Σύγκριση υπολογισμένης συμβολής ανά ζώνη στο σχηματισμό NO, Tier-II & Tier-III

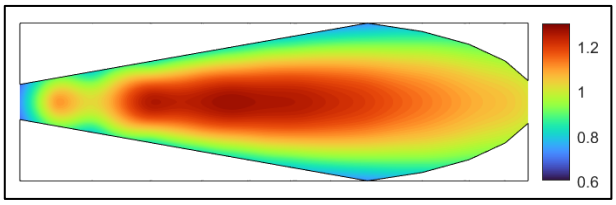

Εικόνα 4-23 Κατανομή λόγου ισοδυναμίας καυσίμου αέρα στη δέσμη 5° μετά την έγχυση, 75% φορτίο με EGR

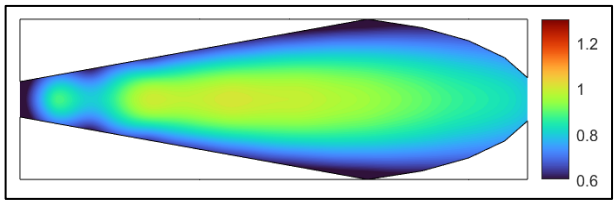

Εικόνα 4-24 Κατανομή λόγου ισοδυναμίας καυσίμου αέρα στη δέσμη 5° μετά την έγχυση, 75% φορτίο χωρίς EGR

4.4.2 Παραμετρική ανάλυση με χρήση του πολυζωνικού μοντέλου καύσης

Τέλος πραγματοποιήθηκε μια παραμετρική ανάλυση για να εξεταστεί η δυνατότητα μείωσης της αύξησης του BSFC κατά τη χρήση EGR μέσω αλλαγών στο χρονισμό έγχυσης. Στην Εικόνα 4-25 παρουσιάζεται η επιτευχθείσα μείωση BSFC. Η αλλαγή στον χρονισμό δίνεται στην Εικόνα 4-26 και η απαιτούμενη αύξηση του λόγου EGR, για διατήρηση χαμηλών εκπομπών NO_x, στην Εικόνα 4-27. Κατά μέσο όρο, θα απαιτηθεί 5% αύξηση του λόγου EGR. Η επίδραση της προπορείας στις τιμές P_{max} παρουσιάζεται στην Εικόνα 4-28. Η αύξηση της πίεσης σε σύγκριση με τις τιμές αναφοράς είναι αρκετά υψηλή, κυρίως σε χαμηλό φορτίο. Γενικά υπάρχει ελάχιστο περιθώριο για αύξηση της πίεσης και περαιτέρω αύξηση του ποσοστού EGR δεν είναι δυνατή. Η επίδραση της αυξημένης προπορείας και του ποσοστού EGR στη θερμοκρασία της ζώνης καύσης ελέγχθηκε και οι αλλαγές που βρέθηκαν ήταν πολύ χαμηλές, καθώς το αυξημένο ποσοστό EGR περιόρισε τις επιπτώσεις της αλλαγής προπορείας, Εικόνα 4-29. Οι αλλαγές χρονισμού δεν επηρέασαν σημαντικά το λόγο αέρα καυσίμου τόσο στον μέσο όρο του κυλίνδρου και εντός της καμένης ζώνης.

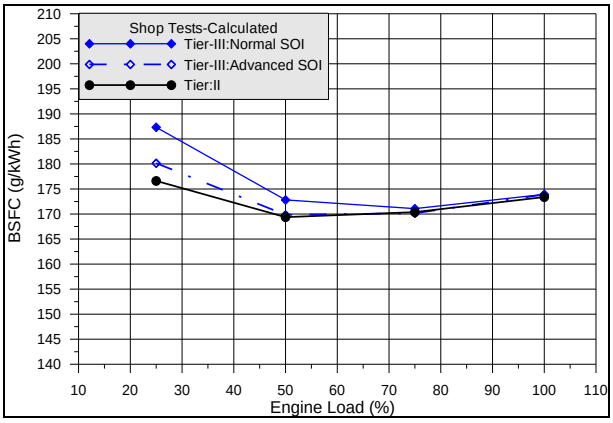

Εικόνα 4-25 BSFC after SOI advance comparison to reference SOI timing Tier-III & Tier-II values; model calculation results

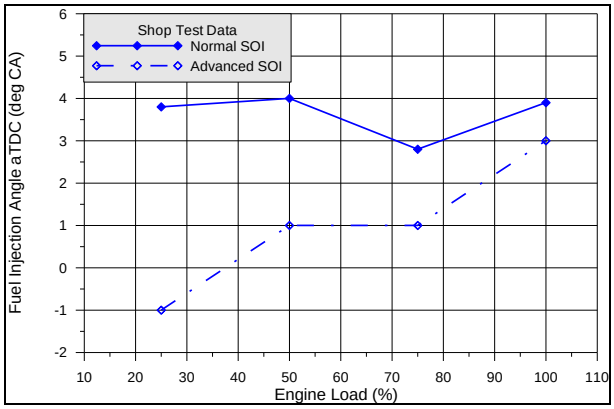

Εικόνα 4-26 SOI advance estimated for Tier-III BSFC optimization

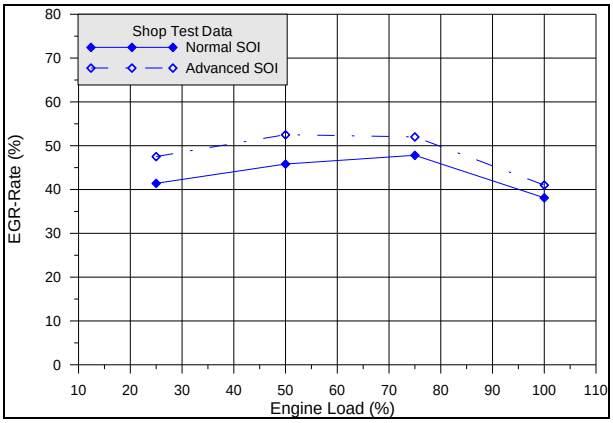

Εικόνα 4-27 EGR rate estimated for Tier-III BSFC optimization via SOI advance

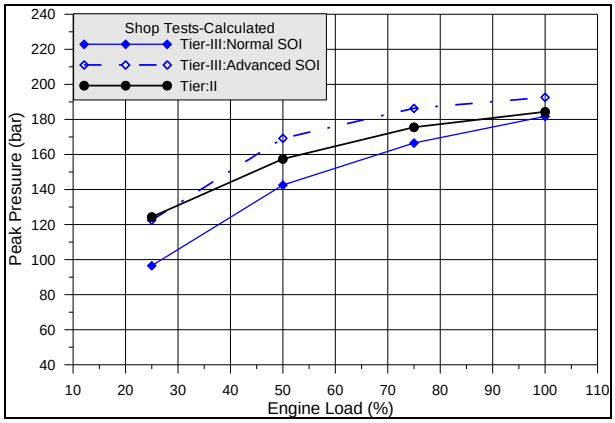

Εικόνα 4-28 Calculated effect of SOI advance on P_{max}, comparison to reference tuning Tier-III & Tier-II values; calculation results

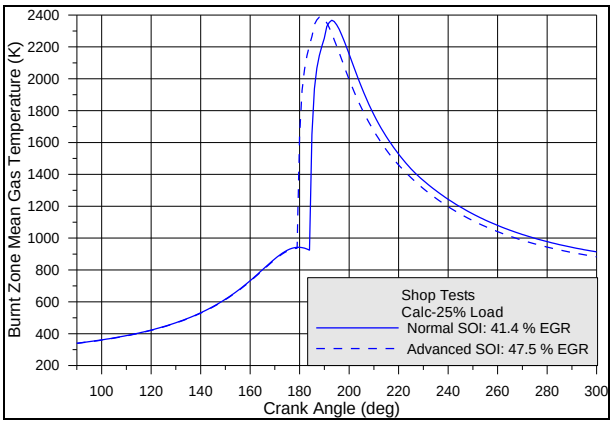

Εικόνα 4-29 Estimated effect of Tier-III SOI advance on burnt zone average temperature; 25% Load

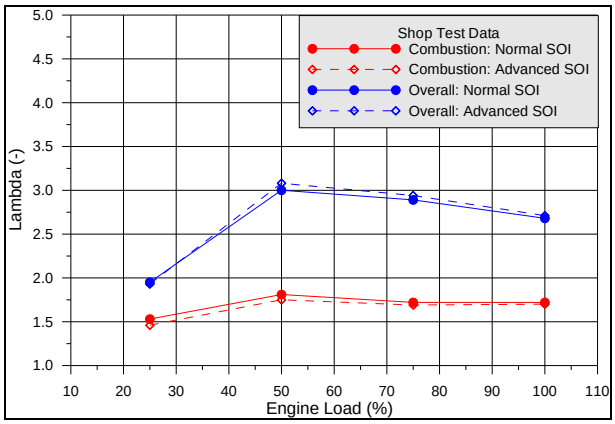

Εικόνα 4-30 Estimated effect of Tier-III SOI advance on overall and burnt zone air-fuel equivalence ratio

5. Επιλεκτική καταλυτική αναγωγή για έλεγχο εκπομπών NO_x σε δίχρονους ναυτικούς κινητήρες

5.1 Υλοποίηση του συστήματος σε ναυτικές μηχανές

Το σύστημα SCR χρησιμοποιεί αμμωνία αποθηκευμένη σε διάλυμα ουρίας νερού και τη χρήση ειδικού καταλύτη για την αποδόμηση των επιβλαβών NO σε N_2 και νερό. Υπάρχουν δύο τύποι εγκατάστασης συστήματος SCR σε ναυτικούς κινητήρες ανάλογα με τη θέση του καταλύτη, πριν ή μετά τον υπερσυμπιεστή, (55), και χαρακτηρίζονται υψηλής πίεσης (HP) και χαμηλής πίεσης (LP) αντίστοιχα. Η κύρια διαφορά μεταξύ τους είναι η ελάχιστη θερμοκρασία καυσαερίων και η μέγιστη περιεκτικότητα σε θείο καυσίμου που μπορεί να χρησιμοποιηθεί, (67). Τα συστήματα HP-SCR μπορούν να λειτουργήσουν με καύσιμα υψηλότερης περιεκτικότητας σε θείο, αλλά τέτοιες εφαρμογές είναι σχετικά ασυνήθιστες λόγω ανησυχιών σχετικά με την διάρκεια ζωής του καταλύτη. Για χαμηλές θερμοκρασίες η παρουσία θείου στα καυσαέριά δημιουργεί επικαθήσεις στα καταλυτικά στοιχεία μειώνοντας την απόδοση της καταλυτικής αντίδρασης. Τα συστήματα HP συνιστώνται για μεγάλους δίχρονους κινητήρες που έχουν χαμηλές θερμοκρασίες καυσαερίων λόγω της διαδικασίας της σάρωσης και της χαμηλής αναλογίας καυσίμου-αέρα, (68). Και σε αυτή την περίπτωση όμως στα χαμηλά φορτία η θερμοκρασία των καυσαερίων μπορεί να είναι χαμηλότερη από την ιδανική. Οι κινητήρες με συστήματα HP-SCR είναι συνήθως εξοπλισμένοι με βαλβίδα παράκαμψης αέρα από τον κύλινδρο (CBV), (55). Με το άνοιγμα της CBV, μέρος του αέρα εισόδου παρακάμπτεται στην πολλαπλή εξαγωγής, μειώνοντας τη μάζα αέρα στον κύλινδρο με αποτέλεσμα την αύξηση της θερμοκρασίας. Το κύριο μειονέκτημα των συστημάτων HP είναι ότι με την τοποθέτησή τους αυξάνεται το έργο εξώθησης και μειώνεται η απόδοση του στροβίλου, αυξάνοντας την κατανάλωση καυσίμου (69,70). Η εφαρμογή LP-SCR είναι πιο κατάλληλη για τις τετράχρονες γεννήτριες καθώς η θερμοκρασία των καυσαερίων τους είναι υψηλή, (68). Η επίδραση στην κατανάλωση καυσίμου είναι ελάχιστη σε αυτό το σύστημα. Αυτή η εφαρμογή χρησιμοποιείται σπάνια σε δίχρονους κινητήρες. Το σύστημα απαιτεί τη χρήση καυσίμου πολύ χαμηλής περιεκτικότητας σε θείο, και αλλαγές στη ρύθμιση του κινητήρα για να αυξηθεί η θερμοκρασία των καυσαερίων, (55). Μία κοινή τεχνική είναι η παράκαμψη καυσαερίων πριν το στρόβιλο για την αύξηση της θερμοκρασίας στην είσοδο του καταλύτη, (55,69) μέσω EGB.

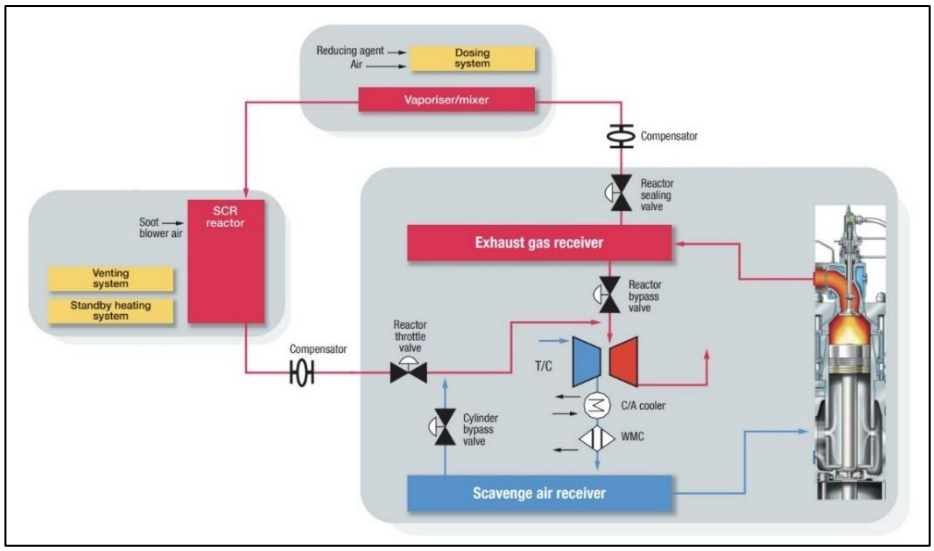

Εικόνα 5-1 Σχηματικό διάγραμμα δίχρονου κινητήρα με σύστημα SCR χαμηλής πίεσης, MAN Energy Solutions, (55)

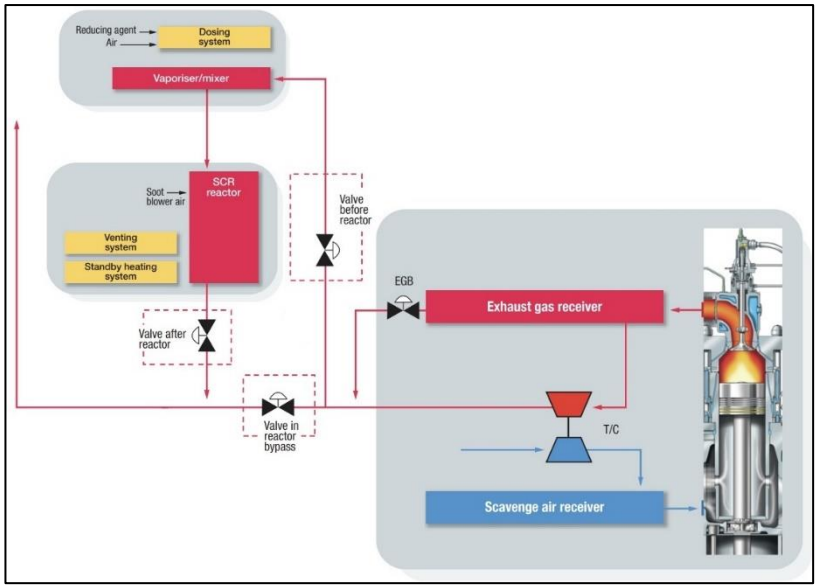

Εικόνα 5-2 Σχηματικό διάγραμμα δίχρονου κινητήρα με σύστημα SCR υψηλής πίεσης, MAN Energy Solutions, (55)

Οι εξεταζόμενοι κινητήρες έχουν τα παρακάτω λειτουργικά στοιχεία, Πίνακας 5-1.

Πίνακας 5-1 Χαρακτηριστικά κινητήρων με SCR

Κινητήρας SCR-LP	**Τιμή**	**Κινητήρας SCR-HP**	**Τιμή**
Μοντέλο	7G80ME-C9.5	Μοντέλο	6G70ME-C9.5
Τύπος	Δίχρονος	Τύπος	Δίχρονος
Αρ. Κυλίνδρων	7	Αρ. Κυλίνδρων	6
Διάμετρος (mm)	800	Διάμετρος (mm)	700
Διαδρομή (mm)	3720	Διαδρομή (mm)	3256
Ον. Ταχύτητα (rpm)	72.0	Ον. Ταχύτητα (rpm)	75.0
Ον. Ισχύς (kW)	26,890	Ον. Ισχύς (kW)	15,745
Τύπος SCR	Χαμηλής πίεσης με EGB	Τύπος SCR	Υψηλής πίεσης με CBV

5.2 Επίδραση του συστήματος LP-SCR στη λειτουργία και απόδοση του κινητήρα

Από τη σύγκριση λειτουργία με και χωρίς SCR, Tier-II και Tier-III αντίστοιχα, εντοπίζεται μεγάλη διαφορά όσον αφορά το λόγο πιέσεων, με αύξηση συμπίεσης λόγω νωρίτερου EVC, Εικόνα 5-3. Αυτό έγινε κυρίως για να αντισταθμιστεί η επίδραση της μειωμένης πίεσης σάρωσής και χαμηλότερης συνολικής μάζας στον κινητήρα, Εικόνα 5-4. Η χαμηλότερη μάζα στους κυλίνδρους και οι παρόμοιες τιμές πίεσης οδηγούν σε αυξημένη θερμοκρασία, Εικόνα 5-5, για ασφαλή λειτουργία του καταλύτη. Η επίδραση του καυσαερίου που παρακάμπτει τον στρόβιλο μέσω του EGB, οδηγεί σε πρόσθετη αύξηση. Η αύξηση της θερμοκρασίας του καυσαερίου ήδη από εντός κυλίνδρου επιτρέπει την επίτευξη της απαιτούμενης θερμοκρασίας με χαμηλότερο ποσοστό καυσαερίων να παρακάμπτει τον στρόβιλο και περιορίζεται η απώλεια έργου. Επιτυγχάνεται σημαντική αύξηση της θερμοκρασίας των καυσαερίων μετά το στρόβιλο, ειδικά σε χαμηλό φορτίο. Οι παραπάνω αλλαγές επηρεάζουν τη συνολική απόδοση του κινητήρα και η επίδραση εκτιμάται από την αλλαγή στην ειδική κατανάλωση καυσίμου. Εντοπίζεται αύξηση BSFC κατά τη λειτουργία του SCR, η οποία αυξάνεται με το φορτίο. Αυτό οφείλεται στο άνοιγμα της EGB και την πτώση πίεσης εντός του καταλύτη που αυξάνει με το φορτίο και ροή μάζας. Η αύξηση του BSFC είναι γενικά μεταξύ, 1,0 – 2,0 g/kWh και σχεδόν μηδενική σε χαμηλό φορτίο.

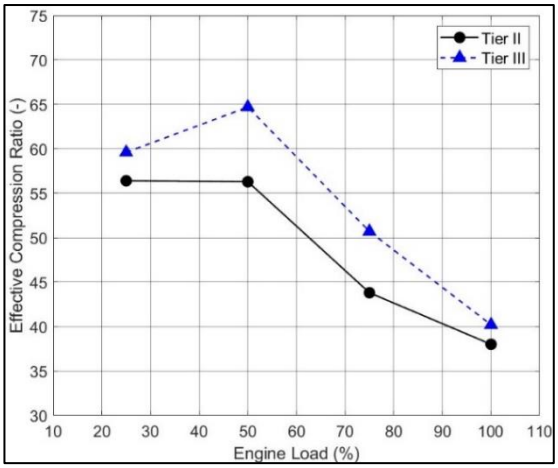

Εικόνα 5-3 Λόγος πιέσεων Tier-II & Tier-III; LP-SCR

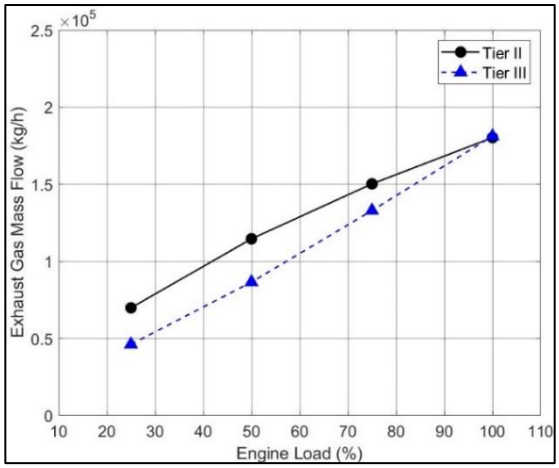

Εικόνα 5-4 Ροή μάζας καυσαερίων, Tier-II & Tier-III; LP-SCR System

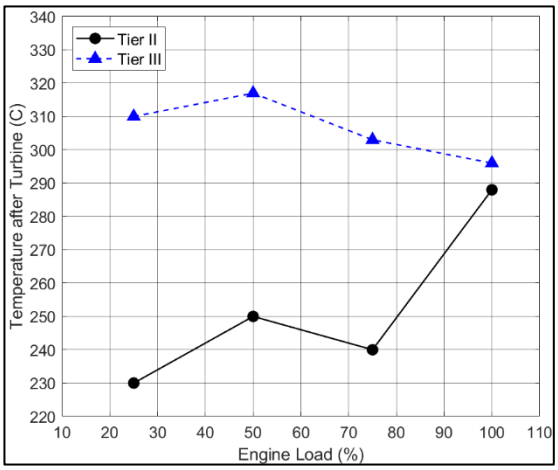

Εικόνα 5-5 Θερμοκρασία καυσαερίων μετά το στρόβιλο; LP-SCR

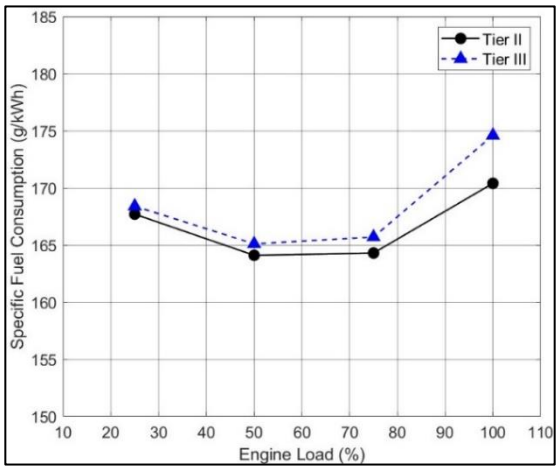

Εικόνα 5-6 Ειδική κατανάλωση καυσίμου, Tier-II & Tier-III; LP- SCR

5.2.1 Επίδραση του συστήματος LP-SCR στις εκπομπές NO_x

Η απόδοση του καταλύτη στη μείωση των NO_x δίνεται στην Εικόνα 5-7. Το επίπεδο μείωσης των NOx κυμαίνεται μεταξύ 68% και 80%. Η μειωμένη απόδοση στα χαμηλά φορτία τονίζει τις προκλήσεις χρήσης ενός συστήματος LP-SCR σε δίχρονο κινητήρα λόγω χαμηλών θερμοκρασιών. Για τη χρήση SCR, η απαιτούμενη κατανάλωση διαλύματος ουρίας έχει μεγάλη σημασία, καθώς η τιμή της μπορεί να πλησιάσει αυτή του HFO. Η ειδική κατανάλωση ουρίας κυμαίνεται μεταξύ 24 – 10 g/kWh ανάλογα με το φορτίο του κινητήρα, όπως φαίνεται στην Εικόνα 5-8 και είναι ιδιαίτερα υψηλή σε χαμηλό και μέσο φορτίο.

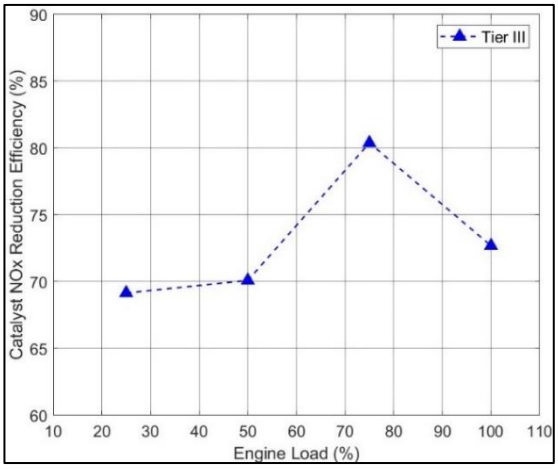

Εικόνα 5-7 Απόδοση καταλύτη στη μείωση NO_x; LP-SCR

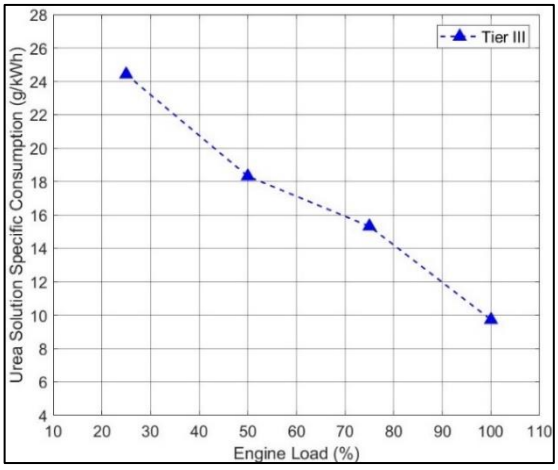

Εικόνα 5-8 Ειδική κατανάλωση διαλύματος ουρίας; LP-SCR

5.3 Επίδραση του συστήματος HP-SCR στη λειτουργία και απόδοση του κινητήρα

Οι βασικές λειτουργικές τιμές και οι ρυθμίσεις λειτουργίας δεν παρουσίασαν πρακτικά καμία μεταβολή για λειτουργία με και χωρίς SCR. Το μόνο σημείο διαφοράς εντοπίστηκε στο χαμηλό φορτίο με το άνοιγμα της CBV. Με χρήση της CBV χαμηλότερη μάζα παγιδεύεται στον κύλινδρο σε παρόμοιες τιμές πίεσης με αποτέλεσμα την αύξηση θερμοκρασίας των καυσαερίων. Οι τιμές θερμοκρασίας εισόδου καταλύτη για λειτουργία με και χωρίς SCR, δίνονται στην Εικόνα 5-9. Για φορτίο 25% η θερμοκρασία των καυσαερίων αυξάνεται σημαντικά λόγω μερικού ανοίγματος της CBV. Επίσης, φαίνεται πως οι τιμές εισόδου στον καταλύτη για το HP-SCR είναι σημαντικά μεγαλύτερες από ότι για το LP-SCR. Η αύξηση της ειδικής κατανάλωσης δίνεται στην Εικόνα 5-10 και είναι χαμηλή, 1.5% κατά μέσο όρο, αλλά είναι μεγαλύτερη από ότι στο σύστημα LP-SCR εξαιτίας μεγαλύτερης πτώσης πίεσης στον καταλύτη. Στο φορτίο 25% περαιτέρω αύξηση εντοπίζεται λόγω ανοίγματος της CBV.

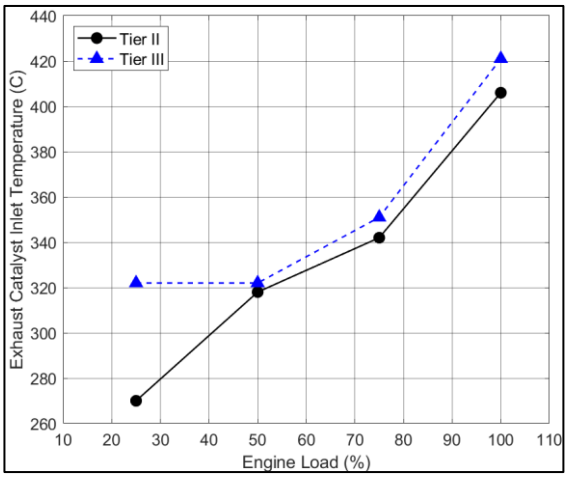

Εικόνα 5-9 Θερμοκρασία καυσαερίων μετά το στρόβιλο, Tier-II & Tier-III; HP SCR

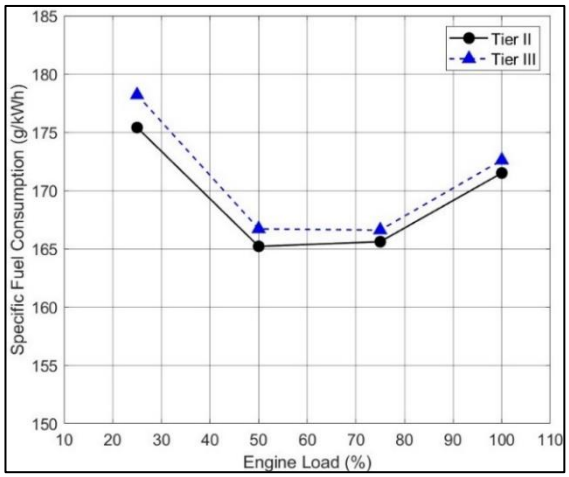

Εικόνα 5-10 Ειδική κατανάλωση καυσίμου, Tier-II vs Tier-III; HP-SCR

5.4 Επίδραση του συστήματος HP-SCR στις εκπομπές NO_x

Η απόδοση του καταλύτη δίνεται στην Εικόνα 5-11. Το επίπεδο μείωσης των NOx κυμαίνεται μεταξύ 75% και 88%. Η μείωσης των εκπομπών NO_x είναι βελτιωμένη σε σχέση με τις δοκιμές LP-SCR, αλλά και τα αποτελέσματα των κινητήρων με EGR. Η ειδική κατανάλωση ουρίας δίνεται στην Εικόνα 5-12. Παρά την αυξημένη θερμοκρασία, η κατανάλωση διαλύματος ουρίας δεν παρουσιάζει βελτιώσεις σε σύγκριση με το σύστημα LP-SCR. Η μέση απαίτηση ουρίας των συστημάτων HP δεν διέφερε σημαντικά από το LP. Μια πιθανή διαφορά στο λειτουργικό κόστος θα μπορούσε να προέλθει από η διάρκεια ζωής του καταλύτη LP σε σύγκριση με τους HP, λόγω των χαμηλότερων τιμών θερμοκρασίας του καυσαερίου. Η μέση διάρκεια ζωής που αναμένεται γενικά είναι τρία έως πέντε χρόνια, (23,55,69). Ένα πλεονέκτημα των συστημάτων HP-SCR είναι η δυνατότητα λειτουργίας με καύσιμα υψηλότερης περιεκτικότητας σε θείο, τα οποία είναι σημαντικά χαμηλότερα σε τιμή. Σε αυτήν την περίπτωση, θα πρέπει να ληφθεί υπόψη το πρόσθετο κόστος λειτουργίας ενός συστήματος πλυντρίδας καυσαερίων (scrubber). Στη διάρκεια δοκιμών εν πλω έγιναν περαιτέρω μετρήσεις σε μηχανές με HP-SCR, σε μία περίπτωση με χρήση HFO. Στην Εικόνα 5-13 παρέχεται η απόδοση του καταλύτη με χρήση HFO, η οποία βρέθηκε μειωμένη σε σύγκριση με τα τεστ MGO. Η αποτελεσματικότητα των άλλων συστημάτων HP-SCR που δοκιμάστηκαν εν πλω (MGO) δίνεται στην Εικόνα 5-14. Για όλες τι δοκιμές οι απόδοση του καταλύτη ήταν μειωμένη σε σχέση με τις μετρήσεις σε εργοστασιακό περιβάλλον. Για το σύστημα με HFO η μείωση ήταν αισθητά μεγαλύτερη.

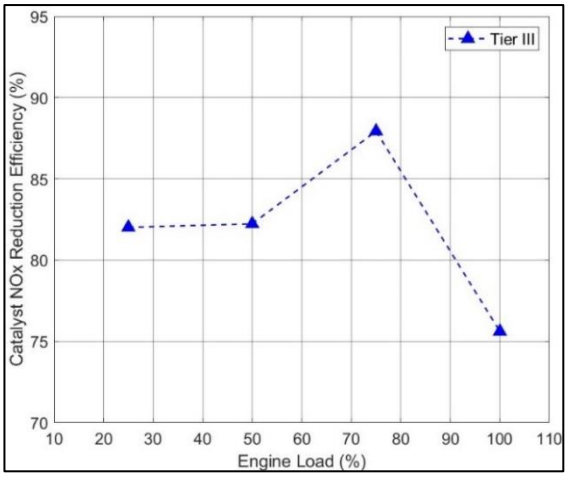

Εικόνα 5-11 Απόδοση καταλύτη στη μείωση NO_x; HP-SCR

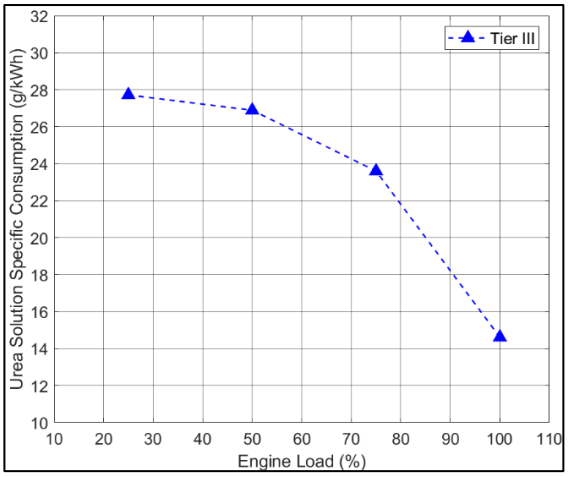

Εικόνα 5-12 Ειδική κατανάλωση ουρίας; HP-SCR

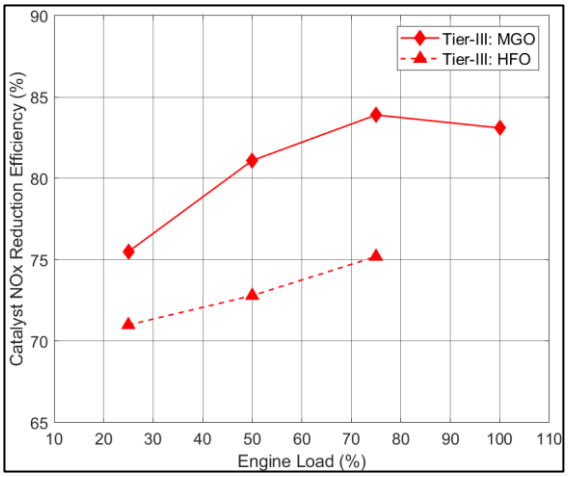

Εικόνα 5-13 Ειδική κατανάλωση ουρίας κατά τη χρήση MGO & HFO; HP-SCR

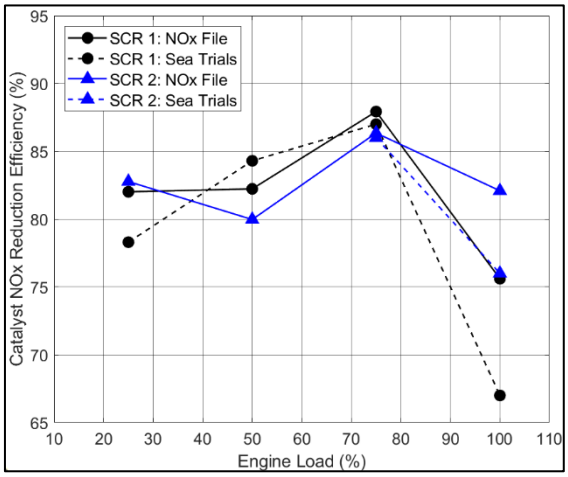

Εικόνα 5-14 Απόδοση καταλύτη στη μείωση NO_x Tier-III, σύγκρισή εργοστασιακών τιμών και δοκίμων εν πλω; HP-SCR

5.5 Συγκριτική ανάλυση συστημάτων EGR & SCR για δίχρονο κινητήρα

Γίνεται σύγκριση μεταξύ των συστημάτων SCR και EGR, με βάση την επίδραση στη λειτουργία του κινητήρα, το κόστος εγκατάστασης και κυρίως το λειτουργικό κόστος. Το SCR έχει μικρή επίδραση στην γενική λειτουργία και την απόδοση των κινητήρων. Το EGR επιφέρει μεγάλες μεταβολές στη λειτουργία και σημαντική αύξηση κατανάλωσης ειδικά σε χαμηλό και μεσαίο φορτίο. Εκτεταμένη βιβλιογραφική έρευνα έδειξε παρόμοιο κόστος εγκατάστασης, που είναι χαμηλότερο για το SCR σε μικρές μηχανές, και αυξάνεται άνω του κόστους EGR σε εγκαταστάσεις μεγάλης ισχύος, (24,71–74). Τέλος με χρήση των μετρημένων καταναλώσεων καυσίμου και τα σημερινά δεδομένα τιμών διαλύματος ουρίας και ναυτικών καυσίμων υπολογίστηκε πως το βασικό κόστος λειτουργίας θα κυμαίνεται από ελαφρώς μεγαλύτερο έως διπλάσιο για το SCR σε σχέση με το EGR. Αυτό ήταν σε συμφωνία με άλλες έρευνες πάνω στο θέμα που όμως χρησιμοποίησαν διαφορετική προσέγγιση και παλαιότερα δεδομένα τιμών (24,72,75,76). Σε αυτά πρέπει να προστεθεί και το κόστος ανανέωσης καταλυτικών στοιχείων κάθε 3 – 5 έτη που αυξάνει περαιτέρω το κόστος, (23,69) με τελικό σημαντικό πλεονέκτημα για το EGR από οικονομική σκοπιά. Παρόλα αυτά το πλεονέκτημα της απλότητας και ελάχιστης επίδρασης στη λειτουργία του κινητήρα για το σύστημα SCR δεν είναι αμελητέο.

Σύνοψη

Μελετήθηκαν τεχνολογίες μείωσης εκπομπών CO_2 και NO_x για ναυτικούς κινητήρες που λειτουργούν με υγρά και αέρια καύσιμα. Η βάση για την έρευνα ήταν δεδομένα μετρήσεων, και συνοδεύτηκαν από περαιτέρω ανάλυση με τη χρήση πολυζωνικού μοντέλου για την προσομοίωση καύσης. Συνολικά 19 κινητήρες μελετήθηκαν, οι περισσότεροι δίχρονοι κινητήρες πρόωσης. Εξετάστηκαν δύο τεχνικές μείωσης για κάθε ρύπο. Για το CO_2 βιοκαύσιμα και υγροποιημένο φυσικό αέριο, και για τον έλεγχο των NO_x ανακύκλωση καυσαερίων και εκλεκτική καταλυτική αναγωγή.

Η χρήση βιοκαυσίμων εξετάστηκε σε δίχρονους και τετράχρονους κινητήρες χρησιμοποιώντας B30, και με συνοδευτικές μετρήσεις με τυπικά ναυτικά καύσιμα. Ελάχιστη επίδραση βρέθηκε στην απόδοση του κινητήρα και στη διαδικασία καύσης, με μια μικρή αύξηση κατανάλωσης, μεγαλύτερη στην περίπτωση των τετράχρονων κινητήρων. Μετρήθηκε αύξηση στις εκπομπές NO_x, που αποδόθηκε στο αυξημένο περιεχομένου του B30 σε O_2 βάσει ανάλυσης των μετρημένων δεδομένων και έρευνας με χρήση του πολυζωνικού μοντέλου. Ο αρνητικός αντίκτυπος στις εκπομπές ήταν μεγαλύτερος για τους τετράχρονους κινητήρες. Για όλους τους κινητήρες, η αύξηση ήταν μέτριου επιπέδου, επιτρέποντας τη λειτουργία εντός των θεσπισμένων ορίων εκπομπών. Αναλύσεις κύκλου ζωής δείχνουν περίπου 25% βελτίωση στις συνολικές εκπομπές άνθρακα χρησιμοποιώντας βιοκαύσιμο.

Η μελέτη χρήσης LNG πραγματοποιήθηκε σε κινητήρες διπλού καυσίμου, δύο συνεχόμενων γενεών, με έγχυση του αερίου σε υψηλή πίεση για λειτουργία μόνο με πετρέλαιο και με χρήση πετρελαίου και αερίου. Βρέθηκε ότι ο προηγούμενης γενεάς κινητήρας ήταν ικανός για σχεδόν ίδια απόδοση μεταξύ των δύο τρόπων λειτουργίας. Η ποσότητα πιλοτικής έγχυσης πετρελαίου που απαιτείται για λειτουργία ΦΑ ήταν χαμηλή. Η κυριότερη διαφορά κατά τη λειτουργία ΦΑ ήταν υψηλότερος αρχικός και μέγιστος ρυθμός καύσης. Η ρύθμιση του κινητήρα αυτού είχε ως στόχο να ελαχιστοποιηθούν οι διαφορές μεταξύ λειτουργίας ενός και δύο καυσίμων. Στον κινητήρα νέας γενεάς μετρήθηκε σημαντική μείωση της απαιτούμενη ποσότητας πιλοτικής έγχυσης. Η οικονομία καυσίμου ήταν σημαντικά καλύτερη κατά τη χρήση ΦΑ. Τα παραπάνω αποδόθηκαν σε βελτιώσεις στο σχεδιασμό του εγχυτήρα και σε διαφορετική ρύθμιση του κινητήρα. Η επίδραση των προηγουμένων στην καύση ήταν εμφανής, με πολύ υψηλότερο ρυθμό καύσης προανάμειξης. Οι εκπομπές NO_x ήταν σχετικά κοντά για τους δύο τρόπους λειτουργίας και κατά τη λειτουργία ΦΑ επηρεάστηκαν από τη μορφή και χρονισμό της πιλοτικής έγχυσης, τις μέγιστες τιμές πίεσης και τη χαμηλότερη θερμοκρασία φλόγας του μεθανίου. Το οφέλη στις εκπομπές CO_2 ήταν περίπου 23% και για τους δύο κινητήρες. Η βελτίωση γενεάς προς γενεά ήταν 7%.

Το EGR δοκιμάστηκε σε έναν δίχρονο κινητήρα πετρελαίου και έναν ΦΑ. Η ανακυκλοφορία καυσαερίων είχε μεγάλη επίδραση στο μηχανισμό καύσης. Ο ρυθμός ήταν πιο αργός και η διάρκειά της αυξήθηκε και στους δύο κινητήρες. Απαιτήθηκαν σημαντικές αλλαγές στη ρύθμιση του κινητήρα. Η επίδραση στο μηχανισμό καύσης οδήγησε σε αύξηση της κατανάλωσης, περίπου 5% για τον κινητήρα με πετρέλαιο και 4% για τον κινητήρα αερίου. Η συνολική αποδοτικότητα μείωσης NO_x ήταν κοντά στο 80%. Δεν βρέθηκε σημαντική διαφορά μεταξύ του κινητήρα αερίου και του κινητήρα πετρελαίου. Το ποσοστό EGR εκτιμήθηκε χρησιμοποιώντας το πολυζωνικό μοντέλο. Τα αποτελέσματα έδειξαν υψηλά ποσοστά ανακυκλοφορίας. Βραδυπορεία στην έγχυση καυσίμου συνέβαλλε στη μείωση του σχηματισμού NO_x. Θεωρητική έρευνα διεξήχθη χρησιμοποιώντας το μοντέλο για διερεύνηση του μηχανισμού μείωσης των NO_x όταν χρησιμοποιείται EGR. Πραγματοποιήθηκε επίσης θεωρητική ανάλυση για τη μείωση της κατανάλωση καυσίμου κατά τη χρήση EGR.

Το SCR δοκιμάστηκε σε δύο διαμορφώσεις πριν και μετά το στρόβιλο σε δίχρονους κινητήρες. Η επίδραση στη λειτουργία του κινητήρα ήταν ελάχιστη, πλην αύξησης της κατανάλωσης καυσίμου περίπου κατά 1.5%. Επιβεβαιώθηκαν απαιτήσεις αλλαγής ρυθμίσεων για αύξηση της θερμοκρασίας εισαγωγής αερίου στον καταλύτη, που συνέβαλαν στην αύξηση της κατανάλωσης. Αξιολογήθηκε η χρήση καταλύτη ικανού να λειτουργεί με βαρύ καύσιμο. Η απόδοση της μείωσης των NO_x ήταν καλή, 85% και 80% για τον καταλύτη πριν και μετά τον στρόβιλο αντίστοιχα. Η κατανάλωση ουρίας ήταν υψηλή, κατά μέσο όρο 18 g/kWh. Αυτό θα οδηγήσει σε υψηλό κόστος λειτουργίας του συστήματος. Σύγκριση μεταξύ EGR και SCR έδειξε σημαντικά υψηλότερο κόστος του συστήματος SCR με βάση τις σύγχρονες τάσεις των τιμών καυσίμων και ουρίας, και

λαμβάνοντας επίσης υπόψη την απαίτηση αντικατάστασης καταλύτη κάθε λίγα χρόνια. Συνολικά, οι τεχνολογίες που διερευνήθηκαν διαπιστώθηκε ότι παρέχουν απτά οφέλη στη μείωση των εκπομπών, ενώ είναι αρκετά ώριμες για τρέχουσα χρήση ενώ ορισμένες έχουν επίσης σημαντικές προοπτικές για μελλοντική εξέλιξη.

Βασικές Συνεισφορές Διατριβής

Συνολικά, παρασχέθηκε μια ουσιαστική συμβολή στο αντικείμενο μελέτης, συμπεριλαμβανομένων τόσο ποιοτικών όσο και ποσοτικών ευρημάτων που μπορούν επίσης να χρησιμοποιηθούν ως βάση ή κατευθυντήρια γραμμή για μελλοντικές εφαρμογές και αναλύσεις.

Μεθοδολογία

Για τους ναυτικούς κινητήρες τα δεδομένα από δοκιμές σε πλήρη κλίμακα είναι εξαιρετικά περιορισμένα στη βιβλιογραφία, καθώς ο προγραμματισμός δοκιμών επί των πλοίων και κατά τη διαδικασία εργοστασιακών δοκιμών παρουσιάζει πολλαπλές δυσκολίες. Για το λόγο αυτό, σχεδιάστηκε μια απλοποιημένη διαδικασία μέτρησης δεδομένων απόδοσης και εκπομπών. Η διεξαγωγή των μετρήσεων επέτρεψε στην ανάλυση να βασίζεται σε πραγματικά δεδομένα και όχι εκτιμήσεις από προσομοιωτές όπως συνήθως, ενώ παρείχε πληροφορίες για τους συμβιβασμούς που απαιτούνται στη ρύθμιση των κινητήρων αυτών σε βαθμό μη δυνατό από προσομοιώσεις. Επίσης, επέτρεψε να ληφθούν υπόψη τα προηγούμενα στη θεωρητική ανάλυση ώστε να παρέχει ακριβέστερες πληροφορίες για τους μηχανισμούς που εμπλέκονται και επηρεάζουν τις επιλογές του εκάστοτε κατασκευαστή.

Καύσιμα χαμηλού αποτυπώματος άνθρακα

Η χρήση πραγματικών δεδομένων για λειτουργία μονού (ντίζελ) και διπλού καυσίμου (ντίζελ και LNG) και η άμεση σύγκρισή τους, επέτρεψαν ακριβείς εκτιμήσεις για τις εκπομπές CO_2 και τα αναμενόμενα οφέλη της χρήσης LNG. Επιπλέον, αποκτήθηκαν πληροφορίες για τον μηχανισμό καύσης και τις ιδιαίτερες απαιτήσεις σε ρυθμίσεις. Η μελέτη κινητήρων διαδοχικής γενιάς παρείχε πληροφορίες για βελτιώσεις και σημαντικές αλλαγές που μπορούν να αναμένονται από αυτή την τεχνολογία. Οι πληροφορίες για δίχρονους κινητήρες ναυτικού διπλού καυσίμου είναι σπάνιες στη διαθέσιμη βιβλιογραφία, ειδικά για μηχανές έγχυσης αερίου σε υψηλή πίεση και για αναλύσεις που βασίζονται σε πραγματικές μετρήσεις. Η έρευνα που διενεργήθηκε για τα βιοκαύσιμα καλύπτει σημαντική έλλειψη τεχνικών και θεωρητικών γνώσεων σχετικά με τη χρήση αυτού του τύπου καυσίμου σε κινητήρες πλοίων. Τη στιγμή συγγραφής της αυτή η εργασία παρέχει την πρώτη πλήρη ανάλυση σχετικά με τη χρήση βιοκαυσίμων σε ναυτικούς κινητήρες, με πληροφορίες για την απόδοση, την καύση και τη διαδικασία σχηματισμού NO_x, συνδυάζοντας δεδομένα μετρήσεων και υπολογιστικά αποτελέσματα.

Τεχνολογίες περιορισμού εκπομπών NO_xΤα δεδομένα που συγκεντρώθηκαν επέτρεψαν να εκτιμηθεί ο αντίκτυπός του EGR στην απόδοση του κινητήρα, την καύση και το σχηματισμό NO_x υπό πραγματικές συνθήκες. Οι απαιτήσεις για τη ρύθμιση του κινητήρα αξιολογήθηκαν σε βαθμό που δεν ήταν δυνατός από προσομοιωτές. Τα εργαλεία προσομοίωσης που χρησιμοποιήθηκαν προετοιμάστηκαν με χρήση των δεδομένα αυτών και επέτρεψαν παραμετρικές έρευνες πιο κοντά στις πραγματικές συνθήκες. Οι έρευνες που χρησιμοποιούν δεδομένα μετρήσεων και παρέχουν ανάλυση για την απόδοση και τις εκπομπές είναι σπάνιες στη διαθέσιμη βιβλιογραφία.

Η εκτεταμένη διερεύνηση της χρήσης SCR παρείχε πληροφορίες σχετικά με την επίδραση στη λειτουργία του κινητήρα και τις αλλαγές που απαιτούνται για να επιτευχθεί το ελάχιστο όριο θερμοκρασίας καυσαερίων στον καταλύτη. Συλλέχθηκαν δεδομένα από διάφορες περιπτώσεις για την κατανάλωση ουρίας που αλλάζει σημαντικά με το φορτίο. Παρά τη μεγάλη επίδρασή της στο λειτουργικό κόστος οι περισσότερες έρευνες χρησιμοποιούν μία μέση τιμή στην ανάλυση που δεν είναι αντιπροσωπευτική των αποτελεσμάτων μετρήσεων. Τέλος, οι δοκιμές και ανάλυση περιλαμβάνουν μία από τις πρώτες δοκιμές που έγιναν με HFO σε συστήματα SCR, που είναι μια νέα και αρκετά σπάνια εφαρμογή.

Αναφορές

1. Fridell E. Emissions and Fuel Use in the Shipping Sector. Green Ports: Inland and Seaside Sustainable Transportation Strategies. 2019 Jan 1;19–33.
2. European Commission. Climate Action Committee. 2016 [cited 2023 Mar 20]. p. 6–8 Reducing emissions from the shipping sector. Available from: https://climate.ec.europa.eu/eu-action/transport-emissions/reducing-emissions-shipping-sector_en
3. Boningari T, Smirniotis PG. Impact of nitrogen oxides on the environment and human health: Mn-based materials for the NOx abatement. Curr Opin Chem Eng. 2016 Aug 1;13:133–41.
4. IMO. International Maritime Organization. 2022 [cited 2023 Mar 20]. Initial IMO GHG Strategy. Available from: https://www.imo.org/en/MediaCentre/HotTopics/Pages/Reducing-greenhouse-gas-emissions-from-ships.aspx
5. Dos Santos VA, da Silva PP, Serrano LMV. The Maritime Sector and Its Problematic Decarbonization: A Systematic Review of the Contribution of Alternative Fuels. Energies 2022, Vol 15, Page 3571 [Internet]. 2022 May 13 [cited 2023 May 24];15(10):3571. Available from: https://www.mdpi.com/1996-1073/15/10/3571/htm
6. ICCT. Vision 2050 - International Council on Clean Transportation [Internet]. 2021 [cited 2023 Jul 2]. Available from: https://theicct.org/vision-2050/
7. DNV GL. Energy Transition Outlook 2020 - A global and regional forecast to 2050. Dnv Gl Energy Transition Outlook [Internet]. 2021;306. Available from: https://eto.dnvgl.com/2020/index.html
8. Alternative fuels: the options - DNV [Internet]. [cited 2023 Jul 1]. Available from: https://www.dnv.com/expert-story/maritime-impact/alternative-fuels.html
9. Deniz C, Zincir B. Environmental and economical assessment of alternative marine fuels. J Clean Prod. 2016 Feb 1;113:438–49.
10. Brief History of IMO [Internet]. [cited 2023 Jul 2]. Available from: https://www.imo.org/en/About/HistoryOfIMO/Pages/Default.aspx
11. IMO. 2020 IMO global 0.50 percent fuel sulphur regulation WinGD operation guideline. 2019.
12. Roadmap to Zero Emission from International Shipping Ministry of Land, Infrastructure, Transport and Tourism. 2020;
13. DNV. Maritime Forecast To 2050 - Energy Transition Outlook 2021. Dnv [Internet]. 2021;118. Available from: https://www.naucher.com/wp-content/uploads/2021/09/DNV_Maritime_Forecast_2050_2021-Web.pdf
14. Jeswani HK, Chilvers A, Azapagic A. Environmental sustainability of biofuels: a review.
15. Hoekman SK. Biofuels in the U.S.-Challenges and Opportunities. 2008;
16. Cho HJ, Kim JK, Ahmed F, Yeo YK. Life-cycle greenhouse gas emissions and energy balances of a biodiesel production from palm fatty acid distillate (PFAD). Appl Energy. 2013 Nov 1;111:479–88.
17. Dufour J, Iribarren D. Life cycle assessment of biodiesel production from free fatty acid-rich wastes. Renew Energy. 2012 Feb 1;38(1):155–62.
18. Hansson J, Månsson S, Brynolf S, Grahn M. Alternative marine fuels: Prospects based on multi-criteria decision analysis involving Swedish stakeholders. Biomass Bioenergy. 2019 Jul 1;126:159–73.
19. Ampah JD, Yusuf AA, Afrane S, Jin C, Liu H. Reviewing two decades of cleaner alternative marine fuels: Towards IMO's decarbonization of the maritime transport sector. J Clean Prod. 2021 Oct 20;320:128871.
20. World LNG Report 2022 | IGU [Internet]. [cited 2023 May 17]. Available from: https://www.igu.org/resources/world-lng-report-2022/
21. Biofuels | ClassNK - English [Internet]. [cited 2023 Mar 20]. Available from: https://www.classnk.or.jp/hp/en/info_service/bio/
22. Lloyd's Register. NOx from marine diesel engines using biofuels NOx from marine diesel engines using biofuels [Internet]. 2022 [cited 2023 Mar 20]. Available from: https://www.lr.org/en/reports/nox-from-marine-diesel-engines-using-biofuels/
23. American Burau of Shipping (ABS). ABS Advisory on NOx Tier III Compliance. 2020.
24. DNV GL NOx TIER III Update - DNV [Internet]. [cited 2023 Jun 30]. Available from: https://www.dnv.com/maritime/publications/NOx-TIER-3-Update-download.html
25. Relating short-term measures to IMO's minimum 2050 emissions reduction target - International Council on Clean Transportation [Internet]. [cited 2023 Mar 20]. Available from: https://theicct.org/publication/relating-short-term-measures-to-imos-minimum-2050-emissions-reduction-target/
26. International Maritime Organization. Fourth IMO GHG Study 2020 [Internet]. London; 2021. Available from: https://wwwcdn.imo.org/localresources/en/OurWork/Environment/Documents/Fourth IMO GHG Study 2020 - Full report and annexes.pdf
27. Lloyd's Register. IMO GHG Strategy – What does it mean ? [Internet]. 2018 [cited 2023 Mar 20]. Available from: https://www.lr.org/en/insights/articles/imo-ghg-strategy-what-does-it-mean/
28. Li K, Wu M, Gu X, Yuen KF, Xiao Y. Determinants of ship operators' options for compliance with IMO 2020. Transp Res D Transp Environ. 2020 Sep 1;86:102459.
29. IMO. IMO. 2022 [cited 2023 Mar 20]. Rules on ship carbon intensity and rating system enter into force. Available from: https://www.imo.org/en/MediaCentre/PressBriefings/pages/CII-and-EEXI-entry-into-force.aspx
30. Sou WS, Goh T, Lee XN, Ng SH, Chai KH. Reducing the carbon intensity of international shipping – The impact of energy efficiency measures. Energy Policy. 2022 Nov 1;170:113239.
31. Chuah LF, Mokhtar K, Mhd Ruslan SM, Bakar AA, Abdullah MA, Osman NH, et al. Implementation of the energy efficiency existing ship index and carbon intensity indicator on domestic ship for marine environmental protection. Environ Res. 2023 Apr 1;222:115348.
32. Comer B, Chen C, Rutherford D. Relating short-term measures to IMO ' s minimum 2050 emissions reduction target [Internet]. ICCT Working Paper 2018-13. 2018 [cited 2023 Mar 20]. Available from: https://theicct.org/wp-content/uploads/2021/06/IMO_Short_term_potential_20181011.pdf%0Ahttps://www.theicct.org/sites/default/files/publications/IMO_Short_term_potential_20181011.pdf

33. MAN Diesel & turbo. MAN B&W ME-GI Dual-fuel, low-speed engine [Internet]. Copenhagen: MAN Diesel & Turbo; 2016 [cited 2022 Dec 5]. Available from: https://mandieselturbo.com/docs/default-source/shopwaredocuments/man-b-w-me-giee40ba7d787543c688da0d9c11628006.pdf?sfvrsn=3
34. Lounici MS, Loubar K, Tarabet L, Balistrou M, Niculescu DC, Tazerout M. Towards improvement of natural gas-diesel dual fuel mode: An experimental investigation on performance and exhaust emissions. Energy. 2014 Jan 1;64:200–11.
35. Li M, Zhang Q, Li G, Shao S. Experimental investigation on performance and heat release analysis of a pilot ignited direct injection natural gas engine. Energy. 2015 Oct 1;90:1251–60.
36. Boretti A. Advances in Diesel-LNG Internal Combustion Engines. Applied Sciences [Internet]. 2020;10(4). Available from: https://www.mdpi.com/2076-3417/10/4/1296
37. MAN Energy Solutions. LNGC-optimised designs of ME-GI engines and fuel gas supply systems. Denmark; 2020.
38. Herdzik J. Decarbonization of Marine Fuels—The Future of Shipping. Energies 2021, Vol 14, Page 4311 [Internet]. 2021 Jul 17 [cited 2023 Jul 2];14(14):4311. Available from: https://www.mdpi.com/1996-1073/14/14/4311/htm
39. Woon KS, Phuang ZX, Taler J, Varbanov PS, Chong CT, Klemeš JJ, et al. Recent advances in urban green energy development towards carbon emissions neutrality. Energy [Internet]. 2023;267:126502. Available from: https://www.sciencedirect.com/science/article/pii/S0360544222033886
40. Sims REH, Mabee W, Saddler JN, Taylor M. An overview of second generation biofuel technologies. Bioresour Technol [Internet]. 2010 Mar 1 [cited 2023 Jan 26];101(6):1570–80. Available from: https://linkinghub.elsevier.com/retrieve/pii/S0960852409015508
41. van der Kroft DFA, Pruyn JFJ. A study into the availability, costs and GHG reduction in drop-in biofuels for shipping under different regimes between 2020 and 2050. Sustainability (Switzerland). 2021;13(17).
42. Naik SN, Goud V V., Rout PK, Dalai AK. Production of first and second generation biofuels: A comprehensive review. Renewable and Sustainable Energy Reviews. 2010 Feb 1;14(2):578–97.
43. Graboski MS, Mccormick RL, Alleman TL, Herring AM. The Effect of Biodiesel Composition on Engine Emissions from a DDC Series 60 Diesel Engine: Final Report; Report 2 in a Series of 6. 2003 [cited 2022 Apr 12]; Available from: http://www.osti.gov/bridge
44. CIMAC. Fuel Quality Guide-Ignition and Combustion, 2011. 2011;
45. Pandey RK, Rehman A, Sarviya RM. Impact of alternative fuel properties on fuel spray behavior and atomization. Vol. 16, Renewable and Sustainable Energy Reviews. Pergamon; 2012. p. 1762–78.
46. Chountalas T, Founti M. Effect of Low-Sulfur Fuel on Auxiliary Engine Combustion and Performance. SNAME 7th International Symposium on Ship Operations, Management and Economics, SOME 2021 [Internet]. 2021 Apr 5 [cited 2023 Jan 28]; Available from: /SNAMESOME/proceedings-abstract/SOME21/2-SOME21/461284
47. Kalligeros S, Zannikos F, Stournas S, Lois E, Anastopoulos G, Teas C, et al. An investigation of using biodiesel/marine diesel blends on the performance of a stationary diesel engine. Biomass Bioenergy. 2003 Feb 1;24(2):141–9.
48. Mueller CJ, Boehman AL, Martin GC. An Experimental Investigation of the Origin of Increased NO_x Emissions When Fueling a Heavy-Duty Compression-Ignition Engine with Soy Biodiesel. SAE Int J Fuels Lubr [Internet]. 2009 Apr 27;2(1):789–816. Available from: http://www.jstor.org/stable/26273427
49. Lin CY. Effects of biodiesel blend on marine fuel characteristics for marine vessels. Energies (Basel) [Internet]. 2013 Sep 24 [cited 2023 Mar 20];6(9):4945–55. Available from: https://www.mdpi.com/1996-1073/6/9/4945/htm
50. Sun J, Caton JA, Jacobs TJ. Oxides of nitrogen emissions from biodiesel-fuelled diesel engines. Prog Energy Combust Sci [Internet]. 2010;36(6):677–95. Available from: https://www.sciencedirect.com/science/article/pii/S0360128510000237
51. Hoekman SK, Robbins C. Review of the effects of biodiesel on NOx emissions. Fuel Processing Technology [Internet]. 2012;96:237–49. Available from: https://www.sciencedirect.com/science/article/pii/S0378382012000021
52. International Maritime Organization. NOx Technical Code 2008, Technical Code on Control of Emission of Nitrogen Oxides from Marine Diesel Engines. 2008.
53. Zheng M, Reader GT, Hawley JG. Diesel engine exhaust gas recirculation—a review on advanced and novel concepts. Energy Convers Manag. 2004 Apr 1;45(6):883–900.
54. Klaus Mollenhauer HT. Handbook of Diesel Engines [Internet]. 1st ed. Mollenhauer K, Tschöke H, editors. Berlin, Heidelberg: Springer Berlin Heidelberg; 2010. 636 p. Available from: http://link.springer.com/10.1007/978-3-540-89083-6
55. MAN Energy Solutions. Emission Project Guide. Copenhagen; 2019.
56. Sun X, Liang X, Shu G, Lin J, Wang Y, Wang Y. Numerical investigation of two-stroke marine diesel engine emissions using exhaust gas recirculation at different injection time. Ocean Engineering. 2017 Nov 1;144:90–7.
57. Wang C, Wang T, Sun K, Lu Z, Gui Y. Effects of EGR and Injection Strategies on the Performance and Emissions of a Two-Stroke Marine Diesel Engine. In: SAE Technical Papers [Internet]. SAE International; 2017 [cited 2023 Mar 13]. Available from: https://www.sae.org/content/2017-01-2249/
58. Yin X, Li W, Zhang W, Lv X, Yang B, Wang Y, et al. Experimental analysis of the EGR rate and temperature impact on combustion and emissions characteristics in a heavy-duty NG engine. Fuel [Internet]. 2022 Feb 15 [cited 2023 May 19];310:122394. Available from: https://linkinghub.elsevier.com/retrieve/pii/S0016236121022663
59. Sun X, Liang X, Shu G, Lin J, Wang Y, Wang Y. Numerical investigation of two-stroke marine diesel engine emissions using exhaust gas recirculation at different injection time. Ocean Engineering. 2017 Nov 1;144:90–7.
60. Agarwal AK, Srivastava DK, Dhar A, Maurya RK, Shukla PC, Singh AP. Effect of fuel injection timing and pressure on combustion, emissions and performance characteristics of a single cylinder diesel engine. Fuel. 2013 Sep 1;111:374–83.
61. Liang X, Zheng Z, Zhang H, Wang Y, Yu H. A Review of Early Injection Strategy in Premixed Combustion Engines. Applied Sciences [Internet]. 2019;9(18). Available from: https://www.mdpi.com/2076-3417/9/18/3737
62. Egnell R. The influence of EGR on heat release rate and NO formation in a di diesel engine. SAE Technical Papers. 2000;
63. Ladommatos N, Abdelhalim SM, Zhao H, Hu. Z. Effects of EGR on heat release in diesel combustion. SAE Technical Papers. 1998;

64. Abd-Alla GH. Using exhaust gas recirculation in internal combustion engines: A review. Energy Convers Manag [Internet]. 2002 [cited 2023 Mar 9];43(8):1027–42. Available from: www.elsevier.com/locate/enconman
65. Zheng M, Reader GT, Hawley JG. Diesel engine exhaust gas recirculation - A review on advanced and novel concepts. Energy Convers Manag. 2004;45(6):883–900.
66. Feng L, Tian J, Long W, Gong W, Du B, Li D, et al. Decreasing NOx of a low-speed two-stroke marine diesel engine by using in-cylinder emission control measures. Energies (Basel) [Internet]. 2016 Apr 21 [cited 2023 Mar 13];9(4):304. Available from: https://www.mdpi.com/1996-1073/9/4/304/htm
67. Zhu Y, Zhang R, Zhou S, Huang C, Feng Y, Shreka M, et al. Performance Optimization of High-Pressure SCR System in a Marine Diesel Engine. Part I: Flow Optimization and Analysis. Top Catal. 2019 Feb 15;62(1–4):27–39.
68. Zhang Y, Xia C, Liu D, Zhu Y, Feng Y. Experimental investigation of the high-pressure SCR reactor impact on a marine two-stroke diesel engine. Fuel. 2023 Mar 1;335:127064.
69. Wintertur Gas & Diesel Ltd. Selective Catalytic Reduction FAQ. ; 2018.
70. Yang ZL, Zhang D, Caglayan O, Jenkinson ID, Bonsall S, Wang J, et al. Selection of techniques for reducing shipping NOx and SOx emissions. Transp Res D Transp Environ [Internet]. 2012 [cited 2023 Mar 9];17(6):478–86. Available from: http://dx.doi.org/10.1016/j.trd.2012.05.010
71. IACCSEA. Marine SCR - Cost Benefit Analysis. 2013.
72. Zhang G, Yan H, Li T, Zhu Y, Zhou S, Feng Y, et al. Relation analysis on emission control and economic cost of SCR system for marine diesels. 2021 [cited 2023 Jun 29]; Available from: https://doi.org/10.1016/j.scitotenv.2021.147856
73. Marine Environment Protection Committee (MEPC), 66th session, 31 March to 4 April 2014 [Internet]. [cited 2023 Jun 30]. Available from: https://www.imo.org/en/MediaCentre/MeetingSummaries/Pages/MEPC66.aspx
74. Zhao Y, Fan Y, Fagerholt K, Zhou J. Reducing sulfur and nitrogen emissions in shipping economically. Transp Res D Transp Environ [Internet]. 2021 Jan 1 [cited 2023 Jun 29];90:102641. Available from: https://linkinghub.elsevier.com/retrieve/pii/S1361920920308269
75. Zhang G, Yan H, Li T, Zhu Y, Zhou S, Feng Y, et al. Relation analysis on emission control and economic cost of SCR system for marine diesels. Science of The Total Environment [Internet]. 2021 Sep 20 [cited 2023 Jun 29];788:147856. Available from: https://linkinghub.elsevier.com/retrieve/pii/S0048969721029272
76. Azzara A, Rutherford D, Wang H. Feasibility of IMO Annex VI Tier III implementation using Selective Catalytic Reduction. 2014;